Bo Yang
Jianke Yang

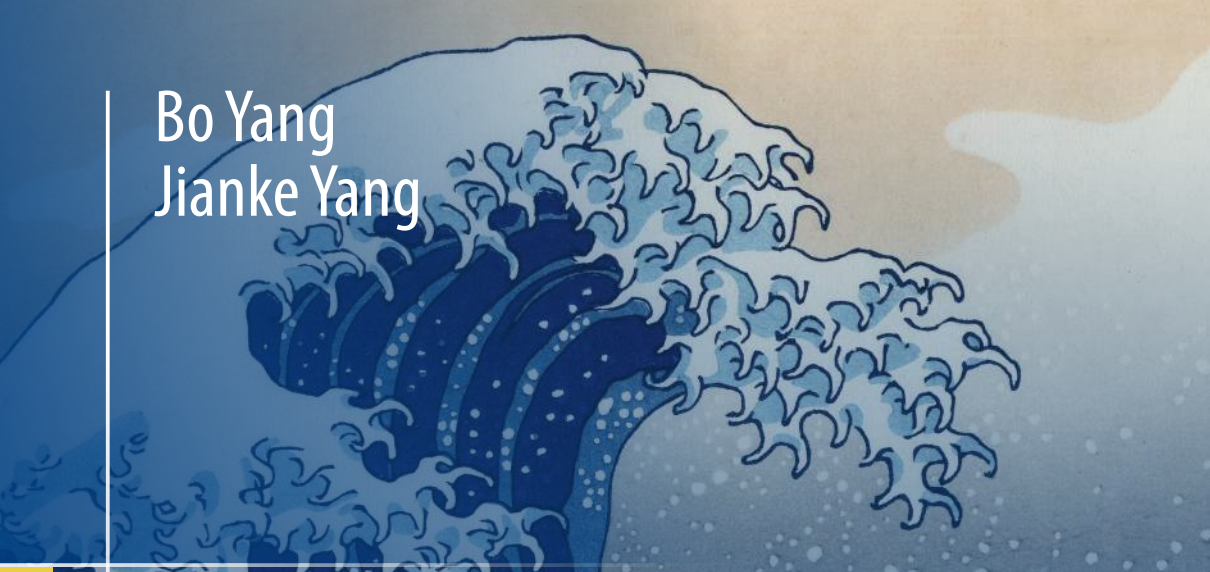

Rogue Waves in Integrable Systems

Springer

Rogue Waves in Integrable Systems

Bo Yang • Jianke Yang

Rogue Waves in Integrable Systems

Springer

Bo Yang
School of Mathematics and Statistics
Ningbo University
Ningbo, China

Jianke Yang
Department of Mathematics and Statistics
University of Vermont
Burlington, VT, USA

ISBN 978-3-031-66792-3 ISBN 978-3-031-66793-0 (eBook)
https://doi.org/10.1007/978-3-031-66793-0

This Springer imprint is published by the registered company Springer Nature Switzerland AG
The registered company address is: Gewerbestrasse 11, 6330 Cham, Switzerland

Preface

Rogue waves, also known as freak waves, monster waves, killer waves, extreme waves, and abnormal waves, are unusually large and suddenly appearing surface waves in the sea (Dysthe et al. 2008; Kharif et al. 2009). Since they appear and disappear without warning, they can be dangerous to ships, even to large ones. The famous Japanese print, *The Great Wave Of Kanagawa*, by Katsushika Hokusai (see cover of this book) can be viewed as an artistic rendering of a rogue wave. In the old days, sailors often talked about rogue waves that they saw in the sea, but such stories were often dismissed as myths or folklore. The first verified measurement of a rogue wave was on January 1, 1995, on the Draupner platform in the North Sea, where a 25.6 m wave was observed—much larger than the background wave field. Subsequently, rogue wave events have been observed in water tanks, thus allowing their physical mechanisms to be better understood. While there could be multiple mechanisms for the appearance of rogue waves, one of them is modulation instability, also called Benjamin-Feir instability, where a uniform nonlinear wavetrain (Stokes wavetrain) is unstable. When this Stokes wavetrain breaks up, it could generate rogue waves if the instability perturbation is seeded properly.

The study of rogue waves has spread from oceanography to other branches of physics such as nonlinear optics, plasma and Bose-Einstein condensates (BEC) because the mathematical model for one-dimensional surface waves in the ocean—the nonlinear Schrödinger (NLS) equation, also governs wave phenomena in those other systems. The NLS equation admits explicit rational solutions that exhibit rogue-wave-like behaviors, which is the underlying mathematical reason for the appearance of rogue water waves in laboratory experiments and possibly in the ocean as well. Since the NLS equation also governs those other physical systems, optical rogue waves, plasma rogue waves, and BEC rogue waves would be expected. Indeed, such rogue waves have been observed in laboratories of optics, plasma, and BEC, thus widening rogue occurrences in the natural world.

It should be recognized that there are also other physical settings where wave behaviors are governed not by the NLS equation but by other model equations

such as the Manakov system and the three-wave resonant interaction system. Such model equations turn out to admit rogue wave solutions as well, due to modulation instability of a uniform background wave. Then, rogue events can be expected in even more diverse physical systems.

Rogue waves can be studied both experimentally and theoretically. In the theoretical approach, one can derive and analyze rogue wave solutions in physically relevant mathematical models in order to gain insight into properties of rogue events. What makes this theoretical treatment possible is that, many physically relevant mathematical models, such as the NLS equation, the Manakov system, the three-wave resonant interaction system, and the long-wave-short-wave resonant interaction system, are all integrable, meaning that they can be solved analytically. Due to their integrability, we are able to derive explicit rogue wave solutions in those systems, which provide us with detailed quantitative information on rogue wave dynamics. In addition, due to the explicitness of these rogue wave solutions, we are able to perform various asymptotic analysis on these solutions, which results in asymptotic predictions of very fascinating rogue wave patterns. These rogue patterns turn out to be closely related to root structures of certain special polynomials, such as the Yablonskii-Vorob'ev polynomial hierarchy, the Okamoto polynomial hierarchies, and Adler-Moser polynomials. This beautiful connection between rogue patterns and special polynomials is a testament of the rich structure of rogue waves in integrable systems.

This book summarizes the current state of knowledge on rogue waves in physically important integrable systems. The first chapter derives many of these integrable systems in physical settings such as water waves, optics, and plasma. This chapter provides physical motivations for our mathematical studies in later chapters. The second chapter derives rogue wave solutions in a wide array of integrable systems, including those obtained in Chap. 1 and much beyond. In the literature, rogue waves in many of those integrable systems were originally derived by generalized Darboux transformation. We will derive these rogue waves almost exclusively by the bilinear method, since rogue wave expressions by the bilinear method are much more explicit than those by Darboux transformation. The third chapter analyzes patterns of rogue waves in certain asymptotic limits such as large internal parameters. Connections between rogue patterns and root structures of special polynomials will be revealed, and universality of these rogue patterns in integrable systems will be established. The fourth chapter describes laboratory experiments on rogue waves in physical settings such as optical fibers, water tanks, plasma, and BEC. The last chapter covers topics that are closely related to rogue waves of the earlier chapters, such as rogue waves arising from a nonuniform background, robustness of rogue waves, partial-rogue waves, and lump patterns in the Kadomtsev-Petviashvili I equation.

This book is intended as a monograph on the theoretical treatments of rogue waves. Its intended readership is researchers and graduate students in diverse

mathematical and physical fields, where rogue waves are an interest of study. Most derivations are self-contained, and the reader should be able to follow them without much help from other sources.

We would like to thank our families for strong support during the writing of this book.

Ningbo, China — Bo Yang
Burlington, VT, USA — Jianke Yang

Contents

Chapter 1
Physical Derivation of Integrable Nonlinear Wave Equations

In this beginning chapter, we derive many integrable systems as governing equations for diverse physical processes. Examples include the nonlinear Schrödinger equation for wave packet propagation in deep water, optical fibers, and unmagnetized plasma, the derivative nonlinear Schrödinger equation for nonlinear Alfvén waves in magnetized plasma, Manakov equations for light transmission in randomly-birefringent optical fibers, the long-wave-short-wave interaction model in water of finite depth, the three-wave resonant interaction system in water waves and optics, and Davey-Stewartson equations for two-dimensional wave packets in water of finite depth. Our method of derivation is the multi-scale perturbation method, the only exception being the optical-fiber case. These physical backgrounds of the underlying integrable systems will not only motivate our mathematical studies of rogue waves in these integrable systems in Chaps. 2 and 3, but also link our mathematical rogue solutions to physical experiments which we will also describe in Chap. 4.

We start with the nonlinear Schrödinger equation.

1.1 Nonlinear Schrödinger Equation

The nonlinear Schrödinger (NLS) equation

$$\mathrm{i}u_t + \frac{1}{2}u_{xx} + |u|^2 u = 0 \tag{1.1}$$

is one of the most important equations that arise in a wide variety of physical processes. In general, this equation governs the evolution of a weakly nonlinear and dispersive wave packet that depends on a single spatial dimension. It was first derived by Benney and Newell (1967) in a general setting. Zakharov (1968) and Hasimoto and Ono (1972) derived this equation for water wave packets on a free

B. Yang, J. Yang, *Rogue Waves in Integrable Systems*,
https://doi.org/10.1007/978-3-031-66793-0_1

surface. Shimizu and Ichikawa (1972) derived this equation for ion wave packets in an unmagnetized plasma. Hasegawa and Tappert (1973) showed that this same equation governs light pulse propagation in an optical fiber. The integrability of this equation was revealed by Zakharov and Shabat (1971).

In this section, we derive this NLS equation in water waves, optical fibers, and plasma.

1.1.1 In Deep Water

We consider the irrotational two-dimensional motion of an inviscid, incompressible, and homogeneous deep water with a free surface, subject to a constant gravitational force g. We take the x axis in the horizontal direction, and z axis in the vertical direction, with $z = 0$ set at the unperturbed free surface. Since the motion is irrotational, the velocity field $\mathbf{u}$ has a potential $\phi(x, z, t)$, where $\mathbf{u} = \nabla\phi$. The free surface is at $z = \zeta(x, t)$. Surface tension will be assumed small and ignored. Waves under gravity and no surface tension are called gravity waves.

The governing equations for these two-dimensional deep-water gravity waves are (Benney and Roskes 1969; Davey and Stewartson 1974)

$$\phi_{xx} + \phi_{zz} = 0, \quad -\infty < z \le \zeta, \tag{1.2}$$

$$\zeta_t + \phi_x \zeta_x = \phi_z, \quad z = \zeta, \tag{1.3}$$

$$\phi_t + g\zeta + \frac{1}{2}(\phi_x^2 + \phi_z^2) = 0, \quad z = \zeta. \tag{1.4}$$

The Laplace equation (1.2) is due to the incompressibility of the fluid, Eq. (1.3) is the kinematic condition on the surface, and Eq. (1.4) is the dynamic condition on the surface. In addition, we impose the bottom condition

$$\phi_z \to 0, \quad z \to -\infty, \tag{1.5}$$

i.e., the water has zero vertical velocity at the infinite bottom.

Derivation of the NLS Equation

We study a progressive wavetrain of wavenumber k and frequency ω travelling in the positive x direction (both k and ω are assumed positive). In the linear theory, valid when the wave amplitude is infinitesimal, this wave can be written as

$$\zeta(x, t) = \zeta_{11} e^{\mathrm{i}(kx-\omega t)} + c.c., \quad \phi(x, z, t) = \phi_{11} e^{\mathrm{i}(kx-\omega t)+kz} + c.c., \tag{1.6}$$

where ζ_{11} and ϕ_{11} are infinitesimal complex constants, and 'c.c.' represents complex conjugates. This ζ function can be rewritten as

$$\zeta(x,t) = 2|\zeta_{11}|\cos\left(kx - \omega t + \arg(\zeta_{11})\right). \tag{1.7}$$

Thus, the wave amplitude of the free surface is $2|\zeta_{11}|$.

The potential function in (1.6) satisfies the Laplace equation (1.2) automatically. Substituting ζ and ϕ in (1.6) into the two surface boundary conditions (1.3)–(1.4) and ignoring nonlinear terms, we get

$$\begin{bmatrix} -\mathrm{i}\omega & -k \\ g & -\mathrm{i}\omega \end{bmatrix} \begin{bmatrix} \zeta_{11} \\ \phi_{11} \end{bmatrix} = \begin{bmatrix} 0 \\ 0 \end{bmatrix}. \tag{1.8}$$

Nontrivial solutions for this linear homogeneous system are possible only when the determinant of the coefficient matrix is zero, which yields the dispersion relation

$$\omega = \sqrt{gk}. \tag{1.9}$$

Now, we consider this progressive wavetrain whose amplitude parameters ζ_{11} and ϕ_{11} are small but not infinitesimal, while the wavenumber k is treated as an $O(1)$ quantity (the latter can be achieved by choosing an appropriate length unit corresponding to the characteristic wavelength of the problem). Physically, this situation is where the surface wave's amplitude is small compared to the wavelength, i.e., the slope of the surface wave is small. We also allow these amplitudes ζ_{11} and ϕ_{11} to slowly vary in space and time. In this case, we use the multiscale perturbation theory to derive the temporal and spatial evolutions of these amplitude functions. In Benney and Roskes (1969) and Davey and Stewartson (1974), such derivations were given for water of finite depth. In deep water, a significant difference is that the amplitude function ϕ_{11} of the potential depends not only on the slow x variable, but also on the slow z variable. As a consequence, our derivation below is noticeably different from those in Benney and Roskes (1969) and Davey and Stewartson (1974) (and in Sect. 1.4 for a higher-dimensional generalization).

We write solutions to Eqs. (1.2)–(1.4) as perturbation series

$$\begin{aligned}\zeta = {} & \epsilon\left(\zeta_{01} + \zeta_{11}e^{\mathrm{i}\theta} + c.c.\right) + \epsilon^2\left(\zeta_{02} + \zeta_{12}e^{\mathrm{i}\theta} + \zeta_{22}e^{2\mathrm{i}\theta} + c.c.\right) + \\ & + \epsilon^3\left(\zeta_{03} + \zeta_{13}e^{\mathrm{i}\theta} + \zeta_{23}e^{2\mathrm{i}\theta} + \zeta_{33}e^{3\mathrm{i}\theta} + c.c.\right) + \cdots,\end{aligned} \tag{1.10}$$

$$\begin{aligned}\phi = {} & \epsilon\left(\phi_{01} + \phi_{11}e^{\mathrm{i}\theta+kz} + c.c.\right) + \epsilon^2\left(\phi_{02} + \phi_{12}e^{\mathrm{i}\theta+kz} + \phi_{22}e^{2\mathrm{i}\theta+2kz} + c.c.\right) + \\ & + \epsilon^3\left(\phi_{03} + \phi_{13}e^{\mathrm{i}\theta+kz} + \phi_{23}e^{2\mathrm{i}\theta+2kz} + \phi_{33}e^{3\mathrm{i}\theta+3kz} + c.c.\right) + \cdots,\end{aligned} \tag{1.11}$$

where $\theta = kx - \omega t$,

$$\zeta_{nj} = \zeta_{nj}(\xi,\tau), \quad \phi_{nj} = \phi_{nj}(\xi, Z, \tau), \tag{1.12}$$

$$\xi = \epsilon(x - c_g t), \quad Z = \epsilon z, \quad \tau = \epsilon^2 t, \tag{1.13}$$

$c_g = \omega'(k) = \omega/(2k)$ is the group velocity, '$c.c.$' represents complex conjugates of only the $e^{in\theta}$ or $e^{in\theta+nkz}$ terms, and ζ_{0j}, ϕ_{0j} are real functions. Here, ϵ is a small positive parameter measuring the slope of the wavy surface. Notice the slow-z dependence of ϕ_{nj} here, which is absent in water of finite depth (Benney and Roskes 1969; Davey and Stewartson 1974).

We first substitute the expansion (1.11) for ϕ into the Laplace equation (1.2) and equate coefficients of $\epsilon^j e^{in\theta+nkz}$ to zero. The results are:

$$\epsilon^3 e^0: \qquad \phi_{01,\xi\xi} + \phi_{01,ZZ} = 0; \tag{1.14}$$

$$\epsilon^2 e^{i\theta+kz}: \qquad \phi_{11,Z} = -i\phi_{11,\xi}; \tag{1.15}$$

$$\epsilon^3 e^{i\theta+kz}: \qquad \phi_{12,Z} = -i\phi_{12,\xi}. \tag{1.16}$$

At other orders of $\epsilon^j e^{in\theta+nkz}$, we get additional relations, but they are not needed for our purpose.

Next, we consider the surface boundary conditions (1.3)–(1.4). Expanding the ϕ function in these boundary conditions around the mean surface level $z = 0$, these boundary conditions up to $O(\epsilon^3)$ become

$$\zeta_t + \zeta_x(\phi_x + \phi_{xz}\zeta) = \phi_z + \phi_{zz}\zeta + \frac{1}{2}\phi_{zzz}\zeta^2, \qquad z = 0, \tag{1.17}$$

$$\phi_t + \phi_{tz}\zeta + \frac{1}{2}\phi_{tzz}\zeta^2 + g\zeta + \frac{1}{2}(\phi_x^2 + \phi_z^2) + \zeta(\phi_x\phi_{xz} + \phi_z\phi_{zz}) = 0, \ z = 0. \tag{1.18}$$

Then, we substitute the above (ζ, ϕ) expansions (1.10)–(1.11) into these new boundary conditions and equate coefficients of $\epsilon^j e^{in\theta}$ to zero. At order ϵe^0, the second boundary condition (1.18) gives

$$\zeta_{01}(\xi, \tau) = 0. \tag{1.19}$$

Utilizing this result, the first boundary condition (1.17) at order $\epsilon^2 e^0$ gives

$$\phi_{01,Z} = 0, \quad Z = 0. \tag{1.20}$$

This condition, together with the Laplace equation (1.14) for ϕ_{01} and boundary condition (1.5) at deep bottom, yields

$$\phi_{01}(\xi, Z, \tau) = \phi_{01}(\tau), \tag{1.21}$$

i.e., the function ϕ_{01} is independent of ξ and Z. This result is important, as it shows that the horizontal velocity ϕ_x from the expansion (1.11) has no $O(\epsilon^2 e^0)$ mean flow. In water of finite depth, however, this $O(\epsilon^2 e^0)$ mean flow would exist, as was shown in Benney and Roskes (1969) and Davey and Stewartson (1974) (see also Sect. 1.4 later).

At $O(\epsilon e^{i\theta})$, the two surface boundary conditions (1.17)–(1.18) give two relations on ζ_{11} and ϕ_{11} at $Z = 0$, which are the same as those in Eq. (1.8). Thus, those relations yield the dispersion relation (1.9), as well as the relation

$$\zeta_{11} = (i\omega/g)\,\phi_{11}|_{Z=0}. \tag{1.22}$$

At $O(\epsilon^2 e^0)$, the second boundary condition (1.18) leads to

$$\zeta_{02}(\xi, \tau) = 0. \tag{1.23}$$

At $O(\epsilon^2 e^{i\theta})$, the two boundary conditions give the following two equations

$$\begin{bmatrix} -i\omega & -k \\ g & -i\omega \end{bmatrix} \begin{bmatrix} \zeta_{12} \\ \phi_{12} \end{bmatrix} = \begin{bmatrix} \phi_{11,Z} + c_g \zeta_{11,\xi} \\ c_g \phi_{11,\xi} \end{bmatrix}, \quad Z = 0. \tag{1.24}$$

Here, the c_g terms come from our choice of the moving coordinate $\xi = \epsilon(x - c_g t)$. This is a linear inhomogeneous system. Since its coefficient matrix has a zero determinant due to the dispersion relation (1.9), this system is solvable only if it satisfies a compatibility condition, which is

$$c_g \phi_{11,\xi} = (i\omega/g)(\phi_{11,Z} + c_g \zeta_{11,\xi}), \quad Z = 0. \tag{1.25}$$

Inserting relations (1.15) and (1.22) into this condition and utilizing the dispersion relation (1.9), we find that this condition is satisfied automatically. This fact simply indicates that the wavepacket indeed travels at the group velocity c_g, i.e., our choice of the moving coordinate ξ is appropriate.

At $O(\epsilon^2 e^{2i\theta})$, the two boundary conditions (1.17)–(1.18) give the following two equations

$$\begin{bmatrix} -2i\omega & -2k \\ g & -2i\omega \end{bmatrix} \begin{bmatrix} \zeta_{22} \\ \phi_{22} \end{bmatrix} = \begin{bmatrix} 2k^2 \phi_{11} \zeta_{11} \\ ik\omega \phi_{11} \zeta_{11} \end{bmatrix}, \quad Z = 0. \tag{1.26}$$

The determinant of its coefficient matrix is nonzero, thus this system has a unique solution, which is

$$\zeta_{22} = -(k^2/g)\phi_{11}^2|_{Z=0}, \quad \phi_{22}|_{Z=0} = 0. \tag{1.27}$$

Here, the formula (1.22) for ζ_{11} has been utilized.

Lastly, we look at $O(\epsilon^3 e^{i\theta})$. At this order, the two boundary conditions give the following two equations

$$\begin{bmatrix} -i\omega & -k \\ g & -i\omega \end{bmatrix} \begin{bmatrix} \zeta_{13} \\ \phi_{13} \end{bmatrix} = \begin{bmatrix} F_1 \\ F_2 \end{bmatrix}, \quad Z = 0, \tag{1.28}$$

where F_1 and F_2 are certain functions. Utilizing Eqs. (1.22), (1.27), as well as the dispersion relation (1.9), F_1 and F_2 can be reduced to

$$F_1 = \phi_{12,Z} + c_g\zeta_{12,\xi} - \zeta_{11,\tau} - \frac{5}{2}\mathrm{i}k^2\omega|\zeta_{11}|^2\zeta_{11}, \tag{1.29}$$

$$F_2 = c_g\phi_{12,\xi} - \phi_{11,\tau} - \frac{3}{2}k^2 g\,|\zeta_{11}|^2\zeta_{11}. \tag{1.30}$$

Due to the zero determinant of its coefficient matrix, the linear inhomogeneous system (1.28) has a solvability condition $F_2 = (\mathrm{i}\omega/k)F_1$. Utilizing the relation (1.16) to replace the $\phi_{12,Z}$ term in F_1, and utilizing the relation (1.22) as well as the dispersion relation (1.9), this solvability condition becomes

$$\mathrm{i}\zeta_{11,\tau} - (\mathrm{i}/4\omega)(-\mathrm{i}\omega\phi_{12} + g\zeta_{12})_\xi - 2k^2\omega|\zeta_{11}|^2\zeta_{11} = 0. \tag{1.31}$$

Here, the ϕ_{12} term is evaluated at $Z = 0$. Finally, we use the second equation in (1.24) to replace the middle term in the above equation and apply the relation (1.22) again. Then we get

$$\mathrm{i}\frac{\partial\zeta_{11}}{\partial\tau} - \frac{\omega}{8k^2}\frac{\partial^2\zeta_{11}}{\partial\xi^2} - 2k^2\omega\,|\zeta_{11}|^2\zeta_{11} = 0. \tag{1.32}$$

This is a NLS equation in temporal-evolution form, and it governs the evolution of the wave envelope ζ_{11} on the free surface. In this equation, $-\omega/(8k^2)$ in front of $\zeta_{11,\xi\xi}$ is called the dispersion coefficient, and $-2k^2\omega$ in front of $|\zeta_{11}|^2\zeta_{11}$ is called the nonlinear coefficient.

To put Eq. (1.32) into a physically more recognizable form, we denote $\epsilon\zeta_{11} = u/2$. Then, from Eqs. (1.10) and (1.19) we see that the water surface elevation $\zeta(x,t)$ is related to $u(x,t)$ as

$$\zeta(x,t) = \mathrm{Re}\{u(x,t)\exp[\mathrm{i}(kx - \omega t)]\} \tag{1.33}$$

to the leading order of wave steepness ϵ. A more accurate relation between $\zeta(x,t)$ and $u(x,t)$, up to the second order of wave steepness ϵ, can be obtained from Eqs. (1.10), (1.19), (1.22), (1.23) and (1.27) as

$$\zeta(x,t) = \mathrm{Re}\left\{u(x,t)e^{\mathrm{i}(kx-\omega t)} + \frac{1}{2}k\,u^2(x,t)e^{2\mathrm{i}(kx-\omega t)}\right\}. \tag{1.34}$$

Here, the $\epsilon^2\zeta_{12}e^{\mathrm{i}(kx-\omega t)}$ term in the ζ expansion (1.10) can be lumped into the $\epsilon\zeta_{11}e^{\mathrm{i}(kx-\omega t)}$ term and is thus dropped.

The temporal-evolution equation for $u(x,t)$ in physical units can be obtained from Eq. (1.32) as

$$\mathrm{i}\frac{\partial u}{\partial t} - \frac{\omega}{8k^2}\frac{\partial^2 u}{\partial\hat{x}^2} - \frac{1}{2}k^2\omega\,|u|^2u = 0, \tag{1.35}$$

where $\hat{x} = x - c_g t$, $c_g = \omega/2k$, and $\omega = \sqrt{gk}$. Introducing nondimensional variables

$$\tilde{u} = u/a, \quad \tilde{x} = \sqrt{2}ak^2\hat{x}, \quad \tilde{t} = -a^2k^2\omega t/2, \tag{1.36}$$

where a is a representative wave-amplitude parameter, the above equation is then reduced to the standard NLS equation

$$\mathrm{i}\frac{\partial \tilde{u}}{\partial \tilde{t}} + \frac{1}{2}\frac{\partial^2 \tilde{u}}{\partial \tilde{x}^2} + |\tilde{u}|^2\tilde{u} = 0, \tag{1.37}$$

which is Eq. (1.1) in tilde notations.

Universal Formula for the Dispersion Coefficient

It is important to notice that, in the above NLS equation (1.32) for ζ_{11}, the dispersion coefficient $-\omega/(8k^2)$ is equal to $\omega''(k)/2$, where $\omega(k)$ is the dispersion relation given in Eq. (1.9). Thus, this NLS equation can be rewritten as

$$\mathrm{i}\zeta_{11,\tau} + \frac{1}{2}\omega''(k)\,\zeta_{11,\xi\xi} - 2k^2\omega|\zeta_{11}|^2\zeta_{11} = 0. \tag{1.38}$$

The fact of this dispersion coefficient being equal to $\omega''(k)/2$ is definitely not an accident. Rather, it is a necessity so that the linear evolution of the free surface function ζ_{11} in Eq. (1.38) matches the linear dispersion relation (1.9). To show this, let us write the linear dispersion relation as $\hat{\omega} = \hat{\omega}(\hat{k})$, where $\hat{k}$ and $\hat{\omega}$ are the wavenumber and frequency of a general linear monochromatic wavetrain (these hatted quantities are introduced to distinguish them from the wavenumber k and frequency ω of the present wavetrain). Here, the exact functional form (1.9) of the dispersion relation, i.e., $\hat{\omega}(\hat{k}) = (g\hat{k})^{1/2}$, is not needed. Then, when $\hat{k}$ is near the wavenumber k of the present wavetrain, i.e., $\hat{k} = k + \tilde{k}$, where $|\tilde{k}| \ll 1$, we have

$$\tilde{\omega} \equiv \hat{\omega}(\hat{k}) - \omega(k) = \omega'(k)\tilde{k} + \frac{1}{2}\omega''(k)\tilde{k}^2 + \cdots. \tag{1.39}$$

The linear partial differential equation for the free surface

$$\zeta(x,t) = \zeta_{11}(x,t)e^{\mathrm{i}(kx-\omega t)} + c.c. \tag{1.40}$$

which features the above dispersion relation (1.39) for the wavetrain $\zeta_{11} \sim e^{\mathrm{i}(\tilde{k}x-\tilde{\omega}t)}$ (up to $O(\tilde{k}^2)$) is

$$(\mathrm{i}\partial_t)\zeta_{11} = \left(\omega'(k)(-\mathrm{i}\partial_x) + \frac{1}{2}\omega''(k)(-\mathrm{i}\partial_x)^2\right)\zeta_{11}. \tag{1.41}$$

In terms of the coordinates $\xi = \epsilon(x - c_g t)$ and $\eta = \epsilon^2 t$ that we have introduced earlier in Eq. (1.13), this equation then becomes

$$\mathrm{i}\zeta_{11,\tau} + \frac{1}{2}\omega''(k)\zeta_{11,\xi\xi} = 0, \tag{1.42}$$

which matches the linear part of the ζ_{11} equation (1.38). Since this derivation did not use the specific form of the dispersion relation (1.9), the dispersion coefficient of the NLS equation (1.32) being $\omega''(k)/2$ is then valid for any physical system where the NLS equation is derived. This certainly includes optical fibers and plasma which we will treat in subsequent subsections. Using similar considerations, one can also write down the linear parts of other nonlinear wave equations derived in physical systems from the linear dispersion relation.

NLS Equation in Spatial Evolution Form

The NLS equation (1.32) for ζ_{11} is written as a temporal evolution equation. In water-tank experiments, a wave-maker (paddle) generates a time-dependent wave at a fixed spatial location (say $x = 0$), and we need to predict how this wave will evolve and deform as it propagates down the water tank. In such a case, it is more convenient to write the NLS equation as a spatial evolution equation. To do so, we define new slow variables

$$T = \epsilon\left(t - \frac{x}{c_g}\right), \quad X = \epsilon^2 x. \tag{1.43}$$

It can be seen that these new slow variables are related to the previous slow variables ξ and τ as $X = c_g\tau + \epsilon\xi$ and $T = -\xi/c_g$. Then for $\xi, \tau = O(1)$, X is asymptotically equal to $c_g\tau$. Thus the derivatives to τ and ξ in Eq. (1.32) can be converted to derivatives to X and T, and we get the NLS equation in spatial-evolution form

$$\mathrm{i}\frac{\partial\zeta_{11}}{\partial X} - \frac{1}{g}\frac{\partial^2\zeta_{11}}{\partial T^2} - 4k^3|\zeta_{11}|^2\zeta_{11} = 0. \tag{1.44}$$

This spatial-evolution form of the NLS equation for ζ_{11} can also be derived directly from the previous multiscale perturbation analysis if we write ζ_{nj} as a function of (X, T) as defined in Eq. (1.43) rather than as a function of (ξ, τ) as in Eq. (1.12). Solutions ζ_{11} out of the two forms (1.32) and (1.44) of the NLS equation are often asymptotically equivalent in the physical (x, t) plane (Chabchoub and Grimshaw 2016)

For the u variable defined through $\epsilon\zeta_{11} = u/2$ as before, the above NLS equation (1.44) in explicit physical units becomes

$$\mathrm{i}\frac{\partial u}{\partial x} - \frac{1}{g}\frac{\partial^2 u}{\partial\hat{t}^2} - k^3|u|^2u = 0, \tag{1.45}$$

where $\hat{t} = t - x/c_g$, $c_g = \omega/2k$, and $\omega = \sqrt{gk}$. The water surface elevation $\zeta(x, t)$ is related to the variable $u(x, t)$ as (1.33) to the first order of wave steepness

and as (1.34) to the second order of wave steepness. Introducing nondimensional variables

$$\tilde{u} = u/a, \quad \tilde{x} = -k^3 a^2 x, \quad \tilde{t} = \sqrt{gk^3 a^2/2}\, \hat{t}, \tag{1.46}$$

where a is a representative wave-amplitude parameter, the above equation is reduced to the standard NLS equation

$$\mathrm{i}\frac{\partial \tilde{u}}{\partial \tilde{x}} + \frac{1}{2}\frac{\partial^2 \tilde{u}}{\partial \tilde{t}^2} + |\tilde{u}|^2 \tilde{u} = 0, \tag{1.47}$$

which is Eq. (1.1) in tilde notations.

Stokes Wave

A special space-independent solution to the NLS equation (1.32) in temporal evolution form is

$$\zeta_{11}(\xi, \tau) = \frac{1}{2} a_0 e^{-\frac{1}{2}\mathrm{i}k^2 \omega a_0^2 \tau}, \tag{1.48}$$

where a_0 is a positive constant. Then, the free-surface elevation $\zeta(x, t)$ from the expansion (1.10) is

$$\zeta(x, t) = a \cos\left[kx - \omega\left(1 + \frac{1}{2}k^2 a^2\right)t\right] + O(a^2), \tag{1.49}$$

where $a \equiv \epsilon a_0$ is small [here the fact of $\zeta_{01} = 0$ from Eq. (1.19) has been used]. This solution describes a nonlinear progressive wavetrain of wavenumber k and amplitude a, whose frequency is amplitude-dependent. The phase velocity of this nonlinear wavetrain is

$$c_p = \frac{\omega}{k}\left(1 + \frac{1}{2}k^2 a^2\right). \tag{1.50}$$

This solution was first derived by Stokes (1847).

The counterpart of the Stokes wave in the NLS equation (1.44) in spatial evolution form is the time-independent solution

$$\zeta_{11}(X, T) = \frac{1}{2} a_0 e^{-\mathrm{i}k^3 a_0^2 X}. \tag{1.51}$$

In this case, the free-surface elevation $\zeta(x, t)$ from the expansion (1.10) is

$$\zeta(x, t) = a \cos\left[k\left(1 - k^2 a^2\right)x - \omega t\right] + O(a^2), \tag{1.52}$$

where $a \equiv \epsilon a_0$ is small.

Benjamin-Feir Instability

The value of the above NLS equations (1.32) and (1.44) for gravity wavepackets goes far beyond the rederivation of the Stokes wavetrain. Another success of these equations is that they can be used to show that this (uniform) Stokes wavetrain is unstable—an instability which was predicted theoretically by Benjamin and Feir (1967) and is often called Benjamin-Feir instability in the literature. Benjamin-Feir instability is equivalent to the modulation instability of monochromatic nonlinear waves in other physical fields such as optics and plasma. In a water tank, this instability means that, the uniform Stokes wave (1.52) generated at the wavemaker ($x = 0$), under weak perturbations, will eventually break up as it propagates down the tank.

To show this instability, we only need to show the time-independent wave envelope solution (1.51) is unstable in the NLS equation (1.32) in spatial evolution form. For this purpose, we perturb this solution by normal modes as

$$\zeta_{11}(X, T) = \left(\frac{1}{2}a_0 + \alpha\, e^{\Lambda X + \mathrm{i}\Omega T} + \beta^* e^{\Lambda^* X - \mathrm{i}\Omega T}\right) e^{-\mathrm{i}k^3 a_0^2 X}, \tag{1.53}$$

where $\epsilon\Omega$ is the frequency of the perturbation in the sideband of the wave's dominant frequency ω, Λ is the spatial exponent of this perturbation, and (α, β) are small complex constants. Stokes waves will be linearly unstable if there exist sideband frequencies $\epsilon\Omega$ of perturbations, such that their corresponding spatial exponents Λ have positive real parts giving rise to exponentially growing perturbations upon propagation down the tank. We insert the perturbed solution (1.53) into the NLS equation (1.44). Dropping nonlinear terms of α and β since they are smaller, and performing simple algebra, we find that (α, β) satisfy the following system of linear homogeneous equations

$$\begin{bmatrix} \Omega^2 g^{-1} - k^3 a_0^2 + \mathrm{i}\Lambda & -k^3 a_0^2 \\ -k^3 a_0^2 & \Omega^2 g^{-1} - k^3 a_0^2 - \mathrm{i}\Lambda \end{bmatrix} \begin{bmatrix} \alpha \\ \beta \end{bmatrix} = \begin{bmatrix} 0 \\ 0 \end{bmatrix}. \tag{1.54}$$

For this system to admit nontrivial solutions, the determinant of its coefficient matrix must be zero, which leads to the expression for the spatial exponent Λ as

$$\Lambda^2 = \frac{\Omega^2}{g}\left(2k^3 a_0^2 - \frac{\Omega^2}{g}\right). \tag{1.55}$$

For sideband frequencies Ω where the right side of the above equation is positive, i.e., $|\Omega| < \sqrt{2}ka_0\omega$, Λ would have a positive part, which makes the uniform Stokes wavetrain (1.52) linearly unstable. In more explicit physical terms, this means for infinitesimal disturbances with frequencies $\omega(1 \pm \delta)$ to the Stokes wavetrain (1.52), if $0 < \delta < \sqrt{2}ka$, where k and a are the wavenumber and amplitude of the wavetrain, then such disturbances would grow exponentially, leading to the

wavetrain's destruction. This sideband instability is what Benjamin and Feir (1967) showed using a different method.

The Stokes wavetrains also exist in water of finite depth. In this case, these uniform wavetrains are unstable only if $kh > 1.363$, where h is the mean depth of water (Benjamin 1967; Whitham 1967). More will be said on this in Sect. 1.4.

The Benjamin-Feir instability of the Stokes wavetrain has been observed in water tanks. In a water tank, an oscillating paddle can make a uniform Stokes wave (1.52). Its instability predicts that this Stokes wave, under sideband-frequency perturbations at the wave maker, will eventually disintegrate as it propagates down the tank. Photographs illustrating this disintegration were shown in Benjamin (1967) and are reproduced in Fig. 1.1. In this experiment, $h = 25$ ft, and $k = 2\pi/7.2 \approx 0.873$/ft, which gives $kh \approx 21.8$. Thus, instability of the Stokes wavetrain is expected to occur. In fact, since $kh \gg 1$ here, the deep-water theory presented in this section applies. Fig. 1.1a shows the wavetrain close to the wavemaker at one end of the basin. Here, the wavetrain is manifestly in a regular periodic condition, except for

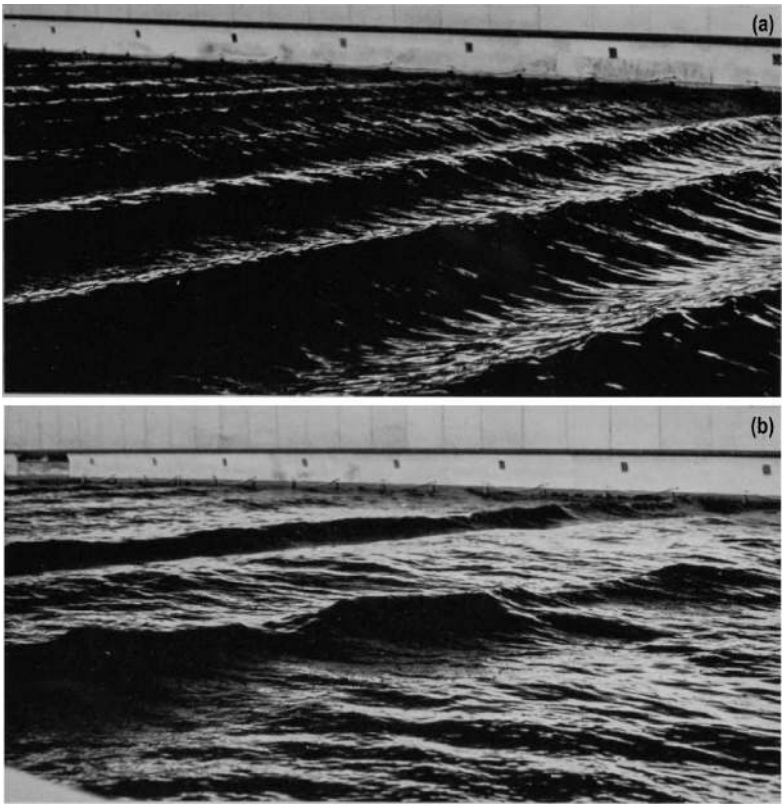

Fig. 1.1 Photographs illustrating the instability and disintegration of Stokes wavetrains in deep water: (**a**) view near to wavemaker; (**b**) view at 200 ft. farther from wavemaker. Fundamental wavelength, 7.2 ft. Depth of water: 25 ft. Taken from Benjamin (1967)

small-scale roughness which is inevitably present when waves are produced on this scale and which is insignificant to the process under question. In contrast, Fig. 1.1b shows the same wavetrain at a distance of 200 ft farther along the tank, and it can be seen that drastic distortions have occurred.

It is important to recognize that disintegration of the Stokes wavetrain is not the only scenario of evolution following the Benjamin-Feir instability. Depending on initial perturbations, other evolution scenarios can also occur. One such example is rogue water waves that arise from the Stokes wavetrain, develop into a localized wave excitation with a much higher amplitude, and then recede back to the same Stokes wavetrain. Such rogue waves will be the focus of this book, and their observations in water tanks will be presented in Chap. 4.

The theory we presented in this section for two-dimensional gravity waves in deep water can be readily generalized to three dimensions. In this case, we still consider the motion of a progressive wavetrain along the horizontal x direction, but allow its amplitudes to also slowly vary along the transverse y direction. In other words, $\zeta \sim \epsilon\,\zeta_{11}(\xi, \eta, \tau)e^{\mathrm{i}(kx-\omega t)}$ now, where $\eta = \epsilon y$ is the slow variable in y. By slightly modifying the above perturbation calculations, we can show that the envelope function $\zeta_{11}(\xi, \eta, \tau)$ is still governed by the NLS equation (1.32), except that an additional linear term $\gamma\,\zeta_{11,\eta\eta}/2$ is added to its left side, where $\gamma = \omega/(2k^2)$ is the dispersion constant along the y direction.

1.1.2 In Optical Fibers

An optical fiber is a flexible, transparent cylinder of glass (silica) that comprises a central core surrounded by a cladding whose refractive index is slightly lower than the core index. The core diameter is typically on the order of 10 μm, the cladding diameter typically on the order of 100 μm, and their refractive index difference typically less than 0.5%. Light is kept in the core by the phenomenon of total internal reflection which causes the fiber to act as a waveguide. Optical fibers are used most often in fiber-optic communications, where they permit transmission over longer distances and at higher data transfer rates than electrical cables. Fibers are used instead of metal wires because the attenuation rates of fibers are much lower, down to only 0.2 dB/km (or about 5% power loss per kilometer) in the 1.55-μm wavelength region. In addition, fibers are immune to electromagnetic interference, a problem metal wires suffer. The response of optical fibers to light becomes nonlinear when the light intensity becomes high, and nonlinear effects are often important in practical situations.

In this subsection, we derive the NLS equation for light transmission in an optical fiber. The NLS equation for optical fibers was first written down by Hasegawa and Tappert (1973), and derived more rigorously by Kodama and Hasegawa (1987). Our treatment follows Agrawal (2001) with some modifications.

Like all electromagnetic phenomena, light transmission in an optical fiber is governed by Maxwell's equations. Since the optical fiber is charge-free and

nonmagnetic, the Maxwell equations take the form

$$\nabla \times \mathbf{E} = -\frac{\partial \mathbf{B}}{\partial t}, \tag{1.56}$$

$$\nabla \times \mathbf{H} = \frac{\partial \mathbf{D}}{\partial t}, \tag{1.57}$$

$$\nabla \cdot \mathbf{D} = 0, \tag{1.58}$$

$$\nabla \cdot \mathbf{B} = 0, \tag{1.59}$$

and the corresponding medium equations are

$$\mathbf{D} = \epsilon_0 \mathbf{E} + \mathbf{P}, \tag{1.60}$$

$$\mathbf{B} = \mu_0 \mathbf{H}. \tag{1.61}$$

Here, $\mathbf{E}$ and $\mathbf{H}$ are the electric and magnetic field vectors, $\mathbf{D}$ and $\mathbf{B}$ are the electric and magnetic displacement vectors, ϵ_0 and μ_0 are the dielectric constant and the medium's permeability in vacuum respectively, and $\mathbf{P}$ is the induced electric polarization.

By taking the curl of Eq. (1.56) and using Eqs. (1.57), (1.60), and (1.61), one can eliminate $\mathbf{B}$ and $\mathbf{D}$ in favor of $\mathbf{E}$ and $\mathbf{P}$ and obtain

$$\nabla \times (\nabla \times \mathbf{E}) = -\frac{1}{c^2}\frac{\partial^2 \mathbf{E}}{\partial t^2} - \mu_0 \frac{\partial^2 \mathbf{P}}{\partial t^2}, \tag{1.62}$$

where $c = 1/\sqrt{\mu_0 \epsilon_0}$ is the speed of light in vacuum.

To complete the description, a relation between the induced polarization $\mathbf{P}$ and the electric field $\mathbf{E}$ is needed. A phenomenological relation between them can be used far from medium resonances, which is the case for optical fibers in the wavelength range 0.5-2 μm that is of interest for the study of nonlinear effects. Since optical fibers are made of silica glass and display inversion symmetry, second-order nonlinear effects vanish identically. Thus, this phenomenological relation up to the third-order nonlinear effects is

$$\mathbf{P}(\mathbf{r}, t) = \mathbf{P}_L(\mathbf{r}, t) + \mathbf{P}_{NL}(\mathbf{r}, t), \tag{1.63}$$

where $\mathbf{r}$ is the spatial vector, $\mathbf{P}_L(\mathbf{r}, t)$ is the linear part of the relation with

$$\mathbf{P}_L(\mathbf{r}, t) = \epsilon_0 \int_{-\infty}^{\infty} \chi^{(1)}(\mathbf{r}, t - t') \cdot \mathbf{E}((\mathbf{r}, t')dt', \tag{1.64}$$

$\mathbf{P}_{NL}(\mathbf{r}, t)$ is the nonlinear (cubic) part of the relation with

$$\mathbf{P}_{NL}(\mathbf{r},t) = \epsilon_0 \int\int\int_{-\infty}^{\infty} \chi^{(3)}(\mathbf{r}, t-t_1, t-t_2, t-t_3)$$

$$\vdots \quad \mathbf{E}((\mathbf{r},t_1)\mathbf{E}((\mathbf{r},t_2)\mathbf{E}((\mathbf{r},t_3)dt_1dt_2dt_3, \tag{1.65}$$

and $\chi^{(j)}$ is a tensor with rank $j+1$.

Equation (1.62) can be simplified under certain conditions. Using a vector identity, its left side can be written as

$$\nabla \times (\nabla \times \mathbf{E}) = \nabla(\nabla \cdot \mathbf{E}) - \nabla^2\mathbf{E}. \tag{1.66}$$

In many cases, such as weakly guided fibers where the refractive index variation between the core and cladding is small, $\nabla \cdot \mathbf{E}$ can be shown to be small and can be neglected (Agrawal 2001). Under this approximation, Eq. (1.62) reduces to

$$\nabla^2\mathbf{E} = \frac{1}{c^2}\frac{\partial^2\mathbf{E}}{\partial t^2} + \mu_0\frac{\partial^2\mathbf{P}_L}{\partial t^2} + \mu_0\frac{\partial^2\mathbf{P}_{NL}}{\partial t^2}, \tag{1.67}$$

where Eq. (1.63) has been utilized.

To solve Eq. (1.67), we will make a few more assumptions. First, the nonlinear response is assumed to be instantaneous so that the time dependence of $\chi^{(3)}$ in Eq. (1.65) is given by the product of three delta functions of the form $\delta(t-t_1)$. In this case, Eq. (1.65) reduces to

$$\mathbf{P}_{NL}(\mathbf{r},t) = \epsilon_0\,\chi^{(3)}(\mathbf{r})\vdots\mathbf{E}(\mathbf{r},t)\mathbf{E}(\mathbf{r},t)\mathbf{E}(\mathbf{r},t). \tag{1.68}$$

The assumption of instantaneous nonlinear response amounts to neglecting the contribution of molecular vibrations to $\chi^{(3)}$ (the Raman effect), which is approximately valid for pulse widths > 1 ps. Second, $\mathbf{P}_{NL}$ is assumed to be a small perturbation to $\mathbf{P}_L$, which is justified because nonlinear changes in the refractive index are less than 10^{-6} in practice. Third, the optical field is assumed to maintain its polarization along the fiber length so that a scalar approach is valid. This is the case in polarization-maintaining fibers, or when birefringence of the fiber is negligible. Fourth, the optical field is assumed to be quasi-monochromatic, i.e., the pulse spectrum, centered at ω_0, is assumed to have a spectral width $\Delta\omega$ such that $\Delta\omega/\omega_0 \ll 1$. Since $\omega_0 \sim 10^{15}\mathrm{s}^{-1}$, the last assumption is valid for pulses as short as 0.1 ps.

Under quasi-monochromatic approximation (i.e., slowly varying envelope approximation), it is useful to separate the rapidly varying part of the electric field by writing it in the form

$$\mathbf{E}(\mathbf{r},t) = \frac{1}{2}\hat{x}\left[E(\mathbf{r},t)e^{-\mathrm{i}\omega_0 t} + c.c.\right], \tag{1.69}$$

where $\hat{x}$ is the polarization unit vector in the transverse plane that is orthogonal to the propagation direction z, and $E(\mathbf{r}, t)$ is a slowly varying function of time (relative to the optical period). The polarization components $\mathbf{P}_L$ and $\mathbf{P}_{NL}$ can also be expressed in a similar way by writing

$$\mathbf{P}_L(\mathbf{r}, t) = \frac{1}{2}\hat{x}\left[P_L(\mathbf{r}, t)e^{-i\omega_0 t} + c.c.\right], \tag{1.70}$$

$$\mathbf{P}_{NL}(\mathbf{r}, t) = \frac{1}{2}\hat{x}\left[P_{NL}(\mathbf{r}, t)e^{-i\omega_0 t} + c.c.\right]. \tag{1.71}$$

When Eq. (1.69) is substituted in Eq. (1.68), $\mathbf{P}_{NL}(\mathbf{r}, t)$ is found to have a term oscillating at ω_0 and another term oscillating at the third-harmonic frequency $3\omega_0$. The latter term requires phase matching and is generally negligible in optical fibers. By making use of Eq. (1.71), $P_{NL}(\mathbf{r}, t)$ is given by

$$P_{NL}(\mathbf{r}, t) \approx \epsilon_0 \epsilon_{NL}(\mathbf{r}, t) E(\mathbf{r}, t), \tag{1.72}$$

where the nonlinear contribution to the dielectric constant is

$$\epsilon_{NL} = \frac{3}{4}\chi^{(3)}_{xxxx}(\mathbf{r})\,|E(\mathbf{r}, t)|^2\,. \tag{1.73}$$

To solve Eq. (1.67) and obtain the wave equation for the slowly varying amplitude $E(\mathbf{r}, t)$, it is more convenient to work in the Fourier domain (with respect to time). This is generally not possible as Eq. (1.67) is nonlinear in $E(\mathbf{r}, t)$ due to the intensity dependence of ϵ_{NL}, and $E(\mathbf{r}, t)$ is time-dependent. However, due to the slowly varying envelope approximation and the perturbative nature of $P_{NL}(\mathbf{r}, t)$, we will treat $E(\mathbf{r}, t)$, and hence ϵ_{NL}, as time-independent during the derivation of the propagation equation. One way to understand this treatment is that, we can first consider the monochromatic case where $E(\mathbf{r}, t)$ is time-independent. In this case, there is only nonlinearity but no dispersion, and our treatment of ϵ_{NL} being time-independent would be valid. This treatment would yield the correct nonlinear parts of the wave equation for $E(\mathbf{r}, t)$. To obtain the linear parts of the wave equation for a quasi-monochromatic wave packet $E(\mathbf{r}, t)$, we can ignore ϵ_{NL} altogether. These two separate treatments of the nonlinear and linear parts of the wave equation can be done together by treating ϵ_{NL} as time-independent, which justifies our approach. A more rigorous derivation of the wave equation for $E(\mathbf{r}, t)$ using multiscale perturbation methods can be found in Kodama and Hasegawa (1987) and Hasegawa and Kodama (1995).

To work in the Fourier domain, we introduce the Fourier transform of an arbitrary function $f(\mathbf{r}, t)$ as

$$\tilde{f}(\mathbf{r}, \omega) = \int_{-\infty}^{\infty} f(\mathbf{r}, t)e^{i\omega t}dt. \tag{1.74}$$

Applying this transform to Eq. (1.67), we find that the Fourier transform $\tilde{E}(\mathbf{r}, \omega - \omega_0)$ satisfies the Helmholtz equation

$$\nabla^2 \tilde{E} + \epsilon(\mathbf{r}, \omega) k^2 \tilde{E} = 0, \tag{1.75}$$

where $k = \omega/c$,

$$\epsilon(\mathbf{r}, \omega) = 1 + \tilde{\chi}^{(1)}_{xx}(\mathbf{r}, \omega) + \epsilon_{NL}(\mathbf{r}), \tag{1.76}$$

and $\tilde{\chi}^{(1)}$ is the Fourier transform of $\chi^{(1)}$. In deriving Eq. (1.75), the treatment of ϵ_{NL} being time-independent has been used. The dielectric constant ϵ can be used to define the refractive index n. Assuming ϵ is real (i.e., neglecting absorption), we define $\epsilon = n^2$. Then for small ϵ_{NL}, n can be approximated as

$$n(\mathbf{r}, \omega) \approx n_0(\mathbf{r}, \omega) + n_2(\mathbf{r}, \omega)|E|^2, \tag{1.77}$$

where $n_0 = [1 + \tilde{\chi}^{(1)}_{xx}(\mathbf{r}, \omega)]^{1/2}$ is the linear refractive index, and

$$n_2 = \frac{3}{8n_0} \chi^{(3)}_{xxxx} \tag{1.78}$$

is the nonlinear index of refraction which is called the Kerr coefficient. Using refractive indices, the dielectric constant ϵ can be approximated as

$$\epsilon \approx n_0^2 + 2n_0 n_2 |E|^2. \tag{1.79}$$

The Helmholtz equation (1.75) can be solved by the method of separation of variables. We assume a solution of the form

$$\tilde{E}(\mathbf{r}, \omega - \omega_0) = \bar{F}(x, y)\tilde{A}(z, \omega - \omega_0) e^{\mathrm{i}\beta_0 z}, \tag{1.80}$$

where $\bar{F}(x, y)$ is a real-valued modal function, $\tilde{A}(z, \omega - \omega_0)$ is a slowly varying complex function of z, and β_0 is the linear propagation constant for frequency ω_0 which will be determined shortly. Substituting this form into the Helmholtz equation (1.75), this equation can be split into two equations for $\bar{F}(x, y)$ and $\tilde{A}(z, \omega - \omega_0)$:

$$\nabla_\perp^2 \bar{F} + (\epsilon k^2 - \bar{\beta}^2)\bar{F} = 0, \tag{1.81}$$

$$2\mathrm{i}\beta_0 \frac{\partial \tilde{A}}{\partial z} + (\bar{\beta}^2 - \beta_0^2)\tilde{A} = 0, \tag{1.82}$$

where $\nabla_\perp^2 = \partial_x^2 + \partial_y^2$. In obtaining these equations, the second derivative $\partial^2 \tilde{A}/\partial z^2$ was neglected since $\tilde{A}(z, \omega - \omega_0)$ is assumed to be a slowly varying function of z. Here, $\bar{\beta}$ is a propagation constant to be determined from the eigenvalue

problem (1.81), subject to the boundary condition of $\bar{F} \to 0$ as $(x, y) \to \infty$. This $\bar{\beta}$ contains both linear and nonlinear effects of the fiber. After $\bar{\beta}$ is obtained, the z-evolution of $\tilde{A}(z, \omega - \omega_0)$ would be derived from Eq. (1.82).

We will solve Eq. (1.81) by perturbation methods, treating the second term of the dielectric constant ϵ in Eq. (1.79) as a small perturbation. The corresponding propagation constant $\bar{\beta}$ and modal function $\bar{F}(x, y)$ can be written as

$$\bar{\beta}(\omega) = \beta(\omega) + \Delta\beta, \quad \bar{F}(x, y) = F(x, y) + \Delta F, \tag{1.83}$$

where $|\Delta\beta| \ll |\beta|$, and $|\Delta F| \ll |F|$.

At the leading order of Eq. (1.81), we get the eigenvalue equation

$$\nabla_\perp^2 F + (n_0^2 k^2 - \beta^2) F = 0, \tag{1.84}$$

with $F(x, y) \to 0$ as $(x, y) \to \infty$. This is the standard equation for the linear propagation constant $\beta(\omega)$ and its corresponding linear modal profile $F(x, y)$, which can be solved numerically or analytically depending on the geometry and material property of the fiber (Agrawal 2001).

At the next order, we get the governing equation for the small correction terms $\Delta\beta$ and ΔF as

$$\left(\nabla_\perp^2 + n_0^2 k^2 - \beta^2\right) \Delta F = 2\beta \Delta\beta F - 2 n_0 n_2 k^2 |E|^2 F, \tag{1.85}$$

subject to the zero boundary condition for ΔF at large (x, y). By taking the inverse Fourier transform of Eq. (1.80), we get

$$E(\mathbf{r}, t) = \bar{F}(x, y) A(z, t) e^{\mathrm{i}\beta_0 z}, \tag{1.86}$$

where A is the inverse Fourier transform of $\tilde{A}$. Thus, $|E|^2$ in Eq. (1.85) can be approximated as $|F(x, y)|^2 |A|^2$.

The linear inhomogeneous Eq. (1.85) is solvable only if it satisfies the Fredholm condition, which is that the right side of this equation is orthogonal to the linear solution $F(x, y)$. This Fredholm condition yields a formula for the correction term $\Delta\beta$ as

$$\Delta\beta = \frac{k^2 \int\int_{-\infty}^{\infty} n_0 n_2 |F(x, y)|^4 dx dy}{\beta \int\int_{-\infty}^{\infty} |F(x, y)|^2 dx dy} |A|^2. \tag{1.87}$$

Due to the quasi-monochromatic approximation, parameters k (i.e., ω/c), $\beta(\omega)$, $n_0(\omega)$, $n_2(\omega)$ and the modal function $F(x, y; \omega)$ here are all evaluated at the central frequency ω_0.

Now we solve Eq. (1.82). The assumption of $\tilde{A}$ slowly varying in z requires $\bar{\beta}^2 - \beta_0^2$ in (1.82) to be relatively small. To achieve that, we choose $\beta_0 = \beta(\omega_0)$, which

is the linear propagation constant of the center frequency ω_0. We also expand $\beta(\omega)$ around the center frequency ω_0 as

$$\beta(\omega) = \beta_0 + \beta_1(\omega - \omega_0) + \frac{1}{2}\beta_2(\omega - \omega_0)^2 + \frac{1}{6}\beta_3(\omega - \omega_0)^3 + \cdots, \tag{1.88}$$

where

$$\beta_m = \left.\frac{d^m\beta}{d\omega^m}\right|_{\omega=\omega_0} \quad (m = 1, 2, \cdots). \tag{1.89}$$

Here, $\beta_1 = 1/c_g$, c_g is the group velocity at frequency ω_0, and β_2 is called the group-velocity-dispersion parameter. The case of $\beta_2 > 0$ is called normal dispersion and the case of $\beta_2 < 0$ is called anomalous dispersion.

The cubic and higher-order terms in the above expansion are generally negligible under the quasi-monochromatic approximation, where $|\omega - \omega_0| \ll \omega_0$. In the special case where $\beta_2 \approx 0$ (in the vicinity of the zero-dispersion wavelength of the fiber), it may be necessary to include the cubic term. In this subsection, we will not consider that special case; thus we will neglect the cubic and higher terms in the above expansion below.

Substituting the $\bar{\beta}(\omega)$ expression in Eq. (1.83) and the above $\beta(\omega)$ expansion into Eq. (1.82), this equation for $\tilde{A}(z, \omega - \omega_0)$ becomes

$$\mathrm{i}\frac{\partial\tilde{A}}{\partial z} + \left[\beta_1(\omega - \omega_0) + \frac{1}{2}\beta_2(\omega - \omega_0)^2 + \Delta\beta\right]\tilde{A} = 0. \tag{1.90}$$

Inserting the $\Delta\beta$ formula in (1.87) into this equation and taking its inverse Fourier transform, and recalling our treatment of $E(\mathbf{r}, t)$ (and hence $A(z, t)$) being time-independent, we find the equation for $A(z, t)$ as

$$\mathrm{i}\frac{\partial A}{\partial z} + \mathrm{i}\beta_1\frac{\partial A}{\partial t} - \frac{1}{2}\beta_2\frac{\partial^2 A}{\partial t^2} + \gamma|A|^2 A = 0, \tag{1.91}$$

where

$$\gamma = \frac{\omega_0^2 \int\int_{-\infty}^{\infty} n_0 n_2 |F(x, y)|^4 dxdy}{c^2\beta_0 \int\int_{-\infty}^{\infty} |F(x, y)|^2 dxdy}. \tag{1.92}$$

In this formula, n_0 and n_2 are kept inside the integral since their values generally depend on the transverse (x, y) coordinates due to different materials in the core and cladding of the fiber. But in many cases such as weakly guided fibers, their values vary very little in the transverse plane, in which case they can be taken out of the integral above.

By recalling Eqs. (1.69) and (1.86), we can write the electric field $\mathbf{E}(\mathbf{r}, t)$ in a more compact form

$$\mathbf{E}(\mathbf{r}, t) = \frac{1}{2}\hat{x}\left[A(z, t)e^{\mathrm{i}(\beta_0 z - \omega_0 t)} + c.c.\right]\bar{F}(x, y). \tag{1.93}$$

So, $A(z, t)$ is the slowly varying envelope of the electric field whose evolution is governed by the NLS equation (1.91).

Finally, we introduce the moving coordinate $\tau = t - \beta_1 z$, upon which the above Eq. (1.91) becomes

$$\mathrm{i}\frac{\partial A}{\partial z} - \frac{1}{2}\beta_2\frac{\partial^2 A}{\partial \tau^2} + \gamma|A|^2 A = 0, \tag{1.94}$$

which is a NLS equation. In this equation, $\gamma > 0$, but β_2 can be positive or negative depending on the type of fiber. Modulation instability and rogue waves will arise when $\beta_2 < 0$, i.e., in the anomalous-dispersion regime. In this case, introducing nondimensional variables

$$u = P_0^{-1/2}A, \quad \xi = \gamma P_0 z, \quad T = (\gamma P_0/|\beta_2|)^{1/2}\tau, \tag{1.95}$$

where P_0 is a characteristic light power, then the dimensional NLS equation (1.94) becomes the normalized one

$$\mathrm{i}u_\xi + \frac{1}{2}u_{TT} + |u|^2 u = 0, \tag{1.96}$$

which is Eq. (1.1) in different notations.

Modulation instability in this NLS equation (1.96) can be seen by noticing that it admits a special monochromatic constant-intensity solution $u(\xi, T) = a_0 e^{\mathrm{i}a_0^2\xi}$, where a_0 is a real constant. But this monochromatic solution is linearly unstable under frequency modulations, following calculations which are very similar to those for Benjamin-Feir instability in the previous subsection. Due to this modulation instability, this monochromatic constant-intensity light under perturbations will break up upon propagation down the fiber. For certain types of perturbations, this light will break up into rogue waves.

1.1.3 In Unmagnetized Plasma

Plasma is called the fourth state of matter after solid, liquid, and gas. It is the most abundant form of ordinary matter in the universe, being mostly associated with stars, including the Sun. It can also be artificially generated by heating a neutral gas or subjecting it to a strong electromagnetic field. A plasma is characterized by the presence of a significant portion of charged unbounded particles in any combination of ions or electrons, with the net charge roughly zero. These charged particles are highly electrically conductive, and long-range electric and magnetic fields dominate

their behaviours. Collective motion of particles is ubiquitous in plasma, resulting in various waves and other types of collective phenomena.

Ion waves in a plasma with no magnetic field has been studied in the physics literature. Shimizu and Ichikawa (1972) showed that the motion of low-amplitude ion wave packets in an unmagnetized plasma comprising isothermal electrons and cold positive ions is governed by a NLS equation. The dispersion coefficient in this NLS equation is always negative for any wavenumber, but the nonlinear coefficient is negative only at high wavenumbers (when the nonlinear coefficient is negative as the dispersion coefficient, modulation instability and rogue waves could arise). However, ion waves with high wavenumbers suffer strong Landau damping, which makes it impossible to observe its modulation instability or rogue waves.

However, if negative ions are also introduced into the plasma, the situation is very different. In this case, Saito et al. (1984) showed that ion wavepackets are still governed by a NLS equation with a negative dispersion coefficient, but its nonlinear coefficient can be negative for all wavenumbers if the negative-ion density is chosen properly. In this setting, modulation instability of ion waves and ion rogue waves can be observed (Bailung and Nakamura 1993; Bailung et al. 2011).

Below, we derive the NLS equation for a wave packet in an unmagnetized plasma comprising electrons and cold positive and negative ions. In this derivation, we use the fluid model, where the positive and negative ions are represented by their densities n_α, n_β, and mean velocities $\mathbf{u}_\alpha$, $\mathbf{u}_\beta$, with all fluctuations about the mean velocities neglected. In this model, the dynamical equations for ions are just continuity and momentum balance. Since ions are assumed cold (i.e., their temperatures are much lower than the temperature of electrons), their pressures are small or zero and thus the pressure gradient terms in the momentum equations are dropped. The electron density is assumed to behave according to the Boltzmann relation.

The continuity equations for the positive and negative ions are

$$\frac{\partial n_\alpha}{\partial t} + \nabla \cdot (n_\alpha \mathbf{u}_\alpha) = 0, \tag{1.97}$$

$$\frac{\partial n_\beta}{\partial t} + \nabla \cdot (n_\beta \mathbf{u}_\beta) = 0. \tag{1.98}$$

Since there is no magnetic field and ions are cold, the momentum equations for the ions are

$$m_\alpha \left(\frac{\partial}{\partial t} + \mathbf{u}_\alpha \cdot \nabla \right) \mathbf{u}_\alpha = e\mathbf{E}, \tag{1.99}$$

$$m_\beta \left(\frac{\partial}{\partial t} + \mathbf{u}_\beta \cdot \nabla \right) \mathbf{u}_\beta = -e\mathbf{E}, \tag{1.100}$$

where $\mathbf{E}$ is the electric field, m_α the mass of the positive ion, m_β the mass of the negative ion, and e the charge of the electron (it is assumed that a positive ion has electric charge e and a negative ion has electric charge $-e$). Due to the absence of

the magnetic field, the Maxwell equations for the electric field, in the international system of units, reduce to

$$\nabla \times \mathbf{E} = 0, \tag{1.101}$$

$$\nabla \cdot \mathbf{E} = \frac{e}{\epsilon_0}(n_\alpha - n_\beta - n_e), \tag{1.102}$$

where n_e is the electron density, and ϵ_0 the vacuum permittivity. The first of these two equations indicates that the electric field is conservative, allowing it to be represented as the gradient of a scalar electrostatic potential ϕ as

$$\mathbf{E} = -\nabla\phi. \tag{1.103}$$

Inserting this equation into (1.102), we get the Poisson equation for the electrostatic potential ϕ as

$$\nabla^2\phi = \frac{e}{\epsilon_0}(n_e + n_\beta - n_\alpha). \tag{1.104}$$

In terms of this electrostatic potential ϕ, the Boltzmann relation is

$$n_e = n_{e0}\exp(e\phi/\kappa T_e), \tag{1.105}$$

where n_{e0} is the central (unperturbed) electron density, κ the Boltzmann constant, and T_e the absolute temperature of electrons (in Kelvin scale).

If the plasma motion is one-dimensional, the above governing equations would be simplified. If we further normalize the densities n_α, n_β and n_e by the unperturbed electron density n_{e0}, the time t by the ion plasma inverse frequency $\omega_{pi}^{-1} \equiv (\epsilon_0 m_\alpha/n_{e0}e^2)^{1/2}$, the distance x by the electron Debye length $\lambda_D \equiv (\epsilon_0\kappa T_e/n_{e0}e^2)^{1/2}$, the electrostatic potential ϕ by $\kappa T_e/e$, then the one-dimensional governing equations would reduce to (Saito et al. 1984)

$$\frac{\partial n_\alpha}{\partial t} + \frac{\partial}{\partial x}(n_\alpha u_\alpha) = 0, \tag{1.106}$$

$$\frac{\partial n_\beta}{\partial t} + \frac{\partial}{\partial x}(n_\beta u_\beta) = 0, \tag{1.107}$$

$$\frac{\partial u_\alpha}{\partial t} + u_\alpha\frac{\partial u_\alpha}{\partial x} = -\frac{\partial\phi}{\partial x}, \tag{1.108}$$

$$\frac{\partial u_\beta}{\partial t} + u_\beta\frac{\partial u_\beta}{\partial x} = \frac{1}{Q}\frac{\partial\phi}{\partial x}, \tag{1.109}$$

$$n_e = e^\phi, \tag{1.110}$$

$$\frac{\partial^2\phi}{\partial x^2} = n_e + n_\beta - n_\alpha, \tag{1.111}$$

where $Q \equiv m_\beta/m_\alpha$ is the mass ratio of the two ions.

Next, we derive the NLS equation for a wave packet in the above plasma by the multiscale perturbation method, following Saito et al. (1984).

First, we expand solutions to the above equations as follows:

$$\begin{bmatrix} n_\alpha \\ n_\beta \\ n_e \\ u_\alpha \\ u_\beta \\ \phi \end{bmatrix} = \begin{bmatrix} n_{\alpha 0} \\ n_{\beta 0} \\ 1 \\ 0 \\ 0 \\ 0 \end{bmatrix} + \sum_{j=1}^{\infty} \epsilon^j \sum_{l=-\infty}^{\infty} \begin{bmatrix} n_{\alpha,l}^{(j)}(\xi,\tau) \\ n_{\beta,l}^{(j)}(\xi,\tau) \\ n_{e,l}^{(j)}(\xi,\tau) \\ u_{\alpha,l}^{(j)}(\xi,\tau) \\ u_{\beta,l}^{(j)}(\xi,\tau) \\ \phi_l^{(j)}(\xi,\tau) \end{bmatrix} e^{\mathrm{i}l(kx-\omega t)}, \tag{1.112}$$

where ϵ is a small real parameter,

$$\xi = \epsilon(x - \lambda t), \quad \tau = \epsilon^2 t, \tag{1.113}$$

λ is the velocity of the wavepacket to be determined, and all quantities satisfy the reality condition such as $n_{\alpha,-l}^{(j)*} = n_{\alpha,l}^{(j)}$, where the asterisk denotes the complex conjugate.

Inserting the above expansions into Eqs. (1.106)–(1.111), at $O(1)$ we get the charge neutrality condition

$$n_{\alpha 0} = 1 + n_{\beta 0}, \tag{1.114}$$

where $n_{\alpha 0}$ and $n_{\beta 0}$ are the undisturbed positive-ion and negative-ion densities.

At $O(\epsilon)$, we get a set of linear homogeneous equations

$$-\mathrm{i}l\omega n_{\alpha,l}^{(1)} + \mathrm{i}lkn_{\alpha 0}u_{\alpha,l}^{(1)} = 0, \tag{1.115}$$

$$-\mathrm{i}l\omega n_{\beta,l}^{(1)} + \mathrm{i}lkn_{\beta 0}u_{\beta,l}^{(1)} = 0, \tag{1.116}$$

$$-\mathrm{i}l\omega n_{\alpha,l}^{(1)} + \mathrm{i}lk\phi_l^{(1)} = 0, \tag{1.117}$$

$$-\mathrm{i}l\omega n_{\beta,l}^{(1)} - Q^{-1}\mathrm{i}lk\phi_l^{(1)} = 0, \tag{1.118}$$

$$n_{e,l}^{(1)} - \phi_l^{(1)} = 0, \tag{1.119}$$

$$-l^2k^2\phi_l^{(1)} - n_{e,l}^{(1)} - n_{\beta,l}^{(1)} + n_{\alpha,l}^{(1)} = 0. \tag{1.120}$$

Setting $l = 1$ or -1, existence of nonzero solutions in this system requires the determinant of its coefficient matrix to be zero, which yields the dispersion relation

$$\omega^2 = \frac{k^2}{1+k^2}\left(n_{\alpha 0} + \frac{n_{\beta 0}}{Q}\right). \tag{1.121}$$

In addition, we get the following relations between its solutions

$$n_{\alpha,\pm1}^{(1)} = n_{\alpha 0}\left(\frac{k}{\omega}\right)^2 \phi_{\pm1}^{(1)}, \quad n_{\beta,\pm1}^{(1)} = -\frac{n_{\beta 0}}{Q}\left(\frac{k}{\omega}\right)^2 \phi_{\pm1}^{(1)}, \tag{1.122}$$

$$u_{\alpha,\pm1}^{(1)} = \left(\frac{k}{\omega}\right)\phi_{\pm1}^{(1)}, \quad u_{\beta,\pm1}^{(1)} = -\frac{1}{Q}\left(\frac{k}{\omega}\right)\phi_{\pm1}^{(1)}, \quad n_{e,\pm1}^{(1)} = \phi_{\pm1}^{(1)}. \tag{1.123}$$

All components with $|l| \geq 2$ such as $n_{\alpha,\pm2}^{(1)}$ vanish because the determinant of the coefficient matrix of the above homogeneous system (1.115)–(1.120) is nonzero.

At $O(\epsilon^2)$, the components of $l = \pm1$ determine λ to be

$$\lambda = \frac{\omega^3}{k^3}\left(n_{\alpha 0} + \frac{n_{\beta 0}}{Q}\right)^{-1}, \tag{1.124}$$

which is simply the group velocity $c_g = \omega'(k)$, i.e., $\lambda = c_g$. This means that our frame ξ is moving at the group velocity, which is the same as in water waves and optical waves before.

From the components of $l = 2$ in order ϵ^2, we obtain $n_{\alpha,2}^{(2)}, n_{\beta,2}^{(2)}, u_{\alpha,2}^{(2)}, u_{\beta,2}^{(2)}$ and $\phi_2^{(2)}$ as a function of the first order quantities with $l = 1$. Utilizing the above relations (1.122)–(1.123) between first-order quantities, all these second-order quantities are found to be proportional to $(\phi_1^{(1)})^2$, with coefficients involving $k, \omega, Q, n_{\alpha 0}$ and $n_{\beta 0}$.

From the components of $l = 0$ in order ϵ^3, we obtain $n_{\alpha,0}^{(2)}, n_{\beta,0}^{(2)}, u_{\alpha,0}^{(2)}, u_{\beta,0}^{(2)}$ and $\phi_0^{(2)}$, which are found to be proportional to $|\phi_1^{(1)}|^2$, with coefficients again involving $k, \omega, Q, n_{\alpha 0}$ and $n_{\beta 0}$.

Finally, the equations of $l = 1$ of order ϵ^3 give rise to the NLS equation

$$\mathrm{i}\frac{\partial \phi_1^{(1)}}{\partial \tau} + p\frac{\partial^2 \phi_1^{(1)}}{\partial \xi^2} + q\left|\phi_1^{(1)}\right|^2 \phi_1^{(1)} = 0, \tag{1.125}$$

where the dispersion coefficient p is

$$p = \frac{1}{2}\omega''(k) = -\frac{3}{2}\frac{\omega^5}{k^4}\left(n_{\alpha 0} + \frac{n_{\beta 0}}{Q}\right)^{-2}, \tag{1.126}$$

and the nonlinear coefficient q is

$$q = \frac{\omega^3}{2k^4(k^4+3k^2+3)}\left[A_1 k^{16} + 12A_1 k^{14} + \frac{61}{2}A_1 k^{12} + \left(152A_1 - \frac{1}{2}A_2\right)k^{10} + \left(\frac{477}{2}A_1 - A_4\right)k^8 + \left(225A_1 + \frac{15}{2}A_3 - 7A_4 + \frac{1}{2}A_5\right)k^6\right.$$

$$+\left(\frac{245}{2}A_1+\frac{35}{2}A_3-14A_4+\frac{4}{3}A_5\right)k^4$$
$$+\left(\frac{75}{2}A_1+15A_3-11A_4+A_5\right)k^2+\frac{9}{2}A_2-3A_4+\frac{1}{2}A_5\Bigg]. \quad (1.127)$$

Here,

$$A_1=\frac{b^2}{a^5}-\frac{bc}{a^4},\quad A_2=\frac{b^2}{a^5},\quad A_3=\frac{bc}{a^4},\quad A_4=\frac{b}{a^3},\quad A_5=\frac{1}{a}, \quad (1.128)$$

and

$$a\equiv n_{\alpha 0}+\frac{n_{\beta 0}}{Q},\quad b\equiv n_{\alpha 0}-\frac{n_{\beta 0}}{Q^2},\quad c\equiv n_{\alpha 0}+\frac{n_{\beta 0}}{Q^3}. \quad (1.129)$$

To connect the function $\phi_1^{(1)}$ to more physical quantities, we first denote $\epsilon\phi_1^{(1)}=\psi/2$. Then, Eq. (1.125) can be written as

$$\mathrm{i}\frac{\partial\psi}{\partial t}+p\frac{\partial^2\psi}{\partial\hat{x}^2}+\frac{q}{4}|\psi|^2\psi=0, \quad (1.130)$$

where $\hat{x}=x-c_gt$ is the normalized distance in moving frame. Notice that $n_e=1+2\epsilon\mathrm{Re}\left[n_{e,1}^{(1)}e^{\mathrm{i}(kx-\omega t)}\right]$ to $O(\epsilon)$ from Eq. (1.112) and $n_{e,1}^{(1)}=\phi_1^{(1)}$ from Eq. (1.119). Thus, defining $\delta n_e\equiv n_e-1$, which is the normalized deviation of the electron density from its unperturbed value, we get

$$\delta n_e=\mathrm{Re}[\psi e^{\mathrm{i}(kx-\omega t)}] \quad (1.131)$$

to the leading order approximation. This δn_e can be experimentally measured and compared to the prediction based on the NLS equation (1.130) for ψ.

The dispersion coefficient p in the NLS equation (1.130) is always negative, but the sign of the nonlinear coefficient $q/4$ depends on the mass ratio Q, density ratio $N\equiv n_{\beta 0}/n_{\alpha 0}$, and the wavenumber k. When $q<0$, Eq. (1.130) can be normalized to the standard NLS equation (1.1) and thus exhibit modulation instability and rogue waves. If we consider the case where the positive ion is Ar^+ and the negative ion is F^-, then the mass ratio $Q=m_\beta/m_\alpha\approx 0.476$. In this case, when $N=0$ (i.e., the negative ion is absent), q would be positive when $k<1.47$ and negative when $k>1.47$. Although carrier waves with $k>1.47$ support modulation instability and rogue waves, their observation is difficult due to strong Landau damping associated with high-wavenumber waves. But at the critical density when $N\approx 0.102$, i.e., $n_{\beta 0}\approx 0.114$, q would be negative for all nonzero wavenumbers k. This critical negative-ion density would facilitate the observation of modulation instability and rogue waves.

1.2 Derivative Nonlinear Schrödinger Equation in Magnetized Plasma

Derivative nonlinear Schrödinger equations have several different forms. One of them is

$$\mathrm{i}\phi_t + \frac{1}{2}\phi_{xx} + \mathrm{i}\left(|\phi|^2\phi\right)_x = 0. \tag{1.132}$$

This equation was shown to govern wave packet propagation in a magnetized plasma (Mio et al. 1976; Spangler and Sheerin 1982), and was shown to be integrable by Kaup and Newell (1978). We derive this equation in a magnetized plasma below.

In a magnetized plasma where an external magnetic field is present, waves in the plasma would behave differently. In such a plasma, Alfvén (1942) first suggested the existence of linear electromagnetic-hydromagnetic waves, which were observed later in lab experiments and space plasmas. These Alfvén waves have since found applications in various parts of plasma physics, including the explanation of why the temperature of the solar corona is hot (about 1 million Kelvins) compared to its surface, which is only a few thousand Kelvins. For the discovery of these waves, Alfvén received the 1970 Nobel Prize in Physics. Our theory below is a nonlinear version of Alfvén's wave theory.

We consider the motion of cold plasma comprising electrons and positive ions in the presence of a magnetic field. We again use the fluid model, where the electrons and ions are represented by their densities and mean velocities. Their governing equations, often referred to as the magnetohydrodynamic (MHD) equations in the literature, are (Kakutani et al. 1968)

$$\frac{\partial n_e}{\partial t} + \nabla \cdot (n_e \mathbf{v}_e) = 0, \tag{1.133}$$

$$\frac{\partial n_i}{\partial t} + \nabla \cdot (n_i \mathbf{v}_i) = 0, \tag{1.134}$$

$$m\left(\frac{\partial}{\partial t} + \mathbf{v}_e \cdot \nabla\right)\mathbf{v}_e = -e\left(\mathbf{E} + \frac{1}{c}\mathbf{v}_e \times \mathbf{B}\right), \tag{1.135}$$

$$M\left(\frac{\partial}{\partial t} + \mathbf{v}_i \cdot \nabla\right)\mathbf{v}_i = e\left(\mathbf{E} + \frac{1}{c}\mathbf{v}_i \times \mathbf{B}\right), \tag{1.136}$$

$$\nabla \times \mathbf{B} - (1/c)\partial\mathbf{E}/\partial t = (4\pi e/c)(n_i\mathbf{v}_i - n_e\mathbf{v}_e), \tag{1.137}$$

$$\nabla \times \mathbf{E} + (1/c)\partial\mathbf{B}/\partial t = 0, \tag{1.138}$$

$$\nabla \cdot \mathbf{B} = 0, \tag{1.139}$$

$$\nabla \cdot \mathbf{E} = 4\pi e(n_i - n_e). \tag{1.140}$$

Here, m is the electron's mass, n_e its density, $\mathbf{v}_e$ its velocity field, M the ion's mass, n_i its density, $\mathbf{v}_i$ its velocity field, $\mathbf{E}$ the electric field, $\mathbf{B}$ the magnetic field, e the elementary charge, and c the speed of light. The first two equations are the continuity equations for electrons and ions. The next two equations are their momentum equations, where the terms on the right hand sides are the Lorentz forces (in Gaussian units), which are a combination of electric and magnetic force on a point charge due to electromagnetic fields. The last four equations are the Maxwell equations in Gaussian units. Since the plasma is cold, pressure gradient terms in Eqs. (1.135) and (1.136) are absent.

One may notice that in the above governing equations for a magnetized plasma, we did not use the Boltzman relation (1.105). The reason is simply that the Boltzman relation is not valid in a magnetized plasma. In fact, the electrostatic potential in this relation does not even exist since the electric field is not conservative here.

We assume that the charge separation can be neglected, i.e., we assume $n_i = n_e \equiv n$, which results in charge neutrality. Under this assumption, one of the two equations (1.133) and (1.134) becomes redundant, since it can be derived from the other equation together with (1.137) and (1.140). We also assume that the displacement current is negligible, i.e., the $(1/c)\partial\mathbf{E}/\partial t$ term in (1.137) can be dropped. This assumption is valid when the Alfvén wave speed (see below) is much less than c, which is generally the case. In addition, using Eq. (1.138), we can readily show that Eq. (1.139) would be automatically satisfied if it is initially valid. Equation (1.140) is used as a criterion for the validity of the neglect of the charge separation. Then, we are left with the following five governing equations

$$\frac{\partial n}{\partial t} + \nabla \cdot (n\mathbf{v}_i) = 0, \tag{1.141}$$

$$m\left(\frac{\partial}{\partial t} + \mathbf{v}_e \cdot \nabla\right)\mathbf{v}_e = -e\left(\mathbf{E} + \frac{1}{c}\mathbf{v}_e \times \mathbf{B}\right), \tag{1.142}$$

$$M\left(\frac{\partial}{\partial t} + \mathbf{v}_i \cdot \nabla\right)\mathbf{v}_i = e\left(\mathbf{E} + \frac{1}{c}\mathbf{v}_i \times \mathbf{B}\right), \tag{1.143}$$

$$\nabla \times \mathbf{B} = (4\pi e/c)n(\mathbf{v}_i - \mathbf{v}_e), \tag{1.144}$$

$$\nabla \times \mathbf{E} + (1/c)\partial\mathbf{B}/\partial t = 0. \tag{1.145}$$

We now eliminate $\mathbf{v}_e$ and $\mathbf{E}$ from these equations. The expression for $\mathbf{v}_e$ can be obtained from Eq. (1.144), and the expression for $\mathbf{E}$ can be obtained from Eq. (1.142). Substituting these $\mathbf{v}_e$ and $\mathbf{E}$ expressions into the other three equations, we get a complete system for n, $\mathbf{v}_i$ and $\mathbf{B}$ as (Kakutani et al. 1968)

$$\frac{\partial n}{\partial t} + \nabla \cdot (n\mathbf{v}_i) = 0, \tag{1.146}$$

$$\frac{\partial \mathbf{B}}{\partial t} - \nabla \times (\mathbf{v}_i \times \mathbf{B}) + (Mc/e)\nabla \times \frac{d\mathbf{v}_i}{dt} = 0, \tag{1.147}$$

$$\begin{aligned}\frac{d\mathbf{v}_i}{dt} &= (1/4\pi)(M+m)^{-1}n^{-1}(\nabla\times\mathbf{B})\times\mathbf{B}\\ &\quad+(mc/4\pi e)(M+m)^{-1}\left[\{(n^{-1}\nabla\times\mathbf{B})\cdot\nabla\}\mathbf{v}_i\right.\\ &\quad\left.+\frac{d}{dt}(n^{-1}\nabla\times\mathbf{B})\right]\\ &\quad-\{mc^2/(4\pi e)^2\}(M+m)^{-1}n^{-1}\{(\nabla\times\mathbf{B})\cdot\nabla\}(n^{-1}\nabla\times\mathbf{B}),\end{aligned}\tag{1.148}$$

where $d/dt = \partial/\partial t + (\mathbf{v}_i\cdot\nabla)$.

When all quantities depend on x and t only, the above equations simplify. The reduced equations are

$$\frac{\partial n}{\partial t}+\frac{\partial(nu)}{\partial x}=0,\tag{1.149}$$

$$\frac{du}{dt}+\frac{1}{4\pi n(M+m)}\frac{\partial}{\partial x}\frac{1}{2}(B_2^2+B_3^2)=0,\tag{1.150}$$

$$\frac{dv}{dt}-\frac{1}{4\pi n(M+m)}B_1\frac{\partial B_2}{\partial x}=-\frac{mc}{4\pi e(M+m)}\frac{d}{dt}\left(n^{-1}\frac{\partial B_3}{\partial x}\right),\tag{1.151}$$

$$\frac{dw}{dt}-\frac{1}{4\pi n(M+m)}B_1\frac{\partial B_3}{\partial x}=\frac{mc}{4\pi e(M+m)}\frac{d}{dt}\left(n^{-1}\frac{\partial B_2}{\partial x}\right),\tag{1.152}$$

$$\frac{dB_2}{dt}-B_1\frac{\partial v}{\partial x}+B_2\frac{\partial u}{\partial x}=\frac{Mc}{e}\frac{\partial}{\partial x}\frac{dw}{dt},\tag{1.153}$$

$$\frac{dB_3}{dt}-B_1\frac{\partial w}{\partial x}+B_3\frac{\partial u}{\partial x}=-\frac{Mc}{e}\frac{\partial}{\partial x}\frac{dv}{dt},\tag{1.154}$$

where $d/dt = \partial/\partial t + u\partial/\partial x$, (u, v, w) are the (x, y, z) components of $\mathbf{v}_i$, (B_1, B_2, B_3) are the (x, y, z) components of $\mathbf{B}$, and B_1 is a constant due to Eq. (1.145).

We first consider small-amplitude (linear) ion waves propagating in a static and uniform magnetic field, whose strength is B_0 and whose direction is along the x-axis (i.e., the wave is propagating in the direction of the magnetic field). The undisturbed ion density is denoted as n_0. Writing

$$n=n_0+\bar{n},\quad u=\bar{u},\quad v=\bar{v},\quad w=\bar{w},\quad B_2=\bar{B}_2,\quad B_3=\bar{B}_3,\tag{1.155}$$

where the barred quantities are small, inserting them into the above governing equations and linearizing, we get the following equations for the linear perturbations,

$$\frac{\partial\bar{n}}{\partial t}+n_0\frac{\partial\bar{u}}{\partial x}=0,\tag{1.156}$$

$$\frac{\partial \bar{u}}{\partial t} = 0, \tag{1.157}$$

$$4\pi n_0 (M+m) B_0^{-1} \frac{\partial \bar{v}}{\partial t} - \frac{\partial \bar{B}_2}{\partial x} = -\omega_{ec}^{-1} \frac{\partial^2 \bar{B}_3}{\partial x \partial t}, \tag{1.158}$$

$$4\pi n_0 (M+m) B_0^{-1} \frac{\partial \bar{w}}{\partial t} - \frac{\partial \bar{B}_3}{\partial x} = \omega_{ec}^{-1} \frac{\partial^2 \bar{B}_2}{\partial x \partial t}, \tag{1.159}$$

$$B_0^{-1} \frac{\partial \bar{B}_2}{\partial t} - \frac{\partial \bar{v}}{\partial x} = \omega_{ic}^{-1} \frac{\partial^2 \bar{w}}{\partial x \partial t}, \tag{1.160}$$

$$B_0^{-1} \frac{\partial \bar{B}_3}{dt} - \frac{\partial \bar{w}}{\partial x} = -\omega_{ic}^{-1} \frac{\partial^2 \bar{v}}{\partial x \partial t}, \tag{1.161}$$

where $\omega_{ec} = eB_0/mc$ and $\omega_{ic} = eB_0/Mc$ are the electron gyrofrequency and ion gyrofrequency, i.e., the angular frequencies of circular motions of an electron and an ion in the plane perpendicular to the magnetic field.

If the frequency of these linear waves is small compared to ω_{ec} and ω_{ic}, then the terms on the right sides of the above equations (1.158)–(1.161) can be dropped. In this case, it is easy to see that quantities $(\bar{v}, \bar{w}, \bar{B}_2, \bar{B}_3)$ all satisfy the linear wave equation of the form

$$\left(\frac{\partial^2}{\partial t^2} - V_A^2 \frac{\partial^2}{\partial x^2} \right) F = 0, \tag{1.162}$$

where F is any of $(\bar{v}, \bar{w}, \bar{B}_2, \bar{B}_3)$, and

$$V_A = \frac{B_0}{\sqrt{4\pi n_0 (M+m)}} \tag{1.163}$$

is the wave speed. These linear waves are the ones that Alfvén (1942) first suggested.

Now we develop a nonlinear theory for these Alfvén waves when their amplitudes are small but finite. For this purpose, we first nondimensionalize the governing equations (1.149)–(1.154). Introducing dimensionless quantities designated by the upper hats through normalizations

$$n = n_0 \hat{n}, \quad \mathbf{B} = B_0 \widehat{\mathbf{B}}, \quad \mathbf{v}_i = V_A \hat{\mathbf{v}}_i, \quad (x, y, z) = L(\hat{x}, \hat{y}, \hat{z}), \quad t = \omega_0^{-1} \hat{t}, \tag{1.164}$$

where n_0 is the mean ion density, B_0 the static magnetic field, V_A the velocity of the linear Alfvén wave given above, L a characteristic length, $\omega_0 = V_A/L$ a characteristic frequency, and dropping the hats, we obtain dimensionless governing equations as

$$\frac{\partial n}{\partial t} + \frac{\partial (nu)}{\partial x} = 0, \tag{1.165}$$

$$\frac{du}{dt} + n^{-1}\frac{\partial}{\partial x}\frac{1}{2}(B_2^2 + B_3^2) = 0, \tag{1.166}$$

$$\frac{dv}{dt} - n^{-1}B_1\frac{\partial B_2}{\partial x} = -R_e^{-1}\frac{d}{dt}\left(n^{-1}\frac{\partial B_3}{\partial x}\right), \tag{1.167}$$

$$\frac{dw}{dt} - n^{-1}B_1\frac{\partial B_3}{\partial x} = R_e^{-1}\frac{d}{dt}\left(n^{-1}\frac{\partial B_2}{\partial x}\right), \tag{1.168}$$

$$\frac{dB_2}{dt} - B_1\frac{\partial v}{\partial x} + B_2\frac{\partial u}{\partial x} = R_i^{-1}\frac{\partial}{\partial x}\frac{dw}{dt}, \tag{1.169}$$

$$\frac{dB_3}{dt} - B_1\frac{\partial w}{\partial x} + B_3\frac{\partial u}{\partial x} = -R_i^{-1}\frac{\partial}{\partial x}\frac{dv}{dt}, \tag{1.170}$$

where $d/dt = \partial/\partial t + u\partial/\partial x$, $R_e \equiv \omega_{ec}/\omega_0$, and $R_i \equiv \omega_{ic}/\omega_0$. Notice that in this general theory, we do not assume the characteristic frequency ω_0 of these waves to be small compared to ω_{ec} and ω_{ic}, i.e., we do not assume R_e and R_i to be large. Thus, the terms on the right sides of Eqs. (1.167)–(1.170) will be kept in our treatment. A consequence of this is that, while linear Alfvén waves under such assumptions are dispersion-less [i.e., their velocities are a constant V_A that is independent of wave frequencies, see Eq. (1.162)], linear Alfvén waves without such assumptions will be dispersive (i.e., the wave velocity will depend on frequency), as we will quickly see below.

We confine our attention to the propagation of Alfvén waves along a static magnetic field. Then, $B_1 = 1$ due to the magnetic field scaling. In addition, we assume that the ion density n fluctuates weakly around its mean value 1 (under the above scaling of n).

The linear dispersion relation of the above system (1.165)–(1.170) will be helpful in our development of the weakly nonlinear theory. Thus, we derive it first. For this purpose, we take

$$n = 1 + \tilde{n}\,e^{\mathrm{i}(kx-\omega t)}, \quad (u, v, w, B_2, B_3) = (\tilde{u}, \tilde{v}, \tilde{w}, \widetilde{B}_2, \widetilde{B}_3)e^{\mathrm{i}(kx-\omega t)}, \tag{1.171}$$

where $(\tilde{n}, \tilde{u}, \tilde{v}, \tilde{w}, \widetilde{B}_2, \widetilde{B}_3)$ are infinitesimal constants. Inserting these expressions into Eqs. (1.165)–(1.170), we get $\tilde{n} = \tilde{u} = 0$. In the linear homogeneous system for $(\tilde{v}, \tilde{w}, \widetilde{B}_2, \widetilde{B}_3)$, the requirement of its matrix' determinant being zero yields the following relation between wavenumber k and frequency ω,

$$\left(1 + R_e^{-1}R_i^{-1}k^2\right)^2\omega^4 - k^2\left[2 + \left(R_e^{-2} + R_i^{-2}\right)k^2\right]\omega^2 + k^4 = 0, \tag{1.172}$$

which can be used to determine the dispersion relation $\omega = \omega(k)$. Clearly, this dispersion relation will not be ω being proportional to k, which indicates that the present waves are dispersive. For long waves (with small $|k|$) propagating along the positive x direction (i.e., $c_p = \omega/k > 0$), this dispersion relation can be expanded as

$$\omega(k) = k \mp \mu k^2 + \cdots, \tag{1.173}$$

where $\mu = (R_i^{-1} - R_e^{-1})/2$. In this dispersion relation, the upper and lower signs denote, respectively, the left and right Alfvén waves.

Now, we consider the nonlinear evolution of small but finite-amplitude Alfvén waves. If these waves are a wavepacket with a nonzero dominant wavenumber k, then the evolution of this wavepacket will be governed by a NLS equation, as was shown in a generic nonlinear system by Benney and Newell (1967). However, for long Alfvén waves ($|k| \ll 1$), the situation will be very different. In this case, a different multiscale calculation is needed, and the resulting governing equation will be a derivative NLS equation rather than the NLS equation. We will show this below, following Mio et al. (1976).

For long Alfvén waves, their group velocity is $c_g = \omega'(0) = 1$ (under velocity normalization introduced before). Thus, we expand solutions to Eqs. (1.165)–(1.170) as the following perturbation series

$$n = 1 + \epsilon n_1 + \epsilon^2 n_2 + \cdots, \tag{1.174}$$

$$u = \quad \epsilon u_1 + \epsilon^2 u_2 + \cdots, \tag{1.175}$$

$$v = \epsilon^{\frac{1}{2}}(v_1 + \epsilon v_2 + \cdots), \tag{1.176}$$

$$w = \epsilon^{\frac{1}{2}}(w_1 + \epsilon w_2 + \cdots), \tag{1.177}$$

$$B_2 = \epsilon^{\frac{1}{2}}(B_{21} + \epsilon B_{22} + \cdots), \tag{1.178}$$

$$B_3 = \epsilon^{\frac{1}{2}}(B_{31} + \epsilon B_{32} + \cdots), \tag{1.179}$$

where ϵ is a small positive parameter,

$$\xi = \epsilon(x - t), \quad \tau = \epsilon^2 t, \tag{1.180}$$

and all variables $n_i, u_i, v_i, w_i, B_{2i}, B_{3i}$ are functions of ξ and τ. Notice that the moving coordinate ξ is moving with the group velocity $\omega'(0) = 1$ of long waves.

To simplify the analysis, we assume that the plasma is in equilibrium state at $\xi \to \pm\infty$, so that all variables $n_i, u_i, v_i, w_i, B_{2i}, B_{3i}$ approach zero there.

Now, we substitute the above perturbation expansions into Eqs. (1.165)–(1.170). At $O(\epsilon^{\frac{3}{2}})$, we find from Eqs. (1.167)–(1.168) that

$$v_1 = -B_{21}, \quad w_1 = -B_{31}. \tag{1.181}$$

At $O(\epsilon^2)$, we find from Eqs. (1.165)–(1.166) that

$$n_1 = u_1 = \frac{1}{2}(B_{21}^2 + B_{31}^2). \tag{1.182}$$

At $O(\epsilon^{\frac{5}{2}})$, we find from Eqs. (1.167)–(1.170) that

$$v_{2,\xi} + B_{22,\xi} = v_{1,\tau} - R_e^{-1} B_{31,\xi\xi\xi}, \tag{1.183}$$

$$w_{2,\xi} + B_{32,\xi} = w_{1,\tau} + R_e^{-1} B_{21,\xi\xi\xi}, \tag{1.184}$$

$$B_{22,\xi} + v_{2,\xi} = B_{21,\tau} + (u_1 B_{21})_\xi + R_i^{-1} w_{1,\xi\xi}, \tag{1.185}$$

$$B_{32,\xi} + w_{2,\xi} = B_{31,\tau} + (u_1 B_{31})_\xi - R_i^{-1} v_{1,\xi\xi}. \tag{1.186}$$

These equations show that

$$v_{1,\tau} - R_e^{-1} B_{31,\xi\xi} = B_{21,\tau} + (u_1 B_{21})_\xi + R_i^{-1} w_{1,\xi\xi}, \tag{1.187}$$

$$w_{1,\tau} + R_e^{-1} B_{21,\xi\xi} = B_{31,\tau} + (u_1 B_{31})_\xi - R_i^{-1} v_{1,\xi\xi}. \tag{1.188}$$

Substituting Eqs. (1.181)–(1.182) into the above two equations, we then obtain two equations for B_{21} and B_{31} as

$$B_{21,\tau} + \frac{1}{4}\left[(B_{21}^2 + B_{31}^2) B_{21}\right]_\xi - \mu B_{31,\xi\xi} = 0, \tag{1.189}$$

$$B_{31,\tau} + \frac{1}{4}\left[(B_{21}^2 + B_{31}^2) B_{31}\right]_\xi + \mu B_{21,\xi\xi} = 0. \tag{1.190}$$

Finally, we define a complex variable

$$\phi \equiv (B_{21} + \mathrm{i} B_{31})/2. \tag{1.191}$$

Then the above two equations can be combined as

$$\mathrm{i}\phi_\tau - \mu\phi_{\xi\xi} + \mathrm{i}\left(|\phi|^2\phi\right)_\xi = 0. \tag{1.192}$$

If $\mu < 0$, i.e., $R_i > R_e$, then after variable rescalings of $\phi = \sqrt{2}\hat{\phi}$, $\xi = |\mu|\hat{\xi}$, and $\tau = |\mu|\hat{\tau}/2$, and dropping the hats, the above equation reduces to

$$\mathrm{i}\phi_\tau + \frac{1}{2}\phi_{\xi\xi} + \mathrm{i}\left(|\phi|^2\phi\right)_\xi = 0, \tag{1.193}$$

which is the derivative NLS equation (1.132) in different notations. If $\mu > 0$, Eq. (1.192) can also be reduced to (1.193) under slightly different variable rescalings.

The above analysis was restricted to cold plasma, where the plasma pressure was small or zero and thus ignored. The more general case of finite plasma pressure was considered by Spangler and Sheerin (1982), where a derivative NLS equation of the same form (1.192) but with a modified nonlinear coefficient was derived.

For short-pulse propagation in a frequency-doubling crystal, the interplay of quadratic and cubic nonlinearities could give rise to a slightly different derivative NLS equation (Moses et al. 2007),

$$\mathrm{i}\phi_\tau + \frac{1}{2}\phi_{\xi\xi} + \mathrm{i}|\phi|^2\phi_\xi = 0. \tag{1.194}$$

This equation was shown to be integrable by Chen et al. (1979).

1.3 Manakov Equations in Randomly-Birefringent Optical Fibers

The Manakov system is

$$\left.\begin{aligned}(\mathrm{i}\partial_t + \partial_x^2)u_1 + \epsilon(|u_1|^2 + |u_2|^2)u_1 = 0,\\ (\mathrm{i}\partial_t + \partial_x^2)u_2 + \epsilon(|u_1|^2 + |u_2|^2)u_2 = 0,\end{aligned}\right\} \tag{1.195}$$

where u_1 and u_2 are complex variables, and $\epsilon = \pm 1$. This system was shown to be integrable by Manakov (1973). The Manakov system governs many physical processes, such as light propagation in randomly birefringent optical fibers (Menyuk 1987; Evangelides et al. 1992; Agrawal 2001), the nonlinear interaction of two incoherent light beams in crystals (Kang et al. 1996; Chen et al. 1979), and evolution of two-component Bose-Einstein condensates (Kevrekidis et al. 2008; Hoefer et al. 2011). In this section, we derive the Manakov system in randomly-birefringent optical fibers.

In the derivation of the NLS equation in optical fibers in Sect. 1.1.2, we assumed that the polarization state of the incident light was preserved during its propagating inside an optical fiber. That is the case only in polarization-maintaining fibers, or in ideal fibers maintaining perfect cylindrical symmetry along its entire length. In practical communication fibers, unintentional variations in the core shape and anisotropic stresses along the fiber length give rise to two orthogonal polarizations along which light propagates at slightly different speeds (i.e., propagation constants along these two polarizations are slightly different). This phenomenon is called modal birefringence. In addition, the degree of modal birefringence and the orientation of the two polarization axes change randomly over a length scale ~ 10 m unless special precautions are taken. In this section, we derive governing equations in randomly birefringent fibers, following Menyuk (1987), Evangelides et al. (1992), and Agrawal (2001).

Fixed-Polarization Case

First, we assume the two polarization axes do not change upon propagation. In this case, the electric field can be written as

$$\mathbf{E}(\mathbf{r},t) = \frac{1}{2}\left[\hat{x}E_x(\mathbf{r},t) + \hat{y}E_y(\mathbf{r},t)\right]e^{-\mathrm{i}\omega_0 t} + c.c., \tag{1.196}$$

where $\hat{x}$ and $\hat{y}$ are the two orthogonal polarization unit vectors on the transverse plane, and E_x, E_y are complex amplitudes along the two polarizations with carrier frequency ω_0.

The nonlinear part of the induced polarization $\mathbf{P}_{NL}$ in Eq. (1.63) is obtained by substituting Eq. (1.196) into Eq. (1.68), i.e., into

$$\mathbf{P}_{NL}(\mathbf{r},t) = \epsilon_0 \chi^{(3)}(\mathbf{r}) \vdots \mathbf{E}(\mathbf{r},t)\mathbf{E}(\mathbf{r},t)\mathbf{E}(\mathbf{r},t). \tag{1.197}$$

This induced polarization inside a dielectric medium (such as the present optical fiber) by an electromagnetic field should not be confused with the state of polarization of that field in Eq. (1.196). In general, the third-order susceptibility $\chi^{(3)}$ is a fourth-rank tensor with 81 elements. In an isotropic medium such as silica glass, only three elements are independent of one another, and the third-order susceptibility can be written in terms of them as (Boyd 2008)

$$\chi^{(3)}_{ijkl} = \chi^{(3)}_{xxyy}\delta_{ij}\delta_{kl} + \chi^{(3)}_{xyxy}\delta_{ik}\delta_{jl} + \chi^{(3)}_{xyyx}\delta_{il}\delta_{jk}, \tag{1.198}$$

where δ_{ij} is the Kronecker delta function defined such that $\delta_{ij} = 1$ when $i = j$ and zero otherwise. Using this result, $\mathbf{P}_{NL}$ in Eq. (1.197) can be written as

$$\mathbf{P}_{NL}(\mathbf{r},t) = \frac{1}{2}\left[\hat{x}P_x(\mathbf{r},t) + \hat{y}P_y(\mathbf{r},t)\right]e^{-\mathrm{i}\omega_0 t} + c.c., \tag{1.199}$$

where P_x and P_y are given by

$$P_i = \frac{3\epsilon_0}{4}\sum_j \left(\chi^{(3)}_{xxyy}E_iE_jE_j^* + \chi^{(3)}_{xyxy}E_jE_iE_j^* + \chi^{(3)}_{xyyx}E_jE_jE_i^*\right), \tag{1.200}$$

and $i, j = x$ or y. From (1.198), we also obtain the relation

$$\chi^{(3)}_{xxxx} = \chi^{(3)}_{xxyy} + \chi^{(3)}_{xyxy} + \chi^{(3)}_{xyyx}, \tag{1.201}$$

where $\chi^{(3)}_{xxxx}$ is the element appearing in Eq. (1.73) of the scalar theory in Sect. 1.1.2 and used in Eq. (1.78) to define the Kerr coefficient n_2.

The relative magnitudes of the three components in Eq. (1.198) depend on the physical mechanisms that contribute to $\chi^{(3)}$. In the case of silica fibers, the dominant contribution is of nonresonant electronic origin (Agrawal 2001; Boyd 2008), and the three components have the same magnitude. In this case the polarization components P_x and P_y in Eq. (1.200) take the form

$$P_x = \frac{3\epsilon_0}{4}\chi^{(3)}_{xxxx}\left[\left(|E_x|^2 + \frac{2}{3}|E_y|^2\right)E_x + \frac{1}{3}E_x^* E_y^2\right], \tag{1.202}$$

$$P_y = \frac{3\epsilon_0}{4}\chi^{(3)}_{xxxx}\left[\left(|E_y|^2 + \frac{2}{3}|E_x|^2\right)E_y + \frac{1}{3}E_y^* E_x^2\right]. \tag{1.203}$$

The propagation equations governing evolution of the two polarization components in Eq. (1.196) can be obtained following the method of Sect. 1.1.2. As in Eq. (1.86), the electric fields E_x and E_y can be factored as

$$E_j(\mathbf{r}, t) = \bar{F}_j(x, y)A_j(z, t)e^{i\beta_{0j}z}, \tag{1.204}$$

where $j = x, y$, $\bar{F}_j$ is the spatial distribution of the fiber mode, β_{0j} is the linear propagation constant at frequency ω_0, and $A_j(z, t)$ is the slowly varying amplitude function, all along the j-polarization. Repeating the calculations of Sect. 1.1.2 for each of the two polarization axes and utilizing Eqs. (1.202)–(1.203), we find that A_x and A_y satisfy the following evolution equations

$$\begin{aligned} i\frac{\partial A_x}{\partial z} &+ i\beta_{1x}\frac{\partial A_x}{\partial t} - \frac{1}{2}\beta_{2x}\frac{\partial^2 A_x}{\partial t^2} + \gamma_x\left(|A_x|^2 + \frac{2}{3}|A_y|^2\right)A_x \\ &+ \frac{\gamma_x}{3}A_x^* A_y^2 e^{-2i\Delta\beta_0 z} = 0, \end{aligned} \tag{1.205}$$

$$\begin{aligned} i\frac{\partial A_y}{\partial z} &+ i\beta_{1y}\frac{\partial A_y}{\partial t} - \frac{1}{2}\beta_{2y}\frac{\partial^2 A_y}{\partial t^2} + \gamma_y\left(|A_y|^2 + \frac{2}{3}|A_x|^2\right)A_y \\ &+ \frac{\gamma_y}{3}A_y^* A_x^2 e^{2i\Delta\beta_0 z} = 0. \end{aligned} \tag{1.206}$$

Here, $\beta_j(\omega)$ is the linear propagation constant at frequency ω along the j-polarization, which is obtained from the eigenvalue problem

$$\nabla_\perp^2 F_j + (n_{0j}^2 k^2 - \beta_j^2)F_j = 0, \quad j = x, y, \tag{1.207}$$

with $n_{0j} = [1 + \tilde{\chi}^{(1)}_{jj}(\mathbf{r}, \omega)]^{1/2}$, $k = \omega/c$, under the zero boundary condition of $F_j(x, y) \to 0$ as $(x, y) \to \infty$,

$$\beta_{0j} = \beta_j(\omega_0), \quad \beta_{1j} = \beta_j'(\omega_0), \quad \beta_{2j} = \beta_j''(\omega_0), \tag{1.208}$$

the prime represents differentiation, $\Delta\beta_0 \equiv \beta_{0x} - \beta_{0y} = 2\pi/L_B$, L_B is the beat length of the birefringent fiber,

$$\gamma_j = \frac{\omega_0^2 \int\int_{-\infty}^{\infty} n_{0j}n_{2j}|F_j(x, y)|^4 dxdy}{c^2\beta_{0j}\int\int_{-\infty}^{\infty}|F_j(x, y)|^2 dxdy}, \tag{1.209}$$

and

$$n_{2j} = \frac{3}{8n_{0j}}\chi^{(3)}_{xxxx}. \tag{1.210}$$

In most cases of fiber optics, $\beta_{2x} \approx \beta_{2y}$ and $\gamma_x \approx \gamma_y$. Thus, we will set

$$\beta_{2x} = \beta_{2y} = \beta_2, \quad \gamma_x = \gamma_y = \gamma \tag{1.211}$$

in Eqs. (1.205)–(1.206).

If we further write

$$A_x = u_1 e^{-\mathrm{i}\Delta\beta_0 z/2}, \quad A_y = u_2 e^{\mathrm{i}\Delta\beta_0 z/2}, \tag{1.212}$$

and introduce the shifted time variable

$$\tau = t - \hat{\beta}_1 z, \tag{1.213}$$

where $\hat{\beta}_1 \equiv (\beta_{1x} + \beta_{1y})/2$, then Eqs. (1.205)–(1.206) would become

$$\mathrm{i}\frac{\partial u_1}{\partial z} + bu_1 + \mathrm{i}\delta\frac{\partial u_1}{\partial \tau} - \frac{1}{2}\beta_2\frac{\partial^2 u_1}{\partial \tau^2} + \gamma\left(|u_1|^2 + \frac{2}{3}|u_2|^2\right)u_1 + \frac{\gamma}{3}u_1^* u_2^2 = 0, \tag{1.214}$$

$$\mathrm{i}\frac{\partial u_2}{\partial z} - bu_2 - \mathrm{i}\delta\frac{\partial u_2}{\partial \tau} - \frac{1}{2}\beta_2\frac{\partial^2 u_2}{\partial \tau^2} + \gamma\left(|u_2|^2 + \frac{2}{3}|u_1|^2\right)u_2 + \frac{\gamma}{3}u_2^* u_1^2 = 0, \tag{1.215}$$

where $b = \Delta\beta_0/2$, and $\delta = (\beta_{1x} - \beta_{1y})/2$.

Random-Polarization Case

In real communication fibers, the two polarization axes and the degree of modal birefringence change randomly over a length scale ~ 10 m due to random variations in the core shape and anisotropic stresses along the fiber length. Next, we consider the leading-order effect of this random birefringence on the evolution equations (1.214)–(1.215).

We first rewrite these coupled equations into a single vector equation,

$$\mathrm{i}\frac{\partial \mathbf{U}}{\partial z} + \sigma_1\left(b\mathbf{U} + \mathrm{i}\delta\frac{\partial \mathbf{U}}{\partial \tau}\right) - \frac{1}{2}\beta_2\frac{\partial^2 \mathbf{U}}{\partial \tau^2} + \gamma s_0\mathbf{U} - \frac{1}{3}\gamma s_3\sigma_3\mathbf{U} = 0, \tag{1.216}$$

where $\mathbf{U} = (u_1, u_2)^T$, i.e., the transpose of (u_1, u_2), σ_1, σ_2, σ_3 are Pauli matrices

$$\sigma_1 = \begin{pmatrix} 1 & 0 \\ 0 & -1 \end{pmatrix}, \quad \sigma_2 = \begin{pmatrix} 0 & 1 \\ 1 & 0 \end{pmatrix}, \quad \sigma_3 = \begin{pmatrix} 0 & -\mathrm{i} \\ \mathrm{i} & 0 \end{pmatrix}, \tag{1.217}$$

s_0, s_1, s_2, s_3 are Stokes parameters defined as

$$s_0 = \mathbf{U}^\dagger U = |u_1|^2 + |u_2|^2, \quad s_1 = \mathbf{U}^\dagger \sigma_1 U = |u_1|^2 - |u_2|^2, \tag{1.218}$$

$$s_2 = \mathbf{U}^\dagger \sigma_2 U = u_1^* u_2 + u_1 u_2^*, \quad s_3 = \mathbf{U}^\dagger \sigma_3 U = -\mathrm{i}(u_1^* u_2 - u_1 u_2^*), \tag{1.219}$$

and $\mathbf{U}^\dagger$ is the conjugate transpose of $\mathbf{U}$. These Stokes parameters satisfy two identities,

$$s_1^2 + s_2^2 + s_3^2 = s_0^2, \tag{1.220}$$

$$s_1 \sigma_1 \mathbf{U} + s_2 \sigma_2 \mathbf{U} + s_3 \sigma_3 \mathbf{U} = s_0 \mathbf{U}. \tag{1.221}$$

Now, we consider how the polarization state varies in the course of propagation in a fiber. The three-dimensional Stokes vector (s_1, s_2, s_3) is a vector whose length equals s_0, and whose end lies on the Poincaré sphere. The phase velocity birefringence, the b term in the propagation Eq. (1.216), only affects the phases of u_1 and u_2 on a length scale $\sim$ 1 m (the beat length). This variation leaves s_0 and s_1 invariant, and so rotates the Stokes vector rapidly around the s_1 axis. Changes in the orientation of the birefringence axes occur randomly over a length scale $\sim$ 10 m. Such changes leave s_0 and s_3 unchanged and thus rotate the Stokes vector around the s_3 axis. The combination of these two types of rotations allows the Stokes vector to sample uniformly all directions on the Poincaré sphere on a length scale $\sim$ 1 km. Then, when we average Eq. (1.216) over random birefringence changes, this average on the phase velocity birefringence b is zero. In addition, this average on the group velocity term δ is also zero, since δ is as often negative as positive. Thus, the two terms containing σ_1 in Eq. (1.216) average out to zero. The last term in Eq. (1.216) requires the average of $s_3 \sigma_3 \mathbf{U}$. This average turns out to be $s_0 \mathbf{U}/3$ when the identity (1.221) is utilized (Evangelides et al. 1992). A more rigorous derivation of this average value can be found in Wai and Menyuk (1996). After this averaging, Eq. (1.216) reduces to

$$\mathrm{i}\frac{\partial \mathbf{U}}{\partial z} - \frac{1}{2}\beta_2 \frac{\partial^2 \mathbf{U}}{\partial \tau^2} + \frac{8}{9}\gamma s_0 \mathbf{U} = 0. \tag{1.222}$$

This equation, in scaler form, is

$$\mathrm{i}\frac{\partial u_1}{\partial z} - \frac{1}{2}\beta_2 \frac{\partial^2 u_1}{\partial \tau^2} + \frac{8}{9}\gamma \left(|u_1|^2 + |u_2|^2\right) u_1 = 0, \tag{1.223}$$

$$\mathrm{i}\frac{\partial u_2}{\partial z} - \frac{1}{2}\beta_2 \frac{\partial^2 u_2}{\partial \tau^2} + \frac{8}{9}\gamma \left(|u_2|^2 + |u_1|^2\right) u_2 = 0, \tag{1.224}$$

and the corresponding electric field can be obtained from Eqs. (1.196), (1.204) and (1.212) as

$$\mathbf{E}(\mathbf{r},t)=\frac{1}{2}\left[\hat{x}\,\bar{F}_x(x,y)u_1(z,\tau)+\hat{y}\,\bar{F}_y(x,y)u_2(z,\tau)\right]e^{\mathrm{i}(\hat{\beta}_0 z-\omega_0 t)}+c.c., \tag{1.225}$$

where $\hat{\beta}_0\equiv(\beta_{0x}+\beta_{0y})/2$.

Equations (1.223)–(1.224) can be normalized. Introducing nondimensional variables

$$\hat{u}_1=P_0^{-1/2}u_1,\quad \hat{u}_2=P_0^{-1/2}u_2,\quad \hat{z}=8\gamma d P_0 z/9,\quad \hat{\tau}=(16\gamma P_0/9|\beta_2|)^{1/2}\tau, \tag{1.226}$$

where P_0 is a representative total power of the solutions and $d=-\mathrm{sgn}(\beta_2)$, these normalized variables (with hats dropped) satisfy the system of equations

$$\mathrm{i}\frac{\partial u_1}{\partial z}+\frac{\partial^2 u_1}{\partial\tau^2}+d\left(|u_1|^2+|u_2|^2\right)u_1=0, \tag{1.227}$$

$$\mathrm{i}\frac{\partial u_2}{\partial z}+\frac{\partial^2 u_2}{\partial\tau^2}+d\left(|u_2|^2+|u_1|^2\right)u_2=0. \tag{1.228}$$

This is the Manakov system (1.195) in different notations.

1.4 Davey-Stewartson Equations in Water of Finite Depth

The Davey-Stewartson (DS) equations are

$$\left.\begin{aligned} iA_t&=A_{xx}+\sigma_0 A_{yy}+(\epsilon|A|^2-2Q)A,\\ Q_{xx}-\sigma_0 Q_{yy}&=\epsilon(|A|^2)_{xx},\end{aligned}\right\} \tag{1.229}$$

where $A(x,y,t)$ is a complex function, $Q(x,y,t)$ is a real function, $\sigma_0=\pm1$, and $\epsilon=\pm1$. They are called DS-I when $\sigma_0=1$ and DS-II when $\sigma_0=-1$. The ϵ value is the sign of nonlinearity ($\epsilon=1$ for focusing and $\epsilon=-1$ for defocusing). Integrability of these equations can be found in Ablowitz and Segur (1981).

Equations of Davey-Stewartson types were first derived by Benney and Roskes (1969) and Davey and Stewartson (1974) for three-dimensional gravity waves in water of finite depth. Such equations were generalized to include surface tension by Djordjevic and Redekopp (1977) and Ablowitz and Segur (1981). Under certain conditions on the wavenumber and surface tension, those equations can be reduced to the above DS equations.

1.4.1 Derivation of Benney-Roskes-Davey-Stewartson Equations

In this subsection, we derive Benney-Roskes-Davey-Stewartson equations in three-dimensional water waves of finite depth with surface tension. Water waves under both gravity and surface tension are called capillary-gravity waves. Our derivation follows Benney and Roskes (1969), Davey and Stewartson (1974), Djordjevic and Redekopp (1977), and Ablowitz and Segur (1979), using the multiscale perturbation method.

We consider the irrotational motion of a progressive capillary-gravity wave moving on the free surface of an inviscid and incompressible liquid of constant depth h. The undisturbed free surface is set as the $z = 0$ plane, and the bottom is located at $z = -h$. The remaining Cartesian coordinates (x, y) are in the plane of the undisturbed free surface, and we choose x to point in the direction of the wave propagation. Since the fluid motion is irrotational, the velocity field $\mathbf{u}$ has a potential $\phi(x, y, z, t)$, where $\mathbf{u} = \nabla\phi$.

The governing equations for these three-dimensional capillary-gravity waves are (Djordjevic and Redekopp 1977)

$$\phi_{xx} + \phi_{yy} + \phi_{zz} = 0, \quad -h < z \le \zeta, \tag{1.230}$$

$$\phi_z = 0, \quad z = -h, \tag{1.231}$$

$$\zeta_t + \phi_x\zeta_x + \phi_y\zeta_y = \phi_z, \quad z = \zeta, \tag{1.232}$$

$$\phi_t + g\zeta + \frac{1}{2}(\phi_x^2 + \phi_y^2 + \phi_z^2) = T\frac{\zeta_{xx}(1+\zeta_y^2) + \zeta_{yy}(1+\zeta_x^2) - 2\zeta_{xy}\zeta_x\zeta_y}{(1+\zeta_x^2+\zeta_y^2)^{\frac{3}{2}}}, \quad z = \zeta, \tag{1.233}$$

where $\zeta(x, y, t)$ denotes the position of the undulating free surface, g is the gravitational constant, and T is the ratio of the surface tension coefficient to the fluid density.

We examine a progressive wavetrain of wavenumber k and frequency ω travelling in the x direction. In the linear theory, this wave can be written as

$$\zeta(x, y, t) = \zeta_{11}\, e^{\mathrm{i}(kx-\omega t)} + c.c., \tag{1.234}$$

$$\phi(x, y, z, t) = \phi_{11}\frac{\cosh k(z+h)}{\cosh kh} e^{\mathrm{i}(kx-\omega t)} + c.c., \tag{1.235}$$

where ζ_{11} and ϕ_{11} are infinitesimal complex constants. The z dependence in this $\phi(x, y, z, t)$ expression is derived from the Laplace equation (1.230) together with the bottom condition (1.231). Inserting these expressions into the two surface boundary conditions (1.232)–(1.233) and dropping nonlinear terms, the compati-

bility condition between the two equations yields the dispersion relation

$$\omega = \{(gk + Tk^3)\tanh kh\}^{1/2}, \tag{1.236}$$

or

$$\omega = \{gk\sigma(1 + \tilde{T})\}^{1/2}, \tag{1.237}$$

where $\tilde{T} = k^2T/g$, and $\sigma = \tanh kh$.

Now, we consider the evolution of this wavetrain whose amplitude is small and slowly modulated in both space and time. We treat $k = O(1)$; hence the slope of the surface wave is small. In addition, we treat $kh = O(1)$. Then, we use the multiscale perturbation theory to derive the temporal and spatial evolutions of this wavetrain.

We write solutions to Eqs. (1.230)–(1.233) as perturbation series

$$\zeta = \epsilon\left(\zeta_{01} + \zeta_{11}e^{\mathrm{i}\theta} + c.c.\right) + \epsilon^2\left(\zeta_{02} + \zeta_{12}e^{\mathrm{i}\theta} + \zeta_{22}e^{2\mathrm{i}\theta} + c.c.\right) + \\ + \epsilon^3\left(\zeta_{03} + \zeta_{13}e^{\mathrm{i}\theta} + \zeta_{23}e^{2\mathrm{i}\theta} + \zeta_{33}e^{3\mathrm{i}\theta} + c.c.\right) + \cdots, \tag{1.238}$$

$$\phi = \epsilon\left(\phi_{01} + \phi_{11}e^{\mathrm{i}\theta} + c.c.\right) + \epsilon^2\left(\phi_{02} + \phi_{12}e^{\mathrm{i}\theta} + \phi_{22}e^{2\mathrm{i}\theta} + c.c.\right) + \\ + \epsilon^3\left(\phi_{03} + \phi_{13}e^{\mathrm{i}\theta} + \phi_{23}e^{2\mathrm{i}\theta} + \phi_{33}e^{3\mathrm{i}\theta} + c.c.\right) + \cdots, \tag{1.239}$$

where $\theta = kx - \omega t$,

$$\zeta_{nj} = \zeta_{nj}(\xi, \eta, \tau), \quad \phi_{nj} = \phi_{nj}(\xi, \eta, z, \tau), \tag{1.240}$$

$$\xi = \epsilon(x - c_g t), \quad \eta = \epsilon y, \quad \tau = \epsilon^2 t, \tag{1.241}$$

$c_g = \omega'(k)$ is the group velocity, '$c.c.$' represents complex conjugates of only the $e^{\mathrm{i}n\theta}$ terms, and ζ_{0j}, ϕ_{0j} are real functions. Here, ϵ is a small positive parameter measuring the slope of the wavy surface. Unlike the deep-water case considered in Sect. 1.1.1, ϕ_{nj} here does not depend on the slow z variable ϵz since the water is of finite depth.

We also expand the ϕ function in surface boundary conditions (1.232)–(1.233) around the unperturbed surface level $z = 0$. Up to $O(\epsilon^3)$, these boundary conditions are

$$\zeta_t + \zeta_x(\phi_x + \phi_{xz}\zeta) + \zeta_y(\phi_y + \phi_{yz}\zeta) = \phi_z + \phi_{zz}\zeta + \frac{1}{2}\phi_{zzz}\zeta^2, \quad z = 0, \tag{1.242}$$

$$\phi_t + \phi_{tz}\zeta + \frac{1}{2}\phi_{tzz}\zeta^2 + g\zeta + \frac{1}{2}(\phi_x^2 + \phi_y^2 + \phi_z^2) + \zeta(\phi_x\phi_{xz} + \phi_y\phi_{yz} + \phi_z\phi_{zz})$$

$$= T\frac{\zeta_{xx}(1+\zeta_y^2)+\zeta_{yy}(1+\zeta_x^2)-2\zeta_{xy}\zeta_x\zeta_y}{(1+\zeta_x^2+\zeta_y^2)^{\frac{3}{2}}}, \quad z=0. \tag{1.243}$$

We first substitute the ϕ expansion (1.239) into the Laplace equation (1.230) and the bottom condition (1.231). Equating coefficients of $\epsilon^j e^{in\theta}$ to zero and solving the resulting equations for ϕ_{nj}, we get

$$\phi_{01} = \phi_{01}(\xi,\eta,\tau), \quad \phi_{11} = A(\xi,\eta,\tau)\frac{\cosh k(z+h)}{\cosh kh}, \tag{1.244}$$

$$\phi_{02} = \phi_{02}(\xi,\eta,\tau), \tag{1.245}$$

$$\phi_{12} = D(\xi,\eta,\tau)\frac{\cosh k(z+h)}{\cosh kh} - \mathrm{i}\frac{(z+h)\sinh k(z+h)}{\cosh kh}A_\xi, \tag{1.246}$$

$$\phi_{22} = F(\xi,\eta,\tau)\frac{\cosh 2k(z+h)}{\cosh 2kh}, \tag{1.247}$$

$$\phi_{03,z} = -(z+h)\left(\phi_{01,\xi\xi}+\phi_{01,\eta\eta}\right), \tag{1.248}$$

$$\phi_{13} = G(\xi,\eta,\tau)\frac{\cosh k(z+h)}{\cosh kh} - \frac{(z+h)\sinh k(z+h)}{2k\cosh kh}\left(2\mathrm{i}kD_\xi + A_{\eta\eta}\right) - \\ -\frac{(z+h)^2\cosh k(z+h)}{2\cosh kh}A_{\xi\xi}. \tag{1.249}$$

Compared to Davey and Stewartson (1974) and Djordjevic and Redekopp (1977), we have lumped all $\cosh k(z+h)$ terms in ϕ_{12} together, which makes its expression simpler. Then, we substitute these ϕ_{nj} solutions and the ζ expansion (1.238) into the two surface boundary conditions (1.242)–(1.243). Equating coefficients of $\epsilon^j e^{in\theta}$ to zero we get

$$\zeta_{01} = 0, \quad g\zeta_{11} = \frac{\mathrm{i}\omega}{1+\tilde{T}}A, \quad g\zeta_{02} = c_g\phi_{01,\xi} - k^2(1-\sigma^2)|A|^2, \tag{1.250}$$

$$g\zeta_{12} = \frac{\mathrm{i}\omega}{1+\tilde{T}}D + \frac{c_p}{1+\tilde{T}}\left(\sigma kh + \frac{c_g}{c_p} - \frac{2\tilde{T}}{1+\tilde{T}}\right)A_\xi, \tag{1.251}$$

$$g\zeta_{22} = \frac{k^2}{2}\frac{\sigma^2-3}{\sigma^2-\tilde{T}(3-\sigma^2)}A^2, \tag{1.252}$$

$$F(\xi,\eta,\tau) = \frac{3\mathrm{i}k^2}{4\omega}\frac{(1+\sigma^2)[1-\sigma^2+\tilde{T}(3-\sigma^2)]}{\sigma^2-\tilde{T}(3-\sigma^2)}A^2, \tag{1.253}$$

where $c_p = \omega/k$ is the phase velocity. Here, ζ_{12} is derived from the $O(\epsilon^2 e^{\mathrm{i}\theta})$ terms of either of the two surface boundary conditions (1.242)–(1.243), and the other surface boundary condition at $O(\epsilon^2 e^{\mathrm{i}\theta})$ is satisfied automatically utilizing the group velocity expression

$$c_g = c_p \left[\frac{\sigma + kh(1-\sigma^2)}{2\sigma} + \frac{\tilde{T}}{1+\tilde{T}} \right], \tag{1.254}$$

which can be derived by differentiating the dispersion relation (1.236).

Notice that the second harmonic terms ϕ_{22} and ζ_{22} are singular when $\tilde{T} = \sigma^2/(3-\sigma^2)$, which for deep water ($\sigma = 1$) yields $\tilde{T} = 1/2$, i.e., $k = [g/(2T)]^{1/2}$. For water, $T \approx 72 \times 10^{-6}\mathrm{m}^3/\mathrm{s}^2$. Thus, the corresponding wavelength is about 2.4 cm. Wavenumbers satisfying this condition have the property that the phase speeds of the first and second harmonic match, resulting in the phenomenon known as 'second-harmonic resonance'. The above analysis breaks down at this wavenumber and a new scaling is required (McGoldrick 1970).

Assuming that the wavenumber k is not close to that for which $\tilde{T} = \sigma^2/(3-\sigma^2)$, we can continue the analysis. Equating the coefficient of $\epsilon^3 e^0$ to zero in the first surface boundary condition (1.242) and utilizing the $\phi_{03,z}$ formula in (1.248), we get the equation

$$(gh - c_g^2)\phi_{01,\xi\xi} + gh\phi_{01,\eta\eta} = -k^2 c_p \left(\frac{c_g}{c_p}(1-\sigma^2) + \frac{2}{1+\tilde{T}} \right) \left(|A|^2 \right)_\xi . \tag{1.255}$$

This equation shows that the horizontal velocity field (ϕ_x, ϕ_y) from the expansion (1.239) has an $O(\epsilon^2 e^0)$ mean flow that is generated by the self-interaction of the progressive wavetrain. In deep water, this mean flow is absent (see later text as well as Sect. 1.1.1). Stokes (1847) first pointed out the existence of this mean flow. But he said it existed in deep water, which is incorrect.

Equating the coefficients of $\epsilon^3 e^{\mathrm{i}\theta}$ to zero in the two surface boundary conditions (1.242)–(1.243) and utilizing the ϕ_{13} solution in (1.249), we get two equations for ζ_{13}, whose compatibility condition gives the following equation for the time evolution of $A(\xi, \eta, \tau)$,

$$\begin{aligned} \mathrm{i}A_\tau + \frac{1}{2}\omega''(k)A_{\xi\xi} + \frac{c_g}{2k}A_{\eta\eta} = k\left[1 + \frac{c_g}{2c_p}(1-\sigma^2)(1+\tilde{T})\right]\phi_{01,\xi}A + \\ + \frac{k^4}{4\omega}\left[\frac{(1-\sigma^2)(9-\sigma^2) + \tilde{T}(3-\sigma^2)(7-\sigma^2)}{\sigma^2 - \tilde{T}(3-\sigma^2)} + \right. \\ \left. + 8\sigma^2 - 2(1-\sigma^2)^2(1+\tilde{T}) - \frac{3\sigma^2\tilde{T}}{1+\tilde{T}}\right]|A|^2 A. \end{aligned} \tag{1.256}$$

These two equations (1.255) and (1.256) govern the evolution of a progressive capillary-gravity wavetrain in water of finite depth, and we will call them Benney-Roskes-Davey-Stewartson (BRDS) equations.

The case of $c_g = (gh)^{1/2}$ is very special, since this is the case where the ϕ_{01} equation (1.255) changes from hyperbolic to elliptic. In this case, the group

velocity of this progressive (short) wavetrain matches the phase velocity of the long wave, and a long-wave/short-wave resonant interaction occurs. Under this condition, the above analysis breaks down, and a different analysis and scaling are required. Relevant equations describing this resonant interaction will be presented in Sect. 1.5. In deep water, this resonance disappears.

In the absence of y-direction variation, we can solve for $\phi_{01,\xi}$ from Eq. (1.255) and then insert it into Eq. (1.256), resulting in a single equation for $A(\xi,\tau)$,

$$\mathrm{i}A_\tau + \frac{1}{2}\omega''(k)A_{\xi\xi} = \nu|A|^2A, \tag{1.257}$$

where ν is a certain constant. A Stokes wavetrain corresponds to a special solution $A(\xi,\tau) = a_0 e^{-\mathrm{i}a_0^2\nu\tau}$ in this equation, where a_0 is a real constant. Performing a linear stability analysis to this special solution similar to what we did in Sect. 1.1.1, we find that this solution is linearly unstable if $\omega''(k)\nu < 0$. Without surface tension ($\tilde{T} = 0$), $\omega''(k)$ is always negative when $kh > 0$, but ν is negative when $kh < 1.363$ and positive when $kh > 1.363$. Thus, the Stokes wavetrain is unstable when $kh > 1.363$—a result which was first reported by Benjamin (1967) and Whitham (1967).

In the deep-water limit ($gh \gg 1$ and $kh \gg 1$), the ϕ_{01} equation (1.255) reduces to a Laplace equation, whose solution is $\phi_{01,\xi} = \phi_{01,\eta} = 0$. Thus, the $O(\epsilon^2)$ mean flow of the horizontal velocity field disappears. In this case, Eq. (1.256) reduces to

$$\mathrm{i}A_\tau + \frac{1}{2}\omega''(k)A_{\xi\xi} + \frac{c_g}{2k}A_{\eta\eta} = \frac{k^4}{4\omega}\frac{8+\tilde{T}+2\tilde{T}^2}{(1-2\tilde{T})(1+\tilde{T})}|A|^2A. \tag{1.258}$$

If we further take the limit of negligible surface tension ($\tilde{T} = 0$) and restrict to the two-dimensional case (independent of the transverse η direction), we get

$$\mathrm{i}A_\tau + \frac{1}{2}\omega''(k)A_{\xi\xi} - \frac{2k^4}{\omega}|A|^2A = 0. \tag{1.259}$$

In this $\tilde{T} = 0$ limit, we see from Eq. (1.250) that $A = g\zeta_{11}/(\mathrm{i}\omega)$. Inserting this expression into the above equation and utilizing the present dispersion relation $\omega = (gk)^{1/2}$, we then recover the evolution equation (1.32) that was derived earlier in Sect. 1.1.1 for the two-dimensional motion of a gravity-wave train in deep water.

1.4.2 Reduction to Davey-Stewartson Equations

Next, we nondimentionalize the BRDS equations (1.255) and (1.256). Introducing nondimensional variables

$$\hat{\xi} = k\xi, \quad \hat{\eta} = k\eta, \quad \hat{\tau} = \omega\tau, \quad \hat{A} = (k^2/\omega)A, \quad \hat{\phi}_{01} = (k^2/\omega)\phi_{01}, \tag{1.260}$$

dropping the hats, and setting $Q = \phi_{01,\xi}$, Eqs. (1.255) and (1.256) become

$$\left.\begin{aligned} \mathrm{i}A_\tau + \lambda A_{\xi\xi} + \mu A_{\eta\eta} &= \chi|A|^2 A + \chi_1 QA, \\ \alpha Q_{\xi\xi} + Q_{\eta\eta} &= -\beta(|A|^2)_{\xi\xi}, \end{aligned}\right\} \tag{1.261}$$

where

$$\lambda = \frac{k^2\omega''(k)}{2\omega}, \quad \mu = \frac{c_g}{2c_p} > 0, \tag{1.262}$$

$$\chi = \frac{1}{4}\left[\frac{(1-\sigma^2)(9-\sigma^2) + \tilde{T}(3-\sigma^2)(7-\sigma^2)}{\sigma^2 - \tilde{T}(3-\sigma^2)} + \right.$$

$$\left. +8\sigma^2 - 2(1-\sigma^2)^2(1+\tilde{T}) - \frac{3\sigma^2\tilde{T}}{1+\tilde{T}}\right], \tag{1.263}$$

$$\chi_1 = 1 + \frac{c_g}{2c_p}(1-\sigma^2)(1+\tilde{T}) > 0, \tag{1.264}$$

$$\alpha = \frac{gh - c_g^2}{gh}, \quad \beta = \frac{c_p^2}{gh}\left(\frac{c_g}{c_p}(1-\sigma^2) + \frac{2}{1+\tilde{T}}\right) > 0. \tag{1.265}$$

Now we determine under what conditions the above BRDS equations can be reduced to the integrable Davey-Stewartson equations (1.229). Through variable scalings

$$\xi = |\alpha|^{\frac{1}{2}}\tilde{\xi}, \quad \tau = -\frac{|\alpha|}{\lambda}\tilde{\tau}, \quad Q = \frac{2\lambda}{\chi_1|\alpha|}\tilde{Q}, \quad A = \left(\frac{2|\lambda|}{\chi_1\beta}\right)^{\frac{1}{2}}\tilde{A}, \tag{1.266}$$

dropping the tildes, and recalling μ, χ_1, β all positive, we find that under parameter conditions of

$$\lambda = -\mu\alpha, \quad 2\chi\alpha = \chi_1\beta, \tag{1.267}$$

the BRDS equations (1.261) would become

$$\left.\begin{aligned} \mathrm{i}A_\tau &= A_{\xi\xi} + \sigma_0 A_{\eta\eta} + (|A|^2 - 2Q)A, \\ Q_{\xi\xi} - \sigma_0 Q_{\eta\eta} &= (|A|^2)_{\xi\xi}, \end{aligned}\right\} \tag{1.268}$$

where $\sigma_0 = \mathrm{sgn}(\lambda)$. These are the DS equations (1.229) with $\epsilon = 1$ under different notations.

In the shallow water limit of $kh \to 0$, defining $\hat{T} \equiv \tilde{T}/(kh)^2 = T/(gh^2)$, we find that

$$\lambda \to \frac{1}{2}\left(-1+3\hat{T}\right)k^2h^2, \quad \mu \to \frac{1}{2}, \quad \chi \to \frac{9}{4(1-3\hat{T})k^2h^2}, \tag{1.269}$$

$$\chi_1 \to \frac{3}{2}, \quad \alpha \to (1-3\hat{T})k^2h^2, \quad \beta \to 3. \tag{1.270}$$

Thus, conditions (1.267) are satisfied, and the BRDS equations (1.261) reduce to the integrable DS equations (1.229) with $\sigma_0 = \mathrm{sgn}(\hat{T} - \frac{1}{3})$ and $\epsilon = 1$.

Interestingly, conditions (1.267) are also satisfied at finite $(\tilde{T}, kh)$ values of

$$\tilde{T} \approx 0.001959, \quad kh \approx 0.1670. \tag{1.271}$$

In this case, the BRDS equations (1.261) also reduce to the integrable DS equations (1.229), with $\sigma_0 = \mathrm{sgn}(\lambda) = -1$ and $\epsilon = 1$. There are no other $(\tilde{T}, kh)$ values or regions where parameter conditions (1.267) are met.

1.5 Long-Wave-Short-Wave Interaction Model in Water of Finite Depth

The Benney-Roskes-Davey-Stewartson equation (1.255) is singular when $c_g^2 = gh$, where the group velocity c_g of the progressive (short) wavetrain matches the phase velocity $(gh)^{1/2}$ of the long wave. In this case, a stronger and faster interaction between the short and long waves is expected. Indeed, this can be anticipated since it is a limiting case of the three-wave resonant interaction (Benney 1977). The governing equations for this interaction were derived by Djordjevic and Redekopp (1977) for capillary-gravity waves in water of finite depth. Similar equations were also derived by Grimshaw (1977) and Funakoshi and Oikawa (1983) for the interaction between long and short internal waves. After scalings, these equations can be written as

$$\left.\begin{aligned} \mathrm{i}A_t - A_{xx} + LA = 0, \\ L_t = -4(|A|^2)_x, \end{aligned}\right\} \tag{1.272}$$

where L is a real function and A a complex one. For the interaction of a Langmuir wave with an ion-sound wave in a plasma, Yajima and Oikawa (1976) derived a system of model equations which can be reduced to the above equations through a coordinate and gauge transformation (Funakoshi and Oikawa 1983). They further showed that the system they derived is integrable.

In this section, we derive the above long-wave-short-wave interaction model for capillary-gravity waves in water of finite depth by the multiscale perturbation method, following Djordjevic and Redekopp (1977) with some corrections.

We consider the irrotational two-dimensional motion of a progressive capillary-gravity wavetrain moving on the free surface of an inviscid and incompressible

liquid of constant depth h. The governing equations for these capillary-gravity waves are (1.230)–(1.233) with the y direction removed, i.e.,

$$\phi_{xx} + \phi_{zz} = 0, \quad -h < z \le \zeta, \tag{1.273}$$

$$\phi_z = 0, \quad z = -h, \tag{1.274}$$

$$\zeta_t + \phi_x \zeta_x = \phi_z, \quad z = \zeta, \tag{1.275}$$

$$\phi_t + g\zeta + \frac{1}{2}(\phi_x^2 + \phi_z^2) = T \frac{\zeta_{xx}}{(1+\zeta_x^2)^{\frac{3}{2}}}, \quad z = \zeta, \tag{1.276}$$

where $\phi(x, z, t)$ is the velocity potential, and $\zeta(x, z, t)$ is the position of the free surface. The linear dispersion relation is (1.237), i.e., $\omega = \{gk\sigma(1+\tilde{T})\}^{1/2}$, where $\tilde{T} = k^2 T/g$ and $\sigma = \tanh kh$. The group velocity of a short wavetrain with wavenumber k is $c_g = \omega'(k)$. The phase velocity of a long wave (with $|k| \ll 1$) is $\omega/k \approx (gh)^{1/2}$. When

$$c_g = (gh)^{1/2}, \tag{1.277}$$

which occurs on a certain curve in the $(\tilde{T}, kh)$ plane (Djordjevic and Redekopp 1977; Ablowitz and Segur 1979), this short wave would interact strongly with the long wave. We derive the model equation for this strong interaction below.

We write solutions to Eqs. (1.273)–(1.276) as perturbation series

$$\begin{aligned}\zeta = {} & \epsilon\left(\zeta_{01} + \zeta_{11}e^{i\theta} + c.c.\right) + \epsilon^{\frac{4}{3}}\left(\zeta_{02} + \zeta_{12}e^{i\theta} + c.c.\right) + \\ & + \epsilon^{\frac{5}{3}}\left(\zeta_{03} + \zeta_{13}e^{i\theta} + c.c.\right) + \epsilon^{2}\left(\zeta_{04} + \zeta_{14}e^{i\theta} + \zeta_{24}e^{2i\theta} + c.c.\right) + \\ & + \epsilon^{\frac{7}{3}}\left(\zeta_{05} + \zeta_{15}e^{i\theta} + \zeta_{25}e^{2i\theta} + c.c.\right) + \epsilon^{\frac{8}{3}}\left(\zeta_{06} + \zeta_{16}e^{i\theta} + \zeta_{26}e^{2i\theta} + c.c.\right) + \\ & + \cdots,\end{aligned} \tag{1.278}$$

$$\begin{aligned}\phi = {} & \epsilon^{\frac{2}{3}}\phi_{00} + \epsilon\left(\phi_{01} + \phi_{11}e^{i\theta} + c.c.\right) + \epsilon^{\frac{4}{3}}\left(\phi_{02} + \phi_{12}e^{i\theta} + c.c.\right) + \\ & + \epsilon^{\frac{5}{3}}\left(\phi_{03} + \phi_{13}e^{i\theta} + c.c.\right) + \epsilon^{2}\left(\phi_{04} + \phi_{14}e^{i\theta} + \phi_{24}e^{2i\theta} + c.c.\right) + \\ & + \epsilon^{\frac{7}{3}}\left(\phi_{05} + \phi_{15}e^{i\theta} + \phi_{25}e^{2i\theta} + c.c.\right) + \epsilon^{\frac{8}{3}}\left(\phi_{06} + \phi_{16}e^{i\theta} + \phi_{26}e^{2i\theta} + c.c.\right) + \\ & \cdots,\end{aligned} \tag{1.279}$$

where $\theta = kx - \omega t$,

$$\zeta_{nj} = \zeta_{nj}(\xi, \tau), \quad \phi_{nj} = \phi_{nj}(\xi, z, \tau), \quad \xi = \epsilon^{\frac{2}{3}}(x - c_g t), \quad \tau = \epsilon^{\frac{4}{3}} t, \tag{1.280}$$

$c_g = \omega'(k)$ is the group velocity of the short wave, '$c.c.$' represents complex conjugates of only the $e^{in\theta}$ terms, and ζ_{0j}, ϕ_{0j} are real functions. In these expansions, the short wave corresponds to the $e^{i\theta}$ modes and their higher harmonics, and the long wave corresponds to the (ζ_{0j}, ϕ_{0j}) terms. These unconventional perturbation expansions are needed in order to balance the short wave's dispersion and its nonlinear interaction with the long wave, and to allow the self-interaction of the short wave to drive the long wave's evolution. The small positive parameter ϵ is the order of the short-wave's amplitude, or equivalently, the order of the slope of the short wave's surface. The mean velocity flow is approximately $\epsilon^{2/3}\phi_{00,x}$, which is $O(\epsilon^{4/3})$. This mean flow is much stronger than that of the non-resonant case treated in Sect. 1.4, which was $O(\epsilon^2)$. The current slow time scale of $O(\epsilon^{-4/3})$ is also much shorter than $O(\epsilon^{-2})$ of the non-resonant case, meaning that the present long-wave-short-wave interaction is much faster.

We also expand the ϕ function in surface boundary conditions (1.275)–(1.276) around the unperturbed surface level $z = 0$. Up to $O(\epsilon^{8/3})$, these boundary conditions are

$$\zeta_t + \zeta_x\phi_x = \phi_z + \phi_{zz}\zeta, \qquad z = 0, \tag{1.281}$$

$$\phi_t + \phi_{tz}\zeta + g\zeta + \frac{1}{2}(\phi_x^2 + \phi_z^2) = T\zeta_{xx}, \qquad z = 0. \tag{1.282}$$

We first substitute the ϕ expansion (1.279) into the Laplace equation (1.273) and the bottom condition (1.274). Equating coefficients of $\epsilon^j e^{in\theta}$ to zero and solving the resulting equations for ϕ_{nj}, we get

$$\phi_{00} = \phi_{00}(\xi, \tau),$$

$$\phi_{01} = \phi_{01}(\xi, \tau), \quad \phi_{11} = A(\xi, \tau)\frac{\cosh k(z+h)}{\cosh kh},$$

$$\phi_{02} = \phi_{02}(\xi, \tau), \quad \phi_{12} = F(\xi, \tau)\frac{\cosh k(z+h)}{\cosh kh},$$

$$\phi_{03} = \phi_{03}(\xi, \tau), \quad \phi_{13} = D(\xi, \tau)\frac{\cosh k(z+h)}{\cosh kh} - \mathrm{i}\frac{(z+h)\sinh k(z+h)}{\cosh kh}A_\xi,$$

$$\phi_{04,z} = -(z+h)\phi_{00,\xi\xi},$$

$$\phi_{14} = H(\xi, \tau)\frac{\cosh k(z+h)}{\cosh kh} - \mathrm{i}\frac{(z+h)\sinh k(z+h)}{\cosh kh}F_\xi,$$

$$\phi_{05,z} = -(z+h)\phi_{01,\xi\xi}, \quad \phi_{15} = G(\xi, \tau)\frac{\cosh k(z+h)}{\cosh kh}$$
$$- \mathrm{i}\frac{(z+h)\sinh k(z+h)}{\cosh kh}D_\xi - \frac{(z+h)^2\cosh k(z+h)}{2\cosh kh}A_{\xi\xi},$$

$$\phi_{06,z} = -(z+h)\phi_{02,\xi\xi}.$$

Then, we substitute these ϕ_{nj} solutions and the ζ expansion (1.278) into the dynamic surface boundary condition (1.282). Equating coefficients of orders up to $\epsilon^2 e^0$ and $\epsilon^2 e^{\mathrm{i}\theta}$ to zero we get

$$\zeta_{01} = 0, \quad g\zeta_{11} = \frac{\mathrm{i}\omega}{1+\tilde{T}} A, \quad g\zeta_{02} = c_g \phi_{00,\xi}, \quad g\zeta_{12} = \frac{\mathrm{i}\omega}{1+\tilde{T}} F,$$

$$g\zeta_{03} = c_g \phi_{01,\xi}, \quad g\zeta_{13} = \frac{\mathrm{i}\omega}{1+\tilde{T}} D + \frac{c_p}{1+\tilde{T}} \left(\sigma kh + \frac{c_g}{c_p} - \frac{2\tilde{T}}{1+\tilde{T}} \right) A_\xi,$$

$$g\zeta_{04} = -\phi_{00,\tau} + c_g \phi_{02,\xi} - k^2 (1-\sigma^2) |A|^2,$$

$$g\zeta_{14} = \frac{\mathrm{i}\omega}{1+\tilde{T}} H + \frac{c_p}{1+\tilde{T}} \left(\sigma kh + \frac{c_g}{c_p} - \frac{2\tilde{T}}{1+\tilde{T}} \right) F_\xi,$$

where $c_p = \omega/k$ is the phase velocity of the short wave. When these ζ_{nj} solutions and the above ϕ_{nj} expressions are inserted into the kinematic boundary condition (1.281), we find that this condition up to $O(\epsilon^2 e^0)$ and $O(\epsilon^2 e^{\mathrm{i}\theta})$ is satisfied automatically due to the dispersion relation, the group-velocity formula (1.254), as well as the resonance condition (1.277).

At $O(\epsilon^{7/3} e^{\mathrm{i}\theta})$, the two surface boundary conditions (1.281)–(1.282) give two linear inhomogeneous equations for ζ_{15} and G. Due to the dispersion relation, these two linear equations are compatible only if a certain condition is satisfied. Utilizing the group-velocity formula (1.254), we find that the D_ξ terms in this compatibility condition cancel out, and the remaining condition becomes

$$\mathrm{i}A_\tau + \frac{1}{2}\omega''(k) A_{\xi\xi} = k \left[1 + \frac{c_g}{2c_p} (1-\sigma^2)(1+\tilde{T}) \right] \phi_{00,\xi} A. \tag{1.283}$$

At $O(\epsilon^{8/3} e^0)$, the kinematic boundary condition (1.281) gives another equation. Substituting the above ϕ_{nj} and ζ_{nj} expressions into this equation and utilizing the resonance condition (1.277) to cancel its $\phi_{02,\xi\xi}$ terms, this equation reduces to

$$\phi_{00,\xi\tau} = -\frac{1}{2} k^2 \left[1 - \sigma^2 + \frac{2c_p}{c_g (1+\tilde{T})} \right] (|A|^2)_\xi. \tag{1.284}$$

Notice that the coefficient in this equation differs from that in Djordjevic and Redekopp (1977). Equations (1.283)–(1.284) are the model equations governing the resonant interaction between a long wave and a short wave.

Finally, we denote $L \equiv \phi_{00,\xi}$ and employ variable scalings of

$$A = \frac{|\omega''|}{\sqrt{|\alpha\beta|}} \tilde{A}, \quad L = \frac{\omega''}{2\alpha} \tilde{L}, \quad \xi = \mathrm{sgn}(\alpha\beta) \tilde{\xi}, \quad \tau = -\frac{2}{\omega''} \tilde{\tau}, \tag{1.285}$$

where α and β are the coefficients of the nonlinear terms on the right sides of Eqs. (1.283)–(1.284), respectively. Then dropping the tildes, the rescaled equations become

$$\left.\begin{aligned} \mathrm{i}A_\tau - A_{\xi\xi} + LA = 0, \\ L_\tau = -4(|A|^2)_\xi, \end{aligned}\right\} \tag{1.286}$$

which are in the standard form (1.272) under different notations.

1.6 Three-Wave Resonant Interaction System

The three-wave resonant interaction system is

$$\left.\begin{aligned} \partial_t u_1 + (\mathbf{c}_1 \cdot \nabla)\, u_1 = \mathrm{i}\gamma_1 u_2^* u_3^*, \\ \partial_t u_2 + (\mathbf{c}_2 \cdot \nabla)\, u_2 = \mathrm{i}\gamma_2 u_1^* u_3^*, \\ \partial_t u_3 + (\mathbf{c}_3 \cdot \nabla)\, u_3 = \mathrm{i}\gamma_3 u_1^* u_2^*, \end{aligned}\right\} \tag{1.287}$$

where (u_1, u_2, u_3) are complex envelope functions of the three waves, $\nabla = (\partial_x, \partial_y)$ is the gradient operator in the (x, y) plane, $(\mathbf{c}_1, \mathbf{c}_2, \mathbf{c}_3)$ are vector velocities of the three waves, and $(\gamma_1, \gamma_2, \gamma_3)$ are real nonlinear coefficients. These nonlinear coefficients can be normalized though. Indeed, employing variable scalings

$$u_1 = -\frac{\mathrm{i}}{\sqrt{|\gamma_2\gamma_3|}}\hat{u}_1, \quad u_2 = -\frac{\mathrm{i}}{\sqrt{|\gamma_1\gamma_3|}}\hat{u}_2, \quad u_3 = -\frac{\mathrm{i}}{\sqrt{|\gamma_1\gamma_2|}}\hat{u}_3, \tag{1.288}$$

and dropping the hats, Eqs. (1.287) reduce to

$$\left.\begin{aligned} \partial_t u_1 + (\mathbf{c}_1 \cdot \nabla)\, u_1 = \epsilon_1 u_2^* u_3^*, \\ \partial_t u_2 + (\mathbf{c}_2 \cdot \nabla)\, u_2 = \epsilon_2 u_1^* u_3^*, \\ \partial_t u_3 + (\mathbf{c}_3 \cdot \nabla)\, u_3 = \epsilon_3 u_1^* u_2^*, \end{aligned}\right\} \tag{1.289}$$

where $\epsilon_j = \mathrm{sgn}(\gamma_j)$.

The three-wave interaction system (1.287) arises in a wide variety of physical systems. Below, we derive them in water waves and optics.

1.6.1 In Water Waves

We consider the irrotational capillary-gravity wave motion of an inviscid, incompressible, and homogeneous fluid in deep water, subject to a constant gravitational force g. Since the motion is irrotational, the velocity field $\mathbf{u}$ has a potential $\phi(x, y, z, t)$, where $\mathbf{u} = \nabla\phi$. The fluid has a free surface at $z = \zeta(x, y, t)$, under the effect of surface tension.

The governing equations for these deep-water capillary-gravity waves are (Djordjevic and Redekopp 1977; Ablowitz and Segur 1979)

$$\nabla^2\phi = 0, \quad -\infty < z \le \zeta, \tag{1.290}$$

$$\zeta_t + \phi_x\zeta_x + \phi_y\zeta_y = \phi_z, \quad z = \zeta, \tag{1.291}$$

$$\phi_t + g\zeta + \frac{1}{2}|\nabla\phi|^2 = T\frac{\zeta_{xx}(1+\zeta_y^2) + \zeta_{yy}(1+\zeta_x^2) - 2\zeta_x\zeta_y\zeta_{xy}}{(1+\zeta_x^2+\zeta_y^2)^{3/2}},$$
$$z = \zeta, \tag{1.292}$$

where T is the ratio of the surface tension coefficient to the fluid density. The Laplace equation here is due to the incompressibility of the fluid, the second equation is the kinematic condition on the surface, and the third equation is the dynamic condition on the surface.

For small-amplitude waves ($\zeta \ll 1$), the kinematic and dynamic conditions at the free surface may be approximated by conditions at the mean level $z = 0$ through Taylor expansion about this value. Assuming the surface slope is of the same order as ζ, i.e., the wavenumbers are $O(1)$, these surface conditions up to the first two order terms become

$$\zeta_t - \phi_z = \phi_{zz}\zeta - \phi_x\zeta_x - \phi_y\zeta_y, \quad z = 0, \tag{1.293}$$

$$\phi_t - T(\zeta_{xx} + \zeta_{yy}) + g\zeta = -\frac{1}{2}|\nabla\phi|^2 - \phi_{zt}\zeta, \quad z = 0. \tag{1.294}$$

Linear capillary-gravity waves are of the form

$$\zeta(\mathbf{x}, t) = u\, e^{\mathrm{i}(\mathbf{k}\cdot\mathbf{x}-\omega t)} + c.c., \quad \phi(\mathbf{x}, z, t) = \psi(z)\, e^{\mathrm{i}(\mathbf{k}\cdot\mathbf{x}-\omega t)} + c.c., \tag{1.295}$$

where $\mathbf{x} \equiv (x, y)$ is the horizontal space vector, $\mathbf{k} \equiv (k, l)$ is the wavenumber vector, ω is the wave frequency, and u is the wave amplitude on the water surface. Substitution of these expressions into Eqs. (1.290) and (1.293)–(1.294) and omission of nonlinear terms give us $\psi(z) = -\mathrm{i}(\omega/\kappa)\, u\, e^{\kappa z}$, as well as the dispersion relation

$$\omega^2 = g\kappa + T\kappa^3, \tag{1.296}$$

where $\kappa \equiv |\mathbf{k}| = \sqrt{k^2 + l^2}$.

Now, we consider the nonlinear interaction of three low-amplitude linear waves with wave vectors $(\mathbf{k}_1, \mathbf{k}_2, \mathbf{k}_3)$ and frequencies $(\omega_1, \omega_2, \omega_3)$. For this interaction to be the strongest, these wave vectors and frequencies must satisfy the resonance conditions

$$\mathbf{k}_1 + \mathbf{k}_2 + \mathbf{k}_3 = 0, \quad \omega_1 + \omega_2 + \omega_3 = 0. \tag{1.297}$$

McGoldrick (1965) showed that these conditions can be satisfied for capillary-gravity waves. Indeed, if these three linear waves propagate in the same horizontal direction, say, x direction, with wavenumbers (k_1, k_2, k_3) respectively, then these conditions will be met if k_1 and k_2 are related by (Craik 1985)

$$\frac{(1+r^2)+(1+r)(1+7r+r^2)^{1/2}}{r(9+14r+9r^2)} = \frac{T}{2g}k_1^2, \tag{1.298}$$

where $r \equiv k_2/k_1$. For waves propagating in different horizontal directions, techniques to find wave vectors $\mathbf{k}_1$ and $\mathbf{k}_2$ to satisfy the resonance conditions (1.297) can be found in McGoldrick (1965) and Simmons (1969).

When these three low-amplitude linear waves interact nonlinearly under resonance conditions (1.297), their amplitudes will be slowly modulated in time, space, or both. To derive their evolution equations, we employ the multi-scale perturbation technique, along the lines of Case and Chiu (1977) but with modifications.

We first consider the case when their amplitudes are slowly varying in time only. Then, the interacting solutions can be written as a multi-scale perturbation series

$$\zeta(\mathbf{x},t) = \epsilon\zeta_1 + \epsilon^2\zeta_2 + \cdots, \quad \phi(\mathbf{x},z,t) = \epsilon\phi_1 + \epsilon^2\phi_2 + \cdots, \tag{1.299}$$

where ϵ is a small wave-amplitude parameter,

$$\zeta_1(\mathbf{x},t) = \sum_{j=1}^{3} u_j(\tau)\, e^{\mathrm{i}(\mathbf{k}_j\cdot\mathbf{x}-\omega_j t)} + c.c., \tag{1.300}$$

$$\phi_1(\mathbf{x},z,t) = \sum_{j=1}^{3} -\mathrm{i}\frac{\omega_j}{\kappa_j} u_j(\tau) e^{\kappa_j z}\, e^{\mathrm{i}(\mathbf{k}_j\cdot\mathbf{x}-\omega_j t)} + c.c., \tag{1.301}$$

$\kappa_j \equiv |\mathbf{k}_j|$, $\omega_j = \omega(\kappa_j)$, and $\tau = \epsilon t$ is the slow time scale. Substituting these expansions into Eqs. (1.293)–(1.294), the equations at $O(\epsilon)$ are satisfied automatically since the first terms of the expansions are slowly-modulated linear modes. At $O(\epsilon^2)$, we get

$$\zeta_{2t} - \phi_{2z} = -\zeta_{1\tau} + \phi_{1zz}\zeta_1 - \phi_{1x}\zeta_{1x} - \phi_{1y}\zeta_{1y}, \quad z = 0, \tag{1.302}$$

$$\phi_{2t} - T(\zeta_{2xx} + \zeta_{2yy}) + g\zeta_2 = -\phi_{1\tau} - \frac{1}{2}|\nabla\phi_1|^2 - \phi_{1zt}\zeta_1, \quad z = 0. \tag{1.303}$$

Inserting the (ζ_1, ϕ_1) expressions (1.300)–(1.301) into the right sides of the above equations and utilizing resonance conditions (1.297), we get

$$\zeta_{2t} - \phi_{2z} = \sum_{j=1}^{3} F_j e^{\mathrm{i}(\mathbf{k}_j\cdot\mathbf{x}-\omega_j t)} + c.c. + \text{other harmonics}, \tag{1.304}$$

$$\phi_{2t} - T(\zeta_{2xx} + \zeta_{2yy}) + g\zeta_2 = \sum_{j=1}^{3} G_j e^{\mathrm{i}(\mathbf{k}_j \cdot \mathbf{x} - \omega_j t)} + c.c. + \text{other harmonics}, \tag{1.305}$$

where the ϕ_2 function is evaluated at $z = 0$,

$$\begin{aligned} F_j &= -u_{j\tau} + \mathrm{i}u_{j+1}^* u_{j+2}^* \left[\omega_{j+1}\kappa_{j+1} + \omega_{j+2}\kappa_{j+2} \right. \\ &\quad \left. + \left(\omega_{j+1}\kappa_{j+1}^{-1} + \omega_{j+2}\kappa_{j+2}^{-1}\right)\mathbf{k}_{j+1} \cdot \mathbf{k}_{j+2}\right], \\ G_j &= \mathrm{i}\omega_j \kappa_j^{-1} u_{j\tau} + u_{j+1}^* u_{j+2}^* \left[\omega_{j+1}^2 + \omega_{j+2}^2 + \omega_{j+1}\omega_{j+2} \right. \\ &\quad \left. - \omega_{j+1}\omega_{j+2}\kappa_{j+1}^{-1}\kappa_{j+2}^{-1}\mathbf{k}_{j+1} \cdot \mathbf{k}_{j+2}\right], \end{aligned}$$

$j = 1, 2, 3$, $u_{j+3} \equiv u_j$, $\omega_{j+3} \equiv \omega_j$, $\kappa_{j+3} \equiv \kappa_j$, and $\mathbf{k}_{j+3} \equiv \mathbf{k}_j$. The (ζ_2, ϕ_2) solutions should not contain secular growth (terms growing linearly in time t). Thus, they have the solution forms

$$\zeta_2(\mathbf{x}, t, \tau) = \sum_{j=1}^{3} \xi_j e^{\mathrm{i}(\mathbf{k}_j \cdot \mathbf{x} - \omega_j t)} + c.c. + \text{other harmonics}, \tag{1.306}$$

$$\phi_2(\mathbf{x}, t, \tau) = \sum_{j=1}^{3} \eta_j e^{\mathrm{i}(\mathbf{k}_j \cdot \mathbf{x} - \omega_j t)} + c.c. + \text{other harmonics}. \tag{1.307}$$

Inserting these solution forms into Eqs. (1.304)–(1.305) and matching the harmonics, we get

$$\begin{pmatrix} -\mathrm{i}\omega_j & -\kappa_j \\ g + T\kappa_j^2 & -\mathrm{i}\omega_j \end{pmatrix} \begin{pmatrix} \xi_j \\ \eta_j \end{pmatrix} = \begin{pmatrix} F_j \\ G_j \end{pmatrix}. \tag{1.308}$$

The matrix in the above linear nonhomogeneous equation is singular, i.e., its determinant is zero, due to the dispersion relation (1.296). Thus, the above linear system is solvable only if it satisfies a solvability condition. Indeed, multiplying its first equation by $-\mathrm{i}\omega_j/\kappa_j$ and adding it to the second equation, the left side of the resulting equation becomes zero. Thus, its right side $G_j - (\mathrm{i}\omega_j/\kappa_j)F_j$ should be zero too. This solvability condition gives us the following evolution equations for the three waves' amplitudes,

$$du_j/d\tau = \mathrm{i}\gamma_j u_{j+1}^* u_{j+2}^*, \quad j = 1, 2, 3, \tag{1.309}$$

where

$$\gamma_j = \frac{1}{2}\left[\omega_{j+1}\kappa_{j+1} + \omega_{j+2}\kappa_{j+2} + (\kappa_j/\omega_j)\left(\omega_{j+1}^2 + \omega_{j+2}^2 + \omega_{j+1}\omega_{j+2}\right)\right]$$
$$+\frac{1}{2}\left[(\omega_{j+1}/\kappa_{j+1}) + (\omega_{j+2}/\kappa_{j+2})\right.$$
$$\left.-(\kappa_j/\omega_j)(\omega_{j+1}\omega_{j+2}/\kappa_{j+1}\kappa_{j+2})\right]\mathbf{k}_{j+1}\cdot\mathbf{k}_{j+2}. \tag{1.310}$$

Some sign differences between this γ_j formula and that in Case and Chiu (1977) are due to our choices of the resonance conditions (1.297), where sums of the three wavenumbers and wave frequencies are zero, while they were $\mathbf{k}_2 = \mathbf{k}_1 + \mathbf{k}_3$ and $\omega_2 = \omega_1 + \omega_3$ in Case and Chiu (1977).

Interestingly, Simmons (1969) has derived the above three-wave resonant interaction equations (1.309) and calculated their γ_j coefficients earlier by a different method—the variational method, and his γ_j formulae are much simpler. After converting to our notations, his γ_j formulae are

$$\gamma_j = \frac{\kappa_j}{\omega_j}\Gamma, \quad \Gamma \equiv -\frac{1}{2}\sum_{i=1}^{3}\omega_i\omega_{i+1}\left(1 + \frac{\mathbf{k}_i\cdot\mathbf{k}_{i+1}}{\kappa_i\,\kappa_{i+1}}\right), \tag{1.311}$$

for $j = 1, 2, 3$. It can be checked that, under resonance conditions (1.297), the above two forms of γ_j formulae are indeed equivalent. Simmons' formulae clearly show that, the three γ_j coefficients cannot all have the same sign, because the three ω_j frequencies cannot all have the same sign due to resonance conditions (1.297).

Now, we generalize the wave interaction equations (1.309) to cases where amplitudes of the three waves are slowly modulated in both time and space, i.e., wave envelope functions u_j in Eq. (1.300) depend on both slow time $\tau = \epsilon t$ and slow space $\mathbf{X} = \epsilon\mathbf{x}$. In this case, nonlinear parts of Eq. (1.309) remain the same, but the linear parts are modified. The generalized equations are

$$\left.\begin{aligned}
\partial_\tau u_1 + (\mathbf{c}_1\cdot\nabla)\,u_1 &= \mathrm{i}\gamma_1 u_2^* u_3^*,\\
\partial_\tau u_2 + (\mathbf{c}_2\cdot\nabla)\,u_2 &= \mathrm{i}\gamma_2 u_1^* u_3^*,\\
\partial_\tau u_3 + (\mathbf{c}_3\cdot\nabla)\,u_3 &= \mathrm{i}\gamma_3 u_1^* u_2^*,
\end{aligned}\right\} \tag{1.312}$$

where $\nabla \equiv [\partial_X, \partial_Y]$, $(X, Y) = \epsilon(x, y)$, and $(\mathbf{c}_1, \mathbf{c}_2, \mathbf{c}_3)$ are group velocities of the three waves, which are $[\partial\omega/\partial k, \partial\omega/\partial l]$ evaluated at the three wavenumber vectors $\mathbf{k}_j = (k_j, l_j)$ for $j = 1, 2, 3$. These group-velocity terms can be derived by the multi-scale perturbation method utilized above, taking into account the slow spatial dependence of envelope functions u_j. But such derivations are generally not needed, since these terms are linear and can be obtained directly from the dispersion relation. Indeed, let us consider a linear plane wave whose wavenumber vector is perturbed from $\mathbf{k}_1$ to $\mathbf{k}_1 + \epsilon\hat{\mathbf{k}}_1$, where $\epsilon \ll 1$, and $\hat{\mathbf{k}}_1$ is an $O(1)$ vector. Then, in view of the dispersion relation, the corresponding frequency of this linear wave is $\omega(\mathbf{k}_1 + \epsilon\hat{\mathbf{k}}_1)$, which can be approximated as

$$\omega(\mathbf{k}_1+\hat{\mathbf{k}}_1) \approx \omega(\mathbf{k}_1)+\epsilon\hat{k}_1 \left.\frac{\partial\omega}{\partial k}\right|_{\mathbf{k}=\mathbf{k}_1} +\epsilon\hat{l}_1 \left.\frac{\partial\omega}{\partial l}\right|_{\mathbf{k}=\mathbf{k}_1} = \omega(\mathbf{k}_1)+\epsilon\hat{\mathbf{k}}_1\cdot\mathbf{c}_1. \quad (1.313)$$

Using these results, the corresponding linear plane wave is then

$$e^{\mathrm{i}[(\mathbf{k}_1+\hat{\mathbf{k}}_1)\cdot\mathbf{x}-\omega(\mathbf{k}_1+\hat{\mathbf{k}}_1)t]} \approx u_1(\tau,\mathbf{X})\, e^{\mathrm{i}[\mathbf{k}_1\cdot\mathbf{x}-\omega(\mathbf{k}_1)t]}, \quad (1.314)$$

where the envelope function is $u_1(\tau,\mathbf{X}) = e^{\mathrm{i}\hat{\mathbf{k}}_1\cdot(\mathbf{X}-\mathbf{c}_1\tau)}$. Thus, $\partial_\tau u_1 + (\mathbf{c}_1\cdot\nabla)\, u_1 = 0$. This equation is derived from linear wave propagation. When nonlinear interactions are brought in, the u_1 equation in (1.312) then appears. The u_2 and u_3 equations in (1.312) can be understood in a similar way.

The above three-wave interaction equations (1.312) are just Eqs. (1.287) in different notations.

It is easy to see that the three-wave interaction equations (1.312) admit two independent conserved quantities,

$$\int_{-\infty}^{\infty}\int_{-\infty}^{\infty}\left(\frac{|u_1|^2}{\gamma_1}-\frac{|u_2|^2}{\gamma_2}\right)dXdY, \quad \int_{-\infty}^{\infty}\int_{-\infty}^{\infty}\left(\frac{|u_1|^2}{\gamma_1}-\frac{|u_3|^2}{\gamma_3}\right)dXdY. \quad (1.315)$$

These conserved quantities, combined with the fact that $(\gamma_1, \gamma_2, \gamma_3)$ cannot all have the same sign, indicate that $\int\int |u_j|^2 dXdY$ is bounded for each wave, as one would expect for capillary-gravity waves.

Experiments on three-wave resonant interactions in capillary-gravity waves can be found in McGoldrick (1970), Phillips (1974), Banerjee and Korpel (1982), and Henderson and Hammack (1987).

1.6.2 In Optics

In this subsection, we derive three-wave resonant interaction equations in optical media exhibiting quadratic nonlinearities. One of the most striking nonlinear optics experiments—a red beam turning blue after passing through a crystal (see photograph in Yariv (1975) and Ablowitz and Segur (1981)), is a special case of this interaction. Our derivation is based on Yariv (1975).

In a charge-free dielectric medium that is nonmagnetic and homogeneous, the Maxwell equations take the form

$$\nabla\times\mathbf{E} = -\frac{\partial\mathbf{B}}{\partial t}, \quad (1.316)$$

$$\nabla\times\mathbf{H} = \frac{\partial\mathbf{D}}{\partial t}, \quad (1.317)$$

$$\nabla \cdot \mathbf{D} = 0, \tag{1.318}$$

$$\nabla \cdot \mathbf{B} = 0, \tag{1.319}$$

and the corresponding medium equations are

$$\mathbf{D} = \epsilon_0 \mathbf{E} + \mathbf{P}, \tag{1.320}$$

$$\mathbf{B} = \mu_0 \mathbf{H}. \tag{1.321}$$

Here, $\mathbf{E}$ and $\mathbf{H}$ are the electric and magnetic field vectors, $\mathbf{D}$ and $\mathbf{B}$ are the electric and magnetic displacement vectors, ϵ_0 and μ_0 are the electric and magnetic permeabilities of vacuum, and $\mathbf{P}$ is the electric polarization of the medium. The polarization $\mathbf{P}$ is made up of a linear and a nonlinear term

$$\mathbf{P} = \epsilon_0 \chi^{(1)} \mathbf{E} + \mathbf{P}_{NL}, \tag{1.322}$$

where the tensor aspect of the linear susceptibility $\chi^{(1)}$ is ignored here. In general, $\chi^{(1)}$ will depend on the wave frequency ω. This can be accommodated by using the linear part of the above equation after the time dependence $e^{-\mathrm{i}\omega t}$ has been taken out. The nonlinear part of the polarization $\mathbf{P}_{NL}$, for a quadratically nonlinear material such as a noncentrosymmetric crystal, is

$$\mathbf{P}_{NL} = \boldsymbol{\chi}^{(2)} : \mathbf{E}\mathbf{E}, \tag{1.323}$$

where $\boldsymbol{\chi}^{(2)}$ is a third-rank nonlinear susceptibility tensor. In most of the nonlinear experiments, $\boldsymbol{\chi}^{(2)}$ is independent of frequency.

The Maxwell equations (1.316)–(1.317) and medium equations (1.320)–(1.321) can be combined as

$$\nabla \times (\nabla \times \mathbf{E}) = -\mu_0 \frac{\partial^2}{\partial t^2} (\epsilon \mathbf{E} + \mathbf{P}_{NL}), \tag{1.324}$$

where $\epsilon = \epsilon_0(1 + \chi^{(1)})$. The left side of the above equation can be rewritten as

$$\nabla \times (\nabla \times \mathbf{E}) = \nabla(\nabla \cdot \mathbf{E}) - \nabla^2 \mathbf{E}, \tag{1.325}$$

which is a vector identity. Since the nonlinear contribution $\mathbf{P}_{NL}$ to $\mathbf{P}$ in (1.322) is generally much smaller than the linear contribution, the Maxwell equation (1.318), combined with our scalar approximation of $\chi^{(1)}$, then leads to $\nabla \cdot \mathbf{E} \approx 0$. Thus, Eq. (1.324) reduces to

$$\nabla^2 \mathbf{E} = \mu_0 \frac{\partial^2}{\partial t^2} (\epsilon \mathbf{E} + \mathbf{P}_{NL}). \tag{1.326}$$

We now consider the interaction of three waves with center frequencies ω_1, ω_2 and ω_3 in this medium. First, we consider the one-dimensional case, where the three waves are propagating in the same direction z, and $\partial/\partial x = \partial/\partial y = 0$. In addition, we assume that each wave has a single frequency ω_j $(j = 1, 2, 3)$. Then, due to the weak nonlinearity $\mathbf{P}_{NL}$ in the medium, the total electric field $\mathbf{E}$ can be approximated as a sum of three linear modes with their amplitudes slowly varying in z, i.e.,

$$\mathbf{E}(z,t) \approx \mathbf{E}_1(z,t) + \mathbf{E}_2(z,t) + \mathbf{E}_3(z,t), \tag{1.327}$$

where

$$\mathbf{E}_j(z,t) = \frac{1}{2}\left[E_j(z)e^{\mathrm{i}(k_j z - \omega_j t)} + \text{c.c.}\right]\mathbf{e}_j, \quad j = 1,2,3, \tag{1.328}$$

k_j is the wavevector of the j-th wave, $\mathbf{e}_j$ is the unit constant vector representing its direction, and $E_j(z)$ is its scalar envelope function. The constant $\mathbf{e}_j$ vectors imply that all three waves are linearly polarized, which is the case for admitted linear modes in the medium (see Yariv (1975), Sec. 5.2). Since $\nabla \cdot \mathbf{E} \approx 0$, the $\mathbf{e}_j$ vectors are orthogonal to the z axis, i.e., they lie on the transverse plane. The wavevector k_j is related to the frequency ω_j through the dispersion relation $k = k(\omega)$, which can be obtained from the linear part of Eq. (1.326). In order for both $e^{\pm\mathrm{i}(k_j z - \omega_j t)}$ in (1.328) to be admissible linear modes, the dispersion relation should satisfy the symmetry $k(-\omega) = -k(\omega)$. If the tensor aspect of the linear susceptibility $\chi^{(1)}(\omega)$ is ignored, then the dispersion relation is

$$k = \omega\sqrt{\mu_0\epsilon} = \omega\sqrt{\mu_0\epsilon_0(1+\chi^{(1)})}. \tag{1.329}$$

The strongest interaction of these three waves occurs when they form a resonant triad, where

$$\omega_1 + \omega_2 + \omega_3 = 0, \quad k_1 + k_2 + k_3 = 0. \tag{1.330}$$

These are called phase-matching conditions in nonlinear optics. These conditions will limit the degrees of freedom that are available in choosing the directions of polarization $\mathbf{e}_j$ in (1.328). Several techniques for choosing $\mathbf{e}_j$ to satisfy these phase-matching conditions are described in Sec. 16.5 of Yariv (1975).

When these resonance conditions are met, we derive evolution equations for the scalar envelope functions $E_j(z)$ of the three waves. To do so, we first substitute Eqs. (1.327)–(1.328) into Eq. (1.326). Since the variation of $E_j(z)$ with z is small, we can neglect the d^2E_j/dz^2 term. Then, picking out the $e^{\mathrm{i}(k_j z - \omega_j t)}$ components, we get

$$\left(-\frac{1}{2}k_j^2 E_j + \mathrm{i}k_j\frac{dE_j}{dz}\right)\mathbf{e}_j = -\mu_0\epsilon(\omega_j)\frac{1}{2}\omega_j^2 E_j\mathbf{e}_j + \mu_0\frac{\partial^2}{\partial t^2}\left(\mathbf{P}_{NL}\right)_j, \tag{1.331}$$

where $(\mathbf{P}_{NL})_j$ is the $e^{\mathrm{i}(k_j z-\omega_j t)}$ component of vector $\mathbf{P}_{NL}$ projected to the $\mathbf{e}_j$ direction. Due to the dispersion relation mentioned above, the first terms on the two sides of the above equation cancel out. Then, calculating $(\mathbf{P}_{NL})_j$ from Eqs. (1.323) and (1.327)–(1.328) and utilizing the resonance conditions (1.330), we get

$$\frac{dE_1}{dz} = \mathrm{i}\gamma_1 E_2^* E_3^*, \tag{1.332}$$

$$\frac{dE_2}{dz} = \mathrm{i}\gamma_2 E_1^* E_3^*, \tag{1.333}$$

$$\frac{dE_3}{dz} = \mathrm{i}\gamma_3 E_1^* E_2^*, \tag{1.334}$$

where

$$\gamma_1 = \frac{\mu_0\omega_1^2}{2k_1} d_{123}, \quad \gamma_2 = \frac{\mu_0\omega_2^2}{2k_2} d_{213}, \quad \gamma_3 = \frac{\mu_0\omega_3^2}{2k_3} d_{312}, \tag{1.335}$$

and

$$d_{ijk} = \mathbf{e}_i \cdot \left(\boldsymbol{\chi}^{(2)} : \mathbf{e_j}\,\mathbf{e_k}\right) \tag{1.336}$$

is the effective quadratic susceptibility coefficient for the electric field of frequency $\omega_j+\omega_k$ in the $\mathbf{e}_i$ direction when electric fields of frequencies ω_j and ω_k are launched along directions $\mathbf{e}_j$ and $\mathbf{e}_k$, respectively. The γ_j formulae (1.335) show that these nonlinear coefficients cannot all have the same sign, because the three wavenumbers k_j cannot due to resonance conditions (1.330).

If the electric fields E_j of the three waves are also slowly varying in time, i.e., their frequency spectrum contains not just the frequency ω_j, but also a narrow sideband around it, then the nonlinear parts of the above interaction equations do not change, but the linear parts do to account for the temporal modulation. The new equations read

$$\frac{\partial E_1}{\partial z} + k'(\omega_1)\frac{\partial E_1}{\partial t} = \mathrm{i}\gamma_1 E_2^* E_3^*, \tag{1.337}$$

$$\frac{\partial E_2}{\partial z} + k'(\omega_2)\frac{\partial E_2}{\partial t} = \mathrm{i}\gamma_2 E_1^* E_3^*, \tag{1.338}$$

$$\frac{\partial E_3}{\partial z} + k'(\omega_3)\frac{\partial E_3}{\partial t} = \mathrm{i}\gamma_3 E_1^* E_2^*, \tag{1.339}$$

where the prime in $k'(\omega)$ denotes differentiation. These linear parts come about so that the linear plane-wave solution $e^{\mathrm{i}[k'(\omega_j)z-t]\Delta\omega_j}$ of these equations, when combined with the carrier plane-wave $e^{\mathrm{i}(k_j z-\omega_j t)}$ in Eq. (1.328), is consistent with the linear plane-wave $e^{\mathrm{i}[k(\omega_j+\Delta\omega_j)z-(\omega_j+\Delta\omega_j)t]}$ of the medium for small $\Delta\omega_j$ under the expansion

$$k(\omega_j + \Delta\omega_j) = k(\omega_j) + k'(\omega_j)\Delta\omega_j + \cdots . \tag{1.340}$$

Equations (1.337)–(1.339) are a special case of the more general three-wave interaction equations (1.287) under different notations.

A special case of the three-wave interaction is the second harmonic generation, where two of the three waves have the same frequencies, and the third frequency is double those two (second harmonic), i.e., $\omega_1 = \omega_2$ and $\omega_3 = -2\omega_1$. In this context, the first nonlinear optics experiment was performed by Franken et al. (1961). In their experiment, an intense ruby laser beam at wavelength 0.6943 μm was launched through a quartz crystal. The radiation exiting the crystal was found to contain the second harmonic at wavelength 0.3471 μm. Since their experiment did not meet the phase-matching condition of $k_3 = -2k_1$, the conversion efficiency was low. Later experiments, using more efficient materials, higher intensity lasers, and phase matching techniques, have greatly improved the conversion efficiency. A beautiful photograph of this, showing a ruby light (red) turning near ultraviolet (blue in photograph) after passing through an ADP (ammonium dihydrogen phosphate) crystal, can be found in Yariv (1975) and Ablowitz and Segur (1981).

In addition to gravity-capillary water waves and optical waves, the three-wave interaction equations (1.287) have also been derived for internal water waves (Ablowitz and Segur 1981; Craik 1985), plasma (Davidson 1972; Kaup et al. 1979), and others.

It is noted that in water waves, optics, and internal waves with no background shear flows, $(\gamma_1, \gamma_2, \gamma_3)$ in the three-wave interaction equations (1.287) cannot all have the same sign. In such cases, all three waves will remain bounded due to integrals of motion such as those in Eq. (1.315). However, in plasma and internal waves with shear flows, $(\gamma_1, \gamma_2, \gamma_3)$ can all have the same sign, giving rise to the explosive case, where the three resonant waves extract energy from the background to produce a singularity in a finite time (Sugaya et al. 1977; Cairns 1979; Craik and Adam 1979).

In addition to the above six integrable systems which have been derived from physical contexts in the above six sections, there are also many others, such as the Boussinesq equation, the complex modified Korteweg-de Vries equation, the massive-Thirring model, and the complex short pulse equation, which would arise in other physical situations. A common feature of all these integrable systems is that constant-amplitude background waves in them exhibit modulation instability (also called Benjamin-Feir instability in water waves). Thus, these constant-amplitude waves are unstable and will break up upon perturbations. For proper perturbations, these constant-amplitude waves will develop into localized waves with significantly higher amplitudes, but will eventually retreat back to those constant-amplitude waves again miraculously. These waves that "come from nowhere and disappear with no trace" (Akhmediev et al. 2009b) are the rogue wave solutions whose behaviors resemble physical rogue wave events. In the next chapter, we will derive these rogue wave solutions in a wide variety of integrable systems.

Chapter 2
Derivation of Rogue Waves in Integrable Systems

In this chapter, we derive general rogue waves in a wide variety of integrable systems, including those obtained in Chap. 1, but also many others, such as the Boussinesq equation, the Ablowitz-Ladik equation, the complex modified Korteweg-de Vries equation, the complex short pulse equation, the massive Thirring model, the Sasa-Satsuma equation, and the parity-time-symmetric NLS equation. We will use the bilinear method in all our derivations, since general rogue wave expressions out of this method are simpler and more explicit than those out of other methods. For the NLS equation, derivation of rogue waves by Darboux transformation is also presented, so that the reader can compare the two methods and their results. Dynamics of low-order rogue waves in these integrable systems are also graphically illustrated.

The bilinear method for the study of integrable systems was developed by R. Hirota and the Japanese school in 1970s–1980s (see Hirota 2004). Its application to derive rogue wave solutions was first performed by Ohta and Yang (2012a) for the nonlinear Schrödinger equation and then extended to many other integrable equations.

In the bilinear derivation of rogue waves, some notations need to be introduced first. One is Hirota's bilinear differential operator D, which is defined by

$$\begin{aligned} &P\left(D_x, D_y, D_t, \ldots\right) F(x, y, t, \ldots) \cdot G(x, y, t, \ldots) \\ &= P\left(\partial_x - \partial_{x'}, \partial_y - \partial_{y'}, \partial_t - \partial_{t'}, \ldots\right) \\ &\quad \times F(x, y, t, \ldots) G(x', y', t', \ldots)|_{x'=x, y'=y, t'=t, \ldots}, \end{aligned} \tag{2.1}$$

where P is a polynomial of $D_x, D_y, D_t, \ldots$. This D operator is the starting point of the bilinear method.

Another is the Schur polynomial $S_k(\boldsymbol{x})$, with $\boldsymbol{x} = (x_1, x_2, \ldots)$, which are defined by the generating function

B. Yang, J. Yang, *Rogue Waves in Integrable Systems*,
https://doi.org/10.1007/978-3-031-66793-0_2

$$\sum_{k=0}^{\infty} S_k(\boldsymbol{x})\epsilon^k = \exp\left(\sum_{k=1}^{\infty} x_k \epsilon^k\right), \tag{2.2}$$

or more explicitly,

$$S_k(\boldsymbol{x}) = \sum_{l_1+2l_2+\cdots+ml_m=k} \left(\prod_{j=1}^{m} \frac{x_j^{l_j}}{l_j!}\right). \tag{2.3}$$

For example we have

$$S_0(\boldsymbol{x}) = 1, \quad S_1(\boldsymbol{x}) = x_1, \quad S_2(\boldsymbol{x}) = \frac{1}{2}x_1^2 + x_2, \quad S_3(\boldsymbol{x}) = \frac{1}{6}x_1^3 + x_1x_2 + x_3. \tag{2.4}$$

In addition, we define $S_k(\boldsymbol{x}) = 0$ if $k < 0$. Schur polynomials $S_k(\boldsymbol{x})$ will be used in the explicit expressions of rogue wave solutions.

2.1 Nonlinear Schrödinger Equation

The nonlinear Schrödinger (NLS) equation

$$\mathrm{i}u_t + \frac{1}{2}u_{xx} + |u|^2 u = 0 \tag{2.5}$$

arises in numerous physical situations such as water waves, optics and plasma (see Sect. 1.1). Constant-amplitude continuous-wave solutions to this equation are modulation unstable to perturbations. Out of this instability, rogue waves may arise. These waves are rational solutions which approach a constant-amplitude continuous-wave background as $x, t \to \pm\infty$, but rise to significantly higher transient amplitudes with localized waveforms at intermediate times. Notice that this NLS equation is Galilean invariant, i.e., if $u(x,t)$ is its solution, so is $u(x - ct, t)e^{\mathrm{i}cx - \frac{1}{2}\mathrm{i}c^2 t}$, where c is an arbitrary velocity parameter. In addition, this equation is also scaling invariant, i.e., if $u(x,t)$ is its solution, so is $\alpha u(|\alpha|x, |\alpha|^2 t)$, where α is an arbitrary complex constant. Using these two invariances, we can normalize the boundary conditions of these rogue waves as

$$u(x,t) \to e^{\mathrm{i}t}, \quad x, t \to \pm\infty, \tag{2.6}$$

without loss of generality.

Rogue waves in the NLS equation have been derived by many researchers using different techniques (Peregrine 1983; Akhmediev et al. 2009a; Dubard et al. 2010; Kedziora et al. 2011; Guo et al. 2012; Ohta and Yang 2012a; Bilman and Miller 2019). Such waves have also been observed in many experiments in water

tanks, optical fibers, plasma, and Bose-Einstein condensates (Kibler et al. 2010; Chabchoub et al. 2011; Bailung et al. 2011; Chabchoub et al. 2012a,b; Xu et al. 2019; Romero-Ros et al. 2024).

2.1.1 Derivation by the Bilinear Method

Rogue waves in the NLS equation have been derived before by Darboux transformation (Akhmediev et al. 2009a; Guo et al. 2012), the bilinear method (Ohta and Yang 2012a), the inverse scattering transform method (Bilman and Miller 2019), and others (Dubard et al. 2010). Of these solutions, the ones by the bilinear method in Ohta and Yang (2012a) are the most explicit. Those bilinear solutions can be further simplified by incorporating a new parameterization into the bilinear derivation (Yang et al. 2020). These simpler expressions of bilinear rogue waves were reported in Yang and Yang (2021a) and are given in the following theorem.

Theorem 2.1 *The NLS equation (2.5) under boundary conditions (2.6) admits the following nonsingular rational rogue wave solutions*

$$u_N(x,t) = \frac{\sigma_1}{\sigma_0} e^{\mathrm{i}t}, \tag{2.7}$$

where the positive integer N represents the order of the rogue wave,

$$\sigma_n = \det_{1\le i,j\le N}\left(\phi^{(n)}_{2i-1,2j-1}\right), \tag{2.8}$$

the matrix elements in σ_n are defined by

$$\phi^{(n)}_{i,j} = \sum_{\nu=0}^{\min(i,j)} \frac{1}{4^\nu} S_{i-\nu}(\boldsymbol{x}^+(n)+\nu \boldsymbol{s})\, S_{j-\nu}(\boldsymbol{x}^-(n)+\nu \boldsymbol{s}), \tag{2.9}$$

vectors $\boldsymbol{x}^{\pm}(n) = \left(x_1^{\pm}, 0, x_3^{\pm}, 0, \cdots\right)$ are defined by

$$x_1^{\pm} = x \pm \mathrm{i}t \pm n, \quad x^+_{2k+1} = \frac{x + 2^{2k}(\mathrm{i}t)}{(2k+1)!} + a_{2k+1}, \quad x^-_{2k+1} = (x^+_{2k+1})^*, \tag{2.10}$$

*with $k \ge 1$ and the asterisk * representing complex conjugation, $\boldsymbol{s} = (0, s_2, 0, s_4, \cdots)$ are coefficients from the expansion*

$$\sum_{k=1}^{\infty} s_k \lambda^k = \ln\left[\frac{2}{\lambda}\tanh\left(\frac{\lambda}{2}\right)\right], \tag{2.11}$$

and a_{2k+1} $(k = 1, 2, \cdots, N-1)$ are free irreducible complex constants.

Since the order N and internal complex parameters $(a_3, a_5, \cdots, a_{2N-1})$ are all free, the above solutions contain a wide variety of rogue waves depending on the values of these free parameters. Physically, these rogue waves arise from a uniform background due to modulation instability (see boundary conditions (2.6)). But to generate rogue waves, perturbations to the uniform background need to be seeded properly according to the above exact solutions; otherwise what is created may not be a rogue wave. This point is important for experimental realizations of rogue waves (see Chap. 4).

We note by passing that another index choice in the above σ_n determinant,

$$\sigma_n = \det_{1\le i,j\le N}\left(\phi^{(n)}_{2i-2,2j-2}\right), \tag{2.12}$$

would also give NLS rogue waves. But as we have shown in a different but similar context (Yang et al. 2020), this other index choice would lead to solutions which are equivalent to those from (2.8).

Next, we derive the NLS rogue wave solutions and prove Theorem 2.1. Since this is our first bilinear derivation of rogue waves, we will provide all details so that the reader can follow it. For later derivations of rogue waves in other integrable systems, we will be more brief.

Proof of Theorem 2.1 Through the variable transformation

$$u = \frac{g}{f}e^{\mathrm{i}t}, \tag{2.13}$$

where f is a real variable and g a complex one, the NLS equation (2.5) can be transformed into the following bilinear form

$$\left.\begin{array}{l}\left(D_x^2+2\right) f\cdot f = 2|g|^2,\\ \left(D_x^2+2\mathrm{i}D_t\right) g\cdot f = 0,\end{array}\right\} \tag{2.14}$$

where D is Hirota's bilinear differential operator defined in Eq. (2.1).

The basic idea of our proof is the following. First, we consider a (2+1)-dimensional generalization of the above bilinear equations,

$$\left.\begin{array}{l}(D_xD_y+2) f\cdot f = 2gh,\\ (D_x^2+2\mathrm{i}D_t) g\cdot f = 0,\end{array}\right\} \tag{2.15}$$

where h is another complex variable. This is in fact the bilinear form of the Davey-Stewartson equations, which is a (2+1)-dimensional generalization of the NLS equation. We construct a wide class of solutions for Eq. (2.15) in the form of Gram determinants. Among these Gram determinant solutions, we extract algebraic solutions satisfying the dimension reduction condition

$$(\partial_x - \partial_y) f = Cf, \tag{2.16}$$

where C is a certain constant. Under this dimension reduction condition, such algebraic solutions would satisfy the (1+1)-dimensional system

$$\left.\begin{aligned}(D_x^2+2)f\cdot f &= 2gh,\\ (D_x^2+2\mathrm{i}D_t)g\cdot f &= 0.\end{aligned}\right\} \tag{2.17}$$

Finally, we impose the complex conjugacy conditions

$$f=f^*,\quad h=g^*. \tag{2.18}$$

Then, the bilinear system (2.17) reduces to the bilinear NLS equation (2.14); hence Eq. (2.13) gives the general rogue wave solutions for the NLS equation (2.5).

Next, we follow the above outline to prove Theorem 2.1.

(a) Gram determinant solution for the (2+1)-dimensional system

We first derive the Gram determinant solution for the (2+1)-dimensional bilinear equations (2.15).

Lemma 2.1 *Let $m_{i,j}^{(n)}$, $\varphi_i^{(n)}$ and $\psi_j^{(n)}$ be functions of x_1, x_2 and x_{-1} satisfying the following differential and difference relations,*

$$\left.\begin{aligned}&\partial_{x_1} m_{i,j}^{(n)} = \varphi_i^{(n)}\psi_j^{(n)},\\ &\partial_{x_k}\varphi_i^{(n)} = \varphi_i^{(n+k)},\quad \partial_{x_k}\psi_j^{(n)} = -\psi_j^{(n-k)},\quad (k=1,2,-1),\end{aligned}\right\} \tag{2.19}$$

and

$$\left.\begin{aligned}&\partial_{x_2} m_{i,j}^{(n)} = \varphi_i^{(n+1)}\psi_j^{(n)} + \varphi_i^{(n)}\psi_j^{(n-1)},\\ &\partial_{x_{-1}} m_{i,j}^{(n)} = -\varphi_i^{(n-1)}\psi_j^{(n+1)},\\ &m_{i,j}^{(n+1)} = m_{i,j}^{(n)} + \varphi_i^{(n)}\psi_j^{(n+1)}.\end{aligned}\right\} \tag{2.20}$$

Then the determinant

$$\tau_n = \det_{1\le i,j\le N}\left(m_{i,j}^{(n)}\right) \tag{2.21}$$

satisfies the bilinear equations

$$\left.\begin{aligned}(D_{x_1}D_{x_{-1}}-2)\tau_n\cdot\tau_n &= -2\tau_{n+1}\tau_{n-1},\\ (D_{x_1}^2 - D_{x_2})\tau_{n+1}\cdot\tau_n &= 0.\end{aligned}\right\} \tag{2.22}$$

Note that the two bilinear equations in (2.22) belong to an extension of the KP-Toda hierarchy (KP stands for Kadomtsev-Petviashvili). Specifically, the first one is the bilinear form of the two-dimensional Toda lattice, and the second one belongs to the first modified KP hierarchy (Jimbo and Miwa 1983).

Proof of Lemma 2.1 First of all, we note that utilizing the former part (2.19) of the differential and difference relations, we can show that the x_1 derivatives of the latter part (2.20) of these relations are automatically satisfied, i.e.,

$$\left.\begin{aligned}
&\partial_{x_1}\left[\partial_{x_2} m_{i,j}^{(n)}\right] = \partial_{x_1}\left[\varphi_i^{(n+1)}\psi_j^{(n)} + \varphi_i^{(n)}\psi_j^{(n-1)}\right],\\
&\partial_{x_1}\left[\partial_{x_{-1}} m_{i,j}^{(n)}\right] = \partial_{x_1}\left[-\varphi_i^{(n-1)}\psi_j^{(n+1)}\right],\\
&\partial_{x_1}\left[m_{i,j}^{(n+1)}\right] = \partial_{x_1}\left[m_{i,j}^{(n)} + \varphi_i^{(n)}\psi_j^{(n+1)}\right]
\end{aligned}\right\} \tag{2.23}$$

automatically hold. For instance, for the first of those latter equations in (2.20), we see from the former relations (2.19) that

$$\partial_{x_1}\left[\partial_{x_2} m_{i,j}^{(n)}\right] = \partial_{x_2}[\varphi_i^{(n)}\psi_j^{(n)}] = \varphi_i^{(n+2)}\psi_j^{(n)} - \varphi_i^{(n)}\psi_j^{(n-2)},$$

and

$$\begin{aligned}
&\partial_{x_1}\left[\varphi_i^{(n+1)}\psi_j^{(n)} + \varphi_i^{(n)}\psi_j^{(n-1)}\right]\\
&= \varphi_i^{(n+2)}\psi_j^{(n)} - \varphi_i^{(n+1)}\psi_j^{(n-1)} + \varphi_i^{(n+1)}\psi_j^{(n-1)} - \varphi_i^{(n)}\psi_j^{(n-2)}\\
&= \varphi_i^{(n+2)}\psi_j^{(n)} - \varphi_i^{(n)}\psi_j^{(n-2)}.
\end{aligned}$$

Thus, the first equation in (2.23) is valid. The other two equations in (2.23) can be similarly verified. However, the validity of the x_1 derivative equations in (2.23) does not guarantee the validity of the original equations in (2.20). This is why we still need to list (2.20) as part of our conditions in addition to (2.19) in Lemma 2.1. With that said, the fact of the x_1 derivative of the latter relations (2.20) being valid [when (2.19) are valid] does suggest that, in practice, if choices of $m_{i,j}^{(n)}$, $\varphi_i^{(n)}$ and $\psi_j^{(n)}$ satisfy the former relations (2.19), then they often satisfy the latter relations (2.20) automatically as well. This fact can be helpful when one looks for appropriate $m_{i,j}^{(n)}$, $\varphi_i^{(n)}$ and $\psi_j^{(n)}$ functions to meet all these differential and difference relations.

We start with the differential formula of determinant,

$$\partial_x \det_{1\le i,j\le N}(a_{ij}) = \sum_{i,j=1}^{N} \Delta_{ij}\partial_x a_{ij}, \tag{2.24}$$

and the expansion formula of bordered determinant,

$$\det\begin{pmatrix} a_{ij} & b_i \\ c_j & d \end{pmatrix} = -\sum_{i,j} \Delta_{ij} b_i c_j + d\det(a_{ij}), \tag{2.25}$$

where Δ_{ij} is the (i, j)-cofactor of the matrix (a_{ij}). By using these determinant formulae as well as the relations (2.19) and (2.20) repeatedly, we can verify that the derivatives and shifts of the τ function (2.21) are expressed by the bordered determinants as follows,

$$\partial_{x_1}\tau_n = \begin{vmatrix} m_{i,j}^{(n)} & \varphi_i^{(n)} \\ -\psi_j^{(n)} & 0 \end{vmatrix},$$

$$\partial_{x_1}^2\tau_n = \begin{vmatrix} m_{i,j}^{(n)} & \varphi_i^{(n+1)} \\ -\psi_j^{(n)} & 0 \end{vmatrix} + \begin{vmatrix} m_{i,j}^{(n)} & \varphi_i^{(n)} \\ \psi_j^{(n-1)} & 0 \end{vmatrix},$$

$$\partial_{x_2}\tau_n = \begin{vmatrix} m_{i,j}^{(n)} & \varphi_i^{(n+1)} \\ -\psi_j^{(n)} & 0 \end{vmatrix} - \begin{vmatrix} m_{i,j}^{(n)} & \varphi_i^{(n)} \\ \psi_j^{(n-1)} & 0 \end{vmatrix},$$

$$\partial_{x_{-1}}\tau_n = \begin{vmatrix} m_{i,j}^{(n)} & \varphi_i^{(n-1)} \\ \psi_j^{(n+1)} & 0 \end{vmatrix},$$

$$(\partial_{x_1}\partial_{x_{-1}} - 1)\tau_n = \begin{vmatrix} m_{i,j}^{(n)} & \varphi_i^{(n-1)} & \varphi_i^{(n)} \\ \psi_j^{(n+1)} & 0 & -1 \\ -\psi_j^{(n)} & -1 & 0 \end{vmatrix},$$

$$\tau_{n+1} = \begin{vmatrix} m_{i,j}^{(n)} & \varphi_i^{(n)} \\ -\psi_j^{(n+1)} & 1 \end{vmatrix},$$

$$\tau_{n-1} = \begin{vmatrix} m_{i,j}^{(n)} & \varphi_i^{(n-1)} \\ \psi_j^{(n)} & 1 \end{vmatrix},$$

$$\partial_{x_1}\tau_{n+1} = \begin{vmatrix} m_{i,j}^{(n)} & \varphi_i^{(n+1)} \\ -\psi_j^{(n+1)} & 0 \end{vmatrix},$$

$$\partial_{x_1}^2\tau_{n+1} = \begin{vmatrix} m_{i,j}^{(n)} & \varphi_i^{(n+2)} \\ -\psi_j^{(n+1)} & 0 \end{vmatrix} + \begin{vmatrix} m_{i,j}^{(n)} & \varphi_i^{(n)} & \varphi_i^{(n+1)} \\ -\psi_j^{(n)} & 0 & 0 \\ -\psi_j^{(n+1)} & 1 & 0 \end{vmatrix},$$

$$\partial_{x_2}\tau_{n+1} = \begin{vmatrix} m_{i,j}^{(n)} & \varphi_i^{(n+2)} \\ -\psi_j^{(n+1)} & 0 \end{vmatrix} - \begin{vmatrix} m_{i,j}^{(n)} & \varphi_i^{(n)} & \varphi_i^{(n+1)} \\ -\psi_j^{(n)} & 0 & 0 \\ -\psi_j^{(n+1)} & 1 & 0 \end{vmatrix}.$$

From the Jacobi formula of determinants,

$$\begin{vmatrix} a_{ij} & b_i & c_i \\ d_j & e & f \\ g_j & h & k \end{vmatrix} \times |a_{ij}| = \begin{vmatrix} a_{ij} & c_i \\ g_j & k \end{vmatrix} \times \begin{vmatrix} a_{ij} & b_i \\ d_j & e \end{vmatrix} - \begin{vmatrix} a_{ij} & b_i \\ g_j & h \end{vmatrix} \times \begin{vmatrix} a_{ij} & c_i \\ d_j & f \end{vmatrix},$$

we immediately obtain the identities,

$$(\partial_{x_1}\partial_{x_{-1}} - 1)\tau_n \times \tau_n = \partial_{x_1}\tau_n \times \partial_{x_{-1}}\tau_n - (-\tau_{n-1})(-\tau_{n+1}),$$
$$\frac{1}{2}(\partial_{x_1}^2 - \partial_{x_2})\tau_{n+1} \times \tau_n = \partial_{x_1}\tau_{n+1} \times \partial_{x_1}\tau_n - \tau_{n+1}\frac{1}{2}(\partial_{x_1}^2 + \partial_{x_2})\tau_n,$$

which are the bilinear equations (2.22). This completes the proof. □

Notice from the first equation in (2.19) that the matrix element $m_{i,j}^{(n)}$ can be written as

$$m_{i,j}^{(n)} = \int^{x_1} \varphi_i^{(n)} \psi_j^{(n)} dx_1. \tag{2.26}$$

For this reason, the determinant (2.21) is often called the Gram determinant. Let us define

$$f = \tau_0, \quad g = \tau_1, \quad h = \tau_{-1}, \tag{2.27}$$

then these are the Gram determinant solutions to the (2+1)-dimensional system,

$$\left.\begin{aligned}(D_{x_1}D_{x_{-1}} - 2)f \cdot f &= -2gh,\\ (D_{x_1}^2 - D_{x_2})g \cdot f &= 0,\end{aligned}\right\} \tag{2.28}$$

which is nothing but the bilinear equations (2.15) by writing $x_1 = x$, $x_2 = \mathrm{i}t/2$ and $x_{-1} = -y$.

(b) Dimensional reduction

Next we derive algebraic solutions satisfying both the (2+1)-dimensional bilinear equations (2.15) and the dimension reduction condition (2.16), hence satisfying the (1+1)-dimensional system (2.17). These solutions are obtained by choosing the matrix elements appropriately in the Gram determinant solution in Lemma 2.1.

Lemma 2.2 *We define matrix elements* $m_{i,j}^{(n)}$ *by*

$$m_{i,j}^{(n)} = \mathcal{A}_i\mathcal{B}_j m^{(n)}|_{p=1,q=1}, \quad m^{(n)} = \frac{(p+1)(q+1)}{p+q}\left(-\frac{p}{q}\right)^n e^{\xi+\eta}, \tag{2.29}$$
$$\xi = \frac{1}{p}x_{-1} + px_1 + p^2x_2 + \xi_0(p), \quad \eta = \frac{1}{q}x_{-1} + qx_1 - q^2x_2 + \eta_0(q), \tag{2.30}$$

where $\mathcal{A}_i$ *and* $\mathcal{B}_j$ *are differential operators with respect to* p *and* q *as*

$$\mathcal{A}_i = \frac{1}{i!}\left(p\partial_p\right)^i, \quad \mathcal{B}_j = \frac{1}{j!}\left(q\partial_q\right)^j, \tag{2.31}$$

and $\xi_0(p)$, $\eta_0(q)$ are arbitrary functions of p, q, respectively. Then the determinant

$$\tau_n = \det_{1\le i,j\le N}\left(m^{(n)}_{2i-1,2j-1}\right) \tag{2.32}$$

satisfies the bilinear equations

$$\left.\begin{aligned}\left(D_{x_1}^2+2\right)\tau_n\cdot\tau_n &= 2\tau_{n+1}\tau_{n-1},\\ \left(D_{x_1}^2-D_{x_2}\right)\tau_{n+1}\cdot\tau_n &= 0.\end{aligned}\right\} \tag{2.33}$$

Proof First let us introduce $\varphi^{(n)}$ and $\psi^{(n)}$ as

$$\varphi^{(n)} = (p+1)p^n e^{\xi}, \quad \psi^{(n)} = (q+1)(-q)^{-n}e^{\eta}, \tag{2.34}$$

where ξ and η are as given in Eq. (2.30). Then, it is easy to see that these functions, together with $m^{(n)}$ in Eq. (2.29), satisfy the differential and difference relations

$$\left.\begin{aligned}&\partial_{x_1}m^{(n)} = \varphi^{(n)}\psi^{(n)},\\ &\partial_{x_k}\varphi^{(n)} = \varphi^{(n+k)}, \quad \partial_{x_k}\psi^{(n)} = -\psi^{(n-k)}, \quad (k=1,2,-1),\end{aligned}\right\} \tag{2.35}$$

and

$$\left.\begin{aligned}&\partial_{x_2}m^{(n)} = \varphi^{(n+1)}\psi^{(n)} + \varphi^{(n)}\psi^{(n-1)},\\ &\partial_{x_{-1}}m^{(n)} = -\varphi^{(n-1)}\psi^{(n+1)},\\ &m^{(n+1)} = m^{(n)} + \varphi^{(n)}\psi^{(n+1)}.\end{aligned}\right\} \tag{2.36}$$

Therefore, by defining

$$\tilde{m}^{(n)}_{i,j} = \mathcal{A}_i\mathcal{B}_j m^{(n)}, \quad \varphi^{(n)}_i = \mathcal{A}_i\varphi^{(n)}, \quad \psi^{(n)}_j = \mathcal{B}_j\psi^{(n)}, \tag{2.37}$$

we see that these $\tilde{m}^{(n)}_{i,j}$, $\varphi^{(n)}_i$ and $\psi^{(n)}_j$ obey the differential and difference relations (2.19)–(2.20) since operators $\mathcal{A}_i$ and $\mathcal{B}_j$ commute with differentials ∂_{x_k}. Lemma 2.1 then tells us that for an arbitrary sequence of indices $(i_1, i_2, \cdots, i_N; j_1, j_2, \cdots, j_N)$, the determinant

$$\tau_n = \det_{1\le\nu,\mu\le N}\left(\tilde{m}^{(n)}_{i_\nu,j_\mu}\right) \tag{2.38}$$

satisfies the (2+1)-dimensional bilinear equations (2.22).

Next we constrain the above determinant τ_n so that it satisfies the dimension reduction condition (2.16). From the Leibniz rule, we have the general operator equation

$$(p\partial_p)^i f(p) = \sum_{l=0}^{i} \binom{i}{l} \left[(p\partial_p)^l f(p)\right] (p\partial_p)^{i-l} \tag{2.39}$$

for any function $f(p)$. Since

$$(p\partial_p)^l (p + \frac{1}{p}) = p + \frac{(-1)^l}{p}, \tag{2.40}$$

the above operator equation then gives

$$(p\partial_p)^i (p + \frac{1}{p}) = \sum_{l=0}^{i} \binom{i}{l} \left(p + \frac{(-1)^l}{p}\right) (p\partial_p)^{i-l}. \tag{2.41}$$

Thus,

$$\begin{aligned} \mathcal{A}_i (p + \frac{1}{p}) &= \frac{1}{i!} \sum_{l=0}^{i} \binom{i}{l} \left(p + \frac{(-1)^l}{p}\right) (p\partial_p)^{i-l} \\ &= \sum_{l=0}^{i} \frac{1}{l!\,(i-l)!} \left(p + \frac{(-1)^l}{p}\right) (p\partial_p)^{i-l} = \sum_{l=0}^{i} \frac{1}{l!} \left(p + \frac{(-1)^l}{p}\right) \mathcal{A}_{i-l}, \end{aligned} \tag{2.42}$$

and similarly

$$\mathcal{B}_j (q + \frac{1}{q}) = \sum_{l=0}^{j} \frac{1}{l!} \left(q + \frac{(-1)^l}{q}\right) \mathcal{B}_{j-l}. \tag{2.43}$$

By using these relations, we find that

$$\begin{aligned} (\partial_{x_1} + \partial_{x_{-1}}) \tilde{m}_{i,j}^{(n)} &= \mathcal{A}_i \mathcal{B}_j (\partial_{x_1} + \partial_{x_{-1}}) m^{(n)} = \mathcal{A}_i \mathcal{B}_j \left(p + q + \frac{1}{p} + \frac{1}{q}\right) m^{(n)} \\ &= \sum_{l=0}^{i} \frac{1}{l!} \left(p + \frac{(-1)^l}{p}\right) \mathcal{A}_{i-l} \mathcal{B}_j m^{(n)} + \sum_{l=0}^{j} \frac{1}{l!} \left(q + \frac{(-1)^l}{q}\right) \mathcal{A}_i \mathcal{B}_{j-l} m^{(n)} \\ &= \sum_{l=0}^{i} \frac{1}{l!} \left(p + \frac{(-1)^l}{p}\right) \tilde{m}_{i-l,j}^{(n)} + \sum_{l=0}^{j} \frac{1}{l!} \left(q + \frac{(-1)^l}{q}\right) \tilde{m}_{i,j-l}^{(n)}. \end{aligned} \tag{2.44}$$

Now let us take $p = 1$ and $q = 1$. Then the above equation shows that $\tilde{m}_{i,j}^{(n)}\Big|_{p=1,q=1}$ satisfies the contiguity relation,

$$(\partial_{x_1}+\partial_{x_{-1}})\,\tilde{m}^{(n)}_{i,j}\Big|_{p=q=1}=2\sum_{\substack{l=0\\ l:\text{even}}}^{i}\frac{1}{l!}\,\tilde{m}^{(n)}_{i-l,j}\Big|_{p=q=1}+2\sum_{\substack{l=0\\ l:\text{even}}}^{j}\frac{1}{l!}\,\tilde{m}^{(n)}_{i,j-l}\Big|_{p=q=1}. \tag{2.45}$$

By using this relation and the formula (2.24), the differential of the determinant

$$\tilde{\tau}_n=\det_{1\le i,j\le N}\left(\tilde{m}^{(n)}_{2i-1,2j-1}\Big|_{p=1,q=1}\right) \tag{2.46}$$

is calculated as

$$\begin{aligned}(\partial_{x_1}+\partial_{x_{-1}})\tilde{\tau}_n&=\sum_{i=1}^{N}\sum_{j=1}^{N}\Delta_{ij}(\partial_{x_1}+\partial_{x_{-1}})\left(\tilde{m}^{(n)}_{2i-1,2j-1}\Big|_{p=q=1}\right)\\
&=\sum_{i=1}^{N}\sum_{j=1}^{N}\Delta_{ij}\left(2\sum_{\substack{l=0\\ l:\text{even}}}^{2i-1}\frac{1}{l!}\,\tilde{m}^{(n)}_{2i-1-l,2j-1}\Big|_{p=q=1}+2\sum_{\substack{l=0\\ l:\text{even}}}^{2j-1}\frac{1}{l!}\,\tilde{m}^{(n)}_{2i-1,2j-1-l}\Big|_{p=q=1}\right)\\
&=2\sum_{i=1}^{N}\sum_{\substack{l=0\\ l:\text{even}}}^{2i-1}\frac{1}{l!}\sum_{j=1}^{N}\Delta_{ij}\,\tilde{m}^{(n)}_{2i-1-l,2j-1}\Big|_{p=q=1}\\
&\quad+2\sum_{j=1}^{N}\sum_{\substack{l=0\\ l:\text{even}}}^{2j-1}\frac{1}{l!}\sum_{i=1}^{N}\Delta_{ij}\,\tilde{m}^{(n)}_{2i-1,2j-1-l}\Big|_{p=q=1},\end{aligned}$$

where Δ_{ij} is the (i,j)-cofactor of the matrix $(\tilde{m}^{(n)}_{2i-1,2j-1}|_{p=1,q=1})$. In the first term on the right-hand side of the above equation, only the term with $l=0$ survives and the other terms vanish, since for $l=2,4,\cdots$, the summation with respect to j is a determinant with two identical rows. Similarly in the second term, only the term with $l=0$ remains. Thus the right side of the above equation becomes

$$2\sum_{i=1}^{N}\sum_{j=1}^{N}\Delta_{ij}\,\tilde{m}^{(n)}_{2i-1,2j-1}\Big|_{p=q=1}+2\sum_{j=1}^{N}\sum_{i=1}^{N}\Delta_{ij}\,\tilde{m}^{(n)}_{2i-1,2j-1}\Big|_{p=q=1}=4N\tilde{\tau}_n. \tag{2.47}$$

Therefore $\tilde{\tau}_n$ satisfies the dimension reduction condition

$$(\partial_{x_1}+\partial_{x_{-1}})\tilde{\tau}_n=4N\tilde{\tau}_n. \tag{2.48}$$

We note that the above derivation of Eq. (2.48) using cofactor expansions can also be done using just determinant notations, which would look simpler. Since $\tilde{\tau}_n$ is

a special case of τ_n in Eq. (2.38), it also satisfies the bilinear equations (2.22) with τ_n replaced by $\tilde{\tau}_n$. From (2.22) and (2.48), we see that $\tilde{\tau}_n$ satisfies the (1+1)-dimensional bilinear equations (2.33). Now we can take $x_{-1} = 0$; then $\tilde{m}^{(n)}_{i,j}|_{p=1,q=1}$ and $\tilde{\tau}_n$ reduce to $m^{(n)}_{i,j}$ and τ_n in Lemma 2.2, and this τ_n satisfies the bilinear equations (2.33). This completes the proof of Lemma 2.2.

The above proof uses the technique of dimension reduction. This reduction is a procedure to derive solutions of a lower dimensional system from those of a higher dimensional one. By using the reduction condition (2.48), the derivative with respect to a variable x_{-1} is replaced by the derivative with respect to another variable x_1. Then in the solution, x_{-1} is just a parameter to which we can substitute any value (such as zero as we did above).

It is remarkable that the determinant expression of the solution (2.32) has a quite unique structure: the indices of matrix elements, which label the degree of polynomial, have the step of 2. This comes from the requirement of the dimension reduction condition (2.48), i.e., since the contiguity relation (2.45) relates matrix elements with indices shifted by even numbers, a determinant with indices of step 2 could satisfy that dimension reduction condition.

From Lemma 2.2, by writing $x_1 = x$ and $x_2 = \mathrm{i}t/2$, we find that $f = \tau_0$, $g = \tau_1$ and $h = \tau_{-1}$ satisfy the (1+1)-dimensional system (2.17).

To introduce explicit free parameters into these (f, g, h) solutions, we expand free functions $\xi_0(p)$ and $\eta_0(q)$ in Eq. (2.30) as power series of $\ln p$ and $\ln q$, i.e.,

$$\xi_0(p) = \sum_{k=1}^{\infty} a_k (\ln p)^k, \quad \eta_0(q) = \sum_{k=1}^{\infty} b_k (\ln q)^k, \tag{2.49}$$

where a_k and b_k are free complex constants. This introduction of free parameters is different from the original one in Ohta and Yang (2012a), and this new way will lead to simpler expressions of rogue waves.

(c) Complex conjugacy conditions and regularity

Now we consider the complex conjugate conditions (2.18). These conditions are

$$\tau_0 = \tau_0^*, \quad \tau_{-1} = \tau_1^*. \tag{2.50}$$

Since $x_1 = x$ is real and $x_2 = \mathrm{i}t/2$ is pure imaginary, the above condition is easily satisfied by taking

$$b_k = a_k^*. \tag{2.51}$$

Indeed, under the condition (2.51) we have

$$(m^{(n)}_{i,j})^* = m^{(n)}_{i,j}\Big|_{a_k \leftrightarrow b_k, x_2 \leftrightarrow -x_2} = m^{(-n)}_{j,i}, \tag{2.52}$$

and therefore

$$\tau_n^* = \tau_{-n}. \tag{2.53}$$

As a result, $f = \tau_0$ and $g = \tau_1$ satisfy the bilinear equations (2.14) of the NLS equation, and hence the function $u = (g/f)e^{\mathrm{i}t}$ is a solution to the NLS equation. In this solution, g/f is a rational function.

We can further show that this u solution is nonsingular, i.e., $f = \tau_0$ is nonzero for all (x, t). To prove it, we notice that τ_0 is the determinant of a Hermitian matrix $M = \underset{1\le i,j\le N}{\mathrm{mat}}\left(m^{(0)}_{2i-1,2j-1}\right)$. For any non-zero column vector $\boldsymbol{v} = (v_1, v_2, \cdots, v_N)^T$ and $\boldsymbol{v}^\dagger$ being its complex transpose, we have

$$\begin{aligned}
\boldsymbol{v}^\dagger M \boldsymbol{v} &= \sum_{i,j=1}^{N} v_i^* m^{(0)}_{2i-1,2j-1} v_j \\
&= \sum_{i,j=1}^{N} v_i^* v_j \, \mathcal{A}_{2i-1}\mathcal{B}_{2j-1} \frac{(p+1)(q+1)}{p+q} e^{\xi+\eta}\Big|_{p=q=1} \\
&= \sum_{i,j=1}^{N} v_i^* v_j \, \mathcal{A}_{2i-1}\mathcal{B}_{2j-1} \int_{-\infty}^{x} (p+1)(q+1) e^{\xi+\eta} dx \Big|_{p=q=1} \\
&= \int_{-\infty}^{x} \sum_{i,j=1}^{N} v_i^* v_j \mathcal{A}_{2i-1}\mathcal{B}_{2j-1}(p+1)(q+1) e^{\xi+\eta}\big|_{p=q=1} \, dx \\
&= \int_{-\infty}^{x} \left| \sum_{i=1}^{N} v_i^* \mathcal{A}_{2i-1}(p+1) e^{\xi}\big|_{p=1} \right|^2 dx > 0,
\end{aligned} \tag{2.54}$$

which proves that the Hermitian matrix M is positive definite. Therefore the denominator $f = \det M > 0$, so the solution u is nonsingular.

(d) Rogue wave solutions in differential operator form

Summarizing the above results, we obtain the following intermediate result on rogue wave solutions in the NLS equation.

Lemma 2.3 *The NLS equation (2.5) admits the following nonsingular rational solutions in differential form,*

$$u_N(x,t) = \frac{\tau_1}{\tau_0} e^{\mathrm{i}t}, \tag{2.55}$$

where

$$\tau_n = \det_{1\le i,j\le N}\left(m^{(n)}_{2i-1,2j-1}\right), \tag{2.56}$$

the matrix elements are defined by

$$m_{i,j}^{(n)} = \mathcal{A}_i \mathcal{B}_j m^{(n)}|_{p=1,q=1}, \quad m^{(n)} = \frac{(p+1)(q+1)}{p+q}\left(-\frac{p}{q}\right)^n e^{\xi+\eta}, \tag{2.57}$$

$$\xi = px + \frac{1}{2}p^2 \mathrm{i}t + \sum_{k=1}^{\infty} a_k (\ln p)^k, \quad \eta = qx - \frac{1}{2}q^2 \mathrm{i}t + \sum_{k=1}^{\infty} a_k^* (\ln q)^k, \tag{2.58}$$

operators $\mathcal{A}_i$ and $\mathcal{B}_j$ are defined in Eq. (2.31), and $a_1, a_2, \cdots, a_{2N-1}$ are arbitrary complex constants.

Compared to the choice of $m^{(n)}$ in Ohta and Yang (2012a), our choice of $m^{(n)}$ in Eq. (2.57) contains an extra factor of $(p+1)(q+1)$. This factor is optional for the above differential form of rogue wave solutions, i.e., functions $u_N(x,t)$ with or without this extra factor both give true rogue wave solutions. The benefit of this extra factor is that it will facilitate our derivation of explicit rogue wave expressions through Schur polynomials, which we will do next.

(e) Explicit rogue wave solutions through Schur polynomials

Finally we simplify the rogue wave solutions in Lemma 2.3 and derive the solution formulae given in Theorem 2.1.

The generator $\mathcal{G}$ of the differential operator $(p\partial_p)^i (q\partial_q)^j$ is

$$\mathcal{G} = \sum_{i=0}^{\infty}\sum_{j=0}^{\infty} \frac{\kappa^i}{i!}\frac{\lambda^j}{j!}(p\partial_p)^i (q\partial_q)^j = \exp(\kappa p\partial_p + \lambda q\partial_q) = \exp(\kappa \partial_{\ln p} + \lambda \partial_{\ln q}). \tag{2.59}$$

Thus, for any function $F(p,q)$, we have

$$\mathcal{G}F(p,q) = F(e^{\kappa}p, e^{\lambda}q). \tag{2.60}$$

This relation can also be seen by expanding its right hand side into Taylor series of (κ, λ) around the point $(0,0)$. By applying this relation to $m^{(n)}$ in Eq. (2.57), we get

$$\begin{aligned} \mathcal{G}m^{(n)} &= \frac{(e^{\kappa}p+1)(e^{\lambda}q+1)}{e^{\kappa}p+e^{\lambda}q}\left(-\frac{e^{\kappa}p}{e^{\lambda}q}\right)^n \\ &\quad \times \exp\left((e^{\kappa}p+e^{\lambda}q)x + \frac{1}{2}(e^{2\kappa}p^2 - e^{2\lambda}q^2)\mathrm{i}t\right) \\ &\quad \times \exp\left(\sum_{k=1}^{\infty} a_k [\ln(e^{\kappa}p)]^k + \sum_{k=1}^{\infty} a_k^* [\ln(e^{\lambda}q)]^k\right). \end{aligned} \tag{2.61}$$

Thus,

$$\begin{aligned}\frac{1}{m^{(n)}}\mathcal{G}m^{(n)}\Big|_{p=q=1} &= \frac{(e^{\kappa}+1)(e^{\lambda}+1)}{2(e^{\kappa}+e^{\lambda})}e^{n(\kappa-\lambda)} \\ &\quad\times\exp\left((e^{\kappa}+e^{\lambda}-2)x+\frac{1}{2}(e^{2\kappa}-e^{2\lambda})\mathrm{i}t\right) \\ &\quad\times\exp\left(\sum_{k=1}^{\infty}a_k\kappa^k+\sum_{k=1}^{\infty}a_k^*\lambda^k\right) \\ &= \frac{1}{1-\frac{(e^{\kappa}-1)(e^{\lambda}-1)}{(e^{\kappa}+1)(e^{\lambda}+1)}}\exp\big(n(\kappa-\lambda)+(e^{\kappa}+e^{\lambda}-2)x \\ &\quad+\frac{1}{2}(e^{2\kappa}-e^{2\lambda})\mathrm{i}t\Big) \\ &\quad\times\exp\left(\sum_{k=1}^{\infty}a_k\kappa^k+\sum_{k=1}^{\infty}a_k^*\lambda^k\right). \end{aligned} \tag{2.62}$$

On the right-hand side of this equation, the exponent can be rewritten as

$$\begin{aligned} &n(\kappa-\lambda)+\sum_{k=1}^{\infty}\frac{\kappa^k}{k!}(x+2^{k-1}\mathrm{i}t)+\sum_{k=1}^{\infty}\frac{\lambda^k}{k!}(x-2^{k-1}\mathrm{i}t)+\sum_{k=1}^{\infty}a_k\kappa^k+\sum_{k=1}^{\infty}a_k^*\lambda^k \\ &\quad=\sum_{k=1}^{\infty}\hat{x}_k^+\kappa^k+\sum_{k=1}^{\infty}\hat{x}_k^-\lambda^k, \end{aligned} \tag{2.63}$$

where

$$\left.\begin{aligned}&\hat{x}_1^+=x+\mathrm{i}t+n+a_1, \quad \hat{x}_1^-=x-\mathrm{i}t-n+a_1^*, \\ &\hat{x}_k^+=\tfrac{1}{k!}(x+2^{k-1}\mathrm{i}t)+a_k, \quad \hat{x}_k^-=(\hat{x}_k^+)^*, \quad k\geq 2,\end{aligned}\right\} \tag{2.64}$$

and the prefactor can be rewritten as

$$\begin{aligned} &\sum_{\nu=0}^{\infty}\left(\frac{(e^{\kappa}-1)(e^{\lambda}-1)}{(e^{\kappa}+1)(e^{\lambda}+1)}\right)^{\nu}=\sum_{\nu=0}^{\infty}\left(\frac{\kappa\lambda}{4}\right)^{\nu}\exp\left(\nu\ln\left(\frac{4}{\kappa\lambda}\tanh\frac{\kappa}{2}\tanh\frac{\lambda}{2}\right)\right) \\ &=\sum_{\nu=0}^{\infty}\left(\frac{\kappa\lambda}{4}\right)^{\nu}\exp\left(\nu\sum_{k=1}^{\infty}s_k(\kappa^k+\lambda^k)\right), \end{aligned} \tag{2.65}$$

where s_k is defined in (2.11). Therefore we obtain

$$\frac{1}{m^{(n)}}\mathcal{G}m^{(n)}\Big|_{p=1,q=1}=\sum_{\nu=0}^{\infty}\left(\frac{\kappa\lambda}{4}\right)^{\nu}\exp\left(\sum_{k=1}^{\infty}(\hat{x}_k^++\nu s_k)\kappa^k+\sum_{k=1}^{\infty}(\hat{x}_k^-+\nu s_k)\lambda^k\right)$$

$$= \sum_{\nu=0}^{\infty} \left(\frac{\kappa\lambda}{4}\right)^{\nu} \sum_{i=0}^{\infty} S_i(\hat{\boldsymbol{x}}^+ + \nu\boldsymbol{s})\kappa^i \sum_{j=0}^{\infty} S_j(\hat{\boldsymbol{x}}^- + \nu\boldsymbol{s})\lambda^j$$

$$= \sum_{i=0}^{\infty}\sum_{j=0}^{\infty}\sum_{\nu=0}^{\infty} \frac{1}{4^\nu} S_i(\hat{\boldsymbol{x}}^+ + \nu\boldsymbol{s}) S_j(\hat{\boldsymbol{x}}^- + \nu\boldsymbol{s})\kappa^{i+\nu}\lambda^{j+\nu}, \tag{2.66}$$

and taking the coefficient of $\kappa^i\lambda^j$ of both sides, we find

$$\frac{\mathcal{A}_i\mathcal{B}_j m^{(n)}\big|_{p=1,q=1}}{m^{(n)}\big|_{p=1,q=1}} = \sum_{\nu=0}^{\min(i,j)} \frac{1}{4^\nu} S_{i-\nu}(\hat{\boldsymbol{x}}^+ + \nu\boldsymbol{s}) S_{j-\nu}(\hat{\boldsymbol{x}}^- + \nu\boldsymbol{s}) \equiv \hat{\phi}_{i,j}^{(n)}, \tag{2.67}$$

where $\hat{\boldsymbol{x}}^\pm$ are defined in Eq. (2.64). Thus, $m_{i,j}^{(n)}$ in Lemma 2.3 is calculated as

$$m_{i,j}^{(n)} = m^{(n)}\Big|_{p=1,q=1} \hat{\phi}_{i,j}^{(n)}, \tag{2.68}$$

and the τ_n determinent in Lemma 2.3 is found to be

$$\tau_n = \left(m^{(n)}\Big|_{p=1,q=1}\right)^N \hat{\sigma}_n, \tag{2.69}$$

where

$$\hat{\sigma}_n = \det_{1\le i,j\le N}\left(\hat{\phi}_{2i-1,2j-1}^{(n)}\right). \tag{2.70}$$

Substituting this relation into Eq. (2.55), and recalling that the NLS equation is invariant if u is changed to $-u$, we see that function $u_N(x,t) = (\hat{\sigma}_1/\hat{\sigma}_0)e^{it}$ satisfies the NLS equation as well.

Now, we simplify $\hat{\sigma}_n$ and show that it can be replaced by σ_n in Theorem 2.1. Through a shift of the x and t axes, we normalize $a_1 = 0$ without loss of generality. Then, $\hat{x}_1^\pm = x_1^\pm$, where $x_1^\pm$ are as defined in Theorem 2.1. In addition, we can show that $\hat{x}_{2k}^\pm$ are dummy variables that do not affect the value of $\hat{\sigma}_n$ and can thus be set as zero, so that $\hat{\boldsymbol{x}}^\pm$ can be replaced by $\boldsymbol{x}^\pm$ of Theorem 2.1, hence $\hat{\sigma}_n$ becoming σ_n of Theorem 2.1. To show this, we split the vectors $\hat{\boldsymbol{x}}^\pm(n)$ into $\boldsymbol{x}^\pm(n) + \boldsymbol{w}^\pm$, where $\boldsymbol{x}^\pm(n)$ is as defined in Theorem 2.1 (see Eq. (2.10)), and $\boldsymbol{w}^\pm = (0, \hat{x}_2^\pm, 0, \hat{x}_4^\pm, \cdots)$. Since $\hat{\boldsymbol{x}}^\pm(n) + \nu\boldsymbol{s} = \boldsymbol{x}^\pm(n) + \nu\boldsymbol{s} + \boldsymbol{w}^\pm$, it is easy to show from the definition of Schur polynomials (2.2) that

$$S_k(\hat{\boldsymbol{x}}^\pm(n) + \nu\boldsymbol{s}) = \sum_{j=0}^{[k/2]} S_j(\hat{\boldsymbol{w}}^\pm) S_{k-2j}(\boldsymbol{x}^\pm(n) + \nu\boldsymbol{s}), \tag{2.71}$$

where $\hat{\boldsymbol{w}}^{\pm} = (\hat{x}_2^{\pm}, \hat{x}_4^{\pm}, \cdots)$. To proceed further, we repeatedly use the formula

$$\det(a_{ij} + b_i c_j) = \det \begin{pmatrix} a_{ij} & b_i \\ -c_j & 1 \end{pmatrix}, \tag{2.72}$$

which allows us to rewrite the determinant $\hat{\sigma}_n$ in Eq. (2.70) into the following $3N \times 3N$ determinant,

$$\hat{\sigma}_n = \begin{vmatrix} \mathbf{O}_{N\times N} & \widehat{\Phi}_{N\times 2N} \\ -\widehat{\Psi}_{2N\times N} & \mathbf{I}_{2N\times 2N} \end{vmatrix}, \tag{2.73}$$

where $\mathbf{O}$ and $\mathbf{I}$ are the zero and unit matrices, $\widehat{\Phi}_{i,j} = 2^{-(j-1)} S_{2i-j}\left[\hat{\boldsymbol{x}}^{+}(n) + (j-1)\boldsymbol{s}\right]$, and $\widehat{\Psi}_{i,j} = 2^{-(i-1)} S_{2j-i}\left[\hat{\boldsymbol{x}}^{-}(n) + (i-1)\boldsymbol{s}\right]$. Then, utilizing the relation (2.71), we can apply row and column manipulations to eliminate all terms involving $\hat{\boldsymbol{w}}^{\pm}$ in this $3N \times 3N$ determinant. The remaining $3N \times 3N$ determinant then becomes

$$\begin{vmatrix} \mathbf{O}_{N\times N} & \Phi_{N\times 2N} \\ -\Psi_{2N\times N} & \mathbf{I}_{2N\times 2N} \end{vmatrix}, \tag{2.74}$$

where

$$\left.\begin{aligned} \Phi_{i,j} &= 2^{-(j-1)} S_{2i-j}\left[\boldsymbol{x}^{+}(n) + (j-1)\boldsymbol{s}\right], \\ \Psi_{i,j} &= 2^{-(i-1)} S_{2j-i}\left[\boldsymbol{x}^{-}(n) + (i-1)\boldsymbol{s}\right]. \end{aligned}\right\} \tag{2.75}$$

This new $3N \times 3N$ determinant (2.74) is nothing but σ_n in Eq. (2.8) of Theorem 2.1, whose matrix element $\phi_{i,j}^{(n)}$ is as given in Eq. (2.9), again by virtue of the formula (2.72). Thus, we have proved that the function $u_N(x,t) = (\sigma_1/\sigma_0)e^{\mathrm{i}t}$ in Eq. (2.7) of Theorem 2.1 satisfies the NLS equation (2.5).

(f) Boundary conditions

Finally, we prove that the solution (2.7) satisfies the boundary conditions (2.6) and is thus a rogue wave.

As we have shown above, σ_n in Eq. (2.8) can be written as the $3N \times 3N$ determinant (2.74), i.e.,

$$\sigma_n = \begin{vmatrix} \mathbf{O}_{N\times N} & \Phi_{N\times 2N} \\ -\Psi_{2N\times N} & \mathbf{I}_{2N\times 2N} \end{vmatrix}, \tag{2.76}$$

where $\Phi_{i,j}$ and $\Psi_{i,j}$ are given in Eq. (2.75). Applying the Laplace expansion to this determinant, we get

$$\sigma_n = \sum_{0\le\nu_1<\nu_2<\cdots<\nu_N\le 2N-1} \det_{1\le i,j\le N}\left[\frac{1}{2^{\nu_j}} S_{2i-1-\nu_j}(\boldsymbol{x}^+(n)+\nu_j \boldsymbol{s})\right] \times \det_{1\le i,j\le N}\left[\frac{1}{2^{\nu_j}} S_{2i-1-\nu_j}(\boldsymbol{x}^-(n)+\nu_j \boldsymbol{s})\right]. \quad (2.77)$$

In order to show the boundary asymptotics (2.6), let us estimate the degree of polynomials of the denominator σ_0 and numerator σ_1 in (2.7). The degree of the polynomial $S_k(\boldsymbol{x}^{\pm}+\nu \boldsymbol{s})$ in (x,t) is k and its leading term appears in the monomial $(x_1^{\pm})^k/k!$, i.e., the leading term is given by $(x \pm \mathrm{i}t)^k/k!$. Therefore both of the degrees of determinants inside the summation of the Laplace expansion (2.77) are given by $1+3+\cdots+(2N-1)-\nu_1-\nu_2-\cdots-\nu_N$. Then, the highest degree term in (2.77) comes from the lowest possible ν_j choices of $\nu_j = j-1$, i.e., $\boldsymbol{\nu} = (0, 1, \cdots, N-1)$. For this choice, the highest degree term in σ_n is nonzero and can be calculated explicitly as (Ohta and Yang 2012a)

$$\left(\frac{0!1!\cdots(N-1)!}{1!3!\cdots(2N-1)!}\right)^2 (x^2+t^2)^{N(N+1)/2}, \quad (2.78)$$

which is independent of n. Hence the $u_N(x,t)$ solution (2.7) satisfies the boundary conditions (2.6).

By now, Theorem 2.1 is fully proved.

Illustration of Low-Order Rogue Waves

Now we graphically illustrate some low-order rogue waves in the NLS equation.

Taking $N=1$ in Theorem 2.1, we get the first-order (fundamental) rogue wave in the NLS equation as

$$u_1(x,t) = \left(1 - \frac{4(1+2\mathrm{i}t)}{1+4x^2+4t^2}\right) e^{\mathrm{i}t}. \quad (2.79)$$

This is the rogue wave first reported by Peregrine (1983) and is often called the Peregrine wave in the literature. This Peregrine wave is displayed in Fig. 2.1 (left column). This wave rises from the unit-amplitude background, reaches a maximum amplitude of three times the background, and then retreats back to the unit background again. In addition, its wave profile features a high hump in the middle, flanked by two dips on the sides.

Taking $N=2$ in Theorem 2.1, we get second-order rogue waves in the NLS equation as

$$u_2(x,t;a_3) = \left(1 - \frac{G_2}{F_2}\right) e^{\mathrm{i}t}. \quad (2.80)$$

where

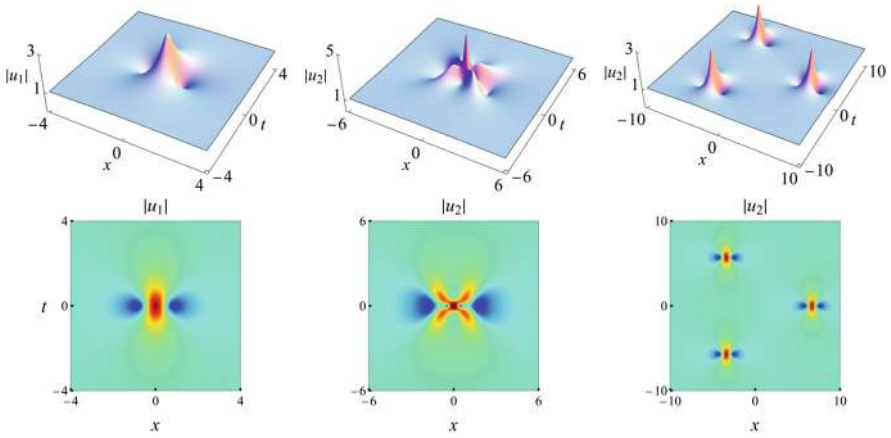

Fig. 2.1 Graphs of NLS rogue waves. Left column: the fundamental rogue (Peregrine) wave in Eq. (2.79); middle column: a second-order rogue wave with $a_3 = 0$ (second-order super rogue wave); right column: a second-order rogue wave with $a_3 = 100$ (a rogue triplet). Upper row: 3D plots; lower row: density plots

$$\begin{aligned} F_2 = \; & 9 + 396t^2 + 432t^4 + 64t^6 + 108x^2 - 288t^2x^2 + 192t^4x^2 + 48x^4 \\ & +192t^2x^4 + 64x^6 + 48a_3[-4\mathrm{i}t^3 + 3x + 12t^2x - 4x^3 + 3\mathrm{i}t(-3 + 4x^2)] \\ & +48a_3^*[4\mathrm{i}t^3 + 3x + 12t^2x - 4x^3 - 3\mathrm{i}t(-3 + 4x^2)] + 576|a_3|^2, \end{aligned} \tag{2.81}$$

and

$$\begin{aligned} G_2 = \; & 12\Big[-3 - 30\mathrm{i}t + 72t^2 + 16\mathrm{i}t^3 + 80t^4 + 32\mathrm{i}t^5 + 24x^2 \\ & -48\mathrm{i}tx^2 + 96t^2x^2 + 64\mathrm{i}t^3x^2 + 16x^4 + 32\mathrm{i}tx^4 \\ & +12(-\mathrm{i} + 2t + 2\mathrm{i}x)^2a_3 - 12(\mathrm{i} - 2t + 2\mathrm{i}x)^2a_3^*\Big]. \end{aligned} \tag{2.82}$$

For two values of $a_3 = 0$ and 100, these two second-order rogue waves are plotted in the middle and right columns of Fig. 2.1, respectively. The solution with $a_3 = 0$ reaches a peak amplitude of five times the background level, which is the highest possible peak value that can be attained among all second-order rogue waves. In the literature, this special N-th order rogue wave that reaches the highest possible peak amplitude among all rogue waves of the N-th order is called a N-th order super rogue wave. Thus, this solution with $a_3 = 0$ in Fig. 2.1 is a second-order super rogue wave. The solution with $a_3 = 100$ in Fig. 2.1 shows a rogue triplet, where this second-order rogue wave splits into three approximate Peregrine waves appearing at different locations in the space-time plane forming a triangle.

2.1.2 Peak Amplitude of the N-th Order Super Rogue Wave

A super rogue wave has the highest possible peak amplitude among rogue waves of the same order. In this subsection, we calculate this maximum peak amplitude of a super rogue wave in the NLS equation, using bilinear expressions of rogue waves in Theorem 2.1.

A super rogue wave of the NLS equation is obtained when all its internal parameters $a_3, a_5, \cdots$ are set as zero. In this case, we can easily see that

$$\boldsymbol{x}^{\pm}(n)|_{x\to -x} = -\boldsymbol{x}^{\mp}(n), \quad \boldsymbol{x}^{\pm}(n)|_{t\to -t} = [\boldsymbol{x}^{\pm}(n)]^*. \tag{2.83}$$

Using this symmetry, we get the spatial-temporal symmetry of a super rogue wave as

$$u_N(-x,t) = u_N(x,t), \quad u_N(x,-t) = u_N^*(x,t), \tag{2.84}$$

i.e., a super rogue wave is symmetric in x and parity-time-symmetric in t. The super rogue wave has a single large hump located at $x = t = 0$, flanked by small and oscillatorily decaying tails (see Fig. 2.1). Due to the above spatial-temporal symmetry, the peak amplitude of a super rogue wave is attained at the origin $(x,t) = (0,0)$. Now, we calculate this peak amplitude.

First of all, we notice that when $x = t = n = 0$, $\boldsymbol{x}^{\pm}(n) = (0,0,\dots)$. Thus, $S_{odd}(\boldsymbol{x}^{\pm}(n) + \nu \boldsymbol{s}) = S_{odd}(\nu \boldsymbol{s}) = 0$. In this case, we can calculate σ_0 directly from that $3N \times 3N$ determinant (2.76) as

$$\sigma_0|_{x=t=0} = \frac{(-1)^N}{2^{2N^2}}. \tag{2.85}$$

When $x = t = 0$ and $n = 1$, $\boldsymbol{x}^{\pm}(n) = (\pm 1, 0, 0, \dots)$. In this case, it can be proved that $\Phi_{i,j}$ and $\Psi_{i,j}$ as defined in Eq. (2.75) satisfy the following relations

$$\Phi_{i,2j} = \frac{1}{2}\left(\Phi_{i,2j-1} + \Phi_{i,2j+1}\right), \qquad i,j = 1,2,\dots, \tag{2.86}$$

$$\Psi_{2i,j} = -\frac{1}{2}\left(\Psi_{2i-1,j} + \Psi_{2i+1,j}\right), \quad i,j = 1,2,\dots, \tag{2.87}$$

i.e., even columns of the Φ matrix are averages of their two neighbor columns, and even rows of the Ψ matrix are averages of their two neighbor rows. As a special case of these two general relations, we have

$$\Phi_{i,2i} = \frac{1}{2}\Phi_{i,2i-1}, \quad \Psi_{2j,j} = -\frac{1}{2}\Psi_{2j-1,j}, \tag{2.88}$$

since $\Phi_{i,2i+1} = \Psi_{2j+1,j} = 0$. In addition, since $\Phi_{i,2i} = 2^{-(2i-1)}$ and $\Psi_{2j,j} = 2^{-(2j-1)}$, we get

$$\Phi_{i,2i-1} = 2^{-(2i-2)}, \quad \Psi_{2j-1,j} = -2^{-(2j-2)}, \quad i, j = 1, 2, \ldots. \tag{2.89}$$

Proofs for the two relations (2.86)–(2.87) are similar; so we will only do so for (2.86). Using the definition (2.75) of the Φ matrix, we can see that the relation (2.86) is equivalent to the relation

$$S_{2i}\left(\boldsymbol{x}^+ + (2j-1)\boldsymbol{s}\right) = S_{2i+1}\left(\boldsymbol{x}^+ + (2j-2)\boldsymbol{s}\right) + \frac{1}{4} S_{2i-1}\left(\boldsymbol{x}^+ + 2j\boldsymbol{s}\right), \tag{2.90}$$

where $\boldsymbol{x}^+ = (1, 0, 0, \ldots)$, and $i, j = 1, 2, \ldots$. To prove this relation, we first recall from the definition (2.2) of Schur polynomials and definition (2.11) of s_k coefficients that

$$\begin{aligned} \sum_{i=0}^{\infty} S_i\left(\boldsymbol{x}^+ + (2j-1)\boldsymbol{s}\right)\epsilon^i &= e^{\epsilon + (2j-1)(s_2\epsilon^2 + s_4\epsilon^4 + \ldots)} \\ &= e^{\epsilon}\left(e^{s_2\epsilon^2 + s_4\epsilon^4 + \ldots}\right)^{2j-1} = e^{\epsilon}\left(\frac{2}{\epsilon}\tanh\frac{\epsilon}{2}\right)^{2j-1}. \end{aligned} \tag{2.91}$$

Similar equations can be written down for the summation series involving $S_i\left(\boldsymbol{x}^+ + 2j\boldsymbol{s}\right)$ and $S_i\left(\boldsymbol{x}^+ + (2j-2)\boldsymbol{s}\right)$. Properly combining these three equations, we get the equation

$$\begin{aligned} &\sum_{i=-1}^{\infty}\left[S_{i+1}\left(\boldsymbol{x}^+ + (2j-2)\boldsymbol{s}\right) + \frac{1}{4}S_{i-1}\left(\boldsymbol{x}^+ + 2j\boldsymbol{s}\right) - S_i\left(\boldsymbol{x}^+ + (2j-1)\boldsymbol{s}\right)\right]\epsilon^i \\ &\quad = \frac{e^{\epsilon}}{\epsilon}\left(\frac{2}{\epsilon}\tanh\frac{\epsilon}{2}\right)^{2j-2} + \frac{\epsilon e^{\epsilon}}{4}\left(\frac{2}{\epsilon}\tanh\frac{\epsilon}{2}\right)^{2j} - e^{\epsilon}\left(\frac{2}{\epsilon}\tanh\frac{\epsilon}{2}\right)^{2j-1} \\ &\quad = \frac{1}{\epsilon}\left(\frac{2}{\epsilon}\tanh\frac{\epsilon}{2}\right)^{2j-2}\operatorname{sech}^2\frac{\epsilon}{2}. \end{aligned} \tag{2.92}$$

Since the right side of this equation is an odd function of ϵ, its even-power expansion coefficients on the left side must be zero. This quickly results in the relation (2.90), and hence (2.86).

Utilizing the relations (2.86)–(2.87) to eliminate even columns of the matrix Φ and even rows of the matrix Ψ in the $3N \times 3N$ determinant (2.76) through row and column operations, and recalling the results in Eq. (2.89), we can reduce this $3N \times 3N$ determinant to

$$\sigma_1|_{x=t=0} = \frac{(-1)^N}{2^{2N^2}} A_N, \tag{2.93}$$

where

$$A_N = \begin{vmatrix} -2 & 1 & 0 & \cdots & 0 & 0 \\ 1 & -2 & 1 & \cdots & 0 & 0 \\ 0 & 1 & -2 & \ddots & \vdots & \vdots \\ \vdots & \vdots & \ddots & \ddots & 1 & 0 \\ 0 & 0 & \cdots & 1 & -2 & 1 \\ 0 & 0 & \cdots & 0 & 1 & -3 \end{vmatrix} \tag{2.94}$$

is a $N \times N$ determinant with $N-1$ number of -2's on the diagonal. Adding the second row of A_N to its first row, and then adding the first row of the resulting determinant to its second row, we find that A_N is equal to $-A_{N-1}$, plus a determinant which can be found by simple row operations to be $2(-1)^N$, i.e.,

$$A_N = -A_{N-1} + 2(-1)^N. \tag{2.95}$$

From this relation and the fact of $A_1 = -3$, we readily find that $A_N = (-1)^N(2N+1)$. Therefore,

$$\sigma_1|_{x=t=0} = \frac{2N+1}{2^{2N^2}}, \tag{2.96}$$

and

$$u_N(0,0) = e^{\mathrm{i}t}\frac{\sigma_1}{\sigma_0}\bigg|_{x=t=0} = (-1)^N(2N+1)e^{\mathrm{i}t}. \tag{2.97}$$

So, the peak amplitude of the N-th order super rogue wave is $2N+1$.

We note that this peak amplitude of NLS super rogue waves has been previously obtained by Wang et al. (2017) by using rogue wave expressions out of Darboux transformation.

2.1.3 *Derivation by Darboux Transformation*

In the literature, rogue waves in integrable systems were often derived by Darboux transformation. For instance, rogue waves in the NLS equation (2.5) were derived by Darboux transformation in Akhmediev et al. (2009a) and Guo et al. (2012). To compare rogue wave derivations and their expressions from the bilinear method and Darboux transformation, we present derivation of NLS rogue waves by Darboux transformation below.

Darboux transformation is a technique that allows one to obtain new solutions of an integrable system from the old ones (Matveev and Salle 1991). The scheme we will use for rogue wave derivations is based on the generalized Darboux transformation first proposed by Matveev and Salle (1991) and then further developed by Guo

et al. (2012). But rogue solutions from that earlier work were not explicit. Here, we will go beyond the earlier work in that we will also derive completely explicit NLS rogue wave solutions through Schur polynomials, similar to what we have done for rogue waves by the bilinear method.

Explicit expressions of NLS rogue waves from Darboux transformation are given by the following theorem.

Theorem 2.2 *The N-th order rogue waves of the NLS equation (2.5) from Darboux transformation are given by the formula*

$$u_N(x,t) = e^{\mathrm{i}t}\left(1 + 2\mathrm{i}\frac{\tau_1}{\tau_0}\right), \tag{2.98}$$

where

$$\tau_0 = \det_{1\le i,j\le N}\left(m^{(i-1,j-1)}\right), \quad \tau_1 = \det\begin{pmatrix} \left(m^{(i-1,j-1)}\right)_{1\le i,j\le N} & \eta^\dagger \\ \mu & 0 \end{pmatrix}, \tag{2.99}$$

$$m^{(i-1,j-1)} = \sum_{\nu=0}^{\min\{i-1,j-1\}} \frac{4^{-\nu}}{2\mathrm{i}}\left(\left[S_{2i-1-2\nu}(\boldsymbol{X}^+)\right]^* S_{2j-1-2\nu}(\boldsymbol{X}^+) + \left[S_{2i-1-2\nu}(\boldsymbol{X}^-)\right]^* S_{2j-1-2\nu}(\boldsymbol{X}^-)\right), \tag{2.100}$$

$$\boldsymbol{X}^\pm(\nu) = \left(X_1^\pm, X_2^\pm, \ldots\right), \tag{2.101}$$

$$X_{2k+1}^\pm = \sqrt{2}\left[\sum_{j=0}^{k} \pm(\delta_{j,0}x + \delta_{[j/2],0}\mathrm{i}t + a_j)\binom{\frac{1}{2}}{k-j}\left(\frac{1}{2}\right)^{k-j} + \frac{(2k)!}{2^{3k+1}(k!)^2}\frac{(-1)^k}{(2k+1)}\right], \tag{2.102}$$

$$X_{2k}^\pm(\nu) = (\nu+1)\left[\frac{(-1)^k}{k\cdot 2^k}\right], \tag{2.103}$$

$$\mu = (\mu_1, \mu_2, \cdots, \mu_N), \quad \eta = (\eta_1, \eta_2, \cdots, \eta_N), \tag{2.104}$$

$$\mu_j = S_{2j-1}(\boldsymbol{Y}^+), \quad \eta_j = S_{2j-1}(\boldsymbol{Y}^-), \quad \boldsymbol{Y}^\pm = \left(Y_1^\pm, Y_2^\pm, \ldots\right), \tag{2.105}$$

$$Y_{2k+1}^\pm = X_{2k+1}^\pm, \quad Y_{2k}^\pm = 0, \tag{2.106}$$

$\delta_{j,0}$ is the Kronecker delta notation (i.e., $\delta_{0,0} = 1$ and zero otherwise), $[j/2]$ represents the integer part of $j/2$,

$$\binom{\alpha}{n} \equiv \frac{\alpha(\alpha-1)\cdots(\alpha-n+1)}{n!}, \quad \binom{\alpha}{0} \equiv 1, \tag{2.107}$$

and $a_0, a_1, \cdots, a_{N-1}$ are free complex constants.

Notice that these rogue wave expressions from Darboux transformation are very different from those presented in Theorem 2.1 by the bilinear method.

Proof We begin with the Lax pair of the NLS equation (Zakharov and Shabat 1971),

$$\Phi_x = U(Q,\lambda)\Phi, \tag{2.108}$$

$$\Phi_t = V(Q,\lambda)\Phi, \tag{2.109}$$

where

$$U(Q,\lambda) = -\mathrm{i}\lambda\sigma_3 + Q, \tag{2.110}$$

$$V(Q,\lambda) = -\mathrm{i}\lambda^2\sigma_3 + \lambda Q + \frac{1}{2}\mathrm{i}\sigma_3\left(Q_x - Q^2\right), \tag{2.111}$$

$$Q(x,t) = \begin{pmatrix} 0 & u(x,t) \\ -u^*(x,t) & 0 \end{pmatrix}, \quad \sigma_3 = \mathrm{diag}(1,-1). \tag{2.112}$$

The compatibility condition of this Lax pair is the zero-curvature equation

$$U_t - V_x + [U,V] = 0, \tag{2.113}$$

which yields the NLS equation (2.5).

To construct the Darboux transformation, we also introduce the adjoint-spectral problem for (2.108)–(2.109):

$$\Psi_x = -\Psi U(Q,\lambda), \tag{2.114}$$

$$\Psi_t = -\Psi V(Q,\lambda). \tag{2.115}$$

Due to the symmetry of the potential matrix Q in Eq. (2.112), it is easy to see that matrices U and V admit the symmetries

$$U^\dagger(x,t,\lambda^*) = -U(x,t,\lambda), \quad V^\dagger(x,t,\lambda^*) = -V(x,t,\lambda), \tag{2.116}$$

where † represents Hermitian, i.e., complex transpose. Using these U, V symmetries and the Lax pair equations (2.108)–(2.109), we get

$$\left[\Phi^\dagger(x,t)\right]_x = \left[\Phi^\dagger(x,t)\right]U(x,t,\lambda^*), \tag{2.117}$$

and

$$\left[\Phi^\dagger(x,t)\right]_t = \left[\Phi^\dagger(x,t)\right]V(x,t,\lambda^*). \tag{2.118}$$

Thus, if $\Phi(x,t)$ is a wave function of the original Lax pair system (2.108)–(2.109) at λ, then $\Phi^\dagger(x,t)$ would be an adjoint wave function of the adjoint linear system (2.114)–(2.115) at λ^*.

For the Lax pair (2.108)–(2.109), its Darboux transformation is (Guo et al. 2012)

$$T = I - \frac{\lambda_1 - \lambda_1^*}{\lambda - \lambda_1^*} P_1, \quad P_1 = \frac{\Phi_1 \Phi_1^\dagger}{\Phi_1^\dagger \Phi_1}, \tag{2.119}$$

where Φ_1 is a (column vector) solution of the original Lax pair (2.108)–(2.109) with spectral parameter $\lambda = \lambda_1$. This Darboux transformation closely mimics the dressing matrix in the Riemann-Hilbert formulation of the inverse scattering transform for the NLS equation (Novikov et al. 1984; Yang 2010). Under this transformation, if $\Phi(x,t,\lambda)$ satisfies the original Lax pair equations (2.108)–(2.109), then the new function

$$\Phi_{[1]} = T\Phi \tag{2.120}$$

would satisfy the same equations, except that the potential matrix Q is transformed to

$$Q_{[1]} = Q + \mathrm{i}(\lambda_1^* - \lambda_1)\,[\sigma_3, P_1]\,, \tag{2.121}$$

where $[\sigma_3, P_1] \equiv \sigma_3 P_1 - P_1 \sigma_3$ is the commutator. In other words, a new NLS solution

$$u_{[1]} = u + 2i(\lambda_1^* - \lambda_1)(P_1)_{1,2} \tag{2.122}$$

is obtained from the old solution u, where $(P_1)_{1,2}$ is the first row, second column element of matrix P_1. This relation between the old and new NLS solutions is the Bäcklund transformation for the NLS equation.

The N-fold Darboux transformation is N iterations of the above elementary Darboux transformation. These N iterations can be lumped together into a single N-fold Darboux matrix, which would yield a concise algebraic expression for the new solutions. There are two different versions of this N-fold Darboux transformation for the NLS equation, one in Guo et al. (2012), and the other in Huang and Ling (2016). The latter version closely resembles the N-fold dressing matrix in the Riemann-Hilbert formulation of the inverse scattering transform for the NLS equation (Novikov et al. 1984; Yang 2010), and this version is presented below.

Lemma 2.4 *The N-fold Darboux transformation matrix for the NLS equation (2.5) is*

$$T_N = I - Y M^{-1} D^{-1} Y^\dagger, \tag{2.123}$$

where

$$Y = [\, \Phi_1,\ \Phi_2,\ \ldots,\ \Phi_N \,]_{2\times N}\,, \tag{2.124}$$

$$M = \left(m_{i,j}\right)_{1\le i,j\le N}\,, \quad m_{i,j} = \frac{\Phi_i^{\dagger}\Phi_j}{\lambda_j - \lambda_i^*}, \tag{2.125}$$

$$D = diag\left(\lambda - \lambda_1^*, \lambda - \lambda_2^*, \ldots, \lambda - \lambda_N^*\right), \tag{2.126}$$

$\lambda_k \in \mathbb{C}_+$ (i.e., λ_k in upper complex plane), and $\Phi_k \equiv \Phi(x,t,\lambda_k)$ solves the Lax pair equations (2.108)–(2.109) at $\lambda = \lambda_k$. The Bäcklund transformation relating the new NLS solution $u_{[N]}$ to the old solution u is

$$u_{[N]} = u - 2\mathrm{i}\left(YM^{-1}Y^{\dagger}\right)_{1,2} = u + 2\mathrm{i}\frac{\begin{vmatrix} M & Y_2^{\dagger} \\ Y_1 & 0 \end{vmatrix}}{|M|}, \tag{2.127}$$

where Y_1 and Y_2 are the first and second rows of matrix Y, respectively.

This N-fold Darboux transformation has been reported by Huang and Ling (2016), and the last expression in Eq. (2.127) can be found in Yang (2010). The proof of this lemma can be given along the lines of Yang (2010) and Bian et al. (2015).

To derive rogue waves, we need general eigenfunctions for the Lax pair system (2.108)–(2.109). Choosing a plane wave solution $u_{[0]} = e^{\mathrm{i}t}$ as the seed solution and introducing a diagonal matrix $\mathcal{D} = \mathrm{diag}\left(e^{\mathrm{i}t/2}, e^{-\mathrm{i}t/2}\right)$, we can derive the general wave function for this linear system as

$$\Phi(x,t) = \mathcal{D}\phi(x,t), \tag{2.128}$$

where

$$\phi(x,t) = \begin{pmatrix} c_1 e^{A} + c_2 e^{-A} \\ c_3 e^{A} + c_4 e^{-A} \end{pmatrix}, \tag{2.129}$$

$$A = \sqrt{-\lambda^2 - 1}(x + \lambda t), \tag{2.130}$$

$$c_3 = c_1\left(\mathrm{i}\lambda + \sqrt{-\lambda^2 - 1}\right), \quad c_4 = c_2\left(\mathrm{i}\lambda - \sqrt{-\lambda^2 - 1}\right), \tag{2.131}$$

and c_1, c_2 are arbitrary complex constants. Here, $A \neq 0$, i.e., $\lambda \neq \pm\mathrm{i}$, in order for (2.128) to be a general wavefunction of the linear system (2.108)–(2.109).

Rogue waves are rational solutions. To derive rogue waves from the above wavefunctions, we need to choose spectral parameters λ so that the exponent A approaches zero under certain limits. These exponents would vanish when $\lambda = \mathrm{i}$. Thus, we will set $\lambda = \mathrm{i}h$ and take the limit of $h \to 1$.

The wavefunction $\phi(x,t)$ in (2.129) can be put in a more convenient form. With a scaling to this wavefunction, one of its two free complex parameters c_1 and c_2 can be removed. Its other free complex parameter can be absorbed into the exponent A. Then, with $\lambda = \mathrm{i}h$, the wavefunction $\phi(x,t)$ in (2.129) can be written equivalently as

$$\phi(x,t;h) = \frac{1}{\sqrt{h-1}} \begin{pmatrix} \sinh\left[A + \frac{1}{2}\ln\left(h+\sqrt{h^2-1}\right)\right] \\ \sinh\left[-A + \frac{1}{2}\ln\left(h+\sqrt{h^2-1}\right)\right] \end{pmatrix}, \tag{2.132}$$

$$A = \sqrt{h^2-1}(x + \mathrm{i}ht + \theta), \tag{2.133}$$

where $\theta = \theta(h)$ is an arbitrary complex parameter. Here, the scaling constant $1/\sqrt{h-1}$ in the wavefunction $\phi(x,t)$ is introduced so that this wavefunction does not approach zero in the limit of $h \to 1$ (i.e., $\lambda \to \mathrm{i}$). This scaling of the wavefunction clearly does not affect the solution.

In the N-fold Darboux transformation in Lemma 2.4, there are N spectral parameters $(\lambda_1, \lambda_2, \cdots, \lambda_N)$, and we want all of them to approach i. Corresponding to these N spectral parameters, there would be N wavefunctions $(\phi_1, \phi_2, \cdots, \phi_N)$ with their own θ parameters $(\theta_1, \theta_2, \cdots, \theta_N)$. Since $\theta_j(h_j)$ is an arbitrary complex parameter, we can expand $\theta_j(h_j)$ through parameters in h_j as well. Thus, we set

$$\lambda_j = \mathrm{i}h_j, \quad h_j = 1 + \epsilon_j, \quad \theta_j = \sum_{k=0}^{\infty} a_k \epsilon_j^k, \quad 1 \le j \le N, \tag{2.134}$$

where $a_0, a_1, \ldots$ are free complex constants. It is important that these complex constants a_k are j-independent, i.e., independent of the spectral parameter λ_j. This fact is needed as we will quickly see below.

We also expand the wave function $\phi_j(x,t)$ in (2.132) at h_j and the adjoint wave function $\phi_j^\dagger(x,t)$ at h_j^* as

$$\phi_j(x,t) = \sum_{k=0}^{\infty} \phi^{(k)}(x,t)\,\epsilon_j^k, \quad \phi_j^\dagger(x,t) = \sum_{k=0}^{\infty} (\phi^{(k)})^\dagger(x,t)\,(\epsilon_j^*)^k, \tag{2.135}$$

and expand the matrix element $m_{i,j}$ in Lemma 2.4 as

$$m_{i,j} = \frac{\Phi_i^\dagger \Phi_j}{\lambda_j - \lambda_i^*} = \frac{\phi_i^\dagger \phi_j}{2\mathrm{i} + \epsilon_j - \epsilon_i^*} = \sum_{k=0}^{\infty}\sum_{l=0}^{\infty} m^{(k,l)}\,(\epsilon_i^*)^k \epsilon_j^l. \tag{2.136}$$

Since expansion coefficients a_k in (2.134) for θ_j are j-independent, we can see that expansions (2.135)–(2.136) for different j or (i,j) are really the same expansions, except for the differences in ϵ_j and ϵ_j^* values. Thus, expansion coefficients in (2.135)–(2.136) are simply

$$\phi^{(k)} = \frac{1}{k!}\frac{\partial^k \phi(x,t;1+\epsilon)}{\partial \epsilon^k}\bigg|_{\epsilon=0}, \tag{2.137}$$

and

$$m^{(k,l)} = \frac{1}{k!l!}\left[\frac{\partial^{k+l}}{(\partial\epsilon^*)^k \partial\epsilon^l}\left(\frac{\phi^\dagger(x,t;1+\epsilon^*)\phi(x,t;1+\epsilon)}{2\mathrm{i}+\epsilon-\epsilon^*}\right)\right]_{\epsilon=\epsilon^*=0}, \tag{2.138}$$

where θ in Eq. (2.132) of the $\phi(x,t;h)$ function is given by the expansion $\theta = \sum_{k=0}^{\infty} a_k \epsilon^k$. These expansion coefficients $\phi^{(k)}$ and $m^{(k,l)}$ are also j-independent or (i,j)-independent (i.e., independent of spectral parameters λ_i and λ_j), which is crucial.

Substituting expansions (2.135)–(2.136) into each matrix element in the Backlünd transformation (2.127), performing determinant manipulations, and taking the limits of $\epsilon_j, \epsilon_j^* \to 0$, we obtain rogue waves which are summarized in the following lemma.

Lemma 2.5 *General N-th order rogue waves in the NLS equation (2.5) are given by the formula*

$$u_N(x,t) = e^{\mathrm{i}t}\left(1 + 2\mathrm{i}\frac{\tau_1}{\tau_0}\right), \tag{2.139}$$

where

$$\tau_0 = \det_{1\le i,j\le N}\left(m^{(i-1,j-1)}\right), \quad \tau_1 = \det\begin{pmatrix}\left(m^{(i-1,j-1)}\right)_{1\le i,j\le n} & \eta^\dagger \\ \mu & 0\end{pmatrix}, \tag{2.140}$$

$m^{(i-1,j-1)}$ is given by Eq. (2.138),

$$\mu = \left[\phi_1^{(0)}, \phi_1^{(1)}, \ldots, \phi_1^{(n-1)}\right], \quad \eta = \left[\phi_2^{(0)}, \phi_2^{(1)}, \ldots, \phi_2^{(n-1)}\right], \tag{2.141}$$

$\phi_1^{(k)}$ and $\phi_2^{(k)}$ are the first and second elements of the vector function $\phi^{(k)}$ given in Eq. (2.137), $\phi(x,t;h)$ in (2.137)–(2.138) is given in Eq. (2.132) with $\theta = \sum_{k=0}^{\infty} a_k \epsilon^k$, and $(a_0, a_1, a_2, \cdots, a_{N-1})$ are free complex parameters.

The above solutions are NLS rogue waves in differential form by Darboux transformation. They are the counterparts of bilinear NLS rogue waves in differential form in Lemma 2.3. Just as in the bilinear case, we can derive explicit NLS rogue waves from Darboux transformation by calculating matrix elements $m^{(k,l)}$ and $\phi^{(k)}$ in Eqs. (2.137)–(2.138) through Schur polynomials. This derivation is very similar to that in Yang and Yang (2020b) for rogue waves in the parity-time-symmetric NLS equation by Darboux transformation. The idea is that, since the matrix elements in the τ_0 and τ_1 determinants of Eq. (2.140) are certain-order derivatives of some ϕ-related functions with respect to ϵ and ϵ^* in view of Eqs. (2.137)–(2.138), all we

have to do is to convert those ϕ-related functions into proper exponential forms, whose exponents are power series of ϵ and ϵ^*. Then, derivatives of those ϕ-related functions would just be Schur polynomials of vectors in those exponents. Following such calculations, explicit NLS rogue waves from Darboux transformation as presented in Theorem 2.2 can be obtained. This completes the proof of Theorem 2.2.

Of the free complex constants $(a_0, a_1, \cdots, a_{N-1})$ in Theorem 2.2, a_0 can be normalized to zero by a shift in the (x, t) axes. So, the irreducible free complex constants are $(a_1, \cdots, a_{N-1})$.

When we take $N = 1$, Theorem 2.2 (with $a_0 = 0$) gives the fundamental rogue wave as

$$u_1(x,t) = \left(-1 + \frac{4(1+2\mathrm{i}t)}{1+4x^2+4t^2}\right) e^{\mathrm{i}t}. \tag{2.142}$$

This rogue wave differs from the Peregrine solution (2.79) by a sign. But the NLS equation (2.5) is invariant under a sign change in $u(x,t)$; thus this rogue wave is equivalent to the Peregrine wave.

When we take higher values of N, we will get higher-order rogue waves. Details are omitted.

Compared to explicit rogue wave expressions by the bilinear method in Theorem 2.1, we can see that these expressions by Darboux transformation in Theorem 2.2 are more complicated. Thus, their asymptotic analysis is expected to be more involved too. For this reason, we will derive explicit rogue wave expressions for all the other integrable systems by only the bilinear method in later sections.

2.2 Derivative Nonlinear Schrödinger Equations

The generalized derivative NLS (GDNLS) equations are (Kundu 1984; Clarkson and Cosgrove 1987)

$$\mathrm{i}\phi_t + \phi_{\xi\xi} + \rho|\phi|^2\phi + \mathrm{i}a\phi\phi^*\phi_\xi + \mathrm{i}b\phi^2\phi_\xi^* + \frac{1}{4}b(2b-a)|\phi|^4\phi = 0, \tag{2.143}$$

where ρ, a, b are arbitrary real constants, and the superscript '*' represents complex conjugation. In fiber optics, these equations model the propagation of short light pulses where, in addition to dispersion and Kerr (cubic) nonlinearity, self-steepening and fifth-order nonlinearity are also accounted for, even though the Raman effect and third-order dispersion are omitted (Hasegawa and Kodama 1995; Agrawal 2001). When $\rho = 0$ and $a = 2b$, these equations reduce to the DNLS equation of Kaup-Newell type (Kaup and Newell 1978), which governs the propagation of nonlinear Alfvén waves in magnetized plasmas (see Sect. 1.2). When $\rho = b = 0$, these equations reduce to the DNLS equation of Chen-Lee-Liu type (Chen et al. 1979), which models short-pulse propagation in a frequency-doubling crystal

through the interplay of quadratic and cubic nonlinearities (Moses et al. 2007). Due to these physical applications, rogue wave formation in these GDNLS equations is a physically significant issue.

There have been a number of studies on rogue waves in these GDNLS equations. For instance, for the Kaup-Newell equation (with $\rho = 0$ and $a = 2b$), special types of rogue waves were derived by Darboux transformation in Xu et al. (2011) and Guo et al. (2013). For the Chen-Lee-Liu equation, with $\rho = b = 0$ in (2.143), the fundamental rogue wave was derived by the bilinear method in Chan et al. (2014), and higher-order rogue waves were derived by Darboux transformation in Zhang et al. (2017). For the Gerdjikov-Ivanov equation (Gerdjikov and Ivanov 1983), with $\rho = a = 0$ in (2.143), fundamental and higher-order rogue waves were derived by Darboux transformation in Xu and He (2012) and Guo et al. (2014). For the GDNLS equations (2.143), general rogue waves were derived by Darboux transformation in Chen et al. (2019) and by the bilinear method in Yang et al. (2020).

In this section, we derive general rogue waves in the GDNLS equations (2.143) with $a \neq b$ by the bilinear method, following Yang et al. (2020) (treatment for the case of $a = b$ can be found in the appendix of Yang et al. (2020)).

First, through a gauge transformation (Kakei et al. 1995)

$$\phi(\xi, t) = \sqrt{\frac{2}{a-b}}\, u(x,t)\ \exp\left\{ \mathrm{i}\frac{\rho}{a-b}x + \mathrm{i}\frac{\rho^2}{(a-b)^2}t \right\}, \tag{2.144}$$

where $x = \xi - 2\rho t/(a-b)$, together with a time scaling, the GDNLS equations (2.143) with $a \neq b$ reduce to

$$\mathrm{i}u_t + \frac{1}{2}u_{xx} + \mathrm{i}\gamma|u|^2u_x + \mathrm{i}(\gamma-1)u^2u_x^* + \frac{1}{2}(\gamma-1)(\gamma-2)|u|^4u = 0, \tag{2.145}$$

where $\gamma = a/(a-b)$. We will work with these normalized GDNLS equations (2.145) in the remainder of this section. These equations become the Kaup-Newell equation when $\gamma = 2$, the Chen-Lee-Liu equation when $\gamma = 1$, and the Gerdjikov-Ivanov equation when $\gamma = 0$.

Rogue waves in the GDNLS equations (2.145) approach a constant-amplitude continuous wave background at large x and t. By simple variable scalings, this constant amplitude can be normalized to be unity. Then, these rogue waves approach the unit-amplitude continuous wave background $e^{\mathrm{i}\kappa x - \mathrm{i}\omega t}$, where κ is a free wavenumber, and $\omega = [\kappa^2 + 2\kappa - (\gamma-1)(\gamma-2)]/2$ is the frequency. In order for rogue waves to arise, these backgrounds must be unstable to perturbations. Simple modulation instability calculations show that these backgrounds are unstable when $\kappa < 1 - \gamma$. Thus, rogue waves in the GDNLS equations (2.145) should approach the following background as $x, t \to \pm\infty$:

$$u(x,t) \to e^{\mathrm{i}(1-\gamma-\alpha)x - \frac{1}{2}\mathrm{i}[\alpha^2 + 2(\gamma-2)\alpha + 1 - \gamma]t}, \tag{2.146}$$

where $\alpha > 0$ is a wavenumber parameter. Unlike the NLS equation, the GDNLS equations (2.145) do not admit Galilean invariance. Thus, α is an irreducible parameter in its rogue waves.

General rogue waves to the GDNLS equations (2.145) are given in the following theorem (Yang et al. 2020).

Theorem 2.3 *The generalized derivative NLS equations (2.145) under boundary conditions (2.146) admit rogue wave solutions*

$$u_N(x,t) = e^{\mathrm{i}(1-\gamma-\alpha)x-\frac{1}{2}\mathrm{i}\left[\alpha^2+2(\gamma-2)\alpha+1-\gamma\right]t}\,\frac{(f_N^*)^{\gamma-1}g_N}{f_N^{\gamma}}, \tag{2.147}$$

where the positive integer N represents the order of the rogue wave,

$$f_N(x,t) = \sigma_{0,0}, \quad g_N(x,t) = \sigma_{-1,1}, \tag{2.148}$$

$$\sigma_{n,k} = \det_{1\le i,j\le N}\left(\phi^{(n,k)}_{2i-1,2j-1}\right), \tag{2.149}$$

the matrix elements in $\sigma_{n,k}$ are defined by

$$\phi^{(n,k)}_{i,j} = \sum_{\nu=0}^{\min(i,j)} \frac{1}{4^{\nu}}\, S_{i-\nu}(\boldsymbol{x}^{+}(n,k)+\nu\boldsymbol{s})\, S_{j-\nu}(\boldsymbol{x}^{-}(n,k)+\nu\boldsymbol{s}), \tag{2.150}$$

vectors $\boldsymbol{x}^{\pm}(n,k) = \left(x_1^{\pm}, 0, x_3^{\pm}, 0, \cdots\right)$ are defined by

$$x_1^{+} = k + \left(n+\frac{1}{2}\right)\left(h_1+\frac{1}{2}\right) + \sqrt{\alpha}x + \sqrt{\alpha}\left[(\alpha-1)+\mathrm{i}\sqrt{\alpha}\right]t, \tag{2.151}$$

$$x_1^{-} = -k - \left(n+\frac{1}{2}\right)\left(h_1^*+\frac{1}{2}\right) + \sqrt{\alpha}x + \sqrt{\alpha}\left[(\alpha-1)-\mathrm{i}\sqrt{\alpha}\right]t, \tag{2.152}$$

$$x_{2r+1}^{+} = \left(n+\frac{1}{2}\right)h_{2r+1} + \frac{1}{(2r+1)!}\left\{\sqrt{\alpha}x + \left[\sqrt{\alpha}(\alpha-1)+2^{2r}\mathrm{i}\alpha\right]t\right\} + a_{2r+1}, \tag{2.153}$$

$$x_{2r+1}^{-} = -\left(n+\frac{1}{2}\right)h_{2r+1}^* + \frac{1}{(2r+1)!}\left\{\sqrt{\alpha}x + \left[\sqrt{\alpha}(\alpha-1)-2^{2r}\mathrm{i}\alpha\right]t\right\} + a_{2r+1}^*, \tag{2.154}$$

$r \ge 1$, $\boldsymbol{s} = (0, s_2, 0, s_4, \cdots)$ is as defined in Eq. (2.11), $h_r(\alpha)$ are coefficients from the expansion

$$\sum_{r=1}^{\infty} h_r(\alpha)\lambda^r = \ln\left(\frac{\mathrm{i}e^{\lambda/2} + \sqrt{\alpha}e^{-\lambda/2}}{\mathrm{i} + \sqrt{\alpha}}\right), \tag{2.155}$$

and $a_3, a_5, \cdots, a_{2N-1}$ *are free irreducible complex constants.*

Proof We first introduce the variable transformation

$$u = e^{\mathrm{i}(1-\gamma-\alpha)x - \frac{1}{2}\mathrm{i}[\alpha^2+2(\gamma-2)\alpha+1-\gamma]t}\,\frac{(f^*)^{\gamma-1}g}{f^{\gamma}}, \tag{2.156}$$

where f and g are complex functions. Under this transformation, the GDNLS equations (2.145) can be decomposed into the following system of four bilinear equations:

$$\left(2\mathrm{i}D_t + D_x^2 + 2\mathrm{i}(1-\alpha)D_x\right) g \cdot f^* = 0, \tag{2.157}$$

$$\left(2\mathrm{i}D_t + D_x^2 + 2\mathrm{i}D_x\right) f \cdot f^* = 0, \tag{2.158}$$

$$(\mathrm{i}D_x - 1)\, f \cdot f^* + |g|^2 = 0, \tag{2.159}$$

$$D_x^2 f \cdot f^* - \mathrm{i}D_x g \cdot g^* + (2\alpha+1)(|f|^2 - |g|^2) = 0, \tag{2.160}$$

where D is Hirota's bilinear differential operator. It is important to notice that these bilinear equations are independent of the equation parameter γ. This means that rogue waves in the whole family of GDNLS equations (2.145), for different values of γ, are given by the same f and g solutions, and the γ-dependence of the rogue waves only appears through the bilinear transformation (2.156). This is a big advantage of the bilinear method for solving the GDNLS equations (2.145).

Interestingly, under the same variable transformation (2.156), the GDNLS equations (2.145) can also be decomposed into a different bilinear system, where the first bilinear equation (2.157) is replaced by a new bilinear equation, while the other three bilinear equations (2.158)–(2.160) remain the same (Yang et al. 2020). Derivations of rogue waves from these two bilinear systems are different, and we will use the above bilinear system (2.157)–(2.160) to derive rogue waves below (derivation from the second bilinear system can be found in Yang et al. (2020)).

Our proof below follows the same idea as in Sect. 2.1.1 for the bilinear derivation of rogue waves in the NLS equation. We first derive algebraic solutions to a higher-dimensional bilinear system. Then we restrict those algebraic solutions so that they satisfy dimension reduction conditions and complex conjugacy conditions. Under those conditions, the restricted algebraic solutions would satisfy the lower-dimensional bilinear system (2.158)–(2.160) of the GDNLS equations.

(a) Gram determinant solutions for a higher-dimensional bilinear system

First, we need to derive algebraic solutions to a higher-dimensional bilinear system, which can reduce to the original lower-dimensional bilinear system (2.157)–(2.160) under certain reductions.

From Lemma 2 of Chen et al. (2018b), section 3.2 of Feng et al. (2017) and additional calculations, we learn that if functions $m_{i,j}^{(n,k)}$, $\varphi_i^{(n,k)}$ and $\psi_j^{(n,k)}$ of variables (x_{-1}, x_1, x_2) satisfy the following differential and difference relations,

$$\left.\begin{array}{l} \partial_{x_1} m_{i,j}^{(n,k)} = \varphi_i^{(n,k)} \psi_j^{(n,k)}, \\ \partial_{x_1} \varphi_i^{(n,k)} = \varphi_i^{(n+1,k)}, \ \partial_{x_1} \psi_j^{(n,k)} = -\psi_j^{(n-1,k)}, \\ \partial_{x_1} \varphi_i^{(n,k)} = c\varphi_i^{(n,k)} + \varphi_i^{(n,k+1)}, \ \partial_{x_1} \psi_j^{(n,k)} = -c\psi_j^{(n,k)} - \psi_j^{(n,k-1)}, \\ \partial_{x_2} \varphi_i^{(n,k)} = \partial_{x_1}^2 \varphi_i^{(n,k)}, \ \partial_{x_2} \psi_j^{(n,k)} = -\partial_{x_1}^2 \psi_j^{(n,k)}, \\ \partial_{x_{-1}} \varphi_i^{(n,k)} = \varphi_i^{(n,k-1)}, \ \partial_{x_{-1}} \psi_j^{(n,k)} = -\psi_j^{(n,k+1)}, \end{array}\right\} \tag{2.161}$$

and

$$\left.\begin{array}{l} \partial_{x_2} m_{i,j}^{(n,k)} = \varphi_i^{(n+1,k)} \psi_j^{(n,k)} + \varphi_i^{(n,k)} \psi_j^{(n-1,k)}, \\ \partial_{x_2} m_{i,j}^{(n,k)} = \varphi_i^{(n,k+1)} \psi_j^{(n,k)} + \varphi_i^{(n,k)} \psi_j^{(n,k-1)} + 2c\varphi_i^{(n,k)} \psi_j^{(n,k)}, \\ \partial_{x_{-1}} m_{i,j}^{(n,k)} = -\varphi_i^{(n,k-1)} \psi_j^{(n,k+1)}, \\ m_{i,j}^{(n+1,k)} = m_{i,j}^{(n,k)} + \varphi_i^{(n,k)} \psi_j^{(n+1,k)}, \\ m_{i,j}^{(n,k+1)} = m_{i,j}^{(n,k)} + \varphi_i^{(n,k)} \psi_j^{(n,k+1)}, \end{array}\right\} \tag{2.162}$$

where c is an arbitrary complex constant, then the determinant

$$\tau_{n,k} = \det_{1 \le i,j \le N} \left(m_{i,j}^{(n,k)} \right) \tag{2.163}$$

would satisfy the following bilinear equations in the extended KP hierarchy

$$\left(D_{x_2} - D_{x_1}^2 - 2cD_{x_1} \right) \tau_{n-1,k+1} \cdot \tau_{n-1,k} = 0, \tag{2.164}$$

$$\left(D_{x_2} - D_{x_1}^2 \right) \tau_{n,k} \cdot \tau_{n-1,k} = 0, \tag{2.165}$$

$$\left(cD_{x_{-1}} - 1 \right) \tau_{n,k} \cdot \tau_{n-1,k} + \tau_{n-1,k+1} \tau_{n,k-1} = 0, \tag{2.166}$$

$$(cD_{x_1} D_{x_{-1}} - D_{x_1} - 2c) \tau_{n,k} \cdot \tau_{n-1,k} + (D_{x_1} + 2c) \tau_{n-1,k+1} \cdot \tau_{n,k-1} = 0. \tag{2.167}$$

We note that utilizing the former part (2.161) of the differential and difference relations, we can show that the x_1 derivatives of the latter part (2.162) of these relations are automatically satisfied. This situation is similar to that for the NLS equation in Sect. 2.1.1.

Now, we introduce functions $m^{(n,k)}$, $\varphi^{(n,k)}$ and $\psi^{(n,k)}$ as

$$m^{(n,k)} = \frac{\mathrm{i}p}{p+q}\left(-\frac{p}{q}\right)^n \left(-\frac{p-c}{q+c}\right)^k \mathrm{e}^{\xi+\eta}, \tag{2.168}$$

$$\varphi^{(n,k)} = (\mathrm{i}p)p^n(p-c)^k e^{\xi}, \tag{2.169}$$

$$\psi^{(n,k)} = (-q)^{-n}\left[-(q+c)\right]^{-k} e^{\eta}, \tag{2.170}$$

where

$$\xi = \frac{1}{p-c}x_{-1} + px_1 + p^2x_2 + \xi_0(p), \tag{2.171}$$

$$\eta = \frac{1}{q+c}x_{-1} + qx_1 - q^2x_2 + \eta_0(q), \tag{2.172}$$

p, q are arbitrary variables, and $\xi_0(p)$, $\eta_0(q)$ are arbitrary complex functions of p and q respectively. It is easy to see that these functions satisfy the differential and difference relations (2.161)–(2.162) with indices i and j ignored. Then, by defining

$$m_{i,j}^{(n,k)} = \mathcal{A}_i\mathcal{B}_j m^{(n,k)}, \quad \varphi_i^{(n,k)} = \mathcal{A}_i\varphi^{(n,k)}, \quad \psi_j^{(n,k)} = \mathcal{B}_j\psi^{(n,k)}, \tag{2.173}$$

where $\mathcal{A}_i$ and $\mathcal{B}_j$ are differential operators with respect to p and q respectively as

$$\mathcal{A}_i = \frac{1}{i!}\left[(p-c)\partial_p\right]^i, \quad \mathcal{B}_j = \frac{1}{j!}\left[(q+c)\partial_q\right]^j, \tag{2.174}$$

these functions would also satisfy the differential and difference relations (2.161)–(2.162) since operators $\mathcal{A}_i$ and $\mathcal{B}_j$ commute with differentials ∂_{x_k}. Consequently, for an arbitrary sequence of indices $(i_1, i_2, \cdots, i_N; j_1, j_2, \cdots, j_N)$, the determinant

$$\tau_{n,k} = \det_{1\le\nu,\mu\le N}\left(m_{i_\nu,j_\mu}^{(n,k)}\right) \tag{2.175}$$

satisfies the higher-dimensional bilinear system (2.164)–(2.167).

We note that without the factor of $\mathrm{i}p$ in Eqs. (2.168)–(2.169), the above $\tau_{n,k}$ function (2.175) would also satisfy the higher-dimensional bilinear system (2.164)–(2.167). However, this $\mathrm{i}p$ factor in (2.168)–(2.169) is needed in order for the resulting $\tau_{n,k}$ to satisfy the complex conjugation condition (2.198), which is coming up in the later text. That complex conjugation condition is also necessary in order for $\tau_{n,k}$ to satisfy the original bilinear equations (2.157)–(2.160) of the GDNLS equations.

Next, we will reduce the higher-dimensional bilinear system (2.164)–(2.167) to the original bilinear system (2.157)–(2.160), so that the higher-dimensional solutions (2.175) become rogue wave solutions to the GDNLS equations (2.145).

In this reduction, we will need to set

$$c = -\mathrm{i}\alpha, \tag{2.176}$$

where c is the parameter in the higher-dimensional system (2.164)–(2.167), and α is the wavenumber parameter in the original bilinear system (2.157)–(2.160).

(b) Dimensional reduction

Next, we reduce the higher-dimensional bilinear system (2.164)–(2.167) to a lower-dimensional one. This reduction will restrict the indices in the determinant (2.175), and select the (p, q) values in its matrix element $m^{(n,k)}_{i_\nu, j_\mu}$.

The dimension reduction condition we impose is

$$\left(\partial_{x_1} + \mathrm{i}c\partial_{x_{-1}}\right)\tau_{n,k} = C\tau_{n,k}, \tag{2.177}$$

where C is some constant. Denoting $\hat{p} \equiv p - c$ and $\hat{q} \equiv q + c$, then $\mathcal{A}_i$ and $\mathcal{B}_j$ in Eq. (2.174) can be rewritten as

$$\mathcal{A}_i = \frac{1}{i!}\left(\hat{p}\partial_{\hat{p}}\right)^i, \quad \mathcal{B}_j = \frac{1}{j!}\left(\hat{q}\partial_{\hat{q}}\right)^j. \tag{2.178}$$

In addition,

$$\begin{aligned}\left(\partial_{x_1} + \mathrm{i}c\partial_{x_{-1}}\right) m^{(n,k)}_{i,j} &= \mathcal{A}_i\mathcal{B}_j\left(\partial_{x_1} + \mathrm{i}c\partial_{x_{-1}}\right) m^{(n,k)} \\ &= \mathcal{A}_i\mathcal{B}_j\left[\hat{p} + \frac{\mathrm{i}c}{\hat{p}} + \hat{q} + \frac{\mathrm{i}c}{\hat{q}}\right] m^{(n,k)}.\end{aligned} \tag{2.179}$$

Using the Leibnitz rule as in Sect. 2.1.1, the above equation reduces to

$$\begin{aligned}\left(\partial_{x_1} + \mathrm{i}c\partial_{x_{-1}}\right) m^{(n,k)}_{i,j} = &\sum_{\mu=0}^{i} \frac{1}{\mu!}\left(\hat{p} + (-1)^\mu \frac{\mathrm{i}c}{\hat{p}}\right) m^{(n,k)}_{i-\mu,j} \\ &+ \sum_{l=0}^{j} \frac{1}{l!}\left(\hat{q} + (-1)^l \frac{\mathrm{i}c}{\hat{q}}\right) m^{(n,k)}_{i,j-l}.\end{aligned} \tag{2.180}$$

Recalling $c = -\mathrm{i}\alpha$ from (2.176), we see that when $\hat{p} = \hat{p}_0$ and $\hat{q} = \hat{q}_0$, where

$$\hat{p}_0 = \hat{q}_0 = \sqrt{\alpha}, \tag{2.181}$$

then $\hat{p}_0 - \mathrm{i}c/\hat{p}_0 = \hat{q}_0 - \mathrm{i}c/\hat{q}_0 = 0$. Thus, the above equation would further simplify to

$$\left(\partial_{x_1} + \mathrm{i}c\partial_{x_{-1}}\right) m_{i,j}^{(n,k)}\Big|_{\hat{p}=\hat{p}_0,\ \hat{q}=\hat{q}_0}$$
$$= 2\sqrt{\alpha}\left(\sum_{\substack{\mu=0,\\ \mu:even}}^{i} \frac{1}{\mu!} m_{i-\mu,j}^{(n,k)} + \sum_{\substack{l=0,\\ l:even}}^{j} \frac{1}{l!} m_{i,j-l}^{(n,k)}\right)\Bigg|_{\substack{\hat{p}=\hat{p}_0,\\ \hat{q}=\hat{q}_0}}. \tag{2.182}$$

Now, we restrict the general determinant (2.175) to

$$\tau_{n,k} = \det_{1\le i,j\le N}\left(m_{2i-1,2j-1}^{(n,k)}\Big|_{\hat{p}=\hat{p}_0,\ \hat{q}=\hat{q}_0}\right). \tag{2.183}$$

Then, using the contiguity relation (2.182) similar to what we did in Sect. 2.1.1, we get

$$\left(\partial_{x_1} + \mathrm{i}c\partial_{x_{-1}}\right)\tau_{n,k} = 4\sqrt{\alpha}N\,\tau_{n,k}, \tag{2.184}$$

which shows that the $\tau_{n,k}$ function (2.183) satisfies the dimension reduction condition (2.177).

When this dimension reduction equation is used to eliminate x_{-1} from the higher-dimensional bilinear system (2.164)–(2.167), and in view of the parameter connection (2.176), we get

$$\left(D_{x_2} - D_{x_1}^2 + 2\mathrm{i}\alpha D_{x_1}\right)\tau_{n-1,k+1}\cdot\tau_{n-1,k} = 0, \tag{2.185}$$

$$\left(D_{x_2} - D_{x_1}^2\right)\tau_{n,k}\cdot\tau_{n-1,k} = 0, \tag{2.186}$$

$$\left(\mathrm{i}D_{x_1} - 1\right)\tau_{n,k}\cdot\tau_{n-1,k} + \tau_{n-1,k+1}\tau_{n,k-1} = 0, \tag{2.187}$$

$$(D_{x_1}^2 + \mathrm{i}D_{x_1} + 2\alpha)\tau_{n,k}\cdot\tau_{n-1,k} - (\mathrm{i}D_{x_1} + 2\alpha)\tau_{n-1,k+1}\cdot\tau_{n,k-1} = 0. \tag{2.188}$$

In addition, using Eq. (2.187), we can replace the last bilinear equation (2.188) by

$$D_{x_1}^2\tau_{n,k}\cdot\tau_{n-1,k} - \mathrm{i}D_{x_1}\tau_{n-1,k+1}\cdot\tau_{n,k-1}$$
$$+(2\alpha+1)(\tau_{n,k}\cdot\tau_{n-1,k} - \tau_{n-1,k+1}\cdot\tau_{n,k-1}) = 0. \tag{2.189}$$

In these reduced bilinear equations, the x_{-1} derivative disappears.

To further reduce the bilinear system (2.185)–(2.187) and (2.189) to the original system (2.157)–(2.160), we set

$$x_1 = x - t, \quad x_2 = \mathrm{i}t/2. \tag{2.190}$$

Under this variable relation, we have

$$\partial_{x_1} = \partial_x, \quad \partial_{x_2} = -2\mathrm{i}\partial_t - 2\mathrm{i}\partial_x. \tag{2.191}$$

Inserting these equations into the bilinear system (2.185)–(2.187) and (2.189), and setting $n = k = 0$, we get

$$\left(2\mathrm{i}D_t + D_x^2 + 2\mathrm{i}(1-\alpha)D_x\right) g \cdot \bar{f} = 0, \tag{2.192}$$

$$\left(2\mathrm{i}D_t + D_x^2 + 2\mathrm{i}D_x\right) f \cdot \bar{f} = 0, \tag{2.193}$$

$$(\mathrm{i}D_x - 1) f \cdot \bar{f} + g\bar{g} = 0, \tag{2.194}$$

$$D_x^2 f \cdot \bar{f} - \mathrm{i}D_x g \cdot \bar{g} + (2\alpha + 1)(f\bar{f} - g\bar{g}) = 0, \tag{2.195}$$

where f, $\bar{f}$, g and $\bar{g}$ are defined as

$$f = \tau_{0,0}, \quad \bar{f} = \tau_{-1,0}, \quad g = \tau_{-1,1}, \quad \bar{g} = \tau_{0,-1}. \tag{2.196}$$

(c) Complex conjugacy conditions

Next, we need to impose complex conjugacy conditions $\bar{f} = f^*$ and $\bar{g} = g^*$, i.e.,

$$\tau_{-1,0} = \tau_{0,0}^*, \quad \tau_{0,-1} = \tau_{-1,1}^*, \tag{2.197}$$

so that the bilinear system (2.192)–(2.195) would reduce to the original bilinear system (2.157)–(2.160). These complex conjugacy conditions would be satisfied if

$$\tau_{n,k}^* = \tau_{-n-1,-k}. \tag{2.198}$$

To satisfy this condition, we impose the parameter constraint $\xi_0 = \eta_0^*$. In this case, since $x_1 = x - t$ is real, $x_2 = \mathrm{i}t/2$ and $c = -\mathrm{i}\alpha$ are pure imaginary, and $\hat{q}_0 = \hat{p}_0^*$, we can easily show that

$$\left[m_{i,j}^{(n,k)} \Big|_{\hat{p}=\hat{p}_0,\ \hat{q}=\hat{q}_0} \right]^* = m_{j,i}^{(-n-1,-k)} \Big|_{\hat{p}=\hat{p}_0,\ \hat{q}=\hat{q}_0}. \tag{2.199}$$

Thus, the complex conjugacy condition (2.198) holds. In meeting Eq. (2.199), the factor $\mathrm{i}p$ in Eqs. (2.168)–(2.169) plays an important role.

(d) Rogue wave solutions in differential operator form

Finally, we need to introduce free parameters into rogue waves. As we did in Sect. 2.1.1 for the NLS equation, we will introduce free parameters through the arbitrary constant ξ_0 in Eq. (2.171). Specifically, we choose ξ_0 as

$$\xi_0(p) = \sum_{r=1}^{\infty} \hat{a}_r \ln^r \left(\frac{\hat{p}}{\hat{p}_0} \right) = \sum_{r=1}^{\infty} \hat{a}_r \ln^r \left(\frac{p + \mathrm{i}\alpha}{\sqrt{\alpha}} \right), \tag{2.200}$$

where $\hat{a}_r$ are free complex constants.

Putting all the above results together, setting $x_{-1} = 0$, and writing the matrix element in the τ function (2.183) through $\hat{p}$ and $\hat{q}$, rational solutions to the GDNLS equations (2.145) in differential form are then given by the following theorem.

Lemma 2.6 *The GDNLS equations (2.145) admit rational solutions*

$$u_N(x,t) = e^{\mathrm{i}(1-\gamma-\alpha)x - \frac{1}{2}\mathrm{i}[\alpha^2+2(\gamma-2)\alpha+1-\gamma]t} \frac{(f_N^*)^{\gamma-1} g_N}{f_N^{\gamma}}, \tag{2.201}$$

where

$$f_N(x,t) = \tau_{0,0}, \quad g_N(x,t) = \tau_{-1,1}, \tag{2.202}$$

$$\tau_{n,k} = \det_{1 \le i,j \le N} \left(m_{2i-1,2j-1}^{(n,k)} \right), \tag{2.203}$$

the matrix elements in $\tau_{n,k}$ are defined by

$$m_{i,j}^{(n,k)} = \frac{\left(\hat{p}\partial_p\right)^i}{i!} \frac{\left(\hat{q}\partial_q\right)^j}{j!} m^{(n,k)} \Big|_{\hat{p}=\hat{p}_0,\ \hat{q}=\hat{q}_0}, \tag{2.204}$$

$$m^{(n,k)} = \frac{\mathrm{i}(\hat{p} - \mathrm{i}\alpha)}{\hat{p} + \hat{q}} \left(-\frac{\hat{p} - \mathrm{i}\alpha}{\hat{q} + \mathrm{i}\alpha} \right)^n \left(-\frac{\hat{p}}{\hat{q}} \right)^k e^{\Theta(x,t)}, \tag{2.205}$$

$$\begin{aligned} \Theta(x,t) = {} & \left(\hat{p} + \hat{q}\right)(x - t) + \frac{1}{2}\left[\hat{p}^2 - \hat{q}^2 - 2\mathrm{i}\alpha(\hat{p} + \hat{q})\right]\mathrm{i}t \\ & + \sum_{r=1}^{\infty} \left(\hat{a}_r \ln^r \left(\frac{\hat{p}}{\hat{p}_0} \right) + \hat{a}_r^* \ln^r \left(\frac{\hat{q}}{\hat{q}_0} \right) \right), \end{aligned} \tag{2.206}$$

$\hat{p}_0 = \hat{q}_0 = \sqrt{\alpha}$, $\alpha > 0$, *and* $\hat{a}_1, \hat{a}_2, \cdots, \hat{a}_{2N-1}$ *are free complex constants.*

(e) Explicit rogue wave solutions through Schur polynomials

Now, we derive explicit rogue wave expressions in Theorem 2.3 from the above differential form in Lemma 2.6.

Introducing the generator $\mathcal{G}$ as

$$\mathcal{G}=\sum_{i=0}^{\infty}\sum_{j=0}^{\infty}\frac{\zeta^i}{i!}\frac{\lambda^j}{j!}\left[\hat{p}\partial_{\hat{p}}\right]^i\left[\hat{q}\partial_{\hat{q}}\right]^j, \tag{2.207}$$

and utilizing the formula (2.60), i.e.,

$$\mathcal{G}F(\hat{p},\hat{q})=F\left(e^{\zeta}\hat{p},e^{\lambda}\hat{q}\right), \tag{2.208}$$

we find that for the $m^{(n,k)}$ function in Lemma 2.6,

$$\begin{aligned}\mathcal{G}m^{(n,k)}\Big|_{\hat{p}=\hat{p}_0,\ \hat{q}=\hat{q}_0}&=\frac{e^{\zeta/2}(\mathrm{i}e^{\zeta/2}+\sqrt{\alpha}e^{-\zeta/2})}{e^{\zeta}+e^{\lambda}}\\&\times(-1)^k e^{(k+\frac{n}{2})(\zeta-\lambda)}\left(\frac{\mathrm{i}e^{\zeta/2}+\sqrt{\alpha}e^{-\zeta/2}}{-\mathrm{i}e^{\lambda/2}+\sqrt{\alpha}e^{-\lambda/2}}\right)^n\\&\times\exp\left\{\sqrt{\alpha}\left(e^{\zeta}+e^{\lambda}\right)(x-t+\alpha t)+\frac{1}{2}\alpha\left(e^{2\zeta}-e^{2\lambda}\right)\mathrm{i}t\right.\\&\left.+\sum_{r=1}^{\infty}\left(\hat{a}_r\zeta^r+\hat{a}_r^*\lambda^r\right)\right\}.\end{aligned} \tag{2.209}$$

Thus,

$$\begin{aligned}\frac{1}{m^{(n,k)}}\mathcal{G}m^{(n,k)}\Big|_{\hat{p}=\hat{p}_0,\ \hat{q}=\hat{q}_0}&=\frac{2}{e^{\zeta}+e^{\lambda}}\left(\frac{\mathrm{i}e^{\zeta/2}+\sqrt{\alpha}e^{-\zeta/2}}{\mathrm{i}+\sqrt{\alpha}}\right)^{n+1}\\&\times\left(\frac{-\mathrm{i}+\sqrt{\alpha}}{-\mathrm{i}e^{\lambda/2}+\sqrt{\alpha}e^{-\lambda/2}}\right)^n\\&\times\exp\left(\frac{1}{2}\zeta+(k+\frac{n}{2})(\zeta-\lambda)+\sqrt{\alpha}\left(e^{\zeta}+e^{\lambda}-2\right)\right.\\&\left.\times(x-t+\alpha t)+\frac{1}{2}\alpha\left(e^{2\zeta}-e^{2\lambda}\right)\mathrm{i}t\right)\\&\times\exp\left(\sum_{r=1}^{\infty}(\hat{a}_r\zeta^r+\hat{a}_r^*\lambda^r)\right).\end{aligned} \tag{2.210}$$

Now, we need to expand the right side of the above equation into power series of ζ and λ. Writing

$$\frac{2}{e^{\zeta}+e^{\lambda}}=\frac{1}{1-\frac{(e^{\zeta}-1)(e^{\lambda}-1)}{(e^{\zeta}+1)(e^{\lambda}+1)}}\exp\left(-\ln\frac{(e^{\zeta}+1)(e^{\lambda}+1)}{4}\right)$$

$$= \sum_{\nu=0}^{\infty} \left(\frac{(e^{\zeta}-1)(e^{\lambda}-1)}{(e^{\zeta}+1)(e^{\lambda}+1)} \right)^{\nu} \exp\left(-\ln \frac{e^{(\zeta+\lambda)/2}(e^{\zeta/2}+e^{-\zeta/2})(e^{\lambda/2}+e^{-\lambda/2})}{4} \right)$$

$$= \sum_{\nu=0}^{\infty} \left(\frac{\zeta\lambda}{4} \right)^{\nu} \exp\left[\nu \ln\left(\frac{4}{\zeta\lambda} \tanh\frac{\zeta}{2} \tanh\frac{\lambda}{2} \right) - \ln\left(\cosh\frac{\zeta}{2} \cosh\frac{\lambda}{2} \right) - \frac{\zeta}{2} - \frac{\lambda}{2} \right]$$

$$= \sum_{\nu=0}^{\infty} \left(\frac{\zeta\lambda}{4} \right)^{\nu} \exp\left(\sum_{r=1}^{\infty} (\nu s_r - c_r) \left(\zeta^r + \lambda^r \right) - \frac{\zeta}{2} - \frac{\lambda}{2} \right), \tag{2.211}$$

where s_r are as defined in Eq. (2.11), and c_r are Taylor coefficients of λ^r in the expansion of $\ln\cosh(\lambda/2)$, then using the h_r expansion in Eq. (2.155), we get

$$\frac{1}{m^{(n,k)}} \mathcal{G} m^{(n,k)} \Big|_{\substack{\hat{p}=\hat{p}_0, \\ \hat{q}=\hat{q}_0}} = \sum_{\nu=0}^{\infty} \left(\frac{\zeta\lambda}{4} \right)^{\nu} \exp\left(\sum_{r=1}^{\infty} \left(x_r^{+} + \nu s_r \right) \zeta^r + \sum_{r=1}^{\infty} \left(x_r^{-} + \nu s_r \right) \lambda^r \right), \tag{2.212}$$

where $x_r^{\pm}(n,k)$ are defined as

$$x_1^{+}(n,k) = \sqrt{\alpha}(x - 2t + 2\alpha t) + 2\mathrm{i}\alpha t + (n+1)h_1 + k + \frac{n}{2} - c_1 + \hat{a}_1, \tag{2.213}$$

$$x_1^{-}(n,k) = \sqrt{\alpha}(x - 2t + 2\alpha t) - 2\mathrm{i}\alpha t - nh_1^{*} - k - \frac{1}{2}(n+1) - c_1 + \hat{a}_1^{*}, \tag{2.214}$$

$$x_r^{+}(n,k) = \frac{1}{r!}\left[\sqrt{\alpha}(x - 2t + 2\alpha t) + 2^r \mathrm{i}\alpha t \right] + (n+1)h_r - c_r + \hat{a}_r, \tag{2.215}$$

$$x_r^{-}(n,k) = \frac{1}{r!}\left[\sqrt{\alpha}(x - 2t + 2\alpha t) - 2^r \mathrm{i}\alpha t \right] - nh_r^{*} - c_r + \hat{a}_r^{*}. \tag{2.216}$$

We further define shifted parameters

$$a_1 = \hat{a}_1 - c_1 + \frac{1}{2}h_1 - \frac{1}{4}, \quad a_r = \hat{a}_r - c_r + \frac{1}{2}h_r \ \ (r \geq 2). \tag{2.217}$$

Notice that the a_r parameters are linearly related to the $\hat{a}_r$ parameters. Then, the above $x_r^{\pm}(n,k)$ reduce to those in Theorem 2.3, except that the above definitions for $x_r^{\pm}(n,k)$ apply for all r indices, including those where r is even. Taking the coefficients of $\zeta^i \lambda^j$ on both sides of Eq. (2.212), we get

$$m_{i,j}^{(n,k)} = m^{(n,k)}\Big|_{\hat{p}=\hat{p}_0, \hat{q}=\hat{q}_0} \times \sum_{\nu=0}^{\min(i,j)} \frac{1}{4^{\nu}} S_{i-\nu}\left(\boldsymbol{x}^{+} + \nu \boldsymbol{s} \right) S_{j-\nu}\left(\boldsymbol{x}^{-} + \nu \boldsymbol{s} \right), \tag{2.218}$$

where $m_{i,j}^{(n,k)}$ is the matrix element defined in Lemma 2.6. Finally, we define

$$\sigma_{n,k} = \frac{\tau_{n,k}}{\left(m^{(n,k)}\big|_{\hat{p}=\hat{p}_0,\hat{q}=\hat{q}_0}\right)^N}. \tag{2.219}$$

One can see that this $\sigma_{n,k}$ satisfies the same bilinear equations as $\tau_{n,k}$. Then the matrix element in $\sigma_{n,k}$ is as given in Theorem 2.3, and the function in Eq. (2.147) is a rational solution to the GDNLS equations (2.145).

By the same technique as in Sect. 2.1.1, we can show that $x_{2r}^{\pm}$ are dummy variables which can be set to zero without affecting the solution. In addition, by a shift of the (x, t) axes, we can normalize $a_1 = 0$. Thus, irreducible parameters in these solutions are $a_3, a_5, \cdots, a_{2N-1}$.

Regarding boundary conditions of these rational solutions, using the Schur polynomial expressions in Theorem 2.3 and the same technique as in Sect. 2.1.1, we can show that when x or t approaches infinity, $f_N(x, t)$ and $g_N(x, t)$ have the same leading term, which is also real. Thus, the rational solution (2.147) satisfies the boundary condition (2.146) and is thus a rogue wave. Theorem 2.3 is then proved.

A remark we would like to make is that, when $a_3 = a_5 = \cdots = a_{2N-1} = 0$, the rogue wave in Theorem 2.3 is parity-time-symmetric, i.e., $u_N^*(-x, -t) = u_N(x, t)$. The significance of this property is that, this parity-time-symmetric rogue wave happens to possess the maximum peak amplitude among rogue waves of that order and is thus a super rogue wave. In addition, this maximum peak amplitude is located at the center of this super rogue wave, i.e., at $x = t = 0$. Thus, to derive the maximum peak amplitude of a GDNLS super rogue wave, we only need to set all its internal parameters a_r as well as (x, t) to zero. Doing so, our explicit calculations for $N = 1, 2, \ldots, 6$ show that (Yang et al. 2020)

$$|f_N(0,0)|_{a_r=0} = \frac{\alpha^{N(N+1)/2}}{2^{2N^2}(\alpha+1)^{N(N+1)/2}}, \quad |g_N(0,0)|_{a_r=0} = \frac{(2N+1)\alpha^{N(N+1)/2}}{2^{2N^2}(\alpha+1)^{N(N+1)/2}}, \tag{2.220}$$

and thus the maximum peak amplitude is

$$|u_N(0,0)|_{a_r=0} = \frac{|g_N(0,0)|_{a_r=0}}{|f_N(0,0)|_{a_r=0}} = 2N+1, \tag{2.221}$$

which is the same as that in the NLS equation (see Sect. 2.1.2). Remarkably, this maximum peak amplitude does not depend on the background wavenumber α, although $|f_N|$ and $|g_N|$ in its numerator and denominator do. While these formulae were obtained for $N \le 6$, we believe they hold for $N > 6$ as well.

When setting $N = 1$ in Theorem 2.3, we get the fundamental GDNLS rogue wave as

$$|u_1(x,t;\alpha)| = \left|\frac{\alpha(x+\alpha t)^2 + (x-t)^2 - \mathrm{i}(x+3\alpha t) - \frac{3}{4}}{\alpha(x+\alpha t)^2 + (x-t)^2 + \mathrm{i}(x+\alpha t) - 2\mathrm{i}t + \frac{1}{4}}\right|. \tag{2.222}$$

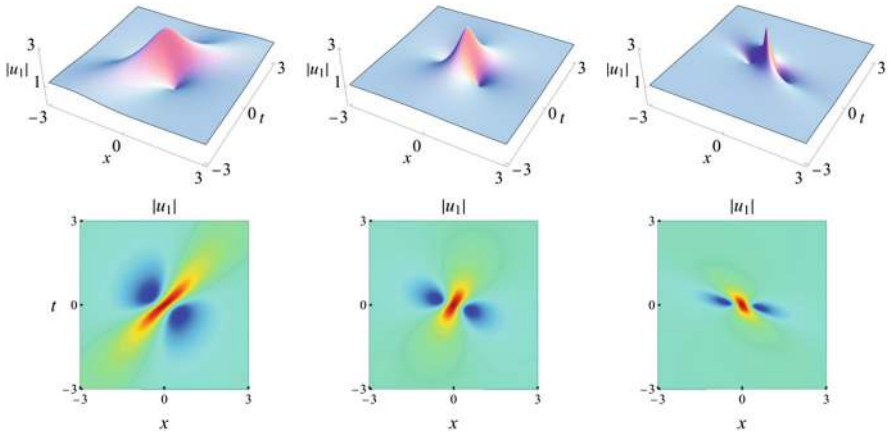

Fig. 2.2 Fundamental GDNLS rogue wave $|u_1(x,t)|$ from Eq. (2.222) for $\alpha = 0.5$, 1 and 2 (from left to right), respectively. Upper row: 3D plots; lower row: density plots

For three different α values of 0.5, 1 and 2, these amplitude fields are plotted in Fig. 2.2. It is seen that α strongly affects the orientation and duration of the rogue wave. Specifically, as the α value increases, the orientation angle (relative to the positive x axis) also increases, but the duration of the rogue wave decreases. However, the peak amplitudes of these rogue waves for different α values are all equal to 3, which are attained at the center $x = t = 0$. Physically, the longer duration of rogue waves at smaller α values can be understood, because in this case, the growth rates of modulation instability can be shown to be smaller, which causes the rogue wave to take longer time to rise from the unit-amplitude background to its peak amplitude of 3. The dependence of the orientation angle on α can also be heuristically understood. It is known that the phase gradient of a pulse generally causes the pulse to move at a velocity which is proportional to this phase gradient. In the present case, the phase gradient of the rogue wave can be estimated from Eq. (2.147) as the wavenumber $1 - \gamma - \alpha$. Then, for a fixed equation parameter γ, larger α causes the velocity to be smaller or negative, leading to a larger orientation angle. To put these results in perspective, we note that for the NLS equation, since the constant-background wavenumber of its rogue waves can be normalized to zero by a Galilean transformation, the background wavenumber only affects the orientation, but not duration, of its rogue waves.

Second-order GDNLS rogue waves can be obtained by setting $N = 2$ in Theorem 2.3. These rogue waves contain one irreducible complex free parameter a_3, in addition to the background wavenumber parameter α and equation parameter γ (the last parameter does not affect the amplitude fields of rogue waves). When we set $\alpha = 1$, then the amplitude fields of rogue waves at three a_3 values of 0, 1/3 and 30 are displayed in the three panels of Fig. 2.3 (from left to right), respectively. The rogue wave at $a_3 = 0$ is a super rogue wave that is parity-time-symmetric, and it reaches peak amplitude 5 at the center $x = t = 0$. The rogue wave at $a_3 = 1/3$

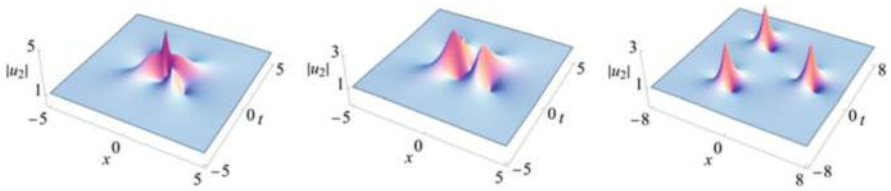

Fig. 2.3 Second-order GDNLS rogue waves $|u_2(x,t)|$ with $\alpha = 1$ and three a_3 values of 0, 1/3, and 30 (from left to right), respectively

exhibits a complex profile with peak amplitude of about 3.3714. The one at $a_3 = 30$ splits into three separate first-order rogue waves and is thus a rogue triplet. This splitting phenomenon is similar to second-order rogue waves of the NLS equation (see Fig. 2.1, third column).

2.3 Boussinesq Equation

In 1871, Boussinesq introduced an equation which governs the propagation of long surface waves on water of constant depth (Boussinesq 1871, 1872; see also Ursell 1953). After variable normalizations, this equation can be written as (Clarkson and Dowie 2017)

$$u_{tt} + u_{xx} - (u^2)_{xx} - \frac{1}{3}u_{xxxx} = 0. \tag{2.223}$$

This equation also arises in many other physical contexts, such as continuum approximations of certain Fermi-Pasta-Ulam chains (Zabusky 1967; Zakharov 1973; Toda 1975), and ion sound waves in a plasma (Scott 1975; Infeld and Rowlands 1990). Remarkably, this equation is integrable. Indeed, its multi-soliton solutions and Lax pair were reported almost simultaneously by Hirota and Zakharov in 1973, respectively (Hirota 1973; Zakharov 1973).

The zero solution in this normalized Boussinesq equation is unstable. As a consequence, rogue waves may arise. Boundary conditions to these rogue waves are then

$$u(x,t) \to 0, \quad x,t \to \pm\infty. \tag{2.224}$$

Fundamental (first-order) rogue waves to the Boussinesq equation (2.223) were derived in Tajiri and Murakami (1991) and Rao et al. (2017) by taking a long-wave limit of the two-soliton solution. Higher-order rogue waves to this equation were considered by Clarkson and Dowie (2017). Converting this equation into a bilinear one, assuming certain polynomial forms for the bilinear solution, equating powers of x, t in the bilinear equation and solving the resulting algebraic equations for the

polynomial coefficients, the authors obtained second- to fifth-order rogue waves with two free real parameters at each order. General rogue waves to this equation were derived by Yang and Yang (2020a) using the bilinear method. However, those bilinear expressions of rogue waves are not in the simplest form. Below, we present simpler expressions of Boussinesq rogue waves using a new parameterization technique as described in Sect. 2.1.1 for the NLS equation.

Theorem 2.4 *The Boussinesq equation (2.223) under boundary conditions (2.224) admits the following general nonsingular rogue waves*

$$u_N(x,t) = 2\partial_x^2 \ln \sigma, \tag{2.225}$$

where

$$\sigma(x,t) = \det_{1\le i,j\le N} \left(\phi_{2i-1,2j-1}\right), \tag{2.226}$$

$$\phi_{i,j} = \sum_{v=0}^{\min(i,j)} \left(\frac{-1}{12}\right)^v S_{i-v}(\boldsymbol{x}^+ + v\boldsymbol{s})\, S_{j-v}(\boldsymbol{x}^- + v\boldsymbol{s}), \tag{2.227}$$

vectors $\boldsymbol{x}^{\pm} = \left(x_1^{\pm}, 0, x_3^{\pm}, 0, \cdots\right)$ *and* $\boldsymbol{s} = (s_1, s_2, \cdots)$ *are defined by*

$$x_{2r+1}^{+} = \frac{\sqrt{3}\,\mathrm{i}}{2\cdot 3^{2r+1}\cdot(2r+1)!}\left(x + 2^{2r}\mathrm{i}t\right) + a_{2r+1}, \quad r = 0, 1, 2, \cdots, \tag{2.228}$$

$$x_{2r+1}^{-} = \frac{\sqrt{3}\,\mathrm{i}}{2\cdot 3^{2r+1}\cdot(2r+1)!}\left(x - 2^{2r}\mathrm{i}t\right) - a_{2r+1}^{*}, \quad r = 0, 1, 2, \cdots, \tag{2.229}$$

$$\sum_{r=1}^{\infty} s_r \lambda^r = \ln\left[\frac{2\mathrm{i}\sqrt{3}}{\lambda}\tanh\frac{\lambda}{6}\tanh\left(\frac{\lambda}{6} + \frac{2\mathrm{i}\pi}{3}\right)\right], \tag{2.230}$$

$a_1 = 0$, *and* $a_3, a_5, \cdots, a_{2N-1}$ *are free irreducible complex constants.*

Note The function $f(\lambda)$ on the right side of Eq. (2.230) satisfies the symmetry $f^*(\lambda) = f(-\lambda)$, where λ is considered real. Because of that, all s_{even} values are real, and all s_{odd} values are purely imaginary. The first few s_k values are

$$s_1 = \frac{2\mathrm{i}}{3\sqrt{3}}, \quad s_2 = -\frac{5}{108}, \quad s_3 = -\frac{5\mathrm{i}}{243\sqrt{3}}. \tag{2.231}$$

Proof First, we introduce the variable transformation

$$u(x,t) = 2\partial_x^2 \ln \sigma(x,t), \tag{2.232}$$

where $\sigma(x,t)$ is a real variable. Under this transformation, the Boussinesq equation (2.223) is converted into the bilinear form

$$\left(D_x^4 - 3D_x^2 - 3D_t^2\right)\sigma\cdot\sigma = 0. \tag{2.233}$$

In order to derive solutions to this bilinear equation, we consider a higher-dimensional bilinear equation

$$\left(D_{x_1}^4 - 4D_{x_1}D_{x_3} + 3D_{x_2}^2\right)\sigma\cdot\sigma = 0, \tag{2.234}$$

which is the bilinear form of the KP equation. We first construct a wide class of algebraic solutions for this higher-dimensional bilinear equation in the form of Gram determinants. Then, we restrict these solutions so that they satisfy the dimensional reduction condition

$$\left(\partial_{x_3} - 3\partial_{x_1}\right)\sigma = C\sigma, \tag{2.235}$$

where C is some constant (our choice of the coefficient 3 in front of ∂_{x_1} is for convenience). Under this condition, the higher-dimensional bilinear equation (2.234) would reduce to

$$\left(D_{x_1}^4 - 12D_{x_1}^2 + 3D_{x_2}^2\right)\sigma\cdot\sigma = 0. \tag{2.236}$$

Finally, we define

$$x_1 = \frac{1}{2}x, \quad x_2 = -\frac{1}{4}\mathrm{i}t, \tag{2.237}$$

and impose the reality condition

$$\sigma^* = \sigma. \tag{2.238}$$

Then, the bilinear equation (2.236) becomes the bilinear equation (2.233) of the Boussinesq equation, and $u = 2\partial_x^2 \ln\sigma$ becomes the rational rogue wave solution of the Boussinesq equation. Next, we execute this strategy.

(a) Gram determinant solutions for a higher-dimensional bilinear system

First, it is well known that when functions $m_{i,j}$, φ_i and ψ_j satisfy the following differential equations

$$\left.\begin{aligned} &\partial_{x_1} m_{i,j} = \varphi_i\psi_j, \\ &\partial_{x_n}\varphi_i = \partial_{x_1}^n\varphi_i, \quad \partial_{x_n}\psi_j = (-1)^{n-1}\partial_{x_1}^n\psi_j, \quad n = 1,2,3, \end{aligned}\right\} \tag{2.239}$$

then the τ function

$$\tau = \det_{1\le i,j\le N}\left(m_{i,j}\right) \tag{2.240}$$

would satisfy the bilinear equation (2.234) of the KP equation, i.e.,

$$\left(D_{x_1}^4 - 4D_{x_1}D_{x_3} + 3D_{x_2}^2\right)\tau\cdot\tau = 0. \tag{2.241}$$

Indeed, substituting the solutions (2.240) into KP's bilinear equation (2.241), this equation reduces to the Jacobi identity of determinants (Hirota 2004).

Now, we introduce functions

$$m_{i,j} = \mathcal{A}_i\mathcal{B}_j m, \quad \varphi_i = \mathcal{A}_i\varphi, \quad \psi_j = \mathcal{B}_j\psi, \tag{2.242}$$

where $\mathcal{A}_i$ and $\mathcal{B}_j$ are differential operators with respect to p and q respectively as

$$\mathcal{A}_i = \frac{1}{i!}\left[f_1(p)\partial_p\right]^i, \quad \mathcal{B}_j = \frac{1}{j!}\left[f_2(q)\partial_q\right]^j, \tag{2.243}$$

$f_1(p)$, $f_2(q)$ are arbitrary functions of p and q,

$$m = \frac{(p-1)(q-1)}{p+q}e^{\xi+\eta}, \quad \varphi = (p-1)e^{\xi}, \quad \psi = (q-1)e^{\eta}, \tag{2.244}$$

$$\xi = px_1 + p^2x_2 + p^3x_3 + \xi_0(p), \quad \eta = qx_1 - q^2x_2 + q^3x_3 + \eta_0(q), \tag{2.245}$$

and $\xi_0(p)$, $\eta_0(q)$ are arbitrary functions of p and q. The factor of $(p-1)(q-1)$ in m above is introduced to simplify later calculations, similar to the factor of $(p+1)(q+1)$ in the $m^{(n)}$ function (2.29) in the NLS case. It is easy to see that these $m_{i,j}$, φ_i and ψ_j functions satisfy the differential equations (2.239), since $m_{i,j} = m$, $\varphi_i = \varphi$ and $\psi_j = \psi$ satisfy them, and operators $\mathcal{A}_i$, $\mathcal{B}_j$ commute with differentials ∂_{x_k}.

Next, we restrict the τ solution (2.240) so that it satisfies the dimension reduction condition (2.235) and the reality condition (2.238).

(b) Dimensional reduction by the $\mathcal{W}$-p treatment

To facilitate the satisfaction of the dimensional reduction condition (2.235), we will utilize the freedom of the $f_1(p)$ and $f_2(q)$ functions and choose them judiciously. This is the so-called $\mathcal{W}$-p treatment we introduced in Yang and Yang (2020a) for the Boussinesq equation and generalized in Yang and Yang (2021b) for the three-wave resonant interaction system.

We start from the dimensional reduction condition (2.235), i.e.,

$$\left(\partial_{x_3} - 3\partial_{x_1}\right)\tau = C\tau, \tag{2.246}$$

where C is a certain constant. In order to calculate the left side of the above equation, we notice from the definitions (2.242) and (2.244) of m and $m_{i,j}$ that

$$\left(\partial_{x_3} - 3\partial_{x_1}\right) m_{i,j} = \mathcal{A}_i \mathcal{B}_j \left[Q_1(p) + Q_2(q)\right] m, \tag{2.247}$$

where

$$Q_1(p) = p^3 - 3p, \quad Q_2(q) = q^3 - 3q. \tag{2.248}$$

To proceed further, we utilize the general Leibnitz-type operator relation,

$$\mathcal{A}_i Q_1(p) = \sum_{l=0}^{i} \frac{1}{l!} \left[\left(f_1 \partial_p\right)^l Q_1(p)\right] \mathcal{A}_{i-l}. \tag{2.249}$$

Note that on the right side of this relation, the operator $\left(f_1 \partial_p\right)^l$ only applies to the function $Q_1(p)$, not to the operator $Q_1(p)\mathcal{A}_{i-l}$. Another relation similar to the above can also be written for $\mathcal{B}_j Q_2(q)$. Using these relations, Eq. (2.247) becomes

$$\begin{aligned}\left(\partial_{x_3} - 3\partial_{x_1}\right) m_{i,j} = &\sum_{\mu=0}^{i} \frac{1}{\mu!} \left[\left(f_1 \partial_p\right)^\mu Q_1(p)\right] m_{i-\mu,j} \\ &+ \sum_{l=0}^{j} \frac{1}{l!} \left[\left(f_2 \partial_q\right)^l Q_2(q)\right] m_{i,j-l}.\end{aligned} \tag{2.250}$$

In order to satisfy the dimensional reduction condition (2.235), we need to select functions $[f_1(p), f_2(q)]$ as well as values of (p, q), so that coefficients of certain indices on the right side of the above relation vanish. Here, we will require coefficients of all odd-indexed terms on the right side of the above relation to vanish. In such a case, this relation would relate matrix elements with indices shifted by even numbers. Then, by choosing indices of matrix elements with jumps of two in the higher-dimensional τ function (2.240), such a τ function would satisfy the dimensional reduction condition (2.235). This situation is similar to that in the NLS case, see Sect. 2.1.1.

To make coefficients of all odd-indexed terms on the right side of the contiguity relation (2.250) to vanish, we first select p_0 to be a root of the following algebraic equation

$$Q_1'(p_0) = 3p_0^2 - 3 = 0. \tag{2.251}$$

There are two roots, $p_0 = \pm 1$. We will choose $p_0 = -1$ without loss of generality. Similarly, we choose q_0 to be a root of $Q_2'(q_0) = 0$, which gives $q_0 = p_0 = -1$. At these (p_0, q_0) values, the $\mu = l = 1$ terms on the right side of Eq. (2.250) will vanish.

To make higher odd terms on the right side of Eq. (2.250) to vanish, we impose a further condition on $f_1(p)$ as

$$\left(f_1\partial_p\right)^2 Q_1(p) = Q_1(p), \tag{2.252}$$

and a similar one on $f_2(q)$. Note that these are differential equations, not operator equations. The reason for this imposition is that under these conditions, as well as the earlier conditions on p_0 and q_0, all odd-μ and l terms on the right side of Eq. (2.250), when evaluated at $p = p_0$ and $q = q_0$, would vanish.

To solve this differential Eq. (2.252), we put $f_1(p)$ in the form

$$f_1(p) = \frac{\mathcal{W}_1(p)}{\mathcal{W}_1'(p)}, \tag{2.253}$$

where $\mathcal{W}_1(p)$ is to be determined. The motivation behind this form of $f_1(p)$ is that, under this form,

$$f_1(p)\partial_p = \frac{\mathcal{W}_1(p)}{\mathcal{W}_1'(p)}\partial_p = \mathcal{W}_1(p)\partial_{\mathcal{W}_1(p)} = \partial_{\ln \mathcal{W}_1}. \tag{2.254}$$

Thus, the condition (2.252) becomes

$$\partial^2_{\ln \mathcal{W}_1} Q_1(p) = Q_1(p). \tag{2.255}$$

Scaling $\mathcal{W}_1(p_0) = 1$, which does not affect the $f_1(p)$ function, the unique solution to the above equation under the condition of $Q_1'(p_0) = 0$ is

$$Q_1(p) = \frac{1}{2}Q_1(p_0)\left(\mathcal{W}_1(p) + \frac{1}{\mathcal{W}_1(p)}\right). \tag{2.256}$$

From this equation, we can solve for $\mathcal{W}_1(p)$ and then get $f_1(p)$ from Eq. (2.253). Explicitly, we get

$$\mathcal{W}_1(p) = \frac{Q_1(p) + \sqrt{Q_1^2(p) - Q_1^2(p_0)}}{Q_1(p_0)}, \quad f_1(p) = \frac{\sqrt{Q_1^2(p) - Q_1^2(p_0)}}{Q_1'(p)}. \tag{2.257}$$

Note that the sign in front of the square root in $\mathcal{W}_1(p)$ can also be minus, in which case the above $f_1(p)$ would change sign; but that would lead to the same rogue wave solutions and thus does not need to be considered. Interestingly, these explicit $\mathcal{W}_1(p)$ and $f_1(p)$ expressions actually will not be needed in our later derivation of rogue expressions through Schur polynomials. A similar treatment can be applied to the q variable, and the formulae for $\mathcal{W}_2(q)$ and $f_2(q)$ are similar to those in Eq. (2.257) for the p variable, except that the subscripts 1 change to 2, and (p, p_0) change to (q, q_0).

Under the above choices of p, q values and $f_1(p)$ and $f_2(q)$ functions, the relation (2.250) simplifies to

$$\left(\partial_{x_3} - 3\partial_{x_1}\right) m_{i,j}\big|_{p=q=-1} = 2 \sum_{\substack{k=0,\\ k:even}}^{i} \frac{1}{k!}\, m_{i-k,j}\big|_{p=q=-1} + 2 \sum_{\substack{l=0,\\ l:even}}^{j} \frac{1}{l!}\, m_{i,j-l}\big|_{p=q=-1}. \tag{2.258}$$

This relation is similar to that we obtained earlier for the NLS equation (see Sect. 2.1.1). Due to this relation, if we choose indices $(i_1, i_2, \cdots, i_N; j_1, j_2, \cdots, j_N)$ in the determinant (2.240) as

$$\tau = \det_{1\le i,j\le N} \left(m_{2i-1,2j-1}\big|_{p=q=-1} \right), \tag{2.259}$$

then the same calculation as in Sect. 2.1.1 would show that this τ function satisfies the dimension reduction condition

$$\left(\partial_{x_3} - 3\partial_{x_1}\right) \tau = 4N\tau. \tag{2.260}$$

Substituting this condition into the higher-dimensional bilinear KP equation (2.234) and utilizing Eq. (2.237), we see that this τ function (2.259) would satisfy the bilinear equation (2.233) of the Boussinesq equation. At this point, we can set $x_3 = 0$ in this τ function since x_3 has become a dummy variable now.

Next, we introduce free parameters in this τ function by choosing

$$\xi_0(p) = \sum_{r=1}^{\infty} a_r \left[\ln \mathcal{W}_1(p)\right]^r, \quad \eta_0(q) = \sum_{r=1}^{\infty} b_r \left[\ln \mathcal{W}_2(q)\right]^r \tag{2.261}$$

in Eq. (2.245), where a_r and b_r are complex constants. In order to meet the reality condition (2.238), i.e., $\sigma^* = \sigma$, these a_r and b_r constants need to be properly constrained.

Now, we briefly summarize our results above. We have found that, the Boussinesq equation (2.223) would admit rational solutions of differential form

$$u_N(x,t) = 2\partial_x^2 \ln \tau, \tag{2.262}$$

where

$$\tau = \det_{1\le i,j\le N} \left(m_{2i-1,2j-1} \right), \tag{2.263}$$

the matrix elements in τ are defined by

$$m_{i,j} = \frac{1}{i!}[f_1(p)\partial_p]^i \frac{1}{j!}[f_2(q)\partial_q]^j m\Big|_{p=q=-1}, \tag{2.264}$$

$$m = \frac{(p-1)(q-1)}{p+q}\exp(\xi+\eta), \tag{2.265}$$

$$\xi = \frac{1}{2}px - \frac{1}{4}p^2 \mathrm{i}t + \sum_{r=1}^{\infty} a_r [\ln \mathcal{W}_1(p)]^r, \tag{2.266}$$

$$\eta = \frac{1}{2}qx + \frac{1}{4}q^2 \mathrm{i}t + \sum_{r=1}^{\infty} b_r [\ln \mathcal{W}_2(q)]^r, \tag{2.267}$$

$f_1(p)$, $\mathcal{W}_1(p)$ are functions given by Eqs. (2.253) and (2.256), $f_2(q)$, $\mathcal{W}_2(q)$ are $f_1(p)$, $\mathcal{W}_1(p)$ with p changing to q and index 1 changing to 2, if complex constants a_r, b_r are properly constrained so that the above τ function is real.

(c) The reality condition

The parameter constraints between a_r and b_r to meet the reality condition are difficult to derive from the above rogue wave expressions in differential form. In addition, we will want to reduce the above differential form to an explicit algebraic form anyway (as we have done before for the other integrable systems). Thus, we will do this form conversion first, and then use the algebraic form to find constraints between a_r and b_r so that τ is real.

The basic idea of this derivation for the explicit solution form is the same as that in Sect. 2.1.1, except that we will work with variables $\mathcal{W}_1(p)$ and $\mathcal{W}_2(q)$ instead of p and q. Introducing the generator $\mathcal{G}$ of the differential operators $\left(f_1(p)\partial_p\right)^k \left(f_2(q)\partial_q\right)^l$ as

$$\mathcal{G} = \sum_{k=0}^{\infty}\sum_{l=0}^{\infty} \frac{\kappa^k}{k!}\frac{\lambda^l}{l!}\left[f_1(p)\partial_p\right]^k \left[f_2(q)\partial_q\right]^l, \tag{2.268}$$

and utilizing Eq. (2.254), we get

$$\mathcal{G} = \sum_{k=0}^{\infty}\sum_{l=0}^{\infty} \frac{\kappa^k}{k!}\frac{\lambda^l}{l!}\left[\partial_{\ln \mathcal{W}_1}\right]^k \left[\partial_{\ln \mathcal{W}_2}\right]^l = \exp\left(\kappa\partial_{\ln \mathcal{W}_1} + \lambda\partial_{\ln \mathcal{W}_2}\right). \tag{2.269}$$

Thus, for any function $F(\mathcal{W}_1, \mathcal{W}_2)$, we have

$$\mathcal{G}F(\mathcal{W}_1, \mathcal{W}_2) = F(e^{\kappa}\mathcal{W}_1, e^{\lambda}\mathcal{W}_2). \tag{2.270}$$

Next, we will apply this generator on the function m in Eq. (2.265). To utilize Eq. (2.270), we need to express p and q in this m as functions of $\mathcal{W}_1$ and $\mathcal{W}_2$. Eq. (2.256) tells us that

$$p^3 - 3p = \mathcal{W}_1 + \frac{1}{\mathcal{W}_1}. \tag{2.271}$$

This equation can be solved and there are three roots. Due to our earlier scaling of $\mathcal{W}_1(p_0) = 1$, i.e., $\mathcal{W}_1(-1) = 1$, the suitable root for p is

$$p(\mathcal{W}_1) = c_1 \mathcal{W}_1^{1/3} + c_1^* \mathcal{W}_1^{-1/3}, \tag{2.272}$$

where $c_1 = \exp(2\mathrm{i}\pi/3)$. Similarly, we have

$$q(\mathcal{W}_2) = c_1 \mathcal{W}_2^{1/3} + c_1^* \mathcal{W}_2^{-1/3}, \tag{2.273}$$

Now, we apply Eq. (2.270) on m and get

$$\begin{aligned} \mathcal{G}m = {} & \frac{[p(e^{\kappa}\mathcal{W}_1) - 1]\,[q(e^{\kappa}\mathcal{W}_2) - 1]}{p(e^{\kappa}\mathcal{W}_1) + q(e^{\lambda}\mathcal{W}_2)} \\ & \times \exp\left(\frac{1}{2}\left[p(e^{\kappa}\mathcal{W}_1) + q(e^{\lambda}\mathcal{W}_2)\right]x - \frac{1}{4}\left[p^2(e^{\kappa}\mathcal{W}_1) - q^2(e^{\lambda}\mathcal{W}_2)\right]\mathrm{i}t\right) \\ & \times \exp\left(\sum_{r=1}^{\infty} a_r\,[\ln e^{\kappa}\mathcal{W}_1(p)]^r + \sum_{r=1}^{\infty} b_r\,[\ln e^{\lambda}\mathcal{W}_2(q)]^r\right). \end{aligned} \tag{2.274}$$

Since $\mathcal{W}_1|_{p=-1} = \mathcal{W}_2|_{q=-1} = 1$, then

$$\begin{aligned} \frac{1}{m}\,\mathcal{G}m|_{p=q=-1} = {} & \frac{[p(e^{\kappa}) - 1][q(e^{\lambda}) - 1]}{-2[p(e^{\kappa}) + q(e^{\lambda})]} \\ & \times \exp\left(\frac{1}{2}\left[p(e^{\kappa}) + q(e^{\lambda}) + 2\right]x - \frac{1}{4}\left[p^2(e^{\kappa}) - q^2(e^{\lambda})\right]\mathrm{i}t\right) \\ & \times \exp\left(\sum_{r=1}^{\infty} a_r\,\kappa^r + \sum_{r=1}^{\infty} b_r\,\lambda^r\right). \end{aligned} \tag{2.275}$$

We need to expand the right side of this equation into double Taylor series in κ and λ. To expand the fraction in front of the exponential term, we notice that for any functions $f(\kappa)$ and $g(\lambda)$,

$$\frac{[f(\kappa) + g(0)][g(\lambda) + f(0)]}{-2[f(\kappa) + g(\lambda)]} = \frac{f(0) + g(0)}{-2}\,\frac{1}{1 - \frac{f(\kappa) - f(0)}{f(\kappa) + g(0)}\,\frac{g(\lambda) - g(0)}{g(\lambda) + f(0)}}$$

$$= \frac{f(0)+g(0)}{-2} \sum_{\nu=0}^{\infty} \left[\frac{f(\kappa)-f(0)}{f(\kappa)+g(0)} \frac{g(\lambda)-g(0)}{g(\lambda)+f(0)} \right]^{\nu}. \tag{2.276}$$

Thus, substituting

$$f(\kappa) = p(e^{\kappa}) = c_1 e^{\kappa/3} + c_1^* e^{-\kappa/3}, \quad g(\lambda) = q(e^{\lambda}) = c_1 e^{\lambda/3} + c_1^* e^{-\lambda/3}, \tag{2.277}$$

and noticing $f(0) = g(0) = -1$, we get

$$\begin{aligned} \frac{[p(e^{\kappa})-1][q(e^{\lambda})-1]}{-2[p(e^{\kappa})+q(e^{\lambda})]} &= \sum_{\nu=0}^{\infty} \left[\frac{f(\kappa)-f(0)}{f(\kappa)+g(0)} \frac{g(\lambda)-g(0)}{g(\lambda)+f(0)} \right]^{\nu} \\ &= \sum_{\nu=0}^{\infty} \left(-\frac{\kappa\lambda}{12} \right)^{\nu} \exp\left(\nu \ln \left[\frac{2\mathrm{i}\sqrt{3}}{\kappa} \tanh\frac{\kappa}{6} \tanh\left(\frac{\kappa}{6} + \frac{2\mathrm{i}\pi}{3} \right) \right] \right) \\ &\qquad \times \exp\left(\nu \ln \left[\frac{2\mathrm{i}\sqrt{3}}{\lambda} \tanh\frac{\lambda}{6} \tanh\left(\frac{\lambda}{6} + \frac{2\mathrm{i}\pi}{3} \right) \right] \right) \\ &= \sum_{\nu=0}^{\infty} \left(-\frac{\kappa\lambda}{12} \right)^{\nu} \exp\left(\nu \sum_{r=1}^{\infty} s_r \left(\kappa^r + \lambda^r \right) \right), \end{aligned} \tag{2.278}$$

where s_r are defined by (2.230) in Theorem 2.4. Regarding the first exponential term in Eq. (2.275), when functions $p(\cdot)$ and $q(\cdot)$ from Eqs. (2.272)–(2.273) are inserted, and after simple Taylor expansions, we find that this first exponential term reduces to

$$\exp\left(\sum_{r=1}^{\infty} \frac{\kappa^r}{r!} \frac{c_1 + (-1)^r c_1^*}{2 \cdot 3^r} \left[x + (-2)^{r-1} \mathrm{i}t \right] + \sum_{r=1}^{\infty} \frac{\lambda^r}{r!} \frac{c_1 + (-1)^r c_1^*}{2 \cdot 3^r} \left[x - (-2)^{r-1} \mathrm{i}t \right] \right).$$

The second exponential term in Eq. (2.275) does not need further treatment.

Combining all these results, Eq. (2.275) reduces to

$$\frac{1}{m} \mathcal{G}m|_{p=q=-1} = \sum_{\nu=0}^{\infty} \left(-\frac{\kappa\lambda}{12} \right)^{\nu} \exp\left(\sum_{r=1}^{\infty} \left(x_r^+ + \nu s_r \right) \kappa^r + \sum_{r=1}^{\infty} \left(x_r^- + \nu s_r \right) \lambda^r \right), \tag{2.279}$$

where

$$x_r^+ = \frac{e^{2i\pi/3} + (-1)^r e^{-2i\pi/3}}{2 \cdot 3^r \cdot r!} \left[x + (-2)^{r-1} it \right] + a_r, \qquad r \geq 1, \tag{2.280}$$

$$x_r^- = \frac{e^{2i\pi/3} + (-1)^r e^{-2i\pi/3}}{2 \cdot 3^r \cdot r!} \left[x - (-2)^{r-1} it \right] + b_r, \qquad r \geq 1. \tag{2.281}$$

Taking the coefficients of $\kappa^k \lambda^l$ on both sides of this equation and noticing $m|_{p=q=-1} = -2e^{-x}$, we get

$$m_{i,j} = -2e^{-x} \sum_{\nu=0}^{\min(k,l)} \left(-\frac{1}{12} \right)^{\nu} S_{k-\nu}\left(\boldsymbol{x}^+ + \nu \boldsymbol{s} \right) S_{l-\nu}\left(\boldsymbol{x}^- + \nu \boldsymbol{s} \right), \tag{2.282}$$

where $m_{i,j}$ is as defined in Eq. (2.264). The exponential term $-2e^{-x}$ in this $m_{i,j}$ eventually drops out after the τ function (2.263) with this matrix element is substituted into the variable transformation (2.262).

The τ function (2.263) with the above explicit $m_{i,j}$ elements has a structure that is identical to that of the τ function (2.69) for the NLS equation. Using the same techniques as those from Eqs. (2.71) to (2.74), we can show that even-indexed $x_{2r}^{\pm}$ elements of the $\boldsymbol{x}^{\pm}$ vectors do not contribute to the determinant of the τ function (2.226) and thus can be set to zero. Then, the above $\boldsymbol{x}^{\pm}$ vectors become $\left(x_1^{\pm}, 0, x_3^{\pm}, 0, \cdots \right)$ as in Theorem 2.4. As a consequence, this τ function contains only odd-indexed parameters a_{2r+1}, b_{2r+1}—there are no even-indexed parameters a_{2r}, b_{2r}.

Then, we have established that the Boussinesq equation (2.223) would admit rational solutions

$$u_N(x,t) = 2\partial_x^2 \ln \sigma, \tag{2.283}$$

where

$$\sigma(x,t) = \det_{1 \leq i,j \leq N} \left(\phi_{2i-1,2j-1} \right), \tag{2.284}$$

$$\phi_{i,j} = \sum_{\nu=0}^{\min(i,j)} \left(\frac{-1}{12} \right)^{\nu} S_{i-\nu}(\boldsymbol{x}^+ + \nu \boldsymbol{s})\, S_{j-\nu}(\boldsymbol{x}^- + \nu \boldsymbol{s}), \tag{2.285}$$

vectors $\boldsymbol{x}^{\pm}$ are as given in Theorem 2.4, and the vector $\boldsymbol{s} = (s_1, s_2, \cdots)$ is as defined by Eq. (2.230), if complex constants a_r, b_r are properly constrained so that the above σ function is real.

Now, we determine constraints between a_r and b_r so that σ is real. Notice that all s_{even} values are real, and all s_{odd} values are purely imaginary (see the note right below Theorem 2.4). Thus, if we constrain parameters a_{2r+1} and b_{2r+1} by

$$b_{2r+1} = -a_{2r+1}^*, \tag{2.286}$$

then

$$[(\boldsymbol{x}^+ + \nu \boldsymbol{s})_{odd}]^* = -(\boldsymbol{x}^- + \nu \boldsymbol{s})_{odd}, \quad [(\boldsymbol{x}^+ + \nu \boldsymbol{s})_{even}]^* = (\boldsymbol{x}^- + \nu \boldsymbol{s})_{even}, \tag{2.287}$$

where the subscripts 'odd' and 'even' represent the odd-indexed and even-indexed elements of the underlying vectors, respectively. Because of this,

$$\left[S_j(\boldsymbol{x}^+ + \nu \boldsymbol{s})\right]^* = (-1)^j S_j(\boldsymbol{x}^- + \nu \boldsymbol{s}). \tag{2.288}$$

Thus, we get from Eq. (2.285) that

$$\left[\phi_{i,j}\right]^* = (-1)^{i+j} \phi_{j,i}, \tag{2.289}$$

which leads to $\sigma^* = \sigma$. Thus, the reality condition is met, and the resulting function (2.283) then satisfies the Boussinesq equation (2.223).

Under the parameter constraint (2.286), the $\boldsymbol{x}^{\pm}$ vectors above become the same as those defined in Theorem 2.4. Thus, the function (2.225) of Theorem 2.4 is a rational solution of the Boussinesq equation. This function contains free parameters $a_1, a_3, \cdots, a_{2N-1}$. But a_1 can be removed by a shift of the (x, t) axes. Thus, irreducible free complex parameters are $a_3, \cdots, a_{2N-1}$.

Using the same techniques as those in Sect. 2.1.1 for the NLS equation, we can also show that these rational solutions (2.225) satisfy the boundary conditions (2.224) and are thus rogue waves. In addition, $\sigma(x, t) > 0$, and thus $u_N(x, t)$ is nonsingular. Theorem 2.4 is then proved.

Setting $N = 1$ in Theorem 2.4, we get the fundamental Boussinesq rogue wave

$$u_1(x, t) = 2\partial_x^2 \ln\left(x^2 + t^2 + 1\right) = \frac{4(1 - x^2 + t^2)}{1 + x^2 + t^2}. \tag{2.290}$$

This solution is plotted in the left panel of Fig. 2.4. It rises from the zero background with a single main hump and reaches the peak amplitude 4 and then decays to the zero background again.

Setting $N = 2$ in Theorem 2.4, we get the second-order Boussinesq rogue wave, whose expression is

$$u_2(x, t) = 2\partial_x^2 \ln\left[F_2(x, t)\right], \tag{2.291}$$

where

$$\begin{aligned} F_2(x, t) = {} & t^6 + 3t^4x^2 + 3t^2x^4 + x^6 + 8t^4x + 16t^2x^3 + 8x^5 + 11t^4 + \\ & 35x^4 + 62t^2x^2 + 120t^2x + 88x^3 + 131t^2 + 107x^2 + 48x + 73 + \\ & 144\Re(a_3)\left(\sqrt{3}t^3 - 3\sqrt{3}tx^2 - 8\sqrt{3}tx - 7\sqrt{3}t + 108\Re(a_3)\right) + \end{aligned}$$

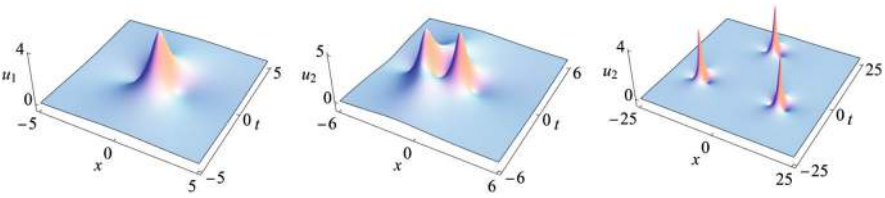

Fig. 2.4 Boussinesq rogue waves $u_N(x,t)$. Left: the fundamental rogue wave. Middle: a second-order rogue wave with $a_3 = 0$. Right: another second-order rogue wave with $a_3 = -30$

$$144\Im(a_3)\left(\sqrt{3}x^3 - 3\sqrt{3}t^2x - 4\sqrt{3}t^2 + 4\sqrt{3}x^2 + 5\sqrt{3}x + 108\Im(a_3)\right). \tag{2.292}$$

For two parameter values of $a_3 = 0$ and -30, this second-order rogue wave is displayed in the right two panels of Fig. 2.4. The $a_3 = 0$ solution exhibits two main humps, while the $a_3 = -30$ solution splits into a rogue triplet.

2.4 Complex Modified Korteweg-de Vries Equation

The complex modified Korteweg-de Vries (CMKdV) equation is

$$u_t + u_{xxx} + 6|u|^2 u_x = 0. \tag{2.293}$$

This equation governs transverse nonlinear waves in a one-dimensional lattice with elastic bonds under longitudinal stress (Gorbacheva and Ostrovsky 1983). In fiber optics, this equation can be gauge-transformed from the Hirota equation (Sasa and Satsuma 1991), which is a modified nonlinear Schrödinger equation for short pulse propagation that takes into account the third-order linear dispersion and self-steepening effects (Hasegawa and Kodama 1995; Agrawal 2001). The CMKdV equation belongs to the Ablowitz-Kaup-Newell-Segur (AKNS) integrable hierarchy (Yang 2010).

Rogue waves up to the third order in the CMKdV equation (2.293) have been derived by Darboux transformation in Zhaqilao (2013) and He et al. (2014). Rogue waves up to the second order in the Hirota equation have also been derived by Darboux transformation in Ankiewicz et al. (2010b). Here, we will derive general rogue waves in the CMKdV equation by the bilinear method.

The CMKdV equation (2.293) is invariant under the scaling of $u \to Au, x \to x/|A|$ and $t \to t/|A|^3$ for an arbitrary complex number A. Thus, we can normalize the background amplitude to unity and write the background as

$$u(x,t) \to e^{\mathrm{i}(\alpha x - \omega t)}, \quad x, t \to \pm\infty, \tag{2.294}$$

where α and ω are the background's wavenumber and frequency. Requiring this background to satisfy Eq. (2.293), we find that $\omega = 6\alpha - \alpha^3$. We seek rogue waves satisfying this boundary condition, i.e.,

$$u(x,t) \to e^{\mathrm{i}[\alpha(x-6t)+\alpha^3 t]}, \quad x,t \to \pm\infty. \tag{2.295}$$

Explicit expressions of general rogue waves in this CMKdV equation are given by the following theorem.

Theorem 2.5 *The complex modified KdV equation (2.293) under boundary conditions (2.295) admits rogue wave solutions of the following form*

$$u_N(x,t) = \frac{g_N(x,t)}{f_N(x,t)} e^{\mathrm{i}[\alpha(x-6t)+\alpha^3 t]}, \tag{2.296}$$

where N is the order of the rogue wave,

$$f_N = \sigma_0, \quad g_N = \sigma_1, \tag{2.297}$$

$$\sigma_k = \det_{1\le i,j\le N} \left(m^{(k)}_{2i-1,2j-1} \right), \tag{2.298}$$

the matrix elements in σ_k are defined by

$$m^{(k)}_{i,j} = \sum_{\nu=0}^{\min(i,j)} \frac{1}{4^\nu} S_{i-\nu}(\boldsymbol{x}^+(k) + \nu \boldsymbol{s})\, S_{j-\nu}(\boldsymbol{x}^-(k) + \nu \boldsymbol{s}), \tag{2.299}$$

vectors $\boldsymbol{x}^{\pm}(k) = \left(x_1^{\pm}, 0, x_3^{\pm}, 0, \cdots\right)$ are defined by

$$\left.\begin{array}{l} x_1^+ = (x-3t) - \beta_1 t + k, \quad x_1^- = (x-3t) - \beta_1^* t - k, \\ x_{2r+1}^+ = \frac{1}{(2r+1)!}(x-3t) - \beta_{2r+1} t + a_{2r+1}, \quad x_{2r+1}^- = (x_{2r+1}^+)^*, \quad r \ge 1, \end{array}\right\} \tag{2.300}$$

the vector $\boldsymbol{s} = (0, s_2, 0, s_4, \cdots)$ is defined by Eq. (2.11), β_r are coefficients from the expansion

$$\left(e^{\kappa} + \mathrm{i}\alpha\right)^3 - (1 + \mathrm{i}\alpha)^3 = \sum_{r=1}^{\infty} \beta_r \kappa^r, \tag{2.301}$$

and $a_3, a_5, \ldots, a_{2N-1}$ are free irreducible complex constants.

Proof We first perform a bilinear variable transformation,

$$u(x,t) = \frac{g(x,t)}{f(x,t)} e^{\mathrm{i}[\alpha(x-6t)+\alpha^3 t]}, \tag{2.302}$$

where f is a real function and g a complex one. Under this transformation, the CMKdV equation (2.293) can be converted to a system of bilinear equations

$$\left(D_x^2 + 2\right) f \cdot f = 2|g|^2, \tag{2.303}$$

$$\left(D_t + D_x^3 + 3\mathrm{i}\alpha D_x^2 + (6 - 3\alpha^2) D_x\right) g \cdot f = 0. \tag{2.304}$$

These two equations can be reduced from the following bilinear equations in the KP hierarchy

$$\left(D_r D_{x_1} - 2\right) \tau_k \cdot \tau_k = -2\tau_{k+1}\tau_{k-1}, \tag{2.305}$$

$$\left(D_{x_1}^2 - D_{x_2} + 2aD_{x_1}\right) \tau_{k+1} \cdot \tau_k = 0, \tag{2.306}$$

$$\left(D_{x_1}^3 + 3D_{x_1}D_{x_2} - 4D_{x_3} + 3a(D_{x_1}^2 + D_{x_2}) + 6a^2 D_{x_1}\right) \tau_{k+1} \cdot \tau_k = 0, \tag{2.307}$$

$$\left(D_r \left(D_{x_1}^2 - D_{x_2} + 2aD_{x_1}\right) - 4D_{x_1}\right) \tau_{k+1} \cdot \tau_k = 0, \tag{2.308}$$

under the dimensional reduction condition of

$$\left(\partial_{x_1} + \partial_r\right) \tau_k = C\tau_k. \tag{2.309}$$

where C is some constant. Indeed, under this dimension reduction, the KP-bilinear equations (2.305) and (2.308) become

$$\left(D_{x_1}^2 + 2\right) \tau_k \cdot \tau_k = 2\tau_{k+1}\tau_{k-1}, \tag{2.310}$$

$$\left(D_{x_1}^3 - D_{x_1}D_{x_2} + 2aD_{x_1}^2 + 4D_{x_1}\right) \tau_{k+1} \cdot \tau_k = 0. \tag{2.311}$$

Then, (2.307)+ 3× (2.311) + $(3a)$×(2.306) gives

$$\left[D_{x_1}^3 + (3a)D_{x_1}^2 + (3a^2 + 6)D_{x_1} - D_{x_3} - 3D_{x_1}\right] \tau_{k+1} \cdot \tau_k = 0. \tag{2.312}$$

The original bilinear system (2.303)–(2.304) can be obtained from Eqs. (2.310) and (2.312) by setting

$$f = \tau_0, \quad g = \tau_1, \quad h = \tau_{-1}, \tag{2.313}$$

$$x_1 = x - 3t, \quad x_3 = -t, \quad a = \mathrm{i}\alpha, \tag{2.314}$$

$x_2 = x_{-1} = 0$, and imposing the conjugation condition

$$\tau_{-k} = \tau_k^*. \tag{2.315}$$

We first construct solutions to the higher-dimensional bilinear system (2.305)–(2.308). Introducing functions $m_{i,j}^{(k)}$, $\varphi_i^{(k)}$ and $\psi_j^{(k)}$ of variables x_1, x_2, x_3 and r satisfying the following differential and difference relations

$$\left.\begin{aligned}
&\partial_{x_1} m_{i,j}^{(k)} = \varphi_i^{(k)} \psi_j^{(k)}, \\
&\partial_{x_1} \varphi_i^{(k)} = a\varphi_i^{(k)} + \varphi_i^{(k+1)}, \quad \partial_{x_1} \psi_j^{(k)} = -a\psi_j^{(k)} - \psi_j^{(k-1)}, \\
&\partial_{x_n} \varphi_j^{(k)} = \partial_{x_1}^n \varphi_j^{(k)}, \ \partial_{x_n} \psi_j^{(k)} = (-1)^{n-1} \partial_{x_1}^n \psi_j^{(k)}, \ (n = 2, 3), \\
&\partial_r \varphi_i^{(k)} = \varphi_i^{(k-1)}, \ \partial_r \psi_j^{(k)} = -\psi_j^{(k+1)},
\end{aligned}\right\} \tag{2.316}$$

$$\left.\begin{aligned}
&\partial_{x_2} m_{i,j}^{(k)} = \varphi_i^{(k+1)} \psi_j^{(k)} + \varphi_i^{(k)} \psi_j^{(k-1)} + 2a\varphi_i^{(k)} \psi_j^{(k)}, \\
&\partial_{x_3} m_{i,j}^{(k)} = \varphi_i^{(k+2)} \psi_j^{(k)} + 3a\varphi_i^{(k+1)} \psi_j^{(k)} + \varphi_i^{(k+1)} \psi_j^{(k-1)} + \\
&\qquad +3a^2 \varphi_i^{(k)} \psi_j^{(k)} + 3a\varphi_i^{(k+1)} \psi_j^{(k-1)} + \varphi_i^{(k)} \psi_j^{(k-2)}, \\
&\partial_r m_{i,j}^{(k)} = -\varphi_i^{(k-1)} \psi_j^{(k+1)}, \\
&m_{i,j}^{(k+1)} = m_{i,j}^{(k)} + \varphi_i^{(k)} \psi_j^{(k+1)},
\end{aligned}\right\} \tag{2.317}$$

where a is an arbitrary complex constant, then the τ function

$$\tau_k = \det_{1 \le \mu, \nu \le N} \left(m_{i_\mu, j_\nu}^{(k)} \right) \tag{2.318}$$

for an arbitrary sequence of indices $(i_1, i_2, \cdots, i_N; j_1, j_2, \cdots, j_N)$ would satisfy the higher-dimensional bilinear equations (2.305)–(2.308). This result is a special case of that reported in Feng et al. (2022b). Again, the former differential and difference relations (2.316) imply the x_1 derivatives of the latter differential and difference relations (2.317) are automatically valid, but not (2.317) themselves.

To get rational solutions, we define matrix elements in the τ function (2.318) as

$$m_{i,j}^{(k)} = \mathcal{A}_i \mathcal{B}_j m^{(k)}, \quad \varphi_i^{(k)} = \mathcal{A}_i \varphi^{(k)}, \quad \psi_j^{(k)} = \mathcal{B}_j \psi^{(k)}, \tag{2.319}$$

where

$$m^{(k)} = \frac{1}{p+q} \left(-\frac{p-a}{q+a} \right)^k e^{\xi(p) + \eta(q)}, \tag{2.320}$$

$$\varphi^{(k)} = (p-a)^k e^{\xi(p)}, \quad \psi^{(k)} = [-(q+a)]^{-k} e^{\eta(q)}, \tag{2.321}$$

$$\xi(p) = px_1 + p^2 x_2 + p^3 x_3 + \frac{1}{p-a} r + \xi_0(p), \tag{2.322}$$

$$\eta(q) = qx_1 - q^2x_2 + q^3x_3 + \frac{1}{q+a}r + \eta_0(q), \tag{2.323}$$

$$\mathcal{A}_i = \frac{1}{i!}\left[(p-a)\partial_p\right]^i, \quad \mathcal{B}_j = \frac{1}{j!}\left[(q+a)\partial_q\right]^j, \tag{2.324}$$

and $\xi_0(p)$, $\eta_0(q)$ are arbitrary functions. It is easy to see that these $m_{i,j}^{(k)}$, $\varphi_i^{(k)}$ and $\psi_j^{(k)}$ functions satisfy the differential and difference relations (2.316) and (2.317), and thus the corresponding τ_k function (2.318) satisfies the higher-dimensional bilinear equations (2.305)–(2.308).

Next, we consider the dimension reduction condition (2.309). Denoting $\hat{p} \equiv p - a$ and $\hat{q} \equiv q + a$, then $\mathcal{A}_i$ and $\mathcal{B}_j$ can be rewritten as

$$\mathcal{A}_i = \frac{1}{i!}\left(\hat{p}\partial_{\hat{p}}\right)^i, \quad \mathcal{B}_j = \frac{1}{j!}\left(\hat{q}\partial_{\hat{q}}\right)^j, \tag{2.325}$$

and

$$(\partial_{x_1}+\partial_r)m_{i,j}^{(k)} = \mathcal{A}_i\mathcal{B}_j(\partial_{x_1}+\partial_r)m^{(k)} = \mathcal{A}_i\mathcal{B}_j\left[\hat{p} + \frac{1}{\hat{p}} + \hat{q} + \frac{1}{\hat{q}}\right]m^{(k)}. \tag{2.326}$$

Using the Leibnitz rule as in Sect. 2.1.1, the above equation reduces to

$$(\partial_{x_1} + \partial_r)m_{i,j}^{(k)} = \sum_{\mu=0}^{i}\frac{1}{\mu!}\left(\hat{p} + \frac{(-1)^\mu}{\hat{p}}\right)m_{i-\mu,j}^{(k)} + \sum_{l=0}^{j}\frac{1}{l!}\left(\hat{q} + \frac{(-1)^l}{\hat{q}}\right)m_{i,j-l}^{(k)}. \tag{2.327}$$

Then, when we take $\hat{p} = \hat{q} = 1$, the above equation gives the contiguity relation

$$(\partial_{x_1} + \partial_r)\, m_{i,j}^{(k)}\Big|_{\hat{p}=\hat{q}=1} = 2\sum_{\substack{l=0\\ l:\text{even}}}^{i}\frac{1}{l!}\, m_{i-l,j}^{(k)}\Big|_{\hat{p}=\hat{q}=1} + 2\sum_{\substack{l=0\\ l:\text{even}}}^{j}\frac{1}{l!}\, m_{i,j-l}^{(k)}\Big|_{\hat{p}=\hat{q}=1}. \tag{2.328}$$

Utilizing this relation and repeating the same algebra as in Sect. 2.1.1, we find that when we restrict the general determinant (2.318) to

$$\tau_k = \det_{1\le i,j\le N}\left(m_{2i-1,2j-1}^{(k)}\Big|_{\hat{p}=\hat{q}=1}\right), \tag{2.329}$$

then

$$(\partial_{x_1} + \partial_r)\tau_k = 4N\,\tau_k. \tag{2.330}$$

Thus, the dimension reduction condition (2.309) is satisfied.

Now, we introduce free parameters in the determinant (2.329). As before, we introduce them through $\xi_0(p)$ and $\eta_0(q)$ of Eqs. (2.322)–(2.323) as

$$\xi_0(p) = \sum_{r=1}^{\infty} a_r \ln^r \hat{p}, \quad \eta_0(q) = \sum_{r=1}^{\infty} b_r \ln^r \hat{q}, \tag{2.331}$$

where a_r, b_r are complex constants.

Regarding the conjugation condition (2.315), it can be satisfied when we take (x_1, x_3, a) as in Eq. (2.314) and constrain $b_r = a_r^*$. Indeed, in this case, $[m_{i,j}^{(k)}]^* = m_{j,i}^{(k)}$ when evaluated at $\hat{p} = \hat{q} = 1$. Thus, $\tau_k^* = \tau_k$.

The above results can be summarized in the following lemma.

Lemma 2.7 *The complex modified KdV equation (2.293) under boundary conditions (2.295) admits rational rogue wave solutions of the following form*

$$u_N(x,t) = \frac{g_N(x,t)}{f_N(x,t)} e^{\mathrm{i}[\alpha(x-6t)+\alpha^3 t]}, \tag{2.332}$$

where N is the order of the rogue wave,

$$f_N = \sigma_0, \quad g_N = \sigma_1, \tag{2.333}$$

$$\sigma_k = \det_{1\le i,j\le N} \left(m_{2i-1,2j-1}^{(k)} \right), \tag{2.334}$$

the matrix elements in σ_k are defined by

$$m_{i,j}^{(k)} = \frac{(\hat{p}\partial_{\hat{p}})^i}{i!} \frac{(\hat{q}\partial_{\hat{q}})^j}{j!} m^{(k)} \Big|_{\hat{p}=\hat{q}=1}, \tag{2.335}$$

$$m^{(k)} = \frac{1}{\hat{p}+\hat{q}} \left(-\frac{\hat{p}}{\hat{q}} \right)^k e^{\xi(\hat{p})+\eta(\hat{q})}, \tag{2.336}$$

$$\xi(\hat{p}) = (\hat{p}+\mathrm{i}\alpha)(x-3t) - (\hat{p}+\mathrm{i}\alpha)^3 t + \sum_{r=1}^{\infty} \hat{a}_r \ln^r \hat{p}, \tag{2.337}$$

$$\eta(\hat{q}) = (\hat{q}-\mathrm{i}\alpha)(x-3t) - (\hat{q}-\mathrm{i}\alpha)^3 t + \sum_{r=1}^{\infty} \hat{a}_r^* \ln^r \hat{q}, \tag{2.338}$$

and $\hat{a}_1, \hat{a}_2, \hat{a}_3, \ldots$ are free complex constants.

Lastly, we remove the differential operators in the matrix elements and derive more explicit expressions of rogue waves through Schur polynomials. This derivation is similar to that for the generalized derivative NLS equations in Sect. 2.2, and the resulting expressions are as given in Theorem 2.5, where parameters a_r are linearly related to $\hat{a}_r$ in the above lemma. This derivation would be a bit simpler if we introduce a factor of $(\hat{p}+1)(\hat{q}+1)$ into Eq. (2.336), in which case this derivation would closely resemble that for the NLS equation in Sect. 2.1.1, and parameters a_r in Theorem 2.5 would be identical to $\hat{a}_r$ in the above lemma. Using the same techniques as in Sect. 2.1.1, we can also set $x_{2r}^{\pm}=0$ in the resulting Schur polynomial expressions. Furthermore, the parameter a_1 can be normalized to zero through a shift of the (x,t) axes. Following these maneuvers, explicit rogue wave expressions as presented in Theorem 2.5 for the CMKdV equation would be derived. This completes the proof of Theorem 2.5.

The fundamental rogue wave can be obtained from the above theorem by setting $N=1$, and we get

$$u_1(x,t)=\left(1+\frac{12\mathrm{i}\alpha t-1}{x^2+9\left(\alpha^4+4\right)t^2+6\left(\alpha^2-2\right)tx+\frac{1}{4}}\right)e^{\mathrm{i}[\alpha(x-6t)+\alpha^3 t]}. \tag{2.339}$$

This rogue wave reaches peak amplitude of 3 at $x=t=0$. Its graph for $\alpha=1$ is plotted in the left column of Fig. 2.5.

Second-order rogue waves can be obtained from Theorem 2.5 by setting $N=2$. These rogue waves contain a free complex parameter a_3, as well as the background wavenumber α. For $\alpha=1$ and two a_3 values of 0 and $30+30\mathrm{i}$, the resulting two second-order rogue waves are plotted in the middle and right columns of Fig. 2.5,

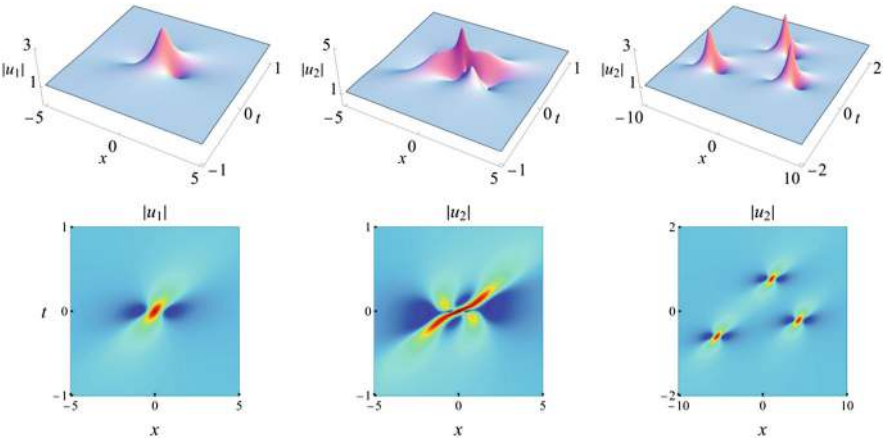

Fig. 2.5 Rogue waves in the complex modified KdV equation (2.293) for $\alpha=1$. Left column: the fundamental rogue wave $|u_1(x,t)|$ in Eq. (2.339). Middle and right columns: second-order rogue waves $|u_2(x,t;a_3)|$ with $a_3=0$ and $30+30\mathrm{i}$, respectively. Upper row: 3D plots. Lower row: density plots

respectively. In the former case, this rogue wave reaches a peak amplitude of 5 at $(x, t) = (0, 0)$. In the latter case, it splits into three fundamental rogue waves as a rogue triplet.

2.5 Complex Short Pulse Equation

The complex short pulse (CSP) equation

$$u_{xt} + u + \frac{1}{2}\left(|u|^2 u_x\right)_x = 0 \tag{2.340}$$

was proposed by Feng (2015) as a model equation to describe ultra-short pulse propagation in optical fibers. Here, $u = u(x, t)$ is a complex-valued function. Since this equation is invariant under the scaling of $u \to Au, x \to |A|x$ and $t \to t/|A|$ for an arbitrary complex number A, we can normalize the background amplitude to unity and thus write the background as

$$u(x, t) \to e^{\mathrm{i}(\kappa x - \omega t)}, \quad x, t \to \pm\infty, \tag{2.341}$$

where κ and ω are the background's wavenumber and frequency. Requiring this background to satisfy Eq. (2.340), we find that $\omega = \kappa/2 - 1/\kappa$.

Rogue waves in the CSP equation (2.340) have been derived by Feng et al. (2022a) using the bilinear method. Here, we follow that paper but with some modifications in the solution expressions.

General rogue waves in the CSP equation are given by the following theorem.

Theorem 2.6 *The complex short pulse equation (2.340) under boundary conditions (2.341) admits rogue wave solutions*

$$u_N(x, t) = \frac{g_N(y, z)}{f_N(y, z)} \exp[\mathrm{i}(y - \frac{1}{\kappa}z)], \tag{2.342}$$

where coordinates (x, t) are related to new coordinates (y, z) through the hodograph transformation

$$x = \frac{1}{\kappa}y - \frac{1}{2}z - 2(\ln f_N)_z, \quad t = -z, \tag{2.343}$$

N is the order of the rogue wave,

$$f_N = \sigma_0, \quad g_N = \sigma_1, \tag{2.344}$$

$$\sigma_n = \det_{1 \le i, j \le N}\left(m^{(n)}_{2i-1, 2j-1}\right), \tag{2.345}$$

$f_N > 0$, the matrix elements in σ_n are given by

$$m_{i,j}^{(n)} = \sum_{\nu=0}^{\min(i,j)} \frac{1}{4^\nu} S_{i-\nu}(\boldsymbol{x}^+(n) + \nu \boldsymbol{s})\, S_{j-\nu}(\boldsymbol{x}^-(n) + \nu \boldsymbol{s}), \tag{2.346}$$

vectors $\boldsymbol{x}^\pm(n) = \left(x_1^\pm, 0, x_3^\pm, 0, \cdots\right)$ are defined by

$$x_1^\pm(n) = \frac{1}{2} z - \frac{\alpha}{(1 \mp \mathrm{i}\alpha)^2} y \pm n, \tag{2.347}$$

$$x_{2r+1}^+ = \beta_{2r+1} z + \gamma_{2r+1} y + a_{2r+1}, \quad x_{2r+1}^- = (x_{2r+1}^+)^*, \tag{2.348}$$

$\beta_r \equiv 1/(2r!)$, γ_r are coefficients from the expansion

$$\frac{\alpha}{e^\lambda - \mathrm{i}\alpha} - \frac{\alpha}{1 - \mathrm{i}\alpha} = \sum_{r=1}^{\infty} \gamma_r \lambda^r, \tag{2.349}$$

the parameter α is related to the background wavenumber κ through $\kappa = 2\alpha/(\alpha^2 - 1)$, the vector $\boldsymbol{s} = (0, s_2, 0, s_4, \cdots)$ is defined in Eq. (2.11), and $a_3, a_5, a_7, \ldots, a_{2N-1}$ are free irreducible complex parameters.

Proof Through a variable transformation

$$u(x,t) = \frac{g(y,z)}{f(y,z)} \exp[\mathrm{i}(y - \frac{1}{\kappa} z)], \tag{2.350}$$

along with the hodograph transformation

$$x = \frac{1}{\kappa} y - \frac{1}{2} z - 2(\ln f)_z, \quad t = -z, \tag{2.351}$$

where $f > 0$ and g is a complex function, the CSP equation (2.340) can be converted into the bilinear form

$$\left.\begin{array}{l} \left(D_y D_z + \mathrm{i} D_z - \frac{1}{\kappa}\mathrm{i} D_y\right) g \cdot f = 0, \\ \left(2D_z^2 + 1\right) f \cdot f = |g|^2. \end{array}\right\} \tag{2.352}$$

To derive rogue wave solutions, we first consider a higher-dimensional generalization of the above bilinear equations,

$$\left.\begin{aligned}
&\left(D_{x_1}D_{x_{-1}}-2\right)\tau_{n,k,l}\cdot\tau_{n,k,l}=-2\tau_{n+1,k,l}\tau_{n-1,k,l},\\
&\left(aD_r-1\right)\tau_{n+1,k,l}\cdot\tau_{n,k,l}=-\tau_{n+1,k-1,l}\tau_{n,k+1,l},\\
&\left(D_{x_1}\left(aD_r-1\right)-2a\right)\tau_{n+1,k,l}\cdot\tau_{n,k,l}=\left(D_{x_1}-2a\right)\tau_{n+1,k-1,l}\tau_{n,k+1,l},\\
&\left(D_{x_1}\left(bD_s-1\right)-2b\right)\tau_{n+1,k,l}\cdot\tau_{n,k,l}=\left(D_{x_1}-2b\right)\tau_{n+1,k,l-1}\tau_{n,k,l+1},
\end{aligned}\right\} \tag{2.353}$$

where x_1, x_{-1}, r, s are four independent variables, and a, b are complex constants. We will construct a large class of rational solutions to this system. Then, we restrict those solutions so that they satisfy the dimensional reduction conditions

$$\left[\partial_{x_1}+\partial_{x_{-1}}\right]\tau_{n,k,l}=C_1\tau_{n,k,l}, \tag{2.354}$$

$$\left[a^2\partial_r-\partial_s\right]\tau_{n,k,l}=C_2\tau_{n,k,l}, \tag{2.355}$$

and the index-reduction condition

$$\tau_{n-1,k+1,l+1}=C_3\tau_{n,k,l}, \tag{2.356}$$

where C_1, C_2, C_3 are certain constants. In this case, the first bilinear equation in (2.353) under the condition (2.354) becomes

$$\left(D_{x_1}^2+2\right)\tau_{n,k,l}\cdot\tau_{n,k,l}=2\tau_{n+1,k,l}\tau_{n-1,k,l}. \tag{2.357}$$

In addition, by letting $b=1/a$, the fourth bilinear equation in (2.353) under conditions (2.355)–(2.356) becomes

$$\left(D_{x_1}\left(aD_r-1\right)-\frac{2}{a}\right)\tau_{n+1,k,l}\cdot\tau_{n,k,l}=-\left(D_{x_1}+\frac{2}{a}\right)\tau_{n+1,k-1,l}\tau_{n,k+1,l}. \tag{2.358}$$

Adding this equation to the third equation of (2.353) and utilizing the second equation of (2.353), we get

$$\left(D_{x_1}\left(aD_r-1\right)-a-\frac{1}{a}\right)\tau_{n+1,k,l}\cdot\tau_{n,k,l}=\left(a+\frac{1}{a}\right)\left(aD_r-1\right)\tau_{n+1,k,l}\cdot\tau_{n,k,l}, \tag{2.359}$$

which simplifies to

$$\left(aD_{x_1}D_r-D_{x_1}-\left(a^2+1\right)D_r\right)\tau_{n+1,k,l}\cdot\tau_{n,k,l}=0. \tag{2.360}$$

Now, we define

$$f = \tau_{0,0,0}, \quad g = \tau_{1,0,0}, \quad h = \tau_{-1,0,0}. \tag{2.361}$$

Then, Eqs. (2.357) and (2.360) would become

$$\left.\begin{aligned} &\left(aD_{x_1}D_r - D_{x_1} - (a^2+1)D_r\right) g \cdot f = 0, \\ &\left(D_{x_1}^2 + 2\right) f \cdot f = 2gh. \end{aligned}\right\} \tag{2.362}$$

Finally, we impose the complex conjugate condition

$$\tau_{n,0,0}^* = \tau_{-n,0,0}, \tag{2.363}$$

which yields f real and $h = g^*$. In addition, we set

$$x_1 = \frac{1}{2}z, \quad r = \alpha y, \quad a = \mathrm{i}\alpha, \quad \kappa = \frac{2\alpha}{\alpha^2 - 1}, \tag{2.364}$$

where α is a real constant determined by the background wavenumber κ. Then, the above bilinear equations (2.362) would become those of the CSP equation in Eq. (2.352), and the corresponding solutions (2.350) would give rogue waves of the CSP equation.

Next, we execute the above plan.

(a) Gram determinant solution for the higher-dimensional system

First, we present Gram determinant solutions for the higher-dimensional bilinear system (2.353).

Lemma 2.8 *Let $m_{i,j}^{(n,k,l)}$, $\varphi_i^{(n,k,l)}$ and $\psi_j^{(n,k,l)}$ be functions of x_1, x_{-1}, r and s satisfying the following differential and difference relations,*

$$\left.\begin{aligned} &\partial_{x_1} m_{i,j}^{(n,k,l)} = \varphi_i^{(n,k,l)} \psi_j^{(n,k,l)}, \\ &\partial_{x_1} \varphi_i^{(n,k,l)} = \varphi_i^{(n+1,k,l)}, \quad \partial_{x_{-1}} \varphi_i^{(n,k,l)} = \varphi_i^{(n-1,k,l)}, \\ &\partial_r \varphi_i^{(n,k,l)} = \varphi_i^{(n,k-1,l)}, \quad \partial_s \varphi_i^{(n,k,l)} = \varphi_i^{(n,k,l-1)}, \\ &\varphi_i^{(n,k+1,l)} = \varphi_i^{(n+1,k,l)} - a\varphi_i^{(n,k,l)}, \quad \varphi_i^{(n,k,l+1)} = \varphi_i^{(n+1,k,l)} - b\varphi_i^{(n,k,l)}, \\ &\partial_{x_1} \psi_j^{(n,k,l)} = -\psi_j^{(n-1,k,l)}, \quad \partial_{x_{-1}} \psi_j^{(n,k,l)} = -\psi_j^{(n+1,k,l)}, \\ &\partial_r \psi_j^{(n,k,l)} = -\psi_j^{(n,k+1,l)}, \quad \partial_s \psi_j^{(n,k,l)} = -\psi_j^{(n,k,l+1)}, \\ &\psi_j^{(n,k-1,l)} = \psi_j^{(n-1,k,l)} - a\psi_j^{(n,k,l)}, \quad \psi_j^{(n,k,l-1)} = \psi_j^{(n-1,k,l)} - b\psi_j^{(n,k,l)}. \end{aligned}\right\} \tag{2.365}$$

Then the determinant

$$\tau_{n,k,l} = \det_{1 \le i,j \le N} \left(m_{i,j}^{(n,k,l)} \right) \tag{2.366}$$

would satisfy the higher-dimensional bilinear system (2.353).

The proof of this lemma is along the lines of the proof of Lemma 2.1 in Sect. 2.1.1; see Feng et al. (2022a) for details (note that the last two equations of (2.365) in Feng et al. (2022a) have typos in the signs in front of the a and b coefficients which we have corrected here).

(b) Dimensional and index reductions

Next we derive algebraic solutions satisfying both the higher-dimensional bilinear equations (2.353), the dimension reduction conditions (2.354)–(2.355), and the index reduction condition (2.356), hence satisfying the (1+1)-dimensional system (2.362). These solutions are obtained by choosing the matrix elements appropriately in the Gram determinant solution in Lemma 2.8.

Lemma 2.9 *We define matrix elements* $m_{i,j}^{(n,k,l)}$ *by*

$$m_{i,j}^{(n,k,l)} = \mathcal{A}_i \mathcal{B}_j m^{(n,k,l)}\Big|_{p=q=1}, \tag{2.367}$$

where

$$\mathcal{A}_i = \frac{1}{i!}\left(p\partial_p\right)^i, \quad \mathcal{B}_j = \frac{1}{j!}\left(q\partial_q\right)^j, \tag{2.368}$$

$$m^{(n,k,l)} = \frac{1}{p+q}\left(-\frac{p}{q}\right)^n \left(-\frac{p-a}{q+a}\right)^k \left(-\frac{p-b}{q+b}\right)^l e^{\xi(p)+\eta(q)}, \tag{2.369}$$

$$\xi(p) = \frac{1}{p}x_{-1} + px_1 + \frac{1}{p-a}r + \frac{1}{p-b}s + \xi_0(p), \tag{2.370}$$

$$\eta(q) = \frac{1}{q}x_{-1} + qx_1 + \frac{1}{q+a}r + \frac{1}{q+b}s + \eta_0(q), \tag{2.371}$$

$b = 1/a$, *and* $\xi_0(p)$, $\eta_0(q)$ *are arbitrary functions of* p, q, *respectively. Then the determinant*

$$\tau_{n,k,l} = \det_{1\le i,j\le N}\left(m_{2i-1,2j-1}^{(n,k,l)}\right) \tag{2.372}$$

would satisfy the bilinear system

$$\left.\begin{aligned} &\left(aD_{x_1}D_r - D_{x_1} - (a^2+1)D_r\right)\tau_{n+1,k,l}\cdot\tau_{n,k,l} = 0,\\ &\left(D_{x_1}^2 + 2\right)\tau_{n,k,l}\cdot\tau_{n,k,l} = 2\tau_{n+1,k,l}\tau_{n-1,k,l}. \end{aligned}\right\} \tag{2.373}$$

Proof It is easy to see that the $m^{(n,k,l)}$ function in (2.369), together with its corresponding $\varphi^{(n,k,l)}$ and $\psi^{(n,k,l)}$ functions, satisfy the differential and difference system (2.365) without indices i and j. Then, since operators $\mathcal{A}_i$ and $\mathcal{B}_j$ commute with differentials ∂_{x_1}, $\partial_{x_{-1}}$, ∂_r and ∂_s, then $\mathcal{A}_i\mathcal{B}_j m^{(n,k,l)}$, with its corresponding $\varphi_i^{(n,k,l)}$ and $\psi_j^{(n,k,l)}$ functions, satisfy the differential and difference system (2.365).

Thus, from Lemma 2.8, we know that for an arbitrary sequence of indices $(i_1, i_2, \cdots, i_N; j_1, j_2, \cdots, j_N)$, the determinant

$$\tau_{n,k,l} = \det_{1\le\nu,\mu\le N}\left(m^{(n,k,l)}_{i_\nu, j_\mu}\right) \tag{2.374}$$

satisfies the higher-dimensional bilinear system (2.353).

Next, we consider dimension reduction conditions (2.354)–(2.355). Introducing linear differential operators $\mathcal{L}_1$ and $\mathcal{L}_2$ as

$$\mathcal{L}_1 = \partial_{x_1} + \partial_{x_{-1}}, \quad \mathcal{L}_2 = a^2\partial_r - \partial_s, \tag{2.375}$$

then we have

$$\mathcal{L}_1 m^{(n,k,l)}_{i,j} = \mathcal{A}_i\mathcal{B}_j\mathcal{L}_1 m^{(n,k,l)} = \mathcal{A}_i\mathcal{B}_j\left[Q_{11}(p) + Q_{12}(q)\right] m^{(n,k,l)}, \tag{2.376}$$

and

$$\mathcal{L}_2 m^{(n,k,l)}_{i,j} = \mathcal{A}_i\mathcal{B}_j\mathcal{L}_1 m^{(n,k,l)} = \mathcal{A}_i\mathcal{B}_j\left[Q_{21}(p) + Q_{22}(q)\right] m^{(n,k,l)}, \tag{2.377}$$

where

$$Q_{11}(p) = p + \frac{1}{p}, \quad Q_{12}(q) = q + \frac{1}{q}. \tag{2.378}$$

$$Q_{21}(p) = \frac{a^2}{p-a} - \frac{1}{p-b}, \quad Q_{22}(q) = \frac{a^2}{q+a} - \frac{1}{q+b}, \tag{2.379}$$

and $b = 1/a$.

We select p_0 and q_0 values to be roots of the following algebraic equations

$$Q'_{11}(p) = 0, \quad Q'_{12}(q) = 0. \tag{2.380}$$

These equations have simple roots ± 1. Without loss of generality, we take

$$p_0 = 1, \quad q_0 = 1. \tag{2.381}$$

Importantly, one can verify that these p_0 and q_0 are simple roots of equations $Q'_{21}(p) = 0$ and $Q'_{22}(q) = 0$ as well, i.e.,

$$Q'_{21}(p_0) = 0, \quad Q'_{22}(q_0) = 0. \tag{2.382}$$

This fact guarantees that both dimension reduction conditions (2.354) and (2.355) will be satisfied simultaneously. A general proof for this using the Faà di Bruno formula can be found in Feng et al. (2022a), and we will use that general proof to

handle a similar situation in the massive Thirring model in Sect. 2.12. Below, we will provide a simpler but less general proof for the simultaneous satisfaction of both dimension reduction conditions (2.354)–(2.355).

Regarding the first dimension reduction condition (2.354), using the Leibnitz rule, we have the operator relation

$$\mathcal{A}_i Q_{11}(p) = \sum_{l=0}^{i} \frac{1}{l!} \left[(p\partial_p)^l Q_{11}(p) \right] \mathcal{A}_{i-l} = \sum_{l=0}^{i} \frac{1}{l!} \left(p + \frac{(-1)^l}{p} \right) \mathcal{A}_{i-l}. \tag{2.383}$$

This relation is the same as that we encountered in Sect. 2.1.1 for the NLS equation. Using this relation and a similar one for $\mathcal{B}_j Q_{12}(q)$, and following similar steps as in Sect. 2.1.1, we get

$$\mathcal{L}_1 m_{i,j}^{(n,k,l)} = \sum_{l=0}^{i} \frac{1}{l!} \left(p + \frac{(-1)^l}{p} \right) m_{i-l,j}^{(n,k,l)} + \sum_{l=0}^{j} \frac{1}{l!} \left(q + \frac{(-1)^l}{q} \right) m_{i,j-l}^{(n,k,l)}. \tag{2.384}$$

Evaluating this relation at $p = q = 1$, we arrive at the first contiguity relation

$$\mathcal{L}_1 \, m_{i,j}^{(n,k,l)} \Big|_{p=q=1} = 2 \sum_{\substack{l=0 \\ l:\text{even}}}^{i} \frac{1}{l!} \, m_{i-l,j}^{(n,k,l)} \Big|_{p=q=1} + 2 \sum_{\substack{l=0 \\ l:\text{even}}}^{j} \frac{1}{l!} \, m_{i,j-l}^{(n,k,l)} \Big|_{p=q=1}. \tag{2.385}$$

Regarding the second dimension reduction condition (2.355), using the Leibnitz rule, we have the operator relation

$$\mathcal{A}_i Q_{21}(p) = \sum_{l=0}^{i} \frac{1}{l!} \left[(p\partial_p)^l Q_{21}(p) \right] \mathcal{A}_{i-l}. \tag{2.386}$$

A similar relation can be written for $\mathcal{B}_j Q_{22}(q)$. Thus,

$$\mathcal{L}_2 m_{i,j}^{(n,k,l)} = \sum_{l=0}^{i} \frac{1}{l!} \left[(p\partial_p)^l Q_{21}(p) \right] m_{i-l,j}^{(n,k,l)} + \sum_{l=0}^{j} \frac{1}{l!} \left[(q\partial_q)^l Q_{22}(q) \right] m_{i,j-l}^{(n,k,l)}. \tag{2.387}$$

Notice that

$$(p\partial_p)^l Q_{21}(p) = \partial_{\ln p}^l Q_{21}(p) = \partial_\epsilon^l Q_{21}(e^\epsilon) \Big|_{\epsilon = \ln p}. \tag{2.388}$$

Then, defining

$$\zeta_l \equiv (p\partial_p)^l Q_{21}(p)\Big|_{p=1}, \tag{2.389}$$

we see that

$$\zeta_l = \partial_\epsilon^l Q_{21}(e^\epsilon)\Big|_{\epsilon=0}. \tag{2.390}$$

But

$$Q_{21}(e^\epsilon) = \frac{a^2}{e^\epsilon - a} - \frac{1}{e^\epsilon - a^{-1}} = \frac{a(1-a^2)}{\left(e^{\epsilon/2} - a\,e^{-\epsilon/2}\right)\left(e^{-\epsilon/2} - a\,e^{\epsilon/2}\right)} \tag{2.391}$$

is an even function of ϵ. Thus, $\zeta_l = 0$ when the index l is odd. Similarly, defining

$$\theta_l \equiv (q\partial_q)^l Q_{22}(q)\Big|_{q=1}, \tag{2.392}$$

we can show that $\theta_l = 0$ when its index l is odd as well. Then, evaluating Eq. (2.387) at $p = q = 1$, we get the second contiguity relation

$$\mathcal{L}_2\, m_{i,j}^{(n,k,l)}\Big|_{p=q=1} = \sum_{\substack{l=0\\ l:\text{even}}}^{i} \frac{\zeta_l}{l!}\, m_{i-l,j}^{(n,k,l)}\Big|_{p=q=1} + \sum_{\substack{l=0\\ l:\text{even}}}^{j} \frac{\theta_l}{l!}\, m_{i,j-l}^{(n,k,l)}\Big|_{p=q=1}. \tag{2.393}$$

Both contiguity relations (2.385) and (2.393) relate matrix elements with indices shifted by even numbers. Then, if we restrict the general τ solutions (2.366) as

$$\tau_{n,k,l} = \det_{1\le i,j\le N}\left(m_{2i-1,2j-1}^{(n,k,l)}\Big|_{p=q=1}\right), \tag{2.394}$$

then for the same reasons as explained in Sect. 2.1.1, we will find that

$$\mathcal{L}_1\tau_{n,k,l} = 4N\,\tau_{n,k,l}, \quad \mathcal{L}_2\tau_{n,k,l} = (\zeta_0+\theta_0)N\,\tau_{n,k,l}, \tag{2.395}$$

or equivalently,

$$\mathcal{L}_1\tau_{n,k,l} = [Q_{11}(p_0) + Q_{12}(q_0)]\,N\,\tau_{n,k,l}, \tag{2.396}$$

$$\mathcal{L}_2\tau_{n,k,l} = [Q_{21}(p_0) + Q_{22}(q_0)]\,N\,\tau_{n,k,l}. \tag{2.397}$$

So both dimensional reduction conditions (2.354)–(2.355) are satisfied simultaneously.

Next, we consider the index-reduction condition (2.356). We start with

$$m_{i,j}^{(n-1,k+1,l+1)} = \mathcal{A}_i \mathcal{B}_j m^{(n-1,k+1,l+1)} = \mathcal{A}_i \mathcal{B}_j \left[\mathcal{H}_1(p)\mathcal{H}_2(q)\right] m^{(n,k,l)}, \tag{2.398}$$

where

$$\mathcal{H}_1(p) = \frac{(p-a)(p-b)}{p}, \quad \mathcal{H}_2(q) = \frac{-q}{(q+b)(q+a)}. \tag{2.399}$$

Applying the Leibnitz rule and following similar calculations as above, we have

$$m_{i,j}^{(n-1,k+1,l+1)}\Big|_{p=q=1} = \sum_{r=0}^{i}\sum_{s=0}^{j} \frac{1}{r!}\frac{1}{s!}\mathcal{H}_{1,r}\mathcal{H}_{2,s}\, m_{i-r,j-s}^{(n,k,l)}\Big|_{p=q=1}, \tag{2.400}$$

where $\mathcal{H}_{1,r}$ and $\mathcal{H}_{2,s}$ are constants defined as

$$\mathcal{H}_{1,r} = (p\partial_p)^r \mathcal{H}_1(p)\big|_{p=1}, \quad \mathcal{H}_{2,s} = (q\partial_q)^s \mathcal{H}_2(q)\big|_{q=1}. \tag{2.401}$$

Since $b = 1/a$, using the same technique as that from Eqs. (2.388)–(2.391), we can show that $\mathcal{H}_{1,r}$ and $\mathcal{H}_{2,s}$ are zero when their indices r and s are odd. Thus, we arrive at the contiguity relation for index reduction

$$m_{i,j}^{(n-1,k+1,l+1)}\Big|_{p=q=1} = \sum_{\substack{r=0 \\ r:\text{even}}}^{i}\sum_{\substack{s=0 \\ s:\text{even}}}^{j} \frac{1}{r!}\frac{1}{s!}\mathcal{H}_{1,r}\mathcal{H}_{2,s}\, m_{i-r,j-s}^{(n,k,l)}\Big|_{p=q=1}. \tag{2.402}$$

Applying this contiguity relation, we can show that

$$\left(m_{2i-1,2j-1}^{(n-1,k+1,l+1)}\Big|_{p=q=1}\right)_{1\le i,j\le N} = L\left(m_{2i-1,2j-1}^{(n,k,l)}\Big|_{p=q=1}\right)_{1\le i,j\le N} U, \tag{2.403}$$

where L and U are lower and upper triangular matrices with diagonal entries as $\mathcal{H}_{1,0}$ and $\mathcal{H}_{2,0}$, respectively. Then, taking the determinant on both sides of this equation, we get

$$\tau_{n-1,k+1,l+1} = K^N \tau_{n,k,l}, \quad K \equiv \mathcal{H}_{1,0}\mathcal{H}_{2,0} = \frac{(1-a)^2}{(1+a)^2}. \tag{2.404}$$

Thus, the index-reduction condition (2.356) is satisfied.

Since our τ function (2.394), i.e., Eq. (2.372) in Lemma 2.9, now satisfies the dimension-reduction conditions (2.354)–(2.355) and the index-reduction con-

dition (2.356), they then satisfy the bilinear system (2.373). Thus, Lemma 2.9 is proved.

Regarding free parameters, they are introduced through $\xi_0(p)$ and $\eta_0(q)$ in Eqs. (2.370)–(2.371) as

$$\xi_0(p) = \sum_{r=1}^{\infty} \hat{a}_r \ln^r p, \quad \eta_0(q) = \sum_{r=1}^{\infty} \hat{b}_r \ln^r q, \tag{2.405}$$

where $\hat{a}_r$ and $\hat{b}_r$ $(r = 1, 2, \dots)$ are complex constants.

Finally, we impose the complex conjugate condition (2.363), i.e., $\tau^*_{n,0,0} = \tau_{-n,0,0}$. After the dimension reduction, we can set $x_{-1} = s = 0$ in the $\xi(p)$ and $\eta(q)$ expressions (2.370)–(2.371). In this case, if we set a to be purely imaginary and denote $a = \mathrm{i}\alpha$, where α is a real parameter, and constrain the parameters in $\xi_0(p)$ and $\eta_0(q)$ above as $\hat{b}_r = \hat{a}^*_r$, then $[m^{(n,0,0)}_{i,j}]^* = m^{(-n,0,0)}_{j,i}$. Thus, the conjugate condition (2.363) is satisfied. After assigning x_1 and r variables and parameter α as in Eq. (2.364), the τ function (2.372) then would give rational solutions to the CSP equation (2.340) through transformations (2.350) and (2.351).

We can also show by the technique of Sect. 2.1.1 that $\tau_{0,0,0} > 0$. In addition, these rational solutions are rogue waves satisfying the boundary conditions (2.341).

Summarizing the above results, we have the following lemma on rogue waves of the CSP equation in differential operator form.

Lemma 2.10 *The complex short pulse equation (2.340) under boundary conditions (2.341) admits rogue wave solutions of the following form*

$$u_N(x,t) = \frac{g_N(y,z)}{f_N(y,z)} \exp[\mathrm{i}(y - \frac{1}{\kappa} z)], \tag{2.406}$$

where coordinates (x,t) are related to new coordinates (y,z) through the hodograph transformation

$$x = \frac{1}{\kappa} y - \frac{1}{2} z - 2(\ln f_N)_z, \quad t = -z, \tag{2.407}$$

N is the order of the rogue wave,

$$f_N = \tau_0, \quad g_N = \tau_1, \tag{2.408}$$

$$\tau_n = \det_{1 \le i,j \le N} \left(m^{(n)}_{2i-1,2j-1} \right), \tag{2.409}$$

$f_N > 0$, the matrix elements in τ_n are defined by

$$m^{(n)}_{i,j} = \frac{(p\partial_p)^i}{i!} \frac{(q\partial_q)^j}{j!} \, m^{(n)} \Big|_{p=q=1}, \tag{2.410}$$

$$m^{(n)} = \left(\frac{1}{p+q}\right)\left(-\frac{p}{q}\right)^n e^{\xi(p)+\eta(q)}, \tag{2.411}$$

$$\xi(p) = \frac{1}{2}pz + \frac{\alpha}{p-\mathrm{i}\alpha}y + \sum_{r=1}^{\infty}\hat{a}_r \ln^r p, \tag{2.412}$$

$$\eta(q) = \frac{1}{2}qz + \frac{\alpha}{q+\mathrm{i}\alpha}y + \sum_{r=1}^{\infty}\hat{a}_r^* \ln^r q, \tag{2.413}$$

α is related to the background wavenumber κ through $\kappa = 2\alpha/(\alpha^2-1)$, and $\hat{a}_1, \hat{a}_2, \hat{a}_3, \ldots, \hat{a}_{2N-1}$ are free complex constants.

Next, we remove differential operators in the above lemma and derive more explicit expressions of rogue waves through Schur polynomials. For the current choice of the $m^{(n)}$ function in Eq. (2.411), this derivation is similar to that for the generalized derivative NLS equations in Sect. 2.2, and the resulting expressions are as given in Theorem 2.6, where parameters a_r are linearly related to $\hat{a}_r$ in the above lemma. This derivation would be a bit simpler if we introduce a factor of $(p+1)(q+1)$ into the $m^{(n)}$ function in Eq. (2.411), in which case this derivation would resemble that for the NLS equation in Sect. 2.1.1, and parameters a_r in Theorem 2.6 would be identical to $\hat{a}_r$ in the above lemma. In addition, using the same techniques as in Sect. 2.1.1, we can set $x_{2r}^{\pm} = 0$ in the resulting Schur polynomial expressions. Skipping these calculations, we arrive at explicit rogue wave expressions of the CSP equation in Schur polynomial form as presented in Theorem 2.6. This completes the proof of Theorem 2.6.

The fundamental rogue wave can be derived from Theorem 2.6 by setting $N = 1$, and we get

$$u_1(x,t) = \left[1 + \frac{16\mathrm{i}\alpha^2 y - 4(1+\alpha^2)^2}{(1+\alpha^2)^2 z^2 - 4\alpha(1-\alpha^2)yz + 4\alpha^2 y^2 + (1+\alpha^2)^2}\right] \times \exp[\mathrm{i}(y - \frac{1}{\kappa}z)]. \tag{2.414}$$

This fundamental rogue wave reaches a peak amplitude of 3 at $x = t = 0$. When $\alpha = 4$, its graph is displayed in Fig. 2.6.

Second-order rogue waves can be obtained from Theorem 2.6 by setting $N = 2$. These solutions have a free complex parameter a_3. For $\alpha = 4$ and two choices of the a_3 values 0 and 50, the corresponding rogue solutions are displayed in Fig. 2.7. In the former case, the rogue wave reaches a peak amplitude of approximately 4.287267. In the latter case, it splits into a rogue triplet.

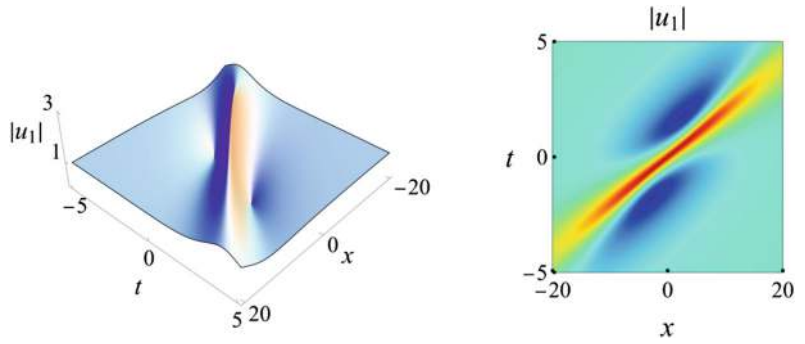

Fig. 2.6 Graph of the fundamental rogue wave (2.414) with $\alpha = 4$ in the complex short pulse equation (2.340). Left: 3D plot; right: density plot

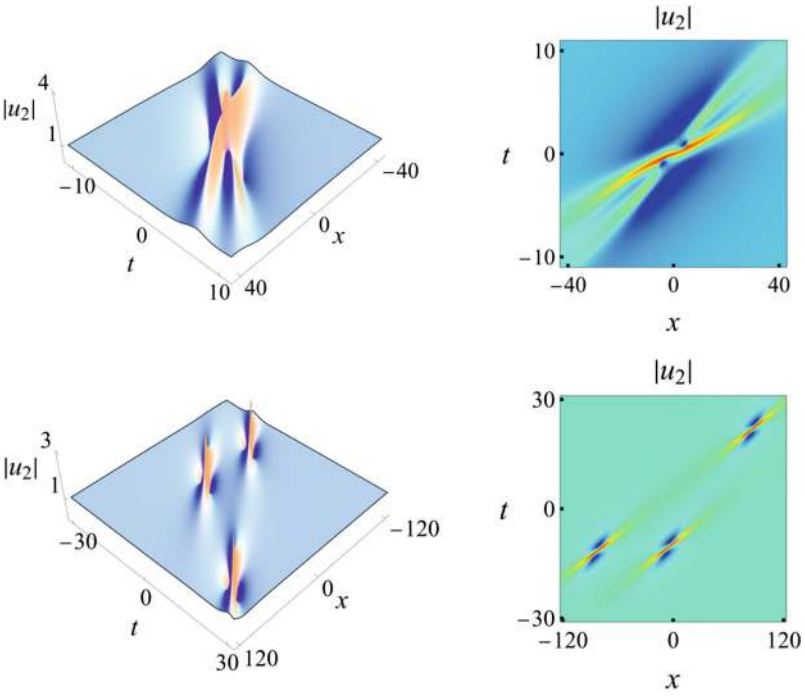

Fig. 2.7 Second-order rogue wave solutions in the complex short pulse equation (2.340) with $\alpha = 4$. Upper row: $a_3 = 0$; lower row: $a_3 = 50$. Left column: 3D plots; right column: density plots

2.6 Sasa-Satsuma Equation

The Sasa-Satsuma equation was proposed as a higher-order nonlinear Schödinger equation for optical pulses that includes some additional physical effects such as

third-order dispersion and self-steepening (Sasa and Satsuma 1991; Hasegawa and Kodama 1995; Agrawal 2001). Through a variable transformation, this equation can be written as

$$u_t = u_{xxx} + 6|u|^2 u_x + 3u(|u|^2)_x. \tag{2.415}$$

Sasa and Satsuma (1991) showed that this equation is integrable.

Through a simple scaling, continuous-wave backgrounds of the Sasa-Satsuma equation can be normalized to have unit amplitude. Hence they can be written as $u(x,t) = e^{\mathrm{i}(\alpha x - \omega t)}$, where α and ω are the wave number and frequency parameters. Inserting this background wave into the Sasa-Satsuma equation (2.415), we find that $\omega = \alpha^3 - 6\alpha$. We seek rogue waves which approach this background at large time and space, i.e.,

$$u(x,t) \to e^{\mathrm{i}[\alpha(x+6t)-\alpha^3 t]}, \quad x,t \to \pm\infty. \tag{2.416}$$

Rogue waves in the Sasa-Satsuma equation have been derived before by Chen (2013), Mu and Qin (2016), Ling (2016), Mu et al. (2020), Feng et al. (2022b), and Wu et al. (2022), by Darboux transformation or the bilinear method. We will use the bilinear method, following Wu et al. (2022) but with modifications in the solution expressions.

General rogue waves in the Sasa-Satsuma equation are given by the following theorem.

Theorem 2.7 *When $|\alpha| > 1/2$ where the algebraic equation $Q_1'(p) = 0$ with*

$$Q_1(p) = \frac{1}{p - \mathrm{i}\alpha} + \frac{1}{p + \mathrm{i}\alpha} + p \tag{2.417}$$

admits a pair of simple complex conjugate roots $(p_{0,1}, p_{0,2})$ with $p_{0,2} = p_{0,1}^*$, the Sasa-Satsuma equation (2.415) under boundary conditions (2.416) admits rogue wave solutions

$$u_N(x,t) = \frac{\sigma_{1,0}}{\sigma_{0,0}} e^{\mathrm{i}[\alpha(x+6t)-\alpha^3 t]}, \tag{2.418}$$

where N is the order of the rogue wave, $\sigma_{k,l}$ is a 2×2 block determinant

$$\sigma_{k,l} = \det \begin{pmatrix} \sigma_{k,l}^{[1,1]} & \sigma_{k,l}^{[1,2]} \\ \sigma_{k,l}^{[2,1]} & \sigma_{k,l}^{[2,2]} \end{pmatrix}, \tag{2.419}$$

$$\sigma_{k,l}^{[I,J]} = \left(m_{2i-1,2j-1}^{(k,l,I,J)} \right)_{1 \le i,j \le N}, \tag{2.420}$$

the matrix elements in $\sigma_{k,l}^{[I,J]}$ are defined by

$$m_{i,j}^{(k,l,I,J)} = \sum_{\nu=0}^{\min(i,j)} \left(\frac{1}{p_{0,I}+p_{0,J}}\right)\left[\frac{p_{1,I}p_{1,J}}{(p_{0,I}+p_{0,J})^2}\right]^{\nu} \times S_{i-\nu}\left(\boldsymbol{x}_{I,J}^{+}(k,l)+\nu \boldsymbol{s}_{I,J}\right) S_{j-\nu}\left(\boldsymbol{x}_{J,I}^{-}(k,l)+\nu \boldsymbol{s}_{J,I}\right), \tag{2.421}$$

vectors $\boldsymbol{x}_{I,J}^{\pm}(k,l) = \left(x_{1,I,J}^{\pm}, x_{2,I,J}^{\pm}, \cdots\right)$ *are defined by*

$$x_{r,I,J}^{+}(k,l) = p_{r,I}(x+6t) + \beta_{r,I}t + k\theta_{r,I} + l\lambda_{r,I} - b_{r,I,J} + a_{r,I}, \tag{2.422}$$

$$x_{r,I,J}^{-}(k,l) = p_{r,I}(x+6t) + \beta_{r,I}t - k\lambda_{r,I} - l\theta_{r,I} - b_{r,I,J} + a_{r,I}, \tag{2.423}$$

$p_{r,I}$, $\beta_{r,I}$, $\theta_{r,I}$, $\lambda_{r,I}$ *and* $b_{r,I,J}$ *are coefficients from the expansions*

$$p_I(\kappa) = \sum_{r=0}^{\infty} p_{r,I}\kappa^r, \quad [p_I(\kappa)]^3 - \left(p_{0,I}\right)^3 = \sum_{r=1}^{\infty} \beta_{r,I}\kappa^r, \tag{2.424}$$

$$\ln\left[\frac{p_I(\kappa)-\mathrm{i}\alpha}{p_{0,I}-\mathrm{i}\alpha}\right] = \sum_{r=1}^{\infty}\theta_{r,I}\kappa^r, \quad \ln\left[\frac{p_I(\kappa)+\mathrm{i}\alpha}{p_{0,I}+\mathrm{i}\alpha}\right] = \sum_{r=1}^{\infty}\lambda_{r,I}\kappa^r, \tag{2.425}$$

$$\ln\left[\frac{p_I(\kappa)+p_{0,J}}{p_{0,I}+p_{0,J}}\right] = \sum_{r=1}^{\infty} b_{r,I,J}\kappa^r, \tag{2.426}$$

the function $p_I(\kappa)$ *is defined by the equation*

$$Q_1[p_I(\kappa)] = Q_1(p_{0,I})\cosh(\kappa), \tag{2.427}$$

the vector $\boldsymbol{s}_{I,J} = (s_{1,I,J}, s_{2,I,J}, \cdots)$ *is defined by the expansion*

$$\ln\left[\frac{1}{\kappa}\left(\frac{p_{0,I}+p_{0,J}}{p_{1,I}}\right)\left(\frac{p_I(\kappa)-p_{0,I}}{p_I(\kappa)+p_{0,J}}\right)\right] = \sum_{r=1}^{\infty} s_{r,I,J}\kappa^r, \tag{2.428}$$

$a_{r,2} = a_{r,1}^*$, *and* $a_{r,1}$ $(r = 1, 2, \ldots, 2N-1)$ *are free complex constants.*

Proof Through a variable transformation,

$$u(x,t) = \frac{g(x,t)}{f(x,t)} e^{\mathrm{i}[\alpha(x+6t)-\alpha^3 t]}, \tag{2.429}$$

where f is real function and g a complex one, the Sasa-Satsuma equation (2.415) can be converted into a set of bilinear equations

$$\left.\begin{aligned}&\left(D_x^2+4\right) f\cdot f=4|g|^2,\\&\left(D_x+2\mathrm{i}\alpha\right) g\cdot g^*=2\mathrm{i}\alpha fh,\\&\left(D_x^3-D_t+3\mathrm{i}\alpha D_x^2-3(\alpha^2-4)D_x+6\mathrm{i}\alpha\right) g\cdot f=6\mathrm{i}\alpha gh,\end{aligned}\right\} \tag{2.430}$$

where h is an auxiliary function.

To get rational solutions, we begin our reduction from the following higher-dimensional bilinear equations in the extended KP hierarchy

$$\left(D_rD_{x_1}-2\right)\tau_{k,l}\cdot\tau_{k,l}=-2\tau_{k+1,l}\tau_{k-1,l}, \tag{2.431}$$

$$\left(D_sD_{x_1}-2\right)\tau_{k,l}\cdot\tau_{k,l}=-2\tau_{k,l+1}\tau_{k,l-1}, \tag{2.432}$$

$$\left(D_{x_1}^2-D_{x_2}+2aD_{x_1}\right)\tau_{k+1,l}\cdot\tau_{k,l}=0, \tag{2.433}$$

$$\left(D_{x_1}^2-D_{x_2}+2bD_{x_1}\right)\tau_{k,l+1}\cdot\tau_{k,l}=0, \tag{2.434}$$

$$\left(D_{x_1}^3+3D_{x_1}D_{x_2}-4D_{x_3}+3a(D_{x_1}^2+D_{x_2})+6a^2D_{x_1}\right)\tau_{k+1,l}\cdot\tau_{k,l}=0, \tag{2.435}$$

$$\left(D_{x_1}^3+3D_{x_1}D_{x_2}-4D_{x_3}+3b(D_{x_1}^2+D_{x_2})+6b^2D_{x_1}\right)\tau_{k,l+1}\cdot\tau_{k,l}=0, \tag{2.436}$$

$$\left(D_r\left(D_{x_1}^2-D_{x_2}+2aD_{x_1}\right)-4D_{x_1}\right)\tau_{k+1,l}\cdot\tau_{k,l}=0, \tag{2.437}$$

$$\left(D_s\left(D_{x_1}^2-D_{x_2}+2bD_{x_1}\right)-4D_{x_1}\right)\tau_{k,l+1}\cdot\tau_{k,l}=0, \tag{2.438}$$

$$\begin{aligned}&\left(D_s\left(D_{x_1}^2-D_{x_2}+2aD_{x_1}\right)-4(D_{x_1}+a-b)\right)\tau_{k+1,l}\cdot\tau_{k,l}+\\&\qquad+4(a-b)\tau_{k+1,l+1}\tau_{k,l-1}=0,\end{aligned} \tag{2.439}$$

$$\begin{aligned}&\left(D_r\left(D_{x_1}^2-D_{x_2}+2bD_{x_1}\right)-4(D_{x_1}+b-a)\right)\tau_{k,l+1}\cdot\tau_{k,l}+\\&\qquad+4(b-a)\tau_{k+1,l+1}\tau_{k-1,l}=0,\end{aligned} \tag{2.440}$$

$$\left(D_{x_1}+a-b\right)\tau_{k+1,l}\cdot\tau_{k,l+1}=(a-b)\tau_{k+1,l+1}\tau_{k,l}. \tag{2.441}$$

We will construct a broad class of algebraic solutions to this bilinear system. Then, we introduce the dimension reduction condition

$$(\partial_r+\partial_s+\partial_{x_1})\tau_{k,l}=C\tau_{k,l}, \tag{2.442}$$

where C is some constant. Under this condition, adding Eqs. (2.431) and (2.432) gives

$$(D_{x_1}^2+4)\tau_{k,l}\cdot\tau_{k,l}=2(\tau_{k+1,l}\tau_{k-1,l}+\tau_{k,l+1}\tau_{k,l-1}). \tag{2.443}$$

In addition, performing

$$3a \times \text{Eq. (2.433)} + \text{Eq. (2.435)} + 3 \times (\text{Eq. (2.437)} + \text{Eq. (2.439)}) \tag{2.444}$$

would eliminate x_2 and yield the equation

$$\left(D_{x_1}^3 - D_{x_3} + 3aD_{x_1}^2 + 3(a^2+2)D_{x_1} + 3(a-b)\right)\tau_{k+1,l} \cdot \tau_{k,l} = 3(a-b)\tau_{k+1,l+1}\tau_{k,l-1}. \tag{2.445}$$

Similarly, performing

$$3b \times \text{Eq. (2.434)} + \text{Eq. (2.436)} + 3 \times (\text{Eq. (2.438)} + \text{Eq. (2.440)}) \tag{2.446}$$

would yield the equation

$$\left(D_{x_1}^3 - D_{x_3} - 3aD_{x_1}^2 + 3(a^2+2)D_{x_1} - 3(a-b)\right)\tau_{k,l+1} \cdot \tau_{k,l} = -3(a-b)\tau_{k+1,l+1}\tau_{k-1,l}. \tag{2.447}$$

Now we set $b = -a$ and $k = l = 0$. Then the bilinear equations (2.441), (2.443), (2.445) and (2.447) become

$$(D_{x_1}^2 + 4)\tau_{0,0} \cdot \tau_{0,0} = 2(\tau_{1,0}\tau_{-1,0} + \tau_{0,1}\tau_{0,-1}), \tag{2.448}$$

$$\left(D_{x_1} + 2a\right)\tau_{1,0} \cdot \tau_{0,1} = 2a\tau_{1,1}, \tag{2.449}$$

$$\left(D_{x_1}^3 - D_{x_3} + 3aD_{x_1}^2 + 3(a^2+2)D_{x_1} + 6a\right)\tau_{1,0} \cdot \tau_{0,0} = 6a\tau_{1,1}\tau_{0,-1}, \tag{2.450}$$

$$\left(D_{x_1}^3 - D_{x_3} - 3aD_{x_1}^2 + 3(a^2+2)D_{x_1} - 6a\right)\tau_{0,1} \cdot \tau_{0,0} = -6a\tau_{1,1}\tau_{-1,0}. \tag{2.451}$$

Then, if we set

$$x_1 = x + 6t, \quad x_3 = t, \quad a = \mathrm{i}\alpha, \quad f = \tau_{0,0}, \quad g = \tau_{1,0}, \quad h = \tau_{1,1}, \tag{2.452}$$

and impose the conjugation and index conditions

$$\tau_{k,k}^* = \tau_{k,k}, \quad \tau_{0,k}^* = \tau_{k,0}, \quad \tau_{k,l} = \tau_{-l,-k} \tag{2.453}$$

for $k, l = 0, 1$, the above bilinear system (2.448)–(2.451) would become the bilinear system (2.430) of the Sasa-Satsuma equation, and algebraic solutions to the higher-dimensional bilinear system (2.431)–(2.441) would give rational rogue wave solutions of the Sasa-Satsuma equation through the bilinear transformation (2.429).

Next, we execute the above plan.

First, we construct a broad class of algebraic solutions to the higher-dimensional bilinear system (2.431)–(2.441). Introducing functions $m_{i,j}^{(k,l)}$, $\varphi_i^{(k,l)}$ and $\psi_j^{(k,l)}$ depending on variables x_1, x_2, x_3, r and s, satisfying differential and difference relations

$$\left.\begin{aligned}
&\partial_{x_1} m_{i,j}^{(k,l)} = \varphi_i^{(k,l)} \psi_j^{(k,l)}, \\
&\partial_{x_1} \varphi_i^{(k,l)} = a\varphi_i^{(k,l)} + \varphi_i^{(k+1,1)} = b\varphi_i^{(k,l)} + \varphi_i^{(k,1+1)}, \\
&\partial_{x_1} \psi_j^{(k,l)} = -a\psi_j^{(k,l)} - \psi_j^{(k-1,1)} = -b\psi_j^{(k,l)} - \psi_j^{(k,1-1)}, \\
&\partial_{x_n} \varphi_j^{(k,l)} = \partial_{x_1}^n \varphi_j^{(k,l)}, \ \partial_{x_n} \psi_j^{(k,l)} = (-1)^{n-1} \partial_{x_1}^n \psi_j^{(k,l)}, \ n = 2, 3, \\
&\partial_r \varphi_i^{(k,l)} = \varphi_i^{(k-1,l)}, \ \partial_r \psi_j^{(k,l)} = -\psi_j^{(k+1,l)}, \\
&\partial_s \varphi_i^{(k,l)} = \varphi_i^{(k,l-1)}, \ \partial_s \psi_j^{(k,l)} = -\psi_j^{(k,l+1)},
\end{aligned}\right\} \tag{2.454}$$

$$\left.\begin{aligned}
&\partial_{x_2} m_{i,j}^{(k,l)} = \varphi_i^{(k+1,l)} \psi_j^{(k,l)} + \varphi_i^{(k,l)} \psi_j^{(k-1,l)} + 2a\varphi_i^{(k,l)} \psi_j^{(k,l)}, \\
&\partial_{x_2} m_{i,j}^{(k,l)} = \varphi_i^{(k,l+1)} \psi_j^{(k,l)} + \varphi_i^{(k,l)} \psi_j^{(k,l-1)} + 2b\varphi_i^{(k,l)} \psi_j^{(k,l)}, \\
&\partial_{x_3} m_{i,j}^{(k,l)} = \varphi_i^{(k+2,l)} \psi_j^{(k,l)} + 3a\varphi_i^{(k+1,l)} \psi_j^{(k,l)} + \varphi_i^{(k+1,l)} \psi_j^{(k-1,l)} + \\
&\qquad +3a^2 \varphi_i^{(k,l)} \psi_j^{(k,l)} + 3a\varphi_i^{(k+1,l)} \psi_j^{(k-1,l)} + \varphi_i^{(k,l)} \psi_j^{(k-2,l)}, \\
&\partial_{x_3} m_{i,j}^{(k,l)} = \varphi_i^{(k,l+2)} \psi_j^{(k,l)} + 3b\varphi_i^{(k,l+1)} \psi_j^{(k,l)} + \varphi_i^{(k,l+1)} \psi_j^{(k,l-1)} + \\
&\qquad +3b^2 \varphi_i^{(k,l)} \psi_j^{(k,l)} + 3b\varphi_i^{(k,l+1)} \psi_j^{(k,l-1)} + \varphi_i^{(k,l)} \psi_j^{(k,l-2)}, \\
&\partial_r m_{i,j}^{(k,l)} = -\varphi_i^{(k-1,l)} \psi_j^{(k+1,l)}, \ \partial_r m_{i,j}^{(k,l)} = -\varphi_i^{(k,l-1)} \psi_j^{(k,l+1)}, \\
&m_{i,j}^{(k+1,l)} = m_{i,j}^{(k,l)} + \varphi_i^{(k,l)} \psi_j^{(k+1,l)}, \ m_{i,j}^{(k,l+1)} = m_{i,j}^{(k,l)} + \varphi_i^{(k,l)} \psi_j^{(k,l+1)},
\end{aligned}\right\} \tag{2.455}$$

where a and b are arbitrary complex constants, then the τ function

$$\tau_{k,l} = \det_{1 \le i,j \le N} \left(m_{i,j}^{(k,l)} \right) \tag{2.456}$$

would satisfy the higher-dimensional bilinear system (2.431)–(2.441) (Ohta and Yang 2012a; Yang and Yang 2021b; Wu et al. 2022).

To get algebraic solutions to this bilinear system, we define matrix elements in the τ function (2.456) as

$$m_{i,j}^{(k,l)} = \mathcal{A}_i \mathcal{B}_j m^{(k,l)}, \tag{2.457}$$

where

$$m^{(k,l)} = \frac{1}{p+q} \left(-\frac{p-a}{q+a} \right)^k \left(-\frac{p-b}{q+b} \right)^l e^{\xi(p)+\eta(q)}, \tag{2.458}$$

$$\xi(p) = px_1 + p^2x_2 + p^3x_3 + \frac{1}{p-a}r + \frac{1}{p-b}s + \xi_0(p), \tag{2.459}$$

$$\eta(q) = qx_1 - q^2x_2 + q^3x_3 + \frac{1}{q+a}r + \frac{1}{q+b}s + \eta_0(q). \tag{2.460}$$

$$\mathcal{A}_i = \frac{[f_1(p)\partial_p]^i}{i!}, \quad \mathcal{B}_j = \frac{[f_2(q)\partial_q]^j}{j!}, \tag{2.461}$$

and $f_1(p)$, $f_2(q)$, $\xi_0(p)$ and $\eta_0(q)$ are arbitrary functions. It is easy to see that these $m_{i,j}^{(k,l)}$ functions and their $\varphi_i^{(k,l)}$ and $\psi_j^{(k,l)}$ counterparts satisfy the differential and difference relations (2.454), and thus the τ function

$$\tau_{k,l} = \det_{1\le\nu,\mu\le N}\left(m_{i_\nu,j_\mu}^{(k,l)}\right) \tag{2.462}$$

for an arbitrary sequence of indices $(i_1, i_2, \cdots, i_N; j_1, j_2, \cdots, j_N)$ would satisfy the higher-dimensional bilinear system (2.431)–(2.441).

Next, we consider the dimensional reduction condition (2.442), following the $\mathcal{W}$-p treatment (see Sect. 2.3). Introducing $\mathcal{L}_0 = \partial_r + \partial_s + \partial_{x_1}$, it is easy to see that

$$\mathcal{L}_0 m_{i,j}^{(k,l)} = \mathcal{A}_i\mathcal{B}_j\mathcal{L}_0 m^{(k,l)} = \mathcal{A}_i\mathcal{B}_j\left[\mathcal{Q}_1(p) + \mathcal{Q}_2(q)\right] m^{(k,l)}, \tag{2.463}$$

where

$$\mathcal{Q}_1(p) = \frac{1}{p-a} + \frac{1}{p+a} + p, \quad \mathcal{Q}_2(q) = \frac{1}{q-b} + \frac{1}{q+b} + q. \tag{2.464}$$

We will select p_0 and q_0 values to be roots of the following algebraic equations

$$\mathcal{Q}_1'(p) = 0, \quad \mathcal{Q}_2'(q) = 0. \tag{2.465}$$

From the text below Eq. (2.447) as well as from Eq. (2.452), we know that

$$a = -b = \mathrm{i}\alpha. \tag{2.466}$$

Thus, the function $\mathcal{Q}_1(p)$ above is the same as that in Eq. (2.417) of Theorem 2.7. The algebraic equation $\mathcal{Q}_1'(p) = 0$ can be written out as

$$p^4 + 2(\alpha^2 - 1)p^2 + \alpha^2(\alpha^2 + 2) = 0, \tag{2.467}$$

whose roots are

$$p_0 = \pm\sqrt{(1-\alpha^2) \pm \sqrt{1-4\alpha^2}}. \tag{2.468}$$

When $|\alpha| < 1/2$, this equation has two pairs of simple real roots. When $|\alpha| = 1/2$, it has one pair of double real roots. When $|\alpha| > 1/2$, it has four simple complex roots which form a quartet of $(p_0, p_0^*, -p_0, -p_0^*)$. The q_0 roots of the $Q_2'(q) = 0$ equation are the same as these p_0's.

The types of Sasa-Satsuma solutions we will get depend on the structure of these four roots. For simple (p_0, q_0) roots, following the $\mathcal{W}$-p treatment for dimension reduction (see Eq. (2.257) in Sect. 2.3), functions $f_1(p)$ and $f_2(q)$ in differential operators $\mathcal{A}_i$ and $\mathcal{B}_j$ would be chosen as

$$f_1(p) = \frac{\sqrt{Q_1^2(p) - Q_1^2(p_0)}}{Q_1'(p)}, \quad f_2(q) = \frac{\sqrt{Q_2^2(q) - Q_2^2(q_0)}}{Q_2'(q)}. \tag{2.469}$$

In this case, we can restrict indices of the general determinant (2.456) to

$$\tau_{k,l} = \det_{1 \le i,j \le N} \left(m_{2i-1,2j-1}^{(k,l)} \Big|_{p=p_0,\ q=q_0} \right). \tag{2.470}$$

Then, repeating the calculations of Sect. 2.3, we get

$$\mathcal{L}_0 \tau_{k,l} = [Q_1(p_0) + Q_2(q_0)]\, N\, \tau_{k,l}. \tag{2.471}$$

Thus, this $\tau_{k,l}$ function satisfies the dimension reduction condition (2.442).

However, this single block τ function (2.470) would only yield a rational solitary wave solution, not a rogue wave. To get rogue waves, roots of the algebraic equation (2.467) should form a quartet of $(p_0, p_0^*, -p_0, -p_0^*)$ which are distinct from each other, which happens when $|\alpha| > 1/2$. In that case, we need to use a pair of its complex conjugate roots $(p_{0,1}, p_{0,2})$, where

$$p_{0,2} = p_{0,1}^*, \tag{2.472}$$

and a pair of q's simple complex conjugate roots $(q_{0,1}, q_{0,2})$ where

$$q_{0,I} = p_{0,I}, \quad I = 1, 2. \tag{2.473}$$

Then, we construct a 2×2 block determinant,

$$\tau_{k,l} = \det \begin{pmatrix} \tau_{k,l}^{[1,1]} & \tau_{k,l}^{[1,2]} \\ \tau_{k,l}^{[2,1]} & \tau_{k,l}^{[2,2]} \end{pmatrix}, \tag{2.474}$$

where

$$\tau_{k,l}^{[I,J]} = \mathrm{mat}_{1 \le i,j \le N} \left(m_{2i-1,2j-1}^{(k,l)} \Big|_{p=p_{0,I},\ q=q_{0,J}} \right), \quad 1 \le I, J \le 2, \tag{2.475}$$

$m_{i,j}^{(k,l)}$ is given by Eq. (2.457) with $[f_1(p), f_2(q)]$ such as in (2.469) replaced by $[f_1^{(I)}(p), f_2^{(J)}(q)]$ and (p_0, q_0) replaced by $(p_{0,I}, q_{0,J})$, ξ_0 is replaced by $\xi_{0,I}$, η_0 is replaced by $\eta_{0,J}$, and N is an arbitrary positive integer. In this case, calculations similar to that in Sect. 2.3 show that

$$\mathcal{L}_0 \tau_{k,l} = \left\{ Q_1(p_{0,1}) + Q_2(q_{0,1}) + Q_1(p_{0,2}) + Q_2(q_{0,2}) \right\} N \tau_{k,l}. \tag{2.476}$$

Thus, this 2×2 block determinant (2.474) also satisfies the dimension reduction condition (2.442).

Next, we consider the conjugation and index conditions (2.453), i.e.,

$$\tau_{k,k}^* = \tau_{k,k}, \quad \tau_{0,k}^* = \tau_{k,0}, \quad \tau_{k,l} = \tau_{-l,-k}. \tag{2.477}$$

If we take

$$q = p, \quad \eta_0(q) = \xi_0(p) \tag{2.478}$$

in $m_{2i-1,2j-1}^{(k,l)}$ of Eq. (2.475) after the differential operation, then we can see that the resulting $\tau_{k,l}$ would satisfy the condition

$$\tau_{k,l} = \tau_{-l,-k} \tag{2.479}$$

due to the (p, q) symmetry in $m_{2i-1,2j-1}^{(k,l)}$ when $b = -a$ and (x_2, r, s) being set to zero after dimensional reduction.

Regarding the remaining conjugation conditions in Eq. (2.477), they can be satisfied when we impose the constraint

$$\xi_{0,2} = \xi_{0,1}^* \tag{2.480}$$

in Eq. (2.475). This constraint, together with $p_{0,2} = p_{0,1}^*$ in Eq. (2.472) and the fact of $b = -a$ being purely imaginary, guarantees that

$$\left[m_{i,j}^{(k,l,3-I,3-J)} \Big|_{p=p_{0,3-I},\ q=p_{0,3-J}} \right]^* = m_{i,j}^{(l,k,I,J)} \Big|_{p=p_{0,I},\ q=p_{0,J}} \tag{2.481}$$

for $I, J = 1, 2$. Thus,

$$\tau_{k,l}^* = \tau_{l,k}, \tag{2.482}$$

which means that the remaining conjugation conditions in Eq. (2.477) are satisfied. As a result, the 2×2 block determinant (2.474), under Eq. (2.452) and the bilinear transformation (2.429), would provide Sasa-Satsuma's rational solutions which turn out to be rogue waves.

Free parameters in these rogue waves can be introduced by expanding the arbitrary function $\xi_{0,1}(p)$ as

$$\xi_{0,1}(p) = \sum_{r=1}^{\infty} a_{r,1} \ln^r \mathcal{W}_1^{(1)}(p), \tag{2.483}$$

where $\mathcal{W}_1^{(1)}(p)$ is given from Eq. (2.257) as

$$\mathcal{W}_1^{(1)}(p) = \frac{Q_1(p) + \sqrt{Q_1^2(p) - Q_1^2(p_{0,1})}}{Q_1(p_{0,1})}, \tag{2.484}$$

which is related to $f_1^{(1)}(p)$ through the equation

$$f_1^{(1)}(p) = \frac{\mathcal{W}_1^{(1)}(p)}{\partial_p[\mathcal{W}_1^{(1)}(p)]}, \tag{2.485}$$

and $a_{1,1}, a_{2,1}, \ldots$ are free complex parameters. This way of introducing free parameters in the $\mathcal{W}$-p treatment has been seen in Sect. 2.3.

Putting all the above results together, general rogue wave solutions for the Sasa-Satsuma equation in differential form would be obtained, and these results are summarized in the following lemma (Wu et al. 2022).

Lemma 2.11 *When $|\alpha| > 1/2$ where the algebraic equation $Q_1'(p) = 0$ in Eq. (2.465) admits a pair of simple complex conjugate roots $(p_{0,1}, p_{0,2})$ with $p_{0,2} = p_{0,1}^*$, the Sasa-Satsuma equation (2.415) admits rogue wave solutions*

$$u_N(x,t) = \frac{\tau_{1,0}}{\tau_{0,0}} e^{\mathrm{i}[\alpha(x+6t)-\alpha^3 t]}, \tag{2.486}$$

where N is the order of the rogue wave, $\tau_{k,l}$ is a 2×2 block determinant

$$\tau_{k,l} = \det \begin{pmatrix} \tau_{k,l}^{[1,1]} & \tau_{k,l}^{[1,2]} \\ \tau_{k,l}^{[2,1]} & \tau_{k,l}^{[2,2]} \end{pmatrix}, \tag{2.487}$$

$$\tau_{k,l}^{[I,J]} = \left(m_{2i-1,2j-1}^{(k,l,I,J)} \right)_{1 \le i,j \le N}, \tag{2.488}$$

matrix elements in $\tau_{k,l}^{[I,J]}$ are defined by

$$m_{i,j}^{(k,l,I,J)} = \frac{\left[f_1^{(I)}(p) \partial_p \right]^i}{i!} \frac{\left[f_2^{(J)}(q) \partial_q \right]^j}{j!} m^{(k,l,I,J)} \Big|_{p=p_{0,I}, q=p_{0,J}}, \tag{2.489}$$

$$f_1^{(I)}(p) = \frac{\sqrt{Q_1^2(p) - Q_1^2(p_{0,I})}}{Q_1'(p)}, \quad f_2^{(J)}(q) = \frac{\sqrt{Q_2^2(q) - Q_2^2(q_{0,J})}}{Q_2'(q)}, \tag{2.490}$$

$$m^{(k,l,I,J)} = \frac{1}{p+q}\left(-\frac{p-\mathrm{i}\alpha}{q+\mathrm{i}\alpha}\right)^k \left(-\frac{p+\mathrm{i}\alpha}{q-\mathrm{i}\alpha}\right)^l e^{\xi_I(p)+\xi_J(q)}, \tag{2.491}$$

$$\xi_I(p) = p(x+6t) + p^3 t + \xi_{0,I}(p), \tag{2.492}$$

$$\xi_{0,1}(p) = \sum_{r=1}^{\infty} a_{r,1} \ln^r \mathcal{W}_1^{(1)}(p), \quad \xi_{0,2}(p) = \sum_{r=1}^{\infty} a_{r,1}^* \ln^r \mathcal{W}_1^{(2)}(p), \tag{2.493}$$

$$\mathcal{W}_1^{(I)}(p) = \frac{Q_1(p) + \sqrt{Q_1^2(p) - Q_1^2(p_{0,I})}}{Q_1(p_{0,I})}, \tag{2.494}$$

and $a_{1,1}, a_{2,1}, \ldots, a_{2N-1,1}$ *are free complex constants.*

More explicit Schur-polynomial expressions for these rogue waves can be further derived by methods we have used earlier, and the corresponding results are as presented in Theorem 2.7. This completes the proof of Theorem 2.7.

Note that for reasons similar to those in Theorem 2.1, $a_{even,1}$ constants in this theorem are dummy variables which do not contribute to the solutions. True free complex parameters in rogue waves of this theorem are only $a_{1,1}, a_{3,1}, a_{5,1}, \ldots, a_{2N-1,1}$. In addition, $a_{1,1}$ can be normalized to zero through a shift of the (x, t) axes. Thus, the irreducible free parameters in these rogue waves are $a_{3,1}, a_{5,1}, \ldots, a_{2N-1,1}$.

To get the fundamental rogue wave of the Sasa-Satsuma equation, we take $N = 1$ in Theorem 2.7. Then, graphs of this fundamental rogue wave for $\alpha = 2$ and 1 are plotted in Fig. 2.8. It is seen that the rogue wave with $\alpha = 2$ has a single hump (with peak amplitude of approximately 2.4495), while the one with $\alpha = 1$ has two humps (with peak amplitude of approximately 2.5671 each).

Second-order rogue waves of the Sasa-Satsuma equation can be obtained by taking $N = 2$ in Theorem 2.7. Four such waves, with $\alpha = 2$ or 1 and $a_{3,1} = 0$ or

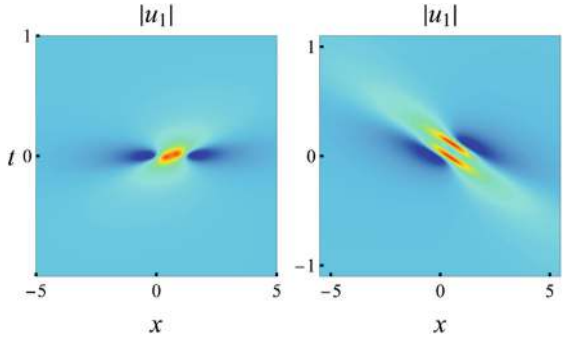

Fig. 2.8 The fundamental rogue wave $|u_1(x,t)|$ in the Sasa-Satsuma equation (2.415). Left: $\alpha = 2$; right: $\alpha = 1$

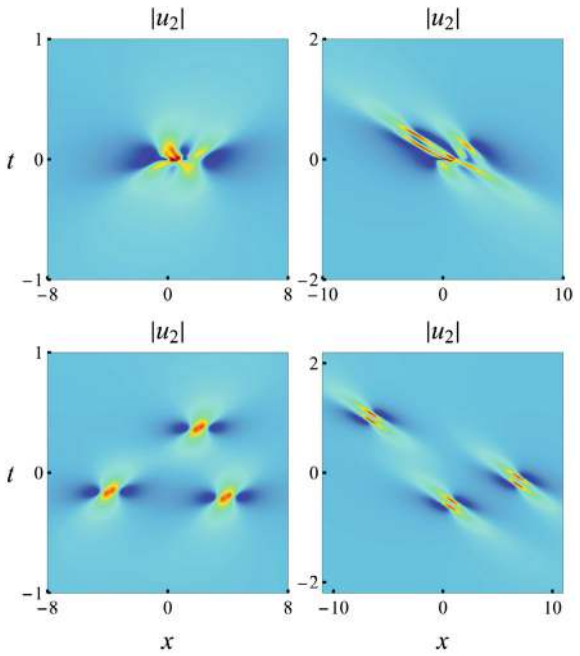

Fig. 2.9 Second-order rogue waves $|u_2(x,t)|$ in the Sasa-Satsuma equation (2.415). Upper left: $\alpha = 2$ and $a_{3,1} = 0$; upper right: $\alpha = 1$ and $a_{3,1} = 0$; lower left: $\alpha = 2$ and $a_{3,1} = 30 - 30\mathrm{i}$; lower right: $\alpha = 1$ and $a_{3,1} = 30 - 30\mathrm{i}$

$30-30\mathrm{i}$, are plotted in Fig. 2.9. It is seen that when $a_{3,1} = 0$, the rogue waves exhibit complicated profiles. But when $a_{3,1} = 30 - 30\mathrm{i}$, they split into three fundamental rogue waves.

2.7 Parity-Time-Symmetric Nonlinear Schrödinger Equation

The nonlocal NLS equation

$$\mathrm{i}u_t(x,t) = u_{xx}(x,t) + 2u^2(x,t)u^*(-x,t) \tag{2.495}$$

was introduced by Ablowitz and Musslimani (2013). The nonlinearity in this equation is nonlocal and parity-time ($\mathcal{PT}$) symmetric (Konotop et al. 2016). Thus, it is called the $\mathcal{PT}$-symmetric NLS equation. A potential physical application of this equation has also been identified in the context of an unconventional system of magnetics (Gadzhimuradov and Agalarov 2016). Since its introduction, this nonlocal NLS equation has been heavily studied (Ablowitz and Musslimani 2016; Wen et al. 2016; Huang and Ling 2016; Gerdjikov and Saxena 2017; Yang 2018; Feng et al. 2018; Santini 2018; Yang and Yang 2019, 2020b). In particular, three families of its rogue waves were derived by Darboux transformation in Yang and Yang (2019), and its more general rogue waves were derived by the bilinear method in Yang and Yang (2020b).

In this section, we derive its rogue waves, using a bilinear method that is based on Yang and Yang (2020b) but is significantly improved. The improvement comes from a better paramaterization (as in Sect. 2.1.1) that leads to much simpler expressions of rogue wave solutions than those in Yang and Yang (2020b).

Through a variable scaling, we can normalize the continuous-wave background to have unit amplitude. Thus, we consider rogue waves with the following boundary conditions

$$u(x,t) \to e^{-2\mathrm{i}t}, \quad x,t \to \pm\infty. \tag{2.496}$$

Our explicit expressions of general rogue wave solutions in the $\mathcal{PT}$-symmetric NLS equation (2.495) are summarized in the following theorem.

Theorem 2.8 *The $\mathcal{PT}$-symmetric nonlinear Schrödinger equation (2.495) under boundary conditions (2.496) admits the following rogue wave solutions*

$$u_N(x,t) = e^{-2\mathrm{i}t}\frac{\tau_1}{\tau_0}, \tag{2.497}$$

where

$$\tau_n = \begin{vmatrix} \Gamma_{1,1}^{(n)} & \Gamma_{1,2}^{(n)} \\ \Gamma_{2,1}^{(n)} & \Gamma_{2,2}^{(n)} \end{vmatrix}, \tag{2.498}$$

$\Gamma_{i,j}^{(n)}$ are $N_i \times M_j$ block matrices defined by

$$\Gamma_{i,j}^{(n)} = \left(m_{2k-i,\,2l-j}^{(n)}\right)_{1\le k\le N_i,\,1\le l\le M_j}, \tag{2.499}$$

N_1, N_2, M_1 and M_2 are arbitrary non-negative integers with the constraint of $N_1 + N_2 = M_1 + M_2 = N$, the matrix elements in $\Gamma_{i,j}^{(n)}$ are defined by

$$m_{i,j}^{(n)} = \sum_{\nu=0}^{\min(i,j)} \frac{1}{4^\nu} S_{i-\nu}(\boldsymbol{x}^+(n) + \nu\boldsymbol{s})\, S_{j-\nu}(\boldsymbol{x}^-(n) + \nu\boldsymbol{s}), \tag{2.500}$$

vectors $\boldsymbol{x}^\pm(n) = \left(x_1^\pm(n), 0, x_3^\pm, 0, \ldots\right)$ are defined by

$$x_1^+(n) = x - 2\mathrm{i}t + n + a_1, \quad x_1^-(n) = x + 2\mathrm{i}t - n + b_1, \tag{2.501}$$

$$x_{2k+1}^+ = \frac{x - 2^{2k}\mathrm{i}t}{(2k+1)!} + a_{2k+1}, \quad x_{2k+1}^- = \frac{x + 2^{2k}\mathrm{i}t}{(2k+1)!} + b_{2k+1}, \ (k \ge 1), \tag{2.502}$$

the vector $\boldsymbol{s} = (0, s_2, 0, s_4, \ldots)$ *is defined in Eq. (2.11),* a_{2k-1}, b_{2k-1} *are complex constants with*

$$\Re(a_{2k-1}) = \Re(b_{2k-1}) = 0, \tag{2.503}$$

$\Re$ *and* $\Im$ *represent the real and imaginary parts of a complex number, and*

$$\{\Im(a_{2k-1}), 1 \le k \le \max(2N_1 - 1, 2N_2 - 2)\},$$
$$\{\Im(b_{2k-1}), 1 \le k \le \max(2M_1 - 1, 2M_2 - 2)\}$$

are free real parameters.

Remark The degrees of polynomials $\sigma_n(x,t)$ in both x and t for rogue waves in Theorem 2.8 are

$$\deg(\sigma_n) = \frac{1}{2}\left[(N_1 - N_2)^2 + (N_1 - N_2) + (M_1 - M_2)^2 + (M_1 - M_2)\right]. \tag{2.504}$$

Proof of Theorem 2.8 First, via the variable transformation

$$u = e^{-2\mathrm{i}t}\frac{g}{f}, \tag{2.505}$$

the $\mathcal{PT}$-symmetric NLS equation (2.495) is transformed into the bilinear form,

$$\left.\begin{array}{l}(D_x^2 + 2) f \cdot f = 2g\bar{g}, \\ (D_x^2 - \mathrm{i}D_t) g \cdot f = 0,\end{array}\right\} \tag{2.506}$$

where the overbar on a function $g(x,t)$ is defined as

$$\bar{g}(x,t) \equiv g^*(-x,t), \tag{2.507}$$

and f is a complex function satisfying the condition

$$\bar{f}(x,t) = f(x,t). \tag{2.508}$$

In order to derive algebraic solutions to the bilinear equations (2.506), we consider a solution reduction from higher-dimensional bilinear equations in the KP-hierarchy. We introduce a Gram determinant

$$\tau_n = \det_{1 \le i,j \le N}\left(m_{i,j}^{(n)}\right), \tag{2.509}$$

where the matrix element $m_{i,j}^{(n)}$ is a function of x_{-1}, x_1 and x_2 defined as

$$m_{i,j}^{(n)} = \mathcal{A}_i \mathcal{B}_j m^{(n)}|_{p=1,q=1}, \quad m^{(n)} = \frac{(p+1)(q+1)}{p+q}\left(-\frac{p}{q}\right)^n e^{\xi+\eta}, \tag{2.510}$$

$$\xi = \frac{1}{p}x_{-1} + px_1 + p^2 x_2 + \xi_0(p), \quad \eta(q) = \frac{1}{q}x_{-1} + qx_1 - q^2 x_2 + \eta_0(q), \tag{2.511}$$

$\mathcal{A}_i$ and $\mathcal{B}_j$ are differential operators with respect to p and q as

$$\mathcal{A}_i = \frac{1}{i!}\left(p\partial_p\right)^i, \quad \mathcal{B}_j = \frac{1}{j!}\left(q\partial_q\right)^j, \tag{2.512}$$

$\xi_0(p)$, $\eta_0(q)$ are arbitrary functions of p and q which can be expanded as

$$\xi_0(p) = \sum_{k=1}^{\infty} a_k (\ln p)^k, \quad \eta_0(q) = \sum_{k=1}^{\infty} b_k (\ln q)^k, \tag{2.513}$$

and a_k, b_k are arbitrary complex constants. Then we have known from Sect. 2.1.1 that for arbitrary sequences of indices $(i_1, i_2, \ldots, i_N; j_1, j_2, \ldots, j_N)$, the determinant

$$\tau_n = \det_{1\le\nu,\mu\le N}\left(m_{i_\nu, j_\mu}^{(n)}\right) \tag{2.514}$$

would satisfy the higher-dimensional bilinear equations

$$\left.\begin{aligned}\left(D_{x_1}D_{x_{-1}} - 2\right)\tau_n\cdot\tau_n &= -2\tau_{n+1}\tau_{n-1}\\ \left(D_{x_1}^2 - D_{x_2}\right)\tau_{n+1}\cdot\tau_n &= 0.\end{aligned}\right\} \tag{2.515}$$

In addition, the matrix element $m_{i,j}^{(n)}$ with $p = q = 1$ satisfies the contiguity relation (2.45), i.e.,

$$\left(\partial_{x_1} + \partial_{x_{-1}}\right) m_{i,j}^{(n)}\Big|_{p=q=1} = 2\sum_{\substack{l=0\\ l:\text{even}}}^{i}\frac{1}{l!}\, m_{i-l,j}^{(n)}\Big|_{p=q=1} + 2\sum_{\substack{l=0\\ l:\text{even}}}^{j}\frac{1}{l!}\, m_{i,j-l}^{(n)}\Big|_{p=q=1}. \tag{2.516}$$

Using this contiguity relation, we can show as in Sect. 2.1.1 that any one of the four determinants

$$\tau_n^{(1)} = \det_{1\le i,j\le N}\left(m_{2i-1,2j-1}^{(n)}\Big|_{p=q=1}\right), \quad \tau_n^{(2)} = \det_{1\le i,j\le N}\left(m_{2i-1,2j-2}^{(n)}\Big|_{p=q=1}\right), \tag{2.517}$$

$$\tau_n^{(3)} = \det_{1\le i,j\le N}\left(m_{2i-2,2j-1}^{(n)}\Big|_{p=q=1}\right), \quad \tau_n^{(4)} = \det_{1\le i,j\le N}\left(m_{2i-2,2j-2}^{(n)}\Big|_{p=q=1}\right), \tag{2.518}$$

satisfies the dimension reduction condition

$$(\partial_{x_1} + \partial_{x_{-1}})\tau_n = 4N\tau_n. \tag{2.519}$$

But more importantly, if we combine the matrix elements of these four determinants into a 2×2-block determinant

$$\tau_n = \left|\begin{matrix}\left(m_{2i-1,2j-1}^{(n)}\right)_{1\le i\le N_1,1\le j\le M_1} & \left(m_{2i-1,2j-2}^{(n)}\right)_{1\le i\le N_1,1\le j\le M_2}\\ \left(m_{2i-2,2j-1}^{(n)}\right)_{1\le i\le N_2,1\le j\le M_1} & \left(m_{2i-2,2j-2}^{(n)}\right)_{1\le i\le N_2,1\le j\le M_2}\end{matrix}\right|_{p=q=1}, \tag{2.520}$$

where $[N_1, N_2, M_1, M_2]$ are arbitrary non-negative integers with $N_1 + N_2 = M_1 + M_2$, then this τ_n would still satisfy the dimension reduction condition

$$(\partial_{x_1} + \partial_{x_{-1}})\tau_n = 4(N_1 + N_2)\tau_n. \tag{2.521}$$

This more general block determinant solution fulfilling the dimension reduction condition allows us to derive a wider class of rogue waves in the $\mathcal{PT}$-symmetric NLS equation (2.495) than in the NLS equation (2.5).

Applying this dimension reduction condition (2.521) to the higher-dimensional bilinear equations (2.515), we see that the block determinant (2.520) would satisfy the $(1 + 1)$-dimensional bilinear equations

$$\left.\begin{matrix}\left(D_{x_1}^2 + 2\right)\tau_n \cdot \tau_n = 2\tau_{n+1}\tau_{n-1}\\ \left(D_{x_1}^2 - D_{x_2}\right)\tau_{n+1} \cdot \tau_n = 0.\end{matrix}\right\} \tag{2.522}$$

Then, if we set $n = 0$ in the above bilinear equations and take

$$f = \sigma_0, \quad g = \sigma_1, \quad \bar{g} = \sigma_{-1}, \quad x_1 = x, \quad x_2 = -\mathrm{i}t, \tag{2.523}$$

$x_{-1} = 0$, and impose the nonlocal reduction condition

$$\bar{\tau}_n = \tau_{-n}, \tag{2.524}$$

these bilinear equations would reduce to the bilinear equations (2.506) of the $\mathcal{PT}$-symmetric NLS equation (2.495).

Before imposing the nonlocal reduction condition (2.524), we first remove the differential operators in the expression (2.510) of the matrix element $m_{i,j}^{(n)}$ and derive

its explicit expressions. Following the same technique as in Sect. 2.1.1, we find that $m_{i,j}^{(n)}$ in the block determinant (2.520) can be written as

$$m_{i,j}^{(n)} = \sum_{\nu=0}^{\min(i,j)} \frac{1}{4^{\nu}} S_{i-\nu}(\boldsymbol{x}^{+}(n) + \nu \boldsymbol{s})\, S_{j-\nu}(\boldsymbol{x}^{-}(n) + \nu \boldsymbol{s}), \tag{2.525}$$

where vectors $\boldsymbol{x}^{\pm}(n) = \left(x_1^{\pm}(n), 0, x_3^{\pm}, 0, \ldots\right)$ are as given in Eqs. (2.501)–(2.502), and the vector $\boldsymbol{s} = (s_1, s_2, \cdots)$ are coefficients from the expansion (2.11).

Finally, we impose the nonlocal reduction condition (2.524), which will constrain the parameters a_{2k-1} and b_{2k-1} in Eqs. (2.501)–(2.502). Given the above algebraic expression of $m_{i,j}^{(n)}$, if we impose the following constraints on these parameters,

$$\Re(a_{2k-1}) = \Re(b_{2k-1}) = 0, \quad k = 1, 2, \ldots, \tag{2.526}$$

then

$$\overline{x}_1^{\pm}(-n) = -x_1^{\pm}(n), \quad \overline{x}_{2k-1}^{\pm} = -x_{2k-1}^{\pm}, \ (k > 1). \tag{2.527}$$

Thus,

$$\overline{\boldsymbol{x}}^{\pm}(-n) + \nu\, \boldsymbol{s} = \mathbf{y}^{\pm}(n) + \nu\, \boldsymbol{s}, \tag{2.528}$$

where vectors $\mathbf{y}^{\pm}$ are defined as

$$\mathbf{y}^{\pm}(n) = \left(-x_1^{\pm}(n), 0, -x_3^{\pm}, 0, \ldots\right). \tag{2.529}$$

Using the fact of $s_1 = s_3 = \cdots = s_{odd} = 0$, we have

$$S_k\left(\overline{\boldsymbol{x}}^{\pm}(-n) + \nu\, \boldsymbol{s}\right) = (-1)^k S_k(\boldsymbol{x}^{\pm}(n) + \nu \boldsymbol{s}). \tag{2.530}$$

Then, we see that the block determinant τ_n in Eq. (2.520) satisfies the condition

$$\overline{\tau}_{-n} = (-1)^{N_2+M_2} \tau_n. \tag{2.531}$$

Thus, by redefining $(-1)^{(N_2+M_2)/2}\tau_n$ as a new τ_n function, which still satisfies the same bilinear equations (2.522), the nonlocal reduction condition (2.524) would be satisfied. This new τ_n leads to the same solution as the original τ_n from Eq. (2.497). Theorem 2.8 is then proved. □

The fundamental singular rogue wave can be obtained by setting $N = 1$ with $N_1 = M_2 = 1$ and $N_2 = M_1 = 0$, and we get

$$u_1(x,t) = \left[1 + \frac{1}{x - 2\mathrm{i}t + a_1}\right] e^{-2\mathrm{i}t}. \tag{2.532}$$

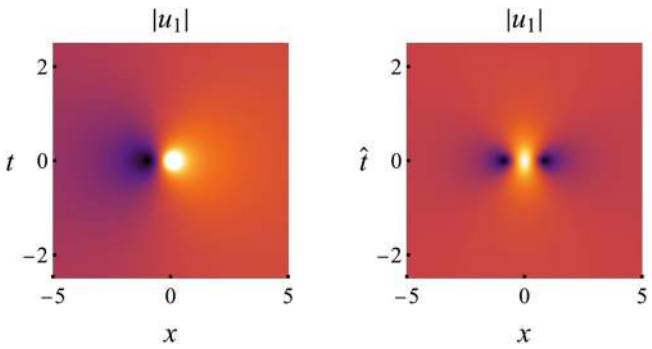

Fig. 2.10 Fundamental rogue waves (with $N = 1$) in the $\mathcal{PT}$-symmetric NLS equation (2.495). Left: the fundamental singular rogue wave (2.532) with $a_1 = 0$. Right: the fundamental nonsingular rogue wave (2.533) with $x_0 = 0$

Since a_1 is imaginary, it can be normalized to zero through a shift of the t axis. The graph of the resulting solution is plotted in Fig. 2.10 (left panel).

The fundamental nonsingular rogue wave can be obtained by setting $N = 1$ with $N_1 = M_1 = 1$ and $N_2 = M_2 = 0$, and we get

$$u_1(x,t) = \left[1 + \frac{4(4\mathrm{i}\hat{t} - 1)}{4\,(x + \mathrm{i}x_0)^2 + 16\hat{t}^2 + 1}\right] e^{-2\mathrm{i}t}, \tag{2.533}$$

where

$$\hat{t} = t + \frac{\Im(a_1) - \Im(b_1)}{2}, \quad x_0 = \frac{\Im(a_1) + \Im(b_1)}{2}. \tag{2.534}$$

This nonsingular rogue wave's peak amplitude is x_0-dependent, ranging between 1 and 3, with 3 reached when $x_0 = 0$. This rogue wave with $x_0 = 0$ is plotted in Fig. 2.10 (right panel).

When we take $N = 2$ in Theorem 2.8, we get second-order rogue waves. Three of these these solutions are displayed in Fig. 2.11. In this figure, all lumps are nonsingular in the left panel, while some lumps are singular in the middle and right panels. Notice that these rogue waves exhibit various geometric shapes such as triangles, diamonds and so on.

2.8 Ablowitz-Ladik Equation

Almost all wave equations considered in this book are continuous wave equations. But discrete wave equations are also important since they can model various physical systems such as wave dynamics in optical lattices (Christodoulides and

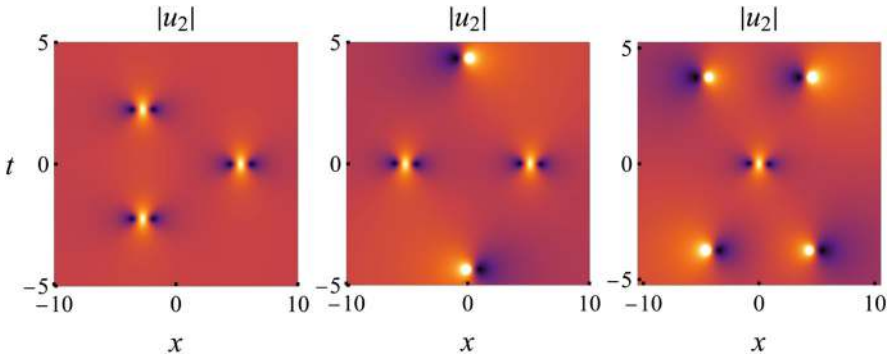

Fig. 2.11 Second order rogue waves in the $\mathcal{PT}$-symmetric NLS equation (2.495) with $[N_1, N_2, M_1, M_2] = [2, 0, 2, 0]$. Left: $a_1 = b_1 = 0$, $a_3 = 50\mathrm{i}$, $b_3 = -50\mathrm{i}$. Middle: $a_1 = b_1 = 3\mathrm{i}$, $a_3 = b_3 = 70\mathrm{i}$. Right: $a_1 = b_1 = 5\mathrm{i}$, $a_3 = b_3 = -40\mathrm{i}$

Joseph 1988). Then an interesting question is rogue wave behaviors in discrete wave systems. In this section, we derive rogue waves in an integrable discrete model—the Ablowitz-Ladik (AL) equation. This equation was proposed by Ablowitz and Ladik (1976) as an integrable discretization of the continuous NLS equation. For the focusing AL equation, non-traveling fundamental rogue waves and special second-order rogue waves were presented by Ankiewicz et al. (2010a). For both focusing and defocusing AL equations, general traveling arbitrary-order rogue waves were derived by Ohta and Yang (2014) using the bilinear method. We follow Ohta and Yang (2014) below, but with a new parameterization as in Sect. 2.1.1 so that the resulting rogue wave expressions are simpler.

The focusing AL equation is

$$\mathrm{i}\frac{d}{dt}u_n = (1 + |u_n|^2)(u_{n+1} + u_{n-1}), \tag{2.535}$$

and the defocusing AL equation is

$$\mathrm{i}\frac{d}{dt}u_n = (1 - |u_n|^2)(u_{n+1} + u_{n-1}). \tag{2.536}$$

These equations admit constant-amplitude background wave solutions

$$u_n^{[b]}(t) = \frac{\rho}{\sqrt{1-\rho^2}} e^{i(\theta n - \omega t)}, \tag{2.537}$$

where ρ, θ are free real constants and $\omega = 2\cos\theta/(1-\rho^2)$. This background wave solution satisfies the focusing AL equation (2.535) when $|\rho| < 1$ and the defocusing AL equation (2.536) when $|\rho| > 1$. However, this background solution is modulation unstable. As a consequence, rogue waves can arise from it. Thus,

boundary conditions for these rogue waves are

$$u_n(t) \to \frac{\rho}{\sqrt{1-\rho^2}} e^{i(\theta n - \omega t)}, \quad n, t \to \pm\infty. \tag{2.538}$$

General rogue waves in these AL equations (2.535)–(2.536) are given in the following theorem.

Theorem 2.9 *General N-th order rogue waves under boundary conditions (2.538) in the Ablowitz-Ladik equations (2.535)–(2.536) are*

$$u_n^{[N]}(t) = \frac{\rho}{\sqrt{1-\rho^2}} \frac{\sigma_{n,1,0}}{\sigma_{n,0,0}} e^{i(\theta n - \omega t)}, \tag{2.539}$$

where ρ and θ are free real constants, $\omega = 2\cos\theta/(1-\rho^2)$,

$$\sigma_{n,k,l} = \det_{1\le i,j\le N} \left(m^{(n,k,l)}_{2i-1,2j-1} \right), \tag{2.540}$$

the matrix elements in $\sigma_{n,k,l}$ are defined by

$$m^{(n,k,l)}_{i,j} = \sum_{\nu=0}^{\min(i,j)} \left(\frac{1-\rho}{1+\rho}\right)^{\nu} \frac{1}{4^{\nu}} S_{i-\nu}(\boldsymbol{x}^{+}(n,k,l) + \nu \boldsymbol{s})\, S_{j-\nu}(\boldsymbol{x}^{-}(n,k,l) + \nu \boldsymbol{s}^{*}), \tag{2.541}$$

vectors $\boldsymbol{x}^{\pm}(n,k,l) = \left(x_1^{\pm}, 0, x_3^{\pm}, 0, \cdots\right)$ are defined by

$$x_r^{+} = \frac{\rho}{r!} x + (1-\rho^2)(r+1) g_{r+1}(\rho) x^{*} + (n+k) g_r(\rho) + l g_r(1/\rho) - k\delta_{r1} + a_r, \tag{2.542}$$

$$x_r^{-} = \frac{\rho}{r!} x^{*} + (1-\rho^2)(r+1) g_{r+1}(\rho) x + (n+l) g_r(\rho) + k g_r(1/\rho) - l\delta_{r1} + a_r^{*}, \tag{2.543}$$

$x \equiv \mathrm{i} t e^{-\mathrm{i}\theta}/(1-\rho^2)$, δ_{r1} denotes the Kronecker delta function which is equal to 1 if $r = 1$ and 0 otherwise, g_r are coefficients from the expansion

$$\ln \frac{1+\rho e^{\lambda}}{1+\rho} = \sum_{r=1}^{\infty} g_r(\rho) \lambda^r, \tag{2.544}$$

the vector $\boldsymbol{s} = (0, s_2, 0, s_4, \cdots)$ is defined in Eq. (2.11), and $(a_1, a_3, \cdots, a_{2N-1})$ are free complex parameters, with $\Im(a_1) = 0$ through a time shift normalization. These rogue waves satisfy the boundary conditions

$$u_n^{[N]}(t) \to \frac{\rho}{\sqrt{1-\rho^2}}\, e^{i(\theta n-\omega t)}, \quad t \to \pm\infty, \tag{2.545}$$

uniformly for all n as long as $\cos\theta \neq 0$. *In addition, when* $|\rho| < 1$, *they satisfy the focusing AL equation (2.535) and are nonsingular; and when* $|\rho| > 1$, *they satisfy the defocusing AL equation (2.536) and may be singular.*

Proof Through the variable transformation

$$u_n = \frac{\rho}{\sqrt{1-\rho^2}} \frac{g_n}{f_n} e^{\mathrm{i}(\theta n-\omega t)}, \tag{2.546}$$

where $\omega = 2\cos\theta/(1-\rho^2)$, the AL equations

$$\mathrm{i}\frac{d}{dt}u_n = (1+\epsilon|u_n|^2)(u_{n+1}+u_{n-1}) \tag{2.547}$$

with $\epsilon = \mathrm{sgn}(1-\rho^2)$ can be transformed to the bilinear equations

$$\left.\begin{array}{c}\left[\mathrm{i}(1-\rho^2)D_t + c + c^*\right] g_n \cdot f_n = c g_{n-1} f_{n+1} + c^* g_{n+1} f_{n-1}, \\ f_{n+1} f_{n-1} - (1-\rho^2) f_n f_n = \rho^2 g_n g_n^*,\end{array}\right\} \tag{2.548}$$

where $c = e^{-\mathrm{i}\theta}$. Thus, when $|\rho| < 1$, the underlying AL equation (2.547) is focusing; and when $|\rho| > 1$, it is defocusing.

The bilinear equations (2.548) can be reduced from the following higher-dimensional bilinear equations of the KP hierarchy,

$$\left.\begin{array}{c}(D_x+1)\,\tau_{n,k-1,l}\cdot\tau_{n,k,l} = \tau_{n+1,k-1,l}\tau_{n-1,k,l}, \\ \left(D_y-1\right)\tau_{n,k,l+1}\cdot\tau_{n,k,l} = -\tau_{n-1,k,l+1}\tau_{n+1,k,l}, \\ \tau_{n+1,k-1,l}\ \tau_{n-1,k,l+1} - (1-\rho^2)\tau_{n,k-1,l}\ \tau_{n,k,l+1} = \rho^2\tau_{n,k-1,l+1}\ \tau_{n,k,l}.\end{array}\right\} \tag{2.549}$$

We will construct a wide class of algebraic solutions to this higher-dimensional system. Then we constrain these solutions so that they admit the index-reduction condition

$$\tau_{n,k+1,l+1} = C\tau_{n,k,l}, \tag{2.550}$$

where C is a certain real positive constant. In this case, $\tau_{n,k,l}$ would satisfy the following bilinear equations

$$\left.\begin{aligned}
&(D_x+1)\,\tau_{n,k,l}\cdot\tau_{n,k+1,l}=\tau_{n+1,k,l}\tau_{n-1,k+1,l},\\
&(D_x+1)\,\tau_{n,k,l+1}\cdot\tau_{n,k,l}=\tau_{n+1,k,l+1}\tau_{n-1,k,l},\\
&\left(D_y-1\right)\tau_{n,k,l+1}\cdot\tau_{n,k,l}=-\tau_{n-1,k,l+1}\tau_{n+1,k,l},\\
&\left(D_y-1\right)\tau_{n,k,l}\cdot\tau_{n,k+1,l}=-\tau_{n-1,k,l}\tau_{n+1,k+1,l},\\
&\tau_{n+1,k,l}\,\tau_{n-1,k,l}-(1-\rho^2)\tau_{n,k,l}\,\tau_{n,k,l}=\rho^2C^{-1}\tau_{n,k+1,l}\,\tau_{n,k,l+1}.
\end{aligned}\right\}\tag{2.551}$$

We now substitute $x=\mathrm{i}ct/(1-\rho^2)$ and $y=-\mathrm{i}c^*t/(1-\rho^2)$, where $c=e^{-\mathrm{i}\theta}$. Then the time derivative becomes $\mathrm{i}(1-\rho^2)\partial_t=-c\partial_x+c^*\partial_y$, and we obtain from the above bilinear equations that

$$\left.\begin{aligned}
&\left[\mathrm{i}(1-\rho^2)D_t+c+c^*\right]\\
&\qquad\tau_{n,k+1,l}\cdot\tau_{n,k,l}=c\tau_{n-1,k+1,l}\tau_{n+1,k,l}+c^*\tau_{n+1,k+1,l}\tau_{n-1,k,l},\\
&\left[-\mathrm{i}(1-\rho^2)D_t+c+c^*\right]\\
&\qquad\tau_{n,k,l+1}\cdot\tau_{n,k,l}=c\tau_{n+1,k,l+1}\tau_{n-1,k,l}+c^*\tau_{n-1,k,l+1}\tau_{n+1,k,l},\\
&\tau_{n+1,k,l}\,\tau_{n-1,k,l}-(1-\rho^2)\tau_{n,k,l}\,\tau_{n,k,l}=\rho^2C^{-1}\tau_{n,k+1,l}\,\tau_{n,k,l+1}.
\end{aligned}\right\}$$

Then, we further impose the complex conjugacy condition

$$\tau_{n,l,k}=\tau^*_{n,k,l},\tag{2.552}$$

and define

$$f_n=\tau_{n,0,0},\quad g_n=C^{-1/2}\tau_{n,1,0}.\tag{2.553}$$

In this case, f_n is real, and $C^{-1/2}\tau_{n,0,1}=g_n^*$, and the above bilinear equations yield AL's bilinear equations (2.548), and the corresponding τ solutions would satisfy the AL equations.

Now, we follow the above plan. First, we construct a wide class of solutions to the higher-dimensional bilinear system (2.549), which are given in the following lemma.

Lemma 2.12 *Let $m_{i,j}^{(n,k,l)}$, $\varphi_i^{(n,k,l)}$ and $\psi_j^{(n,k,l)}$ be functions of continuous independent variables x, y satisfying the following differential and difference relations,*

$$\left.\begin{aligned}
&\partial_x m_{i,j}^{(n,k,l)}=\varphi_i^{(n,k,l)}\psi_j^{(n-1,k,l)},\quad \partial_y m_{i,j}^{(n,k,l)}=\varphi_i^{(n-1,k,l)}\psi_j^{(n,k,l)},\\
&m_{i,j}^{(n+1,k,l)}=(1-\rho^2)m_{i,j}^{(n,k,l)}+\varphi_i^{(n,k,l)}\psi_j^{(n,k,l)},\\
&m_{i,j}^{(n,k+1,l)}=(1-\rho^2)m_{i,j}^{(n,k,l)}-\varphi_i^{(n-1,k+1,l)}\psi_j^{(n,k,l)},\\
&m_{i,j}^{(n,k,l+1)}=(1-\rho^2)m_{i,j}^{(n,k,l)}-\varphi_i^{(n,k,l)}\psi_j^{(n-1,k,l+1)},\\
&\partial_x\varphi_i^{(n,k,l)}=\varphi_i^{(n+1,k,l)},\quad \partial_y\varphi_i^{(n,k,l)}=-(1-\rho^2)\varphi_i^{(n-1,k,l)},\\
&\varphi_i^{(n,k-1,l)}=\varphi_i^{(n,k,l)}-\varphi_i^{(n-1,k,l)},\quad \varphi_i^{(n,k,l+1)}=(1-\rho^2)\varphi_i^{(n,k,l)}-\varphi_i^{(n+1,k,l)},\\
&(\partial_x+1)\psi_j^{(n,k,l)}=-\psi_j^{(n-1,k+1,l)},\quad (\partial_y-1)\psi_j^{(n,k,l)}=\psi_j^{(n+1,k,l-1)},\\
&\psi_j^{(n,k+1,l)}=(1-\rho^2)\psi_j^{(n,k,l)}-\psi_j^{(n+1,k,l)},\quad \psi_j^{(n,k,l-1)}=\psi_j^{(n,k,l)}-\psi_j^{(n-1,k,l)}.
\end{aligned}\right\}\tag{2.554}$$

Then the determinant

$$\tau_{n,k,l} = \det_{1\le i,j\le N}\left(m_{i,j}^{(n,k,l)}\right) \tag{2.555}$$

satisfies the bilinear system (2.549).

The proof of this lemma is along the same lines as the proof of Lemma 2.1, and the details can be found in Ohta and Yang (2014).

A wide class of algebraic solutions to the bilinear system (2.549) can be obtained when we define matrix elements $m_{i,j}^{(n,k,l)}$ by

$$m_{i,j}^{(n,k,l)} = \mathcal{A}_i \mathcal{B}_j m^{(n,k,l)}, \tag{2.556}$$

where

$$m^{(n,k,l)} = \frac{1}{pq-1+\rho^2}(pq)^n \left(\frac{1-\rho^2-q}{1-1/p}\right)^k \left(\frac{1-\rho^2-p}{1-1/q}\right)^l e^{\xi+\eta}, \tag{2.557}$$

$$\xi = px - \frac{1-\rho^2}{p}y + \xi_0(p), \quad \eta = -\frac{1-\rho^2}{q}x + qy + \eta_0(q), \tag{2.558}$$

$\mathcal{A}_i$ and $\mathcal{B}_j$ are differential operators with respect to p and q as

$$\mathcal{A}_i = \frac{1}{i!}\left[(p-1)\partial_p\right]^i, \quad \mathcal{B}_j = \frac{1}{j!}\left[(q-1)\partial_q\right]^j, \tag{2.559}$$

and $\xi_0(p)$, $\eta_0(q)$ are arbitrary functions of p and q. It is easy to see that the above $m^{(n,k,l)}$ and

$$\varphi^{(n,k,l)} = p^n(1-1/p)^{-k}(1-\rho^2-p)^l e^{\xi}, \tag{2.560}$$

$$\psi^{(n,k,l)} = q^n(1-\rho^2-q)^k(1-1/q)^{-l}e^{\eta} \tag{2.561}$$

satisfy the differential and difference relations (2.554) without i and j indices. Then, since the differential operators $\mathcal{A}_i$ and $\mathcal{B}_j$ commute with ∂_x and ∂_y, the above $m_{i,j}^{(n,k,l)}$ and

$$\varphi_i^{(n)}(k,l) = \mathcal{A}_i\varphi^{(n)}(k,l), \quad \psi_j^{(n)}(k,l) = \mathcal{B}_j\psi^{(n)}(k,l) \tag{2.562}$$

would satisfy the differential and difference relations (2.554). Lemma 2.12 then shows that, for any sequences of indices $(I_1, I_2, \cdots, I_N)$ and $(J_1, J_2, \cdots, J_N)$, the determinant

$$\tau_{n,k,l} = \det_{1\le i,j\le N}\left(m^{(n,k,l)}_{I_i,J_j}\right) \tag{2.563}$$

would satisfy the bilinear equations (2.549).

In order for the above $\tau_{n,k,l}$ function to satisfy the index-reduction condition (2.550), we restrict its matrix elements further as

$$\tau_{n,k,l} = \det_{1\le i,j\le N}\left(m^{(n,k,l)}_{2i-1,2j-1}\Big|_{p=q=1+\rho}\right). \tag{2.564}$$

Following the calculation in Ohta and Yang (2014), this determinant satisfies the index-reduction condition (2.550) with $C = (1+\rho)^{4N}$, i.e.,

$$\tau_{n,k+1,l+1} = (1+\rho)^{4N}\tau_{n,k,l}. \tag{2.565}$$

By reparameterizing $p = 1+\rho P$ and $q = 1+\rho Q$, the $\tau_{n,k,l}$ determinant in (2.564) can be rewritten as

$$\tau_{n,k,l} = \det_{1\le i,j\le N}\left(m^{(n,k,l)}_{2i-1,2j-1}\Big|_{P=Q=1}\right), \tag{2.566}$$

where

$$m^{(n,k,l)}_{i,j} = \mathcal{A}_i\mathcal{B}_j m^{(n,k,l)}, \tag{2.567}$$

$$\begin{aligned} m^{(n,k,l)} = {} & \frac{(-1)^{k+l}\rho^{-1}}{P+Q+\rho(1+PQ)}(1+\rho P)^{n+k} \\ & \times (1+\rho Q)^{n+l}\left(\frac{\rho+Q}{P}\right)^k\left(\frac{\rho+P}{Q}\right)^l e^{\xi(P)+\eta(Q)}, \end{aligned} \tag{2.568}$$

$$\begin{aligned} \xi(P)+\eta(Q) = {} & \left(1+\rho P-\frac{1-\rho^2}{1+\rho Q}\right)x+\left(1+\rho Q-\frac{1-\rho^2}{1+\rho P}\right)y \\ & +\xi_0(P)+\eta_0(Q), \end{aligned} \tag{2.569}$$

and

$$\mathcal{A}_i = \frac{1}{i!}\left(P\partial_P\right)^i, \quad \mathcal{B}_j = \frac{1}{j!}\left(Q\partial_Q\right)^j. \tag{2.570}$$

As in Sect. 2.1.1, we introduce free parameters in the $\tau_{n,k,l}$ solution by expanding free functions $\xi_0(P)$ and $\eta_0(Q)$ as

$$\xi_0(P) = \sum_{r=1}^{\infty} a_r \ln^r P, \quad \eta_0(Q) = \sum_{r=1}^{\infty} b_r \ln^r Q, \tag{2.571}$$

where a_r, b_r are complex constants. Then, if we impose the parameter conditions of $b_r = a_r^*$, we can readily see that the $\tau_{n,k,l}$ function would satisfy the complex conjugacy condition (2.552). Hence, the f_n, g_n functions in Eq. (2.553) would give AL's rogue wave solutions through the variable transformation (2.546).

Summarizing the above results, we have the following result on AL's rogue waves in differential operator form.

Lemma 2.13 *General N-th order rogue waves in differential form in the AL equations (2.535)–(2.536) are*

$$u_n^{[N]}(t) = \frac{\rho}{\sqrt{1-\rho^2}} \frac{g_n}{f_n} e^{i(\theta n - \omega t)}, \tag{2.572}$$

where ρ and θ are free real constants, $\omega = 2\cos\theta/(1-\rho^2)$,

$$f_n = \tau_{n,0,0}, \quad g_n = \tau_{n,1,0}/(1+\rho)^{2N}, \tag{2.573}$$

$$\tau_{n,k,l} = \det_{1\le i,j\le N} \left(m_{2i-1,2j-1}^{(n,k,l)} \right), \tag{2.574}$$

the matrix elements in τ_n are defined by

$$m_{i,j}^{(n,k,l)} = \frac{(P\partial_P)^i}{i!} \frac{(Q\partial_Q)^j}{j!} m^{(n,k,l)}\Big|_{P=Q=1}, \tag{2.575}$$

$m^{(n,k,l)}$ is defined by

$$\begin{aligned} m^{(n,k,l)} = {} & \frac{(-1)^{k+l}\rho^{-1}}{P+Q+\rho(1+PQ)} (1+\rho P)^{n+k} \\ & \times (1+\rho Q)^{n+l} \left(\frac{\rho+Q}{P} \right)^k \left(\frac{\rho+P}{Q} \right)^l e^{\Theta}, \end{aligned} \tag{2.576}$$

$$\begin{aligned} \Theta = {} & \left(1+\rho P - \frac{1-\rho^2}{1+\rho Q} \right) x + \left(1+\rho Q - \frac{1-\rho^2}{1+\rho P} \right) y \\ & + \sum_{r=1}^{\infty} \hat{a}_r \ln^r P + \sum_{r=1}^{\infty} \hat{a}_r^* \ln^r Q, \end{aligned} \tag{2.577}$$

and $\hat{a}_r$ ($r = 1, 2, \ldots, 2N-1$) are free complex constants.

Lastly, we remove the differential operators in the above lemma and derive more explicit expressions of rogue waves through Schur polynomials. This calculation is similar to that in Sect. 2.1.1 (see Ohta and Yang (2014) for details). The explicit expressions out of this calculation are as shown in Theorem 2.9, where parameters a_r are linearly related to $\hat{a}_r$ of the above lemma as $a_r = \hat{a}_r - g_r(1)$. This completes the proof of Theorem 2.9.

The fundamental rogue wave expression can be derived from Theorem 2.9 by setting $N = 1$ and we get

$$u_n^{[1]}(t) = \frac{\rho}{\sqrt{1-\rho^2}} e^{\mathrm{i}(\theta n - \omega t)} \left[1 + \frac{2i\rho^2\omega t + (1+\rho)(a_1 - a_1^*) - 1}{\rho^2(1+\rho)^2|R|^2 + \frac{1}{4}(1-\rho^2)} \right], \tag{2.578}$$

where

$$R = \frac{1}{1+\rho} \left[n + \mathrm{i} \left(\frac{e^{-\mathrm{i}\theta}}{1+\rho} - \frac{e^{\mathrm{i}\theta}}{1-\rho} \right) t \right] + \frac{a_1^*}{\rho}. \tag{2.579}$$

Since the AL equation is invariant under a time shift, we can normalize $\Im(a_1) = 0$ through such a time shift (as stated in Theorem 2.9). In this case, by defining a new parameter $n_0 = -(1+\rho)\Re(a_1)/\rho$, the above fundamental rogue waves can be rewritten as

$$u_n^{[1]}(t) = \frac{\rho}{\sqrt{1-\rho^2}} e^{\mathrm{i}(\theta n - \omega t)} \times \left[1 + \frac{2i\rho^2\omega t - 1}{\rho^2 (n + \omega t \tan\theta - n_0)^2 + \rho^4\omega^2 t^2 + \frac{1}{4}(1-\rho^2)} \right], \tag{2.580}$$

where ρ, θ and n_0 are free real parameters. One can see from Eq. (2.580) that θ can be viewed as a velocity parameter of this rogue wave, with the velocity being $-\omega \tan\theta$, i.e., $2\sin\theta/(\rho^2 - 1)$. Thus rogue waves with $\sin\theta = 0$ can be called non-traveling, and those with other θ values called traveling.

When $|\rho| < 1$, these fundamental rogue waves satisfy the focusing AL equation (2.535). Two such solutions, one non-traveling and the other traveling, are displayed in Fig. 2.12. Compared to NLS's fundamental rogue waves (Peregrine solutions), the present rogue waves can reach much higher peak amplitudes (relative to the background amplitude).

When $|\rho| > 1$, these fundamental rogue waves satisfy the defocusing AL equation (2.536). Two such solutions, both non-traveling, are displayed in Fig. 2.13. The left solution reaches peak amplitudes at two lattice sites, because we chose $n_0 = 1/2$. The right solution is unbounded and blows up to infinity in finite time. This solution blowup occurs in the defocusing AL equation, but not in the focusing one.

Second-order rogue waves in the AL equations can be obtained by taking $N = 2$ in Theorem 2.9. Such solutions in the focusing case, for $\rho = 1/2$, $\theta = 0$, $a_1 = 0$ and four different a_3 values of 0, 1/20, 10i and 10, are shown in Fig. 2.14. It is seen

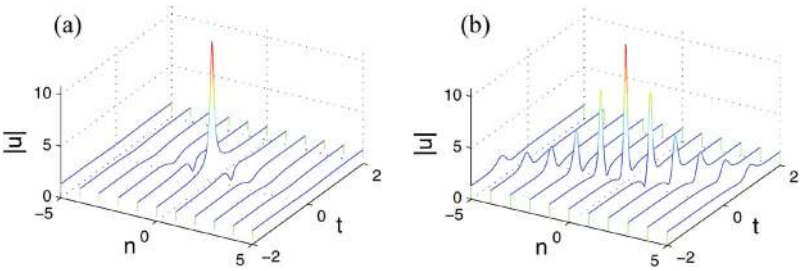

Fig. 2.12 Fundamental rogue waves $u_n^{[1]}(t)$ from Eq. (2.580) in the focusing Ablowitz-Ladik equation (2.535) with $\rho = 0.8$ and $n_0 = 0$. (**a**) A non-traveling rogue wave where $\theta = 0$; (**b**) a traveling rogue wave where $\theta = -1.2$

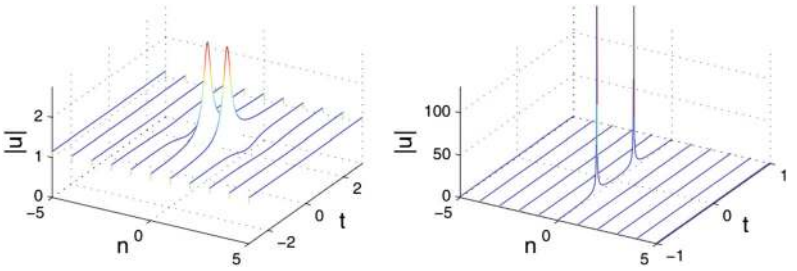

Fig. 2.13 Fundamental rogue waves $u_n^{[1]}(t)$ from Eq. (2.580) in the defocusing Ablowitz-Ladik equation (2.536) with $\rho = 2$ and $\theta = 0$. Left: $n_0 = 1/2$; right: $n_0 = 0$

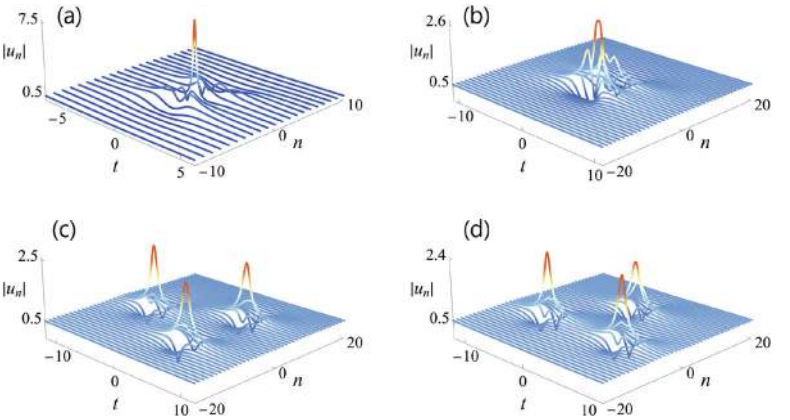

Fig. 2.14 Second-order rogue waves $u_n^{[2]}(t)$ in the focusing Ablowitz-Ladik equation (2.535) for $\rho = 1/2$, $\theta = 0$ and $a_1 = 0$. (**a**) $a_3 = 0$; (**b**) $a_3 = 1/20$; (**c**) $a_3 = 10\mathrm{i}$; (**d**) $a_3 = 10$

that when a_3 is small, the solution concentrates near the origin. When a_3 is large, it splits into three fundamental rogue waves with different peak amplitudes.

2.9 Manakov System

The Manakov system is

$$\left.\begin{aligned}(\mathrm{i}\partial_t + \partial_x^2)u_1 + (\epsilon_1|u_1|^2 + \epsilon_2|u_2|^2)u_1 = 0,\\ (\mathrm{i}\partial_t + \partial_x^2)u_2 + (\epsilon_1|u_1|^2 + \epsilon_2|u_2|^2)u_2 = 0,\end{aligned}\right\} \tag{2.581}$$

where $\epsilon_1 = \pm 1$ and $\epsilon_2 = \pm 1$. These equations govern many physical processes such as the transmission of light in a randomly birefringent optical fiber (see Sect. 1.3), the interaction of two incoherent light beams in crystals (Kang et al. 1996; Chen et al. 1997), and the evolution of two-component Bose-Einstein condensates (Kevrekidis et al. 2008; Hoefer et al. 2011). Integrability of this system for $\epsilon_1 = \epsilon_2$ was reported by Manakov (1973). Integrability of this system for general ϵ_1 and ϵ_2 values was reported in Wang et al. (2010).

This Manakov system admits plane wave solutions

$$u_{1,0}(x,t) = \rho_1 e^{\mathrm{i}(k_1 x + \omega_1 t)}, \quad u_{2,0}(x,t) = \rho_2 e^{\mathrm{i}(k_2 x + \omega_2 t)}, \tag{2.582}$$

where (k_1, k_2) and (ω_1, ω_2) are the wavenumbers and frequencies of the two components, and (ρ_1, ρ_2) are their amplitudes which will be set real using phase invariance of the system. Parameters of these plane waves satisfy the following relations,

$$\omega_1 = \epsilon_1\rho_1^2 + \epsilon_2\rho_2^2 - k_1^2, \quad \omega_2 = \epsilon_1\rho_1^2 + \epsilon_2\rho_2^2 - k_2^2. \tag{2.583}$$

Then, boundary conditions for rogue waves in the Manakov system are

$$u_j(x,t) \to u_{j,0}(x,t), \quad x,t \to \pm\infty, \quad j = 1,2. \tag{2.584}$$

Rogue waves in the Manakov system have been derived by Baronio et al. (2012, 2014), Ling et al. (2014), Chen and Mihalache (2015), and Zhao et al. (2016a) by Darboux transformation, and by Yang and Yang (2021c, 2023a) by the bilinear method. Here, we will derive these rogue waves by the bilinear method, following Yang and Yang (2021c, 2023a).

From a mathematical point of view, there are several types of Manakov rogue waves whose expressions have different determinant structures. In the bilinear framework, these rogue types are determined by non-imaginary roots and their multiplicities of the following algebraic equation

$$Q_1'(p) = 0, \tag{2.585}$$

where

$$Q_1(p) = \frac{\epsilon_1 \rho_1^2}{p - \mathrm{i}k_1} + \frac{\epsilon_2 \rho_2^2}{p - \mathrm{i}k_2} + 2p. \tag{2.586}$$

The reason for this will be seen later. Thus, we will discuss roots of Eq. (2.585) first.

The algebraic equation (2.585) can be rewritten as

$$2(p - \mathrm{i}k_1)^2 (p - \mathrm{i}k_2)^2 - \epsilon_1 \rho_1^2 (p - \mathrm{i}k_2)^2 - \epsilon_2 \rho_2^2 (p - \mathrm{i}k_1)^2 = 0, \tag{2.587}$$

which is a quartic equation for p. Thus, it has four roots (counting multiplicity). These roots are dependent on the parameters in the Manakov system (2.581) and in the boundary conditions (2.584). Notice that if p is a root, so is $-p^*$. Thus, non-imaginary roots appear as pairs of $(p, -p^*)$. Writing $p = \mathrm{i}\tilde{p}$, Eq. (2.587) becomes a quartic equation for $\tilde{p}$ with real coefficients, whose root structure depends only on the sign of its discriminant

$$\begin{aligned} \Delta = 32\epsilon_1\epsilon_2\rho_1^2\rho_2^2 (k_1 - k_2)^2 \Big\{ \Big[2(k_1 - k_2)^2 + \epsilon_1\rho_1^2 + \epsilon_2\rho_2^2 \Big]^3 \\ -27 \Big[2(k_1 - k_2)^2 \epsilon_1\epsilon_2\rho_1^2\rho_2^2 \Big] \Big\}. \end{aligned} \tag{2.588}$$

Below, we delineate this root structure for the three cases of (ϵ_1, ϵ_2) values

$$(\epsilon_1, \epsilon_2) = (1, 1), \quad \text{(focusing case)} \tag{2.589}$$

$$(\epsilon_1, \epsilon_2) = (-1, -1), \quad \text{(defocusing case)} \tag{2.590}$$

$$(\epsilon_1, \epsilon_2) = (1, -1). \quad \text{(focusing-defocusing case)} \tag{2.591}$$

1. In the focusing case (2.589), using the inequality of $(a+b+c)^3 \geq 27abc$ for any non-negative real values of a, b and c, with the equal sign realized if and only if $a = b = c$, it is easy to see that $\Delta \geq 0$, and $\Delta = 0$ if and only if

$$\rho_1 = \rho_2 = \sqrt{2}\,|k_1 - k_2|, \quad k_1 \neq k_2. \tag{2.592}$$

When $\Delta = 0$, i.e., under the above parameter conditions (2.592), Eq. (2.587) admits a pair of double roots:

$$(\hat{p}_0, \hat{p}_0, -\hat{p}_0^*, -\hat{p}_0^*), \tag{2.593}$$

where

$$\hat{p}_0 = \frac{\sqrt{3}}{2}(k_1 - k_2) + \frac{\mathrm{i}}{2}(k_1 + k_2). \tag{2.594}$$

When $\Delta > 0$, i.e., the parameter conditions (2.592) are not met, there cannot be any repeated root. In addition, Eq. (2.587) cannot admit any purely-imaginary root, because such a root would make all terms on the left side of Eq. (2.587) to

have the same sign, whose sum cannot be zero. Thus, the root structure in this case is

$$(p_{0,1}, p_{0,2}, -p_{0,1}^*, -p_{0,2}^*), \tag{2.595}$$

where $p_{0,1} \neq p_{0,2}$, i.e., there are two pairs of non-imaginary simple roots here.

We see that in the focusing case, there are always non-imaginary roots in Eq. (2.585), and such roots can be simple or have multiplicity two. This will imply that rogue waves exist in all parameter regimes in the focusing case. In addition, multiple types of rogue waves exist depending on the multiplicity of those non-imaginary roots.

2. In the defocusing case (2.590) and focusing-defocusing case (2.591), Eq. (2.587) always admits at least two simple imaginary roots. The reason can be seen by dividing that equation with $(p - \mathrm{i}k_1)^2(p - \mathrm{i}k_2)^2$ and setting $p = \mathrm{i}\tilde{p}$, which results in a real equation for $\tilde{p}$ with two rational terms and one constant term. By examining the signs of these terms at $\tilde{p} = \pm\infty$ and near the singularities at $\tilde{p} = k_1$ and k_2, and utilizing the intermediate value theorem, we can readily see that this real $\tilde{p}$ equation has at least two simple real roots, and thus the p equation (2.587) admits at least two simple imaginary roots. The nature of the other two roots of p can be obtained by putting $p = \mathrm{i}\tilde{p}$ into Eq. (2.587), which results in a real quartic equation for $\tilde{p}$. Combining the classical results on the root structure of a real quartic equation with the current information of $\tilde{p}$ admitting at least two simple real roots, we see that the nature of the other two roots of $\tilde{p}$ (and hence p) depends only on the sign of the discriminant Δ in Eq. (2.588). Putting these results together, root structures of the p equation (2.587) in the defocusing and focusing-defocusing cases are summarized as follows.

$\Delta > 0$: four imaginary simple roots;

$\Delta < 0$: a pair of non-imaginary simple roots $(p_0, -p_0^*)$ and two imaginary simple roots;

$\Delta = 0$: one imaginary double root and two imaginary simple roots.

Since only non-imaginary roots could generate rogue waves, we see that in the defocusing and focusing-defocusing cases, the condition of $\Delta < 0$ must be met. Importantly, this condition can indeed be met in both the defocusing and focusing-defocusing cases, albeit in certain parameter regimes only. This means that we can have rogue waves in these two cases under certain parameter conditions. Since these non-imaginary roots are simple, these rogue waves are of a single type. The existence of these rogue waves, especially in the defocusing case, is surprising, since the scalar case of the defocusing NLS equation does not admit rogue waves.

Next, we present three types of Manakov rogue waves according to non-imaginary roots and their multiplicities in the algebraic equation (2.585).

2.9.1 Rogue Waves for a Simple Non-Imaginary Root

Theorem 2.10 *If the algebraic equation (2.585) admits a non-imaginary simple root p_0, then the Manakov system (2.581) under boundary conditions (2.584) would admit nonsingular rogue wave solutions*

$$u_{1,N}(x,t) = \rho_1 \frac{g_{1,N}}{f_N} e^{\mathrm{i}(k_1 x + \omega_1 t)}, \quad u_{2,N}(x,t) = \rho_2 \frac{g_{2,N}}{f_N} e^{\mathrm{i}(k_2 x + \omega_2 t)}, \tag{2.596}$$

where N is an arbitrary positive integer which represents the order of the rogue wave,

$$f_N = \sigma_{0,0}, \quad g_{1,N} = \sigma_{1,0}, \quad g_{2,N} = \sigma_{0,1}, \tag{2.597}$$

$$\sigma_{n,k} = \det_{1 \le i,j \le N} \left(\phi^{(n,k)}_{2i-1,2j-1} \right), \tag{2.598}$$

the matrix elements in $\sigma_{n,k}$ are defined by

$$\phi^{(n,k)}_{i,j} = \sum_{\nu=0}^{\min(i,j)} \left[\frac{|p_1|^2}{(p_0 + p_0^*)^2} \right]^{\nu} S_{i-\nu}(\boldsymbol{x}^+(n,k) + \nu \boldsymbol{s})\, S_{j-\nu}(\boldsymbol{x}^-(n,k) + \nu \boldsymbol{s}^*), \tag{2.599}$$

vectors $\boldsymbol{x}^{\pm}(n,k) = (x_1^{\pm}, 0, x_3^{\pm}, 0, \cdots)$ are defined by

$$x_r^+(n,k) = p_r x + \left(\sum_{i=0}^{r} p_i\, p_{r-i} \right) (\mathrm{i}t) + n\theta_r + k\lambda_r + a_r, \tag{2.600}$$

$$x_r^-(n,k) = p_r^* x - \left(\sum_{i=0}^{r} p_i^*\, p_{r-i}^* \right) (\mathrm{i}t) - n\theta_r^* - k\lambda_r^* + a_r^*, \tag{2.601}$$

$\boldsymbol{s} = (s_1, s_2, \cdots)$, $(p_r, \theta_r, \lambda_r, s_r)$ are coefficients from the expansions

$$p(\kappa) = \sum_{r=0}^{\infty} p_r \kappa^r, \quad \ln\left[\frac{p(\kappa) - \mathrm{i}k_1}{p_0 - \mathrm{i}k_1} \right] = \sum_{r=1}^{\infty} \theta_r \kappa^r, \tag{2.602}$$

$$\ln\left[\frac{p(\kappa) - \mathrm{i}k_2}{p_0 - \mathrm{i}k_2} \right] = \sum_{r=1}^{\infty} \lambda_r \kappa^r, \tag{2.603}$$

$$\ln\left[\frac{1}{\kappa} \left(\frac{p_0 + p_0^*}{p_1} \right) \left(\frac{p(\kappa) - p_0}{p(\kappa) + p_0^*} \right) \right] = \sum_{r=1}^{\infty} s_r \kappa^r, \tag{2.604}$$

the function $p(\kappa)$ is defined by the equation

$$Q_1[p(\kappa)] = Q_1(p_0)\cosh(\kappa), \tag{2.605}$$

$a_1 = 0$, and $a_3, a_5, \cdots, a_{2N-1}$ are free irreducible complex constants.

The proof of this theorem will be presented in Sect. 2.9.4.

As we have explained earlier, this type of rogue waves exists in the focusing case when $\Delta > 0$ and in the defocusing and focusing-defocusing cases when $\Delta < 0$.

The simplest rogue wave of this type can be obtained by setting $N = 1$ in the above theorem and is given by

$$u_{1,1}(x,t) = \hat{u}_1(x,t)e^{\mathrm{i}(k_1x+\omega_1t)}, \quad u_{2,1}(x,t) = \hat{u}_2(x,t)e^{\mathrm{i}(k_2x+\omega_2t)}, \tag{2.606}$$

where

$$\hat{u}_1(x,t) = \rho_1\frac{[p_1x + 2p_0p_1(\mathrm{i}t) + \theta_1]\left[p_1^*x - 2p_0^*p_1^*(\mathrm{i}t) - \theta_1^*\right] + \zeta_0}{|p_1x + 2p_0p_1(\mathrm{i}t)|^2 + \zeta_0}, \tag{2.607}$$

$$\hat{u}_2(x,t) = \rho_2\frac{[p_1x + 2p_0p_1(\mathrm{i}t) + \lambda_1]\left[p_1^*x - 2p_0^*p_1^*(\mathrm{i}t) - \lambda_1^*\right] + \zeta_0}{|p_1x + 2p_0p_1(\mathrm{i}t)|^2 + \zeta_0}, \tag{2.608}$$

$$\theta_1 = \frac{p_1}{p_0 - \mathrm{i}k_1},\ \lambda_1 = \frac{p_1}{p_0 - \mathrm{i}k_2},\ \zeta_0 = \frac{|p_1|^2}{(p_0 + p_0^*)^2}. \tag{2.609}$$

This rogue wave is ratios of second-degree polynomials in x and t, which are the lowest polynomial degrees possible for rogue waves in the Manakov system. Thus, we will call it the fundamental rogue wave of the Manakov system. Note that p_1 actually cancels out in the above formulae; we retain p_1 here so that the reader can easily see how these formulae are obtained from Theorem 2.10. In Fig. 2.15, we plot this fundamental rogue wave in the focusing, focusing-defocusing and defocusing cases under system parameters which are listed in that figure's captions. Interestingly, in the focusing and focusing-defocusing cases, these vector rogue waves are bright in the u_1 component but dark in the u_2 component. In the defocusing case, both components are dark rogue waves. These dark rogue waves strongly contrast the bright Peregrine rogue waves of the NLS equation.

Second-order rogue waves of this type can be obtained by setting $N = 2$ in the above theorem. In these solutions, f_2, $g_{1,2}$ and $g_{2,2}$ are degree-6 polynomials in both x and t. For the same parameter values as in Fig. 2.15, with the additional parameter value of $a_3 = 50$ in the focusing case, $a_3 = 30\mathrm{i}$ in the focusing-defocusing case, and $a_3 = 10\mathrm{i}$ in the defocusing case, the corresponding rogue waves are plotted in Fig. 2.16. In all three cases, the second-order rogue wave splits into three fundamental rogue waves.

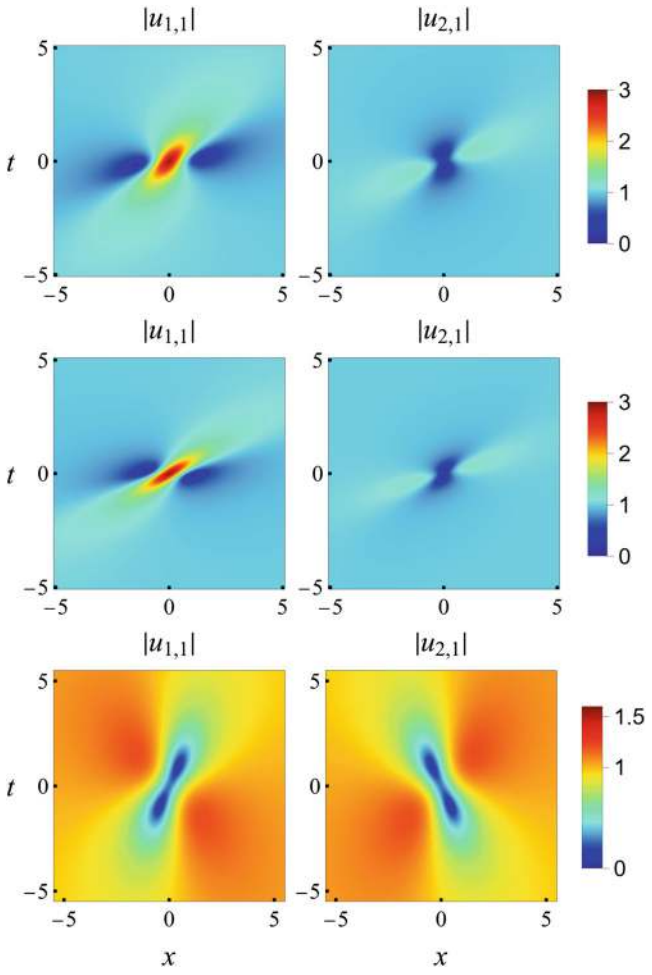

Fig. 2.15 Density plots of the fundamental rogue wave $|u_{1,1}(x,t)|$ and $|u_{2,1}(x,t)|$ in Eq. (2.606) in the Manakov equations with boundary parameters $\rho_1 = \rho_2 = 1$ and $k_1 = -k_2 = 1/2$. Upper row: focusing case ($\epsilon_1 = \epsilon_2 = 1$), with $p_0 \approx 0.6360 + 0.3931\mathrm{i}$. Middle row: focusing-defocusing case ($\epsilon_1 = 1, \epsilon_2 = -1$), with $p_0 \approx 0.7276 + 0.6053\mathrm{i}$. Lower row: defocusing case ($\epsilon_1 = \epsilon_2 = -1$), with $p_0 = [2\sqrt{3} - 3]^{1/2}/2$

2.9.2 *Rogue Waves for Two Simple Non-Imaginary Roots*

Theorem 2.11 *If the algebraic equation (2.585) admits two non-imaginary simple roots $p_{0,1}$ and $p_{0,2}$ with $p_{0,2} \neq -p_{0,1}^*$, which occurs only in the focusing Manakov system (with $\epsilon_1 = \epsilon_2 = 1$) when parameter conditions (2.592) are not met, then this focusing Manakov system (2.581) under boundary conditions (2.584) admits nonsingular (N_1, N_2)-th order rogue wave solutions*

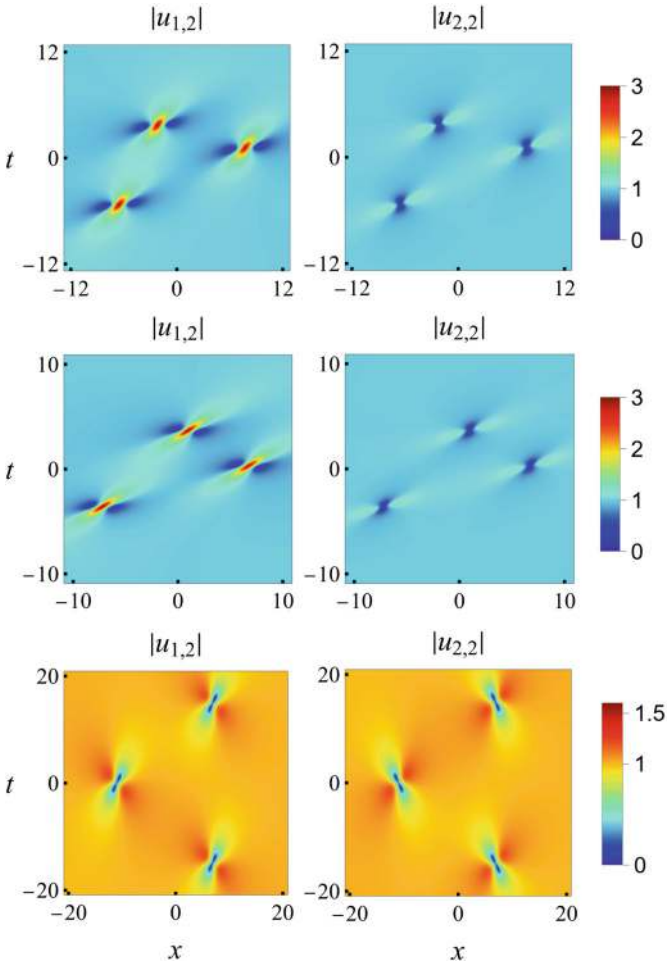

Fig. 2.16 Density plots of the second-order rogue wave $|u_{1,2}(x,t)|$ and $|u_{2,2}(x,t)|$ in Theorem 2.10 in the Manakov equations. Parameter values are the same as in Fig. 2.15, with the additional parameter value as $a_3 = 50$ in the focusing case (upper row), $a_3 = 30\mathrm{i}$ in the focusing-defocusing case (middle row), and $a_3 = 10\mathrm{i}$ in the defocusing case (lower row)

$$u_{1,N_1,N_2}(x,t) = \rho_1 \frac{g_{1,N_1,N_2}}{f_{N_1,N_2}} e^{\mathrm{i}(k_1 x + \omega_1 t)}, \quad u_{2,N_1,N_2}(x,t) = \rho_2 \frac{g_{2,N_1,N_2}}{f_{N_1,N_2}} e^{\mathrm{i}(k_2 x + \omega_2 t)}, \tag{2.610}$$

where N_1, N_2 are arbitrary positive integers,

$$f_{N_1,N_2} = \sigma_{0,0}, \quad g_{1,N_1,N_2} = \sigma_{1,0}, \quad g_{2,N_1,N_2} = \sigma_{0,1}, \tag{2.611}$$

$\sigma_{n,k}$ is a 2×2 block determinant

$$\sigma_{n,k} = \det \begin{pmatrix} \sigma_{n,k}^{[1,1]} & \sigma_{n,k}^{[1,2]} \\ \sigma_{n,k}^{[2,1]} & \sigma_{n,k}^{[2,2]} \end{pmatrix}, \tag{2.612}$$

$$\sigma_{n,k}^{[I,J]} = \left(\phi_{2i-1,2j-1}^{(n,k,I,J)} \right)_{1 \le i \le N_I, 1 \le j \le N_J}, \tag{2.613}$$

the matrix elements in $\sigma_{n,k}^{[I,J]}$ *are defined by*

$$\phi_{i,j}^{(n,k,I,J)} = \sum_{\nu=0}^{\min(i,j)} \left(\frac{1}{p_{0,I} + p_{0,J}^*} \right) \left[\frac{p_{1,I} p_{1,J}^*}{(p_{0,I} + p_{0,J}^*)^2} \right]^{\nu} \times S_{i-\nu} \left(\boldsymbol{x}_{I,J}^{+}(n,k) + \nu \boldsymbol{s}_{I,J} \right) S_{j-\nu} \left(\boldsymbol{x}_{J,I}^{-}(n,k) + \nu \boldsymbol{s}_{J,I}^* \right), \tag{2.614}$$

vectors $\boldsymbol{x}_{I,J}^{\pm}(n,k) = \left(x_{1,I,J}^{\pm}, x_{2,I,J}^{\pm}, \cdots \right)$ *are defined by*

$$x_{r,I,J}^{+}(n,k) = p_{r,I} x + \left(\sum_{i=0}^{r} p_{i,I} p_{r-i,I} \right) (\mathrm{i}t) + n\theta_{r,I} + k\lambda_{r,I} - b_{r,I,J} + a_{r,I}, \tag{2.615}$$

$$x_{r,I,J}^{-}(n,k) = p_{r,I}^* x - \left(\sum_{i=0}^{r} p_{i,I}^* p_{r-i,I}^* \right) (\mathrm{i}t) - n\theta_{r,I}^* - k\lambda_{r,I}^* - b_{r,I,J}^* + a_{r,I}^*, \tag{2.616}$$

$\boldsymbol{s}_{I,J} = \left(s_{1,I,J}, s_{2,I,J}, \cdots \right)$, $p_{r,I}$, $\theta_{r,I}$, $\lambda_{r,I}$, $b_{r,I,J}$ *and* $s_{r,I,J}$ *are coefficients from the expansions*

$$p_I(\kappa) = \sum_{r=0}^{\infty} p_{r,I} \kappa^r, \quad \ln \left[\frac{p_I(\kappa) - \mathrm{i}k_1}{p_{0,I} - \mathrm{i}k_1} \right] = \sum_{r=1}^{\infty} \theta_{r,I} \kappa^r, \tag{2.617}$$

$$\ln \left[\frac{p_I(\kappa) - \mathrm{i}k_2}{p_{0,I} - \mathrm{i}k_2} \right] = \sum_{r=1}^{\infty} \lambda_{r,I} \kappa^r, \quad \ln \left[\frac{p_I(\kappa) + p_{0,J}^*}{p_{0,I} + p_{0,J}^*} \right] = \sum_{r=1}^{\infty} b_{r,I,J} \kappa^r, \tag{2.618}$$

$$\ln \left[\frac{1}{\kappa} \left(\frac{p_{0,I} + p_{0,J}^*}{p_{1,I}} \right) \left(\frac{p_I(\kappa) - p_{0,I}}{p_I(\kappa) + p_{0,J}^*} \right) \right] = \sum_{r=1}^{\infty} s_{r,I,J} \kappa^r, \tag{2.619}$$

$p_I(\kappa)$ is defined by the equation

$$Q_1[p_I(\kappa)] = Q_1(p_{0,I})\cosh(\kappa), \tag{2.620}$$

and $(a_{1,1}, \ldots, a_{2N_1-1,1})$, $(a_{1,2}, \ldots, a_{2N_2-1,2})$ are free complex constants.

The proof of this theorem will be presented in Sect. 2.9.4.

The simplest rogue waves of this type can be obtained by setting $N_1 = N_2 = 1$ in the above theorem. These rogue waves contain two free internal complex parameters $a_{1,1}$ and $a_{1,2}$. Through a shift of the (x, t) axes, we normalize $a_{1,1} = 0$. Then, this rogue wave for two different values of $a_{1,2} = 0$ and 2 is plotted in Fig. 2.17 under system and boundary parameters which are listed in the figure's captions. The rogue wave at $a_{1,2} = 2$ (lower row) comprises two separate simpler rogue waves, which turn out to be fundamental rogue waves (2.606) for the two individual $p_{0,1}$ and $p_{0,2}$ values. Thus, rogue waves in Theorem 2.11 can be viewed as a nonlinear superposition of rogue waves of Theorem 2.10 with two different p_0 values. The rogue wave at $a_{1,2} = 0$ (upper row) in Fig. 2.17 can be regarded as the merging of the two fundamental rogue waves in the lower row. It has a new composite structure.

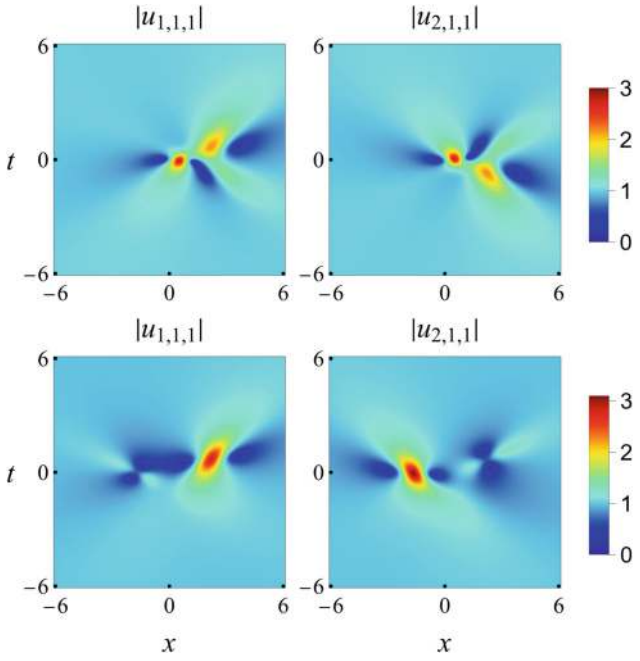

Fig. 2.17 Density plots of the $(1, 1)$-th order rogue wave $|u_{1,1,1}(x, t)|$ and $|u_{2,1,1}(x, t)|$ in Theorem 2.11 in the focusing Manakov equations with parameter values of $\epsilon_1 = \epsilon_2 = 1$, $\rho_1 = \rho_2 = 1$, $k_1 = -k_2 = 1/2$, $p_{0,1} \approx 0.6360 + 0.3931\mathrm{i}$ and $p_{0,2} \approx 0.6360 - 0.3931\mathrm{i}$. Upper row: $a_{1,2} = 0$. Lower row: $a_{1,2} = 2$

2.9.3 Rogue Waves for a Double Non-Imaginary Root

Rogue waves given above for a simple root and two simple roots in the $Q_1'(p) = 0$ equation feature τ functions that involve Schur polynomials with index jumps of 2. If that root is a double root (which only arises in the focusing case), the Manakov system would admit rogue waves whose τ functions involve Schur polynomials with index jumps of 3. These latter rogue waves are given below.

Theorem 2.12 *If the algebraic equation (2.585) admits a non-imaginary double root p_0, which occurs only in the focusing Manakov system (with $\epsilon_1 = \epsilon_2 = 1$) under parameter conditions (2.592), i.e.,*

$$\rho_1 = \rho_2 = \sqrt{2}\,|k_1 - k_2|\,, \quad k_1 \neq k_2, \tag{2.621}$$

then this focusing Manakov system (2.581) under boundary conditions (2.584) would admit nonsingular (N_1, N_2)-th order rogue wave solutions

$$u_{1,N_1,N_2}(x,t) = \rho_1 \frac{g_{1,N_1,N_2}}{f_{N_1,N_2}} e^{\mathrm{i}(k_1 x + \omega_1 t)}, \tag{2.622}$$

$$u_{2,N_1,N_2}(x,t) = \rho_1 \frac{g_{2,N_1,N_2}}{f_{N_1,N_2}} e^{\mathrm{i}(k_2 x + \omega_2 t)}, \tag{2.623}$$

where N_1 and N_2 are arbitrary non-negative integers,

$$f_{N_1,N_2} = \sigma_{0,0}, \quad g_{1,N_1,N_2} = \sigma_{1,0}, \quad g_{2,N_1,N_2} = \sigma_{0,1}, \tag{2.624}$$

$\sigma_{n,k}$ is given by the following 2×2 block determinant

$$\sigma_{n,k} = \det \begin{pmatrix} \sigma_{n,k}^{[1,1]} & \sigma_{n,k}^{[1,2]} \\ \sigma_{n,k}^{[2,1]} & \sigma_{n,k}^{[2,2]} \end{pmatrix}, \tag{2.625}$$

$$\sigma_{n,k}^{[I,J]} = \left(\phi_{3i-I,\,3j-J}^{(n,k,I,J)} \right)_{1 \le i \le N_I,\, 1 \le j \le N_J}, \tag{2.626}$$

the matrix elements in $\sigma_{n,k}^{[I,J]}$ are defined by

$$\phi_{i,j}^{(n,k,I,J)} = \sum_{\nu=0}^{\min(i,j)} \left[\frac{|p_1|^2}{(p_0 + p_0^*)^2} \right]^{\nu} S_{i-\nu}(\boldsymbol{x}_I^+(n,k) + \nu \boldsymbol{s})\, S_{j-\nu}(\boldsymbol{x}_J^-(n,k) + \nu \boldsymbol{s}^*), \tag{2.627}$$

vectors $\boldsymbol{x}_I^+(n,k) = \left(x_{1,I}^+, x_{2,I}^+, \cdots \right)$ and $\boldsymbol{x}_J^-(n,k) = \left(x_{1,J}^-, x_{2,J}^-, \cdots \right)$ are defined by

$$x_{r,I}^{+}(n,k) = p_r x + \left(\sum_{l=0}^{r} p_l p_{r-l}\right)(\mathrm{i}t) + n\theta_r + k\lambda_r + a_{r,I}, \qquad if\, r\ mod 3 \neq 0, \tag{2.628}$$

$$x_{r,J}^{-}(n,k) = p_r^* x - \left(\sum_{l=0}^{r} p_l^* p_{r-l}^*\right)(\mathrm{i}t) - n\theta_r^* - k\lambda_r^* + a_{r,J}^*, \qquad if\, r\ mod 3 \neq 0, \tag{2.629}$$

$$x_{r,I}^{+}(n,k) = x_{r,J}^{-}(n,k) = 0, \qquad if\, r\ mod 3 = 0, \tag{2.630}$$

$\boldsymbol{s} = (s_1, s_2, \cdots)$, $(p_r, \theta_r, \lambda_r, s_r)$ are coefficients from the expansions

$$p(\kappa) = \sum_{r=0}^{\infty} p_r \kappa^r, \quad \ln\left[\frac{p(\kappa) - \mathrm{i}k_1}{p_0 - \mathrm{i}k_1}\right] = \sum_{r=1}^{\infty} \theta_r \kappa^r, \tag{2.631}$$

$$\ln\left[\frac{p(\kappa) - \mathrm{i}k_2}{p_0 - \mathrm{i}k_2}\right] = \sum_{r=1}^{\infty} \lambda_r \kappa^r, \tag{2.632}$$

$$\ln\left[\frac{1}{\kappa}\left(\frac{p_0 + p_0^*}{p_1}\right)\left(\frac{p(\kappa) - p_0}{p(\kappa) + p_0^*}\right)\right] = \sum_{r=1}^{\infty} s_r \kappa^r, \tag{2.633}$$

the function $p(\kappa)$ is defined by the equation

$$Q_1[p(\kappa)] = \frac{Q_1(p_0)}{3}\left[e^{\kappa} + 2e^{-\kappa/2}\cos\left(\frac{\sqrt{3}}{2}\kappa\right)\right], \tag{2.634}$$

and

$$(a_{1,1}, a_{2,1}, a_{4,1}, a_{5,1}, \ldots, a_{3N_1-1,1}), \quad (a_{1,2}, a_{2,2}, a_{4,2}, a_{5,2}, \ldots, a_{3N_2-2,2})$$

are free complex constants.

The proof of this theorem will be presented in Sect. 2.9.4.

Rogue waves in the above theorem contain a wide variety of solutions. For simplicity, we only illustrate solutions with either $N_1 = 0$ or $N_2 = 0$, so that the 2×2-block determinant in the τ function (2.625) degenerates to a single block. In this case, we introduce the terminology:

- *Q-type N-th order rogue waves*: rogue waves when $N_1 = N\ (> 0)$ and $N_2 = 0$;
- *R-type N-th order rogue waves*: rogue waves when $N_1 = 0$ and $N_2 = N\ (> 0)$.

The reason for the word choices of 'Q-type' and 'R-type' here is that patterns of the underlying rogue waves at large internal parameters will be related to Okamoto hierarchy polynomials $Q_N^{[m]}(z)$ and $R_N^{[m]}(z)$ respectively, as we will show in Sect. 3.3 of the next chapter.

For Q-type N-th order rogue waves, $\sigma_{n,k}$ becomes

$$\sigma_{n,k}^{(Q)} = \left(\phi_{3i-1,\,3j-1}^{(n,k)}\right)_{1\le i,j\le N}, \tag{2.635}$$

and for R-type N-th order rogue waves, $\sigma_{n,k}$ is

$$\sigma_{n,k}^{(R)} = \left(\phi_{3i-2,\,3j-2}^{(n,k)}\right)_{1\le i,j\le N}, \tag{2.636}$$

where $\phi_{i,j}^{(n,k)}$ is given by Eq. (2.627) but with indices I and J removed. Internal parameters are $(a_1, a_2, a_4, a_5, \cdots, a_{3N-1})$ for Q-type waves, and $(a_1, a_2, a_4, a_5, \cdots, a_{3N-2})$ for R-type waves. We normalize $a_1 = 0$ by a shift of the (x,t) axes. Then, internal complex parameters in these rogue waves are $(a_2, a_4, a_5, \cdots, a_{3N-1})$ for Q-type, and $(a_2, a_4, a_5, \cdots, a_{3N-2})$ for R-type.

The first (lowest) order Q-type and R-type rogue waves are those with $N = 1$. The first-order R-type rogue wave is

$$u_{1,1}(x,t) = \hat{u}_1(x,t)e^{\mathrm{i}(k_1x+\omega_1t)}, \quad u_{2,1}(x,t) = \hat{u}_2(x,t)e^{\mathrm{i}(k_2x+\omega_2t)}, \tag{2.637}$$

where

$$\hat{u}_1(x,t) = \rho_1\frac{[p_1x+2p_0p_1\,(\mathrm{i}t)+\theta_1]\left[p_1^*x-2p_0^*p_1^*\,(\mathrm{i}t)-\theta_1^*\right]+\zeta_0}{|p_1x+2p_0p_1\,(\mathrm{i}t)|^2+\zeta_0}, \tag{2.638}$$

$$\hat{u}_2(x,t) = \rho_2\frac{[p_1x+2p_0p_1\,(\mathrm{i}t)+\lambda_1]\left[p_1^*x-2p_0^*p_1^*\,(\mathrm{i}t)-\lambda_1^*\right]+\zeta_0}{|p_1x+2p_0p_1\,(\mathrm{i}t)|^2+\zeta_0}, \tag{2.639}$$

$$\theta_1 = \frac{p_1}{p_0-\mathrm{i}k_1},\ \lambda_1 = \frac{p_1}{p_0-\mathrm{i}k_2},\ \zeta_0 = \frac{|p_1|^2}{(p_0+p_0^*)^2}. \tag{2.640}$$

This rogue wave is the fundamental Manakov rogue wave given in Eq. (2.606), except that the background parameters here are under the constraints of (2.621). If we choose background wavenumbers as $k_2 = -k_1$, which is always possible through a Galilean transformation, then p_0 would be real in this case (see Eq. (2.593)). As a result, we can see that this rogue wave admits the symmetry of $\hat{u}_2(x,t) = \hat{u}_1(-x,t)$, i.e., $\hat{u}_2(x,t)$ would be a mirror image of $\hat{u}_1(x,t)$ around the t-axis in the (x,t) plane. To illustrate, let we take $k_1 = -k_2 = 1/\sqrt{12}$, which yields $p_0 = 1/2$. Then, the explicit expression of this first-order R-type rogue wave is

$$u_{1,1}(x,t)=\sqrt{\frac{2}{3}}\,\frac{x^2+t^2-\mathrm{i}(3t-\sqrt{3}x)-2}{x^2+t^2+1}e^{\mathrm{i}(12^{-1/2}x+5t/4)}, \tag{2.641}$$

$$u_{2,1}(x,t)=\sqrt{\frac{2}{3}}\,\frac{x^2+t^2-\mathrm{i}(3t+\sqrt{3}x)-2}{x^2+t^2+1}e^{\mathrm{i}(-12^{-1/2}x+5t/4)}. \tag{2.642}$$

This solution is plotted in the left column of Fig. 2.18. It is seen that both the $|u_1|$ and $|u_2|$ components of this solution have a single elongated hump of equal amplitude, and orientations of these two humps are opposite of each other with respect to the vertical t-axis.

The first-order Q-type Manakov rogue wave can also be obtained from Theorem 2.12. This solution is a ratio of polynomials of degree four in x and t, and it contains an irreducible free complex parameter a_2. When we choose $k_1=-k_2=1/\sqrt{12}$ and $p_0=1/2$, this solution with $a_2=0$ is

$$u_1(x,t)=\rho_1\frac{g_1(x,t)}{f(x,t)}\,e^{\mathrm{i}(k_1x+\omega_1t)},\quad u_2(x,t)=\rho_1\frac{g_2(x,t)}{f(x,t)}\,e^{\mathrm{i}(k_2x+\omega_2t)}, \tag{2.643}$$

where $\rho_1=\sqrt{2/3}$, $\omega_1=\omega_2=5/4$, and

$$\begin{aligned}
f(x,t)&=4+t^4+8x^2+4x^3+x^4+2t^2\left(10+6x+x^2\right),\\
g_1(x,t)&=-2-6\mathrm{i}\sqrt{3}-6\mathrm{i}t^3+t^4-4\mathrm{i}\sqrt{3}x+\left(-1+3\mathrm{i}\sqrt{3}\right)x^2\\
&\quad+\left(4+2\mathrm{i}\sqrt{3}\right)x^3+x^4\\
&\quad+6t\left[-\mathrm{i}+3\sqrt{3}+\left(-3\mathrm{i}+\sqrt{3}\right)x-\mathrm{i}x^2\right]\\
&\quad+t^2\left[5+9\mathrm{i}\sqrt{3}+2\left(6+\mathrm{i}\sqrt{3}\right)x+2x^2\right],\\
g_2(x,t)&=-2+6\mathrm{i}\sqrt{3}-6\mathrm{i}t^3+t^4+4\mathrm{i}\sqrt{3}x\\
&\quad+\left(-1-3\mathrm{i}\sqrt{3}\right)x^2+\left(4-2\mathrm{i}\sqrt{3}\right)x^3+x^4\\
&\quad-6t\left[\mathrm{i}+3\sqrt{3}+\left(3\mathrm{i}+\sqrt{3}\right)x+\mathrm{i}x^2\right]\\
&\quad+t^2\left[5-9\mathrm{i}\sqrt{3}+2\left(6-\mathrm{i}\sqrt{3}\right)x+2x^2\right].
\end{aligned}$$

This solution is plotted in the middle column of Fig. 2.18. It is seen that the profile of this solution is more complicated. If $a_2\neq 0$, the expression for this first-order Q-type solution will be more lengthy and will not be produced here. When we take $a_2=5+5\mathrm{i}$, this solution is plotted in the right column of Fig. 2.18. We can see that this solution splits approximately into two fundamental Manakov rogue waves. This splitting always occurs when the internal parameter $|a_2|$ is large.

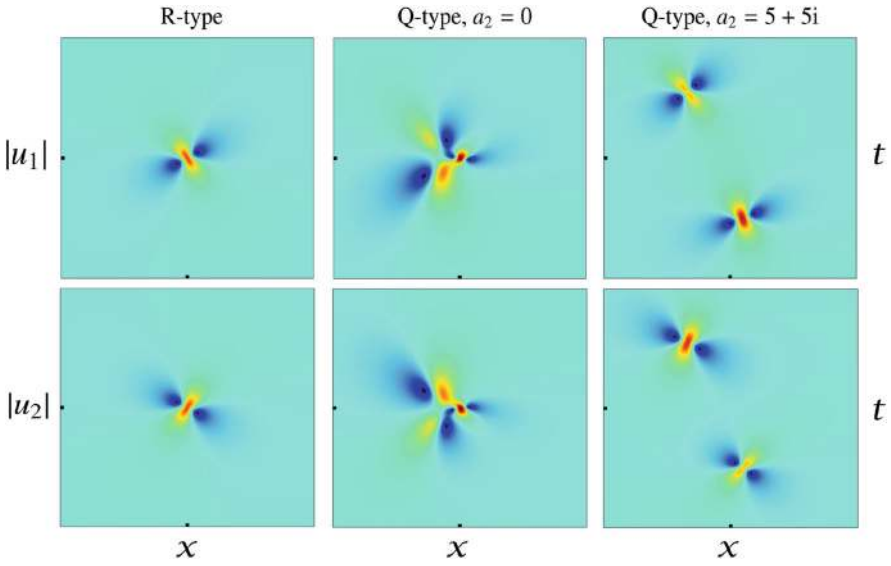

Fig. 2.18 First-order Q-type and R-type rogue waves with $k_1 = -k_2 = 1/\sqrt{12}$ in the focusing Manakov system. Left column: R-type in Eqs. (2.641)–(2.642). Middle column: Q-type with $a_2 = 0$ in Eq. (2.643). Right column: Q-type with $a_2 = 5 + 5\mathrm{i}$. In all panels, $-15 \le x, t \le 15$

2.9.4 Derivation of Rogue Wave Expressions

Next, we derive Manakov bilinear rogue waves presented in the above three theorems.

Under the transformation

$$u_1(x,t) = \rho_1 \frac{g}{f} e^{\mathrm{i}(k_1 x + \omega_1 t)}, \quad u_2(x,t) = \rho_2 \frac{h}{f} e^{\mathrm{i}(k_2 x + \omega_2 t)}, \tag{2.644}$$

where f is a real function and (g, h) complex ones, the Manakov system (2.581) can be converted into the following bilinear equations,

$$\left.\begin{array}{l} \left(D_x^2 + \epsilon_1 \rho_1^2 + \epsilon_2 \rho_2^2\right) f \cdot f = \epsilon_1 \rho_1^2 g g^* + \epsilon_2 \rho_2^2 h h^*, \\ \left(i D_t + D_x^2 + 2 i k_1 D_x\right) g \cdot f = 0, \\ \left(i D_t + D_x^2 + 2 i k_2 D_x\right) h \cdot f = 0. \end{array}\right\} \tag{2.645}$$

This bilinear system can be reduced from the following higher-dimensional bilinear system in the 2-component KP hierarchy (Ohta et al. 2011)

$$\left.\begin{array}{l}(\frac{1}{2}D_xD_r-1)\tau_{n,k}\cdot\tau_{n,k}=-\tau_{n+1,k}\,\tau_{n-1,k},\\(D_x^2-D_y+2aD_x)\tau_{n+1,k}\cdot\tau_{n,k}=0,\\(\frac{1}{2}D_xD_s-1)\tau_{n,k}\cdot\tau_{n,k}=-\tau_{n,k+1}\,\tau_{n,k-1},\\(D_x^2-D_y+2bD_x)\tau_{n,k+1}\cdot\tau_{n,k}=0,\end{array}\right\} \tag{2.646}$$

where n, k are integers, $\tau_{n,k}$ is a function of four independent variables (x, y, r, s), and

$$a=\mathrm{i}k_1,\quad b=\mathrm{i}k_2. \tag{2.647}$$

The solution $\tau_{n,k}$ to these higher-dimensional bilinear equations was given by a certain Gram determinant in Ohta et al. (2011), but that Gram solution was appropriate only for the derivation of dark solitons. For the derivation of rogue waves here, the solution $\tau_{n,k}$ should be chosen as

$$\tau_{n,k}=\det_{1\le\nu,\mu\le N}\left(\phi_{i_\nu,j_\mu}^{(n,k)}\right), \tag{2.648}$$

where $(i_1, i_2, \cdots, i_N)$ and $(j_1, j_2, \cdots, j_N)$ are arbitrary sequences of indices, the matrix element $\phi_{i,j}^{(n,k)}$ is defined as

$$\phi_{i,j}^{(n,k)}=\mathcal{A}_i\mathcal{B}_j\phi^{(n,k)}, \tag{2.649}$$

$$\phi^{(n,k)}=\frac{1}{p+q}\left(-\frac{p-a}{q+a}\right)^n\left(-\frac{p-b}{q+b}\right)^k e^{\xi+\eta}, \tag{2.650}$$

$$\xi=px+p^2y+\frac{1}{p-a}r+\frac{1}{p-b}s+\xi_0(p), \tag{2.651}$$

$$\eta=qx-q^2y+\frac{1}{q+a}r+\frac{1}{q+b}s+\eta_0(q), \tag{2.652}$$

$$\mathcal{A}_i=\frac{1}{i!}\left[f_1(p)\partial_p\right]^i,\quad \mathcal{B}_j=\frac{1}{j!}\left[f_2(q)\partial_q\right]^j, \tag{2.653}$$

p, q are arbitrary complex constants, and $\xi_0(p)$, $\eta_0(q)$, $f_1(p)$, $f_2(q)$ are arbitrary functions of p and q respectively. The reason these functions also satisfy the higher-dimensional bilinear system (2.646) is that these functions satisfy the same differential and difference relations in Ohta et al. (2011).

It is easy to see that the higher-dimensional bilinear system (2.646) is reduced to the original system (2.645) if we set

$$f=\tau_{0,0},\quad g=\tau_{1,0},\quad h=\tau_{0,1},\quad y=\mathrm{i}t, \tag{2.654}$$

impose the dimension reduction condition

$$\mathcal{L}_0 \tau_{n,k} = C\, \tau_{n,k}, \tag{2.655}$$

where

$$\mathcal{L}_0 = 2\partial_x + \epsilon_1 \rho_1^2 \partial_r + \epsilon_2 \rho_2^2 \partial_s, \tag{2.656}$$

and C is some constant, and impose the conjugation condition

$$\tau_{-n,-k} = \tau_{n,k}^*. \tag{2.657}$$

These two reductions proceed as follows.

To meet the dimensional reduction (2.655), we follow the $\mathcal{W}$-p treatment (see sections 2.3 and 2.6). We first see that

$$\mathcal{L}_0 \phi_{i,j}^{(n,k)} = \mathcal{A}_i \mathcal{B}_j \left[Q_1(p) + Q_2(q) \right] \phi^{(n,k)}, \tag{2.658}$$

where

$$Q_1(p) = \frac{\epsilon_1 \rho_1^2}{p-a} + \frac{\epsilon_2 \rho_2^2}{p-b} + 2p, \tag{2.659}$$

which is the same as the earlier expression (2.586) in view of Eq. (2.647), and $Q_2(q)$ is the above $Q_1(p)$ function with p switching to q and (a, b) switching to $(-a, -b)$. To meet the dimensional reduction condition (2.655), we start with the general Leibnitz-type operator relation,

$$\mathcal{A}_i Q_1(p) = \sum_{l=0}^{i} \frac{1}{l!} \left[\left(f_1 \partial_p \right)^l Q_1(p) \right] \mathcal{A}_{i-l}, \tag{2.660}$$

which we have seen before in Eq. (2.249). Another relation similar to the above can also be written for $\mathcal{B}_j Q_2(q)$. Using these relations, Eq. (2.658) gives

$$\mathcal{L}_0\, \phi_{i,j}^{(n,k)} = \sum_{\mu=0}^{i} \frac{1}{\mu!} \left[\left(f_1 \partial_p \right)^\mu Q_1(p) \right] \phi_{i-\mu,j}^{(n,k)} + \sum_{l=0}^{j} \frac{1}{l!} \left[\left(f_2 \partial_q \right)^l Q_2(q) \right] \phi_{i,j-l}^{(n,k)}. \tag{2.661}$$

In order to satisfy the dimensional reduction condition (2.655), we need to select functions $[f_1(p), f_2(q)]$ as well as values of (p, q) so that coefficients of certain indices on the right side of the above equation vanish (see Sect. 2.1.1). For that purpose, we will select p_0 and q_0 values to be roots of the following algebraic equations

$$Q_1'(p_0) = 0, \quad Q_2'(q_0) = 0. \tag{2.662}$$

At these (p_0, q_0) values, the $\mu = l = 1$ terms on the right side of Eq. (2.661) will vanish. Notice that the $Q_1'(p_0) = 0$ equation above is the same as (2.585), whose root structure has been delineated earlier in this section. Roots of the $Q_2'(q_0) = 0$ equation are related to those of $Q_1'(p_0) = 0$ as $q_0 = p_0^*$. Since the $\phi^{(n,k)}$ function in (2.650) has a factor of $1/(p+q)$, in order for $\phi_{i,j}^{(n,k)}$ in (2.649) to be nonsingular when evaluated at $(p, q) = (p_0, q_0)$, the p_0 value cannot be purely imaginary.

To select $f_1(p)$ and $f_2(q)$ functions optimally, we need to impose further conditions, and these conditions will depend on the multiplicity of the root p_0 in the $Q_1'(p) = 0$ equation.

(a) A Simple Root Case

If p_0 is a simple nonimaginary root of the $Q_1'(p) = 0$ equation, the condition on $f_1(p)$ we impose will be

$$\left(f_1 \partial_p\right)^2 Q_1(p) = Q_1(p). \tag{2.663}$$

The reason for this imposition is that under this condition, as well as the earlier condition (2.662), all odd-μ terms on the right side of Eq. (2.661), when evaluated at $p = p_0$, would vanish. Indeed, under this condition and $Q_1'(p_0) = 0$, as well as similar ones for the q variable, we find from Eq. (2.661) that

$$\begin{aligned} \mathcal{L}_0 \, \phi_{i,j}^{(n,k)}\Big|_{p=p_0,\, q=q_0} &= Q_1(p_0) \sum_{\substack{\mu=0 \\ \mu:even}}^{i} \frac{1}{\mu!} \, \phi_{i-\mu,j}^{(n,k)}\Big|_{p=p_0,\, q=q_0} \\ &\quad + Q_2(q_0) \sum_{\substack{l=0 \\ l:even}}^{j} \frac{1}{l!} \, \phi_{i,j-l}^{(n,k)}\Big|_{p=p_0,\, q=q_0}. \end{aligned} \tag{2.664}$$

Then, when we restrict indices of the general determinant (2.648) to

$$\tau_{n,k} = \det_{1 \le i,j \le N} \left(\phi_{2i-1,2j-1}^{(n,k)}\Big|_{p=p_0,\, q=q_0} \right), \tag{2.665}$$

and use the above contiguity relation (2.664) as was done in Sect. 2.1.1, we get

$$\mathcal{L}_0 \tau_{n,k} = [Q_1(p_0) + Q_2(q_0)] \, N \, \tau_{n,k}. \tag{2.666}$$

Thus, the $\tau_{n,k}$ function (2.665) satisfies the dimensional reduction condition (2.655).

The differential equation (2.663) is the same as Eq. (2.252) in Sect. 2.3. So the $f_1(p)$ solution is as given in Eq. (2.257). In addition, by writing $f_1(p) = \mathcal{W}_1(p)/\mathcal{W}_1'(p)$, the corresponding $\mathcal{W}_1(p)$ function is given in Eq. (2.257) as well.

A similar treatment can be applied to the q variable, and the results for $f_2(q)$ and $\mathcal{W}_2(q)$ are the same as in Eq. (2.257), except that the subscript 1 changes to 2, and (p, p_0) change to (q, q_0).

The complex conjugacy condition (2.657) can be met when we choose $\xi_0(p)$ and $\eta_0(q)$ as

$$\xi_0(p) = \sum_{r=1}^{\infty} \hat{a}_r \ln^r \mathcal{W}_1(p), \quad \eta_0(q) = \sum_{r=1}^{\infty} \hat{a}_r^* \ln^r \mathcal{W}_2(q), \tag{2.667}$$

where $\hat{a}_r$ are free complex constants. The reason is that due to $q_0 = p_0^*$ and (a, b) being purely imaginary, we can show that in this case

$$\phi_{j,i}^{(-n,-k)}\Big|_{p=p_0,\ q=q_0} = \left(\phi_{i,j}^{(n,k)}\Big|_{p=p_0,\ q=q_0}\right)^*, \tag{2.668}$$

thus $\tau_{-n,-k} = \tau_{n,k}^*$. The resulting $\tau_{n,k}$ function (2.665) then gives rogue waves of the Manakov system through Eqs. (2.644) and (2.654).

Lastly, we remove the differential operators in the matrix elements of Eq. (2.665) and derive more explicit expressions of rogue waves through Schur polynomials. This derivation is along the lines for the generalized derivative NLS equations in Sect. 2.2 and is very similar to that for the three-wave interaction system in Yang and Yang (2021b). Following such steps, we then obtain the rogue wave expressions given in Theorem 2.10 for the Manakov system, except that the definitions for $x_r^{\pm}(n, k)$ are as given in Eqs. (2.600)–(2.601) for all r indices, including those where $r \bmod 2 = 0$. Parameters a_r in Theorem 2.10 can be found to be linearly related to $\hat{a}_r$ in Eq. (2.667). We note that this derivation would be a bit simpler if we introduce an extra factor of $(p + p_0)(q + q_0)$ into $\phi^{(n,k)}$ of Eq. (2.650), similar to what we did in Eq. (2.29) for the NLS equation. In this latter case, parameters a_r in Theorem 2.10 would be identical to those $\hat{a}_r$ in Eq. (2.667).

Using the same techniques as in Sect. 2.1.1, we can further set $x_{2r}^{\pm} = 0$ in the resulting Schur polynomial expressions. In addition, the parameter a_1 can be normalized to zero through a shift of the (x, t) axes. This completes the proof of Theorem 2.10.

(b) Two-Simple-Root Case

If the $Q_1'(p) = 0$ equation admits two distinct non-imaginary simple roots $p_{0,1}$ and $p_{0,2}$ with $p_{0,2} \neq -p_{0,1}^*$, then we can construct a more general 2×2 block determinant

$$\tau_{n,k} = \det \begin{pmatrix} \tau_{n,k}^{[1,1]} & \tau_{n,k}^{[1,2]} \\ \tau_{n,k}^{[2,1]} & \tau_{n,k}^{[2,2]} \end{pmatrix}, \tag{2.669}$$

where

$$\tau_{n,k}^{[I,J]} = \mathrm{mat}_{1\le i\le N_I,1\le j\le N_J}\left(\phi_{2i-1,2j-1}^{(n,k)}\Big|_{p=p_{0,I},q=q_{0,J}}\right),\quad 1\le I,J\le 2, \tag{2.670}$$

$\phi_{i,j}^{(n,k)}$ is given by Eq. (2.649) with $[f_1(p), f_2(q)]$ replaced by $[f_1^{(I)}(p), f_2^{(J)}(q)]$, the function $f_1^{(I)}(p)$ is provided by Eq. (2.257) with p_0 replaced by $p_{0,I}$, the function $f_2^{(J)}(q)$ is the same as (2.257) but with the subscript 1 changing to 2 and (p, p_0) changing to $(q, q_{0,J})$, with

$$q_{0,J} = p_{0,J}^*, \tag{2.671}$$

ξ_0 is replaced by $\xi_{0,I}$, η_0 is replaced by $\eta_{0,J}$, and N_1, N_2 are arbitrary positive integers. It is easy to see that this 2×2 block determinant (2.669) also satisfies the higher-dimensional bilinear system (2.646).

In the present case, the contiguity relation (2.664) becomes

$$\begin{aligned}\mathcal{L}_0\,\phi_{i,j}^{(n,k)}\Big|_{p=p_{0,I},\,q=q_{0,J}} &= Q_1(p_{0,I})\sum_{\substack{\mu=0\\ \mu:even}}^{i}\frac{1}{\mu!}\,\phi_{i-\mu,j}^{(n,k)}\Big|_{p=p_{0,I},\,q=q_{0,J}} + \\ &\quad + Q_2(q_{0,J})\sum_{\substack{l=0,\\ l:even}}^{j}\frac{1}{l!}\,\phi_{i,j-l}^{(n,k)}\Big|_{p=p_{0,I},\,q=q_{0,J}}.\end{aligned} \tag{2.672}$$

Utilizing this contiguity relation similar to what we did in Sect. 2.1.1, we get

$$\mathcal{L}_0\tau_{n,k} = \left\{\left[Q_1(p_{0,1}) + Q_2(q_{0,1})\right]N_1 + \left[Q_1(p_{0,2}) + Q_2(q_{0,2})\right]N_2\right\}\tau_{n,k}. \tag{2.673}$$

Thus, the 2×2 block determinant (2.669) also satisfies the dimensional reduction condition (2.655).

The complex conjugacy condition (2.657) can be met when we choose $\xi_{0,I}(p)$ and $\eta_{0,J}(q)$ as

$$\xi_{0,I}(p) = \sum_{r=1}^{\infty} a_{r,I}\ln^r \mathcal{W}_1^{(I)}(p),\quad \eta_{0,J}(q) = \sum_{r=1}^{\infty} a_{r,J}^*\ln^r \mathcal{W}_2^{(J)}(q),\quad I,J = 1,2, \tag{2.674}$$

where $\mathcal{W}_1^{(I)}(p)$ is as defined in Eq. (2.257) with p_0 replaced by $p_{0,I}$, $\mathcal{W}_2^{(J)}(q)$ is defined similar to Eq. (2.257) except that the subscript 1 changes to 2 and (p, p_0) change to $(q, q_{0,J})$, and $a_{r,1}, a_{r,2}$ $(r = 1, 2, \dots)$ are free complex constants. Indeed,

since $q_{0,I} = p_{0,I}^*$ and (a, b) purely imaginary, we can show that

$$\phi_{i,j}^{(-n,-k)}\Big|_{p=p_{0,I},\ q=q_{0,J}} = \left(\phi_{j,i}^{(n,k)}\Big|_{p=p_{0,J},\ q=q_{0,I}}\right)^*, \tag{2.675}$$

so that

$$\tau_{-n,-k}^{[I,J]} = \left(\tau_{n,k}^{[J,I]}\right)^*, \tag{2.676}$$

and hence $\tau_{-n,-k} = \tau_{n,k}^*$. The resulting $\tau_{n,k}$ function (2.669) then gives rogue waves of the Manakov system through Eqs. (2.644) and (2.654).

Lastly, we remove differential operators in matrix elements of Eq. (2.669) and derive more explicit expressions of rogue waves through Schur polynomials. This derivation is very similar to that for the three-wave interaction system in Yang and Yang (2021b). Following such steps, we then obtain the rogue wave expressions given in Theorem 2.11 for the Manakov system, where parameters $a_{r,1}$ and $a_{r,2}$ in that theorem are identical to $a_{r,1}$ and $a_{r,2}$ in Eq. (2.674). This completes the proof of Theorem 2.11.

(c) A Double-Root Case

If the algebraic equation $Q_1'(p) = 0$ admits a non-imaginary double root p_0, i.e., $Q_1'(p_0) = Q_1''(p_0) = 0$, the dimension reduction condition (2.655) would be satisfied if we choose $f_1(p)$ to satisfy the differential equation

$$\left(f_1(p)\partial_p\right)^3 Q_1(p) = Q_1(p), \tag{2.677}$$

choose $f_2(q)$ to satisfy a similar equation except to change the index above from 1 to 2 and change p to q, and choose the $\tau_{n,k}$ determinant as

$$\tau_{n,k} = \det\begin{pmatrix} \tau_{n,k}^{[1,1]} & \tau_{n,k}^{[1,2]} \\ \tau_{n,k}^{[2,1]} & \tau_{n,k}^{[2,2]} \end{pmatrix}, \tag{2.678}$$

where

$$\tau_{n,k}^{[I,J]} = \mathrm{mat}_{1\le i\le N_I, 1\le j\le N_J}\left(m_{3i-I,\,3j-J}^{(n,k)}\Big|_{p=p_0,\ q=q_0,\ \xi_0=\xi_{0,I},\ \eta_0=\eta_{0,J}}\right),$$
$$1 \le I, J \le 2, \tag{2.679}$$

$q_0 = p_0^*$, $\xi_{0,I}(p)$, $\eta_{0,J}(q)$ are arbitrary functions of p and q respectively, and N_1, N_2 are arbitrary non-negative integers. The reason is that, in this case,

$$\left(f_1(p)\partial_p\right) Q_1(p)\big|_{p=p_0} = \left(f_1(p)\partial_p\right)^2 Q_1(p)\Big|_{p=p_0} = 0. \tag{2.680}$$

Thus, combined with the condition (2.677) and similar ones for $Q_2(q)$, Eq. (2.661) reduces to

$$\begin{aligned}\mathcal{L}_0\, m_{i,j}^{(n,k)}\Big|_{p=p_0,\ q=q_0} = Q_1(p_0) \sum_{\substack{\mu=0\\ \mu\equiv 0(\mathbf{mod}3)}}^{i} \frac{1}{\mu!}\, m_{i-\mu,j}^{(n,k)}\Big|_{p=p_0,\ q=q_0} + \\ + Q_2(q_0) \sum_{\substack{l=0\\ l\equiv 0(\mathbf{mod}3)}}^{j} \frac{1}{l!}\, m_{i,j-l}^{(n,k)}\Big|_{p=p_0,\ q=q_0}.\end{aligned} \tag{2.681}$$

Using this contiguity relation, we can show as in Sect. 2.1.1 that the 2×2 block determinant (2.678) satisfies the dimensional reduction condition (2.655).

The differential equation (2.677) for $Q_1(p)$ is linear and homogeneous. Writing $f_1(p) = \mathcal{W}_1(p)/\mathcal{W}_1'(p)$, this equation becomes

$$\partial_{\ln \mathcal{W}_1}^3 Q_1(p) = Q_1(p). \tag{2.682}$$

Scaling $\mathcal{W}_1(p_0) = 1$, the unique solution to this equation under the condition of p_0 being a double root of $Q_1'(p) = 0$ is

$$Q_1(p) = \frac{Q_1(p_0)}{3}\left(\mathcal{W}_1(p) + \frac{2}{\sqrt{\mathcal{W}_1(p)}}\cos\left[\frac{\sqrt{3}}{2}\ln \mathcal{W}_1(p)\right]\right). \tag{2.683}$$

From this equation, one can solve for $\mathcal{W}_1(p)$ from $Q_1(p)$ and then obtain $f_1(p)$. A similar equation can be derived for $\mathcal{W}_2(q)$ by replacing p by q and the subscript 1 by 2 in Eq. (2.683). But it turns out the explicit solving for $\mathcal{W}_{1,2}(p)$ and $f_{1,2}(p)$ is not necessary for our goal of obtaining explicit expressions for matrix elements in Eq. (2.678).

Regarding the conjugation condition (2.657), it can be satisfied when we choose

$$\xi_{0,I}(p) = \sum_{r=1}^{\infty} \hat{a}_{r,I} \ln^r \mathcal{W}_1(p), \quad \eta_{0,J}(q) = \sum_{r=1}^{\infty} \hat{a}_{r,J}^* \ln^r \mathcal{W}_2(q), \quad I = 1, 2, \tag{2.684}$$

where $\hat{a}_{r,I}$ are free complex constants. Indeed, in this case, we can show that

$$\tau_{-n,-k}^{[I,J]} = \left(\tau_{n,k}^{[J,I]}\right)^*, \tag{2.685}$$

and hence $\tau_{-n,-k} = \tau_{n,k}^*$. The resulting $\tau_{n,k}$ function (2.678) then gives rogue waves of the Manakov system through Eqs. (2.644) and (2.654).

Next, we remove the differential operators in the matrix elements of (2.678) and derive more explicit expressions of rogue waves through Schur polynomials. This derivation is very similar to that for the three-wave interaction system in Yang and Yang (2021b). Following such steps, we then obtain the rogue wave expressions given in Theorem 2.12 for the Manakov system, except that the definitions for $x^{+}_{r,I}(n,k)$ and $x^{-}_{r,J}(n,k)$ are as given in Eqs. (2.628)–(2.629) for all r indices, including those where $r \bmod 3 = 0$. And those $x^{+}_{r,I}(n,k)$ and $x^{-}_{r,J}(n,k)$ with $r \bmod 3 = 0$ can be removed from the solution, for reasons similar to those in Sect. 2.1.1 where we removed $x^{\pm}_{2r}$ terms in the NLS case. In this calculation, parameters $a_{r,1}$ and $a_{r,2}$ in Theorem 2.12 are linearly related to $\hat{a}_{r,1}$ and $\hat{a}_{r,2}$ in Eq. (2.684). If we had introduced an extra factor of $(p+p_0)(q+q_0)$ into $\phi^{(n,k)}$ of Eq. (2.650), similar to what we did in Eq. (2.29) for the NLS equation, this derivation would have been a bit simpler, and parameters $a_{r,1}$ and $a_{r,2}$ in Theorem 2.12 would be identical to those $\hat{a}_{r,1}$ and $\hat{a}_{r,2}$ in Eq. (2.684). This completes the proof of Theorem 2.12.

2.10 Three-Wave Resonant Interaction System in (1+1)-Dimensions

The (1+1)-dimensional three-wave resonant interaction system is

$$\left.\begin{aligned} (\partial_t + c_1\partial_x)\, u_1 &= \epsilon_1 u_2^* u_3^*, \\ (\partial_t + c_2\partial_x)\, u_2 &= \epsilon_2 u_1^* u_3^*, \\ (\partial_t + c_3\partial_x)\, u_3 &= \epsilon_3 u_1^* u_2^*, \end{aligned}\right\} \tag{2.686}$$

where (c_1, c_2, c_3) are group velocities of the three waves, $(\epsilon_1, \epsilon_2, \epsilon_3)$ are real-valued nonlinear coefficients, and the asterisk '*' represents complex conjugation. This system arises in many physical contexts such as water waves, optics and others (see Sect. 1.6). To remove ambiguity, we order the three group velocities as $c_1 > c_2 > c_3$, and make $c_3 = 0$ by choosing a coordinate system that moves with velocity c_3. The nonlinear coefficients ϵ_n can be normalized to ± 1 by variable scalings (see Sect. 1.6). In addition, we can fix $\epsilon_1 = 1$ without loss of generality.

This interaction system (with $c_3 = 0$) is invariant under the gauge transformation

$$\left.\begin{aligned} u_1(x,t) &\to u_1(x,t)\, e^{\mathrm{i}(kx - kc_1 t)}, \\ u_2(x,t) &\to u_2(x,t)\, e^{\mathrm{i}[-(kc_1/c_2)x + kc_1 t]}, \\ u_3(x,t) &\to u_3(x,t)\, e^{-\mathrm{i}(k - kc_1/c_2)x}, \end{aligned}\right\} \tag{2.687}$$

where k is an arbitrary real constant. In addition, it is invariant under the phase transformation

$$u_k(x,t) \to u_k(x,t)\, e^{\mathrm{i}\theta_k}, \quad k = 1, 2, 3, \tag{2.688}$$

where $\theta_3 = -(\theta_1+\theta_2)$, and θ_1, θ_2 are arbitrary real constants. These two invariances can help us reduce free parameters in the system.

There are three types of three-wave interaction models, which are termed the soliton exchange case, the explosive case, and the stimulated backscatter case in Kaup et al. (1979). These three cases correspond to the following signs of the nonlinear coefficients,

$$(\epsilon_1, \epsilon_2, \epsilon_3) = (1, -1, 1), \quad \text{(soliton-exchange case)} \tag{2.689}$$

$$(\epsilon_1, \epsilon_2, \epsilon_3) = (1, 1, 1), \quad \text{(explosive case)} \tag{2.690}$$

$$(\epsilon_1, \epsilon_2, \epsilon_3) = (1, -1, -1), \quad \text{(stimulated backscatter case)} \tag{2.691}$$

$$(\epsilon_1, \epsilon_2, \epsilon_3) = (1, 1, -1). \quad \text{(stimulated backscatter case)} \tag{2.692}$$

Note that the $(1, -1, -1)$ case can be converted to the $(1, 1, -1)$ case by flipping the sign of x, reordering the (u_1, u_2, u_3) equations in decreasing order of their group velocities, and renormalizing the nonlinear coefficients; thus these two cases belong to the same stimulated backscatter case. Below, we will treat all these cases by allowing $(\epsilon_1, \epsilon_2, \epsilon_3)$ to be arbitrary real parameters.

The above three-wave interaction system (2.686) admits plane wave solutions

$$\left.\begin{aligned} u_{1,0}(x,t) &= \rho_1 e^{\mathrm{i}(k_1 x+\omega_1 t)}, \\ u_{2,0}(x,t) &= \rho_2 e^{\mathrm{i}(k_2 x+\omega_2 t)}, \\ u_{3,0}(x,t) &= \mathrm{i}\rho_3 e^{-\mathrm{i}[(k_1+k_2)x+(\omega_1+\omega_2)t]}, \end{aligned}\right\} \tag{2.693}$$

where (k_1, k_2) and (ω_1, ω_2) are the wavenumbers and frequencies of the first two waves, and (ρ_1, ρ_2, ρ_3) are the complex amplitudes of the three waves. Parameters of these plane waves satisfy the following relations,

$$\left.\begin{aligned} \rho_1\,(\omega_1 + c_1 k_1) &= -\epsilon_1 \rho_2^* \rho_3^*, \\ \rho_2\,(\omega_2 + c_2 k_2) &= -\epsilon_2 \rho_1^* \rho_3^*, \\ \rho_3\,(\omega_1 + \omega_2) &= \epsilon_3 \rho_1^* \rho_2^*. \end{aligned}\right\} \tag{2.694}$$

Below, we assume ρ_1, ρ_2 and ρ_3 all non-zero. In view of the phase invariance (2.688), we can normalize ρ_1 and ρ_2 to be real positive. Then the above relations show that ρ_3 is real as well. In addition, the gauge invariance (2.687) allows us to impose a restriction on the four parameters $(k_1, k_2, \omega_1, \omega_2)$, such as fixing one of them as zero, or equating $k_1 = k_2$, or equating $\omega_1 = \omega_2$, without any loss of generality. Under such a restriction, wavenumber and frequency parameters $(k_1, k_2, \omega_1, \omega_2)$ would be fully determined from the three real background-amplitude parameters (ρ_1, ρ_2, ρ_3) through equations (2.694).

Rogue waves in the three-wave interaction system (2.686) are rational solutions which approach plane-wave solutions (2.693) as $x, t \to \pm\infty$. From the above discussions on plane-wave solutions, we can set the boundary conditions for these rogue waves as

$$\left.\begin{array}{ll} u_1(x,t) \to \rho_1 e^{\mathrm{i}(k_1 x+\omega_1 t)}, & x,t \to \pm\infty, \\ u_2(x,t) \to \rho_2 e^{\mathrm{i}(k_2 x+\omega_2 t)}, & x,t \to \pm\infty, \\ u_3(x,t) \to \mathrm{i}\rho_3 e^{-\mathrm{i}[(k_1+k_2)x+(\omega_1+\omega_2)t]}, & x,t \to \pm\infty, \end{array}\right\} \tag{2.695}$$

where (ρ_1, ρ_2, ρ_3) are free real amplitudes, $\rho_1 > 0, \rho_2 > 0$, and the other parameters $(k_1, k_2, \omega_1, \omega_2)$ are determined by these real amplitudes through equations (2.694) and an extra restriction on them from the gauge invariance (2.687).

Special types of rogue waves in the three-wave system have been derived by Darboux transformation in Baronio et al. (2013), Degasperis and Lombardo (2013), Chen et al. (2015), Wang et al. (2015), and Zhang et al. (2018). General rogue waves in this system were derived by the bilinear method in Yang and Yang (2021b). We will follow Yang and Yang (2021b) below.

In the bilinear framework, rogue-wave expressions will depend on the root structure of the following algebraic equation

$$Q_1'(p) = 0, \tag{2.696}$$

where

$$Q_1(p) = \left(\frac{\gamma_1 c_2}{\gamma_3(c_2-c_1)}\right)\frac{1}{p} - \left(\frac{\gamma_2 c_1}{\gamma_3(c_2-c_1)}\right)\frac{1}{p-\mathrm{i}} - p, \tag{2.697}$$

and

$$\gamma_1 \equiv \epsilon_1 \frac{\rho_2\rho_3}{\rho_1},\ \gamma_2 \equiv \epsilon_2 \frac{\rho_1\rho_3}{\rho_2},\ \gamma_3 \equiv \epsilon_3 \frac{\rho_1\rho_2}{\rho_3}. \tag{2.698}$$

This $Q_1(p)$ function and the associated algebraic equation (2.696) will appear in the dimension reduction of our bilinear derivation of rogue waves.

The algebraic equation (2.696) can be rewritten as

$$\gamma_3(c_1-c_2)p^2(p-\mathrm{i})^2 - \gamma_1 c_2 (p-\mathrm{i})^2 + \gamma_2 c_1 p^2 = 0, \tag{2.699}$$

which is a quartic equation for p. Thus, it has four roots (counting multiplicity). Notice that if p is a root, so is $-p^*$. Thus, non-imaginary roots appear as pairs of $(p, -p^*)$. This quartic equation is similar to Eq. (2.587) of the Manakov system. Using similar techniques, we can obtain the following results on the root structure of this quartic equation for the four cases of $(\epsilon_1, \epsilon_2, \epsilon_3)$ values in Eqs.(2.689)–(2.692).

1. In the soliton-exchange case (2.689), $(\epsilon_1, \epsilon_2, \epsilon_3) = (1, -1, 1)$. In this case, if

$$\rho_2 = \sqrt{\frac{c_1}{c_2}}\rho_1, \quad \rho_3 = \pm\sqrt{\frac{c_1-c_2}{c_2}}\rho_1, \tag{2.700}$$

then the roots of Eq. (2.696) are

$$(\hat{p}_0, \hat{p}_0, -\hat{p}_0^*, -\hat{p}_0^*), \tag{2.701}$$

where

$$\hat{p}_0 = (\sqrt{3} + \mathrm{i})/2, \tag{2.702}$$

which are a pair of non-imaginary double roots. For other (ρ_1, ρ_2, ρ_3) values not satisfying the conditions (2.700), the root structure of Eq. (2.696) is

$$(p_{0,1}, p_{0,2}, -p_{0,1}^*, -p_{0,2}^*), \tag{2.703}$$

where all roots are nonimaginary and simple with $p_{0,1} \neq p_{0,2}$.

2. In the explosive and stimulated backscatter cases with $(\epsilon_1, \epsilon_2, \epsilon_3)$ values given in Eqs.(2.690)–(2.692), root structures of Eq. (2.696) are

$\Delta > 0$: four imaginary simple roots;

$\Delta < 0$: a pair of non-imaginary simple roots $(p_0, -p_0^*)$ and two imaginary simple roots;

$\Delta = 0$: one imaginary double root and two imaginary simple roots,

where

$$\Delta = -16c_1c_2\,(c_1 - c_2)\,\gamma_1\gamma_2\gamma_3 \left\{[\gamma_1 c_2 + \gamma_3(c_1 - c_2) - \gamma_2 c_1]^3 \right.$$
$$\left. +27c_1c_2\,(c_1 - c_2)\,\gamma_1\gamma_2\gamma_3\right\}. \tag{2.704}$$

We can see that these root structure results bear strong similarities to those in the Manakov case. This explains why rogue wave structures in the three-wave system will be very similar to those in the Manakov system.

Now, we present our general rogue-wave solutions in the three-wave interaction system (2.686) according to the root structure of the algebraic equation (2.696).

2.10.1 General Rogue Waves and Their Derivations

Three types of rogue waves in the three-wave system, corresponding to a simple root, two simple roots and a double root of the algebraic equation (2.696), are presented in the following three theorems.

Theorem 2.13 *If the algebraic equation (2.696) admits a non-imaginary simple root p_0, then the three-wave interaction system (2.686) under boundary conditions (2.695) would admit nonsingular N-th order rogue-wave solutions*

$$u_{1,N}(x,t) = \rho_1 \frac{g_{1,N}}{f_N} e^{\mathrm{i}(k_1 x + \omega_1 t)}, \tag{2.705}$$

$$u_{2,N}(x,t) = \rho_2 \frac{g_{2,N}}{f_N} e^{\mathrm{i}(k_2 x + \omega_2 t)}, \tag{2.706}$$

$$u_{3,N}(x,t) = \mathrm{i}\rho_3 \frac{g_{3,N}}{f_N} e^{-\mathrm{i}[(k_1+k_2)x + (\omega_1+\omega_2)t]}, \tag{2.707}$$

where N is an arbitrary positive integer,

$$f_N = \sigma_{0,0}, \quad g_{1,N} = \sigma_{1,0}, \quad g_{2,N} = \sigma_{0,-1}, \quad g_{3,N} = \sigma_{-1,1}, \tag{2.708}$$

$$\sigma_{n,k} = \det_{1 \le i,j \le N} \left(m^{(n,k)}_{2i-1,2j-1} \right), \tag{2.709}$$

the matrix elements in $\sigma_{n,k}$ are defined by

$$m^{(n,k)}_{i,j} = \sum_{\nu=0}^{\min(i,j)} \left[\frac{|p_1|^2}{(p_0 + p_0^*)^2} \right]^{\nu} S_{i-\nu}(\boldsymbol{x}^+(n,k) + \nu \boldsymbol{s})\, S_{j-\nu}(\boldsymbol{x}^-(n,k) + \nu \boldsymbol{s}^*), \tag{2.710}$$

vectors $\boldsymbol{x}^{\pm}(n,k) = \left(x_1^{\pm}, 0, x_3^{\pm}, 0, \cdots\right)$ are defined by

$$x_r^+(n,k) = (\alpha_r - \beta_r)\, x + (c_1 \beta_r - c_2 \alpha_r)\, t + n\theta_r + k\lambda_r + a_r, \tag{2.711}$$

$$x_r^-(n,k) = \left(\alpha_r^* - \beta_r^*\right) x + \left(c_1 \beta_r^* - c_2 \alpha_r^*\right) t - n\theta_r^* - k\lambda_r^* + a_r^*, \tag{2.712}$$

α_r, β_r, θ_r and λ_r are coefficients from the expansions

$$\frac{\gamma_1}{c_1 - c_2} \left(\frac{1}{p(\kappa)} - \frac{1}{p_0} \right) = \sum_{r=1}^{\infty} \alpha_r \kappa^r, \tag{2.713}$$

$$\frac{\gamma_2}{c_1 - c_2} \left(\frac{1}{p(\kappa) - \mathrm{i}} - \frac{1}{p_0 - \mathrm{i}} \right) = \sum_{r=1}^{\infty} \beta_r \kappa^r, \tag{2.714}$$

$$\ln \frac{p(\kappa)}{p_0} = \sum_{r=1}^{\infty} \lambda_r \kappa^r, \quad \ln \frac{p(\kappa) - \mathrm{i}}{p_0 - \mathrm{i}} = \sum_{r=1}^{\infty} \theta_r \kappa^r, \tag{2.715}$$

the vector $\boldsymbol{s} = (s_1, s_2, \cdots)$ is defined by the expansion

$$\ln \left[\frac{1}{\kappa} \left(\frac{p_0 + p_0^*}{p_1} \right) \left(\frac{p(\kappa) - p_0}{p(\kappa) + p_0^*} \right) \right] = \sum_{r=1}^{\infty} s_r \kappa^r, \tag{2.716}$$

the function $p(\kappa)$ is defined by the equation

$$Q_1[p(\kappa)] = Q_1(p_0)\cosh(\kappa), \tag{2.717}$$

with $Q_1(p)$ given in Eq. (2.697), $p_1 \equiv (dp/d\kappa)|_{\kappa=0}$, $a_1 = 0$, and $a_3, a_5, \ldots, a_{2N-1}$ are free irreducible complex constants.

Theorem 2.14 *If the algebraic equation (2.696) admits two distinct non-imaginary simple roots $p_{0,1}$ and $p_{0,2}$ with $p_{0,2} \neq -p_{0,1}^*$, which is only possible in the soliton-exchange case (2.689) with background amplitudes not satisfying conditions (2.700), then the three-wave interaction system (2.686) under boundary conditions (2.695) would admit nonsingular (N_1, N_2)-th order rogue-wave solutions*

$$u_{1,N_1,N_2}(x,t) = \rho_1 \frac{g_{1,N_1,N_2}}{f_{N_1,N_2}} e^{\mathrm{i}(k_1 x + \omega_1 t)}, \tag{2.718}$$

$$u_{2,N_1,N_2}(x,t) = \rho_2 \frac{g_{2,N_1,N_2}}{f_{N_1,N_2}} e^{\mathrm{i}(k_2 x + \omega_2 t)}, \tag{2.719}$$

$$u_{3,N_1,N_2}(x,t) = \mathrm{i}\rho_3 \frac{g_{3,N_1,N_2}}{f_{N_1,N_2}} e^{-\mathrm{i}[(k_1+k_2)x + (\omega_1+\omega_2)t]}, \tag{2.720}$$

where N_1, N_2 are arbitrary positive integers,

$$f_{N_1,N_2} = \sigma_{0,0}, \quad g_{1,N_1,N_2} = \sigma_{1,0}, \quad g_{2,N_1,N_2} = \sigma_{0,-1}, \quad g_{3,N_1,N_2} = \sigma_{-1,1}, \tag{2.721}$$

$\sigma_{n,k}$ is a 2×2 block determinant

$$\sigma_{n,k} = \det \begin{pmatrix} \sigma_{n,k}^{[1,1]} & \sigma_{n,k}^{[1,2]} \\ \sigma_{n,k}^{[2,1]} & \sigma_{n,k}^{[2,2]} \end{pmatrix}, \tag{2.722}$$

$$\sigma_{n,k}^{[I,J]} = \left(m_{2i-1,2j-1}^{(n,k,I,J)} \right)_{1 \le i \le N_I, 1 \le j \le N_J}, \tag{2.723}$$

the matrix elements in $\sigma_{n,k}^{[I,J]}$ are defined by

$$m_{i,j}^{(n,k,I,J)} = \sum_{\nu=0}^{\min(i,j)} \left(\frac{1}{p_{0,I} + p_{0,J}^*} \right) \left[\frac{p_{1,I} p_{1,J}^*}{(p_{0,I} + p_{0,J}^*)^2} \right]^{\nu} \times$$
$$\times S_{i-\nu}\left(\boldsymbol{x}_{I,J}^{+}(n,k) + \nu \boldsymbol{s}_{I,J} \right) S_{j-\nu}\left(\boldsymbol{x}_{J,I}^{-}(n,k) + \nu \boldsymbol{s}_{J,I}^* \right), \tag{2.724}$$

vectors $\boldsymbol{x}_{I,J}^{\pm}(n,k) = \left(x_{1,I,J}^{\pm}, x_{2,I,J}^{\pm}, \cdots \right)$ and $\boldsymbol{s}_{I,J} = \left(s_{1,I,J}, s_{2,I,J}, \cdots \right)$ are defined by

$$x^{+}_{r,I,J}(n,k) = \left(\alpha_{r,I} - \beta_{r,I}\right) x + \left(c_1\beta_{r,I} - c_2\alpha_{r,I}\right) t + n\theta_{r,I} + k\lambda_{r,I} - b_{r,I,J} + a_{r,I}, \tag{2.725}$$

$$x^{-}_{r,I,J}(n,k) = \left(\alpha^{*}_{r,I} - \beta^{*}_{r,I}\right) x + \left(c_1\beta^{*}_{r,I} - c_2\alpha^{*}_{r,I}\right) t - n\theta^{*}_{r,I} - k\lambda^{*}_{r,I} - b^{*}_{r,I,J} + a^{*}_{r,I}, \tag{2.726}$$

$\alpha_{r,I}$, $\beta_{r,I}$, $\theta_{r,I}$, $\lambda_{r,I}$ and $s_{r,I,J}$ are coefficients from the expansions (2.713)–(2.716) with p_0 replaced by $p_{0,I}$, p_1 replaced by $p_{1,I}$, p_0^* replaced by $p^*_{0,J}$, $p(\kappa)$ replaced by $p_I(\kappa)$ which is defined by Eq. (2.717) with p_0 replaced by $p_{0,I}$, $p_{1,I} \equiv (dp_I/d\kappa)|_{\kappa=0}$, $b_{r,I,J}$ is the coefficient from the expansion

$$\ln\left[\frac{p_I(\kappa) + p^*_{0,J}}{p_{0,I} + p^*_{0,J}}\right] = \sum_{r=1}^{\infty} b_{r,I,J}\kappa^r, \tag{2.727}$$

and $a_{r,1}, a_{r,2}$ $(r = 1, 2, \dots)$ are free complex constants.

Theorem 2.15 *If the algebraic equation (2.696) admits a non-imaginary double root p_0, which is only possible in the soliton-exchange case (2.689) with background amplitudes satisfying conditions (2.700), then the three-wave interaction system (2.686) under boundary conditions (2.695) would admit nonsingular (N_1, N_2)-th order rogue-wave solutions $u_{i,N_1,N_2}(x,t)$ $(1 \le i \le 3)$, where N_1 and N_2 are arbitrary non-negative integers, and $u_{i,N_1,N_2}(x,t)$ are of the same forms as (2.718)–(2.721), except that their $\sigma_{n,k}$ is given by the following 2×2 block determinant*

$$\sigma_{n,k} = \det\begin{pmatrix} \sigma^{[1,1]}_{n,k} & \sigma^{[1,2]}_{n,k} \\ \sigma^{[2,1]}_{n,k} & \sigma^{[2,2]}_{n,k} \end{pmatrix}, \tag{2.728}$$

where

$$\sigma^{[I,J]}_{n,k} = \left(m^{(n,k,I,J)}_{3i-I,\,3j-J}\right)_{1\le i\le N_I,\,1\le j\le N_J}, \tag{2.729}$$

the matrix elements in $\sigma^{[I,J]}_{n,k}$ are defined by

$$m^{(n,k,I,J)}_{i,j} = \sum_{\nu=0}^{\min(i,j)} \left[\frac{|p_1|^2}{(p_0 + p_0^*)^2}\right]^{\nu} S_{i-\nu}(\boldsymbol{x}^{+}_{I}(n,k) + \nu\boldsymbol{s})\, S_{j-\nu}(\boldsymbol{x}^{-}_{J}(n,k) + \nu\boldsymbol{s}^*), \tag{2.730}$$

vectors $\boldsymbol{x}^{\pm}_{I}(n,k) = \left(x^{\pm}_{1,I}, x^{\pm}_{2,I}, \cdots\right)$ $(I = 1, 2)$ are given by

$$x^{+}_{r,I}(n,k) = (\alpha_r - \beta_r)\, x + (c_1\beta_r - c_2\alpha_r)\, t$$

$$+n\theta_r + k\lambda_r + a_{r,I}, \quad \text{if } r \bmod 3 \neq 0, \tag{2.731}$$

$$x^-_{r,J}(n,k) = \left(\alpha^*_r - \beta^*_r\right) x + \left(c_1\beta^*_r - c_2\alpha^*_r\right) t$$
$$-n\theta^*_r - k\lambda^*_r + a^*_{r,J}, \quad \text{if } r \bmod 3 \neq 0, \tag{2.732}$$

$$x^+_{r,I}(n,k) = x^-_{r,J}(n,k) = 0, \qquad \text{if } r \bmod 3 = 0, \tag{2.733}$$

α_r, β_r, θ_r and λ_r are defined in Eqs. (2.713)–(2.715), $\boldsymbol{s} = (s_1, s_2, \cdots)$ is defined in Eq. (2.716), the function $p(\kappa)$ which appears in Eqs. (2.713)–(2.716) is defined by the equation

$$Q_1[p(\kappa)] = \frac{Q_1(p_0)}{3}\left[e^{\kappa} + 2e^{-\kappa/2}\cos\left(\frac{\sqrt{3}}{2}\kappa\right)\right], \tag{2.734}$$

$Q_1(p)$ is given by Eq. (2.697), or equivalently

$$Q_1(p) = -\left(\frac{1}{p} + \frac{1}{p-\mathrm{i}} + p\right) \tag{2.735}$$

in view of the parameter restrictions (2.700), $p_1 \equiv (dp/d\kappa)|_{\kappa=0}$, and $a_{r,1}, a_{r,2}$ $(r = 1, 2, \dots)$ are free complex constants.

Proof First, we introduce a variable transformation

$$\left.\begin{aligned} u_1(x,t) &= \rho_1 \frac{g_1}{f} e^{\mathrm{i}(k_1 x + \omega_1 t)}, \\ u_2(x,t) &= \rho_2 \frac{g_2}{f} e^{\mathrm{i}(k_2 x + \omega_2 t)}, \\ u_3(x,t) &= \mathrm{i}\rho_3 \frac{g_3}{f} e^{-\mathrm{i}[(k_1+k_2)x + (\omega_1+\omega_2)t]}, \end{aligned}\right\} \tag{2.736}$$

where f is a real function, and g_1, g_2, g_3 are complex functions. Using this transformation and parameter relations (2.694), the three-wave system (2.686) is converted into the following three bilinear equations

$$\left.\begin{aligned} &(D_t + c_1 D_x - \mathrm{i}\gamma_1)\, g_1 \cdot f = -\mathrm{i}\gamma_1 g^*_2 g^*_3, \\ &(D_t + c_2 D_x - \mathrm{i}\gamma_2)\, g_2 \cdot f = -\mathrm{i}\gamma_2 g^*_1 g^*_3, \\ &(D_t - \mathrm{i}\gamma_3)\, g_3 \cdot f = -\mathrm{i}\gamma_3 g^*_1 g^*_2. \end{aligned}\right\} \tag{2.737}$$

Next, we introduce a coordinate transformation

$$x = \frac{c_1}{\gamma_1} r + \frac{c_2}{\gamma_2} s, \quad t = \frac{1}{\gamma_1} r + \frac{1}{\gamma_2} s, \tag{2.738}$$

or equivalently,

$$r = \frac{\gamma_1}{c_1 - c_2}(x - c_2 t), \quad s = \frac{\gamma_2}{c_2 - c_1}(x - c_1 t). \tag{2.739}$$

Under this coordinate transformation, the bilinear equations (2.737) reduce to

$$\left.\begin{aligned} &(\mathrm{i}D_r + 1)\, g_1 \cdot f = g_2^* g_3^*, \\ &(\mathrm{i}D_s + 1)\, g_2 \cdot f = g_1^* g_3^*, \\ &\left[\frac{\gamma_1 c_2}{\gamma_3(c_2 - c_1)}\mathrm{i}D_r - \frac{\gamma_2 c_1}{\gamma_3(c_2 - c_1)}\mathrm{i}D_s + 1\right] g_3 \cdot f = g_1^* g_2^*. \end{aligned}\right\} \tag{2.740}$$

Bilinear equations (2.740) can be reduced from the following lowest-order bilinear equations in the extended KP hierarchy

$$\left.\begin{aligned} &[(b-a)D_r + 1]\, \tau_{n+1,k} \cdot \tau_{n,k} = \tau_{n,k+1}\tau_{n+1,k-1}, \\ &[(b-a)D_s + 1]\, \tau_{n,k-1} \cdot \tau_{n,k} = \tau_{n-1,k}\tau_{n+1,k-1}, \\ &\left[D_{x_1} + (a-b)\right] \tau_{n-1,k+1} \cdot \tau_{n,k} = (a-b)\tau_{n-1,k}\tau_{n,k+1}, \end{aligned}\right\} \tag{2.741}$$

where we set $a = 0$ and $b = \mathrm{i}$. To reduce (2.741) to (2.740), we impose the dimension reduction condition

$$\mathcal{L}_0 \tau_{n,k} = C\tau_{n,k}, \tag{2.742}$$

where

$$\mathcal{L}_0 = \frac{\gamma_1 c_2}{\gamma_3(c_2 - c_1)}\partial_r - \frac{\gamma_2 c_1}{\gamma_3(c_2 - c_1)}\partial_s - \partial_{x_1}, \tag{2.743}$$

and C is some constant. We also impose the complex conjugation condition

$$\tau_{-n,-k} = \tau_{n,k}^*. \tag{2.744}$$

Under these two conditions, when we set

$$f = \tau_{0,0}, \quad g_1 = \tau_{1,0}, \quad g_2 = \tau_{0,-1}, \quad g_3 = \tau_{-1,1}, \tag{2.745}$$

then the bilinear system (2.741) with $n = k = 0$ would reduce to the original bilinear system (2.740).

A wide class of solutions to the higher-dimensional bilinear system (2.741) can be obtained from the following lemma.

Lemma 2.14 *If functions $m_{i,j}^{(n,k)}$, $\varphi_i^{(n,k)}$ and $\psi_j^{(n,k)}$ of variables (x_1, r, s) satisfy the following differential and difference relations,*

$$\left.\begin{array}{l}
\partial_{x_1} m_{i,j}^{(n,k)} = \varphi_i^{(n,k)} \psi_j^{(n,k)}, \\
\partial_{x_1} \varphi_i^{(n,k)} = \varphi_i^{(n+1,k)}, \ \partial_{x_1} \psi_j^{(n,k)} = -\psi_j^{(n-1,k)}, \\
\partial_r \varphi_i^{(n,k)} = \varphi_i^{(n,k-1)}, \ \partial_r \psi_j^{(n,k)} = -\psi_j^{(n,k+1)}, \\
\partial_s \varphi_i^{(n,k)} = \varphi_i^{(n-1,k)}, \ \partial_s \psi_j^{(n,k)} = -\psi_j^{(n+1,k)}, \\
\varphi_i^{(n+1,k)} = (a-b)\varphi_i^{(n,k)} + \varphi_i^{(n,k+1)}, \ \psi_j^{(n-1,k)} = (a-b)\psi_j^{(n,k)} + \psi_j^{(n,k-1)},
\end{array}\right\} \tag{2.746}$$

where a and b are arbitrary complex constants, then the τ function

$$\tau_{n,k} = \det_{1 \le i,j \le N} \left(m_{i,j}^{(n,k)} \right) \tag{2.747}$$

would satisfy the higher-dimensional bilinear system (2.741).

This lemma can be proved using results in Yang et al. (2020) and some additional similar calculations.

Now, we construct a wide class of algebraic solutions to the bilinear system (2.741) from the above lemma. To do so, we introduce functions $m^{(n,k)}$, $\varphi^{(n,k)}$ and $\psi^{(n,k)}$ as

$$m^{(n,k)} = \frac{1}{p+q} \left(-\frac{p-a}{q+a} \right)^k \left(-\frac{p-b}{q+b} \right)^n \mathrm{e}^{\xi+\eta}, \tag{2.748}$$

$$\varphi^{(n,k)} = (p+1)(p-a)^k (p-b)^n e^{\xi}, \tag{2.749}$$

$$\psi^{(n,k)} = (q+1)\left[-(q+a)\right]^{-k} \left[-(q+b)\right]^{-n} e^{\eta}, \tag{2.750}$$

where

$$\xi = \frac{1}{p-a} r + \frac{1}{p-b} s + (p-b)x_1 + \xi_0(p), \tag{2.751}$$

$$\eta = \frac{1}{q+a} r + \frac{1}{q+b} s + (q+b)x_1 + \eta_0(q), \tag{2.752}$$

and p, q are arbitrary complex constants, and $\xi_0(p)$, $\eta_0(q)$ are arbitrary functions of p and q respectively. It is easy to see that these functions satisfy the differential and difference relations (2.746) with indices i and j ignored. Then, by defining functions

$$m_{i,j}^{(n,k)} = \mathcal{A}_i \mathcal{B}_j m^{(n,k)}, \quad \varphi_i^{(n,k)} = \mathcal{A}_i \varphi^{(n,k)}, \quad \psi_j^{(n,k)} = \mathcal{B}_j \psi^{(n,k)}, \tag{2.753}$$

where $\mathcal{A}_i$ and $\mathcal{B}_j$ are differential operators with respect to p and q respectively as

$$\mathcal{A}_i = \frac{1}{i!} \left[f_1(p) \partial_p \right]^i, \quad \mathcal{B}_j = \frac{1}{j!} \left[f_2(q) \partial_q \right]^j, \tag{2.754}$$

and $f_1(p)$, $f_2(q)$ are arbitrary functions, these functions would also satisfy the differential and difference relations (2.746) since operators $\mathcal{A}_i$ and $\mathcal{B}_j$ commute with differentials. Consequently, for an arbitrary sequence of indices $(i_1, i_2, \cdots, i_N)$ and $(j_1, j_2, \cdots, j_N)$, the determinant

$$\tau_{n,k} = \det_{1\le \nu,\mu\le N} \left(m^{(n,k)}_{i_\nu, j_\mu} \right) \tag{2.755}$$

satisfies the higher-dimensional bilinear system (2.741).

Next, we need to restrict the above solutions so that they satisfy the dimension reduction condition (2.742). To do so, we follow the $\mathcal{W}$-p treatment (see Sects. 2.3, 2.6 and 2.9). We first see that

$$\mathcal{L}_0 m^{(n,k)}_{i,j} = \mathcal{A}_i \mathcal{B}_j \mathcal{L}_0 m^{(n,k)} = \mathcal{A}_i \mathcal{B}_j \left[Q_1(p) + Q_2(q) \right] m^{(n,k)}, \tag{2.756}$$

where $Q_1(p)$ is as defined in Eq. (2.697), and $Q_2(q)$ is $Q_1(p)$ with p changing to q and i to $-$i. To meet the dimensional reduction condition (2.742), we start with the relation,

$$\mathcal{L}_0 m^{(n,k)}_{i,j} = \sum_{\mu=0}^{i} \frac{1}{\mu!} \left[\left(f_1 \partial_p \right)^\mu Q_1(p) \right] m^{(n,k)}_{i-\mu,j} + \sum_{l=0}^{j} \frac{1}{l!} \left[\left(f_2 \partial_q \right)^l Q_2(q) \right] m^{(n,k)}_{i,j-l}, \tag{2.757}$$

which is the same as Eq. (2.661) for the Manakov case in the previous section. In order to satisfy the dimensional reduction condition (2.742), we select functions $[f_1(p), f_2(q)]$ as well as values of (p, q) so that coefficients of certain indices on the right side of the above equation vanish (see Sect. 2.1.1). For that purpose, we will select p_0 and q_0 values to be roots of the following algebraic equations

$$Q_1'(p_0) = 0, \quad Q_2'(q_0) = 0. \tag{2.758}$$

At these (p_0, q_0) values, the $\mu = l = 1$ terms on the right side of Eq. (2.757) will vanish. Notice that the $Q_1'(p_0) = 0$ equation above is the same as (2.696), whose root structure has been delineated earlier in this section. Roots of the $Q_2'(q_0) = 0$ equation are related to those of $Q_1'(p_0) = 0$ as $q_0 = p_0^*$. Since the $m^{(n,k)}$ function in (2.748) has a factor of $1/(p+q)$, in order for $m^{(n,k)}_{i,j}$ in (2.753) to be nonsingular when evaluated at $(p, q) = (p_0, q_0)$, the p_0 value cannot be purely imaginary.

To select $f_1(p)$ and $f_2(q)$ functions, we need to impose further conditions, and these conditions will depend on the multiplicity of the root p_0 in the $Q_1'(p) = 0$ equation. The present situation is very similar to the Manakov case of the previous section; so our discussions will be brief (the reader can see Yang and Yang (2021b) for details).

A Simple Root Case

If p_0 is a simple nonimaginary root to the $Q_1'(p) = 0$ equation, the condition on $f_1(p)$ we impose will be

$$\left(f_1 \partial_p\right)^2 Q_1(p) = Q_1(p). \tag{2.759}$$

This differential equation is the same as Eq. (2.252) in Sect. 2.3. So the $f_1(p)$ solution is as given in Eq. (2.257). In addition, by writing $f_1(p) = \mathcal{W}_1(p)/\mathcal{W}_1'(p)$, the corresponding $\mathcal{W}_1(p)$ function is given in Eq. (2.257) as well. A similar treatment can be applied to the q variable. In this case, when we restrict indices of the general determinant (2.755) to

$$\tau_{n,k} = \det_{1\le i,j\le N}\left(m_{2i-1,2j-1}^{(n,k)}\Big|_{p=p_0,\ q=q_0}\right), \tag{2.760}$$

we will get

$$\mathcal{L}_0 \tau_{n,k} = \left[Q_1(p_0) + Q_2(q_0)\right] N\, \tau_{n,k}. \tag{2.761}$$

Thus, the $\tau_{n,k}$ function (2.760) satisfies the dimensional reduction condition (2.742).

The complex conjugacy condition (2.744) can be met when we choose $\xi_0(p)$ and $\eta_0(q)$ as

$$\xi_0(p) = \sum_{r=1}^{\infty} \hat{a}_r \ln^r \mathcal{W}_1(p), \quad \eta_0(q) = \sum_{r=1}^{\infty} \hat{a}_r^* \ln^r \mathcal{W}_2(q), \tag{2.762}$$

where $\hat{a}_r$ are free complex constants. The resulting $\tau_{n,k}$ function (2.760) then gives rogue waves of the three-wave system through Eqs. (2.736) and (2.745).

Lastly, we remove differential operators in matrix elements of Eq. (2.760) and derive more explicit expressions of rogue waves through Schur polynomials, using techniques we have demonstrated in earlier sections (see Yang and Yang (2021b) for details). Following such steps, we then obtain the rogue wave expressions given in Theorem 2.13 for the three-wave system, where parameters a_r are linearly related to $\hat{a}_r$ in Eq. (2.762). In addition, the parameter a_1 can be normalized to zero through a shift of the (x, t) axes.

Two-Simple-Root Case

If the $Q_1'(p) = 0$ equation admits two distinct non-imaginary simple roots $p_{0,1}$ and $p_{0,2}$ with $p_{0,2} \neq -p_{0,1}^*$, then we can construct a more general 2×2 block determinant

$$\tau_{n,k} = \det \begin{pmatrix} \tau_{n,k}^{[1,1]} & \tau_{n,k}^{[1,2]} \\ \tau_{n,k}^{[2,1]} & \tau_{n,k}^{[2,2]} \end{pmatrix}, \tag{2.763}$$

where

$$\tau_{n,k}^{[I,J]} = \mathrm{mat}_{1\le i\le N_I, 1\le j\le N_J} \left(m_{2i-1,2j-1}^{(n,k)} \Big|_{p=p_{0,I}, q=q_{0,J}} \right), \quad 1 \le I, J \le 2, \tag{2.764}$$

$m_{i,j}^{(n,k)}$ is given by Eqs. (2.748)–(2.753) with $[f_1(p), f_2(q)]$ replaced by $[f_1^{(I)}(p), f_2^{(J)}(q)]$, the function $f_1^{(I)}(p)$ is provided by Eq. (2.257) with p_0 replaced by $p_{0,I}$, the function $f_2^{(J)}(q)$ is the same as (2.257) but with the subscript 1 changing to 2 and (p, p_0) changing to $(q, q_{0,J})$, with

$$q_{0,J} = p_{0,J}^*, \tag{2.765}$$

ξ_0 is replaced by $\xi_{0,I}$, η_0 is replaced by $\eta_{0,J}$, and N_1, N_2 are arbitrary positive integers. This 2×2 block determinant (2.763) also satisfies the higher-dimensional bilinear system (2.741).

In the present case, Eq. (2.761) becomes

$$\mathcal{L}_0 \tau_{n,k} = \left\{ \left[Q_1(p_{0,1}) + Q_2(q_{0,1}) \right] N_1 + \left[Q_1(p_{0,2}) + Q_2(q_{0,2}) \right] N_2 \right\} \tau_{n,k}. \tag{2.766}$$

Thus, the 2×2 block determinant (2.763) also satisfies the dimensional reduction condition (2.742).

The complex conjugacy condition (2.744) can be met when we choose $\xi_{0,I}(p)$ and $\eta_{0,J}(q)$ as

$$\xi_{0,I}(p) = \sum_{r=1}^{\infty} a_{r,I} \ln^r \mathcal{W}_1^{(I)}(p), \quad \eta_{0,J}(q) = \sum_{r=1}^{\infty} a_{r,J}^* \ln^r \mathcal{W}_2^{(J)}(q), \quad I, J = 1, 2, \tag{2.767}$$

where $\mathcal{W}_1^{(I)}(p)$ is as defined in Eq. (2.257) with p_0 replaced by $p_{0,I}$, $\mathcal{W}_2^{(J)}(q)$ is defined similar to Eq. (2.257) except that the subscript 1 changes to 2 and (p, p_0) change to $(q, q_{0,J})$, and $a_{r,1}, a_{r,2}$ $(r = 1, 2, \dots)$ are free complex constants. The resulting $\tau_{n,k}$ function (2.763) then gives rogue waves of the three-wave system through Eqs. (2.736) and (2.745).

Lastly, we remove differential operators in matrix elements of Eq. (2.763) and derive more explicit expressions of rogue waves through Schur polynomials, using techniques we have demonstrated in earlier sections (see Yang and Yang (2021b)

for details). Following such steps, we then obtain the rogue wave expressions given in Theorem 2.14 for the three-wave system.

A Double Root Case

If the algebraic equation $Q_1'(p) = 0$ admits a non-imaginary double root p_0, the dimension reduction condition (2.742) would be satisfied if we choose $f_1(p)$ to satisfy the differential equation

$$\left(f_1(p)\partial_p\right)^3 Q_1(p) = Q_1(p), \tag{2.768}$$

choose $f_2(q)$ to satisfy a similar equation except to change the index above from 1 to 2 and change p to q, and choose the $\tau_{n,k}$ determinant as

$$\tau_{n,k} = \det \begin{pmatrix} \tau_{n,k}^{[1,1]} & \tau_{n,k}^{[1,2]} \\ \tau_{n,k}^{[2,1]} & \tau_{n,k}^{[2,2]} \end{pmatrix}, \tag{2.769}$$

where

$$\tau_{n,k}^{[I,J]} = \mathrm{mat}_{1\le i\le N_I, 1\le j\le N_J}\left(m_{3i-I,\,3j-J}^{(n,k)}\Big|_{p=p_0,\, q=q_0,\, \xi_0=\xi_{0,I},\, \eta_0=\eta_{0,J}} \right),$$
$$1 \le I, J \le 2, \tag{2.770}$$

$q_0 = p_0^*$, $\xi_{0,I}(p)$, $\eta_{0,J}(q)$ are arbitrary functions of p and q respectively, and N_1, N_2 are arbitrary non-negative integers. The differential equation (2.768) is the same as Eq. (2.677) of the Manakov case, and its solution for $Q_1(p)$ is as given in Eq. (2.683) there.

Regarding the conjugation condition (2.657), it can be satisfied when we choose

$$\xi_{0,I}(p) = \sum_{r=1}^{\infty} \hat{a}_{r,I} \ln^r \mathcal{W}_1(p), \quad \eta_{0,J}(q) = \sum_{r=1}^{\infty} \hat{a}_{r,J}^* \ln^r \mathcal{W}_2(q), \quad I = 1, 2, \tag{2.771}$$

where $\hat{a}_{r,I}$ are free complex constants.

Lastly, we remove differential operators in matrix elements of Eq. (2.770) using techniques we have demonstrated in earlier sections. Doing so gives explicit rogue wave expressions given in Theorem 2.15 for the three-wave system, where parameters $a_{r,1}$ and $a_{r,2}$ are linearly related to $\hat{a}_{r,1}$ and $\hat{a}_{r,2}$ above (see Yang and Yang (2021b) for details).

2.10.2 Dynamics of Various Types of Rogue Waves

(a) Rogue Waves for a Simple Root

We first consider rogue waves in Theorem 2.13, which are associated with a non-imaginary simple root in Eq. (2.696). To get the simplest rogue wave in this solution family, we take $N = 1$ in that theorem. Then, we readily find that

$$|u_{i,1}(x,t)| = \left|\rho_i \frac{g_{i,1}}{f_1}\right|, \quad i = 1, 2, 3, \tag{2.772}$$

where

$$\begin{aligned}
f_1 &= |(\alpha_1 - \beta_1)\, x + (c_1\beta_1 - c_2\alpha_1)t|^2 + \zeta_0,\\
g_{1,1} &= [(\alpha_1 - \beta_1)\, x + (c_1\beta_1 - c_2\alpha_1)t + \theta_1]\\
&\quad \times \left[\left(\alpha_1^* - \beta_1^*\right) x + (c_1\beta_1^* - c_2\alpha_1^*)t - \theta_1^*\right] + \zeta_0,\\
g_{2,1} &= [(\alpha_1 - \beta_1)\, x + (c_1\beta_1 - c_2\alpha_1)t - \lambda_1]\\
&\quad \times \left[\left(\alpha_1^* - \beta_1^*\right) x + (c_1\beta_1^* - c_2\alpha_1^*)t + \lambda_1^*\right] + \zeta_0,\\
g_{3,1} &= [(\alpha_1 - \beta_1)\, x + (c_1\beta_1 - c_2\alpha_1)t - \theta_1 + \lambda_1]\\
&\quad \times \left[\left(\alpha_1^* - \beta_1^*\right) x + (c_1\beta_1^* - c_2\alpha_1^*)t + \theta_1^* - \lambda_1^*\right] + \zeta_0,
\end{aligned}$$

and

$$\alpha_1 = -\frac{p_1\epsilon_1\rho_2\rho_3}{p_0^2(c_1 - c_2)\rho_1}, \quad \beta_1 = -\frac{p_1\epsilon_2\rho_1\rho_3}{(p_0 - \mathrm{i})^2(c_1 - c_2)\rho_2},$$

$$\theta_1 = \frac{p_1}{p_0 - \mathrm{i}}, \quad \lambda_1 = \frac{p_1}{p_0}, \quad \zeta_0 = \frac{|p_1|^2}{(p_0 + p_0^*)^2}.$$

This rogue wave is ratios of second-degree polynomials in x and t, which are the lowest polynomial degrees possible for rogue waves in the three-wave system. Thus, we will call it the fundamental rogue wave of the three-wave system. Notice that p_1 cancels out in these $u_{i,1}$ solutions, and thus its formula is not needed here.

To get second-order rogue waves, we take $N = 2$ in Theorem 2.13. These second-order rogue waves have a single free complex parameter a_3. In these solutions, f_2 and $g_{i,2}$ are degree-6 polynomials in both x and t.

To illustrate the dynamics of these rogue waves, we first consider the soliton-exchange case (2.689), i.e., $\epsilon_1 = -\epsilon_2 = \epsilon_3 = 1$. For the background and velocity values of

$$c_1 = 1,\ c_2 = 0.5,\ \rho_1 = 1,\ \rho_2 = 2,\ \rho_3 = 1, \tag{2.773}$$

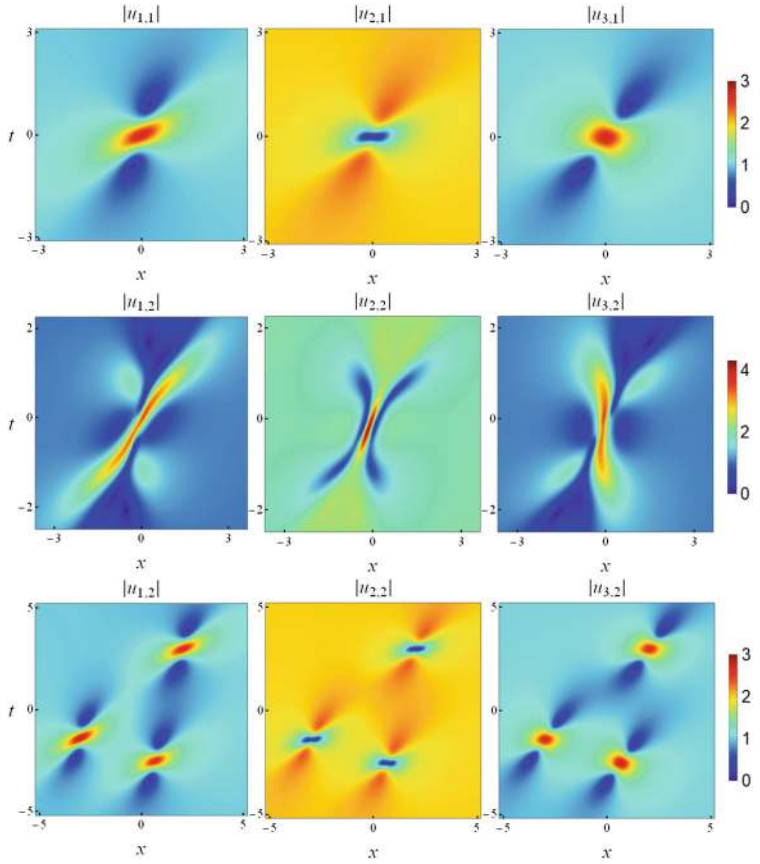

Fig. 2.19 Rogue waves in Theorem 2.13 corresponding to a non-imaginary simple root in the three-wave interaction system in the soliton-exchange case with background and velocity values in Eq. (2.773). Top row: the fundamental rogue wave (2.772); middle row: the second-order rogue wave with $a_3 = 0$; bottom row: the second-order rogue wave with $a_3 = 10 + 10\mathrm{i}$

the roots of Eq. (2.696) are $(p_{0,1}, p_{0,2}, -p_{0,1}^*, -p_{0,2}^*)$, where $p_{0,1} \approx 0.521005 + 0.853553\mathrm{i}$, and $p_{0,2} \approx 0.989219 + 0.146447\mathrm{i}$. Choosing $p_0 = p_{0,1}$, the fundamental rogue wave (2.772) is displayed in Fig. 2.19 (top row). We see that the intensity variation of each component in this rogue wave is along a slanted angle in the (x, t) plane. In addition, while the first and third components peak at the origin $x = t = 0$, the second component bottoms there. Because of this, we can say the first and third components of this rogue wave are bright, but the second component is dark. If we choose $p_0 = p_{0,2}$, the intensity pattern of the resulting rogue wave would also be slanted, but extremely slender, like a needle, in all three components. In addition, the first and third components are now dark, while the second component bright, in this latter case.

The second-order rogue waves involve p_1 and the free parameter a_3. For the chosen value of $p_0 = p_{0,1}$, we find that $p_1 \approx \pm(0.550798 - 0.289323\mathrm{i})$, and choose the plus sign. Then, at two a_3 values of 0 and $10 + 10\mathrm{i}$, the corresponding rogue waves are displayed in Fig. 2.19 (middle and bottom rows respectively). The rogue wave at $a_3 = 0$ exhibits new patterns and higher peak amplitudes. The rogue wave at $a_3 = 10+10\mathrm{i}$ splits into three separate fundamental rogue waves—a phenomenon common in integrable systems.

Next, we illustrate dynamics of rogue waves in the same Theorem 2.13 for a simple root, but for non-soliton-exchange cases. For brevity, we only consider the stimulated backscatter case with $\epsilon_1 = -\epsilon_2 = -\epsilon_3 = 1$. For the background and velocity values of

$$c_1 = 5,\ c_2 = 2,\ \rho_1 = \rho_2 = \rho_3 = 2, \tag{2.774}$$

Eq. (2.696) admits a non-imaginary simple root $p_0 \approx 0.391016 + 0.338012\mathrm{i}$. The corresponding fundamental rogue wave (2.772) is plotted in Fig. 2.20 (upper row). In this rogue wave, the first component is dark, the second a saddle, and the third bright.

In second-order rogue waves, if we choose $a_3 = 0$, the resulting rogue solution is displayed in Fig. 2.20 (middle row). This rogue wave develops strong dips in its first and second components and a strong peak in its third component at the wave center. If we choose $a_3 = 5 + 5\mathrm{i}$, the resulting solution, shown in the bottom row of Fig. 2.20, splits into three separate fundamental rogue waves as a rogue triplet.

(b) Rogue Waves for Two Non-Imaginary Simple Roots

Rogue waves in Theorem 2.14 are associated with two non-imaginary simple roots $p_{0,1}$ and $p_{0,2}$ in Eq. (2.696), with $p_{0,2} \neq -p_{0,1}^*$. These solutions only appear in the soliton-exchange case of $\epsilon_1 = -\epsilon_2 = \epsilon_3 = 1$ when the background amplitudes do not satisfy conditions (2.700). The simplest rogue waves in this family correspond to $N_1 = N_2 = 1$, which contain two free complex parameters $a_{1,1}$ and $a_{1,2}$. To illustrate these rogue waves, we choose background and velocity values as

$$c_1 = 1,\ c_2 = 0.5,\ \rho_1 = \rho_2 = \rho_3 = \sqrt{2}. \tag{2.775}$$

The roots of Eq. (2.696) for this set of values are $(p_{0,1}, p_{0,2}, -p_{0,1}^*, -p_{0,2}^*)$, where

$$p_{0,1} \approx 0.529086 + 0.257066\mathrm{i}, \quad p_{0,2} \approx 1.52909 + 0.742934\mathrm{i}. \tag{2.776}$$

Regarding free complex parameters $a_{1,1}$ and $a_{1,2}$, one of them can be normalized to zero by a shift of x and t, and the other is irreducible. We will normalize $a_{1,1} = 0$. Then, at two $a_{1,2}$ values of 0 and $(2-\mathrm{i})\,p_{1,2}$, the resulting rogue waves are displayed in Fig. 2.21 (the latter choice of $a_{1,2}$ as a multiple of $p_{1,2}$ is because in this case, the parameter $p_{1,2}$ would cancel out in the solution's expression). The rogue wave at $a_{1,2} = (2 - \mathrm{i})\,p_{1,2}$ (lower row) comprises two separate simpler rogue waves, which turn out to be fundamental rogue waves (2.772) of Theorem 2.13 for the

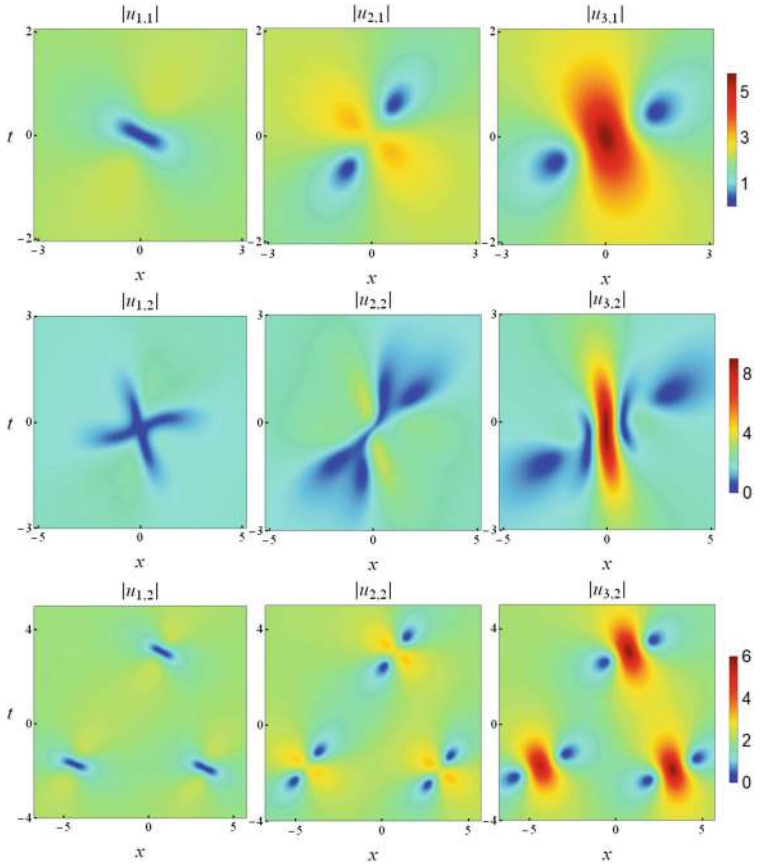

Fig. 2.20 Rogue waves in Theorem 2.13 corresponding to a non-imaginary simple root in the three-wave interaction system in the stimulated backscatter case with background and velocity values in Eq. (2.774). Upper row: the fundamental rogue wave (2.772); middle row: the second-order rogue wave with $a_3 = 0$; bottom row: the second-order rogue wave with $a_3 = 5 + 5\mathrm{i}$

two individual p_0 values in Eq. (2.776). Thus, rogue waves in Theorem 2.14 for two simple roots can be viewed as a nonlinear superposition of rogue waves of Theorem 2.13 for the two simple roots. The rogue wave at $a_{1,2} = 0$ (upper row) is formed by merging the two fundamental rogue waves of the lower row. It has a new composite structure and higher peak amplitude.

(c) Rogue Waves for a Double Root

Rogue waves in Theorem 2.15 for a nonimaginary double root only arise in the soliton-exchange case of $\epsilon_1 = -\epsilon_2 = \epsilon_3 = 1$ when the background amplitudes satisfy conditions (2.700), i.e.,

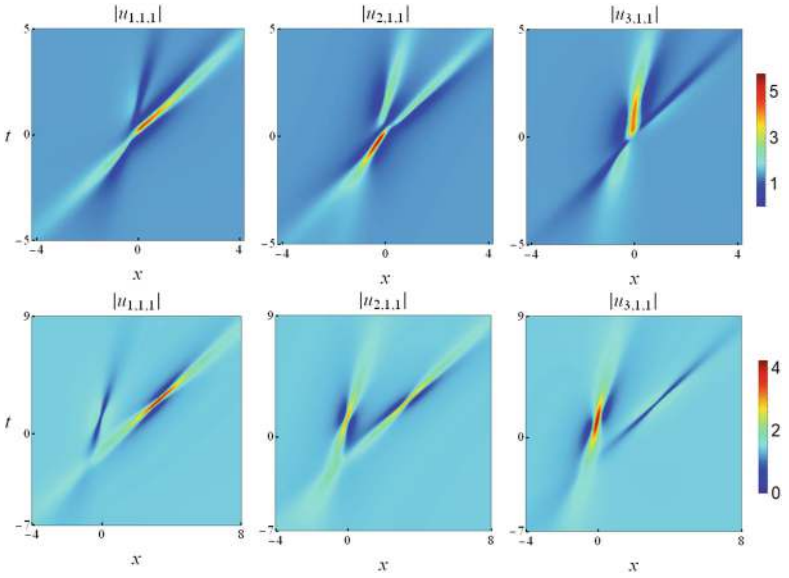

Fig. 2.21 Density plots of the (1, 1)-th order rogue waves in Theorem 2.14 corresponding to two non-imaginary simple roots in the three-wave interaction system in the soliton-exchange case with background and velocity values in Eq. (2.775). Upper row: $a_{1,2} = 0$; lower row, $a_{1,2} = (2-\mathrm{i})p_{1,2}$

$$\rho_2 = \sqrt{\frac{c_1}{c_2}}\rho_1, \quad \rho_3 = \pm\sqrt{\frac{c_1 - c_2}{c_2}}\rho_1. \tag{2.777}$$

In this case, Eq. (2.696) admits a pair of non-imaginary double roots $p_0 = (\pm\sqrt{3} + \mathrm{i})/2$. We will choose $p_0 = (\sqrt{3} + \mathrm{i})/2$. Regarding p_1, which is any one of the three cubic roots of $(3\sqrt{3} + \mathrm{i})/12$, we pick the one in the first quadrant, which is $p_1 \approx 0.759614 + 0.0482053\mathrm{i}$. We also normalize $a_{1,1} = 0$ through a shift in the (x, t) axes.

Rogue waves in Theorem 2.15 are given through a 2×2 block determinant. As in the Manakov case, we will consider only Q-type ($N_1 = N$, $N_2 = 0$) and R-type ($N_1 = 0$ and $N_2 = N$) rogue waves for simplicity.

The first (lowest) order R-type rogue wave can be obtained from Theorem 2.15 by setting $N_1 = 0$ and $N_2 = 1$. This rogue wave is

$$|u_{i,0,1}(x,t)| = \left|\rho_i \frac{g_{i,1}}{f_1}\right|, \quad 1 \le i \le 3, \tag{2.778}$$

where $f_1(x,t)$ and $g_{i,1}(x,t)$ are given in equations below (2.772) under the parameter constraints of Eq. (2.777). Thus, this first-order R-type rogue wave is the fundamental rogue wave (2.772) under parameter constraints (2.777). For the background and velocity choices of $c_1 = 1$, $c_2 = 0.5$, and $\rho_1 = 1$, this rogue wave

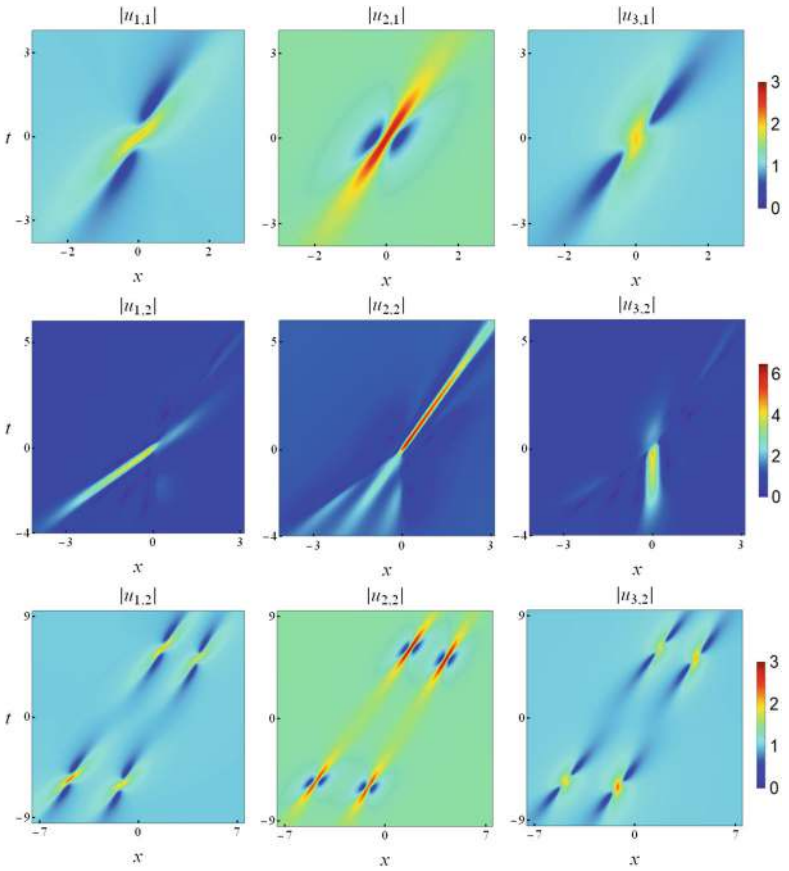

Fig. 2.22 R-type rogue waves in the three-wave interaction system in the soliton-exchange case, with background and velocity values of $c_1 = 1$, $c_2 = 0.5$, $\rho_1 = 1$ under conditions (2.777). Upper row: the first-order rogue wave; middle row: the second-order rogue wave with $a_{2,2} = a_{4,2}$=0; lower row: the second-order rogue wave with $a_{2,2} = 0$ and $a_{4,2} = 50$i

is plotted in Fig. 2.22 (top row). In this rogue wave, all three components are bright at the wave center $x = t = 0$.

Second-order rogue waves of R-type can be obtained from Theorem 2.15 by setting $N_1 = 0$ and $N_2 = 2$. These rogue waves are ratios of degree-eight polynomials in x and t, and they contain three free complex parameters, $a_{1,2}$, $a_{2,2}$ and $a_{4,2}$. We normalize $a_{1,2} = 0$ by a shift in the (x, t) axes. Then, for two choices of $(a_{2,2}, a_{4,2}) = (0, 0)$ and $(0, 50\text{i})$, the corresponding solutions are displayed in the middle and bottom rows of Fig. 2.22, respectively. The solution in the middle row has higher amplitudes, and its three components form a three-needle structure. The solution in the bottom row splits into four fundamental rogue waves.

The first-order Q-type rogue wave in the three-wave system can be obtained from Theorem 2.15 by setting $N_1 = 1$ and $N_2 = 0$. As in the Manakov case, this solution

is a ratio of polynomials of degree four in x and t, and it contains two free complex parameter $a_{1,1}$ and $a_{2,1}$. By a shift of the (x, t) axes, we normalize $a_{1,1} = 0$. For parameter values of $c_1 = 1$, $c_2 = 0.5$ and $\rho_1 = 1$, this solution with $a_{2,1} = 10 + 10\mathrm{i}$ has been plotted in Yang and Yang (2021b). It was seen that this solution splits into two fundamental rogue waves, similar to the Manakov case. When $a_{2,1} = 0$, these two fundamental rogue waves merge together and form a composite structure.

2.11 Long-Wave-Short-Wave Resonant Interaction System

The long-wave-short-wave (LWSW) resonant interaction system is

$$\left.\begin{aligned} \mathrm{i}S_t - S_{xx} + SL = 0, \\ L_t = -4(|S|^2)_x. \end{aligned}\right\} \tag{2.779}$$

This system governs the resonant interaction between long and short waves in many physical systems, such as capillary-gravity waves (Djordjevic and Redekopp 1977), internal waves (Grimshaw 1977; Funakoshi and Oikawa 1983), plasma waves (Yajima and Oikawa 1976), and optical waves (Kivshar 1992; Chowdhury and Tataronis 2008), see Sect. 1.5. Here, S is the complex envelope function of a short wave, and L is the real long-wave function. This system was shown to be integrable by Yajima and Oikawa (1976) and is sometimes called the Yajima-Oikawa system in the literature.

This LWSW system admits a constant-amplitude continuous-wave solution in the S component and zero solution in the L component. Through a simple variable scaling, we can normalize the amplitude of the S component to unity. Then, this solution can be written as $S(x, t) = e^{\mathrm{i}(\alpha x + \alpha^2 t)}$ and $L(x, t) = 0$, where α is a real wavenumber parameter. This background solution is modulation unstable, and rogue waves can arise from it. Thus, we set the boundary conditions of rogue waves as

$$S(x, t) \to e^{\mathrm{i}(\alpha x + \alpha^2 t)}, \quad L(x, t) \to 0, \quad x, t \to \pm\infty. \tag{2.780}$$

Fundamental rogue waves in the LWSW system (2.779) were derived by Chow et al. (2013) using the Hirota method, and by Chen et al. (2014a) and Chen (2014) using Darboux transformation. General rogue waves in the LWSW system were derived by Chen et al. (2018a) using the bilinear method. Rogue wave expressions in Chen et al. (2018a) were complicated though due to their choices of differential operators and parameterizations in the bilinear procedure. Simpler rogue expressions were obtained by He et al. (2023) using the $\mathcal{W}$-p treatment for dimensional reduction (see Sect. 2.3) as well as the new parameterization (see Sect. 2.1.1). Below, we derive general rogue waves in the LWSW system, following Chen et al. (2018a) and He et al. (2023).

General rogue waves in this LWSW system are given in the following theorem.

Theorem 2.16 *The long-wave-short-wave interaction system (2.779) under boundary conditions (2.780) admits N-th order rogue wave solutions*

$$S_N = \frac{g_N}{f_N} e^{\mathrm{i}(\alpha x + \alpha^2 t)}, \quad L_N = -2\frac{\partial^2}{\partial x^2} \ln f_N, \tag{2.781}$$

where N is an arbitrary positive integer,

$$f_N = \sigma_0, \quad g_N = \sigma_1, \tag{2.782}$$

$$\sigma_n = \det_{1 \le i,j \le N} \left(m^{(n)}_{2i-1,2j-1} \right), \tag{2.783}$$

the matrix elements in σ_n are defined by

$$m^{(n)}_{i,j} = \sum_{\nu=0}^{\min(i,j)} \left(\frac{|p_1|^2}{(p_0 + p_0^*)^2} \right)^{\nu} S_{i-\nu}(\boldsymbol{x}^+(n) + \nu \boldsymbol{s})\, S_{j-\nu}(\boldsymbol{x}^-(n) + \nu \boldsymbol{s}^*), \tag{2.784}$$

vectors $\boldsymbol{x}^{\pm}(n) = \left(x_1^{\pm}, 0, x_3^{\pm}, 0, \cdots\right)$ are defined by

$$x_r^+(n) = p_r x - \alpha_r \mathrm{i} t + n\theta_r + a_r, \tag{2.785}$$

$$x_r^-(n) = p_r^* x + \alpha_r^* \mathrm{i} t - n\theta_r^* + a_r^*, \tag{2.786}$$

p_r, α_r and θ_r are coefficients from the expansions

$$p(\kappa) = \sum_{r=0}^{\infty} p_r \kappa^r, \quad p^2(\kappa) - p_0^2 = \sum_{r=1}^{\infty} \alpha_r \kappa^r, \quad \ln\left[\frac{p(\kappa) - \mathrm{i}\alpha}{p_0 - \mathrm{i}\alpha} \right] = \sum_{r=1}^{\infty} \theta_r \kappa^r, \tag{2.787}$$

the vector $\boldsymbol{s} = (s_1, s_2, \cdots)$ is defined by the expansion

$$\ln\left[\frac{1}{\kappa} \left(\frac{p_0 + p_0^*}{p_1} \right) \left(\frac{p(\kappa) - p_0}{p(\kappa) + p_0^*} \right) \right] = \sum_{r=1}^{\infty} s_r \kappa^r, \tag{2.788}$$

the function $p(\kappa)$ is defined by the equation

$$Q_1[p(\kappa)] = Q_1(p_0) \cosh(\kappa), \tag{2.789}$$

with $Q_1(p)$ given by

$$Q_1(p) = p^2 + \frac{2\mathrm{i}}{p - \mathrm{i}\alpha}, \tag{2.790}$$

p_0 is a nonimaginary root of the equation $Q_1'(p) = 0$, $a_1 = 0$, and $(a_3, a_5, \ldots, a_{2N-1})$ are free irreducible complex constants.

Proof To derive rogue waves in the LWSW system, we first introduce variable transformations

$$S = \frac{g}{f} e^{\mathrm{i}(\alpha x + \alpha^2 t)}, \quad L = -2\frac{\partial^2}{\partial x^2} \ln f, \tag{2.791}$$

where f is a real-valued function, and g a complex-valued function. Under this transformation, the LWSW system (2.779) is converted into the following bilinear equations,

$$\left.\begin{aligned} \left(D_x^2 + 2\mathrm{i}\alpha D_x - \mathrm{i}D_t\right) g \cdot f = 0, \\ \left(D_x D_t + 4\right) f \cdot f = 4gg^*. \end{aligned}\right\} \tag{2.792}$$

This bilinear system can be reduced from the following higher-dimensional bilinear equations of the KP hierarchy,

$$\left.\begin{aligned} \left(D_{x_1}^2 + 2aD_{x_1} - D_{x_2}\right) \tau_{n+1} \cdot \tau_n = 0, \\ \left(D_{x_1} D_{x_{-1}} - 2\right) \tau_n \cdot \tau_n = -2\tau_{n+1}\tau_{n-1}, \end{aligned}\right\} \tag{2.793}$$

which is very similar to the higher-dimensional bilinear system (2.22) of the NLS equation, except for the extra $2aD_{x_1}$ term. When we impose the dimensional reduction condition

$$\left(\partial_{x_2} + 2\mathrm{i}\partial_{x_{-1}}\right) \tau_n = C\tau_n, \tag{2.794}$$

where C is some constant, then this system (2.793) would reduce to the (1+1)-dimensional bilinear system

$$\left.\begin{aligned} \left(D_{x_1}^2 + 2aD_{x_1} - D_{x_2}\right) \tau_{n+1} \cdot \tau_n = 0, \\ \left(\mathrm{i}D_{x_1} D_{x_2} - 4\right) \tau_n \cdot \tau_n = -4\tau_{n+1}\tau_{n-1}. \end{aligned}\right\} \tag{2.795}$$

Then, by setting

$$x_1 = x, \quad x_2 = -\mathrm{i}t, \quad a = \mathrm{i}\alpha, \tag{2.796}$$

$$f = \tau_0, \quad g = \tau_1, \quad h = \tau_{-1}, \tag{2.797}$$

and imposing the complex conjugate condition

$$\tau_n^* = \tau_{-n}, \tag{2.798}$$

the bilinear system (2.795) would reduce to the bilinear system (2.792) of the LWSW equations.

First, we construct solutions to the higher-dimensional bilinear system (2.793). We have the following lemma.

Lemma 2.15 *Let $m_{i,j}^{(n)}$, $\varphi_i^{(n)}$ and $\psi_j^{(n)}$ be functions of x_1, x_2 and x_{-1} satisfying the following differential and difference relations,*

$$\left.\begin{aligned} &\partial_{x_1} m_{i,j}^{(n)} = \varphi_i^{(n)} \psi_j^{(n)}, \\ &\varphi_i^{(n+1)} = (\partial_{x_1} - a)\varphi_i^{(n)}, \quad \psi_j^{(n-1)} = -(\partial_{x_1} + a)\psi_j^{(n)}, \\ &\partial_{x_2} \varphi_i^{(n)} = \partial_{x_1}^2 \varphi_i^{(n)}, \quad \partial_{x_2} \psi_j^{(n)} = -\partial_{x_1}^2 \psi_j^{(n)}, \\ &\partial_{x_{-1}} \varphi_i^{(n)} = \varphi_i^{(n-1)}, \quad \partial_{x_{-1}} \psi_j^{(n)} = -\psi_j^{(n+1)}, \end{aligned}\right\} \tag{2.799}$$

and

$$\left.\begin{aligned} &\partial_{x_2} m_{i,j}^{(n)} = [\partial_{x_1} \varphi_i^{(n)}]\psi_j^{(n)} - \varphi_i^{(n)}[\partial_{x_1} \psi_j^{(n)}], \\ &\partial_{x_{-1}} m_{i,j}^{(n)} = -\varphi_i^{(n-1)} \psi_j^{(n+1)}, \\ &m_{i,j}^{(n+1)} = m_{i,j}^{(n)} + \varphi_i^{(n)} \psi_j^{(n+1)}. \end{aligned}\right\} \tag{2.800}$$

Then the determinant

$$\tau_n = \det_{1 \le i,j \le N} \left(m_{i,j}^{(n)} \right) \tag{2.801}$$

satisfies the bilinear system (2.793).

This lemma is similar to Lemma 2.1, and its proof can be found in Chen et al. (2018a). As in Lemma 2.1, if the former part (2.799) of these differential and difference relations hold, then we can show that the x_1 derivatives of the latter part (2.800) of these relations are automatically satisfied.

Based on this lemma, a wide class of algebraic solutions to the higher-dimensional bilinear system (2.793) is

$$\tau_n = \det_{1 \le \nu, \mu \le N} \left(m_{i_\nu, j_\mu}^{(n)} \right), \tag{2.802}$$

where

$$m_{i,j}^{(n)} = \mathcal{A}_i \mathcal{B}_j m^{(n)}, \tag{2.803}$$

$$m^{(n)} = \frac{1}{p+q} \left(-\frac{p-a}{q+a} \right)^n e^{\xi(p) + \eta(q)}, \tag{2.804}$$

$$\xi(p) = px_1 + p^2 x_2 + \frac{1}{p-a} r + \xi_0(p), \tag{2.805}$$

$$\eta(q) = qx_1 - q^2 x_2 + \frac{1}{q+a} r + \eta_0(q), \tag{2.806}$$

$$\mathcal{A}_i = \frac{\left[f_1(p)\partial_p\right]^i}{i!}, \quad \mathcal{B}_j = \frac{\left[f_2(q)\partial_q\right]^j}{j!}, \tag{2.807}$$

$f_1(p)$, $f_2(q)$, $\xi_0(p)$, $\eta_0(q)$ are arbitrary functions, and $(i_1, i_2, \cdots, i_N; j_1, j_2, \cdots, j_N)$ are arbitrary sequences of indices.

Next, we adopt the $\mathcal{W}$-p treatment to meet the dimensional reduction condition (2.794) . Introducing the linear differential operator $\mathcal{L}_0$ as

$$\mathcal{L}_0 = \partial_{x_2} + 2\mathrm{i}\partial_{x_{-1}}, \tag{2.808}$$

then we have

$$\mathcal{L}_0 m_{i,j}^{(n)} = \mathcal{A}_i \mathcal{B}_j \mathcal{L}_0 m^{(n)} = \mathcal{A}_i \mathcal{B}_j \left[Q_1(p) + Q_2(q)\right] m^{(n)}, \tag{2.809}$$

where

$$Q_1(p) = p^2 + \frac{2\mathrm{i}}{p-a}, \quad Q_2(p) = -q^2 + \frac{2\mathrm{i}}{q+a}. \tag{2.810}$$

Note that this $Q_1(p)$ is the same as that in Theorem 2.16.

To meet the dimensional reduction condition (2.794), we will select p_0 and q_0 values to be roots of the following algebraic equations

$$Q_1'(p) = 0, \quad Q_2'(q) = 0. \tag{2.811}$$

Recalling $a = \mathrm{i}\alpha$ from Eq. (2.796), the equation $Q_1'(p) = 0$ can be rewritten as

$$p(p - \mathrm{i}\alpha)^2 = \mathrm{i}. \tag{2.812}$$

When $\alpha > -3/\sqrt[3]{4}$, this equation has one imaginary simple root and a pair of nonimaginary simple complex roots. When $\alpha < -3/\sqrt[3]{4}$, this equation has three imaginary simple roots. When $\alpha = -3/\sqrt[3]{4}$, this equation has one imaginary simple root and another imaginary double root. Only nonimaginary roots can lead to rogue waves. Thus, rogue waves can only be obtained when $\alpha > -3/\sqrt[3]{4}$. In this case, the pair of complex roots are

$$p_0 = \pm\frac{\sqrt{3}(K^2 - 4\alpha^2)}{12K} + \frac{K^2 + 8K\alpha + 4\alpha^2}{12K}\mathrm{i}, \tag{2.813}$$

where $K = (8\alpha^3 + 108 + 12\sqrt{12\alpha^3 + 81})^{1/3}$. Since these complex roots are simple, there can only be one type of rogue waves corresponding to a simple nonimaginary root (which is the counterpart of Theorem 2.10 for the Manakov system and Theorem 2.13 for the three-wave system). The τ_n function for this type of rogue waves is

$$\tau_n = \det_{1\le i,j\le N}\left(m^{(n)}_{2i-1,2j-1}\Big|_{p=p_0,\ q=p_0^*}\right), \tag{2.814}$$

where p_0 is a nonimaginary root of Eq. (2.812), and $f_1(p)$, $f_2(q)$, $\xi_0(p)$, $\eta_0(q)$ are as given in Eqs. (2.257) and (2.667). Lastly, we remove the differential operators in the matrix elements by techniques described in earlier sections, and the final explicit solutions are as given in Theorem 2.16. This completes the proof of Theorem 2.16.

Taking $N = 1$ in Theorem 2.16, we get the fundamental rogue wave

$$S_1 = \frac{g_1}{f_1}e^{\mathrm{i}(\alpha x+\alpha^2 t)}, \quad L_1 = -2\frac{\partial^2}{\partial x^2}\ln f_1, \tag{2.815}$$

where

$$f_1 = |p_1 x - 2p_0 p_1 \mathrm{i}t|^2 + \frac{|p_1|^2}{(p_0+p_0^*)^2},$$

$$g_1 = (p_1 x - 2p_0 p_1 \mathrm{i}t + \theta_1)\left(p_1^* x + 2p_0^* p_1^* \mathrm{i}t - \theta_1^*\right) + \frac{|p_1|^2}{(p_0+p_0^*)^2},\ \theta_1 = \frac{p_1}{p_0 - \mathrm{i}\alpha}.$$

Notice that p_1 cancels out in the S_1 and L_1 solutions; thus its expression is not needed. Graphs of this rogue wave with $\alpha = 1$ and -1 are plotted in the upper and lower rows of Fig. 2.23, respectively. Here, the plus sign is taken in the formula (2.813) for p_0. It is seen that the α value significantly affects the shapes and orientations of this fundamental rogue wave.

Second-order rogue waves can be obtained from Theorem 2.16 by setting $N = 2$. For $\alpha = 1$ and two values of $a_3 = 0$ and 30, the corresponding rogue waves are plotted in the upper and lower rows of Fig. 2.24, respectively (here the plus sign is taken in the formula (2.813) for p_0 as well). In the former case, the rogue wave exhibits an x-shape in its two components. In the latter case, the rogue wave splits into three fundamental rogue waves.

2.12 Massive Thirring Model

The massive Thirring (MT) model arose in the quantum field theory as a completely integrable nonlinear model (Taneda 1958; Mikhailov 1976; Kuznetsov and Mikhailov 1977). In the light-cone coordinates, this model is

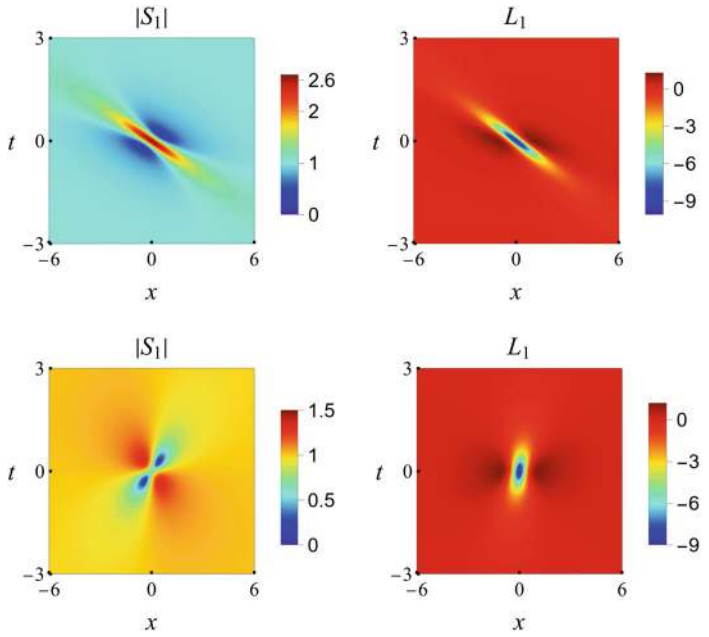

Fig. 2.23 Density plots of the fundamental rogue waves $|S_1(x,t)|$ and $L_1(x,t)$ in the long-wave-short-wave interaction system. Upper row: $\alpha = 1$; lower row: $\alpha = -1$. Left column: $|S_1(x,t)|$; right column: $L_1(x,t)$

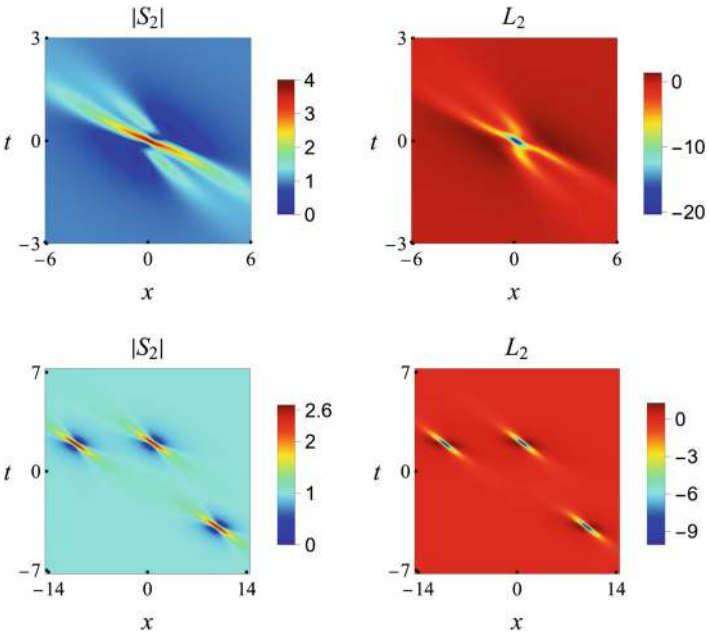

Fig. 2.24 Density plots of second-order rogue waves in the long-wave-short-wave interaction system for $\alpha = 1$. Upper row: $a_3 = 0$; lower row: $a_3 = 30$

$$\left.\begin{aligned} \mathrm{i}u_x + v + \epsilon u|v|^2 = 0, \\ \mathrm{i}v_t + u + \epsilon v|u|^2 = 0, \end{aligned}\right\} \tag{2.816}$$

where $\epsilon = \pm 1$. Note that this model is invariant under the transformation of $v \to -v, x \to -x, t \to -t$ and $\epsilon \to -\epsilon$. Thus, it would suffice to treat one of the $\epsilon = \pm 1$ values only. In the laboratory coordinates (ξ, η) where $\xi = c(x - t)$ and $\eta = x + t$, with c being a velocity constant, the u_x term above would become $u_\eta + cu_\xi$ and v_t become $v_\eta - cv_\xi$. The MT model in these laboratory coordinates is a particular case of the coupled mode equations that describe nonlinear pulse propagation in Bragg optical media (Winful and Cooperman 1982; Christodoulides and Joseph 1989; Aceves and Wabnitz 1989; Eggleton et al. 1999).

Rogue waves in the MT model have been derived in Degasperis (2015), Degasperis et al. (2015), Guo et al. (2017), and Ye et al. (2021) by Darboux transformation, and in Chen et al. (2023) by the bilinear method. Here, we follow Chen et al. (2023).

General rogue waves in the MT system (2.816) are given by the following theorem.

Theorem 2.17 *The massive Thirring model (2.816) admits nonsingular N-th order rogue wave solutions*

$$u_N = \rho_1 \frac{g_N}{f_N^*} e^{\mathrm{i}(1+\epsilon\rho_1\rho_2)\left(\frac{\rho_2}{\rho_1}x + \frac{\rho_1}{\rho_2}t\right)}, \quad v_N = \rho_2 \frac{h_N}{f_N} e^{\mathrm{i}(1+\epsilon\rho_1\rho_2)\left(\frac{\rho_2}{\rho_1}x + \frac{\rho_1}{\rho_2}t\right)}, \tag{2.817}$$

where ρ_1, ρ_2 are free real parameters which satisfy the conditions of $-1 < \rho_1\rho_2 < 0$ for $\epsilon = 1$ or $0 < \rho_1\rho_2 < 1$ for $\epsilon = -1$,

$$f_N = \sigma_{0,0,0}, \quad g_N = C_0^{-1}\sigma_{-1,1,0}, \quad h_N = \sigma_{-1,0,1}, \tag{2.818}$$

$$C_0 = \left[-\frac{p_0}{p_0^*}\left(\frac{p_0 - \mathrm{i}}{p_0^* + \mathrm{i}}\right)\right]^N, \quad p_0 = \sqrt{-\epsilon\rho_1\rho_2(1 + \epsilon\rho_1\rho_2)} + \mathrm{i}(1 + \epsilon\rho_1\rho_2), \tag{2.819}$$

$$\sigma_{n,k,l} = \det_{1\le i,j\le N}\left(m_{2i-1,2j-1}^{(n,k,l)}\right), \tag{2.820}$$

the matrix elements in $\sigma_{n,k,l}$ are defined by

$$m_{i,j}^{(n,k,l)} = \sum_{\nu=0}^{\min(i,j)} \left(\frac{1}{4}\right)^\nu S_{i-\nu}(\boldsymbol{x}^+(n,k,l) + \nu\boldsymbol{s})\, S_{j-\nu}(\boldsymbol{x}^-(n,k,l) + \nu\boldsymbol{s}), \tag{2.821}$$

vectors $\boldsymbol{x}^\pm(n,k,l) = \left(x_1^\pm, 0, x_3^\pm, 0, \cdots\right)$ are defined by

$$x_r^+(n,k,l) = \alpha_r x + \beta_r t + (n+\frac{1}{2})\theta_r + k\lambda_r + l\,\delta_{r1} + a_r, \tag{2.822}$$

$$x_r^-(n,k,l) = \alpha_r x + \beta_r^* t - (n+\frac{1}{2})\theta_r^* - k\lambda_r^* - l\,\delta_{r1} + a_r^*, \tag{2.823}$$

α_r, β_r, θ_r, and λ_r are coefficients from the expansions

$$\frac{\rho_2}{\rho_1}[\hat{\rho}(e^{\kappa}-1)] = \sum_{r=1}^{\infty}\alpha_r\kappa^r, \quad \frac{\rho_1\rho}{\rho_2}\left[\frac{1}{\hat{\rho}+\mathrm{i}\rho} - \frac{1}{e^{\kappa}\hat{\rho}+\mathrm{i}\rho}\right] = \sum_{r=1}^{\infty}\beta_r\kappa^r, \tag{2.824}$$

$$\ln\frac{e^{\kappa}\hat{\rho}+\mathrm{i}\rho}{\hat{\rho}+\mathrm{i}\rho} = \sum_{r=1}^{\infty}\theta_r\kappa^r, \quad \ln\frac{e^{\kappa}\hat{\rho}+\mathrm{i}\epsilon\rho_1\rho_2}{\hat{\rho}+\mathrm{i}\epsilon\rho_1\rho_2} = \sum_{r=1}^{\infty}\lambda_r\kappa^r, \tag{2.825}$$

with $\rho = 1+\epsilon\rho_1\rho_2$ and $\hat{\rho} = \sqrt{-\epsilon\rho_1\rho_2\rho}$, δ_{r1} is the Kronecker delta function which is equal to 1 if $r = 1$ and 0 otherwise, the vector $\boldsymbol{s} = (0, s_2, 0, s_4, \cdots)$ is defined in Eq. (2.11), $a_1 = 0$, and and a_3, a_5, a_{2N-1} are free irreducible complex constants.

Proof Through variable transformations

$$u = \rho_1\frac{g}{f^*}e^{\mathrm{i}(1+\epsilon\rho_1\rho_2)\left(\frac{\rho_2}{\rho_1}x+\frac{\rho_1}{\rho_2}t\right)}, \quad v = \rho_2\frac{h}{f}e^{\mathrm{i}(1+\epsilon\rho_1\rho_2)\left(\frac{\rho_2}{\rho_1}x+\frac{\rho_1}{\rho_2}t\right)}, \tag{2.826}$$

where f, g, h are complex functions and ρ_1, ρ_2 real constants, the MT model (2.816) is transformed into the following bilinear equations

$$(\mathrm{i}D_x - \frac{\rho_2}{\rho_1})g\cdot f = -\frac{\rho_2}{\rho_1}hf^*, \tag{2.827}$$

$$(\mathrm{i}D_x - \epsilon\rho_2^2)f\cdot f^* = -\epsilon\rho_2^2 hh^*, \tag{2.828}$$

$$(\mathrm{i}D_t - \frac{\rho_1}{\rho_2})h\cdot f^* = -\frac{\rho_1}{\rho_2}gf, \tag{2.829}$$

$$(\mathrm{i}D_t - \epsilon\rho_1^2)f^*\cdot f = -\epsilon\rho_1^2 gg^*. \tag{2.830}$$

These bilinear equations can be reduced from the following higher-dimensional bilinear equations in the extended KP hierarchy,

$$\left.\begin{aligned}
&\left(D_{x_1}+a\right)\tau_{n,k+1,l}\cdot\tau_{n+1,k,l} = a\tau_{n+1,k+1,l}\tau_{n,k,l},\\
&\left(bD_{x_{-1}}+1\right)\tau_{n,k,l+1}\cdot\tau_{n,k,l} = \tau_{n-1,k,l+1}\tau_{n+1,k,l},\\
&\left(aD_r-1\right)\tau_{n+1,k,l}\cdot\tau_{n,k,l} = -\tau_{n+1,k-1,l}\tau_{n,k+1,l},\\
&\left(bD_s-1\right)\tau_{n+1,k,l}\cdot\tau_{n,k,l} = -\tau_{n+1,k,l-1}\tau_{n,k,l+1}.
\end{aligned}\right\} \tag{2.831}$$

Indeed, for these higher-dimensional equations, if we impose the dimensional reduction conditions

$$\left[\partial_{x_1} - b(a-b)\partial_s\right]\tau_{n,k,l} = C_1\tau_{n,k,l}, \tag{2.832}$$

$$\left[\partial_{x_{-1}} + \left(\frac{a-b}{b}\right)\partial_r\right]\tau_{n,k,l} = C_2\tau_{n,k,l}, \tag{2.833}$$

as well as the index-reduction condition

$$\tau_{n+1,k+1,l-1} = C_0\tau_{n,k,l}, \tag{2.834}$$

where C_1, C_2 are real constants and C_0 a complex constant with $|C_0| = 1$, then the higher-dimensional system (2.831) would reduce to the (1+1)-dimensional system

$$\left(D_{x_1} + a\right)\tau_{n,k+1,l}\cdot\tau_{n+1,k,l} = a\,C_0\,\tau_{n,k,l+1}\tau_{n,k,l}, \tag{2.835}$$

$$\left(bD_{x_{-1}} + 1\right)\tau_{n,k,l+1}\cdot\tau_{n,k,l} = C_0^*\,\tau_{n,k+1,l}\tau_{n+1,k,l}, \tag{2.836}$$

$$\left(\frac{ab}{a-b}D_{x_{-1}} + 1\right)\tau_{n+1,k,l}\cdot\tau_{n,k,l} = \tau_{n+1,k-1,l}\tau_{n,k+1,l}, \tag{2.837}$$

$$\left(\frac{1}{a-b}D_{x_{-1}} - 1\right)\tau_{n+1,k,l}\cdot\tau_{n,k,l} = -\tau_{n+1,k,l-1}\tau_{n,k,l+1}. \tag{2.838}$$

Then, by setting

$$x_1 = -\frac{\rho_2}{\mathrm{i}a\rho_1}x,\quad x_{-1} = -\frac{\rho_1 b}{\mathrm{i}\rho_2}t,\quad a = \mathrm{i},\quad b = \mathrm{i}(1+\epsilon\rho_1\rho_2), \tag{2.839}$$

$$f = \tau_{0,0,0},\quad f^* = \tau_{-1,0,0},\quad C_0 g = \tau_{-1,1,0}, \tag{2.840}$$

$$h = \tau_{-1,0,1},\quad h^* = \tau_{0,0,-1},\quad C_0^* g^* = \tau_{0,-1,0}, \tag{2.841}$$

and imposing the complex conjugate condition

$$\tau_{n,k,l}^* = \tau_{-1-n,-k,-l}, \tag{2.842}$$

we get the original bilinear equations (2.827)–(2.830).

A wide class of algebraic solutions to the higher-dimensional bilinear system (2.831) is (Chen et al. 2023)

$$\tau_{n,k,l} = \det_{1\le\nu,\mu\le N}\left(m_{i_\nu,j_\mu}^{(n,k,l)}\right), \tag{2.843}$$

where

$$m_{i,j}^{(n,k,l)} = \mathcal{A}_i\mathcal{B}_j m^{(n,k,l)}, \tag{2.844}$$

$$\mathcal{A}_i = \frac{\left[f_1(p)\partial_p\right]^i}{i!}, \quad \mathcal{B}_j = \frac{\left[f_2(q)\partial_q\right]^j}{j!}, \tag{2.845}$$

$$m^{(n,k,l)} = \frac{\mathrm{i}p}{p+q}\left(-\frac{p}{q}\right)^n\left(-\frac{p-a}{q+a}\right)^k\left(-\frac{p-b}{q+b}\right)^l e^{\xi(p)+\eta(q)}, \tag{2.846}$$

$$\xi(p) = \frac{1}{p}x_{-1} + px_1 + \frac{1}{p-a}r + \frac{1}{p-b}s + \xi_0(p), \tag{2.847}$$

$$\eta(q) = \frac{1}{q}x_{-1} + qx_1 + \frac{1}{q+a}r + \frac{1}{q+b}s + \eta_0(q), \tag{2.848}$$

$f_1(p)$, $f_2(q)$, $\xi_0(p)$, $\eta_0(q)$ are arbitrary functions, and $(i_1, i_2, \cdots, i_N; j_1, j_2, \cdots, j_N)$ are arbitrary sequences of indices. The factor $\mathrm{i}p$ in Eq. (2.846) is needed in order for the resulting $m_{i,j}^{(n,k,l)}$ to satisfy the complex conjugacy condition (2.842) (see later text).

Dimensional Reduction

First, we introduce linear differential operators

$$\mathcal{L}_1 = \partial_{x_1} - b(a-b)\partial_s, \quad \mathcal{L}_2 = \partial_{x_{-1}} + \frac{a-b}{b}\partial_r, \tag{2.849}$$

by which the dimensional reduction conditions (2.832) and (2.833) become

$$\mathcal{L}_1\tau_{n,k,l} = C_1\tau_{n,k,l}, \quad \mathcal{L}_2\tau_{n,k,l} = C_2\tau_{n,k,l}. \tag{2.850}$$

It is straightforward to see that

$$\mathcal{L}_1 m_{i,j}^{(n,k,l)} = \mathcal{A}_i\mathcal{B}_j\mathcal{L}_1 m^{(n,k,l)} = \mathcal{A}_i\mathcal{B}_j\left[Q_{11}(p) + Q_{12}(q)\right]m^{(n,k,l)}, \tag{2.851}$$

$$\mathcal{L}_2 m_{i,j}^{(n,k,l)} = \mathcal{A}_i\mathcal{B}_j\mathcal{L}_2 m^{(n,k,l)} = \mathcal{A}_i\mathcal{B}_j\left[Q_{21}(p) + Q_{22}(q)\right]m^{(n,k,l)}, \tag{2.852}$$

where

$$Q_{11}(p) = p - b + \frac{b(b-a)}{p-b}, \quad Q_{12}(q) = q + b + \frac{b(b-a)}{q+b}, \tag{2.853}$$

$$Q_{21}(p) = \frac{1}{p} + \frac{a-b}{b(p-a)}, \quad Q_{22}(q) = \frac{1}{q} + \frac{a-b}{b(q+a)}. \tag{2.854}$$

Using the general Leibnitz-type operator relation (2.249), we get

$$\mathcal{L}_s m_{i,j}^{(n,k,l)} = \sum_{\mu=0}^{i} \frac{1}{\mu!} \left[\left(f_1 \partial_p \right)^{\mu} Q_{s,1}(p) \right] m_{i-\mu,j}^{(n,k,l)} + \sum_{\nu=0}^{j} \frac{1}{\nu!} \left[\left(f_2 \partial_q \right)^{\nu} Q_{s,2}(q) \right] m_{i,j-\nu}^{(n,k,l)}, \tag{2.855}$$

where $s = 1, 2$.

Next, the specific functions $[f_1(p), f_2(q)]$ and values of (p, q) need to be determined to guarantee that coefficients of certain indices vanish in the above summation. To this end, we solve the first two algebraic equations

$$Q'_{11}(p) = 0, \quad Q'_{12}(q) = 0, \tag{2.856}$$

and get the following simple roots:

$$p_0 = \sqrt{b(b-a)} + b, \quad q_0 = \sqrt{b(b-a)} - b. \tag{2.857}$$

Using the a and b values in Eq. (2.839), these roots are

$$\left. \begin{array}{l} p_0 = \sqrt{-\epsilon \rho_1 \rho_2 (1 + \epsilon \rho_1 \rho_2)} + \mathrm{i}(1 + \epsilon \rho_1 \rho_2), \\ q_0 = \sqrt{-\epsilon \rho_1 \rho_2 (1 + \epsilon \rho_1 \rho_2)} - \mathrm{i}(1 + \epsilon \rho_1 \rho_2). \end{array} \right\} \tag{2.858}$$

Since rogue waves can be obtained only when (p_0, q_0) are nonimaginary, the condition for the existence of rogue wave solution is then $-1 < \rho_1 \rho_2 < 0$ for $\epsilon = 1$, or $0 < \rho_1 \rho_2 < 1$ for $\epsilon = -1$. Under these conditions, $q_0 = p_0^*$.

It is important to note that p_0 and q_0 are also simple roots of the equations

$$Q'_{21}(p) = 0, \quad Q'_{22}(q) = 0, \tag{2.859}$$

respectively. The reason is that $Q_{21}(p)$ and $Q_{22}(q)$ are associated with $Q_{11}(p)$ and $Q_{12}(q)$ through the simple relations

$$Q_{21}(p) = \frac{a}{b}[Q_{11}(p) - a + 2b]^{-1}, \quad Q_{22}(q) = \frac{a}{b}[Q_{12}(q) + a - 2b]^{-1}. \tag{2.860}$$

As a consequence, the terms with $\mu = \nu = 1$ on the right side of Eq. (2.855) vanish at (p_0, q_0) for both $s = 1$ and 2.

Following the steps in Sect. 2.3 and the simple root's case in Sects. 2.9 and 2.10, we need to solve the differential equations

$$\left(f_1 \partial_p \right)^2 Q_{11}(p) = Q_{11}(p), \quad \left(f_2 \partial_q \right)^2 Q_{12}(q) = Q_{12}(q). \tag{2.861}$$

From our previous formulae (2.257), the following functions can be derived,

$$\mathcal{W}_1(p) = \frac{p - b}{\sqrt{b(b-a)}}, \quad \mathcal{W}_2(q) = \frac{q + b}{\sqrt{b(b-a)}}, \tag{2.862}$$

and

$$f_1(p) = \frac{\mathcal{W}_1(p)}{\mathcal{W}_1'(p)} = p - b, \quad f_2(q) = \frac{\mathcal{W}_2(p)}{\mathcal{W}_2'(p)} = q + b. \tag{2.863}$$

From the conditions (2.856) and (2.861), we can find that

$$\begin{aligned} \mathcal{L}_1 m_{i,j}^{(n,k,l)}\Big|_{\substack{p=p_0,\\ q=q_0}} &= Q_{11}(p_0) \sum_{\substack{\mu=0,\\ \mu:even}}^{i} \frac{1}{\mu!}\, m_{i-\mu,j}^{(n,k,l)}\Big|_{\substack{p=p_0,\\ q=q_0}} \\ &\quad + Q_{12}(q_0) \sum_{\substack{\nu=0,\\ \nu:even}}^{j} \frac{1}{\nu!}\, m_{i,j-\nu}^{(n,k,l)}\Big|_{\substack{p=p_0,\\ q=q_0}}, \end{aligned} \tag{2.864}$$

From this contiguity relation and similar calculations in Sects. 2.1.1 and 2.3, we then find that if we restrict the general determinant (2.843) to

$$\tau_{n,k,l} = \det_{1\le i,j\le N} \left(m_{2i-1,2j-1}^{(n,k,l)}\Big|_{p=p_0,q=q_0} \right), \tag{2.865}$$

then

$$\mathcal{L}_1 \tau_{n,k,l} = [Q_{11}(p_0) + Q_{12}(q_0)]\, N \tau_{n,k,l} = 4\sqrt{b(b-a)} N \tau_{n,k,l}. \tag{2.866}$$

Thus, the first dimensional reduction condition (2.832) is satisfied.

Now, we prove that the second dimensional reduction condition (2.833) simultaneously holds. The key is that p_0 and q_0 in Eq. (2.857) are simple roots of both Eqs. (2.856) and (2.859) which arise in the two dimension reductions. When this happens, both dimension reduction conditions would hold simultaneously. A similar situation has appeared in the complex short pulse equation in Sect. 2.5, where we proved this fact using a simpler but less general approach. Here, we will prove this fact using a more general approach.

We notice from Eq. (2.860) that $Q_{21}(p)$ can be expressed as a function of $Q_{11}(p)$. Then, let us consider a general function of Q_{11}, $F[Q_{11}(p)] \equiv F(Q_{11})$. By using the Faà di Bruno formula and the relation $f_1 \partial_p = \partial_{\ln \mathcal{W}_1}$, we obtain

$$\begin{aligned} \left(f_1 \partial_p\right)^l F(Q_{11}) &= \partial_{\ln \mathcal{W}_1}^l F(Q_{11}) \\ &= \sum_{m_1+2m_2+\cdots+lm_l=l} \frac{\frac{d^{\hat{m}} F(Q_{11})}{dQ_{11}^{\hat{m}}} \prod_{j=1}^{l} \left[(f_1\partial_p)^j Q_{11}\right]^{m_j}}{(l!)^{-1} \prod_{i=1}^{l} m_i!(i!)^{m_i}}, \end{aligned} \tag{2.867}$$

where $\hat{m} = \sum_{i=1}^{l} m_i$. Furthermore, by using the conditions (2.856) and (2.861), one finds that

$$\left(f_1\partial_p\right)^l F[Q_{11}(p_0)] = 0, \quad (l \text{ is odd}), \tag{2.868}$$

$$\begin{aligned}\left(f_1\partial_p\right)^l F[Q_{11}(p_0)] &= \sum_{\substack{2m_2+\cdots+lm_l=l,\\ m_1=m_3=\cdots=0}} \left.\frac{\frac{d^{\hat{m}}F(Q_{11})}{dQ_{11}^{\hat{m}}}\prod_{j=1}^{l}\left[(f_1\partial_p)^j Q_{11}\right]^{m_j}}{(l!)^{-1}\prod_{i=1}^{l} m_i!(i!)^{m_i}}\right|_{p=p_0} \\ &\triangleq C_{1,l}\left(F[Q_{11}(p_0)]\right), \quad (l \text{ is even}).\end{aligned} \tag{2.869}$$

The similar calculation for a general function $F[Q_{12}(q)] \equiv F(Q_{12})$ gives

$$\left(f_2\partial_q\right)^l F[Q_{12}(q_0)] = 0, \quad (l \text{ is odd}), \tag{2.870}$$

$$\begin{aligned}\left(f_2\partial_q\right)^l F[Q_{12}(q_0)] &= \sum_{\substack{2m_2+\cdots+lm_l=l,\\ m_1=m_3=\cdots=0}} \left.\frac{\frac{d^{\hat{m}}F(Q_{12})}{dQ_{12}^{\hat{m}}}\prod_{j=1}^{l}\left[(f_2\partial_q)^j Q_{12}\right]^{m_j}}{(l!)^{-1}\prod_{i=1}^{l} m_i!(i!)^{m_i}}\right|_{p=p_0} \\ &\triangleq C_{2,l}\left(F[Q_{12}(q_0)]\right), \quad (l \text{ is even}).\end{aligned} \tag{2.871}$$

Applying the above formulae (2.868)–(2.871) to the specific functions $F[Q_{11}(p)] = Q_{21}(p)$ and $F[Q_{12}(q)] = Q_{22}(q)$, it follows that

$$\begin{aligned}\mathcal{L}_2 m_{i,j}^{(n,k,l)}\Big|_{\substack{p=p_0,\\ q=q_0}} &= \sum_{\substack{\mu=0,\\ \mu:even}}^{i} \frac{C_{1,\mu}[Q_{21}(p_0)]}{\mu!}\, m_{i-\mu,j}^{(n,k,l)}\Big|_{\substack{p=p_0,\\ q=q_0}} \\ &\quad + \sum_{\substack{\nu=0,\\ \nu:even}}^{j} \frac{C_{2,\nu}[Q_{22}(q_0)]}{\nu!}\, m_{i,j-\nu}^{(n,k,l)}\Big|_{\substack{p=p_0,\\ q=q_0}}.\end{aligned} \tag{2.872}$$

On the right side of the above equation, the coefficients in the first term of two summations are $C_{1,0}[Q_{21}(p_0)] = Q_{21}(p_0)$ and $C_{2,0}[Q_{22}(q_0)] = Q_{22}(q_0)$, respectively. This contiguity relation for $\mathcal{L}_2 m_{i,j}^{(n,k,l)}$ is similar to (2.864) for $\mathcal{L}_1 m_{i,j}^{(n,k,l)}$. From it, we then find that for the $\tau_{n,k,l}$ function defined in Eq. (2.865),

$$\mathcal{L}_2\tau_{n,k,l} = [Q_{21}(p_0) + Q_{22}(q_0)]\, N\tau_{n,k,l} = -\frac{4\sqrt{b(b-a)}}{ab} N\tau_{n,k,l}, \tag{2.873}$$

and thus the second dimensional reduction condition (2.833) is also satisfied.

Index Reduction

Now we consider the index reduction condition (2.834). From the definition of $m_{i,j}^{(n,k,l)}$, we get

$$m_{i,j}^{(n+1,k+1,l-1)} = \mathcal{A}_i \mathcal{B}_j m^{(n+1,k+1,l-1)} = \mathcal{A}_i \mathcal{B}_j \left[Q_{31}(p) Q_{32}(q) \right] m^{(n,k,l)}, \tag{2.874}$$

where

$$Q_{31}(p) = \frac{p(p-a)}{p-b} = Q_{11}(p) - (a-2b), \tag{2.875}$$

and

$$Q_{32}(q) = -\frac{q+b}{q(q+a)} = -\left[Q_{12}(q) + (a-2b) \right]^{-1}. \tag{2.876}$$

From these connections of $[Q_{31}(p), Q_{32}(q)]$ to $[Q_{11}(p), Q_{12}(q)]$, we get

$$Q'_{31}(p_0) = 0, \quad Q'_{32}(q_0) = 0. \tag{2.877}$$

Furthermore, applying the above formulae (2.868)–(2.871) to the specific functions $F[Q_{11}(p)] = Q_{31}(p)$ and $F[Q_{12}(q)] = Q_{32}(q)$ and utilizing general operator relations (2.249), we arrive at

$$\begin{aligned} m_{i,j}^{(n+1,k+1,l-1)}\Big|_{p=p_0,q=q_0} = & \left[\sum_{\substack{\mu=0,\\ \mu:even}}^{i} \frac{C_{1,\mu}[Q_{31}(p_0)]}{\mu!} \right] \\ & \times \left[\sum_{\substack{\nu=0,\\ \nu:even}}^{j} \frac{C_{2,\nu}[Q_{32}(q_0)]}{\nu!} \right] m_{i-\mu,j-\nu}^{(n,k,l)}\Big|_{p=p_0,q=q_0}. \end{aligned} \tag{2.878}$$

It is easy to see that the coefficients of the first term in the above summations are $C_{1,0}[Q_{31}(p_0)] = Q_{31}(p_0)$ and $C_{2,0}[Q_{32}(q_0)] = Q_{32}(q_0)$. Thus, Eq. (2.878) leads to the following matrix relation

$$\left(m_{2i-1,2j-1}^{(n+1,k+1,l-1)}\Big|_{p=p_0,\ q=q_0} \right)_{1\le i,j\le N} = L \left(m_{2i-1,2j-1}^{(n,k,l)}\Big|_{p=p_0,\ q=q_0} \right)_{1\le i,j\le N} U, \tag{2.879}$$

where L and U are lower and upper triangular matrices with diagonal entries as $Q_{31}(p_0)$ and $Q_{32}(q_0)$, respectively. Taking determinant on both sides of this equation, we get

$$\tau_{n+1,k+1,l-1} = C_0\tau_{n,k,l}, \quad C_0 = [Q_{31}(p_0)Q_{32}(q_0)]^N = \left[-\frac{p_0}{q_0}\left(\frac{p_0-a}{q_0+a}\right)\right]^N. \tag{2.880}$$

Recalling $q_0 = p_0^*$ and $a = \mathrm{i}$ is imaginary, $|C_0| = 1$. Thus, the index reduction condition (2.834) is proved.

Complex Conjugacy Condition

We have known that $q_0 = p_0^*$. Then, by imposing the parameter constraint of $\eta_0 = \xi_0^*$ and noticing that the coordinate transformations $x_1 = \frac{\rho_2}{\rho_1}x$ and $x_{-1} = -\frac{\rho_1(1+\epsilon\rho_1\rho_2)}{\rho_2}t$ are real, one can find that

$$\left[m_{i,j}^{(n,k,l)}\right]^*\Big|_{p=p_0,q=q_0} = \left[m_{j,i}^{(-n-1,-k,-l)}\right]\Big|_{p=p_0,q=q_0}, \tag{2.881}$$

which implies $\tau_{n,k,l}^* = \tau_{-n-1,-k,-l}$. Thus, the complex conjugation condition (2.842) is satisfied.

Finally, we introduce free parameters by expanding $\xi_0(p)$ as

$$\xi_0 = \sum_{r=1}^{\infty}\hat{a}_r\ln^r\mathcal{W}_1(p) = \sum_{r=1}^{\infty}\hat{a}_r\ln^r\left(\frac{p-b}{\sqrt{b(b-a)}}\right), \tag{2.882}$$

where $\hat{a}_r$ are arbitrary complex parameters.

Summarizing the above results, we have the following lemma on rogue waves of the MT system in differential operator form.

Lemma 2.16 *The massive Thirring model (2.816) admits N-th order rogue wave solutions*

$$u_N = \rho_1\frac{g_N}{f_N^*}e^{\mathrm{i}(1+\epsilon\rho_1\rho_2)\left(\frac{\rho_2}{\rho_1}x+\frac{\rho_1}{\rho_2}t\right)}, \quad v_N = \rho_2\frac{h_N}{f_N}e^{\mathrm{i}(1+\epsilon\rho_1\rho_2)\left(\frac{\rho_2}{\rho_1}x+\frac{\rho_1}{\rho_2}t\right)}, \tag{2.883}$$

where

$$f_N = \tau_{0,0,0}, \quad g_N = C_0^{-1}\tau_{-1,1,0}, \quad h_N = \tau_{-1,0,1}, \tag{2.884}$$

$$C_0 = \left[-\frac{p_0}{p_0^*}\left(\frac{p_0-\mathrm{i}}{p_0^*+\mathrm{i}}\right)\right]^N, \quad p_0 = \sqrt{-\epsilon\rho_1\rho_2(1+\epsilon\rho_1\rho_2)} + \mathrm{i}(1+\epsilon\rho_1\rho_2), \tag{2.885}$$

$$\tau_{n,k,l} = \det_{1\le i,j\le N}\left(m_{2i-1,2j-1}^{(n,k,l)}\right), \tag{2.886}$$

$$m_{i,j}^{(n,k,l)} = \frac{\left[(p-b)\partial_p\right]^i}{i!}\frac{\left[(q+b)\partial_q\right]^j}{j!}\, m^{(n,k,l)}\Big|_{p=p_0,\ q=p_0^*}, \tag{2.887}$$

$$m^{(n,k,l)} = \left(\frac{\mathrm{i}p}{p+q}\right)\left(-\frac{p}{q}\right)^n\left(-\frac{p-\mathrm{i}}{q+\mathrm{i}}\right)^k\left(-\frac{p-b}{q+b}\right)^l e^{\Theta}, \tag{2.888}$$

$$\begin{aligned}\Theta = {} & \frac{\rho_2}{\rho_1}(p+q)x + \frac{\mathrm{i}b\rho_1}{\rho_2}\left(\frac{1}{p}+\frac{1}{q}\right)t + \sum_{r=1}^{\infty}\hat{a}_r \ln^r\left(\frac{p-b}{\sqrt{b(b-\mathrm{i})}}\right) \\ & + \sum_{r=1}^{\infty}\hat{a}_r^* \ln^r\left(\frac{q+b}{\sqrt{b(b-\mathrm{i})}}\right),\end{aligned} \tag{2.889}$$

$b = \mathrm{i}(1+\epsilon\rho_1\rho_2)$, *and* $\hat{a}_r$ $(r = 1, 2, \dots)$ *are free complex constants.*

Lastly, we remove the differential operators in the above lemma, using the same technique we have described in earlier sections (see Sect. 2.2 for instance). The final explicit expressions of these rogue waves are then as given in Theorem 2.17, where parameters a_r in that theorem are linearly related to $\hat{a}_r$ in the above lemma. This completes the proof of Theorem 2.17.

Taking $N = 1$ in Theorem 2.17, we obtain the fundamental rogue wave solution as

$$u = \frac{\rho_1 e^{\mathrm{i}\phi_0}}{C_0}\left[1 - \frac{d_2^*(L_1-d_1) - d_2(L_1^*+d_1^*) + |d_2|^2}{(L_1-d_1)(L_1^*+d_1^*) + \frac{d_0^2}{4}}\right], \tag{2.890}$$

$$v = \rho_2 e^{\mathrm{i}\phi_0}\left[1 + \frac{(2d_1^*-d_0)(L_1+d_1) - (2d_1-d_0)(L_1^*-d_1^*) - |2d_1-d_0|^2}{(L_1+d_1)(L_1^*-d_1^*) + \frac{d_0^2}{4}}\right], \tag{2.891}$$

where

$$L_1 = \frac{\rho_2}{\rho_1}x + \frac{4\rho\rho_1 d_1^2}{\rho_2}t,\quad d_1 = \frac{1}{2(\hat{\rho}+\mathrm{i}\rho)},\quad d_2 = \frac{1}{(\hat{\rho}+\mathrm{i}\epsilon\rho_1\rho_2)},\quad d_0 = \frac{1}{\hat{\rho}},$$

$$\phi_0 = \rho\left(\frac{\rho_2}{\rho_1}x + \frac{\rho_1}{\rho_2}t\right),\quad \hat{\rho} = \sqrt{-\epsilon\rho_1\rho_2\rho},\quad \rho = 1+\epsilon\rho_1\rho_2,$$

$$C_0 = -\frac{p_0}{p_0^*}\left(\frac{p_0-\mathrm{i}}{p_0^*+\mathrm{i}}\right).$$

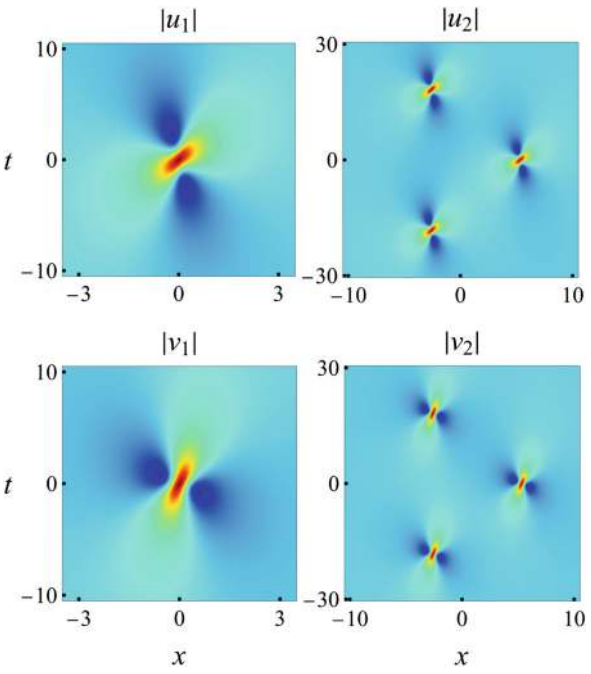

Fig. 2.25 Density plots of the fundamental and a second-order rogue waves in the massive Thirring model (2.816) for $\epsilon = -1,\ \rho_1 = 1/2$ and $\rho_2 = 1$. Left column: the fundamental rogue wave (2.890). Right column: a second-order rogue wave with $a_3 = 50$

Second-order rogue waves can be obtained from Theorem 2.17 by taking $N = 2$, which contains a free complex parameter a_3. Graphs for the fundamental and a second-order rogue wave with $a_3 = 50$ for $\epsilon = -1,\ \rho_1 = 1/2$ and $\rho_2 = 1$ are plotted in Fig. 2.25. The fundamental rogue wave has a single elongated hump in both the u and v components, and the humps in the two components are oriented in different directions. The second-order rogue wave splits into three fundamental rogue waves.

2.13 Davey-Stewartson Equations

Evolution of a two-dimensional wave packet on water of finite depth is governed by the Benney-Roskes-Davey-Stewartson equations; and in the shallow water limit, this equation is integrable (see Sect. 1.4). This integrable equation is sometimes called the Davey-Stewartson (DS) equations in the literature. The DS equations are

$$\left.\begin{aligned} \mathrm{i}A_t &= A_{xx} - \sigma A_{yy} + (\epsilon|A|^2 - 2Q)A, \\ Q_{xx} &+ \sigma Q_{yy} = \epsilon(|A|^2)_{xx}, \end{aligned}\right\} \tag{2.892}$$

where $A(x, y, t)$ is a complex function, and $Q(x, y, t)$ is a real function. When $\sigma = -1$, they are called DSI, and when $\sigma = 1$, they are called DSII. The parameter $\epsilon = \pm 1$ is the sign of nonlinearity.

Fundamental rogue waves in the DSI system have been derived in Tajiri and Arai (1999) by taking a limit to DSI's homoclinic solutions. General rogue waves in DSI and DSII equations have been derived in Ohta and Yang (2012b, 2013) by the bilinear method. However, solution expressions in Ohta and Yang (2012b, 2013) involve differential operators and are not explicit. In addition, parameterizations in them are not optimal. In this section, we derive explicit and simpler expressions of rogue wave solutions in DSI and DSII, following Ohta and Yang (2012b, 2013) but with major improvements.

Under the variable transformation

$$A = \sqrt{2}\frac{g}{f}, \quad Q = \epsilon - (2\ln f)_{xx}, \tag{2.893}$$

where f is a real variable and g a complex one, DS equations (2.892) are reduced to the following bilinear forms

$$\left.\begin{aligned} &(D_x^2 - \sigma D_y^2 - \mathrm{i}D_t)g \cdot f = 0, \\ &(D_x^2 + \sigma D_y^2) f \cdot f = 2\epsilon(f^2 - |g|^2). \end{aligned}\right\} \tag{2.894}$$

With the invertible coordinate transform

$$\left.\begin{aligned} &x_1 = \tfrac{1}{2}(x + \sigma' y), \; x_{-1} = \tfrac{1}{2}\epsilon(x - \sigma' y), \\ &x_2 = -\tfrac{1}{2}\mathrm{i}t, \qquad\quad x_{-2} = \tfrac{1}{2}\mathrm{i}t, \end{aligned}\right\} \tag{2.895}$$

where $\sigma' = \sqrt{-\sigma}$, the bilinear equations (2.894) can be split into the following system

$$\left.\begin{aligned} &(D_{x_1}^2 + D_{x_2}) f \cdot g = 0, \\ &(D_{x_{-1}}^2 - D_{x_{-2}}) f \cdot g = 0, \\ &D_{x_1} D_{x_{-1}} f \cdot f = 2(f^2 - gg^*). \end{aligned}\right\} \tag{2.896}$$

This bilinear system belongs to the extended KP hierarchy,

$$\left.\begin{aligned} &(D_1^2 + D_2)\, \tau_k \cdot \tau_{k+1} = 0, \\ &(D_{-1}^2 - D_{-2})\, \tau_k \cdot \tau_{k+1} = 0, \\ &D_1 D_{-1}\, \tau_k \cdot \tau_k = 2(\tau_k^2 - \tau_{k+1}\tau_{k-1}). \end{aligned}\right\} \tag{2.897}$$

General Gram solutions to these extended KP hierarchy equations can be found in Ohta and Yang (2012b) and Yang and Yang (2022c). To derive rogue wave solutions (which are rational solutions), we specialize those Gram solutions as

$$\tau_k = \det_{1\le i,j\le K}\left(m_{i,j}^{(k)}\right), \tag{2.898}$$

where

$$m_{i,j}^{(k)} = \mathcal{A}_i\mathcal{B}_j\frac{1}{p+q}(-\frac{p}{q})^k e^{\xi_i+\eta_j}\Big|_{p=p_i,\,q=q_j}, \tag{2.899}$$

$$\mathcal{A}_i = \frac{1}{n_i!}(p\partial_p)^{n_i}, \quad \mathcal{B}_j = \frac{1}{m_j!}(q\partial_q)^{m_j}, \tag{2.900}$$

$$\xi_i = \frac{1}{p^2}x_{-2} + \frac{1}{p}x_{-1} + px_1 + p^2x_2 + \sum_{r=1}^{\infty}a_{r,i}\ln^r\left[\frac{p}{p_i}\right], \tag{2.901}$$

$$\eta_j = -\frac{1}{q^2}x_{-2} + \frac{1}{q}x_{-1} + qx_1 - q^2x_2 + \sum_{r=1}^{\infty}b_{r,j}\ln^r\left[\frac{q}{q_j}\right], \tag{2.902}$$

$(n_1, n_2, \ldots, n_K)$, $(m_1, m_2, \ldots, m_K)$ are arbitrary nonnegative integers, and p_i, q_j, $a_{r,i}$, $b_{r,j}$ are free complex constants. Rogue waves (2.893) would be given through these τ functions as

$$f = \tau_0, \quad g = \tau_1, \quad g^* = \tau_{-1}, \tag{2.903}$$

if the above τ_k also satisfies the conjugation condition

$$\tau_{-k} = \tau_k^*. \tag{2.904}$$

This conjugation condition can be met in different ways for DSI and DSII, which will be treated separately below.

2.13.1 Davey-Stewartson-I Equations

For DSI where $\sigma = -1$, the coordinate transform (2.895) reduces to

$$\left.\begin{aligned} x_1 &= \tfrac{1}{2}(x+y),\ x_{-1} = \tfrac{1}{2}\epsilon(x-y),\\ x_2 &= -\tfrac{1}{2}\mathrm{i}t, \qquad x_{-2} = \tfrac{1}{2}\mathrm{i}t, \end{aligned}\right\} \tag{2.905}$$

where (x_1, x_{-1}) are real and (x_2, x_{-2}) purely imaginary. In this case, for τ_n in (2.898) to satisfy conjugacy conditions (2.904), we constrain the parameters as

$$K = N, \quad m_j = n_j, \quad q_j = p_j^*, \quad b_{r,j} = a_{r,j}^*. \tag{2.906}$$

Then,

$$\xi_j^* = \eta_j, \quad \left(m_{i,j}^{(k)}\right)^* = m_{j,i}^{(-k)}, \quad \tau_k^* = \tau_{-k}. \tag{2.907}$$

Thus, conjugation conditions (2.904) are met. The corresponding solutions (2.898)–(2.903) then give DSI rational solutions in differential form.

More explicit expressions of these solutions can be derived by eliminating the differential operators in Eq. (2.900) in favor of Schur polynomials. This is a step which has been taken for every integrable equation covered in previous sections, using a technique carefully explained in Sect. 2.1.1. These more explicit solution expressions are presented in the following theorem (the proof is skipped for brevity).

Theorem 2.18 *The Davey-Stewartson I eqaution admits general rational solutions*

$$A(x, y, t) = \sqrt{2}\frac{g}{f}, \quad Q(x, y, t) = 1 - 2\epsilon \left(\log f\right)_{xx}, \tag{2.908}$$

where

$$f = \tau_0, \quad g = \tau_1, \quad \tau_k = \det_{1\le i,j\le N}\left(m_{i,j}^{(k)}\right), \tag{2.909}$$

N is a positive integer, the matrix elements $m_{i,j}^{(k)}$ of τ_k are defined by

$$m_{i,j}^{(k)} = \sum_{\nu=0}^{\min(n_i,n_j)} \left(\frac{1}{p_i + p_j^*}\right)\left[\frac{p_i p_j^*}{(p_i + p_j^*)^2}\right]^\nu \times S_{n_i-\nu}[\boldsymbol{x}_{i,j}^+(k) + \nu \boldsymbol{s}_{i,j} + \boldsymbol{a}_i]\, S_{n_j-\nu}[\boldsymbol{x}_{j,i}^-(k) + \nu \boldsymbol{s}_{j,i}^* + \boldsymbol{a}_j^*], \tag{2.910}$$

$(n_1, n_2, \ldots, n_N)$ are nonnegative integers, vectors $\boldsymbol{x}_{i,j}^\pm(k) = \left(x_{1,i,j}^\pm, x_{2,i,j}^\pm, \cdots\right)$ are defined by

$$x_{r,i,j}^+(k) = \frac{(-1)^r}{r!p_i}x_{-1} + \frac{(-2)^r}{r!p_i^2}x_{-2} + \frac{1}{r!}p_i x_1 + \frac{2^r}{r!}p_i^2 x_2 + k\delta_{r,1} - c_{r,i,j}, \tag{2.911}$$

$$x_{r,i,j}^-(k) = \frac{(-1)^r}{r!p_i^*}x_{-1} + \frac{(-2)^r}{r!(p_i^*)^2}x_2 + \frac{1}{r!}p_i^* x_1 + \frac{2^r}{r!}(p_i^*)^2 x_{-2} - k\delta_{r,1} - c_{r,i,j}^*, \tag{2.912}$$

$$x_1 = \frac{1}{2}(x + y), \quad x_{-1} = \frac{1}{2}\epsilon(x - y), \quad x_2 = -\frac{1}{2}it, \quad x_{-2} = \frac{1}{2}it, \tag{2.913}$$

p_i are free complex constants, $\delta_{r,1}$ is the Kronecker delta function, vectors $\boldsymbol{s}_{i,j}$ are $(s_{1,i,j}, s_{2,i,j}, \cdots)$, $c_{r,i,j}$ and $s_{r,i,j}$ are coefficients from the expansions

$$\ln\left[\frac{p_i e^{\kappa}+p_j^*}{p_i+p_j^*}\right]=\sum_{r=1}^{\infty}c_{r,i,j}\kappa^r,\quad \ln\left[\frac{p_i+p_j^*}{\kappa}\left(\frac{e^{\kappa}-1}{p_i e^{\kappa}+p_j^*}\right)\right]=\sum_{r=1}^{\infty}s_{r,i,j}\kappa^r, \tag{2.914}$$

vectors $\boldsymbol{a}_i$ *are*

$$\boldsymbol{a}_i=\left(a_{i,1},a_{i,2},\ldots,a_{i,n_i}\right), \tag{2.915}$$

and $a_{i,j}$ $(1\le i\le N, 1\le j\le n_i)$ *are free complex constants.*

The fundamental rational solution is obtained from this theorem by taking $N=1$ and $n_1=1$. In this case, through a simple shift in two of the (x,y,t) axes to remove the $a_{1,1}$ and $c_{1,1,1}$ constants, the corresponding rational solution $A(x,y,t)$ can be written as

$$A(x,y,t)=\sqrt{2}\frac{\tau_1}{\tau_0}, \tag{2.916}$$

where

$$\tau_k=\frac{1}{p_1+p_1^*}\left[(\xi+k)(\xi^*-k)+\Delta\right], \tag{2.917}$$

$$\xi=ax+by+\omega t,\quad \Delta=\frac{p_1p_1^*}{(p_1+p_1^*)^2}, \tag{2.918}$$

and

$$a=\frac{p_1-\epsilon p_1^{-1}}{2},\quad b=\frac{p_1+\epsilon p_1^{-1}}{2},\quad \omega=\frac{p_1^2+p_1^{-2}}{\mathrm{i}}. \tag{2.919}$$

If we separate the real and imaginary part of a, b and ω as

$$a=a_1+\mathrm{i}a_2,\ b=b_1+\mathrm{i}b_2,\ \omega=\omega_1+\mathrm{i}\omega_2, \tag{2.920}$$

then

$$A(x,y,t)=\sqrt{2}\left[1-\frac{2\mathrm{i}(a_2x+b_2y+\omega_2t)+1}{(a_1x+b_1y+\omega_1t)^2+(a_2x+b_2y+\omega_2t)^2+\Delta}\right]. \tag{2.921}$$

This fundamental rational solution has three distinctly different dynamical behaviors depending on the parameter value of p_1^2.

- If p_1^2 is not real, then the solution is a localized soliton moving on a constant background.

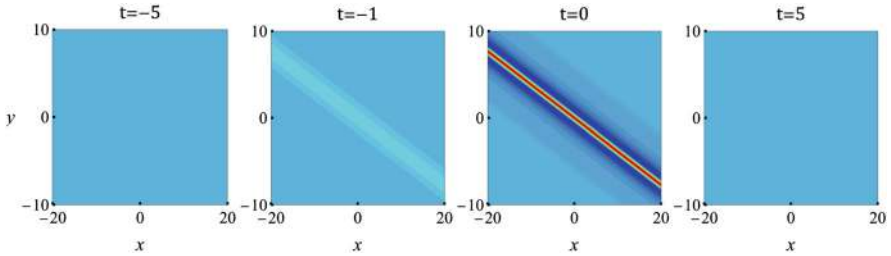

Fig. 2.26 Density plots of the fundamental line-rogue wave $|A(x, y, t)|$ from Eq. (2.921) in the DSI equation at different times for $\epsilon = 1$ and $p_1 = 3/2$

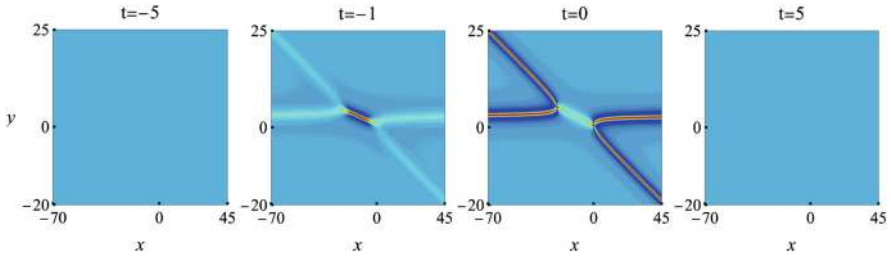

Fig. 2.27 Density plots of a rogue wave solution $|A(x, y, t)|$ in the DSI equation that describes the interaction of two line rogue waves. Parameter choices are $\epsilon = 1$, $N = 2$, $n_1 = n_2 = 1$, $p_1 = 1$, $p_2 = 3/2$, and $a_{1,1} = a_{1,2} = 0$

- If $p_1^2 < 0$, then the solution is a line soliton moving on a constant background.
- If $p_1^2 > 0$, i.e., p_1 is real, then the solution is a line rogue wave which "appears from nowhere and disappears with no trace".

This line rogue wave with $\epsilon = 1$ and $p_1 = 3/2$ is plotted in Fig. 2.26.

If $N > 1$, rational solutions in Theorem 2.18 could describe the interaction between line rogue waves if the p_i values are real. Such an example is shown in Fig. 2.27. In the region of interaction, the solution exhibits a stem connecting two well-separated curvy rogue fronts.

2.13.2 *Davey-Stewartson-II Equations*

For DSII where $\sigma = 1$, the coordinate transform (2.895) becomes

$$\left.\begin{aligned} x_1 &= \tfrac{1}{2}(x + \mathrm{i}y), \quad x_{-1} = \tfrac{1}{2}\epsilon(x - \mathrm{i}y), \\ x_2 &= -\tfrac{1}{2}\mathrm{i}t, \qquad\quad x_{-2} = \tfrac{1}{2}\mathrm{i}t, \end{aligned}\right\} \tag{2.922}$$

where (x_1, x_{-1}) are complex and (x_2, x_{-2}) purely imaginary. This variable transformation means that

$$x_{-1} = \epsilon x_1^*, \quad x_{-2} = x_2^*. \tag{2.923}$$

To derive rogue waves in DSII, we need to constrain parameters in the τ_k solution (2.898) blockwise, so that τ_k becomes a 2×2 block determinant with certain symmetry. Specifically, we constrain the parameters as

$$K = 2N, \quad n_{N+i} = n_i \quad m_{N+j} = m_j, \quad p_{N+i} = \frac{\epsilon}{p_i^*}, \quad q_{N+j} = \frac{\epsilon}{q_j^*}, \tag{2.924}$$

where N is a positive integer. The matrix element $m_{i,j}^{(k)}$ in Eq. (2.898) can be rewritten as

$$m_{i,j}^{(k)} = \widehat{\mathcal{A}}_i \widehat{\mathcal{B}}_j \frac{1}{p_i + q_j} (-\frac{p_i}{q_j})^k e^{\xi_i + \eta_j} \Big|_{p=p_i,\, q=q_j}, \tag{2.925}$$

where

$$\widehat{\mathcal{A}}_i = \frac{1}{n_i!}(p_i \partial_{p_i})^{n_i}, \quad \widehat{\mathcal{B}}_j = \frac{1}{m_j!}(q_j \partial_{q_j})^{m_j}, \tag{2.926}$$

$$\xi_i = \frac{1}{p_i^2} x_{-2} + \frac{1}{p_i} x_{-1} + p_i x_1 + p_i^2 x_2 + \sum_{r=1}^{\infty} a_{r,i} \ln^r \left[\frac{p_i}{p}\right], \tag{2.927}$$

$$\eta_j = -\frac{1}{q_j^2} x_{-2} + \frac{1}{q_j} x_{-1} + q_j x_1 - q_j^2 x_2 + \sum_{r=1}^{\infty} b_{r,j} \ln^r \left[\frac{q_j}{q}\right]. \tag{2.928}$$

Then,

$$\left[m_{i,j}^{(k)}\right]^* = \widehat{\mathcal{A}}_i^* \widehat{\mathcal{B}}_j^* \frac{1}{p_i^* + q_j^*} \left(-\frac{p_i^*}{q_j^*}\right)^k e^{\xi_i^* + \eta_j^*} \Big|_{p=p_i^*,\, q=q_j^*}. \tag{2.929}$$

Using Eqs. (2.923)–(2.924) and (2.926)–(2.928), we find that

$$\begin{aligned} \widehat{\mathcal{A}}_i^* &= \frac{1}{n_i!}(p_i^* \partial_{p_i^*})^{n_i} = \frac{1}{n_i!} \partial_{\ln p_i^*}^{n_i} = \frac{1}{n_i!} \partial_{\ln(\epsilon/p_{N+i})}^{n_i} \\ &= \frac{(-1)^{n_i}}{n_i!} \partial_{\ln(p_{N+i})}^{n_i} = (-1)^{n_i} \widehat{\mathcal{A}}_{N+i}, \end{aligned} \tag{2.930}$$

$$\widehat{\mathcal{B}}_j^* = \frac{1}{m_j!}(q_j^* \partial_{q_j^*})^{m_j} = \frac{1}{m_j!}\partial_{\ln p_j^*}^{m_j} = \frac{1}{m_j!}\partial_{\ln(\epsilon/q_{N+j})}^{m_j}$$
$$= \frac{(-1)^{m_j}}{m_j!}\partial_{\ln(q_{N+j})}^{m_j} = (-1)^{m_j}\widehat{\mathcal{B}}_{N+j}, \tag{2.931}$$

$$\left[m_{i,j}^{(k)}\right]^* = (-1)^{n_i+m_j}\widehat{\mathcal{A}}_{N+i}\widehat{\mathcal{B}}_{N+j}\frac{\epsilon p_{N+i}q_{N+j}}{p_{N+i}+q_{N+j}}\left(-\frac{p_{N+i}}{q_{N+j}}\right)^{-k} e^{\xi_i^*+\eta_j^*}\Big|_{\substack{p=p_{N+i}\\ q=q_{N+j}}}, \tag{2.932}$$

where ξ_i^* and η_j^* can be written as

$$\xi_i^* = \frac{1}{p_{N+i}^2}x_{-2} + \frac{1}{p_{N+i}}x_{-1} + p_{N+i}x_1 + p_{N+i}^2 x_2 + \sum_{r=1}^{\infty}(-1)^r a_{r,i}^* \ln^r\left(\frac{p_{N+i}}{p}\right), \tag{2.933}$$

$$\eta_j^* = -\frac{1}{q_{N+j}^2}x_{-2} + \frac{1}{q_{N+j}}x_{-1} + q_{N+j}x_1 - q_{N+j}^2 x_2 + \sum_{r=1}^{\infty}(-1)^r b_{r,j}^* \ln^r\left(\frac{q_{N+j}}{q}\right). \tag{2.934}$$

The above $\left[m_{i,j}^{(k)}\right]^*$ can be further written as

$$\left[m_{i,j}^{(k)}\right]^* = (-1)^{n_i+m_j}(\epsilon p_{N+i}q_{N+j})\widehat{\mathcal{A}}_{N+i}\widehat{\mathcal{B}}_{N+j}\frac{1}{p_{N+i}+q_{N+j}}\times$$
$$\times\left(-\frac{p_{N+i}}{q_{N+j}}\right)^{-k} e^{\xi_i^*+\eta_j^*+\ln\left(\frac{p_{N+i}}{p}\right)+\ln\left(\frac{q_{N+j}}{q}\right)}\Big|_{\substack{p=p_{N+i}\\ q=q_{N+j}}}. \tag{2.935}$$

Then, by constraining internal parameters as

$$a_{1,N+i} = 1 - a_{1,i}^*,\ \ b_{1,N+j} = 1 - b_{1,j}^*, \tag{2.936}$$

$$a_{r,N+i} = (-1)^r a_{r,i}^*,\ \ b_{r,N+j} = (-1)^r b_{r,j}^*,\ \ r \geq 2, \tag{2.937}$$

we have

$$\begin{aligned}
&\xi_i^* + \ln\left(\frac{p_{N+i}}{p}\right) = \frac{1}{p_{N+i}^2}x_{-2} + \frac{1}{p_{N+i}}x_{-1} + p_{N+i}x_1 + p_{N+i}^2 x_2 \\
&\quad + \sum_{r=1}^{\infty} a_{r,N+i} \ln^r\left(\frac{p_{N+i}}{p}\right) = \xi_{N+i}, \\
&\eta_j^* + \ln\left(\frac{q_{N+j}}{q}\right) = -\frac{1}{q_{N+j}^2}x_{-2} + \frac{1}{q_{N+j}}x_{-1} + q_{N+j}x_1 - q_{N+j}^2 x_2 \\
&\quad + \sum_{r=1}^{\infty} b_{r,N+j} \ln^r\left(\frac{q_{N+j}}{q}\right) = \eta_{N+j}.
\end{aligned}$$

Thus,

$$\left[m_{i,j}^{(k)}\right]^* = (-1)^{n_i+m_j}(\epsilon p_{N+i}q_{N+j})m_{N+i,N+j}^{(-k)},\ 1 \le i, j \le N. \tag{2.938}$$

Similarly,

$$\left[m_{N+i,j}^{(k)}\right]^* = (-1)^{n_i+m_j}(\epsilon p_i q_{N+j})m_{i,N+j}^{(-k)},\ 1 \le i, j \le N. \tag{2.939}$$

Since the τ_k solution can be scaled by an arbitrary constant, we define a scaled τ_k function as

$$\tau_k / \prod_{i=1}^{N}(-1)^{n_i+m_i}\epsilon p_i^* q_i^* \to \tau_k. \tag{2.940}$$

This scaled τ_k function can be written as

$$\tau_k = \begin{vmatrix} m_{i,j}^{(k)} & \frac{(-1)^{m_j}}{q_j^*}m_{i,N+j}^{(k)} \\ \frac{(-1)^{n_i}}{\epsilon p_i^*}m_{N+i,j}^{(k)} & \frac{(-1)^{n_i+m_j}}{\epsilon p_i^* q_j^*}m_{N+i,N+j}^{(k)} \end{vmatrix}_{1\le i,j\le N}. \tag{2.941}$$

Utilizing Eqs. (2.938)–(2.939) as well as the parameter constraints (2.924), this τ_k can be rewritten as

$$\tau_k = \begin{vmatrix} m_{i,j}^{(k)} & \widehat{m}_{i,j}^{(k)} \\ \epsilon\left(\widehat{m}_{i,j}^{(-k)}\right)^* & \left(m_{i,j}^{(-k)}\right)^* \end{vmatrix}_{1\le i,j\le N}, \tag{2.942}$$

where $\widehat{m}_{i,j}^{(k)} \equiv (-1)^{m_j} m_{i,N+j}^{(k)}/q_j^*$. We can see from this form of τ_k that

$$\tau_k = \tau_{-k}^*. \tag{2.943}$$

Thus, the conjugation condition (2.904) is met. The corresponding solutions (2.898)–(2.903) then give DSII rational solutions (in differential form), which are summarized in the following lemma.

Lemma 2.17 *The Davey-Stewartson II eqaution admits rational solutions*

$$A(x,y,t)=\sqrt{2}\frac{g}{f},\quad Q(x,y,t)=\epsilon-2\,(\ln f)_{xx}\,, \tag{2.944}$$

where

$$f=\tau_0,\quad g=\tau_1, \tag{2.945}$$

τ_k is the determinant of a 2×2 block matrix

$$\tau_k=\det_{1\le i,j\le 2N}\left(m_{i,j}^{(k)}\right)=\begin{vmatrix}\left(m_{i,j}^{(k)}\right)_{1\le i,j\le N} & \left(m_{i,N+j}^{(k)}\right)_{1\le i,j\le N}\\ \left(m_{i+N,j}^{(k)}\right)_{1\le i,j\le N} & \left(m_{i+N,j+N}^{(k)}\right)_{1\le i,j\le N}\end{vmatrix}, \tag{2.946}$$

N is a positive integer, the matrix elements in τ_k are defined by

$$m_{i,j}^{(k)}=\frac{\left(p\partial_p\right)^{n_i}}{(n_i)!}\frac{\left(q\partial_q\right)^{m_j}}{(m_j)!}\left[\frac{1}{p+q}\left(-\frac{p}{q}\right)^k e^{\Theta_{i,j}(x,y,t)}\right]\Bigg|_{p=p_i,\ q=q_j}, \tag{2.947}$$

$$\Theta_{i,j}(x,y,t)=\left(\frac{1}{p^2}-\frac{1}{q^2}\right)x_{-2}+\left(\frac{1}{p}+\frac{1}{q}\right)x_{-1}+(p+q)x_1+(p^2-q^2)x_2$$
$$+\sum_{r=1}^{\infty}a_{r,i}\ln^r\left[\frac{p}{p_i}\right]+b_{r,j}\ln^r\left[\frac{q}{q_j}\right], \tag{2.948}$$

$$x_1=\frac{1}{2}(x+\mathrm{i}y),\quad x_{-1}=\frac{1}{2}\epsilon(x-\mathrm{i}y),\quad x_2=-\frac{1}{2}\mathrm{i}t,\quad x_{-2}=\frac{1}{2}\mathrm{i}t, \tag{2.949}$$

n_i, m_j $(1\le i,j\le 2N)$ are nonnegative integers, $p_i, q_j, a_{r,i}, b_{r,j}$ $(1\le i,j\le 2N)$ are complex constants, and they satisfy the following parameter constraints,

$$n_{N+i}=n_i\quad m_{N+j}=m_j,\quad p_{N+i}=\frac{\epsilon}{p_i^*},\quad q_{N+j}=\frac{\epsilon}{q_j^*}, \tag{2.950}$$

$$a_{1,N+i}=1-a_{1,i}^*,\quad b_{1,N+j}=1-b_{1,j}^*, \tag{2.951}$$

$$a_{r,N+i}=(-1)^r a_{r,i}^*,\quad b_{r,N+j}=(-1)^r b_{r,j}^*,\quad r\ge 2. \tag{2.952}$$

More explicit expressions of these solutions can be derived by eliminating the differential operators in Eq. (2.947) in favor of Schur polynomials, using techniques which have been explained in earlier sections (such as Sect. 2.1.1). These more explicit solution expressions are presented in the following theorem (the proof is skipped for brevity).

Theorem 2.19 *The Davey-Stewartson II eqaution admits rational solutions*

$$A(x,y,t)=\sqrt{2}\frac{g}{f},\quad Q(x,y,t)=\epsilon-2\,(\ln f)_{xx}\,, \tag{2.953}$$

where

$$f = \tau_0, \quad g = \tau_1, \tag{2.954}$$

τ_k is the determinant of a 2×2 block matrix

$$\tau_k = \det_{1\le i,j\le 2N}\left(m_{i,j}^{(k)}\right) = \begin{vmatrix} \left(m_{i,j}^{(k)}\right)_{1\le i,j\le N} & \left(m_{i,N+j}^{(k)}\right)_{1\le i,j\le N} \\ \left(m_{i+N,j}^{(k)}\right)_{1\le i,j\le N} & \left(m_{i+N,j+N}^{(k)}\right)_{1\le i,j\le N} \end{vmatrix}, \tag{2.955}$$

N is a positive integer, the matrix elements in τ_k are defined by

$$\begin{aligned} m_{i,j}^{(k)} = & \sum_{v=0}^{\min(n_i,m_j)} \left(\frac{1}{p_i+q_j}\right)\left[\frac{p_i q_j}{(p_i+q_j)^2}\right]^v \\ & \times S_{n_i-v}[\boldsymbol{x}_{i,j}^{+}(k)+v\boldsymbol{s}_{i,j}]\, S_{m_j-v}[\boldsymbol{x}_{j,i}^{-}(k)+v\bar{\boldsymbol{s}}_{j,i}], \end{aligned} \tag{2.956}$$

vectors $\boldsymbol{x}_{i,j}^{\pm}(k) = \left(x_{1,i,j}^{\pm}, x_{2,i,j}^{\pm}, \cdots\right)$ are defined by

$$x_{r,i,j}^{+}(k) = \frac{(-1)^r}{r!p_i}x_{-1} + \frac{(-2)^r}{r!p_i^2}x_{-2} + \frac{1}{r!}p_i x_1 + \frac{2^r}{r!}p_i^2 x_2 + k\delta_{r,1} - c_{r,i,j} + a_{r,i}, \tag{2.957}$$

$$x_{r,i,j}^{-}(k) = \frac{(-1)^r}{r!q_i}x_{-1} + \frac{(-2)^r}{r!q_i^2}x_2 + \frac{1}{r!}q_i x_1 + \frac{2^r}{r!}q_i^2 x_{-2} - k\delta_{r,1} - \bar{c}_{r,i,j} + b_{r,i}, \tag{2.958}$$

$$x_1 = \frac{1}{2}(x+\mathrm{i}y), \quad x_{-1} = \frac{1}{2}\epsilon(x-\mathrm{i}y), \quad x_2 = -\frac{1}{2}\mathrm{i}t, \quad x_{-2} = \frac{1}{2}\mathrm{i}t, \tag{2.959}$$

$\delta_{r,1}$ denotes Kronecker delta function, $\boldsymbol{s}_{i,j} = (s_{1,i,j}, s_{2,i,j}, \cdots)$, $\bar{\boldsymbol{s}}_{i,j} = (\bar{s}_{1,i,j}, \bar{s}_{2,i,j}, \cdots)$, coefficients $c_{r,i,j}$, $\bar{c}_{r,i,j}$, $s_{r,i,j}$ and $\bar{s}_{r,i,j}$ are obtained from the expansions

$$\ln\left[\frac{p_i e^{\kappa}+q_j}{p_i+q_j}\right] = \sum_{r=1}^{\infty} c_{r,i,j}\kappa^r, \quad \ln\left[\frac{q_i e^{\kappa}+p_j}{q_i+p_j}\right] = \sum_{r=1}^{\infty} \bar{c}_{r,i,j}\kappa^r, \tag{2.960}$$

$$\ln\left[\frac{p_i+q_j}{\kappa}\left(\frac{e^{\kappa}-1}{p_i e^{\kappa}+q_j}\right)\right] = \sum_{r=1}^{\infty} s_{r,i,j}\kappa^r, \tag{2.961}$$

$$\ln\left[\frac{q_i+p_j}{\kappa}\left(\frac{e^{\kappa}-1}{q_i e^{\kappa}+p_j}\right)\right] = \sum_{r=1}^{\infty} \bar{s}_{r,i,j}\kappa^r, \tag{2.962}$$

n_i, m_j $(1 \le i, j \le 2N)$ are nonnegative integers, $p_i, q_j, a_{r,i}, b_{r,j}$ $(1 \le i, j \le 2N)$ are complex constants, and they satisfy the following parameter constraints,

$$n_{N+i} = n_i \quad m_{N+j} = m_j, \quad p_{N+i} = \frac{\epsilon}{p_i^*}, \quad q_{N+j} = \frac{\epsilon}{q_j^*}, \tag{2.963}$$

$$a_{1,N+i} = 1 - a_{1,i}^*, \quad b_{1,N+j} = 1 - b_{1,j}^*, \tag{2.964}$$

$$a_{r,N+i} = (-1)^r a_{r,i}^*, \quad b_{r,N+j} = (-1)^r b_{r,j}^*, \quad r \ge 2. \tag{2.965}$$

The simplest rational solution is obtained when $N = 1$, $n_1 = 1$ and $m_1 = 0$. In this case,

$$\tau_k = \begin{vmatrix} m_{1,1}^{(k)} & m_{1,2}^{(k)} \\ m_{2,1}^{(k)} & m_{2,2}^{(k)} \end{vmatrix}, \tag{2.966}$$

where

$$m_{1,1}^{(k)} = \frac{1}{p_1 + q_1}\left(\xi + \theta_{1,1} + k\right), \quad m_{1,2}^{(k)} = \frac{1}{p_1 + q_2}\left(\xi + \theta_{1,2} + k\right),$$

$$m_{2,1}^{(k)} = (-\epsilon p_1^* q_2^*)\left[m_{1,2}^{(-k)}\right]^*, \quad m_{2,2}^{(k)} = (-\epsilon p_1^* q_1^*)\left[m_{1,1}^{(-k)}\right]^*,$$

$$\xi = ax + by + \omega t, \quad a = \frac{p_1 - \epsilon p_1^{-1}}{2}, \quad b = \frac{p_1 + \epsilon p_1^{-1}}{2}\mathrm{i}, \quad \omega = \frac{p_1^2 + p_1^{-2}}{\mathrm{i}},$$

$$\theta_{1,1} = a_{1,1} - \frac{p_1}{p_1 + q_1}, \quad \theta_{1,2} = a_{1,2} - \frac{p_1}{p_1 + q_2},$$

$q_2 = \epsilon/q_1^*$, and $a_{1,2} = -a_{1,1}^*$. This solution seems to have three free complex parameters p_1, q_1 and $a_{1,1}$, but q_1 can be absorbed into $a_{1,1}$ by a reparametrization. Indeed, by defining

$$\theta = a_{1,1} - \frac{p_1}{(|p_1|^2 - \epsilon)(|q_1|^2 - \epsilon)}\left[\frac{|p_1 q_1^* + \epsilon|^2}{p_1 + q_1} - \frac{\epsilon q_1^* |p_1 + q_1|^2}{\epsilon + p_1 q_1^*}\right],$$

then τ_k can be reduced to

$$\tau_k = [(\xi + \theta) + k][(\xi + \theta)^* - k] + \Delta, \quad \Delta = \frac{-\epsilon |p_1|^2}{\left(|p_1|^2 - \epsilon\right)^2} \tag{2.967}$$

up to a constant multiplication; thus this new τ_k yields the same solution, and it contains only two free complex parameters p_1 and θ now. If we separate the real and imaginary part of a, b, ω and θ as

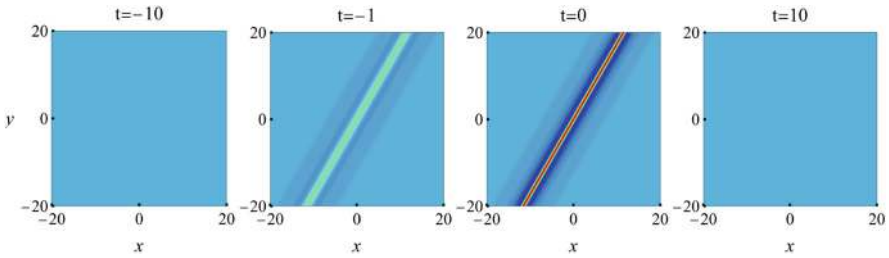

Fig. 2.28 Density plots of the fundamental line rogue wave $|A(x, y, t)|$ from Eq. (2.969) in the Davey-Stewartson II equation for $\epsilon = -1$, $p_1 = e^{\mathrm{i}\pi/6}$ and $\theta = 0$ at different times

$$a = a_1 + \mathrm{i}a_2,\ b = b_1 + \mathrm{i}b_2,\ \omega = \omega_1 + \mathrm{i}\omega_2,\ \theta = \theta_1 + \mathrm{i}\theta_2, \tag{2.968}$$

then the explicit expressions for the fundamental rational solution are:

$$A(x, y, t) = \sqrt{2}\left[1 - \frac{2i(a_2x + b_2y + \omega_2t + \theta_2) + 1}{f}\right] \tag{2.969}$$

$$Q(x, y, t) = \epsilon - (2\ln f)_{xx}\,, \tag{2.970}$$

where

$$f = (a_1x + b_1y + \omega_1t + \theta_1)^2 + (a_2x + b_2y + \omega_2t + \theta_2)^2 + \Delta. \tag{2.971}$$

This fundamental rational solution is nonsingular when $\epsilon = -1$. In this case, the solution exhibits two distinctly different dynamics depending on the parameter value of p_1.

- If $|p_1| \neq 1$, then the solution is a two-dimensional lump moving on a constant background.
- If $|p_1| = 1$, then this line wave is a line rogue wave which "appears from nowhere and disappears with no trace".

This line rogue wave with $\epsilon = -1$, $p_1 = e^{\mathrm{i}\pi/6}$ and $\theta = 0$ is plotted in Fig. 2.28.

If $N > 1$, rational solutions in Theorem 2.19 could describe the interaction between line rogue waves. Such an example is shown in Fig. 2.29.

2.14 Three-Wave Resonant Interaction System in (2+1)-Dimensions

The (2+1)-dimensional three-wave resonant interaction system is (see Sect. 1.6)

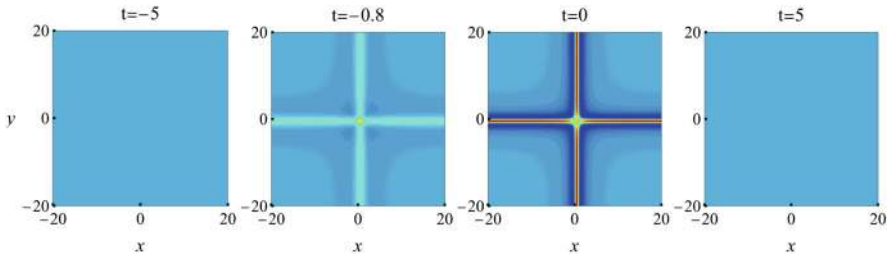

Fig. 2.29 Density plots of a rogue wave solution $|A(x, y, t)|$ in the Davey-Stewartson II equation that describes the interaction of two line rogue waves. Parameter choices are $\epsilon = -1$, $N = 2$, $n_1 = n_2 = 1, m_1 = m_2 = 0$, $p_1 = \mathrm{i}$, $p_2 = 1, q_1 = 1/2,\ q_2 = 2$, and $a_{1,1} = a_{1,2} = 0$

$$\left.\begin{aligned}
(\partial_t + \mathbf{V}_1 \cdot \nabla)\, q_1(x, y, t) &= \epsilon_1 q_2^*(x, y, t) q_3^*(x, y, t), \\
(\partial_t + \mathbf{V}_2 \cdot \nabla)\, q_2(x, y, t) &= \epsilon_2 q_1^*(x, y, t) q_3^*(x, y, t), \\
(\partial_t + \mathbf{V}_3 \cdot \nabla)\, q_3(x, y, t) &= \epsilon_3 q_1^*(x, y, t) q_2^*(x, y, t).
\end{aligned}\right\} \tag{2.972}$$

Here, $\nabla = \left(\partial_x,\ \partial_y\right)$ is the gradient operator in the (x, y) space, and $\mathbf{V}_k = \left(V_{k,1},\ V_{k,2}\right)$ are group-velocity vectors of the three waves. Adopting a coordinate system that moves at the speed of the third wave, we make $\mathbf{V}_3 = (0, 0)$ without loss of generality. In addition, we assume that $\mathbf{V}_1$ and $\mathbf{V}_2$ are not parallel to each other, i.e., $V_{11}V_{22} - V_{12}V_{21} \neq 0$. Parameters ϵ_j are nonlinear coefficients that can be scaled to ± 1. In addition, one can fix $\epsilon_1 = 1$.

The above three-wave system admits plane-wave solutions

$$\left.\begin{aligned}
q_{1,0}(x, y, t) &= \rho_1 e^{\mathrm{i}(k_1 x + \lambda_1 y + \omega_1 t)}, \\
q_{2,0}(x, y, t) &= \rho_2 e^{\mathrm{i}(k_2 x + \lambda_2 y + \omega_2 t)}, \\
q_{3,0}(x, y, t) &= \mathrm{i}\rho_3 e^{\mathrm{i}(k_3 x + \lambda_3 y + \omega_3 t)},
\end{aligned}\right\} \tag{2.973}$$

where wave vectors and frequencies satisfy the resonance relations

$$\omega_1 + \omega_2 + \omega_3 = 0, \quad \lambda_1 + \lambda_2 + \lambda_3 = 0, \quad k_1 + k_2 + k_3 = 0, \tag{2.974}$$

and wave amplitudes (ρ_1, ρ_2, ρ_3) satisfy the following conditions

$$\left.\begin{aligned}
\rho_1 \left(\omega_1 + V_{1,1}k_1 + V_{1,2}\lambda_1\right) &= -\epsilon_1 \rho_2^* \rho_3^*, \\
\rho_2 \left(\omega_2 + V_{2,1}k_2 + V_{2,2}\lambda_2\right) &= -\epsilon_2 \rho_1^* \rho_3^*, \\
\rho_3 \left(\omega_1 + \omega_2\right) &= \epsilon_3 \rho_1^* \rho_2^*.
\end{aligned}\right\} \tag{2.975}$$

These plane-wave solutions have constant amplitudes in the (x, y) space; so we will also call them constant-background solutions.

Below, we assume that the three wave amplitudes $|\rho_1|$, $|\rho_2|$ and $|\rho_3|$ are nonzero. Then, using phase invariance of the three-wave system, we can normalize ρ_1, ρ_2 and ρ_3 to be all real. Thus, in the later text, we assume (ρ_1, ρ_2, ρ_3) real. In addition, we

define three real constants

$$\gamma_1 \equiv \epsilon_1 \frac{\rho_2 \rho_3}{\rho_1}, \ \gamma_2 \equiv \epsilon_2 \frac{\rho_1 \rho_3}{\rho_2}, \ \gamma_3 \equiv \epsilon_3 \frac{\rho_1 \rho_2}{\rho_3}. \tag{2.976}$$

Rogue waves in the three-wave system (2.972) are solutions that approach the above plane-wave solution when $x, t \to \pm\infty$. These rogue waves were first derived by Yang and Yang (2022a) by the bilinear method, and those results are presented below.

Rogue waves are rational solutions. The general rational solutions to the (2+1)-dimensional three-wave system (2.972) in differential form are given in the following lemma.

Lemma 2.18 *The (2+1)-dimensional three-wave system (2.972) admits rational solutions*

$$\left.\begin{aligned} q_1(x, y, t) &= \rho_1 \frac{g_1}{f} e^{i(k_1 x + \lambda_1 y + \omega_1 t)}, \\ q_2(x, y, t) &= \rho_2 \frac{g_2}{f} e^{i(k_2 x + \lambda_2 y + \omega_2 t)}, \\ q_3(x, y, t) &= \mathrm{i}\rho_3 \frac{g_3}{f} e^{\mathrm{i}(k_3 x + \lambda_3 y + \omega_3 t)}, \end{aligned}\right\} \tag{2.977}$$

where

$$f = \tau_{0,0}, \quad g_1 = \tau_{1,0}, \quad g_2 = \tau_{0,-1}, \quad g_3 = \tau_{-1,1}, \tag{2.978}$$

$$\tau_{n,k} = \det_{1 \le i,j \le N} \left(m_{i,j}^{(n,k)} \right), \tag{2.979}$$

N is an arbitrary positive integer, the matrix elements in $\tau_{n,k}$ are defined by

$$m_{i,j}^{(n,k)} = \frac{\left(p\partial_p\right)^{n_i}}{(n_i)!} \frac{\left(q\partial_q\right)^{n_j}}{(n_j)!} \left[\frac{1}{p+q} \left(-\frac{p}{q} \right)^k \left(-\frac{p-\mathrm{i}}{q+\mathrm{i}} \right)^n e^{\Theta_{i,j}(x,y,t)} \right] \Bigg|_{p=p_i, \ q=q_j}, \tag{2.980}$$

$$\begin{aligned} \Theta_{i,j}(x, y, t) = &\left(\frac{1}{p} + \frac{1}{q} \right) z_1 + \left(\frac{1}{p-\mathrm{i}} + \frac{1}{q+\mathrm{i}} \right) z_2 + (p+q) z_3 \\ &+ \sum_{r=1}^{\infty} a_{r,i} \ln^r \left[\frac{p}{p_i} \right] + \sum_{r=1}^{\infty} a_{r,j}^* \ln^r \left[\frac{q}{q_j} \right], \end{aligned} \tag{2.981}$$

$(n_1, n_2, \ldots, n_N)$ are arbitrary nonnegative integers, $(p_1, p_2, \ldots, p_N)$ are free non-imaginary complex constants, $q_j = p_j^*$, variables (z_1, z_2, z_3) are related to (x, y, t) as

$$z_1 = \gamma_1 \frac{V_{22}x - V_{21}y}{V_{11}V_{22} - V_{12}V_{21}}, \tag{2.982}$$

$$z_2 = \gamma_2 \frac{V_{11}y - V_{12}x}{V_{11}V_{22} - V_{12}V_{11}}, \tag{2.983}$$

$$z_3 = \gamma_3 \left[\frac{(V_{12} - V_{22})\,x + (V_{21} - V_{11})\,y}{V_{11}V_{22} - V_{12}V_{21}} + t \right], \tag{2.984}$$

and $a_{r,i}$ $(r = 1, 2, \ldots, n_i;\ i = 1, 2, \ldots, N)$ *are free complex constants.*

Proof Due to the boundary conditions (2.973), we first introduce the bilinear transformation

$$\left.\begin{aligned} q_1(x, y, t) &= \rho_1 \frac{g_1}{f} e^{i(k_1 x + \lambda_1 y + \omega_1 t)}, \\ q_2(x, y, t) &= \rho_2 \frac{g_2}{f} e^{i(k_2 x + \lambda_2 y + \omega_2 t)}, \\ q_3(x, y, t) &= \mathrm{i}\rho_3 \frac{g_3}{f} e^{\mathrm{i}(k_3 x + \lambda_3 y + \omega_3 t)}, \end{aligned}\right\} \tag{2.985}$$

where $f(x, y, t)$ is a real function, and $g_k(x, y, t)\,(k = 1, 2, 3)$ are complex functions. Under this transformation, the three-wave system (2.972) is converted into the following system of bilinear equations

$$\left.\begin{aligned} \left(D_t + V_{1,1}D_x + V_{1,2}D_y - \mathrm{i}\gamma_1\right) g_1 \cdot f &= -\mathrm{i}\gamma_1 g_2^* g_3^*, \\ \left(D_t + V_{2,1}D_x + V_{2,2}D_y - \mathrm{i}\gamma_2\right) g_2 \cdot f &= -\mathrm{i}\gamma_2 g_1^* g_3^*, \\ \left(D_t - \mathrm{i}\gamma_3\right) g_3 \cdot f &= -\mathrm{i}\gamma_3 g_1^* g_2^*. \end{aligned}\right\} \tag{2.986}$$

Next, we introduce the coordinate transformation

$$\begin{pmatrix} x \\ y \\ t \end{pmatrix} = \begin{pmatrix} \frac{V_{1,1}}{\gamma_1} & \frac{V_{2,1}}{\gamma_2} & 0 \\ \frac{V_{1,2}}{\gamma_1} & \frac{V_{2,2}}{\gamma_2} & 0 \\ \frac{1}{\gamma_1} & \frac{1}{\gamma_2} & \frac{1}{\gamma_3} \end{pmatrix} \begin{pmatrix} z_1 \\ z_2 \\ z_3 \end{pmatrix}, \tag{2.987}$$

which is equivalent to Eqs. (2.982)–(2.984) in Lemma 2.18. Under this coordinate transformation, we have

$$\left.\begin{aligned} \partial_t + \mathbf{V}_1 \cdot \nabla &= \gamma_1 \partial_{z_1}, \\ \partial_t + \mathbf{V}_2 \cdot \nabla &= \gamma_2 \partial_{z_2}, \\ \partial_t &= \gamma_3 \partial_{z_3}. \end{aligned}\right\} \tag{2.988}$$

Thus, the bilinear system (2.986) reduces to

$$\left.\begin{aligned}\left(\mathrm{i}D_{z_1}+1\right)g_1\cdot f &= g_2^*g_3^*,\\ \left(\mathrm{i}D_{z_2}+1\right)g_2\cdot f &= g_1^*g_3^*,\\ \left(\mathrm{i}D_{z_3}+1\right)g_3\cdot f &= g_1^*g_2^*.\end{aligned}\right\} \tag{2.989}$$

Below, we will first construct algebraic solutions to the more general bilinear system

$$\left.\begin{aligned}\left(\mathrm{i}D_{z_1}+1\right)g_1\cdot f &= h_2h_3,\\ \left(\mathrm{i}D_{z_2}+1\right)g_2\cdot f &= h_1h_3,\\ \left(\mathrm{i}D_{z_3}+1\right)g_3\cdot f &= h_1h_2,\end{aligned}\right\} \tag{2.990}$$

where h_1, h_2 and h_3 are also complex functions. Afterwards, we will impose the reality conditon for f and complex conjugation conditions

$$h_k^* = g_k, \quad k = 1, 2, 3. \tag{2.991}$$

Then, the bilinear system (2.990) will become the bilinear system (2.989), and the corresponding algebraic solutions will give rational solutions of the three-wave system (2.972) through the above variable and coordinate transformations (2.985) and (2.987).

The bilinear system (2.990) is a special case of the slightly more general bilinear system (2.741) in Sect. 2.10 with $a = 0$ and $b = \mathrm{i}$. Gram solutions to the system (2.741) have been given in Lemma 2.14. Based on that lemma, we see that the τ function

$$\tau_{n,k} = \det_{1\le i,j\le N}\left(m_{i,j}^{(n,k)}\right), \tag{2.992}$$

where

$$m_{i,j}^{(n,k)} = \frac{\left(p\partial_p\right)^{n_i}}{(n_i)!}\frac{\left(q\partial_q\right)^{n_j}}{(n_j)!}\frac{1}{p+q}\left(-\frac{p}{q}\right)^k\left(-\frac{p-\mathrm{i}}{q+\mathrm{i}}\right)^n \mathrm{e}^{\xi_i+\eta_j}\Big|_{p=p_i,\ q=q_j}, \tag{2.993}$$

$$\xi_i = \frac{1}{p}z_1 + \frac{1}{p-\mathrm{i}}z_2 + (p-\mathrm{i})z_3 + \sum_{r=1}^{\infty}a_{r,i}\ln^r\left[\frac{p}{p_i}\right], \tag{2.994}$$

$$\eta_j = \frac{1}{q}z_1 + \frac{1}{q+\mathrm{i}}z_2 + (q+\mathrm{i})z_3 + \sum_{r=1}^{\infty}b_{r,j}\ln^r\left[\frac{q}{q_j}\right], \tag{2.995}$$

n_i, n_j are free nonnegative integers, and $p_i, q_j, a_{r,i}, b_{r,j}$ are free complex constants, would satisfy the following bilinear system

$$\left.\begin{aligned}\left[\mathrm{i}D_{z_1}+1\right]\tau_{n+1,k}\cdot\tau_{n,k}&=\tau_{n,k+1}\tau_{n+1,k-1},\\ \left[\mathrm{i}D_{z_2}+1\right]\tau_{n,k-1}\cdot\tau_{n,k}&=\tau_{n-1,k}\tau_{n+1,k-1},\\ \left[\mathrm{i}D_{z_3}+1\right]\tau_{n-1,k+1}\cdot\tau_{n,k}&=\tau_{n-1,k}\tau_{n,k+1}.\end{aligned}\right\} \tag{2.996}$$

Thus, if we define

$$f=\tau_{0,0},\quad g_1=\tau_{1,0},\quad g_2=\tau_{0,-1},\quad g_3=\tau_{-1,1}, \tag{2.997}$$

and

$$h_1=\tau_{-1,0},\quad h_2=\tau_{0,1},\quad h_3=\tau_{1,-1}, \tag{2.998}$$

the above bilinear system (2.996) would reduce to (2.990), and these τ functions would be solutions to that bilinear system (2.990).

In order to reduce that more general bilinear system (2.990) to the original one in (2.989), we still need to impose the f-reality condition as well as the complex conjugacy conditions of $h_i=g_i^*$. All these conditions would be satisfied if

$$\tau_{n,k}=\left[\tau_{-n,-k}\right]^*. \tag{2.999}$$

To realize this condition, we set

$$q_j=p_j^*,\quad b_{r,j}=a_{r,j}^*. \tag{2.1000}$$

In this case, we can readily show that

$$m_{j,i}^{(-n,-k)}=\left[m_{i,j}^{(n,k)}\right]^*. \tag{2.1001}$$

Thus, the condition (2.999) holds, and the τ functions (2.997) then become solutions to the original bilinear system (2.989). Inserting the above parameter conditions (2.1000) into the matrix element expression (2.993), we then obtain the rational solutions in Lemma 2.18 for the three-wave system (2.972).

More explicit expressions of these solutions can be derived by eliminating the differential operators in Eq. (2.980) in favor of Schur polynomials, using techniques that have been introduced in earlier sections of this chapter. These more explicit solution expressions are presented in the following theorem, and its proof can be found in Yang and Yang (2022a).

Theorem 2.20 *The (2+1)-dimensional three-wave system (2.972) admits rational solutions*

$$\left.\begin{aligned} q_1(x,y,t) &= \rho_1 \frac{g_1}{f} e^{i(k_1 x+\lambda_1 y+\omega_1 t)}, \\ q_2(x,y,t) &= \rho_2 \frac{g_2}{f} e^{i(k_2 x+\lambda_2 y+\omega_2 t)}, \\ q_3(x,y,t) &= \mathrm{i}\rho_3 \frac{g_3}{f} e^{\mathrm{i}(k_3 x+\lambda_3 y+\omega_3 t)}, \end{aligned}\right\} \tag{2.1002}$$

where

$$f = \tau_{0,0}, \quad g_1 = \tau_{1,0}, \quad g_2 = \tau_{0,-1}, \quad g_3 = \tau_{-1,1}, \tag{2.1003}$$

$$\tau_{n,k} = \det_{1\le i,j\le N}\left(m_{i,j}^{(n,k)}\right), \tag{2.1004}$$

N is an arbitrary positive integer, the matrix elements in $\tau_{n,k}$ are defined by

$$\begin{aligned} m_{i,j}^{(n,k)} = &\sum_{\nu=0}^{\min(n_i,n_j)} \left(\frac{1}{p_i+p_j^*}\right)\left[\frac{p_i p_j^*}{(p_i+p_j^*)^2}\right]^{\nu} \\ &\times S_{n_i-\nu}[\boldsymbol{x}_{i,j}^{+}(n,k)+\nu \boldsymbol{s}_{i,j}]\, S_{n_j-\nu}[\boldsymbol{x}_{j,i}^{-}(n,k)+\nu \boldsymbol{s}_{j,i}^{*}], \end{aligned} \tag{2.1005}$$

$(n_1, n_2, \ldots, n_N)$ are arbitrary nonnegative integers, $(p_1, p_2, \ldots, p_N)$ are free non-imaginary complex constants, vectors $\boldsymbol{x}_{i,j}^{\pm}(n,k) = \left(x_{1,i,j}^{\pm}, x_{2,i,j}^{\pm}, \cdots\right)$ are defined by

$$x_{r,i,j}^{+}(n,k) = \frac{(-1)^r}{r!p_i} z_1 + \beta_{r,i} z_2 + \frac{1}{r!} p_i z_3 + n g_{r,i} + k\delta_{1r} - c_{r,i,j} + a_{r,i}, \tag{2.1006}$$

$$x_{r,i,j}^{-}(n,k) = \frac{(-1)^r}{r!p_i^*} z_1 + \beta_{r,i}^* z_2 + \frac{1}{r!} p_i^* z_3 - n g_{r,i}^* - k\delta_{1r} - c_{r,i,j}^* + a_{r,i}^*, \tag{2.1007}$$

δ_{1r} is the Kronecker delta function, $\boldsymbol{s}_{i,j} = (s_{1,i,j}, s_{2,i,j}, \cdots)$, coefficients $\beta_{r,i}$, $g_{r,i}$, $c_{r,i,j}$ and $s_{r,i,j}$ are obtained from the expansions

$$\frac{1}{p_i e^{\kappa}-\mathrm{i}} - \frac{1}{p_i-\mathrm{i}} = \sum_{r=1}^{\infty} \beta_{r,i}\kappa^r, \quad \ln\left(\frac{p_i e^{\kappa}-\mathrm{i}}{p_i-\mathrm{i}}\right) = \sum_{r=1}^{\infty} g_{r,i}\kappa^r, \tag{2.1008}$$

$$\ln\left[\frac{p_i e^{\kappa}+p_j^*}{p_i+p_j^*}\right] = \sum_{r=1}^{\infty} c_{r,i,j}\kappa^r, \quad \ln\left[\frac{p_i+p_j^*}{\kappa}\left(\frac{e^{\kappa}-1}{p_i e^{\kappa}+p_j^*}\right)\right] = \sum_{r=1}^{\infty} s_{r,i,j}\kappa^r, \tag{2.1009}$$

and $a_{r,i}$ $(r = 1, 2, \ldots, n_i; i = 1, 2, \ldots, N)$ are free complex constants.

The above rational solutions contain rogue waves that arise from and decay back to the constant background (2.973), as well as algebraic localized (lump) solitons moving on this constant background and a mixture between these two types of solutions. To get rogue waves, we need to impose conditions on p_i.

To derive these conditions, we consider the fundamental rational solution, where we take $N = 1$ and $n_1 = 1$ in Theorem 2.20. In addition, we normalize $a_{1,1} - c_{1,1,1} = 0$ by a coordinate shift. Performing simple calculations, we can reduce the $\tau_{n,k}$ function to

$$\tau_{n,k} = m_{1,1}^{(n,k)} = \xi\bar{\xi} + \Delta, \quad \Delta = \frac{|p_1|^2}{(p_1 + p_1^*)^2}, \tag{2.1010}$$

where

$$\xi = ax + by + ct + \theta(n,k), \quad \bar{\xi} = a^*x + b^*y + c^*t - \theta^*(n,k), \tag{2.1011}$$

and a, b, c, θ are complex coefficients given by

$$\begin{aligned}
a &= \frac{1}{V_{11}V_{22} - V_{12}V_{21}}\left[-\frac{1}{p_1}\gamma_1 V_{22} + \frac{p_1}{(p_1 - \mathrm{i})^2}\gamma_2 V_{12} + p_1\gamma_3(V_{12} - V_{22})\right], \\
b &= \frac{1}{V_{11}V_{22} - V_{12}V_{21}}\left[\frac{1}{p_1}\gamma_1 V_{21} - \frac{p_1}{(p_1 - \mathrm{i})^2}\gamma_2 V_{11} + p_1\gamma_3(V_{21} - V_{11})\right], \\
c &= \gamma_3 p_1, \quad \theta(n,k) = k + \frac{np_1}{p_1 - \mathrm{i}}.
\end{aligned}$$

To derive the condition for rogue waves, we separate the real and imaginary parts of the above complex variables as

$$p_1 = p_{1,1} + \mathrm{i}p_{1,2},\ a = a_1 + \mathrm{i}a_2,\ b = b_1 + \mathrm{i}b_2,\ c = c_1 + \mathrm{i}c_2,\ \theta = \theta_1 + \mathrm{i}\theta_2. \tag{2.1012}$$

Then, the $\tau_{n,k}$ solution (2.1010) can be rewritten as

$$\tau_{n,k} = \xi_1^2 + \xi_2^2 - 2\mathrm{i}\theta_1\xi_2 + 2\mathrm{i}\theta_2\xi_1 - \theta_1^2 - \theta_2^2 + \Delta, \tag{2.1013}$$

where

$$\xi_1 = a_1x + b_1y + c_1t, \quad \xi_2 = a_2x + b_2y + c_2t. \tag{2.1014}$$

We can readily show that under the velocity assumption of $V_{11}V_{22} - V_{12}V_{21} \neq 0$, the three ratios of $a_1/a_2, b_1/b_2$ and c_1/c_2 cannot be all the same. Then, the above fundamental rational solution has two distinctively different dynamical behaviours depending on the ratio relations between a_1/a_2 and b_1/b_2.

1. If $\frac{a_1}{a_2} \neq \frac{b_1}{b_2}$, then along the $[x(t), y(t)]$ trajectory where

$$a_1 x + b_1 y = -c_1 t, \quad a_2 x + b_2 y = -c_2 t, \tag{2.1015}$$

the above $\tau_{n,k}$ is a constant. The corresponding solution (q_1, q_2, q_3) is an algebraic localized lump soliton moving on the constant background (2.973).

2. If $\frac{a_1}{a_2} = \frac{b_1}{b_2} \neq \frac{c_1}{c_2}$, then the $\frac{a_1}{a_2} = \frac{b_1}{b_2}$ equation yields the following parameter condition

$$\frac{(p_{1,2}-1)(p_{1,1}^2+p_{1,2}^2)^2}{\gamma_1} - \frac{p_{1,2}[p_{1,1}^2+(p_{1,2}-1)^2]^2}{\gamma_2} - \frac{p_{1,1}^2+p_{1,2}^2-p_{1,2}}{\gamma_3} = 0. \tag{2.1016}$$

In this case, the corresponding solution (q_1, q_2, q_3) approaches the constant background (2.973) in the entire (x, y) plane when $t \to \pm\infty$. In the intermediate times, it rises to a higher amplitude. Since $a_1/a_2 = b_1/b_2$, this solution depends on (x, y) through the combination of $a_1 x + b_1 y$. Thus, this is a line rogue wave.

For non-fundamental rational solutions in Theorem 2.20, in order for them to be rogue waves that arise from the constant background (2.973), we need to require all parameters p_i $(1 \leq i \leq N)$ to satisfy the above condition (2.1016), where $p_{1,1}$ is replaced by $p_{i,1}$ and $p_{1,2}$ replaced by $p_{i,2}$, with $(p_{i,1}, p_{i,2})$ being the real and imaginary parts of the complex parameter p_i.

The condition (2.1016) can be further simplified. When $(p_{1,1}, p_{1,2})$ are replaced by the more general $(p_{i,1}, p_{i,2})$, the simplified condition can be expressed as a quartic equation for $p_{i,1}$ as

$$\chi_0 p_{i,1}^4 + \chi_1 p_{i,1}^2 + \chi_2 = 0, \tag{2.1017}$$

where the coefficients are

$$\begin{aligned}
\chi_0 &= (p_{i,2}-1)\gamma_1^{-1} - p_{i,2}\gamma_2^{-1}, \\
\chi_1 &= 2\left(p_{i,2}-1\right) p_{i,2}^2 \gamma_1^{-1} - 2p_{i,2}\left(p_{i,2}-1\right)^2 \gamma_2^{-1} - \gamma_3^{-1}, \\
\chi_2 &= p_{i,2}\left(p_{i,2}-1\right)\left[p_{i,2}^3 \gamma_1^{-1} - \left(p_{i,2}-1\right)^3 \gamma_2^{-1} - \gamma_3^{-1}\right].
\end{aligned}$$

The fundamental rogue wave is given by Eq. (2.1010), with p_1 satisfying the condition (2.1017). This fundamental rogue wave can be written more explicitly as

$$|q_i(x,t)| = \left|\rho_i \frac{g_i}{f}\right|, \quad i = 1, 2, 3, \tag{2.1018}$$

where

$$f = (a_1x + b_1y + c_1t)^2 + \frac{1}{\zeta_0^2}(a_1x + b_1y + \zeta_0c_2t)^2 + \frac{|p_1|^2}{(p_1 + p_1^*)^2},$$

$$g_1 = f - \frac{2i\hat{\theta}_1}{\zeta_0}(a_1x + b_1y + \zeta_0c_2t) + 2i\hat{\theta}_2(a_1x + b_1y + c_1t) - \hat{\theta}_1^2 - \hat{\theta}_2^2,$$

$$g_2 = f + \frac{2i}{\zeta_0}(a_1x + b_1y + \zeta_0c_2t) - 1,$$

$$g_3 = f + \frac{2i(\hat{\theta}_1 - 1)}{\zeta_0}(a_1x + b_1y + \zeta_0c_2t)$$
$$-2i\hat{\theta}_2(a_1x + b_1y + c_1t) - (\hat{\theta}_1 - 1)^2 - \hat{\theta}_2^2,$$

parameters (a_1, b_1, c_1, c_2) are given by Eq. (2.1012), and

$$\zeta_0 = \frac{a_1}{a_2}, \quad \hat{\theta}_1 = \Re\left(\frac{p_1}{p_1 - \mathrm{i}}\right), \quad \hat{\theta}_2 = \Im\left(\frac{p_1}{p_1 - \mathrm{i}}\right).$$

Here, $\Re$ and $\Im$ represent the real and imaginary parts of a complex number respectively.

To demonstrate this fundamental rogue wave, we choose nonlinear coefficients, background amplitudes and velocity values as

$$\epsilon_1 = -\epsilon_2 = \epsilon_3 = 1, \ \rho_1 = \rho_2 = \rho_3 = 1, \ V_{1,1} = 6, \ V_{1,2} = 5, \ V_{2,1} = 4, \ V_{2,2} = 3. \tag{2.1019}$$

In addition, we choose $p_1 = 0.5 + 0.5\mathrm{i}$, which satisfies the condition (2.1017). For these choices of parameters, the corresponding rogue wave is displayed in Fig. 2.30. It is seen that this is a line rogue wave with a single dominant peak.

To get multi-rogue waves, we set $N > 1$ and $n_1 = n_2 = \cdots = n_N = 1$ in the rational solutions of Theorem 2.20, and require all p_i values to satisfy condition (2.1017). To demonstrate, we choose $N = 2$ and the same nonlinear coefficients, background amplitudes and velocity values as in (2.1019). In addition, we choose

$$p_1 = -0.539770966 + 0.3\mathrm{i}, \ \ p_2 = 1.904662796 + 0.65\mathrm{i}, \ \ a_{1,1} = a_{1,2} = 0. \tag{2.1020}$$

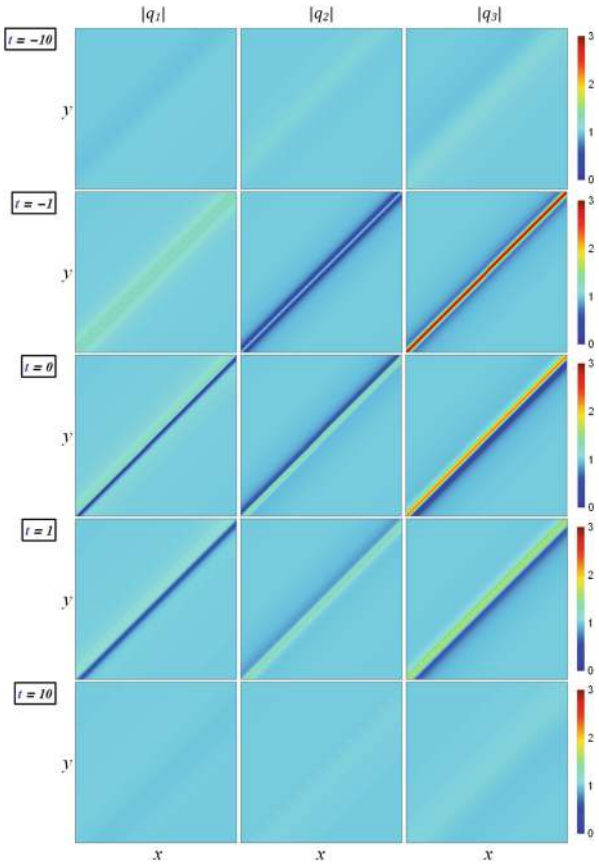

Fig. 2.30 A fundamental line rogue wave in the two-dimensional three-wave system (2.972) with parameter choices (2.1019) and $p = 0.5 + 0.5\mathrm{i}$. In all panels, $-10 \leq x, y \leq 10$

Notice that these (p_1, p_2) values satisfy conditions (2.1017), because we obtained their real parts by solving the quartic equation (2.1017), with their imaginary parts set as 0.3 and 0.65 respectively. The corresponding two-rogue wave solution is displayed in Fig. 2.31. We see that this rogue wave features two intersecting lines, indicating that this solution describes the interaction between two fundamental line rogue waves. Interestingly, at the intersection point between the two line rogue waves, the $|q_2|$ component has higher amplitude, but the $(|q_1|, |q_3|)$ components have lower amplitudes.

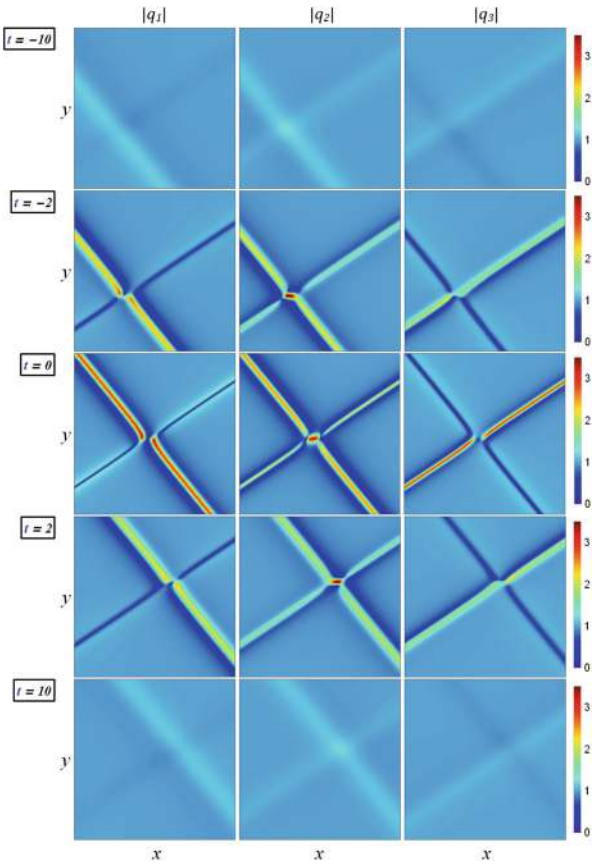

Fig. 2.31 A two-rogue wave solution in the two-dimensional three-wave system (2.972) with parameter choices (2.1019)–(2.1020). In these panels, $-100 \le x \le 0$ and $-50 \le y \le 0$ in the first row, $-50 \le x \le 50$ and $-25 \le y \le 25$ in the second to fourth rows, and $0 \le x \le 100$, $0 \le y \le 50$ in the last row. These (x, y) intervals in different rows are different because the intersection point of the two line rogue waves is moving

Chapter 3
Rogue Wave Patterns

In this chapter, we study rogue wave patterns. This is an important question, because if such patterns are known, this information would allow for the prediction of later rogue wave events from earlier wave forms, providing an opportunity for proactive action in the face of damaging natural events. In the literature, graphs of low-order rogue waves have been plotted for many integrable equations, and simple patterns such as triangles (i.e., rogue triplets) have been reported (see Chap. 2). But richer patterns arising from higher-order rogue wave solutions have been challenging to predict, partially because higher-order rogue wave solutions have more complicated expressions and even their numerical plotting can be difficult. In this chapter, we will develop analytical frameworks to predict rogue patterns for arbitrary orders.

Our basic observation is that, clear rogue patterns would appear when certain internal parameters in the rogue wave solutions get large. The resulting patterns manifest as triangles, pentagons, heptagons, rings, and other shapes, in the spatial-temporal plane or just the spatial plane. Since these patterns arise under large internal parameters, we will develop an asymptotic theory for their prediction. We will show that these patterns can be asymptotically predicted by root structures of certain special polynomials, such as the Yablonskii-Vorob'ev polynomial hierarchy, Adler-Moser polynomials, and Okamoto polynomial hierarchies, in the (1+1)-dimensional case, and by root curves of certain double-real-variable polynomials in the (2+1)-dimensional case. In addition, these patterns are often universal in the sense that they would arise in many different integrable systems. If all internal parameters are zero but the order of the rogue wave is large, one often gets super rogue waves of high order. Asymptotic profiles of super rogue waves at high order in the nonlinear Schrödinger equation will also be presented at the end of this chapter.

We start with universal rogue patterns associated with root structures of the Yablonskii-Vorob'ev polynomial hierarchy.

B. Yang, J. Yang, *Rogue Waves in Integrable Systems*,
https://doi.org/10.1007/978-3-031-66793-0_3

3.1 Rogue Patterns Associated with the Yablonskii-Vorob'ev Polynomial Hierarchy

In many integrable systems, patterns of rogue waves under a single large internal parameter are predicted by root structures of the Yablonskii-Vorob'ev polynomial hierarchy. This finding was first reported by Yang and Yang (2021a) for the nonlinear Schrödinger equation and then extended to several other integrable systems in Yang and Yang (2021c). Such rogue patterns are studied in this section.

3.1.1 The Yablonskii-Vorob'ev Polynomial Hierarchy and Their Root Structures

Yablonskii-Vorob'ev polynomials arose in rational solutions of the second Painlevé (P_{II}) equation

$$w'' = 2w^3 + zw + \alpha, \tag{3.1}$$

where α is an arbitrary constant. This P_{II} equation admits rational solutions if and only if $\alpha = N$ is an integer (Umemura and Watanabe 1998). In this case, the rational solution is unique and is expressed by Yablonskii (1959) and Vorob'ev (1965) as

$$w(z; N) = \frac{d}{dz} \ln \frac{Q_{N-1}(z)}{Q_N(z)}, \quad N \geq 1, \tag{3.2}$$

$$w(z; 0) = 0, \quad w(z; -N) = -w(z; N), \tag{3.3}$$

where polynomials $Q_N(z)$, now called the Yablonskii-Vorob'ev polynomials, are constructed by the following recurrence relation

$$Q_{N+1} Q_{N-1} = z Q_N^2 - 4 \left[Q_N Q_N'' - (Q_N')^2 \right], \tag{3.4}$$

with $Q_0(z) = 1$, $Q_1(z) = z$, and the prime denoting the derivative. Later, a determinant expression for these polynomials was found by Kajiwara and Ohta (1996). Let $p_k(z)$ be the special Schur polynomial defined by

$$\sum_{k=0}^{\infty} p_k(z) \epsilon^k = \exp\left(z\epsilon - \frac{4}{3}\epsilon^3 \right). \tag{3.5}$$

Then, Yablonskii-Vorob'ev polynomials $Q_N(z)$ are given by the $N \times N$ determinant (Kajiwara and Ohta 1996)

$$Q_N(z) = c_N \begin{vmatrix} p_1(z) & p_0(z) & \cdots & p_{2-N}(z) \\ p_3(z) & p_2(z) & \cdots & p_{4-N}(z) \\ \vdots & \vdots & \vdots & \vdots \\ p_{2N-1}(z) & p_{2N-2}(z) & \cdots & p_N(z) \end{vmatrix}, \tag{3.6}$$

where $c_N = \prod_{j=1}^{N}(2j-1)!!$, and $p_k(z) = 0$ if $k < 0$. This determinant is a Wronskian since it is easy to see from Eq. (3.5) that $p_k(z) = p'_{k+1}(z)$. These polynomials are monic with integer coefficients (Clarkson and Mansfield 2003). The first few Yablonskii-Vorob'ev polynomials are

$$\begin{aligned} Q_1(z) &= z, \\ Q_2(z) &= z^3 + 4, \\ Q_3(z) &= z^6 + 20z^3 - 80, \\ Q_4(z) &= z(z^9 + 60z^6 + 11200). \end{aligned}$$

To define the Yablonskii-Vorob'ev polynomial hierarchy, we let $p_k^{[m]}(z)$ be the generalized Schur polynomial defined by

$$\sum_{k=0}^{\infty} p_k^{[m]}(z)\epsilon^k = \exp\left(z\epsilon - \frac{2^{2m}}{2m+1}\epsilon^{2m+1}\right), \tag{3.7}$$

where m is a positive integer. Then, the Yablonskii-Vorob'ev hierarchy $Q_N^{[m]}(z)$ are given by the $N \times N$ determinant (Clarkson and Mansfield 2003)

$$Q_N^{[m]}(z) = c_N \begin{vmatrix} p_1^{[m]}(z) & p_0^{[m]}(z) & \cdots & p_{2-N}^{[m]}(z) \\ p_3^{[m]}(z) & p_2^{[m]}(z) & \cdots & p_{4-N}^{[m]}(z) \\ \vdots & \vdots & \vdots & \vdots \\ p_{2N-1}^{[m]}(z) & p_{2N-2}^{[m]}(z) & \cdots & p_N^{[m]}(z) \end{vmatrix}, \tag{3.8}$$

where $p_k^{[m]}(z) = 0$ if $k < 0$. When $m = 1$, $Q_N^{[1]}(z)$ are the original Yablonskii-Vorob'ev polynomials $Q_N(z)$. When $m > 1$, $Q_N^{[m]}(z)$ give higher members of this polynomial hierarchy. All these $Q_N^{[m]}(z)$ polynomials were conjectured to be monic polynomials with integer coefficients as well (Clarkson and Mansfield 2003). The first few $Q_N^{[2]}(z)$ polynomials are

$$\begin{aligned} Q_1^{[2]}(z) &= z, \\ Q_2^{[2]}(z) &= z^3, \\ Q_3^{[2]}(z) &= z(z^5 - 144), \end{aligned}$$

$$Q_4^{[2]}(z) = z^{10} - 1008z^5 - 48384.$$

These $Q_N^{[m]}(z)$ polynomials, through relations similar to (3.2)–(3.3), provide the unique rational solution for the P_{II} hierarchy (Clarkson and Mansfield 2003; Balogh et al. 2016). It is noted that the determinant (3.8) for $Q_N^{[m]}(z)$ is also a Wronskian, because it is easy to see from Eq. (3.7) that

$$p_k^{[m]}(z) = [p_{k+1}^{[m]}]'(z). \tag{3.9}$$

Root structures of the Yablonskii-Vorob'ev polynomial hierarchy have been studied before (Fukutani et al. 2000; Taneda 2000; Clarkson and Mansfield 2003; Buckingham and Miller 2014; Balogh et al. 2016). Regarding the zero root, its multiplicities in $Q_N(z)$, $Q_N^{[2]}(z)$ and $Q_N^{[3]}(z)$ were presented in Taneda (2000) and Clarkson and Mansfield (2003). Generalizing those results, we have the following theorem (Yang and Yang 2021a).

Theorem 3.1 *The Yablonskii-Vorob'ev hierarchy polynomial $Q_N^{[m]}(z)$ has degree $N(N+1)/2$, and is of the form*

$$Q_N^{[m]}(z) = z^{N_0(N_0+1)/2} q_N^{[m]}(\zeta), \quad \zeta = z^{2m+1}, \tag{3.10}$$

where $q_N^{[m]}(\zeta)$ is a polynomial with a nonzero constant term, and the integer N_0 is determined from (N, m) by the formula

$$N_0 = \begin{cases} N \ mod\ (2m+1), & if\ 0 \le N \ mod\ (2m+1) \le m, \\ 2m - [N \ mod\ (2m+1)], & if\ N \ mod\ (2m+1) > m. \end{cases} \tag{3.11}$$

This theorem gives the multiplicity of the root zero in any $Q_N^{[m]}(z)$ polynomial. It also shows that the root structure of $Q_N^{[m]}(z)$ is invariant under $2\pi/(2m+1)$-angle rotation in the complex z plane. In the particular case of the original Yablonskii-Vorob'ev polynomials $Q_N(z)$ where $m = 1$, the above theorem shows that $0 \le N_0 \le 1$. This means that zero is either not a root or a simple root of $Q_N(z)$, in agreement with previous results in Fukutani et al. (2000) and Taneda (2000).

Regarding nonzero roots, it was shown by Fukutani et al. (2000) that for the original Yablonskii-Vorob'ev polynomials $Q_N(z)$, all nonzero roots are simple. For the higher Yablonskii-Vorob'ev hierarchy polynomials $Q_N^{[m]}(z)$, it was conjectured by Clarkson and Mansfield (2003) that all nonzero roots are also simple. In view of Theorem 3.1, this conjecture implies that the polynomial $Q_N^{[m]}(z)$ has

$$N_p = \frac{1}{2}[N(N+1) - N_0(N_0+1)] \tag{3.12}$$

nonzero simple roots.

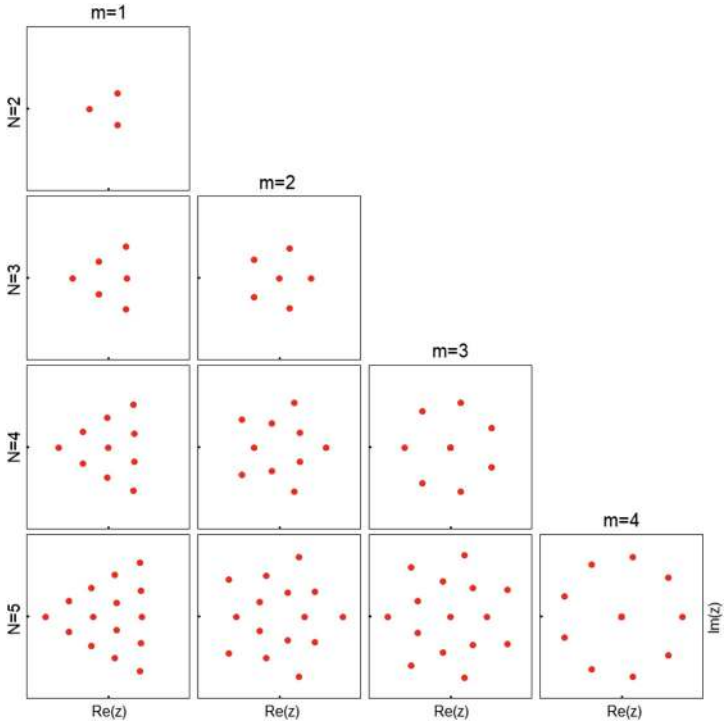

Fig. 3.1 Plots of the roots of the Yablonskii-Vorob'ev polynomial hierarchy $Q_N^{[m]}(z)$ in the complex z plane for $2 \le N \le 5$ and $1 \le m \le N-1$. In all panels, the real and imaginary axes of z are on the same $[-7, 7]$ interval

Roots of many $Q_N^{[m]}(z)$ polynomials were plotted in Clarkson and Mansfield (2003), and highly regular and symmetric patterns were observed. Due to the importance of these root structures to our work, we reproduce those root plots in Fig. 3.1 for $2 \le N \le 5$ and $1 \le m \le N-1$. It is seen that the exteriors of these roots form triangles, pentagons, heptagons, and so on, depending on the value of m. In addition, all nonzero roots are simple, while the zero root may have higher multiplicity according to the above formula (3.10). Boundaries of these roots in $Q_N^{[m]}(z)$ in the large-N limit are analytically determined by Buckingham and Miller (2014) and Balogh et al. (2016).

It turns out that these Yablonskii-Vorob'ev hierarchy polynomials and their root structures play an important role in the prediction of rogue wave patterns in many integrable systems. This will be elaborated in the rest of this section.

3.1.2 Nonlinear Schrödinger Equation

The nonlinear Schrödinger (NLS) equation is

$$\mathrm{i}u_t + \frac{1}{2}u_{xx} + |u|^2 u = 0. \tag{3.13}$$

Rogue patterns in this equation have been studied by Kedziora et al. (2011), He et al. (2013) and Kedziora et al. (2013) through Darboux transformation and numerical simulations. It was observed by Kedziora et al. (2011) that if a N-th order rogue wave exhibits a single-shell ring structure, then the center of the ring is a $(N-2)$-th order rogue wave. This observation was explained analytically by He et al. (2013). Kedziora et al. (2013) observed that NLS rogue patterns could be classified according to the order of the rogue waves and the parameter shifts applied to the Akhmediev breathers in the rogue-wave limit. This latter observation allowed the authors to extrapolate the shapes of rogue waves beyond order six, where numerical plotting of rogue waves became difficult. Rogue patterns in the NLS equation were analytically investigated by Yang and Yang (2021a) when one of the internal parameters in the rogue wave solutions gets large. It was discovered that such rogue patterns could be predicted by root structures of the Yablonskii-Vorob'ev polynomial hierarchy. Those results in Yang and Yang (2021a) are described below.

General rogue waves in the NLS equation (3.13) satisfying the boundary conditions of $u(x,t) \to e^{\mathrm{i}t}$ as $x, t \to \pm\infty$ have been presented in Sect. 2.1.1. For the convenience of the reader, we reproduce those solutions first.

Lemma 3.1 *General nonsingular rogue waves in the NLS equation (3.13) are given by*

$$u_N(x,t) = \frac{\sigma_1}{\sigma_0} e^{\mathrm{i}t}, \tag{3.14}$$

where the positive integer N represents the order of the rogue wave,

$$\sigma_n = \det_{1\le i,j\le N}\left(\phi^{(n)}_{2i-1,2j-1}\right), \tag{3.15}$$

$$\phi^{(n)}_{i,j} = \sum_{\nu=0}^{\min(i,j)} \frac{1}{4^\nu} S_{i-\nu}(\boldsymbol{x}^+(n) + \nu \boldsymbol{s})\, S_{j-\nu}(\boldsymbol{x}^-(n) + \nu \boldsymbol{s}), \tag{3.16}$$

vectors $\boldsymbol{x}^{\pm}(n) = \left(x_1^{\pm}, 0, x_3^{\pm}, 0, \cdots\right)$ are defined by

$$x_1^{\pm} = x \pm it \pm n, \quad x^+_{2k+1} = \frac{x + 2^{2k}(it)}{(2k+1)!} + a_{2k+1}, \quad x^-_{2k+1} = (x^+_{2k+1})^*, \tag{3.17}$$

with $k \geq 1$ *and the asterisk* * *representing complex conjugation,* $\boldsymbol{s} = (0, s_2, 0, s_4, \cdots)$ *are coefficients from the expansion*

$$\sum_{k=1}^{\infty} s_k \lambda^k = \ln\left[\frac{2}{\lambda}\tanh\left(\frac{\lambda}{2}\right)\right], \tag{3.18}$$

and $a_3, a_5, \ldots, a_{2N-1}$ *are free irreducible complex constants.*

Rogue wave solutions in this theorem contain $N-1$ free internal complex parameters $a_3, a_5, \cdots, a_{2N-1}$. In this section, we consider asymptotic patterns of these rogue solutions when one of these internal parameters is large (in amplitude), while the other parameters remain $O(1)$.

Suppose $|a_{2m+1}|$ is large for a certain integer m, where $1 \leq m \leq N-1$, and the other a_{2j+1} parameters are $O(1)$. Then, large-a_{2m+1} asymptotics of rogue waves $u_N(x,t)$ in Lemma 3.1 were obtained by Yang and Yang (2021a) and are summarized in the following two theorems.

Theorem 3.2 *If nonzero roots of the Yablonskii-Vorob'ev hierarchy polynomial* $Q_N^{[m]}(z)$ *are all simple, then far away from the origin of the* (x,t) *plane, with* $\sqrt{x^2+t^2} = O\left(|a_{2m+1}|^{1/(2m+1)}\right)$, *the N-th order rogue wave* $u_N(x,t)$ *would split into* N_p *fundamental (Peregrine) rogue waves, where* N_p *is given in Eq. (3.12). These Peregrine waves are* $\hat{u}_1(x-\hat{x}_0, t-\hat{t}_0)\, e^{it}$, *where*

$$\hat{u}_1(x,t) = 1 - \frac{4(1+2it)}{1+4x^2+4t^2}, \tag{3.19}$$

and their positions $(\hat{x}_0, \hat{t}_0)$ *are given by*

$$\hat{x}_0 + i\hat{t}_0 = \Omega z_0, \tag{3.20}$$

where

$$\Omega = [-(2m+1)2^{-2m} a_{2m+1}]^{1/(2m+1)}, \tag{3.21}$$

and z_0 *is any one of the* N_p *simple nonzero roots of* $Q_N^{[m]}(z)$. *The error of this Peregrine wave approximation is* $O(|a_{2m+1}|^{-1/(2m+1)})$. *Expressed mathematically, when* $(x-\hat{x}_0)^2 + (t-\hat{t}_0)^2 = O(1)$, *we have the following solution asymptotics*

$$u_N(x,t; a_3, a_5, \cdots, a_{2N-1}) = \hat{u}_1(x-\hat{x}_0, t-\hat{t}_0)\, e^{it} + O\left(|a_{2m+1}|^{-1/(2m+1)}\right). \tag{3.22}$$

When (x,t) *is not in the neighborhood of any of these* N_p *Peregrine waves, or* $\sqrt{x^2+t^2}$ *is larger than* $O\left(|a_{2m+1}|^{1/(2m+1)}\right)$, $u_N(x,t)$ *asymptotically approaches the constant background* e^{it} *as* $|a_{2m+1}| \to \infty$.

Theorem 3.3 *In the neighborhood of the origin, where* $x^2 + t^2 = O(1)$, $u_N(x,t)$ *is approximately a lower* N_0*-th order rogue wave* $u_{N_0}(x,t)$*, where* N_0 *is given in Eq. (3.11),* $0 \le N_0 \le N-2$*, and* $u_{N_0}(x,t)$ *is given by Eq. (3.14) with its internal parameters* $a_3, a_5, \cdots, a_{2N_0-1}$ *being the first* $N_0 - 1$ *values in the parameter set* $(a_3, a_5, \cdots, a_{2N-1})$ *of the original rogue wave* $u_N(x,t)$*. The error of this lower-order rogue wave approximation* $u_{N_0}(x,t)$ *is* $O(|a_{2m+1}|^{-1})$*. Expressed mathematically, when* $x^2 + t^2 = O(1)$*,*

$$u_N(x,t;a_3,a_5,\cdots,a_{2N-1}) = u_{N_0}(x,t;a_3,a_5,\cdots,a_{2N_0-1}) + O\left(|a_{2m+1}|^{-1}\right). \tag{3.23}$$

If $N_0 = 0$*, then there will not be such a lower-order rogue wave in the neighborhood of the origin, and* $u_N(x,t)$ *asymptotically approaches the constant background* e^{it} *there as* $|a_{2m+1}| \to \infty$.

These two theorems will be proved later in this section.

Remark 3.1 Theorem 3.2 predicts that when $|a_{2m+1}|$ is large, the N-th order rogue wave (3.14) far away from the origin comprises N_p Peregrine waves. The rogue pattern formed by these Peregrine waves has the same geometric shape as the root structure of the polynomial $Q_N^{[m]}(z)$, and thus this rogue pattern has $2\pi/(2m+1)$-angle rotational symmetry. The only difference between the predicted rogue pattern and the root structure of $Q_N^{[m]}(z)$ is a dilation and rotation between them due to the multiplication factor on the right side of Eq. (3.20). The angle of rotation is equal to the angle of the complex number $-a_{2m+1}$ divided by $2m+1$, and the dilation factor is equal to $[(2m+1)2^{-2m}|a_{2m+1}|]^{1/(2m+1)}$.

Remark 3.2 In Eq. (3.21), we can pick any one of the $(2m+1)$-th root of $-(2m+1)2^{-2m}a_{2m+1}$ as Ω, because roots z_0 of the polynomial $Q_N^{[m]}(z)$ in Eq. (3.20) have $2\pi/(2m+1)$-angle rotational symmetry, see the comment in the paragraph below Theorem 3.1.

Comparison Between True Rogue Patterns and Analytical Predictions

Now, we compare true rogue patterns with our analytical predictions in the above two theorems. For this purpose, we first show in Fig. 3.2 true rogue wave solutions (3.14) from the 2rd to 7th order, with large a_3, a_5, a_7, a_9, a_{11} and a_{13} in the first to sixth columns respectively. The specific value of the large parameter in each panel of this figure is listed in Table 3.1, and the other parameters in each solution are chosen as zero.

It is seen from Fig. 3.2 that these rogue waves comprise a number of Peregrine waves forming triangular patterns for large a_3, pentagon patterns for large a_5, heptagon patterns for large a_7, nonagon patterns for large a_9, hendecagon (eleven-sided polygon) patterns for large a_{11}, and tridecagon (thirteen-sided polygon) patterns for large a_{13}. In addition to these Peregrine waves away from the origin, some of the rogue waves also contain a lower-order rogue wave at their centers.

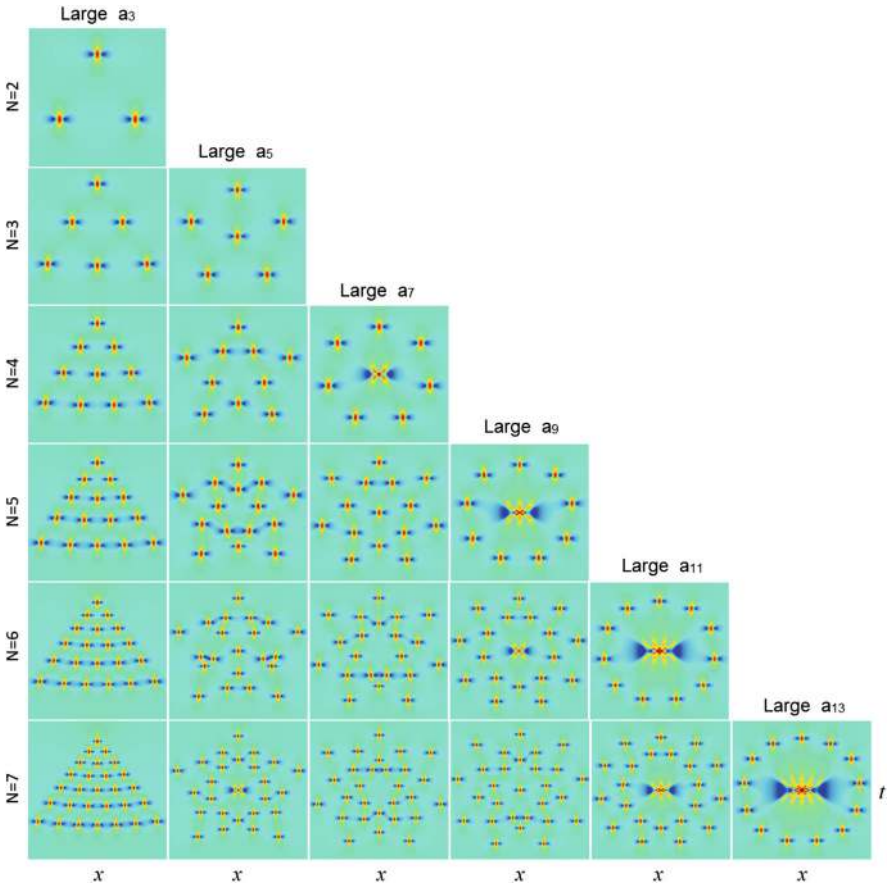

Fig. 3.2 True NLS rogue wave patterns $|u_N(x,t;a_3,a_5,\cdots,a_{2N-1})|$ from solutions (3.14) when N ranges from 2 to 7 and one of the solution parameters is large (the other parameters are set as zero). The large parameter is labeled on top of each column, and its value for each panel is listed in Table 3.1. The center of each panel is always the origin $x = t = 0$, but the (x,t) intervals differ slightly from panel to panel. For instance, in the bottom row, the left-most panel has $-18.5 \le x,t \le 18.5$, and the right-most panel has $-16 \le x,t \le 16$

Table 3.1 Value of the large parameter for NLS rogue waves in Fig. 3.2

N	a_3	a_5	a_7	a_9	a_{11}	a_{13}
2	−100i					
3	−60i	−1000i				
4	−30i	−300i	−3000i			
5	−20i	−100i	−2000i	−12,000i		
6	−20i	−200i	−2000i	−20,000i	−80,000i	
7	−20i	−200i	−2000i	−30,000i	−100,000i	−300,000i

Table 3.2 Predicted (N_p, N_0) values for true NLS rogue waves of Fig. 3.2

N	$m=1$	$m=2$	$m=3$	$m=4$	$m=5$	$m=6$
2	(3, 0)					
3	(6, 0)	(5, 1)				
4	(9, 1)	(10, 0)	(7, 2)			
5	(15, 0)	(15, 0)	(14, 1)	(9, 3)		
6	(21, 0)	(20, 1)	(21, 0)	(18, 2)	(11, 4)	
7	(27, 1)	(25, 2)	(28, 0)	(27, 1)	(22, 3)	(13, 5)

For instance, for the 7-th order rogue waves in the bottom row of Fig. 3.2, the first and fourth panels (with large a_3 and a_9 respectively) exhibit a Peregrine wave in their centers; the second panel (with large a_5) exhibits a second-order rogue wave in the center; the fifth panel (with large a_{11}) exhibits a third-order rogue wave in the center; and the last panel (with large a_{13}) exhibits a fifth-order rogue wave in the center. For our choices of parameters in rogue waves of Fig. 3.2, these lower-order rogue waves in the center are all super-rogue waves, i.e., rogue waves with the highest peak amplitude of their orders.

Now, we compare these true rogue patterns in Fig. 3.2 with our analytical predictions. Our prediction $|u_N^{(p)}(x,t)|$ from Theorems 3.2 and 3.3 can be assembled into a simple formula,

$$\left|u_N^{(p)}(x,t)\right| = \left|u_{N_0}(x,t)\right| + \sum_{j=1}^{N_p} \left(\left|\hat{u}_1(x-\hat{x}_0^{(j)}, t-\hat{t}_0^{(j)})\right| - 1 \right), \tag{3.24}$$

where $\hat{u}_1(x,t)$ is the Peregrine wave given in (3.19), their positions $(\hat{x}_0^{(j)}, \hat{t}_0^{(j)})$ given by (3.20) with z_0 being every one of the N_p simple nonzero roots of $Q_N^{[m]}(z)$, and $u_{N_0}(x,t)$ is the lower-order rogue wave in Eq. (3.23) whose internal parameters $(a_3, a_5, \cdots, a_{2N_0-1})$ are the first $N_0 - 1$ values in the parameter set $(a_3, a_5, \cdots, a_{2N-1})$ of the original rogue wave $u_N(x,t)$. For true rogue waves in Fig. 3.2, all internal parameters except for a_{2m+1} were chosen as zero, and $N_0 \le m$. Then, all internal parameters in the predicted lower-order rogue wave $u_{N_0}(x,t)$ at the origin are zero, which give super rogue waves (see Sect. 2.1.2).

Our predicted (N_p, N_0) values for rogue waves of Fig. 3.2 are displayed in Table 3.2, where $m = 1, 2, \cdots, 6$ correspond to large $a_3, a_5, \cdots, a_{13}$ respectively. These (N_p, N_0) values provide our predictions for the number of Peregrine waves away from the origin $(x,t) = (0,0)$, as well as the order of the reduced rogue wave in the neighborhood of the origin. Visual comparison between Table 3.2 and Fig. 3.2 shows complete agreement.

We further compare our predicted whole solutions (3.24) with the true solutions of Fig. 3.2 for the same sets of $(a_3, a_5, \cdots)$ parameter values. These predicted whole solutions (3.24) are displayed in Fig. 3.3, with identical (x,t) intervals as in Fig. 3.2's true solutions. It is seen that the predicted patterns are strikingly similar to the true ones. In particular, since our predicted Peregrine locations (3.20) in

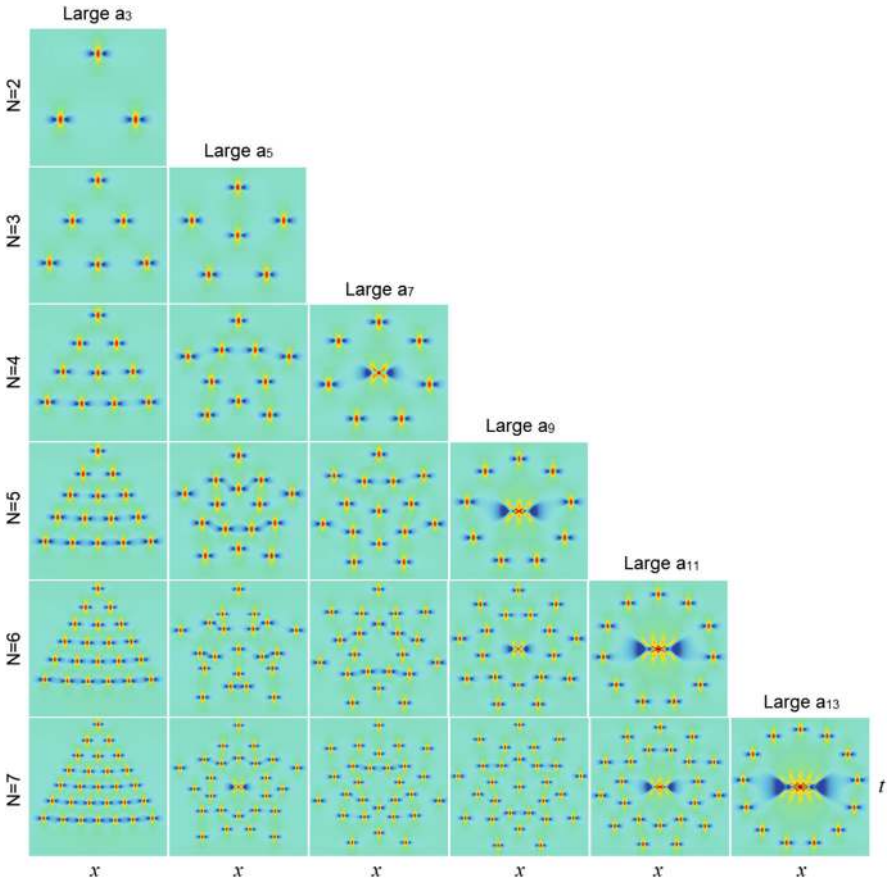

Fig. 3.3 Analytical predictions (3.24) for true rogue waves in Fig. 3.2. The x and t intervals here are identical to those in Fig. 3.2

the (x, t) plane are given by all the non-zero roots of the Yablonskii-Vorob'ev polynomials $Q_N^{[m]}(z)$, multiplied by a fixed complex constant, predicted patterns formed by these Peregrine waves then are simply the root structures of these Yablonskii-Vorob'ev polynomials under certain rotation and dilation, as is evident by comparing predicted rogue waves in Fig. 3.3 to the Yablonskii-Vorob'ev root structures in Fig. 3.1. These predicted Peregrine patterns clearly match the true ones in Fig. 3.2 very well. This visual agreement shows the deep connection between NLS rogue patterns and root structures of the Yablonskii-Vorob'ev hierarchy, as our Theorem 3.2 reveals.

Regarding our predictions $u_{N_0}(x, t)$ for centers of the rogue waves $u_N(x, t)$ in Fig. 3.2, we have shown that they are all lower-order super-rogue waves, which agree with centers of true solutions in Fig. 3.2.

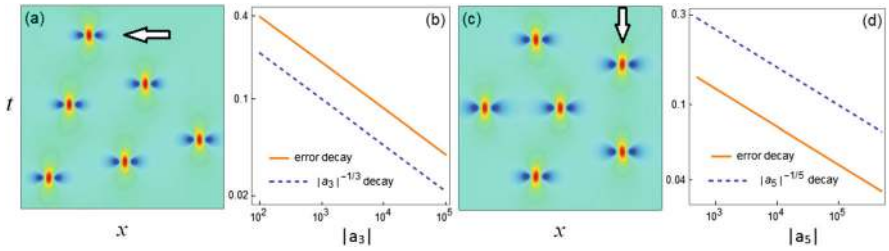

Fig. 3.4 Decay of errors in our prediction (3.20) for the Peregrine location as $|a_3|$ or $|a_5|$ increases. (**a**) A triangle pattern of 3rd-order rogue waves when $|a_3|$ is large and $\arg(a_3) = -\pi/4$. (**b**) Error versus $|a_3|$ for the Peregrine location marked by an arrow in (**a**). (**c**) A pentagon pattern of 3rd-order rogue waves when $|a_5|$ is large with $\arg(a_5) = -\pi/4$. (**b**) Error versus $|a_5|$ for the Peregrine location marked by an arrow in (**c**)

Next, we make quantitative comparisons between true rogue waves and our predictions for large a_{2m+1}, and verify the error decay rate of $O(|a_{2m+1}|^{-1/(2m+1)})$ for the prediction of Peregrine-wave locations far away from the origin in Theorem 3.2, and the error decay rate of $O(|a_{2m+1}|^{-1})$ for the prediction of the lower-order rogue wave at the center in Theorem 3.3.

For the quantitative comparison on Peregrine-wave locations away from the origin, we choose two patterns of 3rd-order rogue waves. One is a triangle pattern from large a_3, and we set $\arg(a_3) = -\pi/4$; and the other is a pentagon pattern from large a_5, and we set a_5 to be real positive. In each pattern, we choose all other parameters of the rogue wave solutions to be zero. These triangul and pentagon patterns are shown schematically in Fig. 3.4a and c respectively. In each of these two patterns, we pick one of its Peregrine waves, which is marked by an arrow, and quantitatively compare its true (x_0, t_0) location with our analytical prediction (3.20) as $|a_3|$ or $|a_5|$ increases. Here, the true location of the Peregrine wave is defined as the (x_0, t_0) location where this Peregrine wave attains its maximum amplitude, and the error of our asymptotic prediction $(\hat{x}_0,\ \hat{t}_0)$ in Eq. (3.20) is defined as

$$\text{error of Peregrine location} = \sqrt{(\hat{x}_0 - x_0)^2 + (\hat{t}_0 - t_0)^2}. \tag{3.25}$$

These errors of Peregrine locations versus $|a_3|$ or $|a_5|$ are plotted as solid lines in panels (b) and (d) of Fig. 3.4 for the triangular and pentagon patterns respectively. For comparison, the decay rates of $|a_3|^{-1/3}$ and $|a_5|^{-1/5}$ are also displayed in these panels as dashed lines. We see that these errors of Peregrine locations indeed decay at the rate of $|a_{2m+1}|^{-1/(2m+1)}$, thus confirming the analytical error estimates (3.22) in Theorem 3.2.

To quantitatively compare our prediction in Theorem 3.3 on the lower-order rogue wave at the center with the true solution, we choose a fifth-order rogue wave $u_5(x, t)$ with large a_9 and the other internal parameters set as zero. This $|u_5(x, t)|$ solution with $a_9 = -5000\mathrm{i}$ is displayed in Fig. 3.5a. The center region of this wave marked by a dashed-line box in panel (a) is amplified and replotted in panel (b).

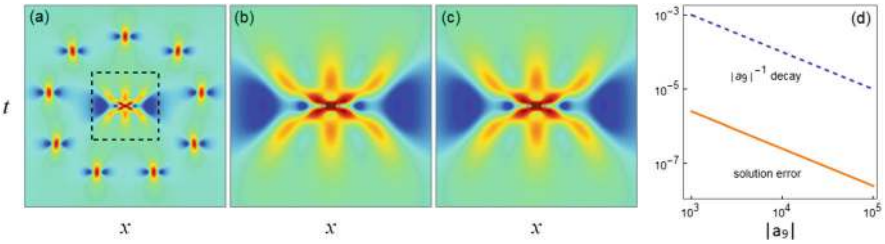

Fig. 3.5 Decay of errors in our prediction $u_3^{[p]}(x,t)$ for the center region of the rogue wave $u_5(x,t)$ with large a_9. (**a**) A true 5-th order rogue wave $|u_5(x,t)|$ with $a_9 = -5000\mathrm{i}$ and the other parameters being zero; the (x,t) intervals here are $-12 \le x, t \le 12$. (**b**) Zoomed-in plot of the center region of the true solution marked by a dashed-line box in panel (**a**). (**c**) Our prediction $|u_3^{[p]}(x,t)|$ for the center region with the same (x,t) intervals as in (**b**). (**d**) Error decay of our predicted solution at the (x,t) location of $(0.5, 0.5)$ as a_9 increases in size with $\arg(a_9) = -\pi/2$

In the present case, $N = 5$ and $m = 4$. Since $5 \equiv -4 \bmod 9$, we get $N_0 = 3$ from Eq. (3.11). Thus, according to Theorem 3.3, this $u_5(x,t)$ solution contains a 3rd-order rogue wave $u_3^{[p]}(x,t)$ in its center region, where all internal parameters (a_3, a_5) in this $u_3^{[p]}(x,t)$ solution are zero. Such a $u_3^{[p]}(x,t)$ solution is a third-order super rogue wave. This predicted $|u_3^{[p]}(x,t)|$ solution is displayed in Fig. 3.5c, with the same (x,t) internals as in the true center-region solution displayed in panel (b). Visually, this predicted center solution in (c) is identical to the true center solution in (b). Quantitatively, we have also obtained the errors in our predicted solution $u_3^{[p]}(x,t)$ at $x = t = 0.5$ of the center region as a_9 increases in magnitude with $\arg(a_9) = -\pi/2$. Our error is defined as

$$\text{error of center region prediction} = \left| u_5(x,t) - u_3^{[p]}(x,t) \right|_{x=t=0.5}. \tag{3.26}$$

The dependence of this error on $|a_9|$ is plotted in Fig. 3.5d. Comparison of this error decay with the $|a_9|^{-1}$ decay [shown as a dashed line in panel (d)] indicates that this error is indeed of $O(|a_9|^{-1})$, confirming the error prediction (3.23) in Theorem 3.3.

Proofs of Pattern Predictions

Below, we prove the analytical predictions on NLS rogue patterns in Theorems 3.2 and 3.3. Our proof is based on an asymptotic analysis of the rogue wave solution (3.14), or equivalently, the determinant σ_n in Eq. (3.15), in the large a_{2m+1} limit.

Proof When a_{2m+1} is large and the other parameters $O(1)$ in the rogue wave solution (3.14), at (x,t) where $\sqrt{x^2+t^2} = O\left(|a_{2m+1}|^{1/(2m+1)}\right)$, by denoting

$$\lambda = a_{2m+1}^{-1/(2m+1)} \tag{3.27}$$

and recalling the definition of Schur polynomials in Eq. (2.2), we have

$$\begin{aligned} S_k(\boldsymbol{x}^+(n)+\nu\boldsymbol{s}) &= S_k\left(x_1^+, \nu s_2, x_3^+, \nu s_4, \cdots\right) \\ &= \lambda^{-k} S_k\left(x_1^+\lambda, \nu s_2\lambda^2, x_3^+\lambda^3, \nu s_4\lambda^4, \cdots\right) \\ &\sim \lambda^{-k} S_k\left[(x+\mathrm{i}t)\lambda, 0, \cdots, 0, 1, 0, \cdots\right] \\ &= S_k\left(x+\mathrm{i}t, 0, \cdots, 0, a_{2m+1}, 0, \cdots\right). \end{aligned} \tag{3.28}$$

Thus,

$$S_k(\boldsymbol{x}^+(n)+\nu\boldsymbol{s}) \sim S_k(\mathbf{v}), \qquad |a_{2m+1}| \gg 1, \tag{3.29}$$

where

$$\mathbf{v} = (x+\mathrm{i}t, 0, \cdots, 0, a_{2m+1}, 0, \cdots). \tag{3.30}$$

From the definition of Schur polynomials, $S_k(\mathbf{v})$ is given by

$$\sum_{k=0}^{\infty} S_k(\mathbf{v})\epsilon^k = \exp\left[(x+\mathrm{i}t)\epsilon + a_{2m+1}\epsilon^{2m+1}\right]. \tag{3.31}$$

Thus, it is related to the polynomial $p_k^{[m]}(z)$ in (3.7) as

$$S_k(\mathbf{v}) = \Omega^k p_k^{[m]}(z), \tag{3.32}$$

where Ω is as defined in Eq. (3.21), and

$$z = \Omega^{-1}(x+\mathrm{i}t). \tag{3.33}$$

Using these formulae, we find that

$$\det_{1\le i,j\le N}\left[S_{2i-j}(\boldsymbol{x}^+(n)+\nu\boldsymbol{s})\right] \sim c_N^{-1}\Omega^{N(N+1)/2} Q_N^{[m]}(z), \quad |a_{2m+1}| \gg 1. \tag{3.34}$$

Similarly,

$$\det_{1\le i,j\le N}\left[S_{2i-j}(\boldsymbol{x}^-(n)+\nu\boldsymbol{s})\right] \sim c_N^{-1}\left(\Omega^*\right)^{N(N+1)/2} Q_N^{[m]}(z^*), \quad |a_{2m+1}| \gg 1. \tag{3.35}$$

To proceed further, we use determinant identities and the Laplace expansion to rewrite σ_n in Eq. (3.15) as

$$\sigma_n = \sum_{0\le\nu_1<\nu_2<\cdots<\nu_N\le 2N-1} \det_{1\le i,j\le N}\left[\frac{1}{2^{\nu_j}} S_{2i-1-\nu_j}(\boldsymbol{x}^+(n)+\nu_j \boldsymbol{s})\right] \times \det_{1\le i,j\le N}\left[\frac{1}{2^{\nu_j}} S_{2i-1-\nu_j}(\boldsymbol{x}^-(n)+\nu_j \boldsymbol{s})\right], \tag{3.36}$$

see Eq. (2.77) in Sect. 2.1.1. Since the highest order term of a_{2m+1} in this σ_n comes from the index choices of $\nu_j = j-1$, then

$$\sigma_n \sim |\alpha|^2 |a_{2m+1}|^{\frac{N(N+1)}{2m+1}} \left|Q_N^{[m]}(z)\right|^2, \qquad |a_{2m+1}| \gg 1, \tag{3.37}$$

where

$$\alpha = 2^{-N(N-1)/2} c_N^{-1} \Omega^{N(N+1)/2}. \tag{3.38}$$

Since α is independent of n, the above equation shows that for large a_{2m+1}, $\sigma_1/\sigma_0 \sim 1$, i.e., the solution $u(x,t)$ is on the unit-amplitude background e^{it}, except at or near (x,t) locations $\left(\hat{x}_0, \hat{t}_0\right)$ where

$$z_0 = \Omega^{-1}(\hat{x}_0 + i\hat{t}_0) \tag{3.39}$$

is a root of the polynomial $Q_N^{[m]}(z)$, when this highest order term (3.37) vanishes. Such $\left(\hat{x}_0, \hat{t}_0\right)$ locations are given by Eq. (3.20) in view of Eq. (3.33).

Next, we show that when (x,t) is in the neighborhood of each of the $\left(\hat{x}_0, \hat{t}_0\right)$ locations given by Eq. (3.20), i.e., when $(x-\hat{x}_0)^2 + (t-\hat{t}_0)^2 = O(1)$, the rogue wave $u_N(x,t)$ in Eq. (3.14) approaches a Peregrine wave $\hat{u}_1(x-\hat{x}_0, t-\hat{t}_0)\, e^{it}$ for large a_{2m+1}. The asymptotic analysis above indicates that when (x,t) is in the neighborhood of $\left(\hat{x}_0, \hat{t}_0\right)$, the highest power term $|a_{2m+1}|^{\frac{N(N+1)}{2m+1}}$ in $\sigma(x,t)$ vanishes. Thus, in order to determine the asymptotics of $u_N(x,t)$ in that (x,t) region, we need to derive the leading order term of a_{2m+1} in Eq. (3.36) whose order is lower than $|a_{2m+1}|^{\frac{N(N+1)}{2m+1}}$. For this purpose, we notice from Eq. (3.28) that when (x,t) is in the neighborhood of $\left(\hat{x}_0, \hat{t}_0\right)$, we have a more refined asymptotics for $S_k(\boldsymbol{x}^+(n)+\nu\boldsymbol{s})$ as

$$\begin{aligned} S_k(\boldsymbol{x}^+(n)+\nu\boldsymbol{s}) &= \lambda^{-k} S_k\left(x_1^+\lambda, 0, \cdots, 0, 1, 0, \cdots\right)\left[1+O(\lambda^2)\right] \\ &= S_k\left(x_1^+, 0, \cdots, 0, a_{2m+1}, 0, \cdots\right)\left[1+O(\lambda^2)\right], \end{aligned} \tag{3.40}$$

i.e.,

$$S_k(\boldsymbol{x}^+(n)+\nu\boldsymbol{s}) = S_k(\hat{\mathbf{v}})\left[1+O\left(a_{2m+1}^{-2/(2m+1)}\right)\right], \tag{3.41}$$

where

$$\hat{\mathbf{v}} = (x + \mathrm{i}t + n, 0, \cdots, 0, a_{2m+1}, 0, \cdots). \tag{3.42}$$

The polynomials $S_k(\hat{\mathbf{v}})$ are related to $p_k^{[m]}(z)$ in (3.7) as

$$S_k(\hat{\mathbf{v}}) = \Omega^k p_k^{[m]}(\hat{z}), \tag{3.43}$$

where Ω is as given in Eq. (3.21), and $\hat{z} = \Omega^{-1}(x + \mathrm{i}t + n)$.

Now, we derive the leading order term of a_{2m+1} in the Laplace expansion (3.36). This leading order term comes from two index choices, one being $\nu = (0, 1, \cdots, N-1)$, and the other being $\nu = (0, 1, \cdots, N-2, N)$.

With the first index choice, in view of Eqs. (3.41) and (3.43), the determinant involving $\boldsymbol{x}^+(n)$ in Eq. (3.36) is

$$\alpha\, a_{2m+1}^{\frac{N(N+1)}{2(2m+1)}}\, Q_N^{[m]}(\hat{z}) \left[1 + O\left(a_{2m+1}^{-2/(2m+1)}\right)\right], \tag{3.44}$$

where α is given in Eq. (3.38). Expanding $Q_N^{[m]}(\hat{z})$ around $\hat{z} = z_0$, where z_0 is given in Eq. (3.39), and recalling $Q_N^{[m]}(z_0) = 0$, we have

$$Q_N^{[m]}(\hat{z}) = \Omega^{-1}\left[(x - \hat{x}_0) + \mathrm{i}(t - \hat{t}_0) + n\right]\left[Q_N^{[m]}\right]'(z_0)\left[1 + O\left(\Omega^{-1}\right)\right]. \tag{3.45}$$

Inserting this equation into (3.44), the determinant involving $\boldsymbol{x}^+(n)$ in Eq. (3.36) becomes

$$\left[(x - \hat{x}_0) + \mathrm{i}(t - \hat{t}_0) + n\right] \hat{\alpha}\, a_{2m+1}^{\frac{N(N+1)-2}{2(2m+1)}} \left[Q_N^{[m]}\right]'(z_0)\left[1 + O\left(a_{2m+1}^{-1/(2m+1)}\right)\right], \tag{3.46}$$

where $\hat{\alpha} = \alpha[-(2m+1)2^{-2m}]^{-1/(2m+1)}$. Similarly, the determinant involving $\boldsymbol{x}^-(n)$ in Eq. (3.36) becomes

$$\left[(x - \hat{x}_0) - \mathrm{i}(t - \hat{t}_0) - n\right] \hat{\alpha}^* \left(a_{2m+1}^*\right)^{\frac{N(N+1)-2}{2(2m+1)}} \left[Q_N^{[m]}\right]'(z_0^*)\left[1 + O\left(a_{2m+1}^{-1/(2m+1)}\right)\right]. \tag{3.47}$$

Next, we consider the contribution in Eq. (3.36) from the second index choice of $\nu = (0, 1, \cdots, N-2, N)$. For this index choice, the determinant involving $\boldsymbol{x}^+(n)$ in Eq. (3.36) is

$$\det_{1 \le i \le N}\left[S_{2i-1}(\boldsymbol{x}^+), \frac{1}{2}S_{2i-2}(\boldsymbol{x}^+ + \boldsymbol{s}), \cdots, \frac{1}{2^{N-2}}S_{2i-(N-1)}[\boldsymbol{x}^+ + (N-2)\,\boldsymbol{s}],\right.$$
$$\left.\frac{1}{2^N}S_{2i-(N+1)}(\boldsymbol{x}^+ + N\boldsymbol{s})\right]. \tag{3.48}$$

Utilizing Eqs. (3.41)–(3.43), this determinant is

$$2^{-N(N-1)/2-1}\Omega^{(N(N+1)-2)/2}\det_{1\le i\le N}\left[p^{[m]}_{2i-1}(\hat{z}),\, p^{[m]}_{2i-2}(\hat{z}),\cdots,\, p^{[m]}_{2i-(N-1)}(\hat{z}),\, p^{[m]}_{2i-(N+1)}(\hat{z})\right]\times\left[1+O\left(a_{2m+1}^{-2/(2m+1)}\right)\right]. \tag{3.49}$$

Recalling Eq. (3.9), we see that $p^{[m]}_{2i-(N+1)}(\hat{z}) = [p^{[m]}_{2i-N}]'(\hat{z})$. Thus, the determinant in the above expression is equal to $c_N^{-1}\left[Q_N^{[m]}\right]'(\hat{z})$, so that the determinant (3.48) becomes

$$\frac{1}{2}\hat{\alpha}\, a_{2m+1}^{\frac{N(N+1)-2}{2(2m+1)}}\left[Q_N^{[m]}\right]'(\hat{z})\left[1+O\left(a_{2m+1}^{-2/(2m+1)}\right)\right]. \tag{3.50}$$

When (x,t) is in the neighborhood of $(\hat{x}_0,\hat{t}_0)$, we expand $\left[Q_N^{[m]}\right]'(\hat{z})$ around $\hat{z}=z_0$ to reduce this expression further to

$$\frac{1}{2}\hat{\alpha}\, a_{2m+1}^{\frac{N(N+1)-2}{2(2m+1)}}\left[Q_N^{[m]}\right]'(z_0)\left[1+O\left(a_{2m+1}^{-1/(2m+1)}\right)\right]. \tag{3.51}$$

Similarly, the determinant involving $\boldsymbol{x}^-(n)$ in Eq. (3.36) becomes

$$\frac{1}{2}\hat{\alpha}^*\,(a^*_{2m+1})^{\frac{N(N+1)-2}{2(2m+1)}}\left[Q_N^{[m]}\right]'(z_0^*)\left[1+O\left(a_{2m+1}^{-1/(2m+1)}\right)\right]. \tag{3.52}$$

Summarizing the above two contributions, we find that

$$\sigma_n(x,t) = |\hat{\alpha}|^2\left|\left[Q_N^{[m]}\right]'(z_0)\right|^2|a_{2m+1}|^{\frac{N(N+1)-2}{(2m+1)}}\times\left[(x-\hat{x}_0)^2+(t-\hat{t}_0)^2-(2\mathrm{i})n\,(t-\hat{t}_0)-n^2+\frac{1}{4}\right]\left[1+O\left(a_{2m+1}^{-1/(2m+1)}\right)\right]. \tag{3.53}$$

Finally, we recall our assumption that nonzero roots of $Q_N^{[m]}(z)$ are all simple. Then, $\left[Q_N^{[m]}\right]'(z_0)\neq 0$. This indicates that the above leading-order asymptotics for $\sigma_n(x,t)$ never vanishes. Therefore, when $|a_{2m+1}|$ is large and (x,t) in the neighborhood of $(\hat{x}_0,\hat{t}_0)$, we get from (3.53) that

$$u_N(x,t) = \frac{\sigma_1}{\sigma_0} e^{\mathrm{i}t} = e^{\mathrm{i}t}\left(1 - \frac{4[1+2\mathrm{i}(t-\hat{t}_0)]}{1+4(x-\hat{x}_0)^2+4(t-\hat{t}_0)^2}\right) + O\left(a_{2m+1}^{-1/(2m+1)}\right), \tag{3.54}$$

which is a Peregrine wave $\hat{u}_1(x-\hat{x}_0, t-\hat{t}_0)\, e^{\mathrm{i}t}$, and the error of this Peregrine prediction is $O\left(a_{2m+1}^{-1/(2m+1)}\right)$. Theorem 3.2 is then proved.

Proof To analyze the large-a_{2m+1} behavior of the rogue wave $u_N(x,t)$ in the neighborhood of the origin, where $x^2 + t^2 = O(1)$, we first rewrite the σ_n determinant (3.15) into a $3N \times 3N$ determinant (Ohta and Yang 2012a)

$$\sigma_n = \begin{vmatrix} \mathbf{O}_{N\times N} & \Phi_{N\times 2N} \\ -\Psi_{2N\times N} & \mathbf{I}_{2N\times 2N} \end{vmatrix}, \tag{3.55}$$

where $\Phi_{i,j} = 2^{-(j-1)} S_{2i-j}\left[\boldsymbol{x}^+(n) + (j-1)\boldsymbol{s}\right]$, and $\Psi_{i,j} = 2^{-(i-1)} S_{2j-i}\left[\boldsymbol{x}^-(n) + (i-1)\boldsymbol{s}\right]$. Defining $\boldsymbol{y}^\pm$ to be the vector $\boldsymbol{x}^\pm$ without the a_{2m+1} term, i.e., let

$$\boldsymbol{x}^+ = \boldsymbol{y}^+ + (0,\cdots,0,a_{2m+1},0,\cdots), \quad \boldsymbol{x}^- = \boldsymbol{y}^- + (0,\cdots,0,a_{2m+1}^*,0,\cdots), \tag{3.56}$$

we find that the Schur polynomials of $\boldsymbol{x}^\pm$ are related to those of $\boldsymbol{y}^\pm$ as

$$S_j(\boldsymbol{x}^+ + \nu\boldsymbol{s}) = \sum_{i=0}^{\left[\frac{j}{2m+1}\right]} \frac{a_{2m+1}^i}{i!} S_{j-(2m+1)i}(\boldsymbol{y}^+ + \nu\boldsymbol{s}), \tag{3.57}$$

$$S_j(\boldsymbol{x}^- + \nu\boldsymbol{s}) = \sum_{i=0}^{\left[\frac{j}{2m+1}\right]} \frac{(a_{2m+1}^*)^i}{i!} S_{j-(2m+1)i}(\boldsymbol{y}^- + \nu\boldsymbol{s}), \tag{3.58}$$

where $[a]$ represents the largest integer less than or equal to a. Using this relation, we express matrix elements of Φ and Ψ in Eq. (3.55) through Schur polynomials $S_k(\boldsymbol{y}^\pm + \nu\boldsymbol{s})$ and powers of a_{2m+1} and a_{2m+1}^*.

We need to determine the highest power term of a_{2m+1} in the determinant (3.55). For that purpose, it may be tempting to retain only the highest power term of a_{2m+1} and a_{2m+1}^* in each element of this determinant. That does not work though because it would result in multiple rows (and columns) which are proportional to each other, making the reduced determinant zero. The correct way is to first judiciously remove certain leading power terms of a_{2m+1} and a_{2m+1}^* from elements of the determinant through row and column manipulations, so that the remaining determinant, after retaining only the highest power term of a_{2m+1} and a_{2m+1}^* in each element, would be nonzero. These row and column manipulations are described below.

Suppose $N \equiv N_0 \bmod (2m+1)$, i.e., $N = k(2m+1) + N_0$ for some positive integer k, with $0 \le N_0 \le m$. We perform the following series of row operations to the matrix Φ so that certain high-power terms of a_{2m+1} in its lower rows are eliminated. In the first round, we use the 1st to m-th rows of Φ to eliminate the highest-power term $a_{2m+1}^{2\nu}$ from the $[\nu(2m+1)+1]$-th up to the $[\nu(2m+1)+m]$-th rows for each $1 \le \nu \le k$, so that the remaining terms in those rows have the highest power $a_{2m+1}^{2\nu-1}$. We also use the $(m+1)$-th to $(2m+1)$-th rows of Φ to eliminate the highest-power term $a_{2m+1}^{2\nu+1}$ from the $[\nu(2m+1)+m+1]$-th to the $[\nu(2m+1)+2m+1]$-th rows for each $1 \le \nu \le k-1$, with the remaining terms in those rows having the highest power $a_{2m+1}^{2\nu}$. In each step, the highest power terms $a_{2m+1}^{2\nu}$ or $a_{2m+1}^{2\nu+1}$ of each row are eliminated simultaneously, because the coefficient vector of those highest power terms in each row below the $(2m+1)$-th is proportional to the coefficient vector of the highest power terms in the corresponding upper row between the 1st and $(2m+1)$-th due to the relation (3.57).

In the second round, we use the $(2m+1+1)$-th to $(2m+1+m)$-th rows of the remaining matrix Φ to eliminate the highest-power term $a_{2m+1}^{2\nu+1}$ from the $[(\nu+1)(2m+1)+1]$-th up to the $[(\nu+1)(2m+1)+m]$-th rows for each $1 \le \nu \le k-1$, so that the remaining terms in those rows have the highest power $a_{2m+1}^{2\nu}$. We also use the $(2m+1+m+1)$-th to $(2m+1+2m+1)$-th rows of Φ to eliminate the highest-power term $a_{2m+1}^{2\nu+2}$ from the $[(\nu+1)(2m+1)+m+1]$-th up to the $[(\nu+1)(2m+1)+2m+1]$-th rows for each $1 \le \nu \le k-2$, with the remaining terms in those rows having the highest power $a_{2m+1}^{2\nu+1}$. This process is repeated k rounds.

At the end of this process, the i-th row of the remaining matrix Φ has the highest power $a_{2m+1}^{[(i+m)/(2m+1)]}$. Then, we keep only the highest power terms of a_{2m+1} in each row. Similar column operations are also performed on the matrix Ψ. With these manipulations, we find that σ_n is asymptotically reduced to

$$\sigma_n = \beta\, |a_{2m+1}|^{k^2(2m+1)+k(2N_0+1)} \begin{vmatrix} \mathbf{O}_{N\times N} & \widetilde{\Phi}_{N\times 2N} \\ -\widetilde{\Psi}_{2N\times N} & \mathbf{I}_{2N\times 2N} \end{vmatrix} \left[1 + O\left(a_{2m+1}^{-1}\right)\right], \tag{3.59}$$

where β is a (m, N)-dependent nonzero constant, matrices $\widetilde{\Phi}_{N\times 2N}$ and $\widetilde{\Psi}_{2N\times N}$ have the structures

$$\widetilde{\Phi}_{N\times 2N} = \begin{pmatrix} \mathbf{L}_{(N-N_0)\times(N-N_0)} & \mathbf{O}_{(N-N_0)\times 2N_0} & \mathbf{O}_{(N-N_0)\times(N-N_0)} \\ \mathbf{M}_{N_0\times(N-N_0)} & \widehat{\Phi}_{N_0\times 2N_0} & \mathbf{O}_{N_0\times(N-N_0)} \end{pmatrix}, \tag{3.60}$$

$$\widetilde{\Psi}_{2N\times N} = \begin{pmatrix} \mathbf{U}_{(N-N_0)\times(N-N_0)} & \widehat{\mathbf{M}}_{(N-N_0)\times N_0} \\ \mathbf{O}_{2N_0\times(N-N_0)} & \widehat{\Psi}_{2N_0\times N_0} \\ \mathbf{O}_{(N-N_0)\times(N-N_0)} & \mathbf{O}_{(N-N_0)\times N_0} \end{pmatrix}, \tag{3.61}$$

$$\mathbf{L}_{i,j} = S_{i-j}\left[\boldsymbol{y}^{+} + (j-1)\boldsymbol{s}\right], \quad \mathbf{U}_{i,j} = S_{j-i}\left[\boldsymbol{y}^{-} + (i-1)\boldsymbol{s}\right], \tag{3.62}$$

$$\widehat{\Phi}_{i,j} = 2^{-(j-1)} S_{2i-j}\left[\boldsymbol{y}^{+}(n) + (j-1+\nu_0)\boldsymbol{s}\right], \tag{3.63}$$

$$\widehat{\Psi}_{i,j} = 2^{-(i-1)} S_{2j-i}\left[\boldsymbol{y}^{-}(n) + (i-1+\nu_0)\boldsymbol{s}\right], \tag{3.64}$$

$\nu_0 = k(2m+1)$, and $\mathbf{M}$, $\widehat{\mathbf{M}}$ are matrices of elements $S_j(\boldsymbol{y}^{+} + \nu\boldsymbol{s})$ and $S_j(\boldsymbol{y}^{-} + \nu\boldsymbol{s})$ respectively. Since $\mathbf{L}$ and $\mathbf{U}$ are respectively lower triangular and upper triangular matrices with unit elements on the diagonal in view that $S_0 = 1$ and $S_j = 0$ for $j < 0$, σ_n in Eq. (3.59) then is

$$\sigma_n = \beta\, |a_{2m+1}|^{k^2(2m+1)+k(2N_0+1)} \begin{vmatrix} \mathbf{O}_{N_0\times N_0} & \widehat{\Phi}_{N_0\times 2N_0} \\ -\widehat{\Psi}_{2N_0\times N_0} & \mathbf{I}_{2N_0\times 2N_0} \end{vmatrix} \left[1 + O\left(a_{2m+1}^{-1}\right)\right]. \tag{3.65}$$

Finally, we notice that $S_j\left[\boldsymbol{y}^{\pm} + (\nu+\nu_0)\boldsymbol{s}\right]$ is related to $S_j\left(\boldsymbol{y}^{\pm} + \nu\boldsymbol{s}\right)$ through

$$S_j\left[\boldsymbol{y}^{\pm} + (\nu+\nu_0)\boldsymbol{s}\right] = \sum_{i=0}^{[j/2]} S_{2i}(\nu_0\boldsymbol{s}) S_{j-2i}(\boldsymbol{y}^{\pm} + \nu\boldsymbol{s}), \tag{3.66}$$

the reason being that the odd elements of the vector $\boldsymbol{s}$ are zero (see Lemma 3.1). Using this relation, the determinant in (3.65) can be reduced to one where ν_0 is set to zero in the above $\widehat{\Phi}$ and $\widehat{\Psi}$ matrices given in Eq. (3.63). Such a determinant for σ_n gives a N_0-th order rogue wave, whose internal parameters $(a_3, a_5, \cdots, a_{2N_0-1})$ are the first $N_0 - 1$ values in the original parameter set $(a_3, a_5, \cdots, a_{2N-1})$. Thus, in the neighborhood of the origin ,

$$\begin{aligned} u_N(x,t;a_3,a_5,\cdots,a_{2N-1}) &= \frac{\sigma_1}{\sigma_0} e^{\mathrm{i}t} \\ &= u_{N_0}(x,t;a_3,a_5,\cdots,a_{2N_0-1})\left[1 + O\left(a_{2m+1}^{-1}\right)\right], \end{aligned} \tag{3.67}$$

which means that the original N-th order rogue wave $u_N(x,t)$ is approximated by a lower N_0-th order rogue wave $u_{N_0}(x,t)$, with the approximation error $O\left(a_{2m+1}^{-1}\right)$.

If $N \equiv -N_0 - 1 \bmod (2m+1)$ with $0 \le N_0 \le m$, Eq. (3.67) can also be derived by similar analysis, and thus the same conclusion holds.

Lastly, we recall that $1 \le m \le N-1$. In addition, $0 \le N_0 \le m$ in view of Theorem 3.1. Furthermore, when $m = N-1$, we find from Eq. (3.11) of Theorem 3.1 that $N_0 = N-2$. As a consequence, $0 \le N_0 \le N-2$. Theorem 3.3 is then proved.

3.1.3 Derivative Nonlinear Schrödinger Equations

The generalized derivative NLS (GDNLS) equations are

$$\mathrm{i}u_t + \frac{1}{2}u_{xx} + \mathrm{i}\gamma|u|^2u_x + \mathrm{i}(\gamma-1)u^2u_x^* + \frac{1}{2}(\gamma-1)(\gamma-2)|u|^4u = 0, \tag{3.68}$$

where γ is a real constant (see Sect. 2.2). These equations contain the Kaup-Newell equation, the Chen-Lee-Liu equation and the Gerdjikov-Ivanov equation as special cases. Boundary conditions of rogue waves in these GDNLS equations are

$$u(x,t) \to e^{\mathrm{i}(1-\gamma-\alpha)x - \frac{\mathrm{i}}{2}\left[\alpha^2+2(\gamma-2)\alpha+1-\gamma\right]t}, \quad x,t \to \pm\infty, \tag{3.69}$$

where $\alpha > 0$ is a free background wave number parameter. Explicit expressions of these rogue waves have been presented in Theorem 2.3 of Sect. 2.2 and will not be repeated here. Importantly, those rogue waves are expressed by determinants of Schur polynomials with index jumps of 2, just like the NLS case. In addition, those rogue waves contain free internal complex parameters $a_3, a_5, \cdots, a_{2N-1}$ as well. We will consider asymptotics of those rogue solutions when one of their internal parameters is large (in amplitude), while the other parameters remain $O(1)$.

Suppose $|a_{2m+1}|$ is large, where $1 \le m \le N-1$, and the other a_{2j+1} parameters are $O(1)$. Then, large-a_{2m+1} asymptotics of rogue waves in the GDNLS equations were derived by Yang and Yang (2021b) and are summarized in the following theorem.

Theorem 3.4 *For the GDNLS rogue wave $u_N(x,t)$ in Theorem 2.3, when $|a_{2m+1}|$ is large and the other internal parameters $O(1)$, then the following statements hold.*

1. *If nonzero roots of the Yablonskii-Vorob'ev hierarchy polynomial $Q_N^{[m]}(z)$ are all simple, then far away from the origin, with $\sqrt{x^2+t^2} = O\left(|a_{2m+1}|^{1/(2m+1)}\right)$, this $u_N(x,t)$ asymptotically would split into N_p fundamental rogue waves, where N_p is given in Eq. (3.12). These fundamental rogue waves are $\hat{u}_1(x-\hat{x}_0, t-\hat{t}_0)\, e^{\mathrm{i}(1-\gamma-\alpha)x - \frac{\mathrm{i}}{2}\left[\alpha^2+2(\gamma-2)\alpha+1-\gamma\right]t}$, where*

$$|\hat{u}_1(x,t)| = \left|\frac{\alpha(x+\alpha t)^2 + (x-t)^2 - \mathrm{i}(x+3\alpha t) - \frac{3}{4}}{\alpha(x+\alpha t)^2 + (x-t)^2 + \mathrm{i}(x+\alpha t) - 2\mathrm{i}t + \frac{1}{4}}\right|, \tag{3.70}$$

and their positions $(\hat{x}_0, \hat{t}_0)$ are given by

$$\hat{x}_0 = \frac{1}{\sqrt{\alpha}}\Re\left[z_0\Omega\right] - \frac{\alpha-1}{\alpha}\Im\left[z_0\Omega\right], \quad \hat{t}_0 = \frac{1}{\alpha}\Im\left[z_0\Omega\right], \tag{3.71}$$

$\Omega = \left(-\frac{2m+1}{2^{2m}}a_{2m+1}\right)^{\frac{1}{2m+1}}$, z_0 is any of the N_p non-zero simple roots of $Q_N^{[m]}(z)$, and $(\Re, \Im)$ represent the real and imaginary parts of a complex number. The error of this fundamental rogue wave approximation is $O(|a_{2m+1}|^{-1/(2m+1)})$. Expressed mathematically, when $|a_{2m+1}| \gg 1$ and $(x-\hat{x}_0)^2 + (t-\hat{t}_0)^2 = O(1)$, we have the following solution asymptotics

$$u_N(x,t;a_3,a_5,\cdots,a_{2N-1}) = \hat{u}_1(x-\hat{x}_0,t-\hat{t}_0)\,e^{\mathrm{i}(1-\gamma-\alpha)x-\frac{\mathrm{i}}{2}[\alpha^2+2(\gamma-2)\alpha+1-\gamma]t} + O\left(|a_{2m+1}|^{-1/(2m+1)}\right). \tag{3.72}$$

When (x,t) is not in the neighborhood of any of these N_p fundamental waves, or $\sqrt{x^2+t^2}$ is larger than $O\left(|a_{2m+1}|^{1/(2m+1)}\right)$, then $u_N(x,t)$ asymptotically approaches the constant-amplitude background $e^{\mathrm{i}(1-\gamma-\alpha)x-\frac{\mathrm{i}}{2}[\alpha^2+2(\gamma-2)\alpha+1-\gamma]t}$ as $|a_{2m+1}|\to\infty$.

2. *In the neighborhood of the origin, where $x^2+t^2=O(1)$, $u_N(x,t)$ is approximately a lower N_0-th order rogue wave $u_{N_0}(x,t)$, where N_0 is determined from (N,m) by Eq. (3.11), $0\le N_0\le N-2$, and $u_{N_0}(x,t)$ is given in Theorem 2.3 with its internal parameters $(a_3,a_5,\cdots,a_{2N_0-1})$ being the first N_0-1 values in the parameter set $\{a_3,a_5,\cdots,a_{2N-1}\}$ of the original rogue wave $u_N(x,t)$. The error of this lower-order rogue wave approximation $u_{N_0}(x,t)$ is $O(|a_{2m+1}|^{-1})$. Expressed mathematically, when $|a_{2m+1}|\gg 1$ and $x^2+t^2=O(1)$,*

$$u_N(x,t;a_3,a_5,\cdots,a_{2N-1}) = u_{N_0}(x,t;a_3,a_5,\cdots,a_{2N_0-1}) + O\left(|a_{2m+1}|^{-1}\right). \tag{3.73}$$

If $N_0=0$, then there will not be such a lower-order rogue wave in the neighborhood of the origin, and $u_N(x,t)$ asymptotically approaches the constant-amplitude background $e^{\mathrm{i}(1-\gamma-\alpha)x-\frac{\mathrm{i}}{2}[\alpha^2+2(\gamma-2)\alpha+1-\gamma]t}$ there as $|a_{2m+1}|\to\infty$.

The proof of this theorem is along the same lines as the proofs of Theorems 3.2–3.3 for the NLS equation and will be omitted here (see Yang and Yang (2021b) for details).

Comparison Between Predictions and True Solutions

According to Theorem 3.4, our predictions for GDNLS' rogue patterns under a large internal parameter a_{2m+1} can be assembled into a single formula

$$|u_N(x,t)| \approx \left|u_{N_0}(x,t)\right| + \sum_{k=1}^{N_p}\left(\left|\hat{u}_1(x-\hat{x}_0^{(k)},t-\hat{t}_0^{(k)})\right|-1\right), \tag{3.74}$$

where N_0 is given from (N,m) by Eq. (3.11), $u_{N_0}(x,t)$ is the lower-order rogue wave at the center whose internal parameters $(a_3,a_5,\cdots a_{2N_0-1})$ are inherited directly from those of the original rogue wave $u_N(x,t)$, the function $\hat{u}_1(x,t)$ is the fundamental rogue wave given in Eq. (3.70), with its position $(\hat{x}_0^{(k)},\hat{t}_0^{(k)})$ given by Eq. (3.71) for every one of the nonzero simple roots $z_0^{(k)}$ of $Q_N^{[m]}(z)$, and N_p is the number of such fundamental rogue waves whose value is given by Eq. (3.12). Then, when we choose $\alpha=16/9$ in the background (3.69), the above solution approximation (3.74) for $2\le N\le 5$, with the large internal parameter a_{2m+1}

Table 3.3 Value of the large parameter for GDNLS rogue waves in Fig. 3.6 with $\alpha = 16/9$

N	a_3	a_5	a_7	a_9
2	−30i			
3	−28i	−500i		
4	−20i	−300i	−1500i	
5	−15i	−250i	−1000i	−3000i

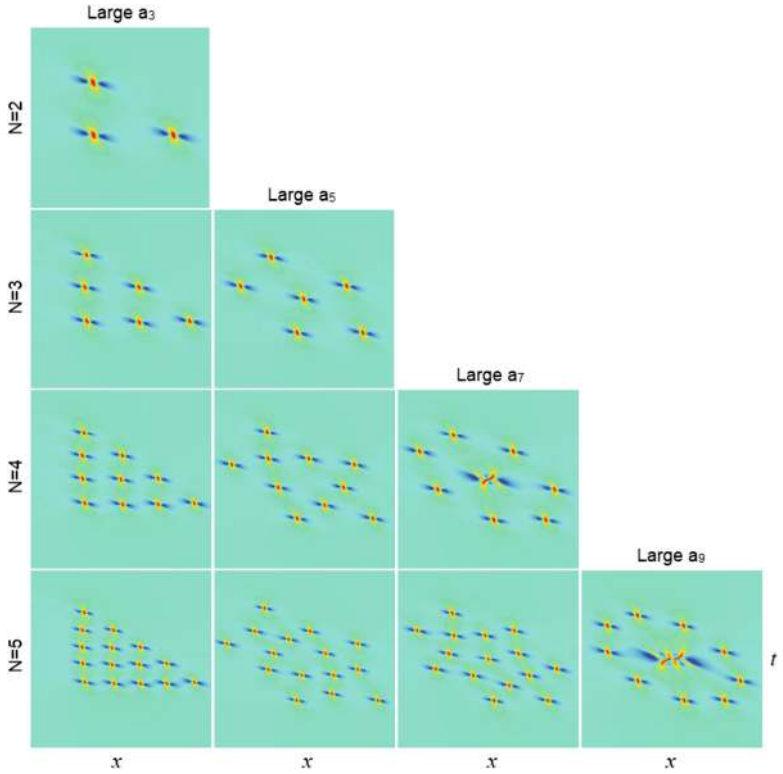

Fig. 3.6 Predicted GDNLS rogue patterns $|u_N(x,t)|$ for the orders $2 \le N \le 5$ and the large parameter a_{2m+1} from $m = 1$ to $N-1$ [the background wavenumber parameter in Eq. (3.69) is chosen as $\alpha = 16/9$]. For each panel, the large parameter a_{2m+1} in the rogue wave is displayed in Table 3.3, with the other internal parameters set as zero. The center of each panel is always the origin $x = t = 0$, but the (x,t) intervals differ slightly from panel to panel. For instance, in the bottom row, the left-most panel has $-12 \le x, t \le 12$, and the right-most panel has $-10 \le x, t \le 10$

ranging from $m = 1$ to $N-1$ and its value taken as in Table 3.3, and with the other internal parameters taken as zero, are displayed in Fig. 3.6. Notice that the predicted patterns are stretched triangles in the first column (for large a_3), stretched pentagons in the second column (for large a_5), stretched heptagons in the third column (for large a_7), and so on.

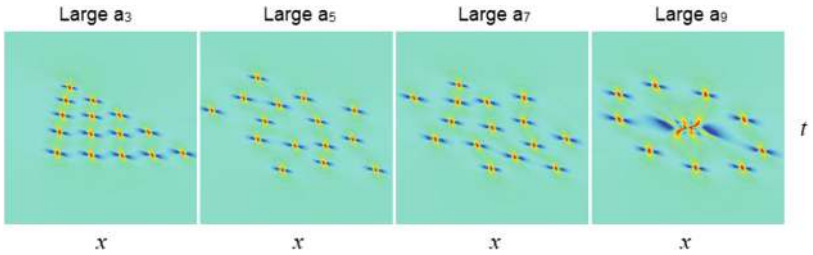

Fig. 3.7 True GDNLS rogue patterns $|u_N(x,t)|$ for $N = 5$. The α value, internal parameters and (x,t) intervals for these true solutions are identical to those in the theoretically predicted patterns shown in the bottom row of Fig. 3.6

Now, we compare these predicted rogue patterns with true ones. For brevity, we only show this comparison for $N = 5$. Under identical α and internal parameter choices and identical (x,t) intervals as in the bottom row of Fig. 3.6, true rogue patterns are displayed in Fig. 3.7. It is seen that the true rogue patterns are almost indistinguishable from the predictions in the bottom row of Fig. 3.6 on all aspects, from the locations of individual fundamental rogue waves, to the overall shapes formed by these fundamental waves, and to the fine details of the lower-order rogue waves at the center. Similar agreements hold for the other panels of Fig. 3.6 as well. These apparent visual agreements testify to the power of our theoretical predictions. The error estimates of $O(|a_{2m+1}|^{-1/(2m+1)})$ away from the origin and $O(|a_{2m+1}|^{-1})$ in the neighborhood of the origin from Theorem 3.4 have been confirmed numerically too.

3.1.4 Boussinesq Equation

The Boussinesq equation is

$$u_{tt} + u_{xx} - (u^2)_{xx} - \frac{1}{3}u_{xxxx} = 0, \tag{3.75}$$

where u is a real variable for water surface elevation. Its rogue waves under boundary conditions of

$$u(x,t) \to 0, \quad x,t \to \pm\infty \tag{3.76}$$

have been given in Theorem 2.4 of Sect. 2.3. These rogue waves contain free complex parameters $a_3, a_5, \cdots, a_{2N-1}$.

Suppose $|a_{2m+1}|$ is large, where $1 \le m \le N-1$, and the other parameters are $O(1)$. Then, large-a_{2m+1} asymptotics of these rogue waves in the Boussinesq equation were derived by Yang and Yang (2021b) and are summarized in the following theorem.

Theorem 3.5 *For the Boussinesq rogue wave $u_N(x,t)$ in Theorem 2.4, when $|a_{2m+1}|$ is large and the other a_{2j+1} parameters $O(1)$, then the following statements hold.*

1. *If nonzero roots of the Yablonskii-Vorob'ev hierarchy polynomial $Q_N^{[m]}(z)$ are all simple, then far away from the origin, with $\sqrt{x^2+t^2} = O\left(|a_{2m+1}|^{1/(2m+1)}\right)$, this $u_N(x,t)$ asymptotically splits into N_p fundamental rogue waves, where N_p is given in Eq. (3.12). These fundamental rogue waves are $u_1(x-\hat{x}_0, t-\hat{t}_0)$, where*

$$u_1(x,t) = 2\partial_x^2 \ln\left(x^2+t^2+1\right), \tag{3.77}$$

and their positions $(\hat{x}_0, \hat{t}_0)$ are given by

$$\hat{x}_0 = \Re\left[\left(-2\mathrm{i}\sqrt{3}\right) z_0 \Omega\right] + \Delta_B, \quad \hat{t}_0 = \Im\left[\left(-2\mathrm{i}\sqrt{3}\right) z_0 \Omega\right], \tag{3.78}$$

$\Omega = \left(-\frac{2m+1}{2^{2m}} a_{2m+1}\right)^{\frac{1}{2m+1}}$, z_0 is any of the N_p non-zero simple roots of $Q_N^{[m]}(z)$, and $\Delta_B = -4(N-1)/3$. The error of this fundamental rogue wave approximation is $O(|a_{2m+1}|^{-1/(2m+1)})$. Expressed mathematically, when $|a_{2m+1}| \gg 1$ and $(x-\hat{x}_0)^2 + (t-\hat{t}_0)^2 = O(1)$, we have the following solution asymptotics

$$u_N(x,t;a_3,a_5,\cdots,a_{2N-1}) = u_1(x-\hat{x}_0, t-\hat{t}_0) + O\left(|a_{2m+1}|^{-1/(2m+1)}\right). \tag{3.79}$$

When (x,t) is not in the neighborhood of any of these N_p fundamental waves, or $\sqrt{x^2+t^2}$ is larger than $O\left(|a_{2m+1}|^{1/(2m+1)}\right)$, then $u_N(x,t)$ asymptotically approaches the zero background as $|a_{2m+1}| \to \infty$.
2. *In the neighborhood of the origin, where $x^2+t^2 = O(1)$, $u_N(x,t)$ is approximately a lower N_0-th order rogue wave $u_{N_0}(x,t)$, where N_0 is determined from (N,m) by Eq. (3.11), $0 \le N_0 \le N-2$, and $u_{N_0}(x,t)$ is given in Theorem 2.4 with its new internal parameters $(\hat{a}_1, \hat{a}_3, \cdots, \hat{a}_{2N_0-1})$ related to the original parameters of $u_N(x,t)$ as*

$$\hat{a}_{2r-1} = a_{2r-1} + (N-N_0)\, s_{2r-1}, \quad r = 1,2,\cdots,N_0. \tag{3.80}$$

The error of this lower-order rogue wave approximation $u_{N_0}(x,t)$ is $O(|a_{2m+1}|^{-1})$. Expressed mathematically, when $|a_{2m+1}| \gg 1$ and $x^2+t^2 = O(1)$,

$$\begin{aligned} u_N(x,t;a_1,a_3,a_5,\cdots,a_{2N-1}) &= u_{N_0}(x,t;\hat{a}_1,\hat{a}_3,\hat{a}_5,\cdots,\hat{a}_{2N_0-1}) \\ &+ O\left(|a_{2m+1}|^{-1}\right). \end{aligned} \tag{3.81}$$

Note that while $a_1 = 0$ in the original rogue wave $u_N(x,t)$ (see Theorem 2.4 in Sect. 2.3), its counterpart $\hat{a}_1$ in the lower-order rogue wave $u_{N_0}(x,t)$ will not be zero. If $N_0 = 0$, then there will not be such a lower-order rogue wave in the neighborhood of the origin, and $u_N(x,t)$ asymptotically approaches the zero background there as $|a_{2m+1}| \to \infty$.

The proof of this theorem is along similar lines as the proofs of Theorems 3.2–3.3 for the NLS equation and will be omitted (see Yang and Yang (2021b) for details).

Comparison Between Predictions and True Solutions

Next, we present comparisons between predictions and true solutions for the Boussinesq equation. In this case, our prediction from Theorem 3.5 for the Boussinesq rogue pattern under a large internal parameter a_{2m+1} can be assembled into the formula

$$u_N(x,t) \approx u_{N_0}(x,t) + \sum_{k=1}^{N_p} u_1\left(x - \hat{x}_0^{(k)}, t - \hat{t}_0^{(k)}\right), \tag{3.82}$$

where $u_{N_0}(x,t)$ is the lower-order rogue wave at the center whose new internal parameters $(\hat{a}_1, \hat{a}_3, \cdots, \hat{a}_{2N_0-1})$ are given by Eq. (3.80), the function $u_1(x,t)$ is the fundamental Boussinesq rogue wave given in Eq. (3.77), with its position $(\hat{x}_0^{(k)}, \hat{t}_0^{(k)})$ given by Eq. (3.78) for every one of the nonzero simple roots $z_0^{(k)}$ of $Q_N^{[m]}(z)$, and N_p is the number of such fundamental rogue waves whose value is given by Eq. (3.12). When the large internal parameter a_{2m+1} is selected as in Table 3.4 for $2 \le N \le 5$ and $1 \le m \le N-1$, with the other internal parameters set as zero, the predicted rogue solutions (3.82) are illustrated in Fig. 3.8.

Now, we compare these predicted Boussinesq rogue patterns in Fig. 3.8 to the true solutions. Again, for brevity, we only do the comparison for the fifth-order rogue waves ($N = 5$). Under the same internal parameter choices and (x,t) intervals as those in the bottom row of Fig. 3.8, the true Boussinesq rogue patterns are displayed in Fig. 3.9. It is seen that again, the true rogue patterns are visually indistinguishable from our theoretical predictions on all aspects, from locations of fundamental rogue waves away from the center, to fine details of lower-order rogue waves at the center, and to the amounts of x-position shifts to the whole structure. Order of accuracy of our predictions as stated in Theorem 3.5 has also been confirmed numerically, with the details omitted.

Table 3.4 Value of the large parameter for Boussinesq rogue waves in Fig. 3.8

N	a_3	a_5	a_7	a_9
2	−20			
3	−16	150		
4	−10	50	−100	
5	−5	20	−80	200

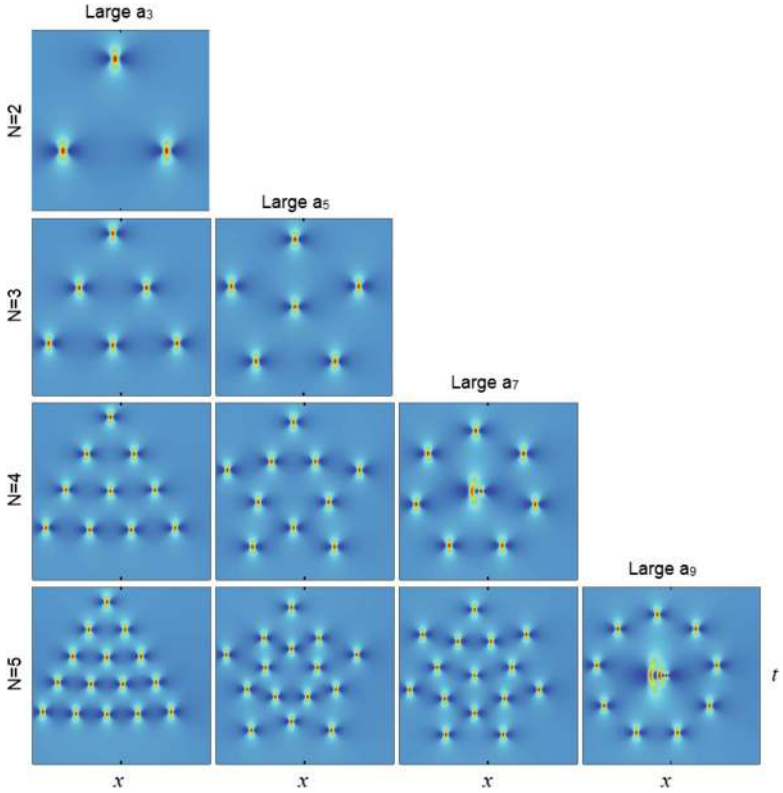

Fig. 3.8 Predicted Boussinesq rogue patterns $u_N(x,t)$ for the orders $2 \leq N \leq 5$ and the large parameter a_{2m+1} from $m = 1$ to $N-1$. For each panel, the large parameter a_{2m+1} in the rogue wave is displayed in Table 3.4, with the other internal parameters set as zero. The center of each panel is always the origin $x = t = 0$, but the (x,t) intervals differ slightly from panel to panel. For instance, in the bottom row, the first two panels have $-32.25 \leq x, t \leq 32.25$ and $-35.25 \leq x, t \leq 35.25$ respectively

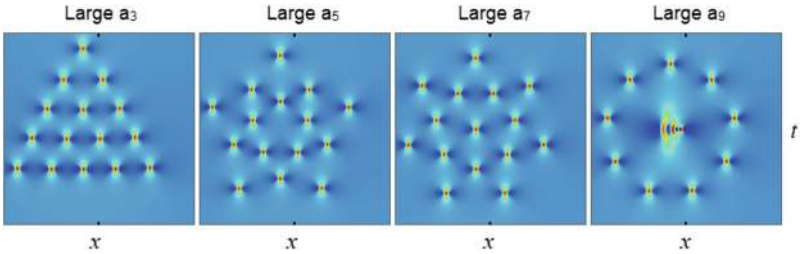

Fig. 3.9 True Boussinesq rogue patterns $u_N(x,t)$ for $N = 5$. The internal parameters and (x,t) intervals for these true solutions are identical to those in the theoretically predicted patterns shown in the bottom row of Fig. 3.8

3.1.5 Manakov System

The Manakov system is

$$\left.\begin{aligned}(\mathrm{i}\partial_t+\partial_x^2)u_1+(\epsilon_1|u_1|^2+\epsilon_2|u_2|^2)u_1=0,\\ (\mathrm{i}\partial_t+\partial_x^2)u_2+(\epsilon_1|u_1|^2+\epsilon_2|u_2|^2)u_2=0,\end{aligned}\right\} \tag{3.83}$$

where $\epsilon_1=\pm1$ and $\epsilon_2=\pm1$. Under the boundary conditions of

$$u_1(x,t)\to\rho_1 e^{\mathrm{i}(k_1x+\omega_1t)},\quad u_2(x,t)\to\rho_2 e^{\mathrm{i}(k_2x+\omega_2t)},\quad x,t\to\pm\infty, \tag{3.84}$$

where parameters ρ_j,k_j,ω_j satisfy algebraic relations (2.583), rogue waves corresponding to a simple root of a certain algebraic equation have been given in Theorem 2.10 of Sect. 2.9. For the convenience of the reader, we reproduce such solutions here.

Lemma 3.2 *If the algebraic equation $\mathcal{F}_1'(p)=0$, with*

$$\mathcal{F}_1(p)=\frac{\epsilon_1\rho_1^2}{p-\mathrm{i}k_1}+\frac{\epsilon_2\rho_2^2}{p-\mathrm{i}k_2}+2p \tag{3.85}$$

and the prime denoting differentiation, admits a non-imaginary simple root p_0, then the Manakov system (3.83) under boundary conditions (3.84) admits rogue wave solutions

$$u_{1,N}(x,t)=\rho_1\frac{g_{1,N}}{f_N}e^{\mathrm{i}(k_1x+\omega_1t)},\quad u_{2,N}(x,t)=\rho_2\frac{g_{2,N}}{f_N}e^{\mathrm{i}(k_2x+\omega_2t)}, \tag{3.86}$$

where N is an arbitrary positive integer which represents the order of the rogue wave,

$$f_N=\sigma_{0,0},\quad g_{1,N}=\sigma_{1,0},\quad g_{2,N}=\sigma_{0,1}, \tag{3.87}$$

$$\sigma_{n,k}=\det_{1\le i,j\le N}\left(\phi_{2i-1,2j-1}^{(n,k)}\right), \tag{3.88}$$

the matrix elements in $\sigma_{n,k}$ are defined by

$$\phi_{i,j}^{(n,k)}=\sum_{\nu=0}^{\min(i,j)}\left[\frac{|p_1|^2}{(p_0+p_0^*)^2}\right]^{\nu}S_{i-\nu}(\boldsymbol{x}^+(n,k)+\nu\boldsymbol{s})\,S_{j-\nu}(\boldsymbol{x}^-(n,k)+\nu\boldsymbol{s}^*), \tag{3.89}$$

the vectors $\boldsymbol{x}^{\pm}(n,k)=(x_1^{\pm},0,x_3^{\pm},0,\cdots)$ are defined by

$$x_r^+(n,k) = p_r x + \left(\sum_{i=0}^{r} p_i p_{r-i}\right)(it) + n\theta_r + k\lambda_r + a_r, \tag{3.90}$$

$$x_r^-(n,k) = p_r^* x - \left(\sum_{i=0}^{r} p_i^* p_{r-i}^*\right)(it) - n\theta_r^* - k\lambda_r^* + a_r^*, \tag{3.91}$$

$\boldsymbol{s} = (s_1, s_2, \cdots)$, p_r, θ_r, λ_r, and s_r are coefficients from the expansions

$$p(\kappa) = \sum_{r=0}^{\infty} p_r \kappa^r, \quad \ln\left[\frac{p(\kappa) - ik_1}{p_0 - ik_1}\right] = \sum_{r=1}^{\infty} \theta_r \kappa^r, \tag{3.92}$$

$$\ln\left[\frac{p(\kappa) - ik_2}{p_0 - ik_2}\right] = \sum_{r=1}^{\infty} \lambda_r \kappa^r, \quad \ln\left[\frac{1}{\kappa}\left(\frac{p_0 + p_0^*}{p_1}\right)\left(\frac{p(\kappa) - p_0}{p(\kappa) + p_0^*}\right)\right] = \sum_{r=1}^{\infty} s_r \kappa^r, \tag{3.93}$$

the function $p(\kappa)$ is defined by the equation

$$\mathcal{F}_1[p(\kappa)] = \mathcal{F}_1(p_0)\cosh(\kappa), \tag{3.94}$$

$a_1 = 0$, and $a_3, a_5, \cdots, a_{2N-1}$ are free irreducible complex constants.

The τ functions of these rogue waves have index jumps of 2 in their matrix elements, and they contain free complex parameters $a_3, a_5, \cdots, a_{2N-1}$.

Suppose $|a_{2m+1}|$ is large, where $1 \le m \le N-1$, and the other parameters are $O(1)$. Then large-a_{2m+1} asymptotics of these Manakov rogue waves in Lemma 3.2 were derived by Yang and Yang (2021b) and are summarized in the following theorem.

Theorem 3.6 *For the Manakov rogue wave $[u_{1,N}(x,t), u_{2,N}(x,t)]$ in Lemma 3.2, when $|a_{2m+1}|$ is large and the other a_{2j+1} parameters $O(1)$, then the following statements hold.*

1. *If nonzero roots of the Yablonskii-Vorob'ev hierarchy polynomial $Q_N^{[m]}(z)$ are all simple, then far away from the origin, with $\sqrt{x^2+t^2} = O\left(|a_{2m+1}|^{1/(2m+1)}\right)$, this $[u_{1,N}(x,t), u_{2,N}(x,t)]$ asymptotically would split into N_p fundamental rogue waves, where N_p is given in Eq. (3.12). These fundamental rogue waves are $[\hat{u}_{1,1}(x-\hat{x}_0, t-\hat{t}_0)\, e^{\mathrm{i}(k_1 x + \omega_1 t)}$, $\hat{u}_{2,1}(x-\hat{x}_0, t-\hat{t}_0)\, e^{\mathrm{i}(k_2 x + \omega_2 t)}]$, where*

$$\hat{u}_{1,1}(x,t) = \rho_1 \frac{[p_1 x + 2p_0 p_1 (it) + \theta_1]\left[p_1^* x - 2p_0^* p_1^* (it) - \theta_1^*\right] + \zeta_0}{|p_1 x + 2p_0 p_1 (it)|^2 + \zeta_0}, \tag{3.95}$$

$$\hat{u}_{2,1}(x,t) = \rho_2 \frac{[p_1 x + 2p_0 p_1 (it) + \lambda_1]\left[p_1^* x - 2p_0^* p_1^* (it) - \lambda_1^*\right] + \zeta_0}{|p_1 x + 2p_0 p_1 (it)|^2 + \zeta_0}, \tag{3.96}$$

$$\theta_1 = \frac{p_1}{p_0 - ik_1},\ \lambda_1 = \frac{p_1}{p_0 - ik_2},\ \zeta_0 = \frac{|p_1|^2}{(p_0 + p_0^*)^2}, \tag{3.97}$$

and their positions $(\hat{x}_0, \hat{t}_0)$ *are given by*

$$\hat{x}_0 = \frac{1}{\Re(p_0)} \Re\left[\frac{z_0 \Omega}{p_1} p_0^*\right] + \Delta_{1M}, \quad \hat{t}_0 = \frac{1}{2\Re(p_0)} \Im\left[\frac{z_0 \Omega}{p_1}\right] + \Delta_{2M}, \tag{3.98}$$

$\Omega = \left(-\frac{2m+1}{2^{2m}} a_{2m+1}\right)^{\frac{1}{2m+1}}$, z_0 *is any of the* N_p *non-zero simple roots of* $Q_N^{[m]}(z)$, *and*

$$\Delta_{1M} = -\frac{1}{\Re(p_0)} \Re\left[\frac{(N-1)s_1}{p_1} p_0^*\right], \quad \Delta_{2M} = -\frac{1}{2\Re(p_0)} \Im\left[\frac{(N-1)s_1}{p_1}\right]. \tag{3.99}$$

The error of this fundamental rogue wave approximation is $O(|a_{2m+1}|^{-1/(2m+1)})$. *Expressed mathematically, when* $|a_{2m+1}| \gg 1$ *and* $(x - \hat{x}_0)^2 + (t - \hat{t}_0)^2 = O(1)$, *we have the following solution asymptotics*

$$u_{j,N}(x, t; a_3, a_5, \cdots, a_{2N-1}) = \hat{u}_{j,1}(x - \hat{x}_0, t - \hat{t}_0)\, e^{\mathrm{i}(k_j x + \omega_j t)} + O\left(|a_{2m+1}|^{-1/(2m+1)}\right), \tag{3.100}$$

where $j = 1, 2$. *When* (x, t) *is not in the neighborhood of any of these* N_p *fundamental waves, or* $\sqrt{x^2 + t^2}$ *is larger than* $O\left(|a_{2m+1}|^{1/(2m+1)}\right)$, *then the solution* $[u_{1,N}(x, t), u_{2,N}(x, t)]$ *asymptotically approaches the constant-amplitude background* $[\rho_1 e^{\mathrm{i}(k_1 x + \omega_1 t)}, \rho_2 e^{\mathrm{i}(k_2 x + \omega_2 t)}]$ *as* $|a_{2m+1}| \to \infty$.

2. *In the neighborhood of the origin, where* $x^2 + t^2 = O(1)$, $[u_{1,N}(x, t), u_{2,N}(x, t)]$ *is approximately a lower* N_0*-th order rogue wave* $[u_{1,N_0}(x, t), u_{2,N_0}(x, t)]$, *where* N_0 *is determined from* (N, m) *by Eq. (3.11),* $0 \le N_0 \le N - 2$, *and* $[u_{1,N_0}(x, t), u_{2,N_0}(x, t)]$ *is given by Lemma 3.2 with its new internal parameters* $(\hat{a}_1, \hat{a}_3, \cdots, \hat{a}_{2N_0-1})$ *related to the original parameters of* $[u_{1,N}(x, t), u_{2,N}(x, t)]$ *as*

$$\hat{a}_{2r-1} = a_{2r-1} + (N - N_0)\, s_{2r-1}, \quad r = 1, 2, \cdots, N_0. \tag{3.101}$$

The error of this lower-order rogue wave approximation is $O(|a_{2m+1}|^{-1})$. *Expressed mathematically, when* $|a_{2m+1}| \gg 1$ *and* $x^2 + t^2 = O(1)$,

$$u_{j,N}(x, t; a_1, a_3, a_5, \cdots, a_{2N-1}) = u_{j,N_0}(x, t; \hat{a}_1, \hat{a}_3, \hat{a}_5, \cdots, \hat{a}_{2N_0-1}) + O\left(|a_{2m+1}|^{-1}\right), \tag{3.102}$$

where $j = 1, 2$. *Note that* $a_1 = 0$ *in the original rogue wave* $[u_{1,N}(x,t), u_{2,N}(x,t)]$, *but its counterpart* $\hat{a}_1$ *in the lower-order rogue wave* $[u_{1,N_0}(x,t), u_{2,N_0}(x,t)]$ *will not be zero. If* $N_0 = 0$, *then there will not be such a lower-order rogue wave in the neighborhood of the origin, and the solution* $[u_{1,N}(x,t), u_{2,N}(x,t)]$ *asymptotically approaches the constant-amplitude background* $[\rho_1 e^{\mathrm{i}(k_1 x+\omega_1 t)}, \rho_2 e^{\mathrm{i}(k_2 x+\omega_2 t)}]$ *there as* $|a_{2m+1}| \to \infty$.

The proof of this theorem is along similar lines as the proofs of Theorems 3.2–3.3 for the NLS equation and will be omitted here (see Yang and Yang (2021b) for details).

Comparison Between Predictions and True Solutions

Our prediction from Theorem 3.6 for Manakov rogue patterns can be assembled into the formulae

$$\left|u_{j,N}(x,t)\right| \approx \left|u_{j,N_0}(x,t)\right| + \sum_{k=1}^{N_p} \left(\left| \hat{u}_{j,1}(x-\hat{x}_0^{(k)}, t-\hat{t}_0^{(k)}) \right| - \rho_j \right), \quad j = 1, 2, \tag{3.103}$$

where $[u_{1,N_0}(x,t), u_{2,N_0}(x,t)]$ is the lower-order rogue wave at the center whose new internal parameters $(\hat{a}_1, \hat{a}_3, \cdots, \hat{a}_{2N_0-1})$ are given by Eq. (3.101), the functions $[\hat{u}_{1,1}(x,t), \hat{u}_{2,1}(x,t)]$ are the fundamental Manakov rogue wave given in Eqs. (3.95)–(3.96), with their positions $(\hat{x}_0^{(k)}, \hat{t}_0^{(k)})$ given by Eq. (3.98) for every one of the nonzero simple roots $z_0^{(k)}$ of $Q_N^{[m]}(z)$, and N_p is the number of such fundamental rogue waves whose value is given by Eq. (3.12). Since the Manakov waves have two components, to show both components, we will make the prediction and comparison for $N = 5$ only. With the system and background parameters chosen as

$$\epsilon_1 = 1, \quad \epsilon_2 = 1, \quad k_1 = \frac{1}{2}, \quad k_2 = -\frac{1}{2}, \quad \rho_1 = 1, \quad \rho_2 = 1, \quad p_0 = \frac{1}{2}\sqrt{1+2\mathrm{i}}, \tag{3.104}$$

and with the large internal parameter a_{2m+1} taken as

$$(a_3, a_5, a_7, a_9) = (40, 400, 3000, 20{,}000) \tag{3.105}$$

respectively, and with the other internal parameters set as zero, the predicted rogue solutions (3.103) are plotted in Fig. 3.10.

Now, we compare these predicted fifth-order Manakov rogue patterns to the true solutions. Under identical system and internal parameter choices and (x,t) intervals as those in Fig. 3.10, the true Manakov rogue patterns are displayed in Fig. 3.11. It is seen that the true rogue patterns closely mimic the predicted ones on all major aspects such as the overall shapes, orientations, and center-rogue-wave profiles.

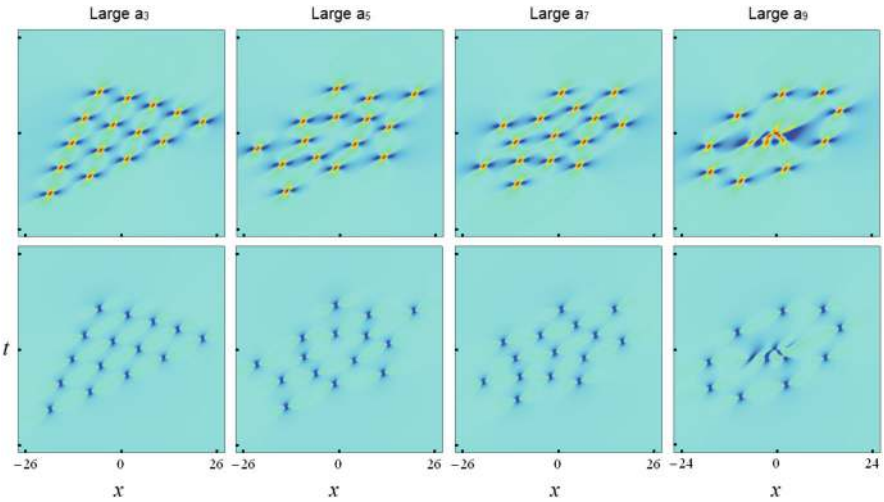

Fig. 3.10 Predicted patterns of fifth-order rogue waves in the Manakov equations under system parameters (3.104) (upper row: $|u_{1,5}|$; lower row: $|u_{2,5}|$). The large internal parameter is as shown in Eq. (3.105), i.e., $a_3 = 40$ in the first column, $a_5 = 400$ in the second column, $a_7 = 3000$ in the third column, $a_9 = 20{,}000$ in the fourth column, and the other internal parameters are set as zero

Some minor differences do exist, such as the three sides of the triangular true-rogue patterns in the first column of Fig. 3.11 are a little more curvy than the predicted ones in the first column of Fig. 3.10. But those differences will diminish if the large parameter a_3 in those panels gets larger. Quantitatively, we have also verified the order of accuracy of our analytical predictions as stated in Theorem 3.6, with details omitted.

3.1.6 Three-Wave Resonant Interaction System

The general (1+1)-dimensional three-wave resonant interaction system is

$$\left.\begin{aligned}(\partial_t + c_1\partial_x)\,u_1 &= \epsilon_1 u_2^* u_3^*,\\ (\partial_t + c_2\partial_x)\,u_2 &= \epsilon_2 u_1^* u_3^*,\\ (\partial_t + c_3\partial_x)\,u_3 &= \epsilon_3 u_1^* u_2^*,\end{aligned}\right\} \tag{3.106}$$

where (c_1, c_2, c_3) are group velocities of the three waves, and $(\epsilon_1, \epsilon_2, \epsilon_3)$ are real-valued nonlinear coefficients which can be normalized to ± 1 with $\epsilon_1 = 1$. To remove ambiguity, we also order the three group velocities as $c_1 > c_2 > c_3$, and make $c_3 = 0$ by choosing a coordinate system that moves with velocity c_3.

Under boundary conditions of

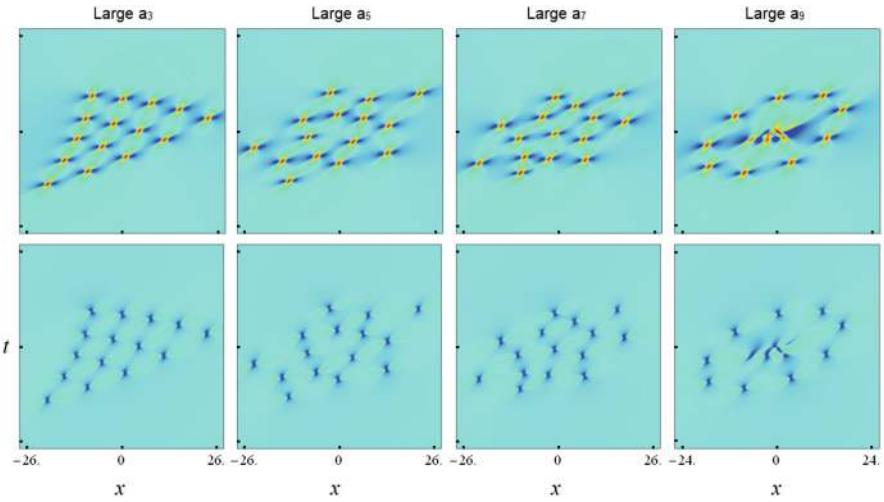

Fig. 3.11 True fifth-order Manakov rogue patterns for system parameters, internal parameters and (x, t) intervals the same as those in the theoretically predicted patterns shown in Fig. 3.10

$$\left.\begin{array}{ll} u_1(x,t) \to \rho_1 e^{\mathrm{i}(k_1 x+\omega_1 t)}, & x,t \to \pm\infty, \\ u_2(x,t) \to \rho_2 e^{\mathrm{i}(k_2 x+\omega_2 t)}, & x,t \to \pm\infty, \\ u_3(x,t) \to \mathrm{i}\rho_3 e^{-\mathrm{i}[(k_1+k_2)x+(\omega_1+\omega_2)t]}, & x,t \to \pm\infty, \end{array}\right\} \tag{3.107}$$

where background parameters ρ_j, k_j, ω_j satisfy algebraic conditions (2.694) in Sect. 2.10, rogue waves in the above three-wave system corresponding to a simple root of a certain algebraic equation have been given in Theorem 2.13 of Sect. 2.10. The τ functions of those rogue waves have index jumps of 2 in their matrix elements, and they contain free complex parameters $a_3, a_5, \ldots, a_{2N-1}$.

Suppose $|a_{2m+1}|$ is large, where $1 \le m \le N-1$, and the other parameters are $O(1)$. Then our results on the large-a_{2m+1} asymptotics of those rogue waves in Theorem 2.13 are summarized in the following theorem.

Theorem 3.7 *For the rogue wave* $[u_{1,N}(x,t), u_{2,N}(x,t), u_{3,N}(x,t)]$ *of the three-wave system in Theorem 2.13, when* $|a_{2m+1}|$ *is large and the other internal parameters* $O(1)$*, then the following statements hold.*

1. *If nonzero roots of the Yablonskii-Vorob'ev hierarchy polynomial* $Q_N^{[m]}(z)$ *are all simple, then far away from the origin, with* $\sqrt{x^2+t^2} = O\left(|a_{2m+1}|^{1/(2m+1)}\right)$*, this* $[u_{1,N}(x,t), u_{2,N}(x,t), u_{3,N}(x,t)]$ *asymptotically would split into* N_p *fundamental rogue waves, where* N_p *is given in Eq. (3.12). These fundamental rogue waves are* $[\hat{u}_{1,1}(x-\hat{x}_0, t-\hat{t}_0)\, e^{\mathrm{i}(k_1 x+\omega_1 t)}$, $\hat{u}_{2,1}(x-\hat{x}_0, t-\hat{t}_0)\, e^{\mathrm{i}(k_2 x+\omega_2 t)}$, $\hat{u}_{3,1}(x-\hat{x}_0, t-\hat{t}_0)\, e^{-\mathrm{i}[(k_1+k_2)x+(\omega_1+\omega_2)t]}]$*, where functions* $[\hat{u}_{1,1}(x,t), \hat{u}_{2,1}(x,t), \hat{u}_{3,1}(x,t)]$ *are given in Eq. (2.772) of Sect. 2.10, and positions* $(\hat{x}_0, \hat{t}_0)$ *of these fundamental rogue waves are given by*

$$\hat{x}_0 = \frac{\Im\left[\frac{z_0\Omega - \Delta_M}{c_1\beta_1 - c_2\alpha_1}\right]}{\Im\left[\frac{\alpha_1-\beta_1}{c_1\beta_1-c_2\alpha_1}\right]}, \quad \hat{t}_0 = \frac{\Im\left[\frac{z_0\Omega - \Delta_M}{\alpha_1-\beta_1}\right]}{\Im\left[\frac{c_1\beta_1-c_2\alpha_1}{\alpha_1-\beta_1}\right]}, \tag{3.108}$$

$\Omega = \left(-\frac{2m+1}{2^{2m}}a_{2m+1}\right)^{\frac{1}{2m+1}}$, z_0 is any of the N_p non-zero simple roots of $Q_N^{[m]}(z)$, and $\Delta_M = (N-1)s_1$. The error of this fundamental rogue wave approximation is $O(|a_{2m+1}|^{-1/(2m+1)})$. Expressed mathematically, when $|a_{2m+1}| \gg 1$ and $(x-\hat{x}_0)^2 + (t-\hat{t}_0)^2 = O(1)$, we have the following solution asymptotics

$$u_{j,N}(x,t;a_3,a_5,\cdots,a_{2N-1}) = \hat{u}_{j,1}(x-\hat{x}_0, t-\hat{t}_0)\, e^{\mathrm{i}(k_j x+\omega_j t)} + O\left(|a_{2m+1}|^{-1/(2m+1)}\right), \quad j=1,2,3. \tag{3.109}$$

When (x,t) is not in the neighborhood of any of these N_p fundamental waves, or $\sqrt{x^2+t^2}$ is larger than $O\left(|a_{2m+1}|^{1/(2m+1)}\right)$, then $[u_{1,N}(x,t), u_{2,N}(x,t), u_{3,N}(x,t)]$ would asymptotically approach the constant-amplitude background (3.107) as $|a_{2m+1}| \to \infty$.

2. *In the neighborhood of the origin, where $x^2+t^2 = O(1)$, this N-th order rogue wave $[u_{1,N}(x,t), u_{2,N}(x,t), u_{3,N}(x,t)]$ is approximately a lower N_0-th order rogue wave $[u_{1,N_0}(x,t), u_{2,N_0}(x,t), u_{3,N_0}(x,t)]$, where N_0 is determined from (N,m) by Eq. (3.11), $0 \le N_0 \le N-2$, and $[u_{1,N_0}(x,t), u_{2,N_0}(x,t), u_{3,N_0}(x,t)]$ is given by Theorem 2.13 with its new internal parameters $(\hat{a}_1, \hat{a}_3, \cdots, \hat{a}_{2N_0-1})$ related to the original parameters of $[u_{1,N}(x,t), u_{2,N}(x,t), u_{3,N}(x,t)]$ as*

$$\hat{a}_{2r-1} = a_{2r-1} + (N-N_0)\, s_{2r-1}, \quad r = 1,2,\cdots,N_0. \tag{3.110}$$

The error of this lower-order rogue wave approximation is $O(|a_{2m+1}|^{-1})$. Expressed mathematically, when $|a_{2m+1}| \gg 1$ and $x^2+t^2 = O(1)$,

$$u_{j,N}(x,t;a_1,a_3,a_5,\cdots,a_{2N-1}) = u_{j,N_0}(x,t;\hat{a}_1,\hat{a}_3,\hat{a}_5,\cdots,\hat{a}_{2N_0-1}) + O\left(|a_{2m+1}|^{-1}\right), \quad j=1,2,3. \tag{3.111}$$

Note that $a_1 = 0$ in the original rogue wave $[u_{1,N}(x,t), u_{2,N}(x,t), u_{3,N}(x,t)]$, but its counterpart $\hat{a}_1$ in the lower-order rogue wave $[u_{1,N_0}(x,t), u_{2,N_0}(x,t), u_{3,N_0}(x,t)]$ will not be zero. If $N_0 = 0$, then there will not be such a lower-order rogue wave in the neighborhood of the origin, and $[u_{1,N}(x,t), u_{2,N}(x,t), u_{3,N}(x,t)]$ would asymptotically approach the constant-amplitude background (3.107) there as $|a_{2m+1}| \to \infty$.

These results have not been reported before to the authors' knowledge. The proof of this theorem is along similar lines as the proofs of Theorems 3.2–3.3 for the NLS equation and will be omitted here.

Comparison Between Predictions and True Solutions

Our prediction from Theorem 3.7 on rogue patterns in the three-wave system can be assembled into the formulae

$$\left|u_{j,N}(x,t)\right| \approx \left|u_{j,N_0}(x,t)\right| + \sum_{k=1}^{N_p} \left(\left| \hat{u}_{j,1}(x-\hat{x}_0^{(k)}, t-\hat{t}_0^{(k)}) \right| - \rho_j \right), \quad j=1,2,3, \tag{3.112}$$

where $\{u_{j,N_0}(x,t)(j=1,2,3)\}$ is the lower-order rogue wave at the center whose new internal parameters $(\hat{a}_1, \hat{a}_3, \cdots, \hat{a}_{2N_0-1})$ are given by Eq. (3.110), the functions $\hat{u}_{j,1}(x,t)\,(j=1,2,3)$ are the fundamental rogue wave given in Eq. (2.772) of Sect. 2.10, with their positions $(\hat{x}_0^{(k)}, \hat{t}_0^{(k)})$ given by Eq. (3.108) for every one of the nonzero simple roots $z_0^{(k)}$ of $Q_N^{[m]}(z)$, and N_p is the number of such fundamental rogue waves whose value is given by Eq. (3.12). For the fourth-order rogue waves $(N=4)$, with the system and background parameters chosen as

$$\left.\begin{array}{l} (\epsilon_1,\epsilon_2,\epsilon_3)=(1,-1,1), \quad (c_1,c_2)=(1,0.5), \\ (\rho_1,\rho_2,\rho_3)=(1,2,1), \quad k_1=0, \quad p_0 \approx 0.521005+0.853553\mathrm{i}, \end{array}\right\} \tag{3.113}$$

and with the large internal parameter a_{2m+1} taken as

$$(a_3,a_5,a_7)=(50,500,5000) \tag{3.114}$$

respectively, and with the other internal parameters set as zero in each case, the predicted rogue solutions (3.112) are plotted in Fig. 3.12.

Now, we compare these predicted fourth-order rogue patterns to the true solutions. Under identical system and internal parameter choices and (x,t) intervals as those in Fig. 3.12, the true rogue patterns are displayed in Fig. 3.13. It is seen that the true rogue patterns closely mimic the predicted ones on all major aspects such as the overall shapes, orientations, and center-rogue-wave profiles. Quantitatively, we have also verified the order of accuracy of our analytical predictions as stated in Theorem 3.7, with details omitted.

3.1.7 Long-Wave-Short-Wave Resonant Interaction System

The long-wave-short-wave (LWSW) resonant interaction system is (see Sect. 2.11)

$$\left.\begin{array}{l} \mathrm{i}S_t - S_{xx} + SL = 0, \\ L_t = -4(|S|^2)_x. \end{array}\right\} \tag{3.115}$$

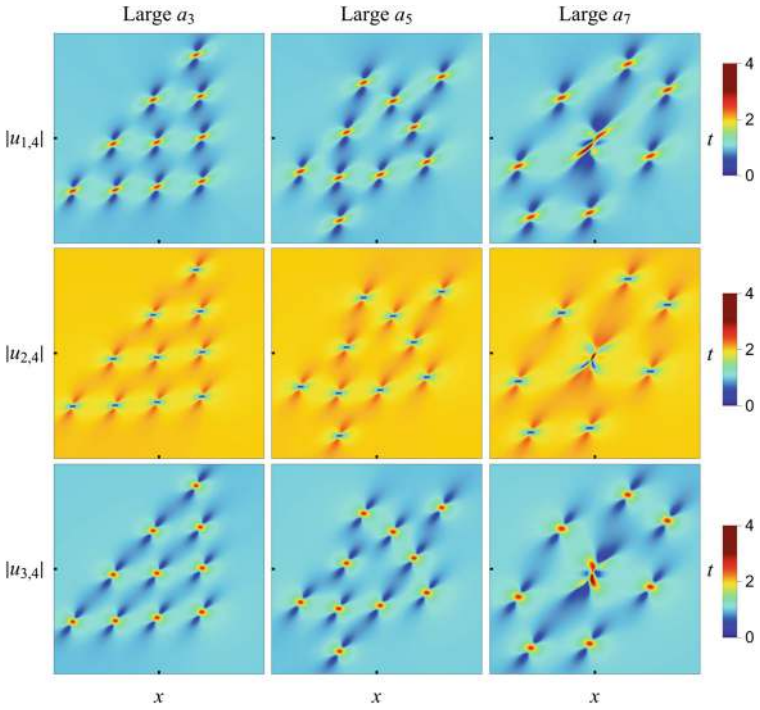

Fig. 3.12 Predicted patterns of fourth-order rogue waves in the three-wave resonant interaction system under system parameters (3.113). The large internal parameter is as shown in Eq. (3.114), i.e., $a_3 = 50$ in the first column, $a_5 = 500$ in the second column, $a_7 = 5000$ in the third column, and the other internal parameters are set as zero in each case. The (x, t) intervals in the three columns are $-15 \le x, t \le 15$, $-14 \le x, t \le 14$, and $-12 \le x, t \le 12$, respectively

Under the boundary conditions of

$$S(x,t) \to e^{\mathrm{i}(\alpha x+\alpha^2 t)}, \quad L(x,t) \to 0, \quad x,t \to \pm\infty, \tag{3.116}$$

where α is a real background wavenumber parameter, rogue waves in this system have been presented in Theorem 2.16 of Sect. 2.11. These rogue waves contain free complex parameters $a_3, a_5, \ldots, a_{2N-1}$. When one of these complex parameters is large, rogue patterns in the LWSW system are given in the following theorem.

Theorem 3.8 *For the rogue wave* $[S_N(x,t), L_N(x,t)]$ *in the LWSW system (3.115) in Theorem 2.16, when* $|a_{2m+1}|$ *is large and the other internal parameters* $O(1)$*, then the following statements hold.*

1. *If nonzero roots of the Yablonskii-Vorob'ev hierarchy polynomial* $Q_N^{[m]}(z)$ *are all simple, then far away from the origin, with* $\sqrt{x^2+t^2} = O\left(|a_{2m+1}|^{1/(2m+1)}\right)$*, this* $[S_N(x,t), L_N(x,t)]$ *asymptotically would split into* N_p *fundamental rogue*

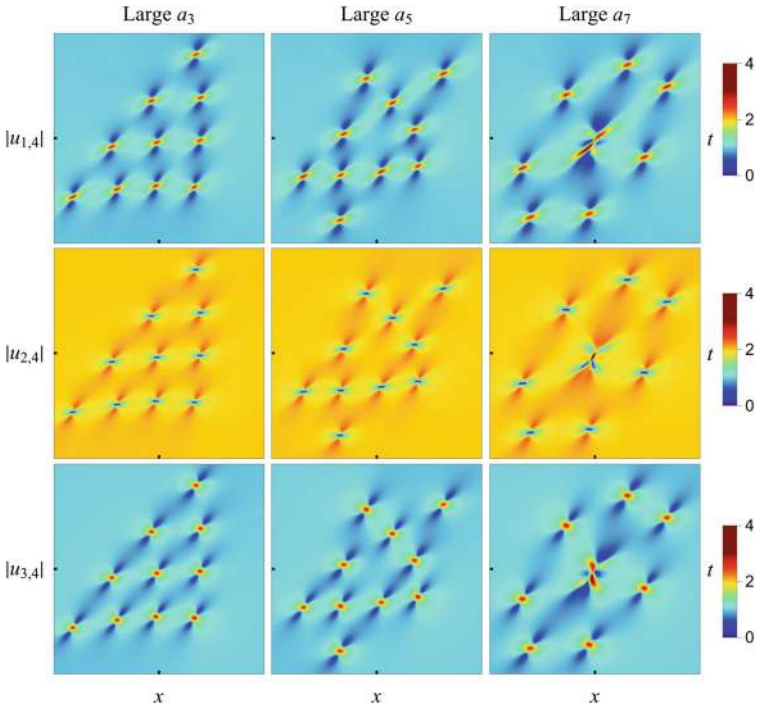

Fig. 3.13 True fourth-order rogue patterns in the three-wave resonant interaction system for system parameters, internal parameters and (x, t) intervals the same as those in the theoretically predicted patterns shown in Fig. 3.12

waves, where N_p is given in Eq. (3.12). These fundamental rogue waves are $\left[\hat{S}_1(x-\hat{x}_0, t-\hat{t}_0)\, e^{i(\alpha x+\alpha^2 t)},\ \hat{L}_1(x-\hat{x}_0, t-\hat{t}_0)\right]$, *where*

$$\hat{S}_1(x,t) = \frac{(p_1 x - 2p_0 p_1 i t + \theta_1)\left(p_1^* x + 2p_0^* p_1^* i t - \theta_1^*\right) + \frac{|p_1|^2}{(p_0+p_0^*)^2}}{|p_1 x - 2p_0 p_1 i t|^2 + \frac{|p_1|^2}{(p_0+p_0^*)^2}}, \quad (3.117)$$

$$\hat{L}_1(x,t) = -2\partial_x^2 \ln\left[|p_1 x - 2p_0 p_1 i t|^2 + \frac{|p_1|^2}{(p_0+p_0^*)^2}\right], \quad (3.118)$$

$\theta_1 = p_1/(p_0 - i\alpha)$, *and their positions* $(\hat{x}_0, \hat{t}_0)$ *are given by*

$$\hat{x}_0 = \frac{1}{\Re(\frac{p_1}{\alpha_1})}\Re\left[\frac{z_0\Omega - \Delta}{\alpha_1}\right], \quad \hat{t}_0 = -\frac{1}{\Re(\frac{\alpha_1}{p_1})}\Im\left[\frac{z_0\Omega - \Delta}{p_1}\right], \quad (3.119)$$

$\Omega = \left(-\frac{2m+1}{2^{2m}} a_{2m+1}\right)^{\frac{1}{2m+1}}$, z_0 *is any of the* N_p *non-zero simple roots of* $Q_N^{[m]}(z)$, *and* $\Delta = (N-1)s_1$. *The error of this fundamental rogue wave approximation is* $O(|a_{2m+1}|^{-1/(2m+1)})$. *Expressed mathematically, when* $|a_{2m+1}| \gg 1$ *and* $(x - \hat{x}_0)^2 + (t - \hat{t}_0)^2 = O(1)$, *we have the following solution asymptotics*

$$S_N(x,t;a_3,a_5,\cdots,a_{2N-1}) = \hat{S}_1(x-\hat{x}_0, t-\hat{t}_0)\, e^{i(\alpha x+\alpha^2 t)} + O\left(|a_{2m+1}|^{-1/(2m+1)}\right),$$

$$L_N(x,t;a_3,a_5,\cdots,a_{2N-1}) = \hat{L}_1(x-\hat{x}_0, t-\hat{t}_0) + O\left(|a_{2m+1}|^{-1/(2m+1)}\right).$$

When (x,t) *is not in the neighborhood of any of these* N_p *fundamental waves, or* $\sqrt{x^2+t^2}$ *is larger than* $O\left(|a_{2m+1}|^{1/(2m+1)}\right)$, *then* $[S_N(x,t), L_N(x,t)]$ *asymptotically approaches the constant-amplitude background* $[e^{\mathrm{i}(\alpha x+\alpha^2 t)},\ 0]$ *as* $|a_{2m+1}| \to \infty$.

2. *In the neighborhood of the origin, where* $x^2 + t^2 = O(1)$, $[S_N(x,t), L_N(x,t)]$ *is approximately a lower* N_0*-th order rogue wave* $[S_{N_0}(x,t), L_{N_0}(x,t)]$, *where* N_0 *is determined from* (N,m) *by Eq. (3.11),* $0 \le N_0 \le N-2$, *and new internal parameters* $(\hat{a}_1, \hat{a}_3, \cdots, \hat{a}_{2N_0-1})$ *in this* N_0*-th order rogue wave are related to the original internal parameters of* $[S_N(x,t), L_N(x,t)]$ *as*

$$\hat{a}_{2r-1} = a_{2r-1} + (N-N_0)\, s_{2r-1}, \quad r = 1,2,\cdots,N_0. \tag{3.120}$$

The error of this lower-order rogue wave approximation is $O(|a_{2m+1}|^{-1})$. *Expressed mathematically, when* $|a_{2m+1}| \gg 1$ *and* $x^2 + t^2 = O(1)$,

$$S_N(x,t;a_1,a_3,a_5,\cdots,a_{2N-1}) = S_{N_0}(x,t;\hat{a}_1,\hat{a}_3,\hat{a}_5,\cdots,\hat{a}_{2N_0-1}) + O\left(|a_{2m+1}|^{-1}\right),$$

$$L_N(x,t;a_1,a_3,a_5,\cdots,a_{2N-1}) = L_{N_0}(x,t;\hat{a}_1,\hat{a}_3,\hat{a}_5,\cdots,\hat{a}_{2N_0-1}) + O\left(|a_{2m+1}|^{-1}\right).$$

Note that $a_1 = 0$ *in the original rogue wave* $[S_N(x,t), L_N(x,t)]$, *but its counterpart* $\hat{a}_1$ *in the lower-order rogue wave* $[S_{N_0}(x,t), L_{N_0}(x,t)]$ *will not be zero. If* $N_0 = 0$, *then there will not be such a lower-order rogue wave in the neighborhood of the origin, and* $[S_N(x,t), L_N(x,t)]$ *asymptotically would approach the constant-amplitude background* $[e^{i(\alpha x+\alpha^2 t)},\ 0]$ *there as* $|a_{2m+1}| \to \infty$.

These results have not been reported before to the authors' knowledge. The proof of this theorem is along similar lines as the proofs of Theorems 3.2–3.3 for the NLS equation and will be omitted here.

Comparison Between Predictions and True Solutions

Our prediction for rogue patterns in $S_N(x,t)$ from Theorem 3.8 can be assembled into the formulae

$$|S_N(x,t)| \approx \left|S_{N_0}(x,t)\right| + \sum_{k=1}^{N_p} \left(\left| \hat{S}_1(x-\hat{x}_0^{(k)}, t-\hat{t}_0^{(k)}) \right| - 1 \right), \tag{3.121}$$

where $S_{N_0}(x,t)$ is the lower-order rogue wave at the center whose new internal parameters $(\hat{a}_1, \hat{a}_3, \cdots, \hat{a}_{2N_0-1})$ are given by Eq. (3.120), the function $\hat{S}_1(x,t)$ is the fundamental rogue wave given in Eq. (3.117), with their positions $(\hat{x}_0^{(k)}, \hat{t}_0^{(k)})$ given by Eq. (3.119) for every one of the nonzero simple roots $z_0^{(k)}$ of $Q_N^{[m]}(z)$, and N_p is the number of such fundamental rogue waves whose value is given by Eq. (3.12). A similar prediction formula for $L_N(x,t)$ can also be written down.

Now, we compare these predictions with true solutions for fourth-order rogue waves ($N = 4$). For this purpose, we take $\alpha = 1/2$ and the plus sign in p_0 from Eq. (2.813) in Sect. 2.11. We also take the large a_{2m+1} parameter respectively as

$$a_3 = -30, \quad a_5 = -500, \quad a_7 = -5000, \tag{3.122}$$

with the other internal parameters set as zero in each case. True $|S_4(x,t)|$ solutions for these parameter choices are displayed in the upper row of Fig. 3.14. The predicted solutions from Eq. (3.121) are displayed in the lower row of Fig. 3.14. It is seen that the predicted rogue patterns closely match true rogue patterns on all major aspects such as the overall shapes, orientations, and center-rogue-wave profiles. Quantitatively, we have also verified the order of accuracy of our analytical predictions as stated in Theorem 3.8, with details omitted.

3.1.8 Ablowitz-Ladik Equation

The Ablowitz-Ladik (AL) equation is

$$\mathrm{i}\frac{d}{dt}u_n = (1+\epsilon|u_n|^2)(u_{n+1}+u_{n-1}), \tag{3.123}$$

where $\epsilon = \pm 1$. Its general N-th order rogue waves $u_n^{[N]}(t)$ under boundary conditions

$$u_n(t) \to \frac{\rho}{\sqrt{1-\rho^2}} e^{\mathrm{i}(\theta n - \omega t)}, \quad n, t \to \pm\infty, \tag{3.124}$$

have been presented in Theorem 2.9 of Sect. 2.8. Here, ρ, θ are real background parameters and $\omega = 2\cos\theta/(1-\rho^2)$. These rogue waves $u_n^{[N]}(t)$ contain free

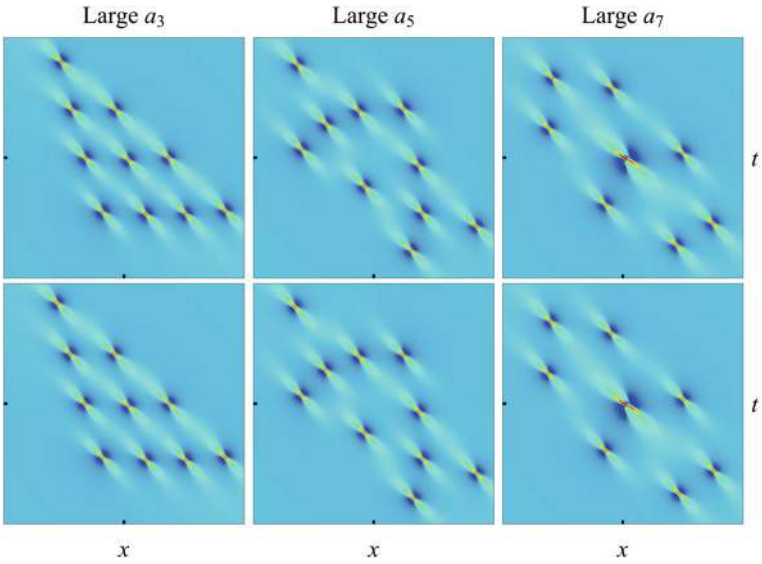

Fig. 3.14 Comparison between true rogue solutions $|S_4(x,t)|$ (upper row) and their analytical predictions (lower row) in the long-wave-short-wave interaction system (3.115) with $\alpha = 1/2$, $p_0 \approx 0.844701 + 0.848715\mathrm{i}$ and parameters (a_3, a_5, a_7) from the left to right columns as $(-30, 0, 0)$, $(0, -500, 0)$, and $(0, 0, -5000)$, respectively. In all panels, $-27 \le x \le 27$, $-11 \le t \le 11$

internal real parameter $\Re(a_1)$ and complex parameters $a_3, a_5, \ldots, a_{2N-1}$ (note that $\Im(a_1)$ has been normalized to zero through a time shift). The real parameter $\Re(a_1)$ can be kept $O(1)$ through a lattice shift (i.e., a shift of the lattice index n). Then, when one of the complex internal parameters $\{a_3, a_5, \ldots, a_{2N-1}\}$ is large, rogue patterns in the AL system are given by the following theorem.

Theorem 3.9 *For the N-th order rogue wave $u_n^{[N]}(t)$ in the AL equation (3.123) with $\Im(a_1) = 0$, when $|a_{2m+1}|$ is large ($m \ge 1$) and the other internal parameters $O(1)$, then the following statements hold.*

1. *If nonzero roots of the Yablonskii-Vorob'ev hierarchy polynomial $Q_N^{[m]}(z)$ are all simple, then far away from the origin, with $\sqrt{t^2+n^2} = O\left(|a_{2m+1}|^{1/(2m+1)}\right)$, the N-th order rogue wave $u_n^{[N]}(t)$ splits into N_p fundamental rogue waves, where N_p is given in Eq. (3.12). These fundamental rogue waves are $e^{i(\theta n - \omega t)}\hat{u}_{n-\hat{n}_0}(t-\hat{t}_0)$, where*

$$\hat{u}_n(t) = \frac{\rho}{\sqrt{1-\rho^2}}\left[1 + \frac{2i\rho^2\omega t - 1}{\rho^2\,(n+\omega t\tan\theta)^2 + \rho^4\omega^2 t^2 + \frac{1}{4}(1-\rho^2)}\right], \tag{3.125}$$

and their temporal and spatial positions $(\hat{t}_0, \hat{n}_0)$ *are given by*

$$\hat{t}_0 = \frac{(1+\rho)(1-\rho^2)}{2\rho^2 \cos\theta} \Im\left(z_0 \Omega\right), \tag{3.126}$$

$$\hat{n}_0 = \frac{1+\rho}{\rho}\left[\Re\left(z_0\Omega\right) - \frac{\tan\theta}{\rho}\Im\left(z_0\Omega\right) - \Re(a_1)\right], \tag{3.127}$$

$\Omega = \left(-\frac{2m+1}{2^{2m}} a_{2m+1}\right)^{\frac{1}{2m+1}}$, *and* z_0 *is any one of the* N_p *simple nonzero roots of* $Q_N^{[m]}(z)$. *The error of this approximation is* $O(|a_{2m+1}|^{-1/(2m+1)})$. *Expressed mathematically, when* $(t-\hat{t}_0)^2 + (n-\hat{n}_0)^2 = O(1)$, *we have the following solution asymptotics*

$$u_n^{[N]}(t; a_1, a_3, a_5, \cdots, a_{2N-1}) = e^{i(\theta n - \omega t)} \hat{u}_{n-\hat{n}_0}(t-\hat{t}_0) + O\left(|a_{2m+1}|^{-1/(2m+1)}\right). \tag{3.128}$$

When (t, n) *is not in the neighborhood of any of these* N_p *fundamental rogue waves, or* $\sqrt{t^2+n^2}$ *is larger than* $O\left(|a_{2m+1}|^{1/(2m+1)}\right)$, $u_n^{[N]}(t)$ *asymptotically approaches the constant background* $\frac{\rho}{\sqrt{1-\rho^2}} e^{i(\theta n - \omega t)}$ *as* $|a_{2m+1}| \to \infty$.

2. *In the neighborhood of the origin, where* $t^2 + n^2 = O(1)$, $u_n^{[N]}(t)$ *is approximately a lower* N_0*-th order rogue wave* $u_n^{[N_0]}(t)$, *where* N_0 *is determined from* (N, m) *by Eq. (3.11),* $0 \le N_0 \le N-2$, *and the internal parameters* $a_1, a_3, a_5, \cdots, a_{2N_0-1}$ *in* $u_n^{[N_0]}(t)$ *are the first* N_0 *values in the parameter set* $(a_1, a_3, a_5, \cdots, a_{2N-1})$ *of the original rogue wave* $u_n^{[N]}(t)$. *The error of this lower-order rogue wave approximation* $u_n^{[N_0]}(t)$ *is* $O(|a_{2m+1}|^{-1})$. *Expressed mathematically, when* $t^2 + n^2 = O(1)$,

$$u_n^{[N]}(t; a_1, a_3, a_5, \cdots, a_{2N-1}) = u_n^{[N_0]}(t; a_1, a_3, a_5, \cdots, a_{2N_0-1}) + O\left(|a_{2m+1}|^{-1}\right). \tag{3.129}$$

If $N_0 = 0$, *then there will not be such a lower-order rogue wave in the neighborhood of the origin, and* $u_n^{[N]}(t)$ *asymptotically approaches the constant background* $\frac{\rho}{\sqrt{1-\rho^2}} e^{i(\theta n - \omega t)}$ *there as* $|a_{2m+1}| \to \infty$.

Since the results in this theorem have not been reported before, and the AL equation is very different from the other fully-continuous integrable equations covered in earlier sections, we will give a proof of this theorem here.

Proof of Theorem 3.9 The proof of this theorem is along similar lines as proofs of Theorems 3.2–3.3 for the NLS equation. Thus, our proof will be brief.

First, we prove the statement in the outer region. Suppose $|a_{2m+1}|$ is large, where $1 \le m \le N-1$, and the other parameters are $O(1)$. It is easy to see that

$$g_1(\rho) = \frac{\rho}{1+\rho}, \quad g_1(1/\rho) = \frac{1}{1+\rho}, \quad g_2(\rho) = \frac{\rho}{2(1+\rho)^2}. \tag{3.130}$$

Thus,

$$\begin{aligned} x_1^+(n,k,0) &= \frac{\rho}{1+\rho}\left[n + \mathrm{i}t\left(\frac{e^{-\mathrm{i}\theta}}{1-\rho} - \frac{e^{\mathrm{i}\theta}}{1+\rho}\right) + \frac{1+\rho}{\rho}\Re(a_1) - \frac{k}{\rho}\right] \\ &= \frac{\rho}{1+\rho}\left[n - n_{0a} + \mathrm{i}t\left(\frac{e^{-\mathrm{i}\theta}}{1-\rho} - \frac{e^{\mathrm{i}\theta}}{1+\rho}\right) - \frac{k}{\rho}\right], \end{aligned} \tag{3.131}$$

where $n_{0a} \equiv -(1+\rho)\Re(a_1)/\rho$. Similarly,

$$x_1^-(n,k,0) = \frac{\rho}{1+\rho}\left[n - n_{0a} - \mathrm{i}t\left(\frac{e^{\mathrm{i}\theta}}{1-\rho} - \frac{e^{-\mathrm{i}\theta}}{1+\rho}\right) + \frac{k}{\rho}\right]. \tag{3.132}$$

When $|a_{2m+1}| \gg 1$ and $\sqrt{t^2+n^2} = O\left(|a_{2m+1}|^{1/(2m+1)}\right)$, we have the asymptotics

$$S_j(\boldsymbol{x}^+(n,k,0) + \nu\boldsymbol{s}) = S_j(\boldsymbol{v}^+)\left(1 + O\left(a_{2m+1}^{-2/(2m+1)}\right)\right), \tag{3.133}$$

where

$$\boldsymbol{v}^+ = \left[x_1^+(n,k,0), 0, \cdots, 0, a_{2m+1}, 0, \cdots\right]. \tag{3.134}$$

We can write $S_j(\boldsymbol{v}^+)$ as

$$S_j(\boldsymbol{v}^+) = \Omega^j p_k^{[m]}(z^+), \quad z^+ \equiv \Omega^{-1} x_1^+(n,k,0), \tag{3.135}$$

where Ω is as defined in Theorem 3.9. Thus,

$$S_j(\boldsymbol{x}^+(n,k,0) + \nu\boldsymbol{s}) = \Omega^j p_k^{[m]}(z^+)\left(1 + O\left(a_{2m+1}^{-2/(2m+1)}\right)\right). \tag{3.136}$$

Similarly,

$$S_j(\boldsymbol{x}^-(n,k,0) + \nu\boldsymbol{s}) = \Omega^{*j} p_k^{[m]}(z^-)\left(1 + O\left(a_{2m+1}^{-2/(2m+1)}\right)\right), \tag{3.137}$$

where $z^- \equiv (\Omega^*)^{-1} x_1^-(n,k,0)$. Using these formulae, we find that

$$\begin{aligned} &\det_{1\le i,j\le N}\left[S_{2i-j}(\boldsymbol{x}^+(n,k,0) + (j-1)\boldsymbol{s})\right] \\ &\quad = c_N^{-1}\Omega^{N(N+1)/2} Q_N^{[m]}(z^+)\left(1 + O\left(a_{2m+1}^{-2/(2m+1)}\right)\right), \end{aligned} \tag{3.138}$$

and

$$\det_{1\le i,j\le N}\left[S_{2i-j}(\boldsymbol{x}^-(n,k,0)+(j-1)\boldsymbol{s})\right]$$
$$=c_N^{-1}\Omega^{*N(N+1)/2}Q_N^{[m]}(z^-)\left(1+O\left(a_{2m+1}^{-2/(2m+1)}\right)\right). \tag{3.139}$$

Defining real parameters $\hat{t}_0$ and n_{0b} through the equation

$$z_0\Omega=\frac{\rho}{1+\rho}\left[n_{0b}+\mathrm{i}\hat{t}_0\left(\frac{e^{-\mathrm{i}\theta}}{1-\rho}-\frac{e^{\mathrm{i}\theta}}{1+\rho}\right)\right], \tag{3.140}$$

where z_0 is a root of $Q_N^{[m]}(z)$, then

$$z^+=z_0+\Omega^{-1}\frac{\rho}{1+\rho}\left[n-\hat{n}_0+\mathrm{i}(t-\hat{t}_0)\left(\frac{e^{-\mathrm{i}\theta}}{1-\rho}-\frac{e^{\mathrm{i}\theta}}{1+\rho}\right)-\frac{k}{\rho}\right], \tag{3.141}$$

where $\hat{n}_0=n_{0a}+n_{0b}$. Note that this $\hat{n}_0$ and the above $\hat{t}_0$ can be found to be given in Eqs. (3.126)–(3.127). Similarly,

$$z^-=z_0^*+(\Omega^*)^{-1}\frac{\rho}{1+\rho}\left[n-\hat{n}_0-\mathrm{i}(t-\hat{t}_0)\left(\frac{e^{\mathrm{i}\theta}}{1-\rho}-\frac{e^{-\mathrm{i}\theta}}{1+\rho}\right)+\frac{k}{\rho}\right]. \tag{3.142}$$

Inserting these equations into (3.138) and (3.139), expanding $Q_N^{[m]}(z^\pm)$ around z_0 and z_0^* respectively, and recalling that z_0 is a root of $Q_N^{[m]}(z)$, we get

$$\det_{1\le i,j\le N}\left[S_{2i-j}(\boldsymbol{x}^+(n,k,0)+(j-1)\boldsymbol{s})\right]$$
$$=2^{-N(N-1)/2}c_N^{-1}\Omega^{N(N+1)/2}\left[Q_N^{[m]}\right]'(z_0)$$
$$\times\frac{\rho}{1+\rho}\left[n-\hat{n}_0-\mathrm{i}(t-\hat{t}_0)\left(\frac{e^{\mathrm{i}\theta}}{1-\rho}-\frac{e^{-\mathrm{i}\theta}}{1+\rho}\right)-\frac{k}{\rho}\right]$$
$$\times\left(1+O\left(a_{2m+1}^{-1/(2m+1)}\right)\right), \tag{3.143}$$

and

$$\det_{1\le i,j\le N}\left[S_{2i-j}(\boldsymbol{x}^-(n,k,0)+(j-1)\boldsymbol{s})\right]$$
$$=2^{-N(N-1)/2}c_N^{-1}\Omega^{*N(N+1)/2}\left[Q_N^{[m]}\right]'(z_0^*)$$

$$\times \frac{\rho}{1+\rho}\left[n-\hat{n}_0+\mathrm{i}(t-\hat{t}_0)\left(\frac{e^{-\mathrm{i}\theta}}{1-\rho}-\frac{e^{\mathrm{i}\theta}}{1+\rho}\right)+\frac{k}{\rho}\right]$$
$$\times\left(1+O\left(a_{2m+1}^{-1/(2m+1)}\right)\right). \tag{3.144}$$

Using these formulae and the Laplace expansion [see Eq. (2.77)]

$$\sigma_{n,k,0}=\sum_{0\le\nu_1<\nu_2<\cdots<\nu_N\le 2N-1}\det_{1\le i,j\le N}\left[\frac{1}{2^{\nu_j}}S_{2i-1-\nu_j}(\boldsymbol{x}^+(n,k,0)+\nu_j\boldsymbol{s})\right]$$
$$\times\det_{1\le i,j\le N}\left[\frac{1}{2^{\nu_j}}S_{2i-1-\nu_j}(\boldsymbol{x}^-(n,k,0)+\nu_j\boldsymbol{s})\right], \tag{3.145}$$

we find that the leading order contributions to $\sigma_{n,k,0}$ come from two index choices, one being $\nu=(0,1,\cdots,N-1)$, and the other being $\nu=(0,1,\cdots,N-2,N)$, and their combined contributions are

$$\sigma_{n,k,0}=2^{-N(N-1)}c_N^{-2}\Omega^{N(N+1)}\left|\left[Q_N^{[m]}\right]'(z_0)\right|^2$$
$$\times\frac{\rho^2}{(1+\rho)^2}\left\{\left[n-\hat{n}_0-\mathrm{i}(t-\hat{t}_0)\left(\frac{e^{\mathrm{i}\theta}}{1-\rho}-\frac{e^{-\mathrm{i}\theta}}{1+\rho}\right)-\frac{k}{\rho}\right]\right.$$
$$\left.\times\left[n-\hat{n}_0+\mathrm{i}(t-\hat{t}_0)\left(\frac{e^{-\mathrm{i}\theta}}{1-\rho}-\frac{e^{\mathrm{i}\theta}}{1+\rho}\right)+\frac{k}{\rho}\right]+\frac{1-\rho^2}{4\rho^2}\right\}$$
$$\times\left(1+O\left(a_{2m+1}^{-1/(2m+1)}\right)\right). \tag{3.146}$$

According to our assumption of z_0 being a simple root of $Q_N^{[m]}(z)$, $\left[Q_N^{[m]}\right]'(z_0)\neq 0$. Thus, the above leading order asymptotics of $\sigma_{n,k,0}$ does not vanish. Inserting this asymptotics into the formula $u_n^{[N]}(t)=(\rho/\sqrt{1-\rho^2})e^{\mathrm{i}(\theta n-\omega t)}\sigma_{n,1,0}/\sigma_{n,0,0}$ and simplifying, we then get

$$u_n^{[N]}(t)=e^{\mathrm{i}(\theta n-\omega t)}\hat{u}_{n-\hat{n}_0}(t-\hat{t}_0)+O\left(|a_{2m+1}|^{-1/(2m+1)}\right), \tag{3.147}$$

where $\hat{u}_n(t)$ is as given in Eq. (3.125). This completes the proof in the outer region.

The proof for the inner region is almost identical to that for Theorem 3.3 of the NLS equation. This completes the proof of Theorem 3.9. □

Comparison Between True Rogue Patterns and Analytical Predictions

From Theorem 3.9, we get predictions for rogue patterns in $u_n^{[N]}(t)$, which can be assembled into the formula

$$\left|u_n^{[N]}(t)\right| \approx \left|u_n^{[N_0]}(t)\right| + \sum_{k=1}^{N_p} \left(\left| \hat{u}_{n-\hat{n}_0^{(k)}}(t - \hat{t}_0^{(k)}) \right| - 1 \right), \tag{3.148}$$

where $\hat{u}_n(t)$ is the fundamental AL rogue wave given in Eq. (3.125), their positions $(\hat{n}_0^{(j)}, \hat{t}_0^{(j)})$ given by (3.126)–(3.127) with z_0 being every one of the N_p simple nonzero roots of $Q_N^{[m]}(z)$, and $u_n^{[N_0]}(t)$ is the lower-order rogue wave at the center with its internal parameters $a_3, a_5, \cdots, a_{2N_0-1}$ being the first $N_0 - 1$ values in the parameter set $(a_3, a_5, \cdots, a_{2N-1})$ of the original rogue wave $u_n^{[N]}(t)$.

Now, we compare these predictions with true solutions for the fourth-order rogue waves ($N = 4$). For this purpose, we take $\rho = 0.5$ and $\theta = 0$ in the boundary conditions (3.124). We also take the large a_{2m+1} parameter respectively as

$$a_3 = 30, \quad a_5 = 500 \tag{3.149}$$

with the other internal parameters set as zero in each case. True $|u_n^{[4]}(t)|$ solutions for these parameter choices are displayed in the upper row of Fig. 3.15. The predicted solutions from Eq. (3.148) are displayed in the lower row of Fig. 3.15. It can be seen that the predicted and true patterns match well. Differences between the predicted and true solutions are also visible, but we have verified that such differences would gradually disappear as the $|a_{2m+1}|$ value in these solutions gets larger, which quantitatively confirms the correctness of Theorem 3.9.

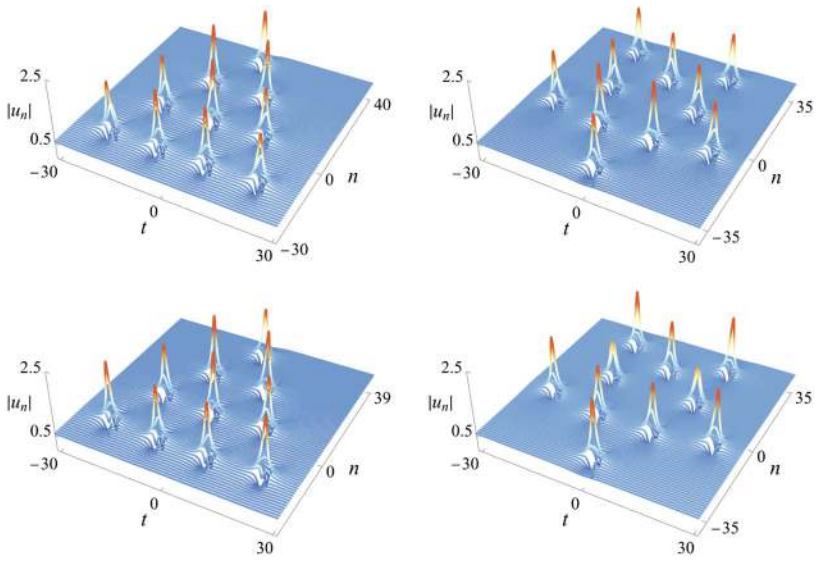

Fig. 3.15 Comparison between true rogue solutions $|u_n^{[4]}(t)|$ (upper row) and their analytical predictions (lower row) in the Ablowitz-Ladik equation (3.123), for parameters $(a_3, a_5, a_7) = (30, 0, 0)$ in the left column and $(0, 500, 0)$ in the right column. The other parameter values are $\rho = 0.5, \theta = 0$, and $\Re(a_1) = 0$

3.1.9 Universality of Rogue Patterns Associated with the Yablonskii-Vorob'ev Polynomial Hierarchy

One can clearly see from theorems in the previous subsections that rogue patterns under the large-parameter limit in these integrable systems have a lot in common. In all cases, the center of the wave pattern is a lower-order rogue wave, and the order of this center rogue wave depends only on the order of the original rogue wave and the index of the large internal parameter. Away from the center, the rogue pattern comprises fundamental rogue waves, whose number is equal to the number of nonzero simple roots of the Yablonskii-Vorob'ev polynomial $Q_N^{[m]}(z)$, and whose (x,t) or (n,t) locations are linearly dependent on the real and imaginary parts of these nonzero simple roots. To put it mathematically, the location $(\hat{x}_0, \hat{t}_0)$ of each fundamental rogue wave inside the rogue structure is given by the real and imaginary parts of each nonzero simple root z_0 of $Q_N^{[m]}(z)$ through a linear transformation

$$\begin{bmatrix} \hat{x}_0 \\ \hat{t}_0 \end{bmatrix} = \mathbf{B} \begin{bmatrix} \Re(z_0) \\ \Im(z_0) \end{bmatrix} + \begin{bmatrix} \Delta_1 \\ \Delta_2 \end{bmatrix}, \tag{3.150}$$

where $\mathbf{B}$ is a constant matrix and (Δ_1, Δ_2) a constant vector (for the Ablowitz-Ladik equation, $\hat{x}_0$ in this transformation will be replaced by its counterpart $\hat{n}_0$). For example, for the NLS equation, we can see from Eq. (3.20) of Theorem 3.2 that

$$\mathbf{B} = \begin{bmatrix} \Re(\Omega) & -\Im(\Omega) \\ \Im(\Omega) & \Re(\Omega) \end{bmatrix}, \qquad \begin{bmatrix} \Delta_1 \\ \Delta_2 \end{bmatrix} = \begin{bmatrix} 0 \\ 0 \end{bmatrix}, \tag{3.151}$$

where $\Omega = [-(2m+1)2^{-2m} a_{2m+1}]^{1/(2m+1)}$. For the GDNLS equations, we can see from Eq. (3.71) of Theorem 3.4 that

$$\mathbf{B} = \begin{bmatrix} \frac{1}{\sqrt{\alpha}}\Re(\Omega) - \frac{\alpha-1}{\alpha}\Im(\Omega) & -\frac{1}{\sqrt{\alpha}}\Im(\Omega) - \frac{\alpha-1}{\alpha}\Re(\Omega) \\ \frac{1}{\alpha}\Im(\Omega) & \frac{1}{\alpha}\Re(\Omega) \end{bmatrix}, \qquad \begin{bmatrix} \Delta_1 \\ \Delta_2 \end{bmatrix} = \begin{bmatrix} 0 \\ 0 \end{bmatrix}. \tag{3.152}$$

For the Boussinesq equation, Eq. (3.78) of Theorem 3.5 gives

$$\mathbf{B} = 2\sqrt{3} \begin{bmatrix} \Im(\Omega) & \Re(\Omega) \\ -\Re(\Omega) & \Im(\Omega) \end{bmatrix}, \qquad \begin{bmatrix} \Delta_1 \\ \Delta_2 \end{bmatrix} = \begin{bmatrix} \Delta_B \\ 0 \end{bmatrix}, \tag{3.153}$$

where Δ_B is provided in Theorem 3.5. For the Manakov system, Eq. (3.98) of Theorem 3.6 gives

$$\mathbf{B} = \frac{1}{\Re(p_0)} \begin{bmatrix} \Re\left(\frac{p_0^* \Omega}{p_1}\right) & -\Im\left(\frac{p_0^* \Omega}{p_1}\right) \\ \frac{1}{2}\Im\left(\frac{\Omega}{p_1}\right) & \frac{1}{2}\Re\left(\frac{\Omega}{p_1}\right) \end{bmatrix}, \qquad \begin{bmatrix} \Delta_1 \\ \Delta_2 \end{bmatrix} = \begin{bmatrix} \Delta_{1M} \\ \Delta_{2M} \end{bmatrix}, \tag{3.154}$$

where $(\Delta_{1M}, \Delta_{2M})$ are provided by Eq. (3.99). This linear transformation can be similarly written down for the other three integrable systems covered in earlier subsections, namely, the three-wave system, the long-wave-short-wave resonant interaction system, and the Ablowitz-Ladik equation. For the massive Thirring model not covered in this section, this linear transformation has been derived by Chen et al. (2023) as well.

It is important to notice that the constant matrix $\mathbf{B}$ and the constant vector (Δ_1, Δ_2) are both independent of the root z_0, which is why (3.150) is a linear transformation from the z-plane to the (x, t) or (n, t) plane. This linear transformation means that the whole rogue pattern formed by fundamental rogue waves in the (x, t) or (n, t) plane is just a linear transformation matrix $\mathbf{B}$ applied to the root structure of the Yablonskii-Vorob'ev polynomial $Q_N^{[m]}(z)$ in the complex z plane, plus a constant position shift (Δ_1, Δ_2).

To get a visual impression of the linear transformation (3.150), we plot in Fig. 3.16 its effects on the root structures of $Q_5^{[m]}(z)$ with $1 \leq m \leq 4$ for the NLS equation, the GDNLS equations, the Boussinesq equation, and the Manakov system. The reader is reminded that these root structures of $Q_5^{[m]}(z)$ have been plotted in the bottom row of Fig. 3.1. In the first row of Fig. 3.16, images of the transformation (3.150) on these root structures are displayed for the NLS equation with the large internal parameter a_{2m+1} respectively as

$$(a_3, a_5, a_7, a_9) = (-20\mathrm{i}, -100\mathrm{i}, -2000\mathrm{i}, -12{,}000\mathrm{i}). \tag{3.155}$$

These parameter values are the same as those in NLS' predicted rogue patterns shown in Fig. 3.3 for $N = 5$. In the second row of Fig. 3.16, images of this transformation are displayed for the GDNLS equations with the background wavenumber $\alpha = 16/9$ and the large internal parameter a_{2m+1} respectively as

$$(a_3, a_5, a_7, a_9) = (-15\mathrm{i}, -250\mathrm{i}, -1000\mathrm{i}, -3000\mathrm{i}). \tag{3.156}$$

These parameter values are the same as those in GDNLS' predicted rogue patterns shown in Fig. 3.6 for $N = 5$. The third row of Fig. 3.16 are images of this transformation for the Boussinesq equation with the large parameter a_{2m+1} respectively as

$$(a_3, a_5, a_7, a_9) = (-5, 20, -80, 200). \tag{3.157}$$

These parameter values are the same as those in Boussinesq' predicted rogue patterns shown in Fig. 3.8 for $N = 5$. In the last row of Fig. 3.16, images of this transformation for the Manakov equations are illustrated under system and background parameter choices in Eq. (3.104), with the large parameter a_{2m+1} as in Eq. (3.105) respectively. These parameter values are the same as those in Manakov's predicted rogue patterns shown in Fig. 3.10 (for $N = 5$).

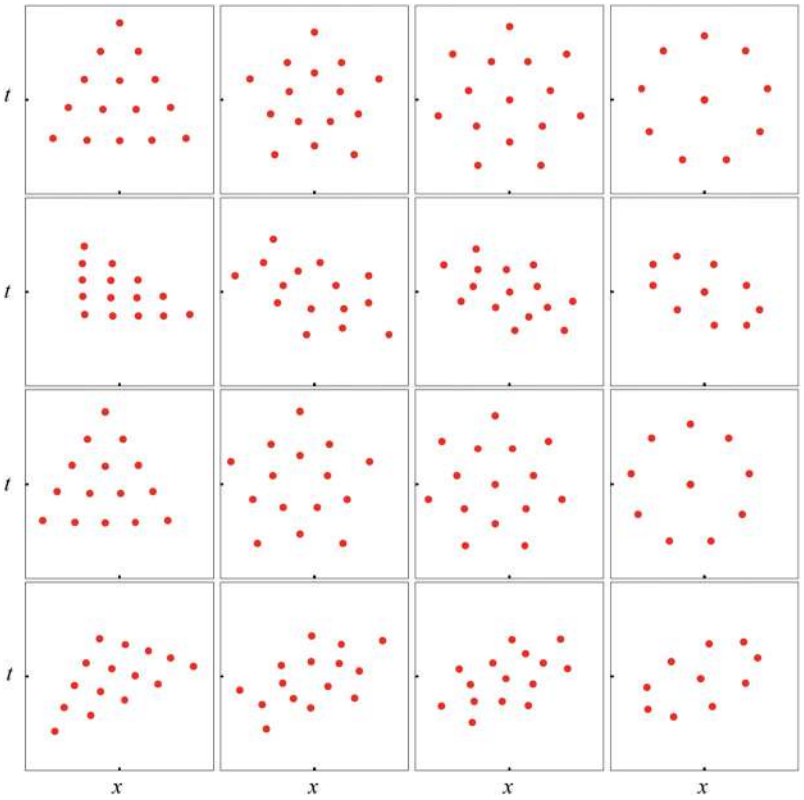

Fig. 3.16 The (x, t) plane images of the linear transformation (3.150) on the root structures of $Q_5^{[m]}(z)$ with $1 \le m \le 4$, for the NLS equation, the GDNLS equations, the Boussinesq equation, and the Manakov system, with the respective large internal parameter a_{2m+1} and other system parameters provided by Eqs. (3.155)–(3.157) and (3.104)–(3.105). First row: images for the NLS equation, where $-15 \le x, t \le 15$. Second row: images for the GDNLS equations, where $-13 \le x, t \le 13$. Third row: images for the Boussinesq equation, where $-35 \le x, t \le 35$. Fourth row: images for the Manakov system, where $-28 \le x, t \le 28$

By comparing these images to the original root structures at the bottom row of Fig. 3.1, we can see that in the NLS and Boussinesq cases, the images have the same shapes of the root structures. In the GDNLS and Manakov cases, however, the images are stretched versions of the root structures. The reasons for these different shapes of images are due to the properties of the underlying transformation matrix **B**.

By comparing these images to the predicted and true rogue patterns shown in Figs. 3.2 and 3.3 and Figs. 3.6, 3.7, 3.8, 3.9, 3.10, and 3.11 under the same parameter values and (x, t) intervals, we can see clearly that the predicted and true rogue patterns are simply the flesh-out of the images of the linear transformation (3.150) on the Yablonskii-Vorob'ev root structures, where the image of each nonzero root is replaced by a fundamental rogue wave, and the image of the zero root is replaced

by a lower-order rogue wave. This fact is true not only for the NLS, GDNLS, Boussinesq and Manakov equations, but also for other integrable equations covered in this section, namely, the three-wave system, the long-wave-short-wave resonant interaction system, and the Ablowitz-Ladik equation. In addition, it has been shown to be true for the massive Thirring model as well (Chen et al. 2023). Furthermore, numerical evidence indicates that this fact should also hold for the Sasa-Satsuma equation and the complex short pulse equation (Wu et al. 2022, Feng et al. 2022a). A common feature of all these integrable systems is that their rogue waves can be expressed by τ functions whose matrix elements are Schur polynomials with index jumps of two. In such cases, rogue patterns in shapes of the Yablonskii-Vorob'ev hierarchy's root structures under linear transformations would always appear, and they constitute a class of universal rogue patterns in integrable systems.

3.2 Rogue Patterns Associated with Adler-Moser Polynomials

The previous section showed that rogue patterns under a single large internal parameter are predicted by root structures of the Yablonskii-Vorob'ev polynomial hierarchy. When multiple internal parameters in rogue wave solutions are large, new rogue patterns would appear, and their shapes could be predicted asymptotically by root structures of Adler-Moser polynomials. We study these rogue patterns below, following Yang and Yang (2024a).

3.2.1 Adler-Moser Polynomials and Their Root Structures

Adler-Moser polynomials were proposed by Adler and Moser (1978), who expressed rational solutions of the Korteweg-de Vries equation in terms of those polynomials. In a different context of point vortex dynamics, it was discovered unexpectedly that the zeros of these polynomials also form stationary vortex configurations when the vortices have the same strength but positive or negative orientations, and the numbers of those positive and negative vortices are consecutive triangular numbers (Aref 2007; Clarkson 2009).

Adler-Moser polynomials $\Theta_N(z)$ can be written as a determinant (Clarkson 2009)

$$\Theta_N(z) = c_N \begin{vmatrix} \theta_1(z) & \theta_0(z) & \cdots & \theta_{2-N}(z) \\ \theta_3(z) & \theta_2(z) & \cdots & \theta_{4-N}(z) \\ \vdots & \vdots & \vdots & \vdots \\ \theta_{2N-1}(z) & \theta_{2N-2}(z) & \cdots & \theta_N(z) \end{vmatrix}, \tag{3.158}$$

where $\theta_k(z)$ are Schur polynomials defined by

$$\sum_{k=0}^{\infty}\theta_k(z)\epsilon^k=\exp\left(z\epsilon+\sum_{j=1}^{\infty}\kappa_j\epsilon^{2j+1}\right), \tag{3.159}$$

$\theta_k(z)\equiv 0$ if $k<0$, $c_N=\prod_{j=1}^{N}(2j-1)!!$, and $(\kappa_1,\kappa_2,\ldots,\kappa_{N-1})$ are arbitrary complex constants. Note that our κ_j constant is slightly different from that in Clarkson (2009) by a factor of $-1/(2j+1)$, and this different parameter definition will be more convenient for our purpose. The determinant in (3.158) is a Wronskian since we can see from Eq. (3.159) that $\theta_k'(z)=\theta_{k-1}(z)$, where the prime denotes differentiation. In addition, these $\Theta_N(z)$ polynomials are monic with degree $N(N+1)/2$, which can be seen by noticing that the highest z term of $\theta_k(z)$ is $z^k/k!$, and the determinant in (3.158) with $\theta_k(z)$ replaced by its highest z term can be explicitly calculated as $z^{N(N+1)/2}$ (Ohta and Yang 2012a). Adler-Moser polynomials reduce to the Yablonskii-Vorob'ev polynomial hierarchy when all κ_j constants are set as zero except for one of them (see Sect. 3.1.1). Thus, Adler-Moser polynomials are generalizations of the Yablonskii-Vorob'ev polynomial hierarchy.

The first few Adler-Moser polynomials are

$$\begin{aligned}
\Theta_1(z)&=z,\\
\Theta_2(z)&=z^3-3\kappa_1,\\
\Theta_3(z)&=z^6-15\kappa_1z^3+45\kappa_2z-45\kappa_1^2,\\
\Theta_4(z)&=z^{10}-45\kappa_1z^7+315\kappa_2z^5-1575\kappa_3z^3\\
&\quad+4725\kappa_1\kappa_2z^2-4725\kappa_1^3z-4725\kappa_2^2+4725\kappa_1\kappa_3.
\end{aligned}$$

Root structures of Adler-Moser polynomials are important to us, since we will link them to rogue wave patterns in the later text. Due to the free complex parameters $\{\kappa_j\}$ in them, their root structures will be understandably very diverse—much more diverse than root structures of Yablonskii-Vorob'ev hierarchy polynomials. Indeed, when setting all $\{\kappa_j\}$ as zero except for one of them, we get root structures of Yablonskii-Vorob'ev hierarchy polynomials which are in the shape of triangles, pentagons, heptagons, and so on. When we continuously change those $\{\kappa_j\}$ values, we will get root structures which smoothly deform from one type of Yablonskii-Vorob'ev root structure to another, such as from a triangle to a pentagon. In this process, uncountably infinite new root shapes will be generated. These roots are generically simple roots. Indeed, if a root happens to be a multiple root, it will split into simple roots when the complex parameters $\{\kappa_j\}$ are slightly perturbed. For this reason, we will focus on the case when all roots of $\Theta_N(z)$ are simple in this article. In this case, $\Theta_N(z)$ will have $N(N+1)/2$ roots.

Of the uncountably infinite root structures of Adler-Moser polynomials, we illustrate only three of them for brevity. These three samples are for $\Theta_5(z;\kappa_1,\kappa_2,\kappa_3,\kappa_4)$,

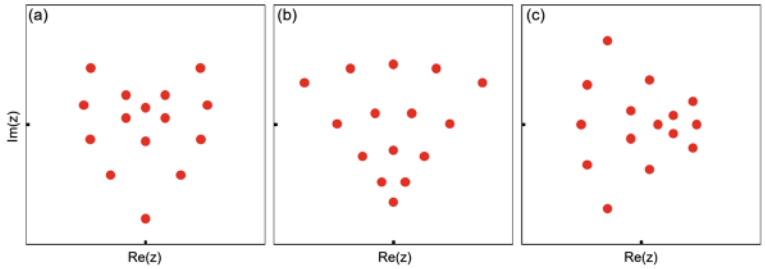

Fig. 3.17 Three sample root structures of the Adler-Moser polynomial $\Theta_5(z)$ for parameter values $(\kappa_1, \kappa_2, \kappa_3, \kappa_4)$ given in Eq. (3.160). In all panels, $-7 \le \mathrm{Re}(z), \mathrm{Im}(z) \le 7$

with three sets of $(\kappa_1, \kappa_2, \kappa_3, \kappa_4)$ values as

$$(\mathrm{i}, \mathrm{i}, \mathrm{i}, \mathrm{i}), \ \ (5\mathrm{i}/3, -\mathrm{i}, 5\mathrm{i}/7, -5\mathrm{i}/9), \ \ (1, 1, 1, 1). \tag{3.160}$$

Their root structures are displayed in Fig. 3.17a–c, respectively. In these panels, every root is a simple root. The (a) panel shows a heart-shaped structure, (b) shows a fan-shaped circular sector, and (c) shows a two-arc structure combined with a triangle.

It turns out that root structures of Adler-Moser polynomials describe rogue patterns in many integrable systems when multiple internal parameters in their rogue waves are large. We present detailed results for two such integrable systems below.

3.2.2 Nonlinear Schrödinger Equation

For the NLS equation

$$\mathrm{i}u_t + \frac{1}{2}u_{xx} + |u|^2 u = 0, \tag{3.161}$$

its rogue wave solutions $u_N(x,t)$ have been presented in Theorem 2.1 of Chap. 2 (see also Lemma 3.1 of this chapter). These solutions contain $N-1$ free internal complex parameters $a_3, a_5, \cdots, a_{2N-1}$. If only one of those parameters is large, then the resulting rogue pattern is predicted by root structures of Yablonskii-Vorob'ev hierarchy polynomials, see the previous section. In this section, we consider patterns of these rogue solutions when *multiple* of these internal parameters are large.

Specifically, suppose parameters $a_3, a_5, \cdots, a_{2N-1}$ in $u_N(x,t)$ are of the following form

$$a_{2j+1} = \kappa_j A^{2j+1}, \quad 1 \le j \le N-1, \tag{3.162}$$

where $A \gg 1$ is a large positive constant, and $(\kappa_1, \kappa_2, \ldots, \kappa_{N-1})$ are $O(1)$ complex constants not being all zero. Suppose also that roots of the Adler-Moser polynomial $\Theta_N(z)$ with parameters $(\kappa_1, \kappa_2, \ldots, \kappa_{N-1})$ are all simple. Then, our analytical prediction on the pattern of this rogue wave solution $u_N(x,t)$ is given by the following theorem.

Theorem 3.10 *If all roots of $\Theta_N(z)$ with parameters $(\kappa_1, \kappa_2, \ldots, \kappa_{N-1})$ are simple, then the N-th order rogue wave $u_N(x,t)$ of the NLS equation in Eq. (3.14) with its internal large parameters as given by Eq. (3.162) would asymptotically split into $N(N+1)/2$ fundamental (Peregrine) rogue waves of the form $\hat{u}_1(x-\hat{x}_0, t-\hat{t}_0)\, e^{it}$, where $\hat{u}_1(x,t)$ is given in Eq. (3.19), and positions $(\hat{x}_0, \hat{t}_0)$ of these Peregrine waves are given by*

$$\hat{x}_0 + i\hat{t}_0 = z_0 A, \tag{3.163}$$

with z_0 being every one of the $N(N+1)/2$ simple roots of $\Theta_N(z)$. The error of this Peregrine wave approximation is $O(A^{-1})$. Expressed mathematically, when $(x-\hat{x}_0)^2 + (t-\hat{t}_0)^2 = O(1)$, we have the following solution asymptotics

$$u_N(x,t;a_3,a_5,\cdots,a_{2N-1}) = \hat{u}_1(x-\hat{x}_0, t-\hat{t}_0)\, e^{it} + O\left(A^{-1}\right). \tag{3.164}$$

When (x,t) is not in the neighborhood of any of these Peregrine waves, $u_N(x,t)$ would asymptotically approach the constant-amplitude background e^{it} as $A \to +\infty$.

This theorem indicates that the rogue pattern is asymptotically a simple dilation of the root structure of the underlying Adler-Moser polynomial by a factor of A, with each root predicting the location of a Peregrine wave in the (x,t) plane according to Eq. (3.163). Thus, this theorem establishes a direct connection between rogue patterns and root structures of Adler-Moser polynomials.

One may notice that in the present case of multiple large parameters, the rogue pattern is a simple dilation of the root structure of an Adler-Moser polynomial (by a factor of A), while in the case of a single large parameter as studied in Sect. 3.1.2, the rogue pattern was a dilation *and rotation* of the root structure of a Yablonskii-Vorob'ev hierarchy polynomial (see Theorem 3.2). The reason our current rogue pattern does not involve rotation to the root structure is that, the Adler-Moser polynomial contains free complex constants $\{\kappa_j\}$, which automatically put its root structure in proper orientation to match the rogue pattern. Comparatively, a Yablonskii-Vorob'ev hierarchy polynomial does not contain such free complex constants, and thus the orientation of its root structure is fixed. In this case, in order for its root structure to match the orientation of the rogue wave, a proper rotation is needed.

Proof of Theorem 3.10 The main idea of our proof resembles that for Theorem 3.2 for a single large internal parameter case, and we will only sketch the main differences below.

To derive the large-parameter asymptotics of the rogue wave solution $u_N(x,t)$ in Eq. (3.14), we need asymptotic expressions for the determinant σ_n in Eq. (3.15). As before, we first use determinant identities and the Laplace expansion to rewrite σ_n as

$$\sigma_n = \sum_{0\le\nu_1<\nu_2<\cdots<\nu_N\le 2N-1} \det_{1\le i,j\le N}\left[\frac{1}{2^{\nu_j}} S_{2i-1-\nu_j}(\boldsymbol{x}^+(n)+\nu_j \boldsymbol{s})\right] \times \det_{1\le i,j\le N}\left[\frac{1}{2^{\nu_j}} S_{2i-1-\nu_j}(\boldsymbol{x}^-(n)+\nu_j \boldsymbol{s})\right], \tag{3.165}$$

see Eqs. (2.77) and (3.36).

When internal parameters $(a_3, a_5, \cdots, a_{2N-1})$ are of the form (3.162) with $A \gg 1$, and $x, t = O(A)$ or smaller, we have

$$\begin{aligned} S_k(\boldsymbol{x}^+(n)+\nu \boldsymbol{s}) &= S_k\left(x_1^+, \nu s_2, x_3^+, \nu s_4, \cdots\right) \\ &= S_k\left(x_1^+, 0, \kappa_1 A^3, 0, \kappa_2 A^5, \cdots\right)\left[1+O(A^{-2})\right] \\ &= S_k(\hat{\mathbf{v}})\left[1+O(A^{-2})\right], \end{aligned} \tag{3.166}$$

where $\hat{\mathbf{v}} = \left(x+\mathrm{i}t+n, 0, \kappa_1 A^3, 0, \kappa_2 A^5, 0, \cdots\right)$. From the definition (2.2) of Schur polynomials, one can see that the polynomial $S_k(\hat{\mathbf{v}})$ is related to $\theta_k(z)$ in (3.159) as

$$S_k(\hat{\mathbf{v}}) = A^k \theta_k(\hat{z}), \tag{3.167}$$

where $\hat{z} \equiv A^{-1}(x+\mathrm{i}t+n)$.

The dominant contribution in the Laplace expansion (3.165) of σ_n comes from two index choices, $\nu = (0, 1, \cdots, N-1)$, and $\nu = (0, 1, \cdots, N-2, N)$.

With the first index choice, in view of Eqs. (3.41)–(3.43), the determinant involving $\boldsymbol{x}^+(n)$ inside the summation of (3.165) is asymptotically

$$\alpha\, A^{\frac{N(N+1)}{2}} \Theta_N(\hat{z})\left[1+O\left(A^{-2}\right)\right], \tag{3.168}$$

where $\alpha = 2^{-N(N-1)/2} c_N^{-1}$. Let us define $(\hat{x}_0, \hat{t}_0)$ by Eq. (3.163), i.e., $z_0 = A^{-1}(\hat{x}_0 + \mathrm{i}\hat{t}_0)$, where z_0 is a simple root of the Adler-Moser polynomial $\Theta_N(z)$. Then, when (x,t) is in the $O(1)$ neighborhood of $(\hat{x}_0, \hat{t}_0)$, we expand $\Theta_N(\hat{z})$ around $\hat{z} = z_0$. Recalling $\Theta_N(z_0) = 0$, we get

$$\Theta_N(\hat{z}) = A^{-1}\left[(x-\hat{x}_0) + \mathrm{i}(t-\hat{t}_0) + n\right]\Theta_N'(z_0)\left[1+O\left(A^{-1}\right)\right]. \tag{3.169}$$

Inserting this equation into (3.168), the determinant involving $\boldsymbol{x}^+(n)$ inside the summation of (3.165) becomes

$$\left[(x-\hat{x}_0)+\mathrm{i}(t-\hat{t}_0)+n\right]\alpha\, A^{\frac{N(N+1)}{2}}\Theta_N'(z_0)\left[1+O\left(A^{-1}\right)\right]. \tag{3.170}$$

Similarly, the determinant involving $\boldsymbol{x}^-(n)$ inside this summation becomes

$$\left[(x-\hat{x}_0)-\mathrm{i}(t-\hat{t}_0)-n\right]\alpha\, A^{\frac{N(N+1)}{2}}\Theta_N'(z_0^*)\left[1+O\left(A^{-1}\right)\right]. \tag{3.171}$$

Next, we consider the contribution from the second index choice of $\nu = (0, 1, \cdots, N-2, N)$. For this index choice, the determinant involving $\boldsymbol{x}^+(n)$ inside the summation of (3.165) becomes

$$\frac{1}{2}\alpha\, A^{\frac{N(N+1)-2}{2}}\Theta_N'(\hat{z})\left[1+O\left(A^{-2}\right)\right]. \tag{3.172}$$

When (x, t) is in the $O(1)$ neighborhood of $(\hat{x}_0, \hat{t}_0)$, the above term is asymptotically equal to

$$\frac{1}{2}\alpha\, A^{\frac{N(N+1)-2}{2}}\Theta_N'(z_0)\left[1+O\left(A^{-1}\right)\right]. \tag{3.173}$$

Similarly, the determinant involving $\boldsymbol{x}^-(n)$ inside the summation of (3.165) becomes

$$\frac{1}{2}\alpha\, A^{\frac{N(N+1)-2}{2}}\Theta_N'(z_0^*)\left[1+O\left(A^{-1}\right)\right]. \tag{3.174}$$

Summarizing the above two dominant contributions in the Laplace expansion (3.165), we find that

$$\begin{aligned}\sigma_n(x,t) = \alpha^2\,&\left|\Theta_N'(z_0)\right|^2 A^{N(N+1)-2}\\ &\times\left[(x-\hat{x}_0)^2+(t-\hat{t}_0)^2-2in\,(t-\hat{t}_0)-n^2+\frac{1}{4}\right]\\ &\times\left[1+O\left(A^{-1}\right)\right].\end{aligned} \tag{3.175}$$

Since the root z_0 has been assumed simple, $\Theta_N'(z_0)\neq 0$. Thus, the above leading-order asymptotics for $\sigma_n(x,t)$ does not vanish. Therefore, when A is large and (x,t) in the O(1) neighborhood of $(\hat{x}_0, \hat{t}_0)$, we get from (3.175) that

$$u_N(x,t)=\frac{\sigma_1}{\sigma_0}e^{\mathrm{i}t}=e^{\mathrm{i}t}\left(1-\frac{4[1+2\mathrm{i}(t-\hat{t}_0)]}{1+4(x-\hat{x}_0)^2+4(t-\hat{t}_0)^2}\right)+O\left(A^{-1}\right), \tag{3.176}$$

which is a Peregrine wave $\hat{u}_1(x - \hat{x}_0, t - \hat{t}_0)\, e^{it}$, and the error of this Peregrine prediction is $O\left(A^{-1}\right)$. Theorem 3.10 is then proved. □

Numerical Confirmation

Now, we numerically verify Theorem 3.10 by comparing its predictions with true rogue-wave solutions. This comparison will be done only for fifth-order rogue waves $u_5(x, t)$ for brevity. Such fifth-order solutions have internal complex parameters (a_3, a_5, a_7, a_9).

We will do this comparison on three examples. Internal parameter values in these three examples are of the form (3.162) with $A = 5$, which is large as desired, and their $(\kappa_1, \kappa_2, \kappa_3, \kappa_4)$ values are given in Eq. (3.160). These κ_j values are used since root structures of Adler-Moser polynomials $\Theta_5(z)$ for these values have been displayed in Fig. 3.17. For these three sets of internal parameters, true rogue wave solutions are plotted in the upper three panels of Fig. 3.18, respectively. It is seen that each panel comprises 15 lumps (Peregrine waves) in the (x, t) plane. In the first panel, these 15 Peregrine waves form a heart-shaped structure, with another mini-heart in its interior. In the second panel, these 15 Peregrine waves form a fan-shaped structure. In the third panel, these 15 Peregrine waves form two vertically-oriented arcs plus a smaller triangle on their right side.

Our analytical predictions $|u_5^{(p)}(x, t)|$ for these rogue waves from Theorem 3.10 can be assembled into a simple formula,

$$\left|u_5^{(p)}(x,t)\right| = 1 + \sum_{j=1}^{15} \left(\left|\hat{u}_1(x - \hat{x}_0^{(j)}, t - \hat{t}_0^{(j)})\right| - 1\right), \tag{3.177}$$

where $\hat{u}_1(x, t)$ is the Peregrine wave given in (3.19), and their positions $(\hat{x}_0^{(j)}, \hat{t}_0^{(j)})$ are given by (3.163) with z_0 being every one of the $N(N+1)/2 = 15$ simple roots of the Adler-Moser polynomial $\Theta_5(z)$. These predicted solutions for the same (a_3, a_5, a_7, a_9) values as in the true solutions are plotted in the lower three panels of Fig. 3.18. When compared to the root structures of the Adler-Moser polynomial $\Theta_5(z)$ in Fig. 3.17, our predicted rogue patterns in these lower panels are obviously a simple dilation of those root structures, by a factor of $A = 5$, with each root replaced by a Peregrine wave, as Theorem 3.10 says.

When comparing the true rogue solutions in the upper row to their analytical predictions in the lower row, we can clearly see that they agree with each other very well. In fact, one can hardly notice the difference between them, which is an indication that our prediction in Theorem 3.10 is highly accurate.

Quantitatively, we have also measured the error of our analytical predictions versus the A value, similar to what we did in Fig. 3.4 for the NLS equation under a single large internal parameter. That error analysis confirmed that the error does decay in proportion to A^{-1}, as Theorem 3.10 predicts. Thus, Theorem 3.10 is fully confirmed numerically. Details of this quantitative comparison are omitted here for brevity.

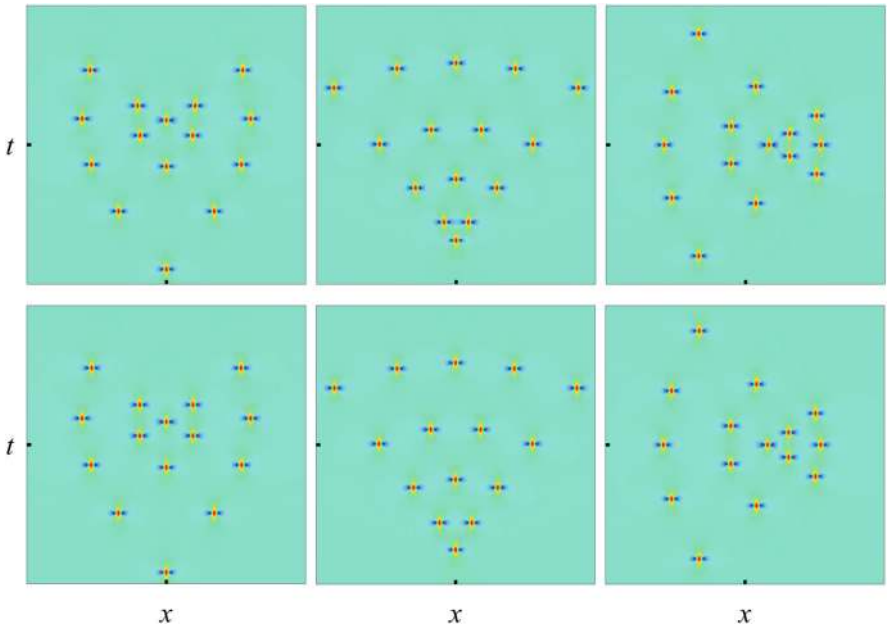

Fig. 3.18 Comparison between true rogue waves $|u_5(x,t)|$ (upper row) and their analytical predictions (lower row) in the NLS equation under multiple large parameters (3.162) with $A = 5$. From left to right columns: $(\kappa_1, \kappa_2, \kappa_3, \kappa_4) = (\mathrm{i}, \mathrm{i}, \mathrm{i}, \mathrm{i})$, $(5\mathrm{i}/3, -\mathrm{i}, 5\mathrm{i}/7, -5\mathrm{i}/9)$, $(1, 1, 1, 1)$. In all panels, $-30 \le x, t \le 30$

3.2.3 *Derivative Nonlinear Schrödinger Equations*

The normalized generalized derivative nonlinear Schrödinger (GDNLS) equations are

$$\mathrm{i}u_t + \frac{1}{2}u_{xx} + \mathrm{i}\gamma|u|^2u_x + \mathrm{i}(\gamma-1)u^2u_x^* + \frac{1}{2}(\gamma-1)(\gamma-2)|u|^4u = 0, \qquad (3.178)$$

where γ is a real constant (see Sect. 2.2). These equations contain the Kaup-Newell equation ($\gamma = 2$), the Chen-Lee-Liu equation ($\gamma = 1$) and the Gerdjikov-Ivanov equation ($\gamma = 0$) as special cases. Rogue waves in the GDNLS equations have been presented in Theorem 2.3 of Sect. 2.2. Those rogue waves contain free internal complex parameters $a_3, a_5, \cdots, a_{2N-1}$. Suppose these parameters are of the form (3.162), i.e.,

$$a_{2j+1} = \kappa_j A^{2j+1}, \quad 1 \le j \le N-1, \qquad (3.179)$$

where $A \gg 1$ is a large positive constant, and $(\kappa_1, \kappa_2, \ldots, \kappa_{N-1})$ are $O(1)$ complex constants not being all zero. Then, we have the following theorem on the pattern of these rogue waves.

Theorem 3.11 *If all roots of $\Theta_N(z)$ with parameters $(\kappa_1, \kappa_2, \ldots, \kappa_{N-1})$ are simple, then the GDNLS rogue wave $u_N(x,t)$ with its large internal parameters as given by Eq. (3.179) would asymptotically split into $N(N+1)/2$ fundamental rogue waves of the form $\hat{u}_1(x-\hat{x}_0, t-\hat{t}_0)\, e^{\mathrm{i}(1-\gamma-\alpha)x - \frac{\mathrm{i}}{2}[\alpha^2+2(\gamma-2)\alpha+1-\gamma]t}$, where*

$$|\hat{u}_1(x,t)| = \left| \frac{\alpha(x+\alpha t)^2 + (x-t)^2 - \mathrm{i}(x+3\alpha t) - \frac{3}{4}}{\alpha(x+\alpha t)^2 + (x-t)^2 + \mathrm{i}(x+\alpha t) - 2\mathrm{i}t + \frac{1}{4}} \right|, \tag{3.180}$$

and their positions $(\hat{x}_0, \hat{t}_0)$ are given by

$$\hat{x}_0 = \frac{1}{\sqrt{\alpha}} \Re\left[z_0 A\right] - \frac{\alpha-1}{\alpha} \Im\left[z_0 A\right], \quad \hat{t}_0 = \frac{1}{\alpha} \Im\left[z_0 A\right], \tag{3.181}$$

with z_0 being any one of the $N(N+1)/2$ simple roots of $\Theta_N(z)$. The error of this fundamental rogue wave approximation is $O(A^{-1})$. Expressed mathematically, when $(x-\hat{x}_0)^2 + (t-\hat{t}_0)^2 = O(1)$, we have the following solution asymptotics

$$u_N(x,t;a_3,a_5,\cdots,a_{2N-1}) = \hat{u}_1(x-\hat{x}_0, t-\hat{t}_0)\, e^{\mathrm{i}(1-\gamma-\alpha)x - \frac{\mathrm{i}}{2}[\alpha^2+2(\gamma-2)\alpha+1-\gamma]t} + O\left(A^{-1}\right). \tag{3.182}$$

When (x,t) is not in the neighborhood of any of these fundamental waves, then $u_N(x,t)$ would asymptotically approach the constant-amplitude background wave $e^{\mathrm{i}(1-\gamma-\alpha)x - \frac{\mathrm{i}}{2}[\alpha^2+2(\gamma-2)\alpha+1-\gamma]t}$ as $A \to +\infty$.

The proof of this theorem is similar to that for Theorem 3.10 and will be omitted.

Numerical Confirmation

Next, we numerically verify Theorem 3.11 by comparing its predictions with true rogue-wave solutions. This comparison will be done for fifth-order rogue waves $u_5(x,t)$. Such fifth-order solutions have internal complex parameters (a_3, a_5, a_7, a_9). Our analytical predictions $|u_5^{(p)}(x,t)|$ for these rogue waves from Theorem 3.11 can be assembled into a simple formula,

$$\left|u_5^{(p)}(x,t)\right| \approx 1 + \sum_{j=1}^{15} \left(\left| \hat{u}_1(x-\hat{x}_0^{(j)}, t-\hat{t}_0^{(j)}) \right| - 1 \right), \tag{3.183}$$

where $\hat{u}_1(x,t)$ is the fundamental rogue wave given by Eq. (3.180), and their positions $(\hat{x}_0^{(j)}, \hat{t}_0^{(j)})$ are given by Eq. (3.181) with z_0 being every one of the $N(N+1)/2 = 15$ simple roots of the Adler-Moser polynomial $\Theta_5(z)$.

We will do this comparison on three different patterns. Internal parameter values in these three examples are of the form (3.179) with $A = 5$, which is large as desired, and their $(\kappa_1, \kappa_2, \kappa_3, \kappa_4)$ values are given in Eq. (3.160). These κ_j values are used since root structures of Adler-Moser polynomials $\Theta_5(z)$ for these values have been displayed in Fig. 3.17. Then, when we choose $\alpha = 16/9$ in the background wave, true rogue wave solutions for these three sets of internal parameters are plotted in the upper three panels of Fig. 3.19, respectively. It is seen that each panel comprises 15 lumps (fundamental rogue waves) in the (x, t) plane. In the first panel, these 15 fundamental rogue waves form a heart-shaped structure, with another mini-heart in its interior. In the second panel, these 15 fundamental rogue waves form a fan-shaped structure. In the third panel, these 15 fundamental rogue waves form two vertically-oriented arcs plus a smaller triangle on their right side.

Predicted rogue solutions from Theorem 3.10 for the same (a_3, a_5, a_7, a_9) values as in the true solutions are plotted in the lower three panels of Fig. 3.19. When comparing these predictions to the true solutions, we can clearly see that they agree with each other very well. In fact, one can hardly notice the difference between them, which is an indication that our prediction in Theorem 3.11 is highly accurate. When comparing these rogue patterns to root structures of Adler-Moser polynomials $\Theta_5(z)$ in Fig. 3.17, we see that these rogue patterns are stretched from Adler-Moser

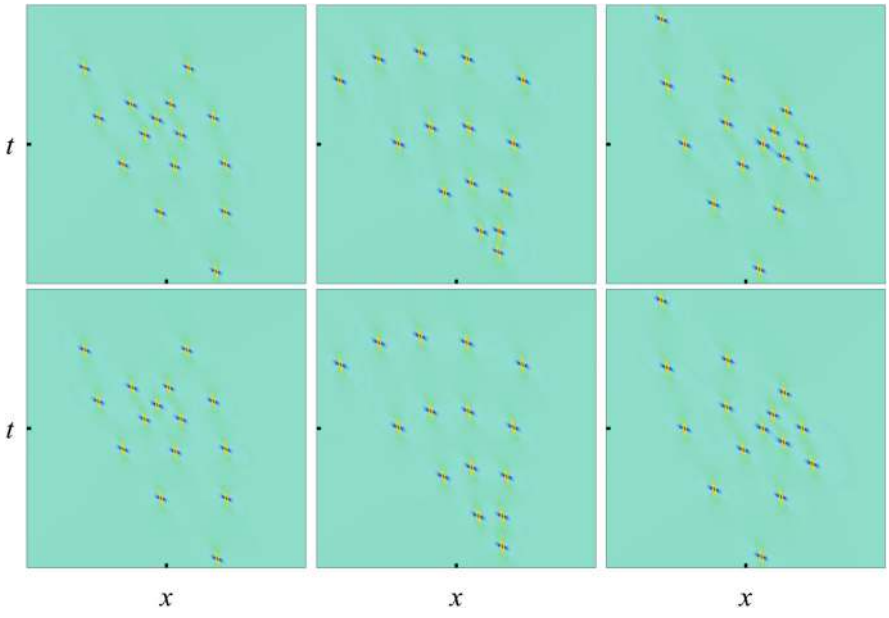

Fig. 3.19 Comparison between true rogue solutions $|u_5(x, t)|$ (upper row) and their analytical predictions (lower row) in the GDNLS equations under multiple large parameters (3.179) with $A = 5$ and $\alpha = 16/9$. From left to right columns: $(\kappa_1, \kappa_2, \kappa_3, \kappa_4) = (\mathrm{i}, \mathrm{i}, \mathrm{i}, \mathrm{i})$, $(5\mathrm{i}/3, -\mathrm{i}, 5\mathrm{i}/7, -5\mathrm{i}/9)$, $(1, 1, 1, 1)$. In the first column, $-33 \le x, t \le 33$. In the second and third columns, $-30 \le x, t \le 30$

root structures, because the linear transformation from the root-z plane to the (x, t) plane in Eq. (3.181) involves stretching.

Quantitatively, we have also measured the error of our analytical predictions versus the A value. That error analysis confirmed that the error does decay in proportion to A^{-1}, as Theorem 3.11 predicts. Thus, Theorem 3.11 is fully confirmed numerically. Details of this quantitative comparison are omitted for brevity.

To conclude this section, we point out that these rogue patterns associated with Adler-Moser polynomials are also universal and would arise in many other integrable systems as well if their rogue waves can be expressed by τ functions whose matrix elements are Schur polynomials with index jumps of two, and when multiple internal parameters in their rogue waves are large as in Eq. (3.162). Examples include the Boussinesq equation, the Manakov system, the three-wave interaction system, the long-wave-short-wave interaction system, the Ablowitz-Ladik equation, the massive Thirring model, and others. Details are omitted.

3.3 Rogue Patterns Associated with Okamoto Polynomial Hierarchies

Yablonskii-Vorob'ev polynomial hierarchies and Adler-Moser polynomials are associated with rogue patterns in integrable systems whose rogue waves can be expressed by τ functions whose matrix elements are Schur polynomials with index jumps of two. However, there exist other rogue waves in certain integrable systems whose τ functions do not feature Schur polynomials with index jumps of two. For example, the Manakov system and three-wave interaction system admit rogue waves whose τ functions contain Schur polynomials with index jumps of three. In such cases, rogue patterns would be associated with another type of special polynomials—the Okamoto polynomial hierarchies (Yang and Yang 2023a). This prospect will be examined in this section.

3.3.1 Okamoto Polynomials and Their Hierarchies

Okamoto polynomials first arose in Okamoto's study of rational solutions to the Painlevé IV equation (Okamoto 1986). He showed that a class of such rational solutions can be expressed as the logarithmic derivative of certain special polynomials, which are now called Okamoto polynomials. Later, determinant expressions of these polynomials were discovered by Kajiwara and Ohta (1998). Let $p_j(z)$ be Schur polynomials defined by

$$\sum_{j=0}^{\infty} p_j(z)\epsilon^j = \exp\left(z\epsilon + \epsilon^2\right), \tag{3.184}$$

with $p_j(z) \equiv 0$ for $j < 0$. Then, the monic Okamoto polynomials $Q_N(z)$ and $R_N(z)$ with $N \geq 1$ are defined as (Kajiwara and Ohta 1998; Clarkson 2003)

$$Q_N(z) = c_N \begin{vmatrix} p_2(z) & p_1(z) & \cdots & p_{3-N}(z) \\ p_5(z) & p_4(z) & \cdots & p_{6-N}(z) \\ \vdots & \vdots & \vdots & \vdots \\ p_{3N-1}(z) & p_{3N-2}(z) & \cdots & p_{2N}(z) \end{vmatrix}, \tag{3.185}$$

and

$$R_N(z) = d_N \begin{vmatrix} p_1(z) & p_0(z) & \cdots & p_{2-N}(z) \\ p_4(z) & p_3(z) & \cdots & p_{5-N}(z) \\ \vdots & \vdots & \vdots & \vdots \\ p_{3N-2}(z) & p_{3N-3}(z) & \cdots & p_{2N-1}(z) \end{vmatrix}, \tag{3.186}$$

where

$$c_N = 3^{-\frac{1}{2}N(N-1)} \frac{2!5! \cdots (3N-1)!}{0!1! \cdots (N-1)!}, \tag{3.187}$$

and

$$d_N = 3^{-\frac{1}{2}N(N-1)} \frac{1!4! \cdots (3N-2)!}{0!1! \cdots (N-1)!}. \tag{3.188}$$

Note that these two determinants are both Wronskians, because $p'_{j+1}(z) = p_j(z)$ from the definition of $p_j(z)$ in Eq. (3.184), where the prime denotes differentiation. The first three $Q_N(z)$ and $R_N(z)$ polynomials are

$$\begin{aligned} Q_1(z) &= z^2 + 2, \\ Q_2(z) &= z^6 + 10z^4 + 20z^2 + 40, \\ Q_3(z) &= z^{12} + 28z^{10} + 260z^8 + 1120z^6 + 2800z^4 + 11200z^2 + 11200, \\ R_1(z) &= z, \\ R_2(z) &= z^4 + 4z^2 - 4, \\ R_3(z) &= z(z^8 + 16z^6 + 56z^4 - 560). \end{aligned}$$

Compared to the Okamoto polynomials introduced in Okamoto (1986), Kajiwara and Ohta (1998) and Clarkson (2003), the polynomials above are related to them through a simple scaling in z and (Q_N, R_N).

Like the Yablonskii-Vorob'ev polynomials, these Okamoto polynomials can also be generalized to hierarchies (Yang and Yang 2023a). Let $p_j^{[m]}(z)$ be Schur

polynomials defined by

$$\sum_{j=0}^{\infty} p_j^{[m]}(z)\epsilon^j = \exp\left(z\epsilon + \epsilon^m\right), \tag{3.189}$$

where m is a positive integer larger than one, and $p_j^{[m]}(z) \equiv 0$ if $j < 0$. Then, we define the monic Okamoto polynomial hierarchies $R_N^{[m]}(z)$ and $Q_N^{[m]}(z)$ by the Wronskians

$$Q_N^{[m]}(z) = c_N \begin{vmatrix} p_2^{[m]}(z) & p_1^{[m]}(z) & \cdots & p_{3-N}^{[m]}(z) \\ p_5^{[m]}(z) & p_4^{[m]}(z) & \cdots & p_{6-N}^{[m]}(z) \\ \vdots & \vdots & \vdots & \vdots \\ p_{3N-1}^{[m]}(z) & p_{3N-2}^{[m]}(z) & \cdots & p_{2N}^{[m]}(z) \end{vmatrix}, \tag{3.190}$$

and

$$R_N^{[m]}(z) = d_N \begin{vmatrix} p_1^{[m]}(z) & p_0^{[m]}(z) & \cdots & p_{2-N}^{[m]}(z) \\ p_4^{[m]}(z) & p_3^{[m]}(z) & \cdots & p_{5-N}^{[m]}(z) \\ \vdots & \vdots & \vdots & \vdots \\ p_{3N-2}^{[m]}(z) & p_{3N-3}^{[m]}(z) & \cdots & p_{2N-1}^{[m]}(z) \end{vmatrix}. \tag{3.191}$$

If $m \bmod 3 = 0$, then $Q_N^{[m]}(z) = z^{N(N+1)}$ and $R_N^{[m]}(z) = z^{N^2}$ (Yang and Yang 2023a). But such m values turn out to be irrelevant to our rogue pattern problem. Thus, we require $m \bmod 3 \neq 0$, i.e., $m = 2, 4, 5, 7, 8, 10, \cdots$. When $m = 2$, $Q_N^{[2]}(z)$ and $R_N^{[2]}(z)$ are the Okamoto polynomials $Q_N(z)$ and $R_N(z)$. When $m > 2$, $Q_N^{[m]}(z)$ and $R_N^{[m]}(z)$ give higher members of Okamoto hierarchies.

3.3.2 *Root Structures of Okamoto Polynomial Hierarchies*

Root structures of Okamoto-hierarchy polynomials will play a key role in our analytical study of rogue wave patterns. For Okamoto polynomials $Q_N(z)$ and $R_N(z)$, their root structures have been investigated by Kametaka (1983), Fukutani et al. (2000) and Clarkson (2003). It has been shown that for every positive integer N, $Q_N(z)$ and $R_N(z)$ have simple roots (Kametaka 1983; Fukutani et al. 2000). In addition, graphs of root locations for many $Q_N(z)$ and $R_N(z)$ polynomials have been plotted, and double-triangle as well as rhombus-shaped root structures have been observed (Clarkson 2003).

In this subsection, we examine root structures of Okamoto hierarchies $Q_N^{[m]}(z)$ and $R_N^{[m]}(z)$. Defining integer N_0 as the remainder of N divided by m, i.e.,

$$N_0 \equiv N \bmod m, \tag{3.192}$$

and denoting $[a]$ as the largest integer less than or equal to a real number a, then our results are summarized by the following two theorems (Yang and Yang 2023a).

Theorem 3.12 *The Okamoto hierarchy polynomial $Q_N^{[m]}(z)$ is monic with degree $N(N+1)$, and is of the form*

$$Q_N^{[m]}(z) = z^{N_Q} q_N^{[m]}(\zeta), \quad \zeta \equiv z^m, \tag{3.193}$$

where $q_N^{[m]}(\zeta)$ is a monic polynomial of ζ with all-real coefficients and a nonzero constant term. The non-negative integer N_Q is the multiplicity of the zero root in $Q_N^{[m]}(z)$ and is given by the formula

$$N_Q = N_{1Q}(N_{1Q} - N_{2Q} + 1) + N_{2Q}^2, \tag{3.194}$$

where N_{1Q} and N_{2Q} are non-negative integers. If $m > 1$ and $m \bmod 3 = 1$, these (N_{1Q}, N_{2Q}) values are

$$(N_{1Q}, N_{2Q}) = \begin{cases} (N_0, 0), & \text{when } 0 \le N_0 \le \left[\frac{m}{3}\right], \\ \left(\left[\frac{m}{3}\right], N_0 - \left[\frac{m}{3}\right]\right), & \text{when } \left[\frac{m}{3}\right] + 1 \le N_0 \le 2\left[\frac{m}{3}\right], \\ (m-1-N_0,\, m-1-N_0), & \text{when } 2\left[\frac{m}{3}\right] + 1 \le N_0 \le m-1; \end{cases} \tag{3.195}$$

and if $m \bmod 3 = 2$, these (N_{1Q}, N_{2Q}) values are

$$(N_{1Q}, N_{2Q}) = \begin{cases} (N_0, 0), & \text{when } 0 \le N_0 \le \left[\frac{m}{3}\right], \\ \left(N_0 - \left[\frac{m}{3}\right] - 1, \left[\frac{m}{3}\right]\right), & \text{when } \left[\frac{m}{3}\right] + 1 \le N_0 \le 2\left[\frac{m}{3}\right], \\ (m-1-N_0,\, m-1-N_0), & \text{when } 2\left[\frac{m}{3}\right] + 1 \le N_0 \le m-1. \end{cases} \tag{3.196}$$

If $N_Q = 0$, then zero is not a root of $Q_N^{[m]}(z)$.

Theorem 3.13 *The Okamoto hierarchy polynomial $R_N^{[m]}(z)$ is monic with degree N^2, and is of the form*

$$R_N^{[m]}(z) = z^{N_R} r_N^{[m]}(\zeta), \quad \zeta \equiv z^m, \tag{3.197}$$

where $r_N^{[m]}(\zeta)$ is a monic polynomial of ζ with all-real coefficients and a nonzero constant term. The non-negative integer N_R is the multiplicity of the zero root in $R_N^{[m]}(z)$ and is given by the formula

$$N_R = N_{1R}(N_{1R} - N_{2R} + 1) + N_{2R}^2, \tag{3.198}$$

where N_{1R} and N_{2R} are non-negative integers. If $m > 1$ and $m \bmod 3 = 1$, these (N_{1R}, N_{2R}) values are

$$(N_{1R}, N_{2R}) = \begin{cases} (0, N_0), & \text{when } 0 \le N_0 \le \left[\frac{m}{3}\right], \\ \left(\left[\frac{m}{3}\right] - 1, N_0 - 1 - \left[\frac{m}{3}\right]\right), & \text{when } \left[\frac{m}{3}\right] + 1 \le N_0 \le 2\left[\frac{m}{3}\right], \\ (m - 1 - N_0, m - N_0), & \text{when } 2\left[\frac{m}{3}\right] + 1 \le N_0 \le m - 1; \end{cases} \tag{3.199}$$

and if $m \bmod 3 = 2$, these (N_{1R}, N_{2R}) values are

$$(N_{1R}, N_{2R}) = \begin{cases} (0, N_0), & \text{when } 0 \le N_0 \le \left[\frac{m}{3}\right], \\ \left(N_0 - 1 - \left[\frac{m}{3}\right], \left[\frac{m}{3}\right] + 1\right), & \text{when } \left[\frac{m}{3}\right] + 1 \le N_0 \le 2\left[\frac{m}{3}\right], \\ (m - 1 - N_0, m - N_0), & \text{when } 2\left[\frac{m}{3}\right] + 1 \le N_0 \le m - 1. \end{cases} \tag{3.200}$$

If $N_R = 0$, then zero is not a root of $R_N^{[m]}(z)$.

Proofs of these two theorems can be found in Yang and Yang (2023a).

The most significant piece of information in these two theorems is the formulae for N_Q and N_R, which give the multiplicities of the zero root in $Q_N^{[m]}(z)$ and $R_N^{[m]}(z)$ polynomials. These root-multiplicity formulae are particularly important for the analysis of rogue waves in the inner region under a large parameter (see later text). Compared to the multiplicity formula of the zero root in the Yablonskii-Vorob'ev polynomial hierarchy as given in Theorem 3.1, the present multiplicity formulae for Okamoto hierarchies are more involved, but their connection to the multiplicity formula of the Yablonskii-Vorob'ev hierarchy is still visible. For Okamoto polynomials $Q_N(z)$ and $R_N(z)$ (where $m = 2$), these multiplicity formulae show that $N_Q = 0$ for all N values, and $N_R = 0$ if N is even and $N_R = 1$ if N is odd. This means that for any N, zero is not a root of $Q_N(z)$. In addition, for $R_N(z)$, zero is not a root when N is even and is a simple root when N is odd.

Another piece of information from formulae (3.193) and (3.197) of these theorems is that, root structures of both $Q_N^{[m]}(z)$ and $R_N^{[m]}(z)$ polynomials are invariant under $2\pi/m$-angle rotation in the complex z plane. This rotational symmetry of the root structures will have implications on shapes of rogue patterns away from the origin under a large parameter, as we will see later.

The only major piece of information missing from the above two theorems is multiplicities of *nonzero* roots in these $Q_N^{[m]}(z)$ and $R_N^{[m]}(z)$ polynomials. For Okamoto polynomials $Q_N(z)$ and $R_N(z)$ (where $m = 2$), it has been shown that all their roots are simple (Kametaka 1983; Fukutani et al. 2000). For higher members of these hierarchies, their zero root clearly can be non-simple in view of the above N_Q and N_R formulae. However, it is unclear whether their nonzero roots can also be non-simple. Our numerical evidence suggests that their nonzero roots are all simple. Assuming this is true, then from Theorems 3.12–3.13, numbers of nonzero roots in $Q_N^{[m]}(z)$ and $R_N^{[m]}(z)$ would be

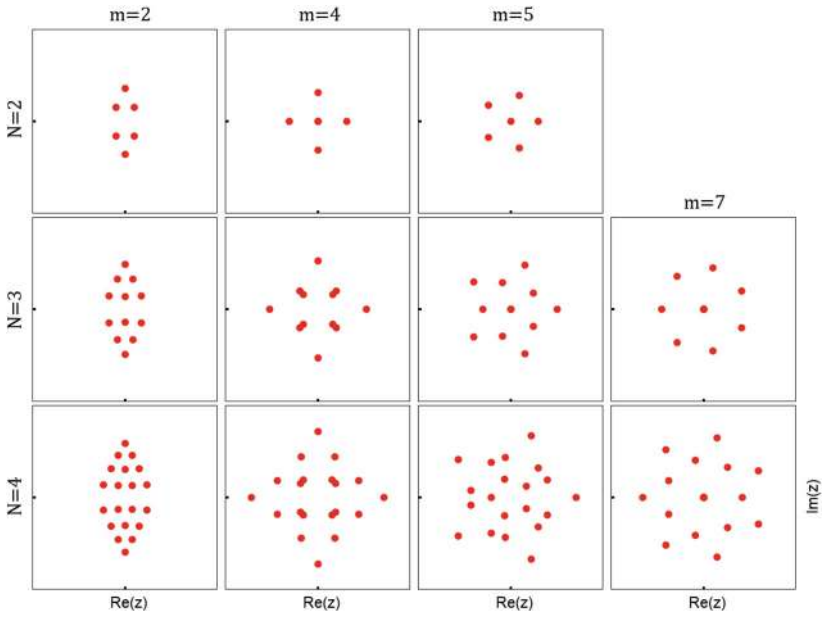

Fig. 3.20 Root structures of the $Q_N^{[m]}(z)$ polynomial hierarchy for $2 \le N \le 4$ and $m = 2, 4, 5, 7$. In all panels, $-8 \le \mathrm{Re}(z), \mathrm{Im}(z) \le 8$

$$M_Q = N(N+1) - N_Q, \quad M_R = N^2 - N_R, \tag{3.201}$$

respectively, where N_Q and N_R are given in Eqs. (3.194) and (3.198).

To get a visual impression of root structures in Okamoto polynomial hierarchies, we plot in Figs. 3.20 and 3.21 roots of the $Q_N^{[m]}(z)$ and $R_N^{[m]}(z)$ hierarchies in the complex z plane with $2 \le N \le 4$ and $m = 2, 4, 5, 7$. The first column of Fig. 3.20 (with $m = 2$), for roots of Okamoto polynomials $Q_N(z)$, exhibit "double triangles" as reported in Clarkson (2003). We caution the reader that sides of these double triangles are not exactly straight; thus our use of the term "double triangles" is only in an approximate sense. The second column of this figure, for roots of $Q_N^{[4]}(z)$ polynomials, exhibit a "square" shape with curved sides, intricate interiors, and some very close roots. The third column, for roots of $Q_N^{[5]}(z)$, exhibit a pentagon shape; while the fourth column, for roots of $Q_N^{[7]}(z)$, exhibit a heptagon shape. Compared to root shapes of the Yablonskii-Vorob'ev polynomial hierarchy, the present double-triangle and square shapes are new. The pentagon and heptagon shapes are not new, as they have appeared in the Yablonskii-Vorob'ev hierarchy before (see Fig. 3.1). However, compared to pentagons and heptagons of Yablonskii-Vorob'ev-hierarchy roots, the current pentagons and heptagons of Okamoto-hierarchy roots have different interiors.

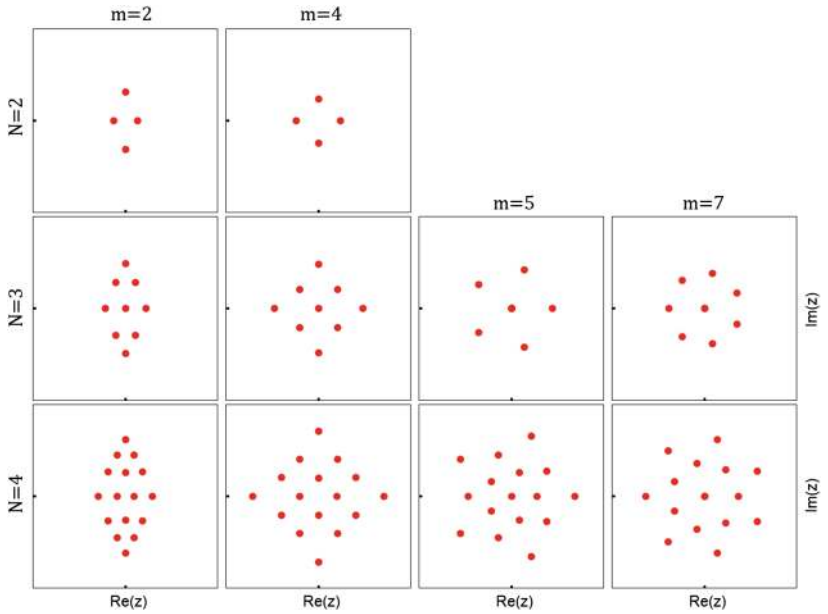

Fig. 3.21 Root structures of the $R_N^{[m]}(z)$ polynomial hierarchy for $2 \le N \le 4$ and $m = 2, 4, 5, 7$. In all panels, $-7 \le \mathrm{Re}(z), \mathrm{Im}(z) \le 7$

In Fig. 3.21 for the $R_N^{[m]}(z)$ hierarchy, shapes of their roots are somewhat similar to their counterparts for $Q_N^{[m]}(z)$ in the previous figure, but plenty of differences also exist between them. One difference is that, while the first column of Fig. 3.20 exhibit two separate triangles, the first column of the current figure exhibit two triangles that are joined together at the base to form a rhombus. Another difference is that, interior roots in the second column of the current figure are more orderly than their counterparts in Fig. 3.20. A third difference is that, even though shapes of roots in the fourth columns of the two figures are quite similar to each other, zero roots in corresponding panels actually have different multiplicities. For example, the zero root has multiplicity 5 in the upper panel of the fourth column of Fig. 3.20, but has multiplicity 2 in the corresponding panel of Fig. 3.21.

Geometric shapes of rogue waves in certain integrable systems are closely related with root structures of Okamoto polynomial hierarchies. We consider two such integrable systems below.

3.3.3 Manakov System

The Manakov system of focusing type is

$$\left.\begin{aligned}(\mathrm{i}\partial_t + \partial_x^2)u_1 + (|u_1|^2 + |u_2|^2)u_1 = 0,\\ (\mathrm{i}\partial_t + \partial_x^2)u_2 + (|u_1|^2 + |u_2|^2)u_2 = 0.\end{aligned}\right\} \tag{3.202}$$

Under the boundary conditions of

$$\left.\begin{aligned}u_1(x,t) \to \rho_1 e^{\mathrm{i}(k_1 x + \omega_1 t)}, \quad x,t \to \pm\infty,\\ u_2(x,t) \to \rho_2 e^{\mathrm{i}(k_2 x + \omega_2 t)}, \quad x,t \to \pm\infty,\end{aligned}\right\} \tag{3.203}$$

where

$$\rho_1 = \rho_2 = \sqrt{2}\,|k_1 - k_2|\,, \quad k_1 \neq k_2, \tag{3.204}$$

and

$$\omega_1 = \epsilon_1\rho_1^2 + \epsilon_2\rho_2^2 - k_1^2, \quad \omega_2 = \epsilon_1\rho_1^2 + \epsilon_2\rho_2^2 - k_2^2, \tag{3.205}$$

this Manakov system admits a class of rogue waves whose τ functions are made of Schur polynomials with index jumps of three, and such rogue waves have been presented in Theorem 2.12 of Chap. 2. For the convenience of the reader, those results are reproduced in the following lemma.

Lemma 3.3 *Under parameter conditions (3.204), the focusing Manakov system (3.202) admits the following rogue wave solutions*

$$u_{1,N_1,N_2}(x,t) = \rho_1 \frac{g_{1,N_1,N_2}}{f_{N_1,N_2}} e^{\mathrm{i}(k_1 x + \omega_1 t)}, \quad u_{2,N_1,N_2}(x,t) = \rho_1 \frac{g_{2,N_1,N_2}}{f_{N_1,N_2}} e^{\mathrm{i}(k_2 x + \omega_2 t)}, \tag{3.206}$$

where N_1 and N_2 are arbitrary nonnegative integers,

$$f_{N_1,N_2} = \sigma_{0,0}, \quad g_{1,N_1,N_2} = \sigma_{1,0}, \quad g_{2,N_1,N_2} = \sigma_{0,1}, \tag{3.207}$$

$\sigma_{n,k}$ is a 2×2 block determinant

$$\sigma_{n,k} = \det\begin{pmatrix}\sigma_{n,k}^{[1,1]} & \sigma_{n,k}^{[1,2]}\\ \sigma_{n,k}^{[2,1]} & \sigma_{n,k}^{[2,2]}\end{pmatrix}, \quad \sigma_{n,k}^{[I,J]} = \left(\phi_{3i-I,\,3j-J}^{(n,k,I,J)}\right)_{1\le i\le N_I,\,1\le j\le N_J}, \tag{3.208}$$

the matrix elements in $\sigma_{n,k}^{[I,J]}$ are defined by

$$\phi_{i,j}^{(n,k,I,J)} = \sum_{\nu=0}^{\min(i,j)} \left[\frac{|p_1|^2}{(p_0+p_0^*)^2}\right]^{\nu} S_{i-\nu}(\boldsymbol{x}_I^+(n,k) + \nu\boldsymbol{s})\, S_{j-\nu}(\boldsymbol{x}_J^-(n,k) + \nu\boldsymbol{s}^*), \tag{3.209}$$

vectors $\boldsymbol{x}_I^+(n,k) = \left(x_{1,I}^+, x_{2,I}^+, \cdots\right)$ *and* $\boldsymbol{x}_J^-(n,k) = \left(x_{1,J}^-, x_{2,J}^-, \cdots\right)$ *are defined by*

$$x_{r,I}^+(n,k) = p_r x + \left(\sum_{l=0}^{r} p_l p_{r-l}\right)(\mathrm{i}t) + n\theta_r + k\lambda_r + a_{r,I}, \qquad \text{if } r \bmod 3 \neq 0, \tag{3.210}$$

$$x_{r,J}^-(n,k) = p_r^* x - \left(\sum_{l=0}^{r} p_l^* p_{r-l}^*\right)(\mathrm{i}t) - n\theta_r^* - k\lambda_r^* + a_{r,J}^*, \qquad \text{if } r \bmod 3 \neq 0, \tag{3.211}$$

$$x_{r,I}^+(n,k) = x_{r,J}^-(n,k) = 0, \qquad \text{if } r \bmod 3 = 0, \tag{3.212}$$

$\boldsymbol{s} = (s_1, s_2, \cdots)$, $(p_r, \theta_r, \lambda_r, s_r)$ *are coefficients from the expansions*

$$p(\kappa) = \sum_{r=0}^{\infty} p_r \kappa^r, \quad \ln\left[\frac{p(\kappa) - \mathrm{i}k_1}{p_0 - \mathrm{i}k_1}\right] = \sum_{r=1}^{\infty} \theta_r \kappa^r, \tag{3.213}$$

$$\ln\left[\frac{p(\kappa) - \mathrm{i}k_2}{p_0 - \mathrm{i}k_2}\right] = \sum_{r=1}^{\infty} \lambda_r \kappa^r, \tag{3.214}$$

$$\ln\left[\frac{1}{\kappa}\left(\frac{p_0 + p_0^*}{p_1}\right)\left(\frac{p(\kappa) - p_0}{p(\kappa) + p_0^*}\right)\right] = \sum_{r=1}^{\infty} s_r \kappa^r, \tag{3.215}$$

the function $p(\kappa)$ *is defined by the equation*

$$Q_1[p(\kappa)] = \frac{Q_1(p_0)}{3}\left[e^{\kappa} + 2e^{-\kappa/2}\cos\left(\frac{\sqrt{3}}{2}\kappa\right)\right], \tag{3.216}$$

and $(a_{1,1}, a_{2,1}, a_{4,1}, a_{5,1}, \ldots, a_{3N_1-1,1})$, $(a_{1,2}, a_{2,2}, a_{4,2}, a_{5,2}, \ldots, a_{3N_2-2,2})$ *are free complex constants.*

Regarding coefficients s_r in Eq. (3.215), we can show that $s_r = 0$ when $r \bmod 3 \neq 0$ (Yang and Yang 2023a). This fact will be useful in the determination of rogue patterns in the inner regions below.

In the special cases where these block determinants degenerate to a single block, i.e., when $(N_1, N_2) = (N, 0)$ or $(0, N)$, the resulting rogue waves are called Q-type and R-type of N-th order respectively. For these special waves, $\sigma_{n,k}$ in Eq. (3.208) becomes

$$\sigma_{n,k}^{(Q)} = \left(\phi_{3i-1,3j-1}^{(n,k)}\right)_{1\leq i,j\leq N}, \quad \sigma_{n,k}^{(R)} = \left(\phi_{3i-2,3j-2}^{(n,k)}\right)_{1\leq i,j\leq N}, \tag{3.217}$$

where $\phi_{i,j}^{(n,k)}$ is given by Eq. (3.209) but with indices I and J removed. Internal free complex parameters are $(a_1, a_2, a_4, a_5, \cdots, a_{3N-1})$ for Q-type waves, and $(a_1, a_2, a_4, a_5, \cdots, a_{3N-2})$ for R-type waves. We normalize $a_1 = 0$ by a shift of the (x, t) axes. Then, internal parameters in these rogue waves are $(a_2, a_4, a_5, \cdots, a_{3N-1})$ for Q-type, and $(a_2, a_4, a_5, \cdots, a_{3N-2})$ for R-type.

When one of these internal parameters is large, patterns of these rogue waves are summarized in the following two theorems (Yang and Yang 2023a).

Theorem 3.14 *For the Q-type rogue wave $[u_{1,N,0}(x,t), u_{2,N,0}(x,t)]$ in the Manakov system (3.202), suppose $|a_m| \gg 1$ and all other internal parameters $O(1)$. In addition, suppose all nonzero roots of $Q_N^{[m]}(z)$ are simple. Then, the following statements for this rogue wave hold.*

1. *In the outer region on the (x,t) plane, where $\sqrt{x^2+t^2} = O(|a_m|^{1/m})$, this rogue wave asymptotically separates into M_Q isolated fundamental rogue waves, where M_Q is given in Eq. (3.201). These fundamental rogue waves are $[\hat{u}_1(x - \hat{x}_0, t - \hat{t}_0)\, e^{\mathrm{i}(k_1 x + \omega_1 t)},\ \hat{u}_2(x - \hat{x}_0, t - \hat{t}_0)\, e^{\mathrm{i}(k_2 x + \omega_2 t)}]$, where $[\hat{u}_1(x,t), \hat{u}_2(x,t)]$ are given in Eqs. (3.95)–(3.96), and their positions $(\hat{x}_0, \hat{t}_0)$ are given by*

$$\left.\begin{aligned} \hat{x}_0 &= \tfrac{1}{\Re(p_0)} \Re\left[\tfrac{p_0^*}{p_1}\left(z_0 a_m^{1/m} - \Delta_Q\right)\right], \\ \hat{t}_0 &= \tfrac{1}{2\Re(p_0)} \Im\left[\tfrac{1}{p_1}\left(z_0 a_m^{1/m} - \Delta_Q\right)\right], \end{aligned}\right\} \tag{3.218}$$

   where $\Re$ and $\Im$ represent the real and imaginary parts of a complex number, z_0 is each of the M_Q nonzero simple roots of $Q_N^{[m]}(z)$, and Δ_Q is a z_0-dependent $O(1)$ quantity whose formula will be given by Eq. (3.246) in later text. The error of this fundamental rogue wave approximation is $O(|a_m|^{-1/m})$. Expressed mathematically, when $|a_m| \gg 1$ and $(x - \hat{x}_0)^2 + (t - \hat{t}_0)^2 = O(1)$, we have the following solution asymptotics

$$\left.\begin{aligned} u_{1,N,0}(x,t) &= \hat{u}_1(x - \hat{x}_0, t - \hat{t}_0)\, e^{\mathrm{i}(k_1 x + \omega_1 t)} + O(|a_m|^{-1/m}), \\ u_{2,N,0}(x,t) &= \hat{u}_2(x - \hat{x}_0, t - \hat{t}_0)\, e^{\mathrm{i}(k_2 x + \omega_2 t)} + O(|a_m|^{-1/m}). \end{aligned}\right\} \tag{3.219}$$

2. *If zero is a root of the Okamoto-hierarchy polynomial $Q_N^{[m]}(z)$, then in the neighborhood of the origin (the inner region), where $x^2 + t^2 = O(1)$, this rogue wave is approximately a lower (N_{1Q}, N_{2Q})-th order rogue wave $[u_{1,N_{1Q},N_{2Q}}(x,t), u_{2,N_{1Q},N_{2Q}}(x,t)]$ as given in Lemma 3.3, where (N_{1Q}, N_{2Q}) are provided in Theorem 3.12. Internal parameters $(\hat{a}_{1,1}, \hat{a}_{2,1}, \ldots, \hat{a}_{3N_{1Q}-1,\,1})$ and $(\hat{a}_{1,2}, \hat{a}_{2,2}, \ldots, \hat{a}_{3N_{2Q}-2,\,2})$ in this lower-order rogue wave are the same as those in the original rogue wave, i.e.,*

$$\hat{a}_{j,1} = \hat{a}_{j,2} = a_j, \quad j = 1, 2, 4, 5, \cdots. \tag{3.220}$$

The error of this lower-order rogue wave approximation is $O(|a_m|^{-1})$. *Expressed mathematically, when* $|a_m| \gg 1$ *and* $x^2 + t^2 = O(1)$,

$$\left.\begin{aligned} u_{1,N,0}(x,t;a_2,a_4,a_5,\cdots) &= u_{1,N_{1Q},N_{2Q}}(x,t;\hat{a}_{j,1},\hat{a}_{j,2},\, j=1,2,4,5,\ldots) \\ &\quad + O(|a_m|^{-1}), \\ u_{2,N,0}(x,t;a_2,a_4,a_5,\cdots) &= u_{2,N_{1Q},N_{2Q}}(x,t;\hat{a}_{j,1},\hat{a}_{j,2},\, j=1,2,4,5,\ldots) \\ &\quad + O(|a_m|^{-1}). \end{aligned}\right\} \tag{3.221}$$

If zero is not a root of $Q_N^{[m]}(z)$, *then in the inner region, this rogue wave approaches the uniform background* $[\rho_1 e^{\mathrm{i}(k_1 x+\omega_1 t)}, \rho_1 e^{\mathrm{i}(k_2 x+\omega_2 t)}]$ *when* $|a_m| \gg 1$.

Theorem 3.15 *For the R-type rogue wave* $[u_{1,0,N}(x,t), u_{2,0,N}(x,t)]$ *in the Manakov system (3.202), suppose* $|a_m| \gg 1$ *and all other internal parameters* $O(1)$. *In addition, suppose all nonzero roots of* $R_N^{[m]}(z)$ *are simple. Then, the following asymptotics for this rogue wave holds.*

1. *In the outer region, where* $\sqrt{x^2+t^2} = O(|a_m|^{1/m})$, *this rogue wave asymptotically separates into* M_R *isolated fundamental rogue waves, where* M_R *is given in Eq. (3.201). These fundamental rogue waves are* $[\hat{u}_1(x-\hat{x}_0, t-\hat{t}_0)\, e^{\mathrm{i}(k_1 x+\omega_1 t)}, \hat{u}_2(x-\hat{x}_0, t-\hat{t}_0)\, e^{\mathrm{i}(k_2 x+\omega_2 t)}]$, *where* $[\hat{u}_1(x,t), \hat{u}_2(x,t)]$ *are given in Eqs. (3.95)–(3.96), and their positions* $(\hat{x}_0, \hat{t}_0)$ *are given by*

$$\left.\begin{aligned} \hat{x}_0 &= \tfrac{1}{\Re(p_0)} \Re\left[\tfrac{p_0^*}{p_1}\left(z_0 a_m^{1/m} - \Delta_R\right)\right], \\ \hat{t}_0 &= \tfrac{1}{2\Re(p_0)} \Im\left[\tfrac{1}{p_1}\left(z_0 a_m^{1/m} - \Delta_R\right)\right], \end{aligned}\right\} \tag{3.222}$$

where z_0 *is each of the* M_R *nonzero simple roots of* $R_N^{[m]}(z)$, *and* Δ_R *is a* z_0*-dependent* $O(1)$ *quantity given by Eq. (3.264) in later text. The error of this fundamental rogue wave approximation is* $O(|a_m|^{-1/m})$. *Expressed mathematically, when* $|a_m| \gg 1$ *and* $(x-\hat{x}_0)^2 + (t-\hat{t}_0)^2 = O(1)$, *we have the following solution asymptotics*

$$\left.\begin{aligned} u_{1,0,N}(x,t) &= \hat{u}_1(x-\hat{x}_0, t-\hat{t}_0)\, e^{\mathrm{i}(k_1 x+\omega_1 t)} + O(|a_m|^{-1/m}), \\ u_{2,0,N}(x,t) &= \hat{u}_2(x-\hat{x}_0, t-\hat{t}_0)\, e^{\mathrm{i}(k_2 x+\omega_2 t)} + O(|a_m|^{-1/m}). \end{aligned}\right\} \tag{3.223}$$

2. *If zero is a root of the Okamoto-hierarchy polynomial* $R_N^{[m]}(z)$, *then in the inner region, where* $x^2 + t^2 = O(1)$, *this rogue wave is approximately a lower* (N_{1R}, N_{2R})*-th order rogue wave* $[u_{1,N_{1R},N_{2R}}(x,t),\ u_{2,N_{1R},N_{2R}}(x,t)]$ *as given in Lemma 3.3, where* (N_{1R}, N_{2R}) *are provided in Theorem 3.13. Internal parameters* $(\hat{a}_{1,1}, \hat{a}_{2,1}, \ldots, \hat{a}_{3N_{1R}-1,\,1})$ *and* $(\hat{a}_{1,2}, \hat{a}_{2,2}, \ldots, \hat{a}_{3N_{2R}-2,\,2})$ *in this lower-order rogue wave are the same as those in the original rogue wave, i.e.,*

$$\hat{a}_{j,1} = \hat{a}_{j,2} = a_j, \quad j = 1, 2, 4, 5, \cdots. \tag{3.224}$$

The error of this lower-order rogue wave approximation is $O(|a_m|^{-1})$. *Expressed mathematically, when* $|a_m| \gg 1$ *and* $x^2 + t^2 = O(1)$,

$$\left.\begin{aligned} u_{1,0,N}(x,t;a_2,a_4,a_5,\cdots) &= u_{1,N_{1R},N_{2R}}(x,t;\hat{a}_{j,1},\hat{a}_{j,2},j=1,2,4,5,\ldots) \\ &\quad +O(|a_m|^{-1}), \\ u_{2,0,N}(x,t;a_2,a_4,a_5,\cdots) &= u_{2,N_{1R},N_{2R}}(x,t;\hat{a}_{j,1},\hat{a}_{j,2},j=1,2,4,5,\ldots) \\ &\quad +O(|a_m|^{-1}). \end{aligned}\right\} \tag{3.225}$$

If zero is not a root of $R_N^{[m]}(z)$, *then in the inner region, this rogue wave approaches the uniform background* $[\rho_1 e^{\mathrm{i}(k_1 x+\omega_1 t)}, \rho_1 e^{\mathrm{i}(k_2 x+\omega_2 t)}]$ *when* $|a_m| \gg 1$.

Proofs of these two theorems will be provide later in this section.

Theorems 3.14 and 3.15 show that, when the internal parameter $|a_m|$ is large, then in the outer region, patterns of Q- and R-type Manakov rogue waves comprise isolated fundamental rogue waves, which are the same with each other, except for their locations that are determined by root structures of $Q_N^{[m]}(z)$ and $R_N^{[m]}(z)$ polynomials through formula (3.218) and (3.222). To the leading order of these positions, i.e., to $O(|a_m|^{1/m})$, rogue patterns formed by these fundamental rogue waves are linear transformations of the underlying root structures. However, the next-order corrections of size $O(1)$ to these leading-order terms, induced by Δ_Q and Δ_R in Eqs. (3.218) and (3.222), depend on the root z_0 in a nonlinear way (see Eqs. (3.246) and (3.264) in later text). These next-order nonlinear corrections will introduce deformations to rogue patterns and make them look different from linear transformations of root structures, as we will see graphically below. This behavior contrasts rogue patterns reported in Sect. 3.1 for some other types of rogue waves, where those patterns are just linear transformations of root structures of the Yablonskii-Vorob'ev polynomial hierarchy, even after next-order position corrections are included. We do note, though, that these nonlinear deformations of rogue patterns in the present case are subdominant compared to the leading-order term, and will become less significant as $|a_m|$ gets larger. In other words, as $|a_m|$ increases, rogue patterns for Q- and R-type Manakov rogue waves will look more and more like the linear transformation of root structures of $Q_N^{[m]}(z)$ and $R_N^{[m]}(z)$.

Theorems 3.14 and 3.15 also show that, when the internal parameter $|a_m|$ is large, then in the inner region, the original rogue wave reduces to a lower-order rogue wave, or to the uniform background, depending on whether zero is a root of $Q_N^{[m]}(z)$ or $R_N^{[m]}(z)$. If zero is a root, then its multiplicity will determine the order of this reduced rogue wave.

In these theorems, which internal parameter a_m is taken to be large has profound consequences on the prediction of rogue patterns. Once the index m of the large parameter a_m is fixed, that choice would determine not only the size of the outer region and the convergence rates of predictions, but also the polynomial $Q_N^{[m]}(z)$ or

$R_N^{[m]}(z)$ whose roots predict the locations of isolated fundamental rogue waves in the outer region.

It may be interesting to notice from these theorems that in the outer region, both the Q-type and R-type rogue waves, under a large internal parameter, split into a number of the lowest-order R-type rogue waves (the fundamental rogue waves) *only*, never to the lowest-order Q-type rogue waves. There are two ways to understand this. An intuitive way is that, the lowest-order R-type rogue wave (with $N_1 = 0$ and $N_2 = 1$) is the fundamental rogue wave with degree-two polynomials. The lowest-order Q-type rogue wave (with $N_1 = 1$ and $N_2 = 0$), however, is a ratio of degree-four polynomials. This latter solution should be viewed as a composition of two fundamental rogue waves, and it would split up into two separate fundamental rogue waves when its internal parameter a_2 is large (see Fig. 2.18 in the previous chapter). A mathematical way to understand this is that, as long as the nonzero roots in $Q_N^{[m]}(z)$ and $R_N^{[m]}(z)$ are simple, then under a large internal parameter, both the Q-type and R-type rogue waves in the outer region would reduce to ratios of degree-two polynomials (see later text), which can only be the fundamental Manakov rogue waves, not the lowest-order Q-type rogue waves of degree-four polynomials.

Comparison Between Predictions and True Solutions

Now, we compare predictions from Theorems 3.14–3.15 with true solutions. For this purpose, we choose background wavenumbers $k_1 = -k_2 = 1/\sqrt{12}$. Then background amplitudes are obtained from conditions (3.204) as $\rho_1 = \rho_2 = \sqrt{2/3}$, and background wave frequencies can be obtained from equations (3.205).

Q-Type

First, we consider Q-type Manakov rogue waves. Specifically, we take $N = 2$; thus these are second-order waves with three internal parameters (a_2, a_4, a_5). We set one of these parameters large and the other parameters zero. Then, when that large parameter is chosen as one of

$$a_2 = 30\mathrm{i}, \quad a_4 = 400, \quad a_5 = 3000\mathrm{i}, \tag{3.226}$$

the three predicted rogue waves from Theorem 3.14 are displayed in the three columns of Fig. 3.22, respectively. The top row of this figure shows the predicted $(\hat{x}_0, \hat{t}_0)$ locations by formulae (3.218) applied to all roots of $Q_2^{[m]}(z)$. In these formulae, $p_0 = 1/2$, $(p_1, p_2) = \left(12^{-1/3}, 144^{-1/3}\right)$, and Δ_Q is calculated from Eq. (3.246). Note that these $(\hat{x}_0, \hat{t}_0)$ predictions contain not only the dominant $O(|a_m|^{1/m})$ contribution, but also the subdominant $O(1)$ contribution.

According to Theorem 3.14, at each of the $(\hat{x}_0, \hat{t}_0)$ locations obtained from formulae (3.218) for nonzero roots of $Q_2^{[m]}(z)$, a fundamental Manakov rogue wave is predicted. The amplitude fields of these predicted fundamental rogue waves in the outer region are plotted in the middle and bottom rows of Fig. 3.22, for $|u_1|$ and $|u_2|$, respectively.

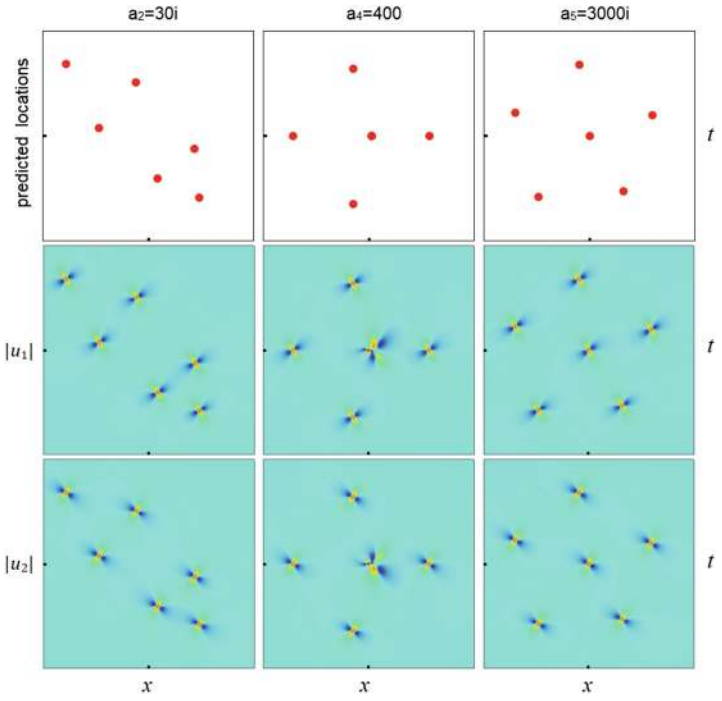

Fig. 3.22 Predicted patterns of Q-type second-order Manakov rogue waves from Theorem 3.14. Each column is for a rogue wave with a single large parameter a_m, whose value is indicated on top, and all other internal parameters are set as zero. Top row: predicted $(\hat{x}_0, \hat{t}_0)$ locations by formulae (3.218) applied to all roots of $Q_2^{[m]}(z)$. Middle row: predicted $|u_1(x,t)|$. Bottom row: predicted $|u_2(x,t)|$. These $(|u_1|, |u_2|)$ predictions are assembled as $|u_k^{(p)}(x,t)| = |u_{k,N_{1Q},N_{2Q}}(x,t)| + \sum_{j=1}^{M_Q} \left(|\hat{u}_k(x - \hat{x}_0^{(j)}, t - \hat{t}_0^{(j)})| - \rho_k \right)$, where $k = 1, 2$, $u_{k,N_{1Q},N_{2Q}}(x,t)$ are the predicted inner solutions on the right sides of Eqs. (3.221), M_Q is given in Eq. (3.201), $[\hat{u}_1(x,t), \hat{u}_2(x,t)]$ are given in Eqs. (3.95)–(3.96), and $[\hat{x}_0^{(j)}, \hat{t}_0^{(j)}]$ are the predicted locations (3.218) of outer fundamental rogue waves in the top row (with $z_0 \neq 0$). In all panels, $-40 \leq x, t \leq 40$

Theorem 3.14 also predicts that, if zero is a root of $Q_2^{[m]}(z)$, as is the case for $m = 4$ and 5, then in the inner region, i.e., the region near the $(\hat{x}_0, \hat{t}_0)$ location from formulae (3.218) with $z_0 = 0$, a lower (N_{1Q}, N_{2Q})-th order rogue wave would appear. These (N_{1Q}, N_{2Q}) values are calculated from Theorem 3.12 as

$$(N_{1Q}, N_{2Q}) = (0,0),\ (1,1),\ (0,1), \tag{3.227}$$

for the three solutions in Fig. 3.22, respectively. The first set $(0, 0)$ indicates that zero is not a root of $Q_2^{[2]}(z)$, hence no lower-order rogue wave in the inner region. The third set $(0, 1)$ indicates that the lower-order rogue wave in the inner region is a fundamental rogue wave, while the second set $(1, 1)$ indicates that the rogue wave

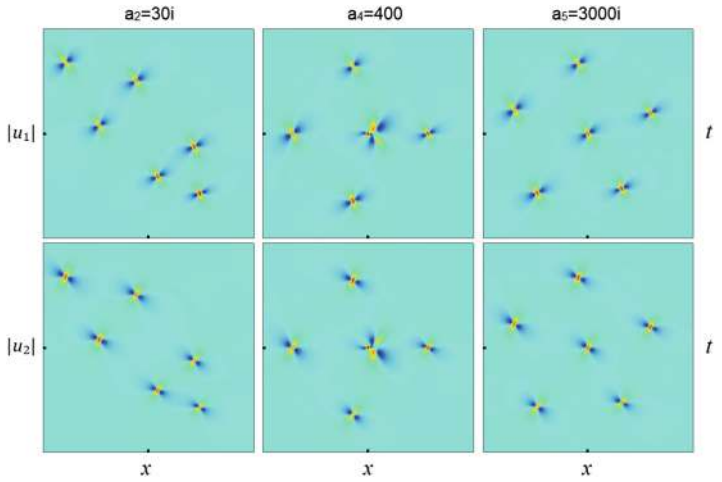

Fig. 3.23 True Q-type second-order Manakov rogue waves for the same parameters and (x, t) intervals as in Fig. 3.22

in the inner region is a non-fundamental rogue wave. Internal parameters in these predicted lower (N_{1Q}, N_{2Q})-th order rogue waves are all zero, due to our choices of internal parameters in the original rogue waves. Plotting these (N_{1Q}, N_{2Q})-th order rogue waves, we get the center-region predictions for rogue waves in the middle and bottom rows of Fig. 3.22.

Looking at these predicted rogue solutions in Fig. 3.22, we see that the large-a_2 solution exhibits a skewed double-triangle, reminiscent of the double-triangle root structure of $Q_2^{[2]}(z)$ in Fig. 3.20. The large-a_4 solution exhibits a square, reminiscent of the square-shaped root structure of $Q_2^{[4]}(z)$ in Fig. 3.20. The large-a_5 solution exhibits a pentagon, reminiscent of the pentagon-shaped root structure of $Q_2^{[5]}(z)$ in Fig. 3.20. This pentagon-shaped rogue pattern has been seen in the NLS and other equations before (see Sect. 3.1), but the double-triangle and square patterns are new.

Now, we compare these predictions to true solutions. The corresponding true solutions are plotted directly from Lemma 3.3 and displayed in Fig. 3.23. Comparing these true solution graphs with the predicted ones in Fig. 3.22, they clearly match each other very well.

To quantitatively compare our prediction with the true solution and verify Theorem 3.14's error decay rates with the large parameter a_m, we choose a_4 to be the large parameter, corresponding to the second-column solution in Figs. 3.22 and 3.23. For simplicity, we choose all a_4 to be real. As before, the other two internal parameters (a_2, a_5) in the rogue wave will be set as zero. We will vary this a_4 value, from 400 to 400,000, and for each value, we measure the errors of our prediction in the outer and inner regions and then plot these errors versus a_4. In the outer region, this error is defined as the distance in the (x, t) plane between the predicted and true positions of the fundamental rogue wave marked by the lower arrow in panel (a) of

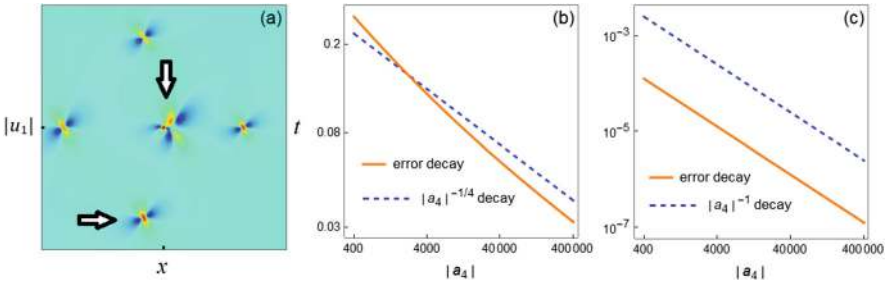

Fig. 3.24 Decay of errors in our predictions of Theorem 3.14 for the outer and inner regions of the Q-type second-order Manakov rogue wave with various large real values of a_4, while the other internal parameters are set as zero. (**a**) $|u_1(x,t)|$ of the true rogue wave with $a_4 = 400$. (**b**) Decay of error versus a_4 for the outer fundamental rogue wave marked by the lower arrow in panel (**a**), together with the $|a_4|^{-1/4}$ decay for comparison. (**c**) Decay of error versus a_4 at $x = t = 0$ of the inner region marked by the upper arrow in panel (**a**), together with the $|a_4|^{-1}$ decay for comparison

Fig. 3.24. In the inner region, marked by the upper arrow in panel (a), the error is defined as the magnitude of the difference between the predicted and true solution values at the origin $x = t = 0$. These error curves are plotted in panels (b) and (c), for the outer and inner regions, respectively. For comparison, decay rates of $|a_4|^{-1/4}$ and $|a_4|^{-1}$ are also plotted in the corresponding panels. These error curves clearly show that, the error decay rate is $|a_4|^{-1/4}$ in the outer region and $|a_4|^{-1}$ in the inner region, which fully agree with our theoretical predictions in Theorem 3.14.

R-Type

Next, we compare R-type rogue waves. Here, we set $N = 3$. Thus, these are third-order waves with internal parameters (a_2, a_4, a_5, a_7). We choose one of these parameters large and the other parameters zero. Then, when that large parameter is chosen as one of

$$a_2 = 30\mathrm{i}, \quad a_4 = 300, \quad a_5 = 1000\mathrm{i}, \quad a_7 = 3000, \tag{3.228}$$

the four predicted rogue waves from Theorem 3.15 are displayed in the four columns of Fig. 3.25, respectively. The top row of this figure shows the predicted $(\hat{x}_0, \hat{t}_0)$ locations by formulae (3.222) applied to all roots of $R_3^{[m]}(z)$. At each of the $(\hat{x}_0, \hat{t}_0)$ locations resulting from nonzero roots of $R_3^{[m]}(z)$, Theorem 3.15 predicts a fundamental Manakov rogue wave, whose amplitude fields $|u_1|$ and $|u_2|$ are plotted in the middle and bottom rows of Fig. 3.25, respectively. Our prediction for the center regions in these rows is based on Eq. (3.225) of Theorem 3.15. In this prediction, the (N_{1R}, N_{2R}) values for these four rogue solutions are obtained from Theorem 3.13 as

$$(N_{1R}, N_{2R}) = (0,1),\ (0,1),\ (1,2),\ (1,0), \tag{3.229}$$

respectively. These values show that the center region of the first two rogue solutions hosts a fundamental rogue wave, while that region in the last two rogue solutions

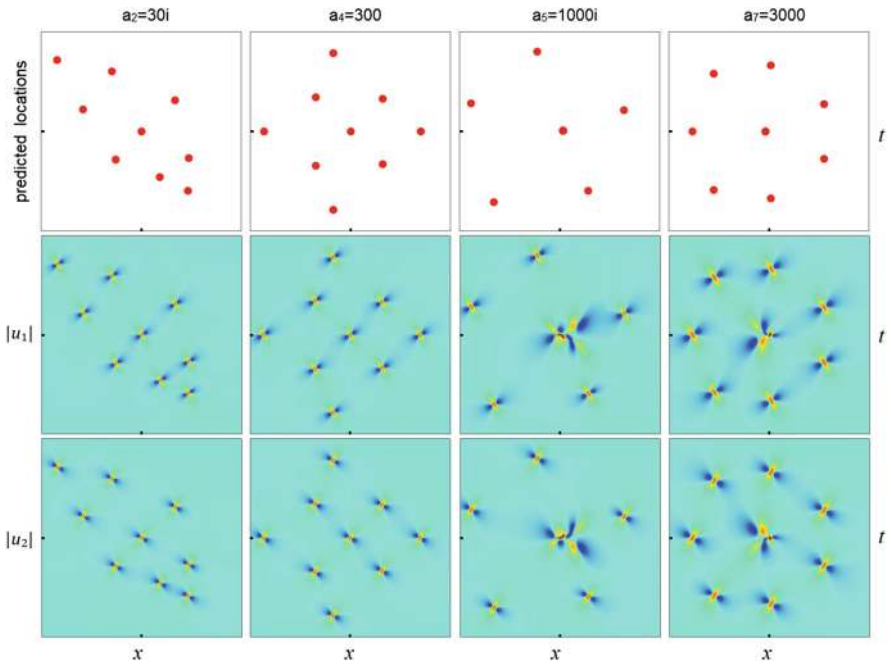

Fig. 3.25 Predicted R-type third-order Manakov rogue waves from Theorem 3.15. Each column is for a rogue wave with a single large parameter a_m, whose value is indicated on top, and all other internal parameters are set as zero. Top row: predicted $(\hat{x}_0, \hat{t}_0)$ locations by formulae (3.222) applied to all roots of $R_3^{[m]}(z)$. Middle row: predicted $|u_1(x,t)|$. Bottom row: predicted $|u_2(x,t)|$. The (x,t) intervals in the four columns are $-46 \le x,t \le 46$, $-41 \le x,t \le 41$, $-35 \le x,t \le 35$, and $-28 \le x,t \le 28$, respectively

hosts a non-fundamental rogue wave. Internal parameters in these predicted lower (N_{1R}, N_{2R})-th order rogue waves of the center region are all zero, due to our choices of internal parameters in the original rogue waves. Plotting these (N_{1R}, N_{2R})-th order rogue waves from Lemma 3.3, we get the center-region predictions for rogue waves in the middle and bottom rows of Fig. 3.25.

These predicted rogue solutions in Fig. 3.25 exhibit various patterns, such as a skewed and deformed rhombus (first column), a deformed square (second column), a deformed pentagon (third column), and a heptagon (last column). Of these patterns, rhombus-shaped and square-shaped ones are new.

Now, we compare these predictions to true solutions. The corresponding true solutions are plotted directly from Lemma 3.3 and displayed in Fig. 3.26. These true solutions clearly match the predicted ones in Fig. 3.25 very well.

In addition to this visual agreement, we have also performed error analysis for predictions of these R-type waves, similar to what we have done for Q-type waves in Fig. 3.24. This error analysis confirmed the error decay rates we predicted in Theorem 3.15 for the outer and inner regions. Details are omitted for brevity.

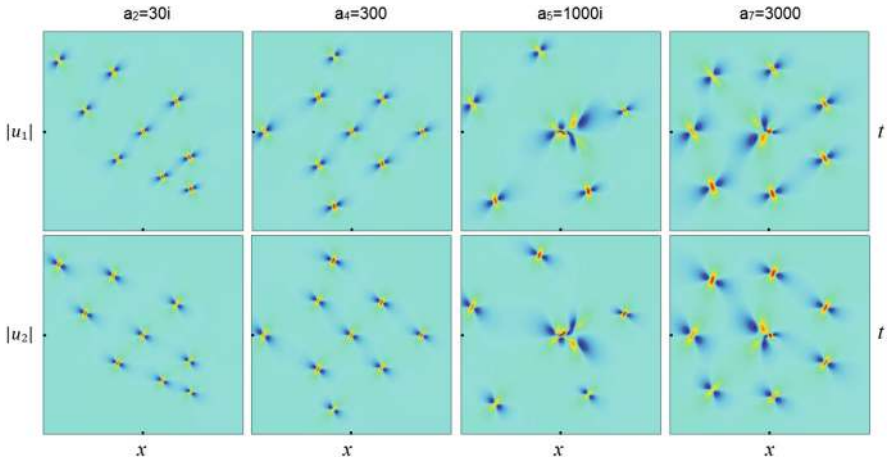

Fig. 3.26 True R-type third-order Manakov rogue waves for the same parameters and (x, t) intervals as in Fig. 3.25

Effect of Parameter Size on Rogue Shapes

From the above comparisons, we have established that Manakov rogue patterns can be accurately predicted by root structures of Okamoto-hierarchy polynomials through mappings (3.218) and (3.222). The reader may have noticed that, rogue shapes in the above figures are often twisted and less orderly, even though their corresponding root structures of Okamoto-hierarchy polynomials are very orderly. For example, in the R-type third-order rogue wave of Figs. 3.25–3.26 with large a_4, the upper-left and lower-left sides of rogue patterns are strongly bent in, resulting in an irregular square, but the corresponding root structure of $R_3^{[4]}(z)$ in Fig. 3.21 is like a regular square.

The reason for this irregularity in rogue patterns is apparently due to the next-order correction term in mappings (3.218) and (3.222) from the root structure of Okamoto-hierarchy polynomials to rogue peak positions in the (x, t) plane. While the leading term of $O(|a_m|^{1/m})$ in those formulae is a linear mapping, the next-order correction term of $O(1)$ is a nonlinear mapping in view of formulae (3.246) and (3.264). This nonlinear part of the mappings causes deformations in rogue shapes and makes them irregular even if the underlying root structures are. But this next-order correction term is subdominant, and its relative effect should get weaker when $|a_m|$ gets larger. In other words, if we increase $|a_m|$, this irregularity in rogue shape should diminish. To confirm this prediction, we take that R-type third-order rogue wave of Figs. 3.25–3.26 with large a_4, and vary its a_4 value, with other internal parameters still set as zero. For three a_4 values of 30, 300 and 3000, predicted rogue locations $(\hat{x}_0, \hat{t}_0)$ from formulae (3.222) of Theorem 3.15 are plotted in the upper row of Fig. 3.27, and true solutions (only the $|u_1|$ part) are plotted in the lower row. We see that when $a_4 = 30$, both the predicted and true solutions

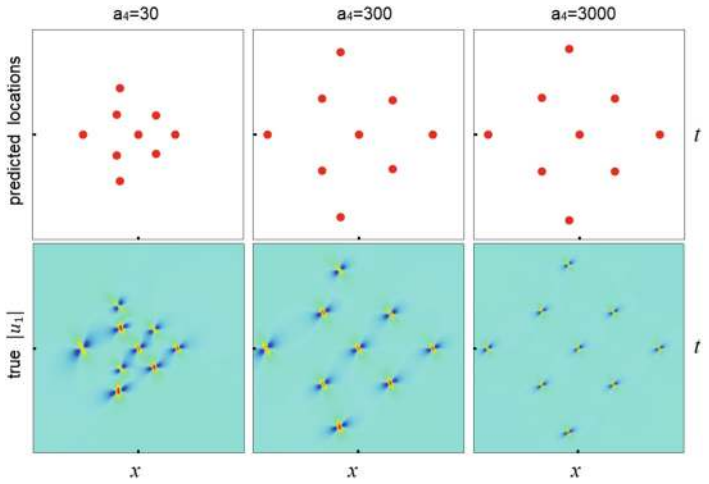

Fig. 3.27 Effect of parameter size a_4 on R-type third-order Manakov rogue shapes (all other internal parameters are set as zero). Upper row: predicted $(\hat{x}_0, \hat{t}_0)$ locations by formulae (3.222) applied to all roots of $R_3^{[4]}(z)$. Lower row: true $|u_1(x,t)|$. The (x,t) intervals in the three columns are $-41 \le x, t \le 41$, $-41 \le x, t \le 41$, and $-70 \le x, t \le 70$, respectively

are highly irregular, almost random-like. But as a_4 increases to 300, this irregularity is significantly reduced and is visible only at the upper-left and lower-left sides of the figure. When a_4 further increases to 3000, this irregularity is almost completely gone, and the rogue shape closely resembles the root structure of $R_3^{[4]}(z)$ as shown in Fig. 3.21.

Proofs of Theorems 3.14–3.15

Now we prove the Q-type and R-type Manakov rogue patterns presented in Theorems 3.14–3.15. Our proof is based on an asymptotic analysis of rogue wave solutions, or equivalently, the determinant $\sigma_{n,k}^{(Q,R)}$ in Eq. (3.217), in the large $|a_m|$ limit.

(1) Proof of Theorem 3.14 for the outer region

First, we use determinant identities and the Laplace expansion to rewrite $\sigma_{n,k}^{(Q)}$ in Eq. (3.217) as

$$\sigma_{n,k}^{(Q)} = \sum_{0\le\nu_1<\nu_2<\cdots<\nu_N\le 3N-1} \det_{1\le i,j\le N}\left[(h_0)^{\nu_j} S_{3i-1-\nu_j}(\boldsymbol{x}^+(n,k)+\nu_j \boldsymbol{s})\right] \times \det_{1\le i,j\le N}\left[(h_0^*)^{\nu_j} S_{3i-1-\nu_j}(\boldsymbol{x}^-(n,k)+\nu_j \boldsymbol{s}^*)\right], \quad (3.230)$$

similar to what we did in Eq. (2.77). Here, $h_0 = p_1/(p_0+p_0^*)$. We need to derive the asymptotics of this $\sigma_{n,k}^{(Q)}$ when $|a_m|$ is large and the other parameters $O(1)$. In this

parameter regime, when (x,t) is in the outer region of $\sqrt{x^2+t^2} = O(|a_m|^{1/m})$, we have

$$S_j(\boldsymbol{x}^+(n,k)+\nu\boldsymbol{s}) = S_j(x_1^+, x_2^+, \nu s_3, x_4^+, x_5^+, \nu s_6, \cdots, x_m^+ + \nu s_m, \cdots) \sim S_j(\mathbf{v}), \tag{3.231}$$

where

$$\mathbf{v} = (p_1 x + 2p_0 p_1 \mathrm{i}t,\ 0, \cdots, 0, a_m, 0, \cdots). \tag{3.232}$$

Here, the fact of $s_r = 0$ for $r \bmod 3 \neq 0$ has been used (Yang and Yang 2023a).

Next, we see from the definition of Schur polynomials that

$$\sum_{j=0}^{\infty} S_j(\mathbf{v})\epsilon^j = e^{\epsilon(p_1 x + 2p_0 p_1 \mathrm{i}t) + \epsilon^m a_m}. \tag{3.233}$$

Introducing the scaled variable $\hat{\epsilon} = \epsilon a_m^{1/m}$, we can write the right side of the above equation as $e^{\hat{\epsilon} z + \hat{\epsilon}^m}$, where

$$z = a_m^{-1/m}(p_1 x + 2p_0 p_1 \mathrm{i}t). \tag{3.234}$$

This $e^{\hat{\epsilon} z + \hat{\epsilon}^m}$ term is the same as the right side of Eq. (3.189), except for a notational change of ϵ to $\hat{\epsilon}$. Using that Eq. (3.189) with ϵ changed to $\hat{\epsilon}$ and combining the result with the above Eq. (3.233), we get

$$\sum_{j=0}^{\infty} S_j(\mathbf{v})\,\epsilon^j = \sum_{j=0}^{\infty} p_j^{[m]}(z)\,\hat{\epsilon}^j. \tag{3.235}$$

Then, recalling $\hat{\epsilon} = \epsilon a_m^{1/m}$, we arrive at the relation

$$S_j(\mathbf{v}) = a_m^{j/m} p_j^{[m]}(z). \tag{3.236}$$

To proceed further, we notice that the highest order term of a_m in Eq. (3.230) for $\sigma_{n,k}^{(Q)}$ comes from the index choice of $\nu_j = j-1$. For this index choice, using the formulae (3.231) and (3.236), as well as the definition of $Q_N^{[m]}(z)$ in Eq. (3.190), we find that

$$\begin{aligned}\det_{1\le i,j\le N}\left[S_{3i-1-\nu_j}(\boldsymbol{x}^+(n,k)+\nu_j\boldsymbol{s})\right] &= \det_{1\le i,j\le N}\left[S_{3i-j}\left(\boldsymbol{x}^+(n,k)+(j-1)\boldsymbol{s}\right)\right] \\ &\sim c_N^{-1} a_m^{N(N+1)/m} Q_N^{[m]}(z).\end{aligned} \tag{3.237}$$

Similarly,

$$\det_{1\le i,j\le N}\left[S_{3i-1-\nu_j}(\boldsymbol{x}^-(n,k)+\nu_j\boldsymbol{s}^*)\right]\sim c_N^{-1}\left(a_m^*\right)^{N(N+1)/m}Q_N^{[m]}(z^*). \tag{3.238}$$

Thus,

$$\sigma_{n,k}^{(Q)}\sim|\alpha|^2\,|a_m|^{2N(N+1)/m}\left|Q_N^{[m]}(z)\right|^2, \tag{3.239}$$

where $\alpha=(h_0)^{N(N-1)/2}c_N^{-1}$. Since this leading-order asymptotics of $\sigma_{n,k}^{(Q)}$ is independent of n and k, it implies that, for $|a_m|\gg 1$, we would have $\sigma_{1,0}/\sigma_{0,0}\sim 1$ and $\sigma_{0,1}/\sigma_{0,0}\sim 1$, i.e., the solution $[u_{1,N,0}(x,t),u_{2,N,0}(x,t)]$ would be on the uniform background $[\rho_1 e^{\mathrm{i}(k_1x+\omega_1t)},\rho_1 e^{\mathrm{i}(k_2x+\omega_2t)}]$, except when z is near a root z_0 of the polynomial $Q_N^{[m]}(z)$, where this leading-order asymptotics in (3.239) vanishes. In terms of x and t, this means that the solution $[u_{1,N,0}(x,t),u_{2,N,0}(x,t)]$ would be on the uniform background, except when (x,t) is in an $O(1)$ neighborhood of the location $\left(\tilde{x}_0,\tilde{t}_0\right)$, where

$$z_0=a_m^{-1/m}(p_1\tilde{x}_0+2\mathrm{i}p_0p_1\tilde{t}_0). \tag{3.240}$$

Such $\left(\tilde{x}_0,\tilde{t}_0\right)$ locations are the leading-order terms of $(\hat{x}_0,\hat{t}_0)$ in Eqs. (3.218) of Theorem 3.14. Due to the requirement of $\sqrt{x^2+t^2}=O(|a_m|^{1/m})$, z_0 should not be zero here.

Next, we show that when (x,t) is in an $O(1)$ neighborhood of each of the $\left(\tilde{x}_0,\tilde{t}_0\right)$ locations given by Eq. (3.240), the Q-type Manakov rogue wave approaches a fundamental Manakov rogue wave that is located within $O(1)$ distance from $\left(\tilde{x}_0,\tilde{t}_0\right)$. In order to derive this more refined asymptotics, we need to calculate terms in Eq. (3.230) whose order is lower than $|a_m|^{2N(N+1)/m}$, since that highest order term (3.239) vanishes at $\left(\tilde{x}_0,\tilde{t}_0\right)$.

First, we denote

$$\hat{x}_2^+(x,t)=p_2x+(2p_0p_2+p_1^2)(\mathrm{i}t), \tag{3.241}$$

which are the dominant terms of $x_2^+(x,t)$ from Lemma 3.3 with the index 'I' removed when (x,t) is in the outer region. Then, for (x,t) in the $O(1)$ neighborhood of $\left(\tilde{x}_0,\tilde{t}_0\right)$, we have a more refined asymptotics for $S_j(\boldsymbol{x}^+(n,k)+\nu\boldsymbol{s})$ as

$$\begin{aligned}S_j(\boldsymbol{x}^+(n,k)+\nu\boldsymbol{s})&=S_j(x_1^+,x_2^+,\nu s_3,x_4^+,x_5^+,\nu s_6,\cdots,x_m^++\nu s_m,\cdots)\\&=\left[S_j(\hat{\mathbf{v}})+\hat{x}_2^+(\tilde{x}_0,\tilde{t}_0)S_{j-2}(\hat{\mathbf{v}})\right]\left[1+O(|a_m|^{-2/m})\right],\qquad |a_m|\gg 1,\end{aligned} \tag{3.242}$$

where

$$\begin{aligned}\hat{\mathbf{v}}&=\left(x_1^+,0,\cdots,0,a_m,0,\cdots\right)\\&=\left(p_1x+2p_0p_1\mathrm{i}t+n\theta_1+k\lambda_1,0,\cdots,0,a_m,0,\cdots\right).\end{aligned} \tag{3.243}$$

Here, the normalization of $a_1 = 0$ in x_1^+ has been used, and the second equation in (3.242) is obtained by using the definition of Schur polynomials and splitting the $\boldsymbol{x}^+(n,k)+\nu\boldsymbol{s}$ vector into $\hat{\mathbf{v}}$ and the rest. Polynomials $S_j(\hat{\mathbf{v}})$ are related to $p_j^{[m]}(z)$ in Eq. (3.189) as

$$S_j(\hat{\mathbf{v}}) = a_m^{j/m} p_j^{[m]}(\hat{z}), \tag{3.244}$$

where $\hat{z} = a_m^{-1/m}(p_1 x + 2p_0 p_1 \mathrm{i} t + n\theta_1 + k\lambda_1)$.

Now, we derive leading order terms of a_m in the Laplace expansion (3.230) when (x,t) is in the $O(1)$ neighborhood of $(\tilde{x}_0, \tilde{t}_0)$. These leading order terms come from two index choices, the first being $\boldsymbol{\nu} = (0,1,\cdots,N-1)$, and the second being $\boldsymbol{\nu} = (0,1,\cdots,N-2,N)$.

With the first index choice, applying the more refined asymptotics (3.242) to the Laplace expansion (3.230), the determinant involving $\boldsymbol{x}^+(n,k)$ in Eq. (3.230) can be found as (Yang and Yang 2023a)

$$\begin{aligned}&\alpha\, a_m^{[N(N+1)-1]/m}\left[p_1(x-\tilde{x}_0)+2p_0p_1\mathrm{i}(t-\tilde{t}_0)+n\theta_1+k\lambda_1+\Delta_Q\right]\\&\times\left[Q_N^{[m]}\right]'(z_0)\left[1+O(|a_m|^{-1/m})\right],\end{aligned} \tag{3.245}$$

where

$$\Delta_Q = \frac{\hat{x}_2^+(\tilde{x}_0,\tilde{t}_0)}{a_m^{1/m}}\frac{\sum_{j=1}^N \det_{1\le i\le N}\left[p_{3i-1}^{[m]}(z_0),\cdots,p_{3i-j-2}^{[m]}(z_0),\cdots,p_{3i-N}^{[m]}(z_0)\right]}{\left[Q_N^{[m]}\right]'(z_0)}. \tag{3.246}$$

Here, the determinant inside the summation is the determinant of $Q_N^{[m]}(z_0)$, i.e., $\det_{1\le i,j\le N}\left[p_{3i-j}^{[m]}(z_0)\right]$, except that the sub-indices of its j-th column are reduced by two. Using the $(\tilde{x}_0,\tilde{t}_0)$ expressions as obtained from Eq. (3.240), we have

$$\frac{\hat{x}_2^+(\tilde{x}_0,\tilde{t}_0)}{a_m^{1/m}} = \frac{p_2}{p_1}z_0 + \frac{\mathrm{i}p_1^2}{2\Re(p_0)}\frac{\Im\left(z_0 e^{\mathrm{i}\varphi_m}/p_1\right)}{e^{\mathrm{i}\varphi_m}}, \tag{3.247}$$

where $\varphi_m \equiv \arg\left(a_m^{1/m}\right)$. This Δ_Q is an $O(1)$ quantity. Absorbing it into $(\tilde{x}_0,\tilde{t}_0)$ in Eq. (3.245), we find that the contribution to the first determinant in the Laplace expansion (3.230) under the index choice of $\boldsymbol{\nu} = (0,1,\cdots,N-1)$ is

$$\begin{aligned}&\alpha\, a_m^{[N(N+1)-1]/m}\left[p_1(x-\hat{x}_0)+2p_0p_1\mathrm{i}(t-\hat{t}_0)+n\theta_1+k\lambda_1\right]\left[Q_N^{[m]}\right]'(z_0)\\&\times\left[1+O(|a_m|^{-1/m})\right],\end{aligned}$$

where $(\hat{x}_0, \hat{t}_0)$ are given in Eqs. (3.218) of Theorem 3.14. Similarly, the second determinant involving $\boldsymbol{x}^-(n,k)$ in Eq. (3.230) under the index choice of $\boldsymbol{\nu} = (0, 1, \cdots, N-1)$ is found to be

$$\alpha^* (a_m^*)^{[N(N+1)-1]/m} \left[p_1^*(x-\hat{x}_0) - 2p_0^* p_1^* \mathrm{i}(t-\hat{t}_0) - n\theta_1^* - k\lambda_1^*\right] \left[Q_N^{[m]}\right]' (z_0^*) \times$$
$$\times \left[1 + O(|a_m|^{-1/m})\right].$$

Under the second index choice of $\boldsymbol{\nu} = (0, 1, \cdots, N-2, N)$ in the Laplace expansion (3.230), the leading-order contribution to the first determinant involving $\boldsymbol{x}^+(n,k)$ can be calculated from the asymptotics (3.231) and the relation (3.236) as

$$h_0 \alpha\, a_m^{[N(N+1)-1]/m} \left[Q_N^{[m]}\right]' (z_0) \left[1 + O(|a_m|^{-1/m})\right].$$

Similarly, the second determinant involving $\boldsymbol{x}^-(n,k)$ in Eq. (3.230) contributes

$$h_0^* \alpha^* (a_m^*)^{[N(N+1)-1]/m} \left[Q_N^{[m]}\right]' (z_0^*) \left[1 + O(|a_m|^{-1/m})\right].$$

Summarizing the above contributions to the Laplace expansion (3.230) of $\sigma_{n,k}^{(Q)}$, we find that

$$\begin{aligned}
\sigma_{n,k}^{(Q)} = |\alpha|^2 & \left|\left[Q_N^{[m]}\right]' (z_0)\right|^2 |a_m|^{[N(N+1)-1]/m} \\
& \times \Big(\left[p_1(x-\hat{x}_0) + 2\mathrm{i}p_0 p_1 (t-\hat{t}_0) + n\theta_1 + k\lambda_1\right] \\
& \times \left[p_1^*(x-\hat{x}_0) - 2\mathrm{i}p_0^* p_1^* (t-\hat{t}_0) - n\theta_1^* - k\lambda_1^*\right] + |h_0|^2\Big) \\
& \times \left[1 + O(|a_m|^{-1/m})\right]. \qquad (3.248)
\end{aligned}$$

Under our assumption of all nonzero roots of $Q_N^{[m]}(z)$ being simple, $\left[Q_N^{[m]}\right]' (z_0) \neq 0$. Thus, the above leading-order asymptotics for $\sigma_{n,k}^{(Q)}(x,t)$ does not vanish. It is easy to see that this expression of $\sigma_{n,k}^{(Q)}$ gives a fundamental rogue wave $[\hat{u}_1(x-\hat{x}_0, t-\hat{t}_0)\, e^{\mathrm{i}(k_1 x+\omega_1 t)},\ \hat{u}_2(x-\hat{x}_0, t-\hat{t}_0)\, e^{\mathrm{i}(k_2 x+\omega_2 t)}]$ as given in Theorem 3.14, and the error of this fundamental rogue wave prediction is $O(|a_m|^{-1/m})$. This completes the proof of Theorem 3.14 for the outer region.

(2) Proof of Theorem 3.14 for the inner region

To analyze the large-a_m behavior of Q-type Manakov rogue waves in the inner region, where $x^2 + t^2 = O(1)$, we first rewrite the $\sigma_{n,k}^{(Q)}$ determinant (3.217) into a $4N \times 4N$ determinant

$$\sigma_{n,k}^{(Q)} = \begin{vmatrix} \mathbf{O}_{N\times N} & \Phi_{N\times 3N} \\ -\Psi_{3N\times N} & \mathbf{I}_{3N\times 3N} \end{vmatrix}, \tag{3.249}$$

where

$$\Phi_{i,j} = \left(\frac{p_1}{p_0+p_0^*}\right)^{j-1} S_{3i-j}\left[\boldsymbol{x}^+(n,k) + (j-1)\boldsymbol{s}\right], \tag{3.250}$$

$$\Psi_{i,j} = \left(\frac{p_1^*}{p_0+p_0^*}\right)^{i-1} S_{3j-i}\left[\boldsymbol{x}^-(n,k) + (i-1)\boldsymbol{s}^*\right]. \tag{3.251}$$

Defining $\boldsymbol{y}^\pm$ to be the vector $\boldsymbol{x}^\pm$ without the a_m term, i.e., let

$$\boldsymbol{x}^+ = \boldsymbol{y}^+ + (0,\cdots,0,a_m,0,\cdots), \quad \boldsymbol{x}^- = \boldsymbol{y}^- + (0,\cdots,0,a_m^*,0,\cdots), \tag{3.252}$$

it is easy to see from the definition of Schur polynomials that the Schur polynomials of $\boldsymbol{x}^\pm$ are related to those of $\boldsymbol{y}^\pm$ as

$$\left.\begin{aligned} S_j(\boldsymbol{x}^+ + \nu\boldsymbol{s}) &= \textstyle\sum_{l=0}^{[j/m]} \frac{a_m^l}{l!} S_{j-lm}(\boldsymbol{y}^+ + \nu\boldsymbol{s}), \\ S_j(\boldsymbol{x}^- + \nu\boldsymbol{s}^*) &= \textstyle\sum_{l=0}^{[j/m]} \frac{(a_m^*)^l}{l!} S_{j-lm}(\boldsymbol{y}^- + \nu\boldsymbol{s}^*). \end{aligned}\right\} \tag{3.253}$$

The notation of $[a]$ here represents the largest integer less than or equal to a. Using these relations, we express matrix elements of Φ and Ψ in Eq. (3.249) through Schur polynomials $S_j(\boldsymbol{y}^+ + \nu\boldsymbol{s})$, $S_j(\boldsymbol{y}^- + \nu\boldsymbol{s}^*)$, and powers of a_m and a_m^*.

Next, we perform row operations to the Φ matrix in order to remove certain power terms of a_m. For this purpose, we notice that when $m = 3j+1$ ($j \geq 1$), coefficients of the highest a_m power terms in Φ's first column are proportional to

$$\hat{S}_2, \hat{S}_5, \cdots, \hat{S}_{3j-1}, \hat{S}_1, \hat{S}_4, \cdots, \hat{S}_{3j-2}, \hat{S}_0, \hat{S}_3, \cdots, \hat{S}_{3j}, \tag{3.254}$$

and repeating, where $\hat{S}_j \equiv S_j(\boldsymbol{y}^+ + \nu\boldsymbol{s})$. When $m = 3j+2$ ($j \geq 0$), these coefficients of the highest a_m power terms in Φ's first column are proportional to

$$\hat{S}_2, \hat{S}_5, \cdots, \hat{S}_{3j-1}, \hat{S}_0, \hat{S}_3, \cdots, \hat{S}_{3j}, \hat{S}_1, \hat{S}_4, \cdots, \hat{S}_{3j+1}, \tag{3.255}$$

and repeating. In the second and higher columns of Φ, elements are of the same form as those in the first column, except that the index j of every $\hat{S}_j$ in them decreases by one with each higher column, and $\hat{S}_j \equiv 0$ for $j < 0$. Using the first m rows, we perform row operations to remove the highest powers of a_m from the second m rows, leaving the second-highest power terms of a_m with coefficients proportional to $\hat{S}_{j+m}$, where $\hat{S}_j$ is the highest a_m-power coefficient of each element just being removed. Then, we use the first m rows and the resulting second m rows to eliminate

the highest and second-highest power terms of a_m from the third m rows, leaving the third-highest power terms of a_m with coefficients proportional to $\hat{S}_{j+2m}$ in them. This process is continued to all later rows of Φ. Similar column operations are also applied to the matrix Ψ in Eq. (3.249).

After these row and column operations, we then keep only the highest remaining power of a_m in each matrix element of Φ and the highest remaining power of a_m^* in each matrix element of Ψ. Using these manipulations and the sequence structures in Eqs. (3.254) and (3.255), we find that $\sigma_{n,k}^{(Q)}$ in (3.249) is asymptotically reduced to

$$\sigma_{n,k}^{(Q)} = \widehat{\beta}\,|a_m|^{\widehat{K}} \begin{vmatrix} \mathbf{O}_{(N_{1Q}+N_{2Q})\times(N_{1Q}+N_{2Q})} & \widehat{\Phi}_{(N_{1Q}+N_{2Q})\times\widehat{N}} \\ -\widehat{\Psi}_{\widehat{N}\times(N_{1Q}+N_{2Q})} & \mathbf{I}_{\widehat{N}\times\widehat{N}} \end{vmatrix} \left[1 + O(|a_m|^{-1})\right], \tag{3.256}$$

where $\widehat{\beta}$ is an (m, N)-dependent nonzero constant, $\widehat{K}$ is an (m, N)-dependent positive integer, (N_{1Q}, N_{2Q}) are nonnegative integers given in Theorem 3.12, $\widehat{N} = \max(3N_{1Q}, 3N_{2Q} - 1)$,

$$\widehat{\Phi} = \begin{pmatrix} \widehat{\Phi}^{(1)}_{N_{1Q}\times\widehat{N}} \\ \\ \widehat{\Phi}^{(2)}_{N_{2Q}\times\widehat{N}} \end{pmatrix}, \quad \widehat{\Psi} = \left(\widehat{\Psi}^{(1)}_{\widehat{N}\times N_{1Q}} \ \widehat{\Psi}^{(2)}_{\widehat{N}\times N_{2Q}}\right), \tag{3.257}$$

$$\widehat{\Phi}^{(I)}_{i,j} = (h_0)^{-(j-1)} S_{3i-I}\left[\boldsymbol{y}^+(n,k) + (j-1+\nu_0)\boldsymbol{s}\right], \tag{3.258}$$

$$\widehat{\Psi}^{(J)}_{i,j} = (h_0^*)^{-(i-1)} S_{3j-J}\left[\boldsymbol{y}^-(n,k) + (i-1+\nu_0)\boldsymbol{s}^*\right], \tag{3.259}$$

and $\nu_0 = N - N_{1Q} - N_{2Q}$. Since the constant factor $\widehat{\beta}\,|a_m|^{\widehat{K}}$ in (3.256) does not affect the solution and can be dropped, the remaining determinant in (3.256) can be rewritten as

$$\sigma_{n,k}^{(Q)} = \det\begin{pmatrix} \sigma_{n,k}^{[1,1]} & \sigma_{n,k}^{[1,2]} \\ \sigma_{n,k}^{[2,1]} & \sigma_{n,k}^{[2,2]} \end{pmatrix}\left[1 + O(|a_m|^{-1})\right], \tag{3.260}$$

$$\sigma_{n,k}^{[I,J]} = \left(\phi^{(n,k,I,J)}_{3i-I,\,3j-J}\right)_{1\le i\le N_{IQ},\,1\le j\le N_{JQ}}, \tag{3.261}$$

where the matrix elements in $\sigma_{n,k}^{[I,J]}$ are defined by

$$\begin{aligned}\phi^{(n,k,I,J)}_{i,j} = \sum_{\nu=0}^{\min(i,j)} \left[\frac{|p_1|^2}{(p_0+p_0^*)^2}\right]^{\nu} & S_{i-\nu}\left(\boldsymbol{y}^+(n,k) + \nu_0\boldsymbol{s} + \nu\boldsymbol{s}\right) \\ & \times S_{j-\nu}\left(\boldsymbol{y}^-(n,k) + \nu_0\boldsymbol{s}^* + \nu\boldsymbol{s}^*\right).\end{aligned} \tag{3.262}$$

The largest index j of S_j involved in the above reduced solution is $\max(3N_{1Q} - 1, 3N_{2Q} - 2)$. It is easy to see from Theorem 3.12 that $\max(3N_{1Q} - 1, 3N_{2Q} - 2) < m$. Thus, the above solution only depends on S_j polynomials with $j < m$, and hence only depends on $y_j^{\pm}(n,k)$ with $j < m$. From the definition (3.252), we see that $y_j^{\pm}(n,k) = x_j^{\pm}(n,k)$ when $j < m$. This means that in Eq. (3.262), $\boldsymbol{y}^{\pm}(n,k)$ can be replaced by $\boldsymbol{x}^{\pm}(n,k)$. Finally, we lump each constant $v_0 s_j$ into a_j of $x_j^{+}(n,k)$, and similarly lump each $v_0 s_j^*$ into a_j^* of $x_j^{-}(n,k)$. When $j \bmod 3 = 0$, $x_j^{\pm}(n,k) = 0$ per Lemma 3.3 and does not contain a_j. In such a case, we just lump $v_0 s_j$ into $x_j^{+}(n,k)$ and $v_0 s_j^*$ into $x_j^{-}(n,k)$, which eventually can be eliminated from the solution for the same reason as in Lemma 3.3. After these treatments, the above determinant in (3.260) becomes a $\left(N_{1Q}, N_{2Q}\right)$-th order Manakov rogue wave $[u_{1,N_{1Q},N_{2Q}}(x,t), u_{2,N_{1Q},N_{2Q}}(x,t)]$ as given in Lemma 3.3, whose internal parameters $(\hat{a}_{1,1}, \hat{a}_{2,1}, \hat{a}_{4,1}, \hat{a}_{5,1}, \ldots, \hat{a}_{3N_{1Q}-1,1})$ and $(\hat{a}_{1,2}, \hat{a}_{2,2}, \hat{a}_{4,2}, \hat{a}_{5,2}, \ldots, \hat{a}_{3N_{2Q}-2,2})$ are related to those in the original rogue wave as

$$\hat{a}_{j,1} = \hat{a}_{j,2} = a_j + v_0 s_j, \quad j = 1, 2, 4, 5, \cdots, \tag{3.263}$$

which is the same as the relation (3.220) in Theorem 3.14 since $s_j = 0$ for $j \bmod 3 \neq 0$. The error of this lower-order rogue wave approximation is $O(|a_m|^{-1})$ in view of Eq. (3.260). This completes the proof of Theorem 3.14 for the inner region.

(3) Proof of Theorem 3.15

The proof of Theorem 3.15 for R-type Manakov rogue waves is very similar to that for Theorem 3.14. For that reason, we will only list the differences here.

In the outer region, due to the different matrix indices in Eq. (3.217) for R-type rogue waves, the corresponding polynomials whose roots give leading-order locations of fundamental rogue waves are naturally R-type Okamoto hierarchy polynomials $R_N^{[m]}(z)$. The remaining difference is the calculation of the next-order position shift, i.e., the formula for Δ_R in Eqs. (3.222). Repeating earlier calculations for the different R-type matrix indices, we can easily find that

$$\Delta_R = \left(\frac{p_2}{p_1} z_0 + \frac{\mathrm{i} p_1^2}{2\Re(p_0)} \frac{\Im\left(z_0 e^{i\varphi_m}/p_1\right)}{e^{i\varphi_m}} \right) \times \frac{\sum_{j=1}^{N} \det_{1\le i\le N} \left[p_{3i-1-1}^{[m]}(z_0), \cdots, p_{3i-j-1-2}^{[m]}(z_0), \cdots, p_{3i-N-1}^{[m]}(z_0) \right]}{\left[R_N^{[m]} \right]'(z_0)}. \tag{3.264}$$

Here, the determinant inside the summation of the above formula is the determinant of $R_N^{[m]}(z_0)$, i.e., $\det_{1\le i,j\le N}\left[p_{3i-j-1}^{[m]}(z_0) \right]$, except that sub-indices of its j-th column are reduced by two.

In the inner region, where $x^2 + t^2 = O(1)$, we also rewrite the $\sigma_{n,k}^{(R)}$ determinant (3.217) into a $4N \times 4N$ determinant, and then use relations (3.253) to rewrite every matrix element of Φ and Ψ into powers of a_m and a_m^* respectively. For R-type rogue waves, when $m = 3j + 1$ ($j \geq 1$), coefficients of the highest a_m power terms in Φ's first column are proportional to

$$\hat{S}_1, \hat{S}_4, \cdots, \hat{S}_{3j-2}, \hat{S}_0, \hat{S}_3, \cdots, \hat{S}_{3j}, \hat{S}_2, \hat{S}_5, \cdots, \hat{S}_{3j-1}, \tag{3.265}$$

and repeating, and when $m = 3j + 2$ ($j \geq 0$), these coefficients are proportional to

$$\hat{S}_1, \hat{S}_4, \cdots, \hat{S}_{3j+1}, \hat{S}_2, \hat{S}_5, \cdots, \hat{S}_{3j-1}, \hat{S}_0, \hat{S}_3, \cdots, \hat{S}_{3j}, \tag{3.266}$$

and repeating. Using these sequence structures and performing the same row and column operations as described earlier to remove certain high powers of a_m in the Φ and Ψ matrices, we find that $\sigma_{n,k}^{(R)}$ can be asymptotically reduced to (3.256)–(3.259), except that (N_{1Q}, N_{2Q}) are replaced by (N_{1R}, N_{2R}) as given in Theorem 3.13, and $(\widehat{\beta}, \widehat{K})$ are different constants. The rest of the proof is the same as before, and Theorem 3.15 is then proved.

3.3.4 Three-Wave Resonant Interaction System

The (1+1)-dimensional three-wave resonant interaction system of soliton-exchange case is

$$\left.\begin{aligned} (\partial_t + c_1\partial_x)\, u_1 &= u_2^* u_3^*, \\ (\partial_t + c_2\partial_x)\, u_2 &= -u_1^* u_3^*, \\ (\partial_t + c_3\partial_x)\, u_3 &= u_1^* u_2^*, \end{aligned}\right\} \tag{3.267}$$

where (c_1, c_2, c_3) are group velocities of the three waves. In this soliton-exchange case, under the boundary conditions

$$\left.\begin{aligned} u_1(x,t) &\to \rho_1 e^{\mathrm{i}(k_1 x + \omega_1 t)}, && x, t \to \pm\infty, \\ u_2(x,t) &\to \rho_2 e^{\mathrm{i}(k_2 x + \omega_2 t)}, && x, t \to \pm\infty, \\ u_3(x,t) &\to \mathrm{i}\rho_3 e^{-\mathrm{i}[(k_1+k_2)x + (\omega_1+\omega_2)t]}, && x, t \to \pm\infty, \end{aligned}\right\} \tag{3.268}$$

and parameter constraints

$$\rho_2 = \sqrt{\frac{c_1}{c_2}}\rho_1, \quad \rho_3 = \pm\sqrt{\frac{c_1 - c_2}{c_2}}\rho_1, \tag{3.269}$$

the above three-wave system admits a class of rogue waves whose τ functions are 2×2 block determinants of Schur polynomials with index jumps of 3, similar to the

focusing Manakov case. These rogue waves have been presented in Theorem 2.15 of Chap. 2. When those 2×2 block determinants degenerate to single blocks, we also get Q-type and R-type rogue waves. Patterns of these rogue waves under a large internal parameter are summarized in the following two theorems (Yang and Yang 2023a).

Theorem 3.16 *For the Q-type rogue wave* $[u_{1,N,0}(x,t), u_{2,N,0}(x,t), u_{3,N,0}(x,t)]$ *in the three-wave resonant interaction system (3.267), suppose* $|a_m| \gg 1$ *and all other internal parameters* $O(1)$*. In addition, suppose all nonzero roots of* $Q_N^{[m]}(z)$ *are simple. Then, the following statements for this rogue wave hold.*

1. *In the outer region, where* $\sqrt{x^2+t^2} = O(|a_m|^{1/m})$*, this rogue wave asymptotically separates into* M_Q *isolated fundamental rogue waves, where* M_Q *is given in Eq. (3.201). These fundamental rogue waves are* $[\hat{u}_1(x-\hat{x}_0, t-\hat{t}_0)\, e^{\mathrm{i}(k_1 x+\omega_1 t)}, \hat{u}_2(x-\hat{x}_0, t-\hat{t}_0)\, e^{\mathrm{i}(k_2 x+\omega_2 t)}, \hat{u}_3(x-\hat{x}_0, t-\hat{t}_0)\, e^{-\mathrm{i}[(k_1+k_2)x+(\omega_1+\omega_2)t]}]$*, where functions* $\hat{u}_j(x,t)$ *are given in Eq. (2.772) of Sect. 2.10, and their positions* $(\hat{x}_0, \hat{t}_0)$ *are given by*

$$\hat{x}_0 = \frac{\Im\left[\frac{z_0 a_m^{1/m} - \hat{\Delta}_Q}{c_1\beta_1 - c_2\alpha_1}\right]}{\Im\left[\frac{\alpha_1-\beta_1}{c_1\beta_1-c_2\alpha_1}\right]}, \quad \hat{t}_0 = \frac{\Im\left[\frac{z_0 a_m^{1/m} - \hat{\Delta}_Q}{\alpha_1-\beta_1}\right]}{\Im\left[\frac{c_1\beta_1-c_2\alpha_1}{\alpha_1-\beta_1}\right]}, \tag{3.270}$$

where z_0 *is each of the* M_Q *nonzero simple roots of* $Q_N^{[m]}(z)$*,* (α_1, β_1) *are given in the expansions of Theorem 2.15, and* $\hat{\Delta}_Q$ *is a* z_0*-dependent* $O(1)$ *quantity. The error of this fundamental rogue wave approximation is* $O(|a_m|^{-1/m})$*. Expressed mathematically, when* $|a_m| \gg 1$ *and* $(x-\hat{x}_0)^2 + (t-\hat{t}_0)^2 = O(1)$*, we have the following solution asymptotics*

$$\left.\begin{aligned} u_{1,N,0}(x,t) &= \hat{u}_1(x-\hat{x}_0, t-\hat{t}_0)\, e^{\mathrm{i}(k_1 x+\omega_1 t)} + O(|a_m|^{-1/m}), \\ u_{2,N,0}(x,t) &= \hat{u}_2(x-\hat{x}_0, t-\hat{t}_0)\, e^{\mathrm{i}(k_2 x+\omega_2 t)} + O(|a_m|^{-1/m}), \\ u_{3,N,0}(x,t) &= \hat{u}_3(x-\hat{x}_0, t-\hat{t}_0)\, e^{-\mathrm{i}[(k_1+k_2)x+(\omega_1+\omega_2)t]} + O(|a_m|^{-1/m}). \end{aligned}\right\} \tag{3.271}$$

2. *If zero is a root of the Okamoto-hierarchy polynomial* $Q_N^{[m]}(z)$*, then in the inner region, where* $x^2 + t^2 = O(1)$*, this rogue wave is approximately a lower* (N_{1Q}, N_{2Q})*-th order rogue wave* $[u_{1,N_{1Q},N_{2Q}}(x,t), u_{2,N_{1Q},N_{2Q}}(x,t), u_{3,N_{1Q},N_{2Q}}(x,t)]$*, where* (N_{1Q}, N_{2Q}) *are provided in Theorem 3.12. Internal parameters in this lower-order rogue wave,* $(\hat{a}_{1,1}, \hat{a}_{2,1}, \ldots, \hat{a}_{3N_{1Q}-1,1})$ *and* $(\hat{a}_{1,2}, \hat{a}_{2,2}, \ldots, \hat{a}_{3N_{2Q}-2,2})$*, are the same as those in the original rogue wave, i.e.,*

$$\hat{a}_{j,1} = \hat{a}_{j,2} = a_j, \quad j = 1, 2, 4, 5, \cdots. \tag{3.272}$$

The error of this lower-order rogue wave approximation is $O(|a_m|^{-1})$*. Expressed mathematically, when* $|a_m| \gg 1$ *and* $x^2 + t^2 = O(1)$*,*

$$u_{k,N,0}(x,t;a_2,a_4,a_5,\cdots) = u_{k,N_{1Q},N_{2Q}}(x,t;\hat{a}_{j,1},\hat{a}_{j,2},\, j=1,2,4,5,\ldots) + O(|a_m|^{-1}), \tag{3.273}$$

where $k = 1, 2, 3$. If zero is not a root of $Q_N^{[m]}(z)$, then in the inner region, this rogue wave approaches the uniform background $[\rho_1 e^{\mathrm{i}(k_1 x+\omega_1 t)}, \rho_2 e^{\mathrm{i}(k_2 x+\omega_2 t)}, \mathrm{i}\rho_3 e^{-\mathrm{i}[(k_1+k_2)x+(\omega_1+\omega_2)t]}]$ when $|a_m| \gg 1$.

Theorem 3.17 *For the R-type rogue wave $[u_{1,0,N}(x,t), u_{2,0,N}(x,t), u_{3,0,N}(x,t)]$ in the three-wave resonant interaction system (3.267), suppose $|a_m| \gg 1$ and all other internal parameters $O(1)$. In addition, suppose all nonzero roots of $R_N^{[m]}(z)$ are simple. Then, the following statements for this rogue wave hold.*

1. *In the outer region, where $\sqrt{x^2+t^2} = O(|a_m|^{1/m})$, this rogue wave asymptotically separates into M_R isolated fundamental rogue waves, where M_R is given in Eq. (3.201). These fundamental rogue waves are $[\hat{u}_1(x-\hat{x}_0, t-\hat{t}_0)\, e^{\mathrm{i}(k_1 x+\omega_1 t)}, \hat{u}_2(x-\hat{x}_0, t-\hat{t}_0)\, e^{\mathrm{i}(k_2 x+\omega_2 t)}, \hat{u}_3(x-\hat{x}_0, t-\hat{t}_0)\, e^{-\mathrm{i}[(k_1+k_2)x+(\omega_1+\omega_2)t]}]$, where functions $\hat{u}_j(x,t)$ are given in Eq. (2.772) of Sect. 2.10, and their positions $(\hat{x}_0, \hat{t}_0)$ are given by*

$$\hat{x}_0 = \frac{\Im\left[\frac{z_0 a_m^{1/m} - \hat{\Delta}_R}{c_1\beta_1 - c_2\alpha_1}\right]}{\Im\left[\frac{\alpha_1-\beta_1}{c_1\beta_1-c_2\alpha_1}\right]}, \quad \hat{t}_0 = \frac{\Im\left[\frac{z_0 a_m^{1/m} - \hat{\Delta}_R}{\alpha_1-\beta_1}\right]}{\Im\left[\frac{c_1\beta_1-c_2\alpha_1}{\alpha_1-\beta_1}\right]}, \tag{3.274}$$

where z_0 is each of the M_R nonzero simple roots of $R_N^{[m]}(z)$, (α_1, β_1) are given in the expansions of Theorem 2.15, and $\hat{\Delta}_R$ is a z_0-dependent $O(1)$ quantity. The error of this fundamental rogue wave approximation is $O(|a_m|^{-1/m})$. Expressed mathematically, when $|a_m| \gg 1$ and $(x-\hat{x}_0)^2 + (t-\hat{t}_0)^2 = O(1)$, we have the following solution asymptotics

$$\left.\begin{aligned} u_{1,0,N}(x,t) &= \hat{u}_1(x-\hat{x}_0, t-\hat{t}_0)\, e^{\mathrm{i}(k_1 x+\omega_1 t)} + O(|a_m|^{-1/m}),\\ u_{2,0,N}(x,t) &= \hat{u}_2(x-\hat{x}_0, t-\hat{t}_0)\, e^{\mathrm{i}(k_2 x+\omega_2 t)} + O(|a_m|^{-1/m}),\\ u_{3,0,N}(x,t) &= \hat{u}_3(x-\hat{x}_0, t-\hat{t}_0)\, e^{-\mathrm{i}[(k_1+k_2)x+(\omega_1+\omega_2)t]} + O(|a_m|^{-1/m}). \end{aligned}\right\} \tag{3.275}$$

2. *If zero is a root of the Okamoto-hierarchy polynomial $R_N^{[m]}(z)$, then in the inner region, where $x^2 + t^2 = O(1)$, this rogue wave is approximately a lower (N_{1R}, N_{2R})-th order rogue wave $[u_{1,N_{1R},N_{2R}}(x,t), u_{2,N_{1R},N_{2R}}(x,t), u_{3,N_{1R},N_{2R}}(x,t)]$, where (N_{1R}, N_{2R}) are provided in Theorem 3.13. Internal parameters $(\hat{a}_{1,1}, \hat{a}_{2,1}, \ldots, \hat{a}_{3N_{1R}-1,1})$ and $(\hat{a}_{1,2}, \hat{a}_{2,2}, \ldots, \hat{a}_{3N_{2R}-2,2})$ in this lower-order rogue wave are the same as those in the original rogue wave, i.e.,*

$$\hat{a}_{j,1} = \hat{a}_{j,2} = a_j, \quad j = 1, 2, 4, 5, \cdots. \tag{3.276}$$

The error of this lower-order rogue wave approximation is $O(|a_m|^{-1})$. *Expressed mathematically, when* $|a_m| \gg 1$ *and* $x^2 + t^2 = O(1)$,

$$u_{k,0,N}(x,t;a_2,a_4,a_5,\cdots) = u_{k,N_{1R},N_{2R}}(x,t;\hat{a}_{j,1},\hat{a}_{j,2},\, j=1,2,4,5,\ldots) + O(|a_m|^{-1}), \tag{3.277}$$

where $k = 1, 2, 3$. *If zero is not a root of* $R_N^{[m]}(z)$, *then in the inner region, this rogue wave approaches the uniform background* $[\rho_1 e^{\mathrm{i}(k_1 x+\omega_1 t)}, \rho_2 e^{\mathrm{i}(k_2 x+\omega_2 t)}, \mathrm{i}\rho_3 e^{-\mathrm{i}[(k_1+k_2)x+(\omega_1+\omega_2)t]}]$ *when* $|a_m| \gg 1$.

Proofs of these theorems are very similar to those for the Manakov system and are omitted here (see Yang and Yang (2023a) for details).

These theorems indicate that, similar to the Manakov case, patterns of Q- and R-type rogue waves in the three wave system are also linear transformations of root structures of $Q_N^{[m]}(z)$ and $R_N^{[m]}(z)$ polynomials to the leading order, but are nonlinear transformations of those root structures when the next-order position corrections are included.

Comparison Between Predictions and True Solutions

Now, we compare predictions from Theorems 3.16–3.17 to true solutions. For this purpose, we choose velocity values as $(c_1, c_2, c_3) = (1, 9/20, 0)$, and the first wave's background amplitude $\rho_1 = 1$. Then, the other two waves' background amplitudes can be derived from Eq. (3.269) as $\rho_2 = 2\sqrt{5}/3$ and $\rho_3 = \sqrt{11}/3$ (we have taken the plus signs).

Q-Type

We first compare Q-type rogue waves of the three-wave system and set $N = 2$. Regarding their three internal parameters (a_2, a_4, a_5), we choose one of them large and the other two zero. Then, when that large parameter is taken as one of

$$a_2 = 40\mathrm{i}, \quad a_4 = 300, \quad a_5 = 3000\mathrm{i}, \tag{3.278}$$

the three predicted rogue waves from Theorem 3.16 are displayed in the three columns of Fig. 3.28, respectively. The first row of this figure shows the predicted $(\hat{x}_0, \hat{t}_0)$ locations from formulae (3.270) applied to all roots of $Q_2^{[m]}(z)$. At each of the $(\hat{x}_0, \hat{t}_0)$ locations resulting from nonzero roots of $Q_2^{[m]}(z)$, a fundamental rogue wave of the three-wave system is predicted. Our prediction for the center regions is based on Eq. (3.273) of Theorem 3.16. In this prediction, the (N_{1Q}, N_{2Q}) values for these three rogue waves are the same as those given in Eq. (3.227) earlier. Internal parameters in these predicted lower (N_{1Q}, N_{2Q})-th order rogue waves in the center region are all zero due to our choices of internal parameters in the original rogue waves. These predictions for $(|u_1|, |u_2|, |u_3|)$ in the outer and inner regions are

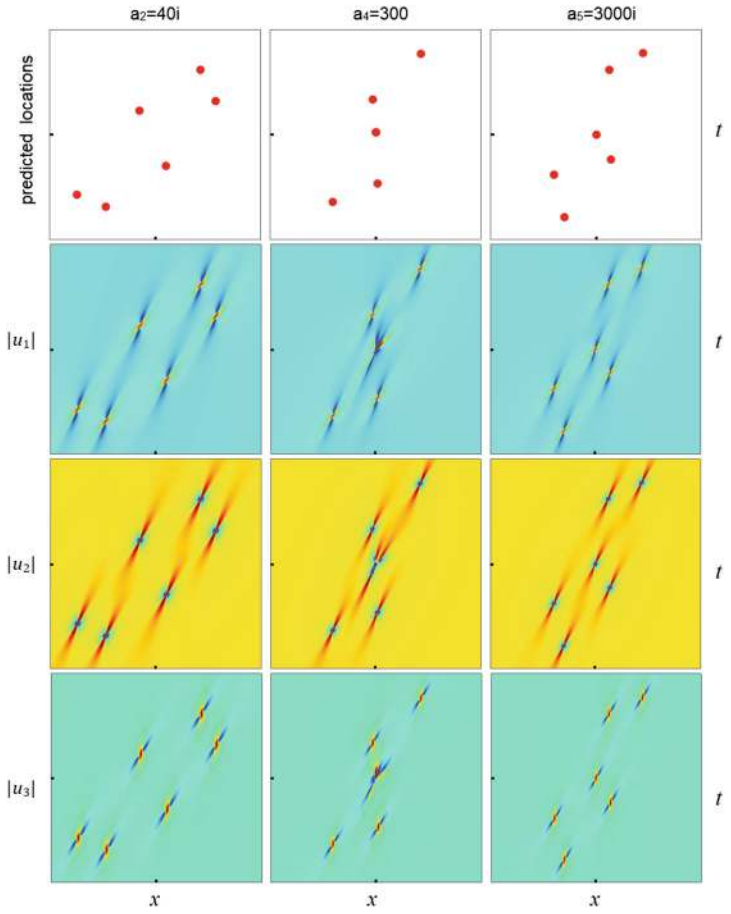

Fig. 3.28 Predicted Q-type second-order rogue waves from Theorem 3.16 in the three-wave system. Each column shows a predicted rogue wave with a single large parameter a_m, whose value is indicated on top, and all other internal parameters are set as zero. First row: predicted $(\hat{x}_0, \hat{t}_0)$ locations from formulae (3.270) applied to all roots of $Q_2^{[m]}(z)$. Second row: predicted $|u_1(x,t)|$. Third row: predicted $|u_2(x,t)|$. Last row: predicted $|u_3(x,t)|$. The (x,t) intervals in the three columns are $-19 \le x,t \le 19$, $-23 \le x,t \le 23$, and $-25 \le x,t \le 25$, respectively

assembled together similar to that explained in the caption of Fig. 3.22 and plotted in the second to fourth rows of Fig. 3.28, respectively.

It is easy to see that these predicted rogue patterns in Fig. 3.28, although being produced from the root structures of $Q_2^{[m]}(z)$ polynomials in Fig. 3.20, look totally different from those root structures. The reason is the nonlinear mapping of the next-order correction term in formulae (3.270), which induces strong deformations to the linearly mapped result from the leading-order term in (3.270). These deformations, under our current velocity choices of (c_1, c_2, c_3), are much stronger than in the previous Manakov case, at comparable a_m values. However, as we have explained

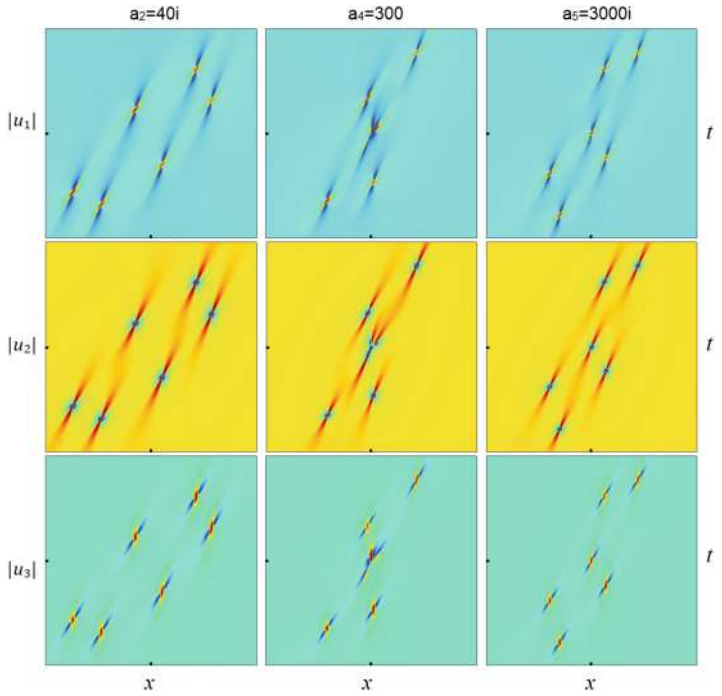

Fig. 3.29 True Q-type second-order rogue waves of the three-wave system for the same parameters and (x, t) intervals as in Fig. 3.28

in the previous subsection, if we increase the $|a_m|$ values, these deformations will become weaker, and rogue patterns will approach linearly transformed root structures of Okamoto-hierarchy polynomials and will thus be more recognizable

To compare these predictions to true solutions, we plot in Fig. 3.29 the corresponding true solutions. It is easy to see that the agreement is excellent, confirming the validity of Theorem 3.16. This agreement also indicates that, predictions from our Theorem 3.16 are highly accurate, even when rogue patterns are strongly deformed from Okamoto-hierarchy root structures.

R-Type

Next, we consider R-type rogue waves, and set $N = 3$. Regarding their internal parameters (a_2, a_4, a_5, a_7), we choose one of them large, and the others zero. Then, when that large parameter a_m is taken as one of

$$a_2 = 30\mathrm{i}, \quad a_4 = 200, \quad a_5 = 600\mathrm{i}, \quad a_7 = 5000, \tag{3.279}$$

predicted rogue waves from Theorem 3.17 are displayed in the first two rows of Fig. 3.30. The first row of this figure shows the predicted $(\hat{x}_0, \hat{t}_0)$ locations by formulae (3.274) applied to all roots of $R_3^{[m]}(z)$. The second row shows the predicted

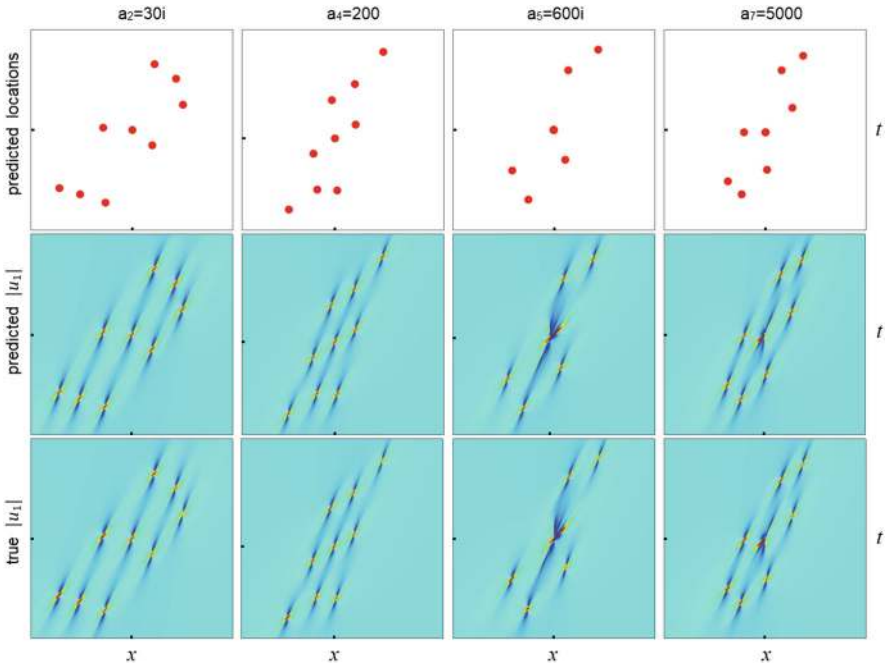

Fig. 3.30 Comparison between predicted and true R-type third-order rogue waves of the three-wave system. Each column is for a rogue wave with a single large parameter a_m, whose value is indicated on top, and all other internal parameters are set as zero. Top row: predicted $(\hat{x}_0, \hat{t}_0)$ locations by formulae (3.274) applied to all roots of $R_3^{[m]}(z)$. Middle row: predicted $|u_1(x,t)|$. Third row: true $|u_1(x,t)|$. The (x,t) intervals in the four columns are $-21 \le x,t \le 21$, $-23 \le x,t \le 27$, $-24 \le x,t \le 24$, and $-23 \le x,t \le 23$, respectively

amplitude fields $|u_1|$ (the other two fields $|u_2|$ and $|u_3|$ are not shown for brevity). These amplitude fields in the outer region are predicted by the fundamental rogue waves in Theorem 3.17, and these fields in the inner region are predicted by the lower (N_{1R}, N_{2R})-th order rogue waves with all-zero internal parameters, and their (N_{1R}, N_{2R}) values are as given in Eq. (3.229).

As in the earlier Q-case, predicted rogue patterns in Fig. 3.30 also look very different from the underlying root structures of $R_3^{[m]}(z)$ polynomials in Fig. 3.21.

In the bottom row of this same figure, the corresponding true solutions $|u_1|$ are plotted. Again, perfect agreement is seen between our predictions and the true solutions, confirming the predictive power of our Theorem 3.17.

3.4 Rogue Curves Associated with Double-Real-Variable Polynomials in the Davey-Stewartson I Equation

The Davey-Stewartson I equation admits a class of rogue wave solutions whose wave crests form closed or open curves in the spatial plane, which we call rogue curves. These rogue curves come in various striking shapes, such as rings, double rings, and many others. They emerge from a uniform background (possibly with a few lumps on it), reach high amplitude in such striking shapes, and then disappear into the same background again. These rogue curves would arise when an internal parameter in bilinear expressions of the rogue waves is real and large, and they can be predicted by root curves of certain types of double-real-variable polynomials. These results were first reported in Yang and Yang (2024b) and will be described below.

3.4.1 Rogue Curves in the Davey-Stewartson I Equation

The Davey-Stewartson-I (DSI) equation is

$$\left.\begin{aligned} \mathrm{i}A_t &= A_{xx} + A_{yy} + (\epsilon|A|^2 - 2Q)A, \\ Q_{xx} - Q_{yy} &= \epsilon(|A|^2)_{xx}, \end{aligned}\right\} \tag{3.280}$$

where $\epsilon = \pm 1$ is the sign of nonlinearity. Explicit rogue wave solutions in this equation have been presented in Theorem 2.18 of Chap. 2. Those rogue waves contain various types of solutions, such as multi-rogue waves and higher-order rogue waves, depending on whether the spectral parameters in them are the same or different. In addition, those solutions contain many free internal parameters. In this section, we consider the higher-order rogue waves where all the spectral parameters are the same, and their internal parameters are under certain restrictions. Expressions of such higher-order rogue waves are simpler and are given in the following lemma.

Lemma 3.4 *The Davey-Stewartson I eqaution (3.280) admits higher-order rogue wave solutions*

$$A_\Lambda(x, y, t) = \sqrt{2}\frac{g}{f}, \quad Q_\Lambda(x, y, t) = 1 - 2\epsilon\,(\log f)_{xx}\,, \tag{3.281}$$

where $\Lambda = (n_1, n_2, \ldots, n_N)$ is an order-index vector, N is the length of Λ, each n_i is a nonnegative integer, $n_1 < n_2 < \cdots < n_N$,

$$f = \tau_0, \quad g = \tau_1, \quad \tau_k = \det_{1\le i,j\le N}\left(m_{i,j}^{(k)}\right), \tag{3.282}$$

the matrix elements $m_{i,j}^{(k)}$ *of* τ_k *are given by*

$$m_{i,j}^{(k)} = \sum_{\nu=0}^{\min(n_i,n_j)} \frac{1}{4^\nu} S_{n_i-\nu}[\boldsymbol{x}^+(k)+\nu\boldsymbol{s}]\, S_{n_j-\nu}[\boldsymbol{x}^-(k)+\nu\boldsymbol{s}], \tag{3.283}$$

vectors $\boldsymbol{x}^\pm(k) = \left(x_1^\pm, x_2^\pm, \cdots\right)$ *are defined as*

$$x_r^+(k) = \frac{(-1)^r}{r!p}x_{-1} + \frac{(-2)^r}{r!p^2}x_{-2} + \frac{1}{r!}px_1 + \frac{2^r}{r!}p^2x_2 + k\delta_{r,1} + a_r, \tag{3.284}$$

$$x_r^-(k) = \frac{(-1)^r}{r!p}x_{-1} + \frac{(-2)^r}{r!p^2}x_2 + \frac{1}{r!}px_1 + \frac{2^r}{r!}p^2x_{-2} - k\delta_{r,1} + a_r^*, \tag{3.285}$$

$$x_1 = \frac{1}{2}(x+y), \quad x_{-1} = \frac{1}{2}\epsilon(x-y), \quad x_2 = -\frac{1}{2}it, \quad x_{-2} = \frac{1}{2}it, \tag{3.286}$$

p *is a real constant,* $\delta_{r,1}$ *is the Kronecker delta function which is equal to 1 when* $r = 1$ *and 0 otherwise,* $\boldsymbol{s} = (0, s_2, 0, s_4, \cdots)$ *are coefficients from the expansion*

$$\sum_{k=1}^{\infty} s_k\lambda^k = \ln\left[\frac{2}{\lambda}\tanh\left(\frac{\lambda}{2}\right)\right], \tag{3.287}$$

and $a_1, a_2, \ldots, a_{n_N}$ *are free complex constants.*

Derivation of this lemma from Theorem 2.18 is simple and can be found in Yang and Yang (2024b).

Notice that the free internal complex parameter a_1 can be absorbed into (x,t) or (y,t) through a coordinate shift. In addition, under the variable transformation of $Q \to Q + \epsilon|A|^2$, $x \leftrightarrow y$, and $\epsilon \to -\epsilon$, the DSI equation (3.280) is invariant. Thus, we will set

$$\epsilon = 1, \quad a_1 = 0, \tag{3.288}$$

in this section without loss of generality. In addition, we denote $\boldsymbol{a} = (0, a_2, \ldots, a_{n_N})$.

To demonstrate rogue curves in DSI, we show two examples. In the first example, we choose

$$p = 1, \quad \Lambda = (1,4), \quad \boldsymbol{a} = (0,0,0,5000). \tag{3.289}$$

The corresponding solution $|A|$ from Lemma 3.4 at four time values of $t = -3, -1, 0$ and 3 is shown in Fig. 3.31. It is seen that a rogue wave in the shape of two separate open curves symmetric with respect to the x-axis arises from the uniform background in the (x,y) plane. This rogue curve reaches peak amplitude of $3\sqrt{2}$ at $t = 0$, and then retreats to the same uniform background again. The

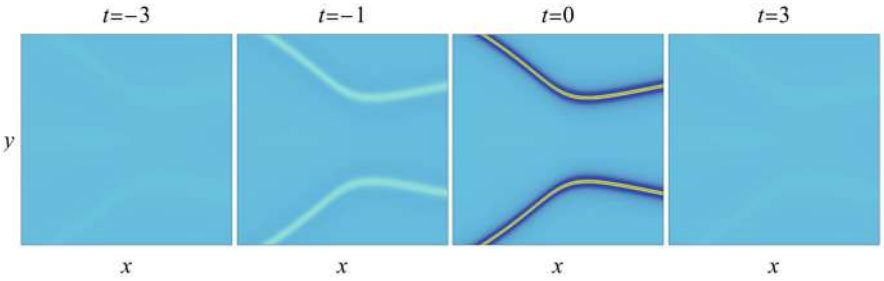

Fig. 3.31 A rogue curve ($|A|$) in the DSI equation (3.280) at four time values of $t = -3, -1, 0$ and 3 for parameter choices in Eq. (3.289). In all panels, $-500 \le x \le 500$, and $-30 \le y \le 30$

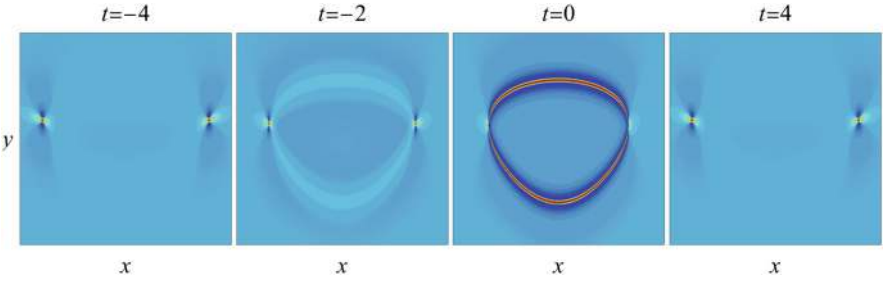

Fig. 3.32 A rogue ring ($|A|$) in the DSI equation (3.280) at four time values of $t = -4, -2, 0$ and 4 for parameter choices in Eq. (3.290). In all panels, $-500 \le x \le 500$, and $-10 \le y \le 40$

shape of this rogue curve is not parabolas but more complex, and its appearance is mysterious.

An even more interesting example comes when we choose

$$p = 1, \quad \Lambda = (2, 3), \quad \boldsymbol{a} = (0, 0, 2000), \tag{3.290}$$

and the corresponding solution $|A|$ from Lemma 3.4 at four time values of $t = -4, -2, 0$ and 4 is shown in Fig. 3.32. It is seen that at large times ($t = \pm 4$), the solution contains two lumps on the uniform background. But at the intermediate time of $t = -2$, a rogue wave whose crests form a closed curve in the (x, y) plane starts to appear between the two lumps (we call this rogue closed curve a rogue ring). This rogue ring reaches peak amplitude of $3\sqrt{2}$ at $t = 0$, after which it starts to disappear and becomes invisible when $t = 4$. The appearance of this rogue ring is more mysterious.

How can we understand these rogue curves? In particular, how can we analytically predict the shapes and locations of these rogue curves? This will be done in the next subsections.

3.4.2 A Class of Double-Real-Variable Polynomials and Their Root Curves

It turns out that the rogue curves such as those in Figs. 3.31 and 3.32 can be predicted through a certain class of double-real-variable polynomials and their root curves. Such polynomials and their root curves are described below.

We introduce a class of special polynomials in two real variables (z_1, z_2), which can be written as a determinant

$$\mathcal{P}_{\Lambda}^{[m]}(z_1,z_2)=\begin{vmatrix} \mathcal{S}_{n_1}^{[m]}(z_1,z_2) & \mathcal{S}_{n_1-1}^{[m]}(z_1,z_2) & \cdots & \mathcal{S}_{n_1-N+1}^{[m]}(z_1,z_2) \\ \mathcal{S}_{n_2}^{[m]}(z_1,z_2) & \mathcal{S}_{n_2-1}^{[m]}(z_1,z_2) & \cdots & \mathcal{S}_{n_2-N+1}^{[m]}(z_1,z_2) \\ \vdots & \vdots & \vdots & \vdots \\ \mathcal{S}_{n_N}^{[m]}(z_1,z_2) & \mathcal{S}_{n_N-1}^{[m]}(z_1,z_2) & \cdots & \mathcal{S}_{n_N-N+1}^{[m]}(z_1,z_2) \end{vmatrix}, \tag{3.291}$$

where $\mathcal{S}_k^{[m]}(z_1, z_2)$ are Schur polynomials in two variables defined by

$$\sum_{k=0}^{\infty}\mathcal{S}_k^{[m]}(z_1,z_2)\epsilon^k=\exp\left(z_2\epsilon+z_1\epsilon^2+\epsilon^m\right),\quad m\geq 3, \tag{3.292}$$

$\Lambda = (n_1, n_2, \ldots, n_N)$ is an order-index vector, and $\mathcal{S}_k^{[m]}(z_1, z_2) \equiv 0$ if $k < 0$. This determinant is a Wronskian (in z_2) since we can see from Eq. (3.292) that

$$\frac{\partial}{\partial z_2}\mathcal{S}_k^{[m]}(z_1,z_2)=\mathcal{S}_{k-1}^{[m]}(z_1,z_2). \tag{3.293}$$

A few such polynomials are given below by choosing specific m and Λ values,

$$m=4,\ \Lambda=(1,4):\ \mathcal{P}_{\Lambda}^{[m]}(z_1,z_2)=\left(z_2^4+4z_1z_2^2-4z_1^2-8\right)/8, \tag{3.294}$$

$$m=3,\ \Lambda=(2,3):\ \mathcal{P}_{\Lambda}^{[m]}(z_1,z_2)=\left(z_2^4+12z_1^2-12z_2\right)/12, \tag{3.295}$$

$$m=4,\ \Lambda=(2,4):\ \mathcal{P}_{\Lambda}^{[m]}(z_1,z_2)=z_2\left(z_2^4+4z_1z_2^2+12z_1^2-24\right)/24, \tag{3.296}$$

$$m=5,\ \Lambda=(4,5):\ \mathcal{P}_{\Lambda}^{[m]}(z_1,z_2)=\frac{1}{2880}\left(z_2^8+16z_1z_2^6+120z_1^2z_2^4 +720z_1^4-480z_2^3-2880z_1z_2\right). \tag{3.297}$$

By setting

$$\mathcal{P}_{\Lambda}^{[m]}(z_1,z_2)=0 \tag{3.298}$$

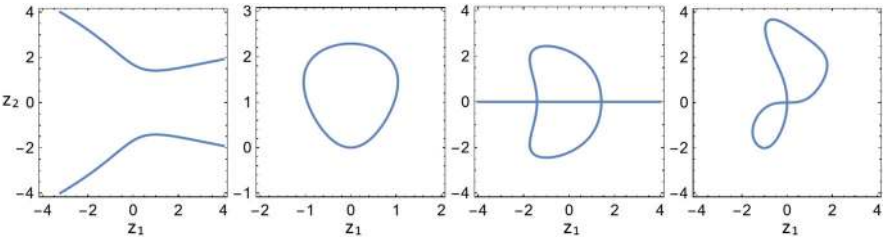

Fig. 3.33 Root curves $z_2 = \mathcal{R}_{\Lambda,m}(z_1)$ of the double-real-variable polynomial $\mathcal{P}_{\Lambda}^{[m]}(z_1, z_2)$ in the (z_1, z_2) plane for parameter choices in Eqs. (3.294)–(3.297), from left to right, respectively

for real values of (z_1, z_2), we get root curves of this equation in the (z_1, z_2) plane. Let us denote these root curve solutions as

$$z_2 = \mathcal{R}_{\Lambda,m}(z_1). \tag{3.299}$$

For the above four examples of $\mathcal{P}_{\Lambda}^{[m]}(z_1, z_2)$, their root curves are displayed in Fig. 3.33. As one can see, these root curves may be an open curve, as in the first example, or a closed curve, as in the second and fourth examples, or a mixture of open and closed curves, as in the third example. For closed curves, they can be a single loop as in the second example, or a connected double loop as in the fourth example. Other varieties of these curves are also possible for other examples of $\mathcal{P}_{\Lambda}^{[m]}(z_1, z_2)$, such as disconnected double loops and so on.

On a root curve, there may exist some special points where

$$\frac{\partial \mathcal{P}_{\Lambda}^{[m]}(z_1, z_2)}{\partial z_2} = 0. \tag{3.300}$$

Such special points will be important to us, and we will call them exceptional points of the root curve. These exceptional points satisfy both Eqs. (3.298) and (3.300). To easily see where these exceptional points are located on a root curve, it is helpful to consider the dynamical system

$$\frac{dz_2}{dt} = \mathcal{P}_{\Lambda}^{[m]}(z_1, z_2), \tag{3.301}$$

where z_2 is treated as a real function of time t, and z_1 is treated as a real parameter. For this dynamical system, the root curve (3.299) gives its bifurcation diagram, while Eq. (3.300) is the bifurcation condition on this diagram. From this point of view, it is then clear that the exceptional points of the root curve are the bifurcation points of this root curve (when this root curve is viewed as a bifurcation diagram). This realization then makes it very easy to identify exceptional points of the root curve. For example, on the root curve in the second panel of Fig. 3.33, the left and right edge points of the curve are exceptional points because saddle-node

bifurcations occur there. The root curve in the third panel of Fig. 3.33 has four exceptional points. Two of them are in the lower and upper half planes where saddle-node bifurcations occur, while the other two are on the z_1 axis where pitchfork bifurcations occur. The root curve in the fourth panel of Fig. 3.33 also has four exceptional points; three of them are where saddle-node bifurcations occur, while the fourth one is at the intersection between the upper and lower loops where a transcritical bifurcation occurs. The first panel of Fig. 3.33 does not have exceptional points since no bifurcation occurs here.

One may notice that the first two root curves in Fig. 3.33 resemble the shapes of rogue curves in Figs. 3.31 and 3.32. Indeed, the root curve of $\mathcal{P}_{\Lambda}^{[m]}(z_1, z_2)$ turns out to be closely related to rogue curves in DSI, as we will show in the next subsection.

3.4.3 *Analytical Prediction of Rogue Curves Through Root Curves*

In this subsection, we analytically predict the shapes of rogue waves in DSI. For this purpose, we make the following restrictions on parameters in DSI's rogue waves in Lemma 3.4.

1. We set $p = 1$.
2. For a certain $m \geq 3$, a_m is real, $a_m \gg 1$ when m is even and $|a_m| \gg 1$ when m is odd, and the other a_j values in $\boldsymbol{a}$ are $O(1)$ and complex.

The other cases of $p \neq 1$ and large negative a_m when m is even will be briefly discussed at the end of this subsection.

One may notice that the parameter choices (3.289)–(3.290) for Figs. 3.31 and 3.32 meet these restrictions. In both cases, $p = 1$. In addition, in (3.289), $a_4 = 5000$ is large positive. In (3.290), $a_3 = 2000$ is large.

Under the above parameter restrictions, we will show that rogue curves in DSI would appear, and their shapes in the (x, y) plane would be predicted by the root curves of $\mathcal{P}_{\Lambda}^{[m]}(z_1, z_2)$. To present these results, we first introduce some definitions.

Let us define a curve $y = y_c(x)$ in the (x, y) plane, which we call the critical curve, as

$$x = 2z_1 a_m^{2/m}, \quad y_c(x) = z_2 a_m^{1/m}, \tag{3.302}$$

where (z_1, z_2) is every point on the root curve of $\mathcal{P}_{\Lambda}^{[m]}(z_1, z_2)$. Alternatively, the critical curve can be defined by the equation

$$\mathcal{P}_{\Lambda}^{[m]}\left(\frac{x}{2a_m^{2/m}}, \frac{y_c(x)}{a_m^{1/m}}\right) = 0, \tag{3.303}$$

or

$$y_c(x) = a_m^{1/m} \mathcal{R}_{\Lambda,m}\left(\frac{x}{2a_m^{2/m}}\right), \tag{3.304}$$

using the notation in Eq. (3.299). This critical curve may also contain exceptional points where

$$\frac{\partial}{\partial y_c} \mathcal{P}_{\Lambda}^{[m]}\left(\frac{x}{2a_m^{2/m}}, \frac{y_c}{a_m^{1/m}}\right) = 0. \tag{3.305}$$

Such points are also bifurcation points of the critical curve when this curve is viewed as a bifurcation diagram, because a dynamical system point of view similar to Eq. (3.301) also applies here. It is easy to see that an exceptional point $(x^{(e)}, y_c^{(e)})$ of the critical curve is related to an exceptional point $(z_1^{(e)}, z_2^{(e)})$ of the root curve as

$$x^{(e)} = 2a_m^{2/m} z_1^{(e)}, \quad y_c^{(e)} = a_m^{1/m} z_2^{(e)}. \tag{3.306}$$

Thus, the two exceptional points are simply related by a stretching along the horizontal and vertical axes.

Under these definitions, we have the following theorem.

Theorem 3.18 *Let $A_\Lambda(x, y, t)$ be a DSI's rogue wave with order-index vector $\Lambda = (n_1, n_2, \ldots, n_N)$ in Eq. (3.281) of Lemma 3.4. Under the parameter restrictions mentioned above and when time $t = O(1)$, we have the following asymptotic result on the solution $A_\Lambda(x, y, t)$ in the (x, y) plane for large $|a_m|$.*

1. *If (x, y) is not in the $O(1)$ neighborhood of the critical curve $y = y_c(x)$, then the solution $A_\Lambda(x, y, t)$ approaches the constant background $\sqrt{2}$ as $|a_m| \to +\infty$.*
2. *If (x, y) is in the $O(1)$ neighborhood of the critical curve $y = y_c(x)$, but not in the $O(1)$ neighborhood of its exceptional points, then the solution $A_\Lambda(x, y, t)$ at large $|a_m|$ would asymptotically form a rogue curve $A_R(x, y, t)$, whose expression is*

$$A_R(x, y, t) = \sqrt{2}\left[1 + \frac{4\mathrm{i}t - 1}{[y - y_c(x)]^2 + 4t^2 + \frac{1}{4}}\right]. \tag{3.307}$$

The error of this rogue curve approximation is $O(a_m^{-1/m})$. Expressed mathematically, when $(x, y_c(x))$ is not an exceptional point of the critical curve and $|y(x) - y_c(x)| = O(1)$, we have the following solution asymptotics

$$A_\Lambda(x, y, t) = A_R(x, y, t) + O\left(|a_m|^{-1/m}\right). \tag{3.308}$$

The proof of this theorem can be found in Yang and Yang (2024b).

Notice that $A_R(x, y, t)$ in Eq. (3.307) is the same as the Peregrine rogue wave of the nonlinear Schrödinger equation (along the y direction), except for a y-directional shift. The peak location of $|A_R(x, y, t)|$ at each y value is at $y = y_c(x)$. All these peak locations from different x values fall precisely on the critical curve $y = y_c(x)$. Thus, we can say the critical curve $y = y_c(x)$ predicts the spatial location of the rogue curve. The full rogue curve surrounding that critical curve is predicted by the function $A_R(x, y, t)$. The root curves of $\mathcal{P}_{\Lambda}^{[m]}(z_1, z_2)$ involved in Eq. (3.302) for those predictions are precisely the ones shown in the left two panels of Fig. 3.33. In cases where the root curve is closed so that z_1 of the root curve is only on a limited interval (see the second panel of Fig. 3.33 for an example), this $A_R(x, y, t)$ prediction would be only for a limited x interval as well in view of Eq. (3.302). Outside that x interval, our prediction of $A_\Lambda(x, y, t)$ would be the background value $\sqrt{2}$ as long as (x, y) is not in the $O(1)$ neighborhood of the critical curve $y = y_c(x)$, according to the first statement of Theorem 3.18.

The only (x, y) places where Theorem 3.18 does not make a solution prediction are $O(1)$ neighborhoods of the exceptional points on the critical curve $y = y_c(x)$. In such special neighborhoods, a more elaborate analysis is needed in order to predict the solution behavior there.

Next, we compare analytical predictions of rogue curves in Theorem 3.18 to true solutions. Since parameter choices (3.289)–(3.290) for Figs. 3.31 and 3.32 meet the assumptions of Theorem 3.18, we will compare Theorem 3.18's predictions on them to the true solutions in Figs. 3.31 and 3.32.

For the first parameter choices (3.289), $m = 4, \quad a_m = 5000, \quad \Lambda = (1, 4)$. In this case, the corresponding root curve of $\mathcal{P}_{\Lambda}^{[m]}(z_1, z_2)$ has been plotted in the first panel of Fig. 3.33. Using that root curve, we can obtain the predicted rogue curve $A_R(x, y, t)$ from Eqs. (3.302) and (3.307). At four time values of $t = -3, -1, 0$ and 3, corresponding to the time values chosen in Fig. 3.31, this $A_R(x, y, t)$ prediction is plotted in Fig. 3.34. Comparing this figure to Fig. 3.31, we see that they closely match each other.

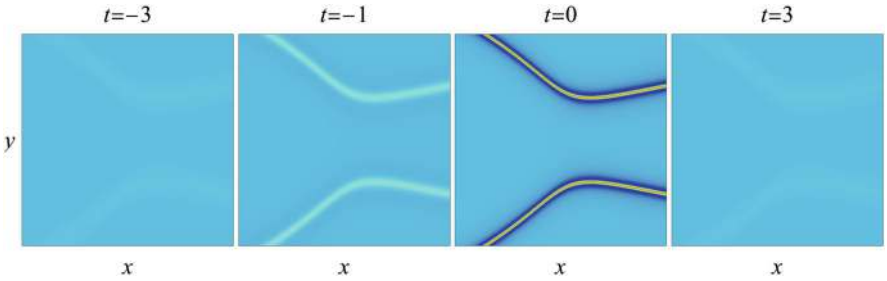

Fig. 3.34 Analytical predictions of the rogue curve in the DSI equation (3.280) for the parameter choices of (3.289) at four time values of $t = -3, -1, 0$ and 3. The (x, y) intervals here are the same as those in Fig. 3.31 for easy comparison

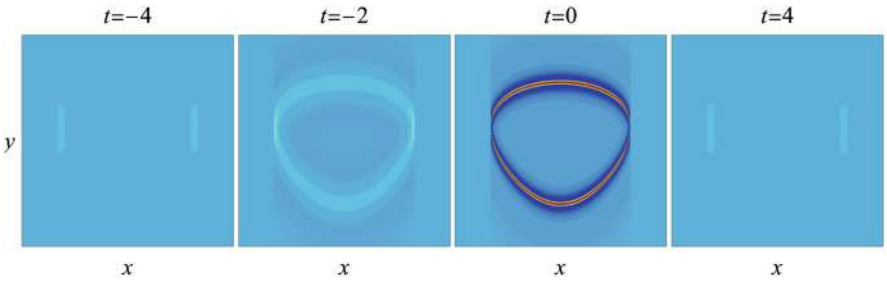

Fig. 3.35 Analytical predictions of the rogue ring in the DSI equation (3.280) for the parameter choices of (3.290) at four time values of $t = -4, -2, 0$ and 4. The (x, y) intervals here are the same as those in Fig. 3.32 for easy comparison

For the second parameter choices (3.290), $m = 3, \quad a_m = 2000, \quad \Lambda = (2, 3)$. In this case, the corresponding root curve of $\mathcal{P}_{\Lambda}^{[m]}(z_1, z_2)$ has been plotted in the second panel of Fig. 3.33. Using that root curve, we obtain the predicted rogue curve $A_R(x, y, t)$ from Eqs. (3.302) and (3.307). This $A_R(x, y, t)$ prediction only holds for the x interval of $\left(2z_{1,L}a_m^{2/m}, 2z_{1,R}a_m^{2/m}\right)$, where $(z_{1,L}, z_{1,R})$ is the z_1 interval of the underlying root curve in the second panel of Fig. 3.33. For this root curve, $z_{1,R} = -z_{1,L} = 3^{2/3}/2 \approx 1.0400$. Thus, the x interval of this $A_R(x, y, t)$ prediction is $|x| < 6000^{2/3} \approx 330.19$. Outside this x interval, we will use the uniform background $\sqrt{2}$ prediction for $A_{\Lambda}(x, y, t)$ according to the first statement of Theorem 3.18. At four time values of $t = -4, -2, 0$ and 4, corresponding to the time values chosen in Fig. 3.32, this $A_R(x, y, t)$ prediction is plotted in Fig. 3.35. Note that in this example, the critical curve $y = y_c(x)$ contains two exceptional points, which correspond to the left and right edge points of the rogue ring seen in the second and third panels of Fig. 3.35. According to Theorem 3.18, our predicted solutions in all four panels of Fig. 3.35 are not expected to be valid in the $O(1)$ neighborhoods of those edge points.

Comparing our predicted solution in Fig. 3.35 to the true one in Fig. 3.32, we see that the predicted rogue ring closely matches the true one in its shape and location.

The predicted solution in Fig. 3.35 and the true one in Fig. 3.32 also have notable differences though, and those differences are mostly at or near the left and right edges of the rogue ring. At those edges, the true solution shows a lump there, which is very narrow and hardly visible at $t = 0$ but becomes wider and more visible as $|t|$ increases. The predicted solution, however, does not exhibit such lumps. The reason for this difference is clearly due to the fact that those edge points are exceptional points of the critical curve, where our predicted solution does not hold according to Theorem 3.18. So, there are no contradictions between the analytical theory and the true solution here.

The results of Theorem 3.18 are for the case of $p = 1$ in rogue waves of Lemma 3.4. If $p \neq 1$, rogue curves can also be predicted, and such rogue curves

would be a linear transformation of those for $p = 1$ in the (x, y) plane (see Yang and Yang (2024b) for details).

The results of Theorem 3.18 also exclude the case of large negative a_m when m is even. In that case, rogue curves can also arise, but they will be predicted analytically through root curves of slightly modified double-real-variable polynomials, where the matrix elements $\mathcal{S}_k^{[m]}(z_1, z_2)$ in Eq. (3.291) are replaced by $\hat{\mathcal{S}}_k^{[m]}(z_1, z_2)$, which are defined slightly differently as

$$\sum_{k=0}^{\infty} \hat{\mathcal{S}}_k^{[m]}(z_1, z_2)\epsilon^k = \exp\left(z_2\epsilon + z_1\epsilon^2 - \epsilon^m\right), \quad m \geq 3. \tag{3.309}$$

See Yang and Yang (2024b) for details.

3.5 Super Rogue Wave of High Order in the Nonlinear Schrödinger Equation

In previous sections, the rogue patterns occur when certain internal parameters in the rogue wave solutions were large. In (1+1)-dimensional systems, such as the NLS equation and many others, those rogue waves under large internal parameters would often split into a number of fundamental rogue waves, plus possibly a lower-order rogue wave at the center. Because of such splitting, rogue waves with large internal parameters are generally not the super rogue waves, i.e., rogue waves with the highest peak amplitude among all rogue waves of a certain order.

Super rogue waves are important, because they would cause the greatest damage should they occur in nature. For this reason, profiles of super rogue waves are of great interest. At low order, such profiles can be numerically plotted. At high order, it is possible to analytically determine such profiles by asymptotic methods. So far, this large-order asymptotic profile of the super rogue wave has been derived for the NLS equation by Bilman et al. (2020), and their results are described below.

The NLS equation (3.13), under a gauge transformation of $u(x, t) = e^{\mathrm{i}t}\psi(x, t)$, can be rewritten as

$$\mathrm{i}\psi_t + \frac{1}{2}\psi_{xx} + (|\psi|^2 - 1)\psi = 0. \tag{3.310}$$

Super rogue waves in this equation were derived by Guo et al. (2012) using Darboux transformation, and their expressions are as follows. Let quantities $F_l(x, t)$ and $G_l(x, t)$ be defined by generating functions

$$(1 - \mathrm{i}\lambda)\frac{\sin\left[(x + \lambda t)\sqrt{\lambda^2 + 1}\right]}{\sqrt{\lambda^2 + 1}} = \sum_{l=0}^{\infty}\left(\frac{1}{2}\mathrm{i}\right)^l F_l(x, t)(\lambda - \mathrm{i})^l, \tag{3.311}$$

$$\cos\left[(x+\lambda t)\sqrt{\lambda^2+1}\right]=\sum_{l=0}^{\infty}\left(\frac{1}{2}\mathrm{i}\right)^l G_l(x,t)(\lambda-\mathrm{i})^l. \tag{3.312}$$

Define a $k\times k$ matrix $\boldsymbol{K}^{(k)}(x,t)$ by

$$K_{pq}^{(k)}(x,t)=\sum_{\mu=0}^{p-1}\sum_{\nu=0}^{q-1}\binom{\mu+\nu}{\mu}\left(F_{q-\nu-1}(x,t)^*F_{p-\mu-1}(x,t)\right.$$
$$\left.+G_{q-\nu-1}(x,t)^*G_{p-\mu-1}(x,t)\right), \tag{3.313}$$

where $1\le p,q\le k$, and a $k\times k$ rank-one perturbation $\boldsymbol{H}^{(k)}(x,t)$ by

$$H_{pq}^{(k)}(x,t)=-2\left(F_{p-1}(x,t)+G_{p-1}(x,t)\right)\left(F_{q-1}(x,t)^*\right.$$
$$\left.-G_{q-1}(x,t)^*\right),\quad 1\le p,q\le k. \tag{3.314}$$

Then, the super rogue wave of order k in Eq. (3.310) is

$$\psi_k(x,t)=(-1)^k\frac{\det\left(\boldsymbol{K}^{(k)}(x,t)+\boldsymbol{H}^{(k)}(x,t)\right)}{\det\left(\boldsymbol{K}^{(k)}(x,t)\right)}. \tag{3.315}$$

It can be shown that (Bilman et al. 2020)

$$\psi_k(0,0)=(-1)^k(2k+1). \tag{3.316}$$

Thus, the peak amplitude of the k-th order super rogue wave is $2k+1$. This result is consistent with Eq. (2.97) that was obtained for super rogue waves from the bilinear method.

Using the determinant formula (3.315), the first four super rogue waves are plotted in Fig. 3.36. One can see that the amplitude of the super rogue wave of order k increases with k, and the extreme amplitude is achieved at a central peak located at the origin. In addition, the solution near the origin changes more and more rapidly in x and t as k increases. Furthermore, the solution becomes more complex as k increases, with the formation of more and more subordinate peaks in amplitude.

The above determinant solution (3.315) allows a representation via a Riemann-Hilbert Problem. In this latter formulation, the asymptotic description of the solution $\psi(x,t)$ at high order k can be obtained in the near-field limit, i.e., for (x,t) in a small neighborhood of the origin that is shrinking in size as $k\to\infty$. This asymptotic near-field profile is given in the following theorem (Bilman et al. 2020).

Theorem 3.19 *Let $\psi_k(x,t)$ be the super rogue wave (3.315) of the NLS equation (3.310). Then, if $k=2n$,*

$$n^{-1}\psi_{2n}(n^{-1}X,n^{-2}T)=\Psi^+(X,T)+O(n^{-1}),\quad n\to\infty, \tag{3.317}$$

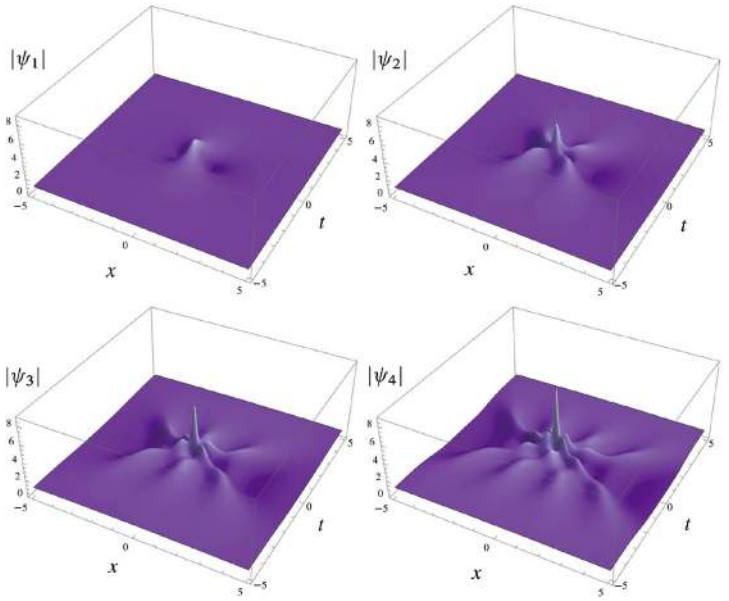

Fig. 3.36 The NLS super rogue waves $|\psi_k(x,t)|$ for $k = 1, 2, 3, 4$. Taken from Bilman et al. (2020)

while if $k = 2n - 1$,

$$n^{-1}\psi_{2n-1}(n^{-1}X, n^{-2}T) = \Psi^{-}(X,T) + O(n^{-1}), \quad n \to \infty. \tag{3.318}$$

The functions $\Psi^{\pm}(X,T)$*, called super rogue waves of infinite order, are global solutions of the NLS equation*

$$\mathrm{i}\Psi_T + \frac{1}{2}\psi_{XX} + |\Psi|^2\Psi = 0, \tag{3.319}$$

and they are given by

$$\Psi^{\pm}(X,T) = 2\mathrm{i}\lim_{\Lambda\to\infty} \Lambda P_{12}^{\pm}(\Lambda; X, T), \tag{3.320}$$

where $P_{12}^{\pm}(\Lambda; X, T)$ *is the first row, second column of a* 2×2 *matrix function* $\boldsymbol{P}^{\pm}(\Lambda; X, T)$ *that is analytic in the complex* Λ *plane for* $|\Lambda| \neq 1$*. Across the unit circle* $|\Lambda| = 1$*,* $\boldsymbol{P}^{\pm}(\Lambda; X, T)$ *are connected by the jump condition*

$$\boldsymbol{P}_{+}^{\pm}(\Lambda; X, T) = \boldsymbol{P}_{-}^{\pm}(\Lambda; X, T)e^{-\mathrm{i}(\Lambda X + \Lambda^2 T)\sigma_3}\boldsymbol{Q}e^{\mp 2\mathrm{i}\Lambda^{-1}\sigma_3}\boldsymbol{Q}^{-1}e^{\mathrm{i}(\Lambda X + \Lambda^2 T)\sigma_3},$$
$$|\Lambda| = 1, \tag{3.321}$$

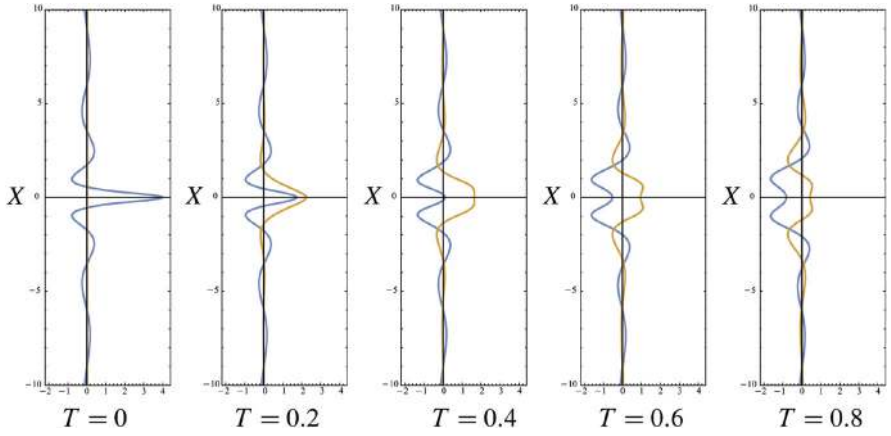

Fig. 3.37 Graphs of $\mathrm{Re}(\Psi(X,T))$ (blue) and $\mathrm{Im}(\Psi(X,T))$ (maize), from left to right for $T = 0, 0.2, 0.4, 0.6, 0.8$. Taken from Bilman et al. (2020)

where

$$Q = \frac{1}{\sqrt{2}}\begin{pmatrix} 1 & -1 \\ 1 & 1 \end{pmatrix}, \quad \sigma_3 = \begin{pmatrix} 1 & 0 \\ 0 & -1 \end{pmatrix}. \tag{3.322}$$

At infinity of the complex Λ plane, the normalization condition of $\boldsymbol{P}^{\pm}(\Lambda; X, T)$ is

$$\boldsymbol{P}^{\pm}(\Lambda; X, T) \to \boldsymbol{I}, \quad \Lambda \to \infty, \tag{3.323}$$

where $\boldsymbol{I}$ is the identity matrix.

The functions $\Psi^{+}(X,T)$ and $\Psi^{-}(X,T)$ are related as

$$\Psi^{-}(X,T) = -\Psi^{+}(X,T). \tag{3.324}$$

In addition, they satisfy the following symmetry relations,

$$\Psi^{\pm}(-X,T) = \Psi^{\pm}(X,T), \quad \Psi^{\pm}(X,-T) = \Psi^{\pm}(X,T)^{*}. \tag{3.325}$$

Furthermore, $\Psi^{\pm}(0,0) = \pm 4$. Graphs of $\Psi^{+}(X,T)$ at various T values are displayed in Fig. 3.37. These super rogue waves of infinite order $\Psi^{\pm}(X,T)$ give the asymptotic predictions of super rogue waves at high order through the scalings (3.317)–(3.318).

Chapter 4
Experiments on Rogue Waves

Rogue waves predicted by the nonlinear Schrödinger equation and the Manakov equations have been observed in various physical systems such as optical fibers, water waves, plasma, and Bose-Einstein condensates. In this chapter, we describe these observations.

4.1 Observation of NLS Rogue Waves in Optical Fibers

Evolution of light transmission in optical fibers in the anomalous-dispersion regime is described by the normalized NLS equation (1.96), i.e.,

$$\mathrm{i}u_\xi + \frac{1}{2}u_{TT} + |u|^2 u = 0, \tag{4.1}$$

where u is the complex envelope of the light's electric field normalized by $P_0^{1/2}$, ξ is the propagation distance z normalized by $(\gamma P_0)^{-1}$, and $T \equiv t - \beta_1 z$ is the retarded time normalized by $(|\beta_2|/\gamma P_0)^{1/2}$. Here, P_0 is a characteristic light power, β_1^{-1} is the carrier wave's group velocity, β_2 is the group-velocity-dispersion parameter which is negative in the anomalous-dispersion regime, and γ is the nonlinear coefficient.

The Peregrine rogue wave in Eq. (4.1) is

$$u(\xi, T) = \left[1 - \frac{4(1 + 2\mathrm{i}\xi)}{1 + 4T^2 + 4\xi^2}\right] e^{\mathrm{i}\xi}. \tag{4.2}$$

This wave in physical units can be obtained from the above variable normalizations. It was first observed in optical fibers as a limit of the Akhmediev breather by Kibler et al. (2010). Akhmediev breathers are a family of T-periodic and ξ-localized

B. Yang, J. Yang, *Rogue Waves in Integrable Systems*,
https://doi.org/10.1007/978-3-031-66793-0_4

waves in the NLS equation (4.1) and were first reported by Akhmediev and Korneev (1986). Their expressions are

$$u(\xi, T) = \left[\frac{(1-4a)\cosh(b\xi) + \mathrm{i}b\sinh(b\xi) + \sqrt{2a}\cos(\Omega T)}{\sqrt{2a}\cos(\Omega T) - \cosh(b\xi)} \right] e^{\mathrm{i}\xi}, \tag{4.3}$$

where $b = [8a(1-2a)]^{1/2}$, $\Omega = [4(1-2a)]^{1/2}$, and $0 < a < 1/2$ is a free parameter. When $|\xi| \gg 1$, this breather's tail behaves as

$$u(\xi, T) \approx \left[4a - 1 - \mathrm{i}b\,\mathrm{sgn}(\xi) + \alpha\cos(\Omega T)\right] e^{\mathrm{i}\xi}, \tag{4.4}$$

where α is a ξ-related small parameter. At $\xi = 0$, this wave reaches a peak amplitude of $1 + 2\sqrt{2a}$. Importantly, when $a \to 1/2$, this Akhmediev breather approaches the Peregrine wave (4.2).

The experimental setup by Kibler et al. (2010) is shown in Fig. 4.1 (left panel). The initial signals (pump and seed) were generated from two telecommunications-grade external-cavity lasers, with the pump laser at wavenumber $\lambda_p = 1554.53$ nm and the seed laser at a nearby wavenumber λ_s. The fiber used was 900 m of highly nonlinear fiber with $\beta_2 = -8.85 \times 10^{-28}\mathrm{s}^2\mathrm{m}^{-1}$ and $\gamma = 0.01\mathrm{W}^{-1}\mathrm{m}^{-1}$ at λ_p. The fiber was dispersion-flattened to have low third-order dispersion. Fibre loss was 1 dB/km. A phase modulator was used to broaden the narrow intrinsic external-cavity-laser linewidths so as to suppress Brillouin scattering in the fiber at the power levels used in our experiments. Both the pump and the seed were then amplified to the power levels used in the experiments by means of an erbium-doped fiber amplifier. The injection set-up was all-polarization maintaining to maximize the modulation-instability process occurring in the optical fiber. A low-noise amplifier was used so as to clearly favour the induced wave dynamics over spontaneous broadband modulation instability.

In the experiment, an input field $A(z = z_0, \tau) = \sqrt{P_0}[1 + \alpha_{mod}\exp(\mathrm{i}\omega_{mod}\tau)]$ was injected into the fiber. The input power was P_0, and α_{mod}, ω_{mod} were the modulation strength and frequency. By comparing this input field with the tail (4.4) of the Akhmediev breather, we see that the frequency ω_{mod} here is related to the modulation parameter a of Eq. (4.4) by $a = [1 - \omega_{mod}^2/(4\gamma P_0/|\beta_2|)]/2$. To observe the Peregrine rogue wave, a should be made as close to $1/2$ as possible. It is acknowledged that this experimental input is not the ideal one for the Peregrine rogue wave (it is not even ideal for the Akhmediev breather, see Eq. (4.4)). Thus, deviations between experiments and the true Peregrine wave should be expected, especially at longer distances (these deviations were later studied in Hammani et al. (2011) and Erkintalo et al. (2011)).

When the input field was taken as $P_0 = 0.30$ W, $\omega_{mod} = 241$ GHz $= 1.514 \times 10^{12}$ rad/s, and $\alpha_{mod} = 0.225$, the measured temporal intensity profile of the maximally compressed pulse (at nondimensional propagation distance $\xi = 2.5$) is displayed as the blue line with markers in Fig. 4.1 (right panel). The peak power of the retrieved profile was calculated from the measured output power with no free

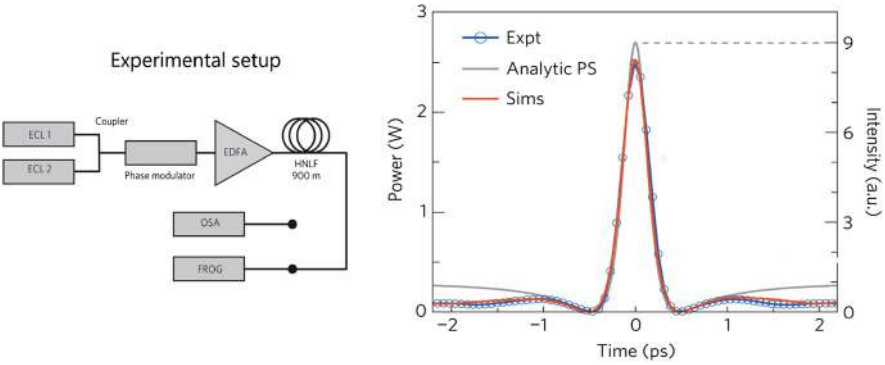

Fig. 4.1 Observation of Peregrine rogue wave in an optical fiber. Left panel: experimental setup. ECL: external-cavity laser; EDFA: erbium-doped fiber amplifier; HNLF: highly nonlinear fiber; OSA: optical spectrum analyser; FROG: frequency-resolved optical gating. Right panel: experimental results showing the measured temporal intensity profile of the maximally compressed pulse (blue line with circles), and comparison with the NLS simulation result (red) and the ideal Peregrine wave (grey). Taken from Kibler et al. (2010)

parameters. At these P_0 and ω_{mod} values, $a \approx 0.42$, which is close to the Peregrine wave condition. Indeed, the observed peak intensity of the maximally compressed pulse is seen from this figure as close to 9 times that of the input field (i.e., the observed peak amplitude is close to 3 times that of the input field), which matches the Peregrine wave. The observed intensity profile of the maximally compressed pulse was also compared to the maximal-intensity profile of the Peregrine wave (4.2) (grey line), and they match as well. These measurements confirm the expected temporal features of the Peregrine wave—a temporally localized peak (400 fs duration) surrounded by a non-zero background. The FROG measurements also confirm the different signs of the peak and background amplitudes through the measured relative π phase difference.

Due to the imperfect initial excitation in the above experiment, after the first stage of growth the return to the initial stage is only partial and the nonlinear structure tends to split into several higher-order structures (Hammani et al. 2011; Erkintalo et al. 2011), which contrasts the Peregrine dynamics. To better observe the Peregrine wave, a more advanced experiment was performed by Xu et al. (2019). Their experimental setup is shown in Fig. 4.2. A frequency comb centered at wavenumber $\lambda_p = 1550\,\text{nm}$ with a 20-GHz line spacing is first generated by the nonlinear evolution of a sinusoidal beating in a fiber. In order to have input conditions as close as possible to the ideal Peregrine wave, the discrete spectral components are then spectrally shaped in amplitude as well as in phase using a liquid crystal on a silicon based programmable filter (Waveshaper device). This method is able to synthesize as an initial condition a close-to-ideal Peregrine wave at any propagation length. Note that a phase modulator is also inserted in the initial comb source, in order to prevent the deleterious effects of Brillouin backscattering. Next, the resulting shaped wave is amplified by a high-power erbium doped fiber amplifier up to average

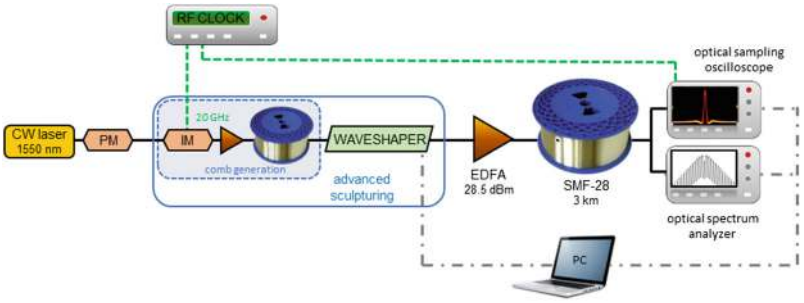

Fig. 4.2 A more advanced experimental setup for observation of the Peregrine rogue wave in a standard single-mode optical fiber. PM: phase modulator; IM: intensity modulator; EDFA: erbium-doped fiber amplifier. Taken from Xu et al. (2019)

powers of 28.5 dBm (i.e., 0.708 W). The propagation takes place in a combination of segments of variable lengths made of the most standard fiber that is currently available, i.e., the single-mode fiber SMF-28, where $\beta_2 = -2.1 \times 10^{-26} \mathrm{s}^2\mathrm{m}^{-1}$ and $\gamma = 0.0011 \mathrm{W}^{-1}\mathrm{m}^{-1}$ at λ_p. Given the high value of β_2, the impact of third-order dispersion is negligible in the spectral bandwidth under study. After propagation into the fiber, the output field is recorded in the temporal domain taking advantage of an optical sampling oscilloscope that allows a temporal resolution of the order of picoseconds. The output spectral properties are also recorded using an optical spectrum analyzer with a spectral resolution of 2.5 GHz.

In the experiment of Xu et al. (2019), longitudinal evolution of temporal and spectral intensity profiles of the synthesized initial waveform was investigated in detail. The input profile programmed on the spectral waveshaper corresponded to the Peregrine-like structure (4.2) at a normalized distance of $\xi = \gamma P_0 z = -1.2$ and is shown as the red curve in Fig. 4.3b. A total of 22 longitudinal measurements were carried out, involving fiber lengths up to 3 km, corresponding to a normalized length from $\xi = -1.2$ to 1.2. Spatiotemporal intensity measurements are shown in Fig. 4.3a1. These experimental measurements nicely reproduce the spatiotemporal localization of the ideal Peregrine wave (Fig. 4.3a2) and are in excellent agreement with the analytical Peregrine evolution. The point of maximum temporal compression occurs after 1.5 km of nonlinear propagation. It is worth mentioning that contrary to previous experimental realizations in Kibler et al. (2010), Hammani et al. (2011), and Erkintalo et al. (2011), which were based on approximate sinusoidal inputs, the input here is much closer to the initial ideal Peregrine wave. As a result, the recorded longitudinal evolution in Fig. 4.3a1 is rather symmetric and does not show any sign of pulse splitting.

Details of the temporal phase and intensity profiles at the point of maximum temporal compression are provided in Fig. 4.3b and c. The temporal profile retrieved at a distance $z = 1.5$ km exhibits the typical signatures of the Peregrine wave. Compared to the initial localized perturbation (red line) obtained after accurate phase and amplitude sculpturing of the frequency comb, the wave has been

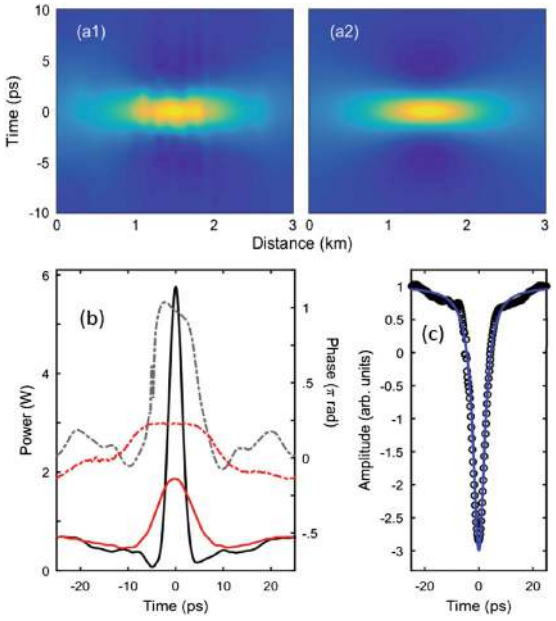

Fig. 4.3 A more advanced observation of Peregrine rogue wave in a standard single mode fiber. (**a1**) Measured longitudinal evolution of temporal intensity profiles. (**a2**) Analytical intensity evolution of an ideal Peregrine wave (4.2) using dimensional units of experiments. (**b**) Experimental intensity and phase profiles (solid and dash-dotted lines, respectively) obtained for the generated Peregrine-like wave. Black colors: experimental results retrieved at the point of maximum compression. Red colors: the initial synthesized waveform input. (**c**) Real part of the amplitude profile at the point of maximum compression. Black circles: experimental results; blue lines: analytical shape of the corresponding Peregrine wave. Taken from Xu et al. (2019)

significantly compressed down to a full width at half maximum of 3 ps. The ratio between the background and the central peak is up to 8, which is close to 9 of the Peregrine wave. The sharp phase shift between the central part and the continuous background has also increased up to a value that becomes close to π. Therefore, the reconstructed field passes twice through the zero value and is in convincing agreement with the typical Peregrine profile corresponding to the parameters involved in the experiment.

4.2 Observation of NLS Rogue Waves in Water Tanks

Evolution of one-dimensional gravity-wave packets in deep water with a free surface is described by the NLS equation, see Sect. 1.1.1. This NLS equation has two forms, the temporal-evolution form (1.32) and the spatial-evolution form (1.44). For experiments in a water tank where the temporal movement of the wave-

maker at one end of the tank is prescribed, the spatial-evolution form (1.44) is more natural. However, to observe special solutions of the NLS equation such as rogue waves, explicit dimensional expressions of such solutions in the physical (x, t) space are available from either form of the NLS equation. In addition, those explicit dimensional expressions out of the two forms of the NLS equation are often asymptotically equivalent (Chabchoub and Grimshaw 2016). In such a case, it does not matter which NLS form is used, as long as the motion of the wave-maker at its spatial location is prescribed according to the explicit (x, t) expression of that special solution.

In most papers of water wave experiments on rogue waves, the temporal-evolution form of the NLS equation was used. In nondimensional variables, this NLS equation is (1.37), i.e.,

$$\mathrm{i}\frac{\partial \tilde{u}}{\partial \tilde{t}} + \frac{1}{2}\frac{\partial^2 \tilde{u}}{\partial \tilde{x}^2} + |\tilde{u}|^2\tilde{u} = 0, \tag{4.5}$$

where

$$\tilde{u} = u/a, \quad \tilde{x} = \sqrt{2}ak^2(x - c_g t), \quad \tilde{t} = -a^2k^2\omega t/2, \tag{4.6}$$

$c_g = \omega/2k$, $\omega = \sqrt{gk}$, and a is a representative wave-amplitude parameter which we will set as the amplitude of the background wave in rogue wave experiments. The variable $u(x, t)$ is related to the water surface elevation $\zeta(x, t)$ as (1.33), i.e.,

$$\zeta(x, t) = \mathrm{Re}\{u(x, t)\exp[\mathrm{i}(kx - \omega t)]\}, \tag{4.7}$$

to the first order of wave steepness, and as (1.34), i.e.,

$$\zeta(x, t) = \mathrm{Re}\left\{u(x, t)e^{\mathrm{i}(kx-\omega t)} + \frac{1}{2}ku^2(x, t)e^{2\mathrm{i}(kx-\omega t)}\right\}, \tag{4.8}$$

to the second order of wave steepness.

4.2.1 *Peregrine Rogue Wave*

The Peregrine (fundamental) rogue wave in the NLS equation (4.5) on a uniform background is (2.79), which can be written equivalently as

$$\tilde{u}(\tilde{x}, \tilde{t}) = \left(-1 + \frac{4\left(1 + 2\mathrm{i}\tilde{t}\right)}{1 + 4\tilde{x}^2 + 4\tilde{t}^2}\right)e^{\mathrm{i}\tilde{t}}. \tag{4.9}$$

Converting to physical units through Eq. (4.6), this Peregrine wave is

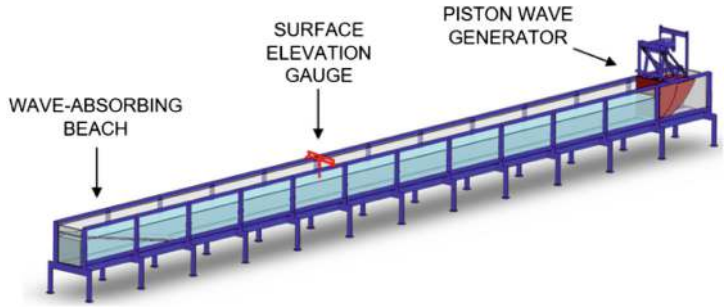

Fig. 4.4 Schematic illustration of the water tank for rogue wave observation. Taken from Xu et al. (2020)

$$u(x,t) = a\left(-1 + \frac{4\left(1 - \mathrm{i}a^2k^2\omega t\right)}{1 + 8a^2k^4(x - c_g t)^2 + a^4k^4\omega^2t^2}\right)e^{-\mathrm{i}a^2k^2\omega t/2}. \tag{4.10}$$

The experiment to observe this Peregrine rogue wave was performed by Chabchoub et al. (2011). The water tank used in this experiment was 15 m long, 1.6 m wide, and 1.5 m deep, and the tank was filled with water with mean height of 1 m. A schematic illustration of the water tank setup is shown in Fig. 4.4. A single-flap paddle activated by a hydraulic cylinder is located at one end of the tank. To avoid wave reflections from the opposite end of the tank, there is a wave-absorbing beach there. The surface elevation of water at a given point is measured by a capacitance wave gauge with a sensitivity of 1.06 V/cm and a sampling frequency of 500 Hz.

In the experiment, the dimensional far-field amplitude of the background was selected to be $a = 0.01\mathrm{m}$. The wavelength λ of the carrier was set to 0.54 m, corresponding to a wave number $k = 2\pi/\lambda \approx 11.63/\mathrm{m}$ and frequency $\omega = \sqrt{gk} \approx 10.7/\mathrm{s}$. These values have been chosen in order to ensure that the wavelength is large enough to ignore effects of surface tension but still small enough to have sufficient tank length to develop the wave evolution described by Eq. (4.10). The wavelength also has to be small enough for the whole arrangement to be sufficiently close to the deep water limit.

The position where the rogue wave develops its maximum amplitude depends on the initial conditions at the wave maker. In order to demonstrate the evolution of a nearly periodic Stokes wave towards the most extreme wave state, the position of the maximum was chosen 9 m along the tank. Water surface-height data was collected at ten positions, with equal separations of 1 m, along the direction of wave propagation.

Under these experimental conditions, the nondimensional Peregrine wave (4.9) is displayed in the left panel of Fig. 4.5, and the theoretical leading-order water surface elevation $\mathrm{Re}\{u(x,t)\exp[\mathrm{i}(kx - \omega t)]\}$ associated with the dimensional Peregrine wave (4.10) versus time at spatial locations of $x = -9, -8, \cdots, 0\,\mathrm{m}$ are displayed in the right panel of Fig. 4.5.

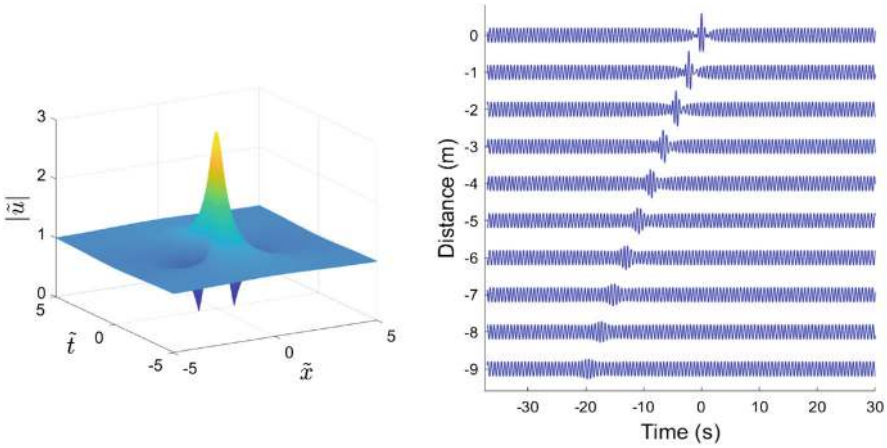

Fig. 4.5 Left: the nondimensional Peregrine solution $|\tilde{u}(\tilde{x},\tilde{t})|$ in Eq. (4.9). Right: theoretical leading-order water surface elevation $\mathrm{Re}\{u(x,t)\exp[\mathrm{i}(kx-\omega t)]\}$ associated with the dimensional Peregrine wave (4.10) versus time at spatial locations of $x=-9,-8,\cdots,0$ m under experimental conditions of Chabchoub et al. (2011)

Experimentally, prescribing the initial condition at the wave maker to resemble the one in Fig. 4.5 (right panel) with $x=-9$ m, the measurement results of water surface elevations down the tank are displayed in the left panel of Fig. 4.6. This figure shows that the wave is essentially sinusoidal when close to the flap. This can be seen from the wave profile measured at 10 cm next to the mean flap position. The flap motion produces a periodic wave with about 1 cm amplitude, with a brief increase of modulation above that level to about 1.4 cm in the middle of the packet. Measurements at further distances from the wave maker show the process of amplitude growth of this perturbation which remains strongly localized and moves along with group velocity, confirming the existence of rogue waves "that appear from nowhere". These experimental results agree well with the theoretical predictions as shown in Fig. 4.5.

The theoretical prediction from the Peregrine solution suggests that the carrier wave surface elevation should be amplified by a factor of 3. The measurements came very close to this value. The right panel of Fig. 4.6 represents a surface-height measurement at a position close to the presumed maximum envelope amplitude. While the carrier wave has an amplitude of about one centimeter, the surface height of the "maximum wave" almost exactly reaches a value of three centimeters. By comparing the measured time series (solid line) with the curve predicted by the Peregrine solution (dashed line), good agreement can be seen.

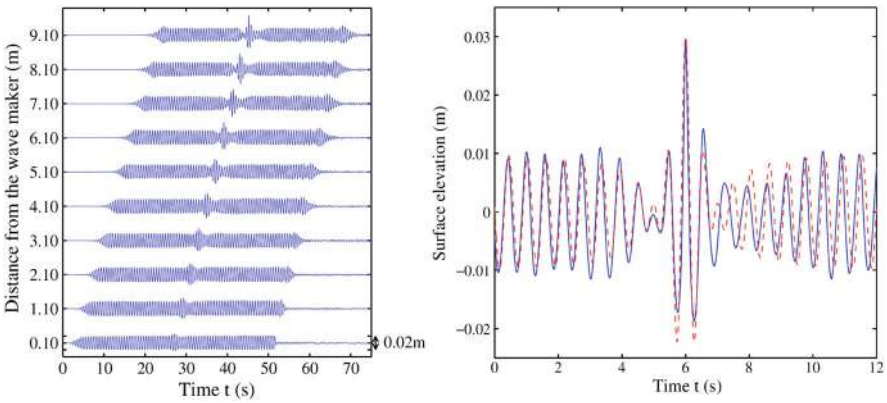

Fig. 4.6 Observation of the Peregrine rogue wave in a water tank. Left: temporal evolution of the water surface height at various distances from the wave maker. Right: comparison of measured surface height at the position of maximum rogue wave amplitude (solid line) with the theoretical Peregrine solution (dashed line) at maximum wave amplitude. Taken from Chabchoub et al. (2011)

4.2.2 Higher-Order Rogue Waves

Second-order NLS rogue waves have also been observed in water tanks. Analytical expressions of these 2nd-order waves have been displayed in Eq. (2.80) of Sect. 2.1.1. Their equivalent expressions for Eq. (4.5) are (Ankiewicz et al. 2011)

$$\tilde{u}(\tilde{x},\tilde{t}) = \left(1 + \frac{G_2(\tilde{x},\tilde{t}) + \mathrm{i}K_2(\tilde{x},\tilde{t})}{D_2(\tilde{x},\tilde{t})}\right) e^{\mathrm{i}\tilde{t}}, \tag{4.11}$$

where

$$G_2 = 12\left[3 - 16\tilde{x}^4 - 24\tilde{x}^2(4\tilde{t}^2+1) - 4\beta\tilde{x} - 80\tilde{t}^4 - 72\tilde{t}^2 + 4\gamma\tilde{t}\right],$$

$$K_2 = 24\left[\tilde{t}(15 - 16\tilde{x}^4 + 24\tilde{x}^2 - 4\beta\tilde{x}) - 8(4\tilde{x}^2+1)\tilde{t}^3 - 16\tilde{t}^5 + \gamma\left(2\tilde{t}^2 - 2\tilde{x}^2 - \frac{1}{2}\right)\right],$$

$$D_2 = 64\tilde{x}^6 + 48\tilde{x}^4(4\tilde{t}^2+1) + 12\tilde{x}^2(3-4\tilde{t}^2)^2 + 64\tilde{t}^6 + 432\tilde{t}^4 + 396\tilde{t}^2 + 9 + \\ + \beta\left[\beta + 4\tilde{x}(12\tilde{t}^2 - 4\tilde{x}^2 + 3)\right] + \gamma\left[\gamma + 4\tilde{t}(12\tilde{x}^2 - 4\tilde{t}^2 - 9)\right],$$

and β, γ are arbitrary real constants. These solutions in physical units can be obtained through Eq. (4.6). Since these waves contain free parameters, they can exhibit various shapes depending on the choices of parameter values. For two choices of $(\beta, \gamma) = (0, 0)$ and $(50, -50)$, the corresponding solutions are shown

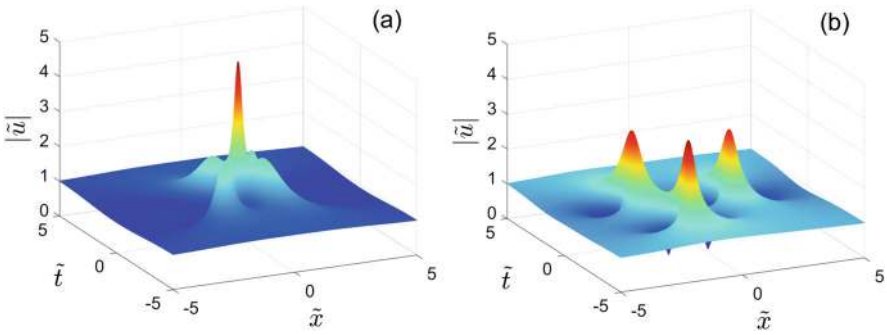

Fig. 4.7 Second-order NLS rogue waves (4.11) in Eq. (4.5) with $(\beta, \gamma) = (0, 0)$ in (**a**) and $(\beta, \gamma) = (50, -50)$ in (**b**)

in Fig. 4.7. The solution with $(\beta, \gamma) = (0, 0)$ is the super rogue wave which has the highest amplitude 5 among this family of solutions, and the one with $(\beta, \gamma) = (50, -50)$ gives a rogue triplet, where three Peregrine waves appear at different space-time locations.

These second-order NLS rogue waves have also been observed in water tanks. Observation of the super rogue wave was performed by Chabchoub et al. (2012a). The water tank and its setup here are the same as those in the Peregrine experiment of Chabchoub et al. (2011) described in the earlier text (see Fig. 4.4). As before, the analytical solution (4.11) is written in dimensional form and shifted in space in order to observe the formation of the rogue wave at a desired location in the wave tank. This furnishes the solution at the wave maker and consequently the signal that drives the paddle. However, a significant difference from the previous Peregrine experiment is that, since the present super rogue wave is steeper than the Peregrine wave, in order to get a good agreement between theory and experiment, the theoretical surface elevation $\zeta(x, t)$ used to drive the wave maker needs to be calculated from the solution $u(x, t)$ of the NLS equation (4.5) to the second order in steepness through Eq. (4.8).

The experiment of the super rogue wave was conducted for a carrier amplitude of $a = 0.001$ m. The carrier wavenumber was $k = 30$/m, corresponding to a frequency of $\omega = \sqrt{gk} \approx 17.2$/s. Close to the wave maker, at a distance of 1 m, the regular background wave was locally perturbed in the middle of the wave train. The limited length of the wave tank, however, was not long enough to directly observe the full evolution of the super rogue wave from a very small amplitude to its maximum in a single run. As the growth of the amplitude was algebraic rather than exponential, even the use of longer wave tanks remained problematic. To overcome this difficulty, the experiment was split into several stages. Namely, starting the wave generation repetitively with different boundary conditions given from theory, the wave profile at the other end of the tank was measured. Each time, the final profile was checked and found to follow the theoretical prediction. Deviations between theoretical and experimental profiles were minimal and mainly manifested

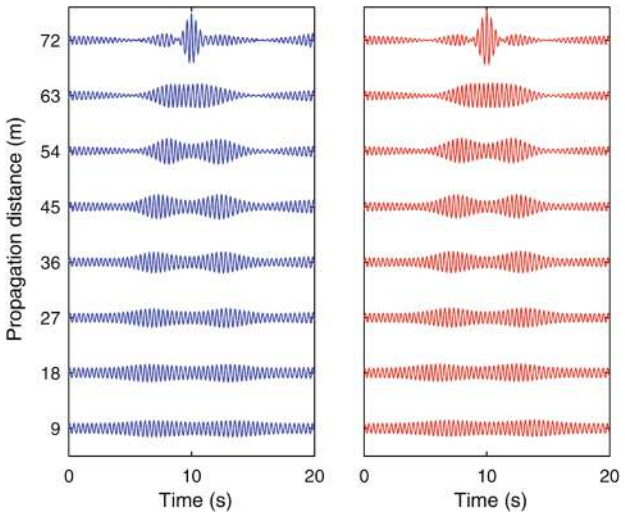

Fig. 4.8 Observation of the second-order super NLS rogue wave in a water tank by the split-propagation technique. The left panel shows experimental profiles at the end of each split propagation, while the right panel shows theoretical ones. The time axis of each wave profile is shifted by the amount of x/c_g, so that the shifted time follows the wave center. Taken from Chabchoub et al. (2012a)

in their left-right asymmetry. This process was repeated 7 times, thus multiplying the propagation length of 9 meters 8 times. This way, the propagation distance of 72 m was reached, which corresponded to the point of maximum amplitude. The left panel in Fig. 4.8 shows the profiles measured at the end of each propagation segment. The right panel of this figure shows the corresponding theoretical curves. The comparison between the measured wave profiles and the theoretical curves shows very good agreement and justifies the experimental approach.

Observation of rogue triplets such as the one in Fig. 4.7b was performed by Chabchoub and Akhmediev (2013). The experimental facility is the same as that used to observe the second-order super rogue wave in the earlier text. Here, the theoretical surface elevation $\zeta(x,t)$ is also calculated from the solution $u(x,t)$ of the NLS equation (4.5) to the second order in steepness by the formula (4.8). To observe these triplets, the propagation distance needed is also significantly longer than the actual length of the water tank—the same difficulty that was encountered in the observation of super rogue waves. To overcome this difficulty, the experiment was also done in sequences, but with minor technical differences from that in the super rogue experiment. Here, the tank's length was effectively increased by recording a signal measured at a specific position from the paddle in the first part of the sequence and regenerating the measured wave profile in the second part of the sequence. Repeating this procedure with sufficiently high accuracy, the effective tank length could be increased multiple times.

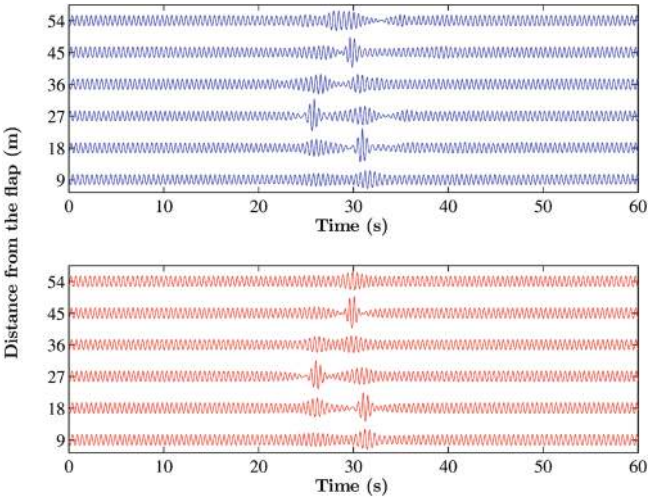

Fig. 4.9 Water-tank observation of the NLS rogue wave triplet in Fig. 4.7b by the split-propagation and profile-regeneration techniques. Upper blue curves show experimental profiles of surface elevations at the end of each split propagation, while the lower red curves show the corresponding theoretical predictions expected at the same positions. The time axis of each wave profile is shifted by the amount of x/c_g. Taken from Chabchoub and Akhmediev (2013)

The set of experiments was conducted for a carrier amplitude of $a = 0.005$ m. The carrier wavenumber was $k = 16$/m, corresponding to a frequency of $\omega = \sqrt{gk} \approx 12.53$/s. To observe the rogue triplet shown in Fig. 4.7b, the corresponding physical solution $u(x,t)$ was first obtained through Eq. (4.6), which yielded the theoretical surface elevation $\zeta(x,t)$ through Eq. (4.8). In the first experiment, the theoretical surface elevation profile at $x_{\text{initial}} = -30$ m was used to drive the paddle of the wave maker. After 9 m of propagation down the tank, the profile was recorded, and this recorded profile was then used as the initial condition for the second experiment. This process was repeated 5 times, resulting in 54 m of effective propagation. The recorded profiles at the end of each propagation are shown in Fig. 4.9 (blue curves). This evolution shows clearly the appearance of three Peregrine waves at various positions in the space-time domain, which is the main feature of a rogue triplet. The corresponding theoretical predictions of wave profiles at the same positions are shown as red curves in the same figure. Good agreement between the experiment and the theory can be seen.

NLS rogue waves of even higher orders, up to the fifth order, have also been observed in water tanks; see Chabchoub et al. (2012b) for details.

4.3 Observation of NLS Rogue Waves in Plasma

Propagation of low-amplitude ion-acoustic wave packets in a plasma comprising electrons, cold positive ions and negative ions is governed by the NLS equation (1.130), i.e.,

$$\mathrm{i}\frac{\partial \psi}{\partial t} + p\frac{\partial^2 \psi}{\partial \hat{x}^2} + \frac{q}{4}|\psi|^2 \psi = 0, \tag{4.12}$$

where the envelop function ψ is related to the normalized deviation δn_e of the electron density from its unperturbed value as

$$\delta n_e = \mathrm{Re}[\psi e^{\mathrm{i}(kx-\omega t)}] \tag{4.13}$$

to the leading order approximation, t is the time normalized by the ion plasma period $\omega_{pi}^{-1} \equiv (\epsilon_0 m_\alpha / n_{e0} e^2)^{1/2}$, $\hat{x} = x - c_g t$ is the distance in moving frame normalized by the electron Debye length $\lambda_D \equiv (\epsilon_0 \kappa T_e / n_{e0} e^2)^{1/2}$, m_α is the positive ion mass, n_{e0} is the unperturbed electron density, ϵ_0 is the vacuum permittivity, κ is Boltzmann constant, T_e is the absolute temperature of electrons, e is the charge of the electron, $c_g = \omega'(k)$ is the group velocity, $p = \omega''(k)/2$ is the dispersion coefficient, $\omega(k)$ is the dispersion relation given in Eq. (1.121), k is the normalized wavenumber of the carrier wave, and q is the nonlinear coefficient given in Eq. (1.127).

In the NLS equation (4.12), the dispersion coefficient p is always negative. When the nonlinear coefficient q is also negative, which is the case for all wavenumbers k at a critical negative-ion density value, this NLS equation admits the Peregrine rogue wave

$$\psi(\hat{x}, t) = 2|q|^{-1/2}\left(-1 + \frac{4\,(1-2\mathrm{i}t)}{1 + 2\hat{x}^2/|p| + 4t^2}\right) e^{-\mathrm{i}t}. \tag{4.14}$$

This solution, when substituted into Eq. (4.13), gives a predicted plasma Peregrine rogue wave for the normalized electron density perturbation which can be measured.

This plasma Peregrine rogue wave was observed by Bailung et al. (2011). The experiment was carried out in a multidipole double-plasma machine. The diameter of the device was 30 cm and its total length was 120 cm. The device was separated into a source and a target section with a floating grid. The grid consisted of a stainless steel mesh 50 lines/inch with 83% transparency. The cathodes consisted of 0.1 mm diameter tungsten filaments and were placed 6 cm from the surface of the anode. Each section had five filaments with a length of 6 cm. The chamber was evacuated down to 2.0×10^{-4} Pa with an oil diffusion pump. Argon (Ar) and sulfur hexafluoride (SF_6) were introduced independently into the chamber under continuous pumping. The pressure of Ar was 5.7×10^{-2} Pa and the pressure of SF_6 was varied from 0 to 1×10^{-3} Pa. The discharge voltage was 70 V and the discharge currents of the two sections were 10-50 mA. Plasma parameters as

measured with a Langmuir probe of 6 mm diameter were: the electron temperature T_e was approximately 1.1 eV (i.e., 1.28×10^4 K) and the electron density n_{e0} was approximately 3.8×10^8 cm^{-3}. The mass m_α of the positive Ar^+ ion is 39.9 Dalton (or 6.63×10^{-26} kg), and the mass m_β of the negative F^- ion is 19.0 Dalton. Wave signals were detected with the axially movable Langmuir probe which was biased positively with respect to the plasma potential ($\approx$ 1.5 V) to collect the electron saturation current and was therefore sensitive to the perturbed electron density.

In the experiment, both Ar and SF_6 were introduced into the chamber so that the density ratio between F^- and Ar^+ was 0.1, which is approximately the critical density where the nonlinear coefficient q is always negative for all wavenumbers (see Sect. 1.1.3). Then, a slowly varying amplitude-modulated continuous sinusoidal signal was applied to the source anode and ion-acoustic perturbations were excited. Examples of observed signals at different distances from the separation grid for fixed carrier amplitude (5.4 V peak to peak) are shown in Fig. 4.10. The carrier frequency is 350 kHz and modulation frequency is 31 kHz. Close to the grid the observed signals resemble the applied signal. With increasing distance the compression of the wave packet sets in and the first Peregrine wave emerges at 10.5 cm. The perturbation grows in amplitude and reaches a maximum at 12.5 cm. The observed maximum amplitude is 2.5 times the nearby carrier wave. At further distances ($\geq$ 14.5 cm) the perturbation decays. The perturbation moves with group velocity measured to be 2.1×10^5 cm/s. These observations are in reasonable agreement with theoretical Peregrine wave predictions in plasma.

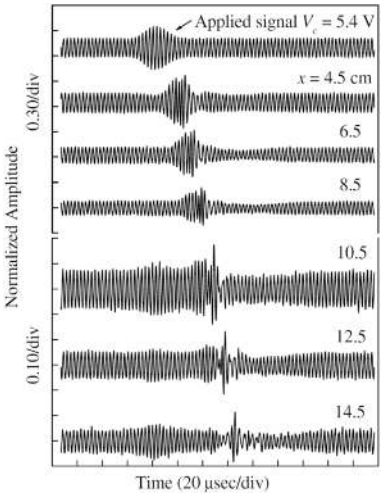

Fig. 4.10 Observation of the Peregrine rogue wave in plasma. The figure shows observed signals of normalized electron density perturbation at different probe positions from the separation grid. The top trace is the applied signal with carrier and modulation frequencies 350 and 31 kHz, respectively. Peak to peak amplitude of the applied carrier wave (V_c) is fixed at 5.4 V. Signals observed at 10.5–14.5 cm are shown with different amplitude scale (0.10/div) for better resolution. Taken from Bailung et al. (2011)

4.4 Observation of NLS Rogue Waves in Bose-Einstein Condensates

A Bose-Einstein condensate (BEC) is a dilute gas of weakly interacting boson particles confined in an external potential and cooled to temperatures very close to absolute zero. Under such conditions, a large fraction of the bosons collapse into the lowest quantum state of the external potential, and all wave functions overlap each other, at which point quantum effects become apparent on a macroscopic scale. This state of matter was first predicted by S.N. Bose and A. Einstein in 1924–1925, and then experimentally observed by E. Cornell, W. Ketterle and C. Wieman in 1995 [Anderson et al. (1995), Davis et al. (1995)]. For their work, Cornell, Ketterle and Wieman jointly won the Nobel Prize in Physics in 2001.

In quantum mechanics, the motion of a boson in a potential well is described by a wave function satisfying a linear Schödinger equation. But since many bosons in a BEC are in the same lowest quantum state and their wave functions overlap, the state of BEC can be described by a collective wave function $\psi(\mathbf{x}, t)$, where $\mathbf{x}$ is the three-dimensional spatial coordinate, $|\psi|^2$ is interpreted as the particle density, and the total number of atoms is $\int |\psi|^2 d\mathbf{x}$. In addition, due to interactions between bosons which give rise to nonlinear effects, this collective wave function $\psi(\mathbf{x}, t)$ satisfies a NLS equation with an external potential:

$$i\hbar\psi_t = \left[-\frac{\hbar^2}{2m}\nabla^2 + V(\mathbf{x}) + g|\psi|^2\right]\psi, \tag{4.15}$$

where $\hbar$ is the Planck constant, m is the mass of the boson, $V(\mathbf{x})$ is the external potential, $g = 4\pi\hbar^2 a_s/m$ is the nonlinear coefficient, and a_s is the scattering length of two interacting bosons. This equation was first derived by Gross (1961) and Pitaevskii (1961) and is now called the Gross-Pitaevskii equation. It provides a good description of the collective behavior of a single-component BEC.

If the potential $V(\mathbf{x})$ is slowly varying in $\mathbf{x}$, then it may be approximated as a constant and scaled to zero. In this case, the Gross-Pitaevskii equation (4.15), when restricted to one spatial dimension x, becomes

$$i\hbar\psi_t + \frac{\hbar^2}{2m}\psi_{xx} - g|\psi|^2\psi = 0. \tag{4.16}$$

Since $g > 0$, this is a defocusing NLS equation, which does not admit modulation instability or rogue waves.

In order to derive a focusing NLS model in BEC, an idea was proposed by Dutton and Clark (2005), Bakkali-Hassani et al. (2021) and Romero-Ros et al. (2022). This idea is based on a two-component Bose gas, where the minority component immersed in a bath defined by the other component is well described by an effective single-component NLS equation with focusing nonlinearity.

We consider atoms of mass m in states $|1\rangle$ and $|2\rangle$ with repulsive interactions. The intracomponent (g_{11}, g_{22}) and intercomponent (g_{12}) interaction parameters are thus all positive, where $g_{ij} = 4\pi\hbar^2 a_{ij}/m$, and a_{ij} are the s-wave scattering lengths for binary collisions between atoms in internal states $|i\rangle$ and $|j\rangle$. Such a mixture is well described in the zero-temperature limit by two coupled nonlinear Schrödinger equations. In the weak depletion regime, one can assume that the dynamics of the dense bath of atoms in state $|1\rangle$ occurs on a short timescale compared to the minority component dynamics. The bath is then always at equilibrium on the timescale of the evolution of the minority component in state $|2\rangle$. In this case, based on some approximations and numerical evidence, the collective wave function ψ_2 for the minority component can be approximated by the following NLS equation ((Dutton and Clark 2005; Bakkali-Hassani et al. 2021))

$$i\hbar\frac{\partial\psi_2}{\partial t} = \left[-\frac{\hbar^2}{2m}\nabla^2 + V_{\text{eff}}(\mathbf{x}) + g_{\text{eff}}|\psi_2|^2\right]\psi_2, \tag{4.17}$$

where $V_{\text{eff}}(\mathbf{x})$ is an effective potential, and g_{eff} is an effective nonlinear coefficient that is determined by g_{11}, g_{12} and g_{22}. This g_{eff} value was quoted as

$$g_{\text{eff}}^{[\text{DC}]} = g_{11} + g_{22} - 2g_{12}, \quad g_{\text{eff}}^{[\text{BH}]} = g_{22} - \frac{g_{12}^2}{g_{11}}, \tag{4.18}$$

in Dutton and Clark (2005) and Bakkali-Hassani et al. (2021), respectively. In physical situations, g_{11}, g_{22} and g_{12} are very close to each other within a few percent. In such a case, these two different formulae for g_{eff} give approximately the same effective nonlinear coefficients. For example, for ^{87}Rb atoms, if we take the $|1\rangle$ state as $|F, m_F\rangle = |1, 0\rangle$ and the $|2\rangle$ state as $|F, m_F\rangle = |2, 0\rangle$, then $g_{12} = 0.98g_{11}$, and $g_{22} = 0.94g_{11}$ (Altin et al. 2011). In this case, the two g_{eff} formulae in (4.18) give $-0.02g_{11}$ and $-0.0204g_{11}$ respectively, which differ by only 2%.

The formulae in Eq. (4.18) show that the effective nonlinearity in the NLS model (4.17) for the minority component can be negative, as is the case in the above ^{87}Rb example. In this case, if the effective potential $V_{\text{eff}}(\mathbf{x})$ is slowly varying in $\mathbf{x}$, then the effective NLS model (4.17) restricted to one dimension would reduce to

$$i\hbar\psi_{2t} + \frac{\hbar^2}{2m}\psi_{2xx} - g_{\text{eff}}|\psi_2|^2\psi_2 = 0, \tag{4.19}$$

which is a focusing NLS equation that admits rogue waves.

Employing this approach, the formation of Peregrine rogue waves in a ^{87}Rb BEC of approximately $N = 9 \times 10^5$ atoms were experimentally demonstrated by Romero-Ros et al. (2024). In the experiment, the atoms initially occupied the single hyperfine state $|F, m_F\rangle = |1, -1\rangle$. The BEC was confined in a highly elongated, cigar-shaped harmonic trap where a 100 : 1 aspect ratio ensures effectively one-dimensional dynamics. An additional attractive optical potential was present in the

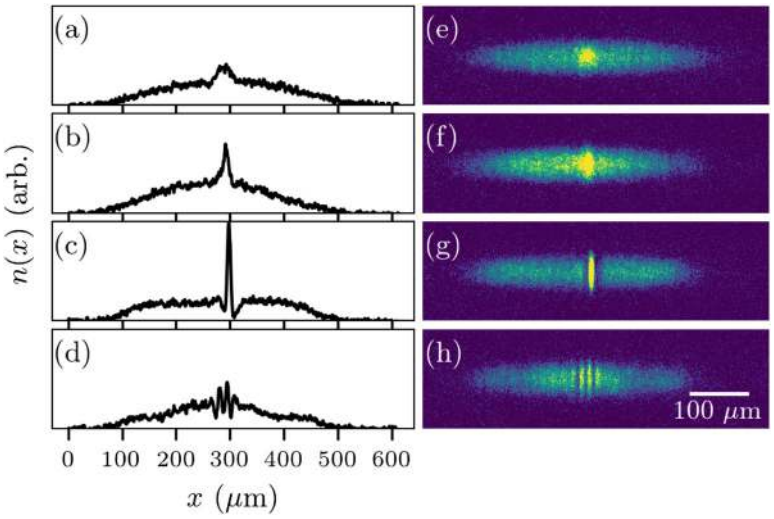

Fig. 4.11 Observation of Peregrine rogue wave in a two-component ^{87}Rb Bose-Einstein condensate. Panels (**a**)–(**d**) are cross sections corresponding to panels (**e**)–(**h**) showing absorption images after 10, 30, 50, and 80 ms of evolution, respectively. Taken from Romero-Ros et al. (2024)

central part of the BEC producing a small density hump in the center of the cloud. This optical potential was radially uniform but has a Gaussian shape along the long axis of the BEC. From this static initial condition, instability was induced by rapidly transferring a small fraction (typically 15%) of the atoms to the $|F, m_F\rangle = |2, 0\rangle$ hyperfine state with a brief, 55 µs microwave pulse, and transferring the remaining atoms to the $|F, m_F\rangle = |1, 0\rangle$ state in a 102 µs RF pulse. Both pulses were applied uniformly across the whole BEC.

Dynamics of the $|F, m_F\rangle = |2, 0\rangle$ hyperfine state (minority component) was the focus of study, for which an effective self-focusing NLS model (4.19) applies. Experimental snapshots of its density distributions at four evolution times are presented in Fig. 4.11. The experimental images are taken after 9 ms of time-of-flight to avoid image saturation of the high density peak. The initially prepared Gaussian hump in the center of the BEC is seen to evolve into a narrow, high peak after approximately 50 ms of evolution (Fig. 4.11c and g). The peak is flanked by two clear dips on either side. These dips are a characteristic feature of a Peregrine wave and are related to the formation of a π phase jump of the wave function in the peak region relative to the surrounding BEC, leading to destructive interference at the position of the dips. Subsequently, the peak height decreases, leading to the emergence of side peaks and excitations on either side as shown in Fig. 4.11d and h after 80 ms of evolution. We note that the observed timescales are highly reproducible, indicating that the dynamics are not triggered by a random instability, but rather are a consequence of the initial conditions prepared in the experiment. Numerical simulations were also performed by Romero-Ros et al. (2024) using a

system of two coupled three-dimensional Gross-Pitaevskii equations under experimental conditions, and good agreement was obtained between simulation results and experimental observations.

4.5 Observation of Manakov Dark Rogue Waves in Optical Fibers

Light propagation in randomly birefringent optical fibers is governed by the Manakov equations (1.227)–(1.228) in Sect. 1.3, i.e.,

$$\mathrm{i}\frac{\partial u_1}{\partial \xi} + \frac{\partial^2 u_1}{\partial \tau^2} + d\left(|u_1|^2 + |u_2|^2\right) u_1 = 0, \tag{4.20}$$

$$\mathrm{i}\frac{\partial u_2}{\partial \xi} + \frac{\partial^2 u_2}{\partial \tau^2} + d\left(|u_2|^2 + |u_1|^2\right) u_2 = 0. \tag{4.21}$$

Here, (u_1, u_2) are slowly varying envelopes of the light's electric field at center frequency ω_0 along two transverse orthogonal polarizations, normalized by $P_0^{1/2}$ where P_0 is a representative total power of the solutions, $\xi = d\hat{\gamma} P_0 z$ is the normalized distance, $\tau = (2\hat{\gamma} P_0/|\beta_2|)^{1/2}(t - \hat{\beta}_1 z)$ is the normalized retarded time, $\hat{\beta}_1 = (\beta_{1x} + \beta_{1y})/2$, (β_{1x}, β_{1y}) are inverse group velocities along the two polarizations, β_2 is the group velocity dispersion, $\hat{\gamma} = 8\gamma/9$ is the effective Kerr nonlinear coefficient, and $d = -\mathrm{sgn}(\beta_2)$.

We note that in the two experimental papers Frisquet et al. (2016) and Baronio et al. (2018) to be quoted below, the Manakov system was written for envelopes (U, V) of the light's electric field at frequencies $\omega_0 \pm \Delta\omega/2$ along the two polarizations. Thus, our (u_1, u_2) variables are related to their (U, V) by $u_1 = Ue^{-\mathrm{i}(\Delta\omega/2)t}$ and $u_2 = Ve^{\mathrm{i}(\Delta\omega/2)/t}$ in physical units.

Rogue waves in the above Manakov system have been derived in Sect. 2.9. Dark rogue waves (in both components) exist in the defocusing Manakov equations, where $d = -1$ (the normal dispersion regime). Unlike most other bright rogue waves (such as Peregrine waves in the focusing NLS equation), where the solution reaches transient higher intensity from a uniform background, a dark rogue wave is the opposite. It develops a transient hole of almost zero intensity from a uniform background instead. Both fundamental and second-order dark rogue waves have been observed in the above optical setting in the normal dispersion regime.

4.5.1 Fundamental Dark Rogue Wave

Assuming the background waves of the two components have equal amplitudes ρ, analytical expressions of fundamental dark rogue waves in the Manakov sys-

tem (4.20)–(4.21) can be obtained from Eq. (2.606) after proper change of variable notations and a little simplification as

$$u_1(\tau,\xi) = \hat{u}_1(\tau,\xi)e^{\mathrm{i}(k_1\xi-\omega_1\tau)}, \quad u_2(\tau,\xi) = \hat{u}_2(\tau,\xi)e^{\mathrm{i}(k_2\xi-\omega_2\tau)}, \tag{4.22}$$

where

$$\hat{u}_1(\tau,\xi) = \rho\frac{\left[\tau+2p_0\,(\mathrm{i}\xi)+\hat{\theta}_1\right]\left[\tau-2p_0^*\,(\mathrm{i}\xi)-\hat{\theta}_1^*\right]+\hat{\zeta}_0}{|\tau+2p_0\,(\mathrm{i}\xi)|^2+\hat{\zeta}_0}, \tag{4.23}$$

$$\hat{u}_2(\tau,\xi) = \rho\frac{\left[\tau+2p_0\,(\mathrm{i}\xi)+\hat{\lambda}_1\right]\left[\tau-2p_0^*\,(\mathrm{i}\xi)-\hat{\lambda}_1^*\right]+\hat{\zeta}_0}{|\tau+2p_0\,(\mathrm{i}\xi)|^2+\hat{\zeta}_0}, \tag{4.24}$$

$$\hat{\theta}_1 = \frac{1}{p_0+\mathrm{i}\omega_1},\ \hat{\lambda}_1 = \frac{1}{p_0+\mathrm{i}\omega_2},\ \hat{\zeta}_0 = \frac{1}{(p_0+p_0^*)^2}, \tag{4.25}$$

and p_0 is a nonimaginary root of the algebraic equation

$$\frac{\rho^2}{(p+\mathrm{i}\omega_1)^2}+\frac{\rho^2}{(p+\mathrm{i}\omega_2)^2}+2=0. \tag{4.26}$$

This equation admits a pair of non-imaginary simple roots $(p_0,-p_0^*)$ only when $\Delta<0$ (see Sect. 2.9), i.e., when $|\omega_2-\omega_1|<2\rho$ in the present situation. The total power of this solution is $|u_1|^2+|u_2|^2=2\rho^2$. Converting this solution into physical units using the variable normalizations described above, then under physical parameters of the total power of $P=1.9\,\mathrm{W}$, $\beta_2=18\,\mathrm{ps}^2\,\mathrm{km}^{-1}$, $\hat{\gamma}=2.4\,\mathrm{W}^{-1}\,\mathrm{km}^{-1}$, and a pump spacing of 100 GHz (i.e., $\omega_1=-\omega_2=3.14\times10^{11}$ rad/s in dimensional units), this solution is plotted in Fig. 4.12. In nondimensional units, this solution corresponds to (4.22) with $\rho=1/\sqrt{2}$ and $\omega_1=-\omega_2\approx0.44$.

This fundamental dark rogue wave was observed in randomly birefringent optical fibers by Frisquet et al. (2016). The experimental setup is shown in Fig. 4.13. Two pump waves with 100 GHz frequency spacing were superposed with a polarization maintaining fiber optical coupler with a 50:50 coupling ratio. An intensity modulator (EOM1) driven by a 35-GHz RF clock was used to generate sidebands on either side of both pumps. An erbium-doped fiber amplifier (EDFA1) was used to compensate the insertion loss introduced by the electro-optic modulator. The sinusoidal perturbation on each pump with adjustable frequency and amplitude then seeds the modulation-instability process. The perturbation frequency (35 GHz) was chosen to be half of the value that leads to peak modulation-instability gain for 2.5 W total input power. This choice stems from the trade-off of imposing the slowest modulation on the one side, while still having sufficient sideband gain to observe the emergence of dark rogue waves within the 3 km fiber length. Such value of fiber length was chosen to satisfy the requirement that fiber losses have virtually no

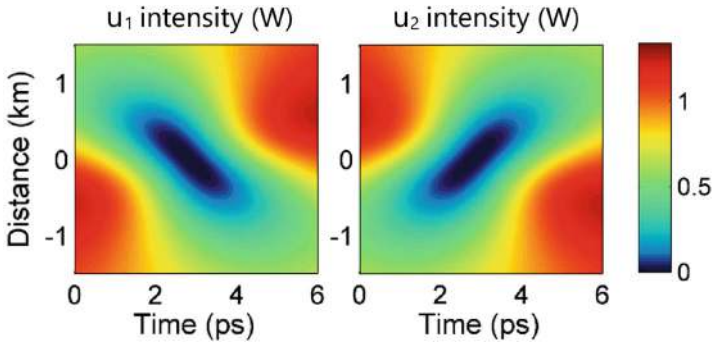

Fig. 4.12 Spatio-temporal intensity fields of the optical fundamental dark rogue wave in the Manakov system for $P = 1.9\,\mathrm{W}$, $\beta_2 = 18\,\mathrm{ps}^2\,\mathrm{km}^{-1}$, $\hat{\gamma} = 2.4\,\mathrm{W}^{-1}\mathrm{km}^{-1}$, and a pump spacing of 100 GHz. The horizontal axis (time) refers to the retarded time $t - \hat{\beta}_1 z$. Taken from Frisquet et al. (2016)

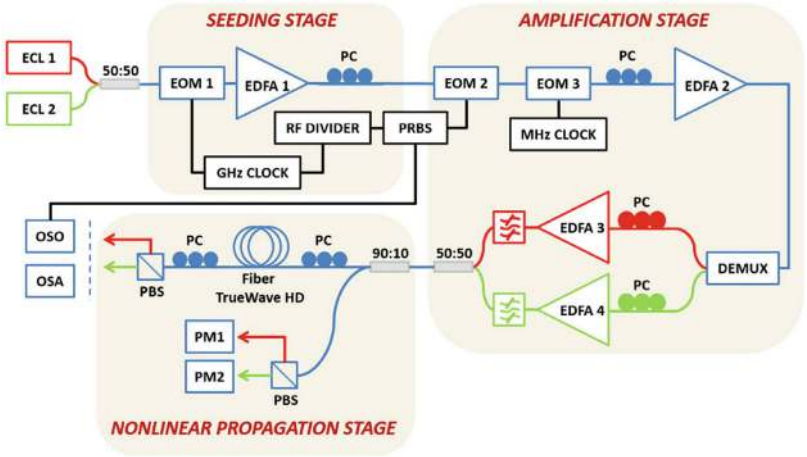

Fig. 4.13 Schematic illustration of the experimental setup for observation of Manakov dark rogue waves in randomly birefringent optical fibers. Red and green lines depict the two wavelength-division-multiplexed and orthogonally polarized pumps. ECL: external-cavity diode laser; 50:50 & 90:10: fiber couplers; EOM: (intensity or phase) electro-optic modulator; EDFA: Erbium doped fiber amplifier; PRBS: pseudo-random binary sequence generator; PC: polarization controller; PM: power-meter; OSO: optical sampling oscilloscope; OSA: optical spectrum analyzer. Taken from Frisquet et al. (2016)

impact on the propagation dynamics. The perturbation amplitude of the continuous-wave field was set properly in order to observe the dark rogue wave at precisely 3 km in the fiber with the available pump power. To suppress stimulated Brillouin scattering (SBS) that may occur in the optical fiber, a phase modulator (EOM3) was inserted into the setup in order to increase the spectral linewidth of the two pump waves. The phase modulator was driven by a 67-MHz RF signal, thus enabling one

to work at relatively high pump powers, still being far below the SBS threshold. The two pump waves were spectrally separated by means of a programmable optical filter (DEMUX). A pair of polarization controllers (PCs) were used to obtain two pumps with orthogonal linear states of polarization. The pumps were finally recombined after their independent amplification by high power erbium-doped fiber amplifiers (EDFA3&4) and before injection into the optical fiber. The optical fiber used in the experiment was a reverse-TrueWave fiber with the chromatic dispersion of $\beta_2 = 18\,\mathrm{ps}^2\,\mathrm{km}^{-1}$ (or $D = -14\,\mathrm{ps/nm/km}$), the effective nonlinear coefficient $\hat{\gamma} = 2.4\,\mathrm{W}^{-1}\mathrm{km}^{-1}$ and the attenuation of 0.25 dB/km at wavelength $\lambda_0 = 1554.7\,\mathrm{nm}$. At the fiber output, a polarization beam splitter (PBS) selects the output light propagating in the two orthogonal linear polarizations. The output light was simultaneously analyzed both in the spectral and temporal domain by means of an optical spectrum analyzer (OSA) and an optical sampling oscilloscope (OSO). Spectral measurements were carried out with 0.02 nm resolution bandwidth. The optical sampling oscilloscope had 0.8 ps resolution.

The experimental results are displayed in Fig. 4.14. Here, the input and output intensities (after 3 km of optical fiber propagation) are shown from the experiments with an input periodic intensity modulation, together with their corresponding analytical dark rogue wave solutions. As can be seen, an overall excellent quantitative agreement (with no adjustable parameters) is obtained between theory and

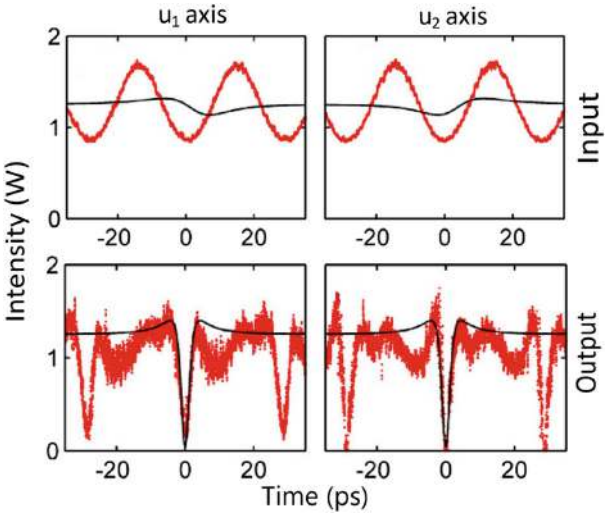

Fig. 4.14 Experimental observation of fundamental Manakov dark rogue waves in randomly birefringent optical fibers. Upper row: temporal intensity profiles in the u_1 and u_2 polarization axes at the fiber input. Lower row: output intensities after 3 km of optical fiber. Red solid traces: experimental measurements; black solid lines: analytical dark rogue wave solution. Physical parameters are $P = 2.5\,\mathrm{W}$ (total power), $\beta_2 = 18\,\mathrm{ps}^2\,\mathrm{km}^{-1}$, $\hat{\gamma} = 2.4\,\mathrm{W}^{-1}\mathrm{km}^{-1}$, and a pump spacing of 100 GHz. Taken from Frisquet et al. (2016)

experiments. Only slight discrepancies appear due to the non-ideal initial conditions used in the experimental generation of dark rogue waves.

Cut-back measurements were also done by Frisquet et al. (2016) to verify the kinematics of the dark rogue wave generation and disappearance at distances before and after the rogue center point (3 km).

4.5.2 Second-Order Dark Rogue Waves

The defocusing Manakov system (4.20)–(4.21) (with $d = -1$) admits not only fundamental dark rogue waves but also higher-order dark rogue waves. General expressions of these higher-order dark rogue waves can be found in Sect. 2.9. For second-order dark rogue waves, their alternative expressions can be found in Chen et al. (2014b). Assuming the background waves of the two polarization components have equal amplitudes ρ, then these higher-order dark rogue waves would exist under the same condition of $|\omega_2 - \omega_1| < 2\rho$ of fundamental dark rogue waves. In addition, they contain irreducible free parameters that affect their shapes. For physical parameters of the total power of $P = 2.5\,\mathrm{W}$, $\beta_2 = 18\,\mathrm{ps}^2\,\mathrm{km}^{-1}$, $\hat{\gamma} = 2.4\,\mathrm{W}^{-1}\mathrm{km}^{-1}$, and a pump spacing of 100 GHz, a second-order dark rogue solution was shown in Baronio et al. (2013) and is reproduced in Fig. 4.15. This solution exhibits a nonlinear superposition of three fundamental dark rogue waves arising at different space-time locations and is a dark rogue triplet.

Such a dark rogue triplet was observed in randomly birefringent optical fibers by Baronio et al. (2018). Their experimental setup is similar to Fig. 4.13. Two external-cavity diode lasers generated the pump waves at frequencies ω_1 and ω_2, which were fixed around the central frequency ω_0 (with $\omega_0 = 2\pi c/\lambda_0$ and $\lambda_0 = 1554.7\,\mathrm{nm}$), and the frequency spacing was $\Delta\omega = 2\pi\Delta f$, where $\Delta f = 100\,\mathrm{GHz}$. The two pumps were superimposed with a polarization maintaining fiber

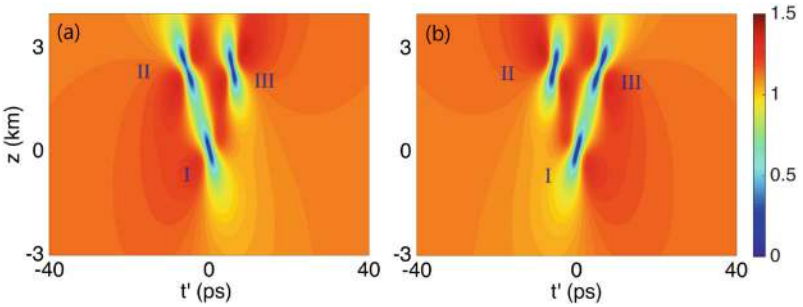

Fig. 4.15 Spatial-temporal amplitude fields of a theoretical optical dark rogue triplet in the Manakov system for $P = 2.5\,\mathrm{W}$, $\beta_2 = 18\,\mathrm{ps}^2\,\mathrm{km}^{-1}$, $\hat{\gamma} = 2.4\,\mathrm{W}^{-1}\mathrm{km}^{-1}$, and a pump spacing of 100 GHz. (**a**) $|u_1|$; (**b**) $|u_2|$. The horizontal axis $t' \equiv t - \hat{\beta}_1 z$ is the retarded time. Taken from Baronio et al. (2018)

optical coupler with a 50:50 coupling ratio. An electro-optic modulator, driven by a 35-GHz RF clock, was used to induce the initial sinusoidal perturbations to the pumps. A pair of polarization controllers were used to manage two pumps with orthogonal linear states of polarization, amplified independently by erbium-doped fiber amplifiers, and finally recombined and injected into the fiber. The total input power was $P = 2.5\,\mathrm{W}$. The optical fiber used in the experiment was a reverse-TrueWave fiber with the chromatic dispersion of $\beta_2 = 18\,\mathrm{ps}^2\,\mathrm{km}^{-1}$ (or $D = -14\,\mathrm{ps/nm/km}$), the effective nonlinear coefficient $\hat{\gamma} = 2.4\,\mathrm{W}^{-1}\mathrm{km}^{-1}$ and the attenuation of 0.25 dB/km at wavelength $\lambda_0 = 1554.7\,\mathrm{nm}$. Two fiber spans were used in the experiments: a 3 km-long span, and a 5 km-long span. In these experimental conditions, higher-order dispersion, material absorption and Raman effects can be safely neglected.

In the experiments, the initial perturbations to the uniform background waves were sinusoidal, unlike such perturbations in true dark rogue triplets. Thus, Baronio et al. (2018) first investigated numerically the possibility to experimentally generate the dark rogue triplet under realistic (non-ideal) experimental conditions at the input of the optical fiber. To this end, the Manakov system (4.20)–(4.21) in physical units were simulated, using physical parameters as quoted above. Corresponding to the experiments, the initial conditions were taken as

$$u_1(t', z=0) = \left[\sqrt{P/2} - \epsilon\cos(2\pi f_m t')\right] e^{-\mathrm{i}(\Delta\omega/2)t}, \tag{4.27}$$

$$u_2(t', z=0) = \left[\sqrt{P/2} - \epsilon\cos(2\pi f_m t')\right] e^{\mathrm{i}(\Delta\omega/2)t}, \tag{4.28}$$

where $t' \equiv t - \hat{\beta}_1 z$ is the retarded time, $P = 2.5\,\mathrm{W}$ is the total power, $\Delta\omega = 2\pi\Delta f$ is the frequency detuning between the two polarizations with $\Delta f = 100\,\mathrm{GHz}$, $\epsilon = 0.13$ is the perturbation strength, and $f_m = 35\,\mathrm{GHz}$ is the modulation frequency of the perturbation. These initial conditions differ from those quoted in Baronio et al. (2018) by the exponential factors, the reason being notational differences in writing the Manakov system as explained at the beginning of this section.

Simulation results of the Manakov system (4.20)–(4.21) under the above physical parameters and initial conditions are shown in Fig. 4.16. As can be seen, one observes the generation of time-periodic notch structures, which are localized both in time and in space. This figure shows that each individual dark structure within the periodic wave train closely matches the shape of the dark rogue triplet that was previously presented in Fig. 4.15 (with a 3 km translation of the longitudinal z coordinate). Thus, these dark rogue triplets are observable under experimental conditions.

Observation results of these dark rogue triplets are presented in Fig. 4.17, where the measured temporal traces of wave amplitudes emerging from orthogonal polarizations are displayed at the fiber input, after 3 km, and after 5 km. The corresponding numerical simulation results from Fig. 4.16 are also shown for comparison. Quite remarkably, experimental observations are in excellent quantitative agreement, with no adjustable parameters, with theoretical predictions.

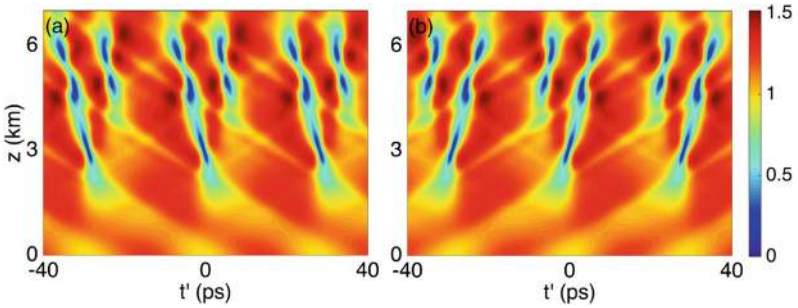

Fig. 4.16 Contour plots of the two orthogonal polarization waves (**a**) $u_1(t', z)$ and (**b**) $u_2(t', z)$ describing the numerical excitation of a dark rogue triplet under experimental conditions in the Manakov system (4.20)–(4.21). Physical parameters used are $P = 2.5\,\mathrm{W}$ (total power), $\beta_2 = 18\,\mathrm{ps}^2\,\mathrm{km}^{-1}$, $\hat{\gamma} = 2.4\,\mathrm{W}^{-1}\mathrm{km}^{-1}$, and a pump spacing of 100 GHz. The initial modulated condition is given in Eqs. (4.27)–(4.28). The horizontal axis $t' \equiv t - \hat{\beta}_1 z$ is the retarded time. Taken from Baronio et al. (2018)

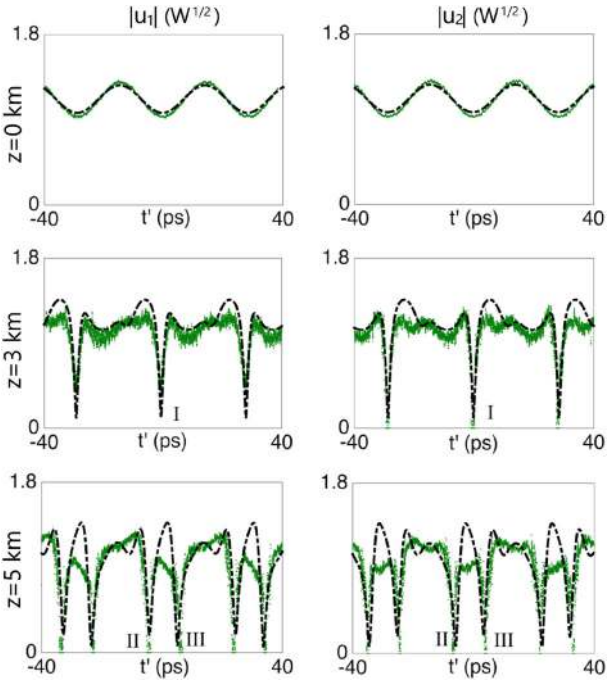

Fig. 4.17 Observation of optical dark rogue triplets in randomly birefringent fibers. Shown are temporal profiles of $|u_1|$ (left column) and $|u_2|$ (right column) at the input (upper row), after 3 km of optical fiber (middle row), and after 5 km of optical fiber (bottom row). Green solid lines are experimental measurements, and black dashed lines are numerical simulations from the Manakov system (these numerical solutions refer to those in Fig. 4.16). Physical parameters are $P = 2.5\,\mathrm{W}$ (total power), $\beta_2 = 18\,\mathrm{ps}^2\,\mathrm{km}^{-1}$, $\hat{\gamma} = 2.4\,\mathrm{W}^{-1}\mathrm{km}^{-1}$, and a pump spacing of 100 GHz. The horizontal axis $t' \equiv t - \hat{\beta}_1 z$ is the retarded time. Taken from Baronio et al. (2018)

Chapter 5
Related Topics

In this chapter, we cover several topics which are different from rogue waves in previous chapters but yet are closely related to them. One topic is rogue waves on a nonuniform-amplitude background, which contrasts such rogue waves in earlier chapters which sit on a uniform-amplitude background. Another topic is robustness of rogue waves under perturbations, which is a physically important question. The third topic is partial-rogue waves, which "come from nowhere but leave with a trace", as opposed to rogue waves which "come from nowhere and disappear with no trace". The last topic is patterns of higher-order lumps in the Kadomtsev-Petviashvili I equation. Although this last topic is very different from rogue patterns, the phenomena and mathematical treatments of the two have a lot in common.

We start with rogue waves on a nonuniform-amplitude background, using the nonlinear Schrödinger (NLS) equation as an example.

5.1 Rogue Waves on Nonuniform-Amplitude Background in the NLS Equation

Rogue waves in the NLS equation as described in Sect. 2.1 arise from a background that has uniform amplitude. It turns out that NLS rogue waves can also arise from nonuniform-amplitude backgrounds. Such rogue waves are described in this section.

5.1.1 Solution Derivation by Darboux Transformation

Rogue waves on a nonuniform-amplitude background in the NLS equation have been studied either analytically or numerically by Kedziora et al. (2014), Agafontsev and Zakharov (2016), Wright (2016), Bertola and Tovbis (2016), Bertola and Tovbis

B. Yang. J. Yang, *Rogue Waves in Integrable Systems*,
https://doi.org/10.1007/978-3-031-66793-0_5

(2017), Calini and Schober (2017), and Chen and Pelinovsky (2018). Below, we analytically derive fundamental NLS rogue waves on a stationary spatially-periodic background through Darboux transformation, following Chen and Pelinovsky (2018).

The NLS equation

$$\mathrm{i}u_t + u_{xx} + 2|u|^2 u = 0 \tag{5.1}$$

appears as a compatibility condition of the following Lax pair of linear equations on φ:

$$\varphi_x = U\varphi, \quad U = \begin{pmatrix} \lambda & u \\ -u^* & -\lambda \end{pmatrix}, \tag{5.2}$$

and

$$\varphi_t = V\varphi, \quad V = \mathrm{i}\begin{pmatrix} 2\lambda^2 + |u|^2 & u_x + 2\lambda u \\ u_x^* - 2\lambda u^* & -2\lambda^2 - |u|^2 \end{pmatrix}. \tag{5.3}$$

The basic idea to derive fundamental rogue waves on a periodic-amplitude background is to use onefold Darboux transformation

$$\tilde{u} = u + \frac{4\,\mathrm{Re}(\lambda_1)\hat{p}_1\hat{q}_1^*}{|\hat{p}_1|^2 + |\hat{q}_1|^2}, \tag{5.4}$$

where u is a x-periodic background solution of the NLS equation, $\varphi = (\hat{p}_1, \hat{q}_1)^T$ is a non-periodic solution of the linear system (5.2)–(5.3) for the periodic background solution u, 'Re' represents the real part of a complex number, and $\lambda = \lambda_1$ is a branch point of the band-gap spectrum in the linear spectral problem (5.2) associated with the periodic background wave u. Note that at a branch point λ_1, the linear system (5.2)–(5.3) admits one periodic solution and one non-periodic solution. The periodic solution, when inserted into the above Darboux transformation, only leads to a trivial NLS solution $\tilde{u}$. Only that non-periodic solution of the linear system (5.2)–(5.3) leads to the desired rogue waves on a periodic background.

First, we look for standing x-periodic background solutions of the NLS equation in the form

$$u(x,t) = U(x)e^{\mathrm{i}ct}, \tag{5.5}$$

where the periodic function $U(x)$ is real and satisfies the equation

$$U_{xx} + 2U^3 = cU, \tag{5.6}$$

and c is a real constant. This equation can be integrated once to give

$$U_x^2 + U^4 = cU^2 + d, \tag{5.7}$$

where d is another real constant. This latter equation admits two particular families of periodic wave solutions expressed by the Jacobian elliptic functions dn and cn. The positive-definite dn-periodic waves are

$$U(x) = \mathrm{dn}(x;k), \quad c = 2 - k^2, \quad d = k^2 - 1, \quad k \in (0,1), \tag{5.8}$$

and the sign-indefinite cn-periodic waves are

$$U(x) = k\,\mathrm{cn}(x;k), \quad c = 2k^2 - 1, \quad d = k^2(1-k^2), \quad k \in (0,1). \tag{5.9}$$

Below, we will derive rogue waves on these dn- and cn-periodic backgrounds. We will focus on the dn-waves, and will only quote the results for the cn-waves for brevity.

Using differential constraints on the periodic potential that are obtained from the Lax pair (5.2)–(5.3), it can be found that the branch points of the band-gap spectrum in the linear spectral problem (5.2) associated with the dn periodic wave are

$$\lambda_\pm = \frac{1}{2}(1 \pm \sqrt{1-k^2}) \tag{5.10}$$

in the right-half plane, and two symmetric points $-\lambda_\pm$ in the left half-plane. If we take $\lambda_1 = \lambda_+$, then the periodic solution $(p_1, q_1)^T$ of the linear system (5.2)–(5.3) is of the form

$$p_1(x,t) = P_1(x)e^{\mathrm{ict}/2}, \quad q_1(x,t) = Q_1(x)e^{-\mathrm{ict}/2}, \tag{5.11}$$

where $P_1(x)$ and $Q_1(x)$ are real and periodic functions. Substituting these expressions into the linear system (5.2)–(5.3), we obtain the following relations

$$P_1(x)Q_1(x) = -\frac{1}{4\lambda_+}\left[U^2(x) + \sqrt{1-k^2}\right], \tag{5.12}$$

and

$$P_1^2(x) + Q_1^2(x) = U(x), \quad 2\lambda_+[P_1^2(x) - Q_1^2(x)] = U'(x). \tag{5.13}$$

Next, we construct the nonperiodic solution $(\hat{p}_1, \hat{q}_1)^T$ of the linear system (5.2)–(5.3) at the periodic potential u and branch point λ_1. These nonperiodic solutions can be set as

$$\hat{p}_1 = \frac{\theta - 1}{q_1}, \quad \hat{q}_1 = \frac{\theta + 1}{p_1}, \tag{5.14}$$

where $\theta(x,t)$ is a new function. Substituting these expressions into (5.2), we get an equation for $\partial\theta/\partial x$ that can be simplified to

$$\frac{\partial\theta}{\partial x} = \theta U \frac{Q_1^2 - P_1^2}{P_1 Q_1} + U \frac{Q_1^2 + P_1^2}{P_1 Q_1}. \tag{5.15}$$

For the dn-periodic wave $U(x) = \mathrm{dn}(x;k)$, substituting Eqs. (5.12)–(5.13) into (5.15) and solving for $\theta(x,t)$, we get

$$\theta(x,t) = \left[U^2(x) + \sqrt{1-k^2}\right]\left[-4\lambda_+ \int_0^x \frac{U^2(y)}{\left(U^2(y) + \sqrt{1-k^2}\right)^2} dy + \theta_0(t)\right], \tag{5.16}$$

where θ_0 is a constant of integration in x that may depend on t. To determine $\theta_0(t)$, we substitute expressions (5.14) into (5.3) and obtain an equation for $\partial\theta/\partial t$. Utilizing relations (5.13), this $\partial\theta/\partial t$ equation reduces to

$$\frac{\partial\theta}{\partial t} = 8\mathrm{i}\,\mathrm{Re}(\lambda_1) P_1(x) Q_1(x). \tag{5.17}$$

Substituting the relation (5.12) into the above equation, we get $\theta_0'(t) = -2\mathrm{i}$. Thus,

$$\theta_0(t) = -2\mathrm{i}t, \tag{5.18}$$

where the constant of integration in t is neglected due to translational invariance of the NLS equation with respect to t.

Finally, we substitute the above nonperiodic solution $(\hat{p}_1, \hat{q}_1)^T$ into the onefold Darboux transformation (5.4) and obtain a new solution to the NLS equation as

$$\tilde{u}(x,t) = \left[\mathrm{dn}(x,k) + \frac{F(x,t)}{G(x,t)}\right] e^{\mathrm{i}(2-k^2)t}, \tag{5.19}$$

where

$$\begin{aligned}
F(x,t) &= \left[1 - 2\mathrm{i}\,\mathrm{Im}\{\theta(x,t)\} - |\theta(x,t)|^2\right]\left[\mathrm{dn}(x,k)^2 + \sqrt{1-k^2}\right], \\
G(x,t) &= \left[|\theta(x,t)|^2 + 1\right]\mathrm{dn}(x,k) \\
&\quad + 2\left(1 - \sqrt{1-k^2}\right)\mathrm{Re}\{\theta(x,t)\}\mathrm{sn}(x,k)\mathrm{cn}(x,k), \\
\theta(x,t) &= -\left[\mathrm{dn}(x,k)^2 + \sqrt{1-k^2}\right] \times \\
&\quad \times \left[2(1+\sqrt{1-k^2}) \int_0^x \frac{\mathrm{dn}(\tau,k)^2}{[\mathrm{dn}(\tau,k)^2 + \sqrt{1-k^2}]^2} d\tau + 2\mathrm{i}t\right],
\end{aligned}$$

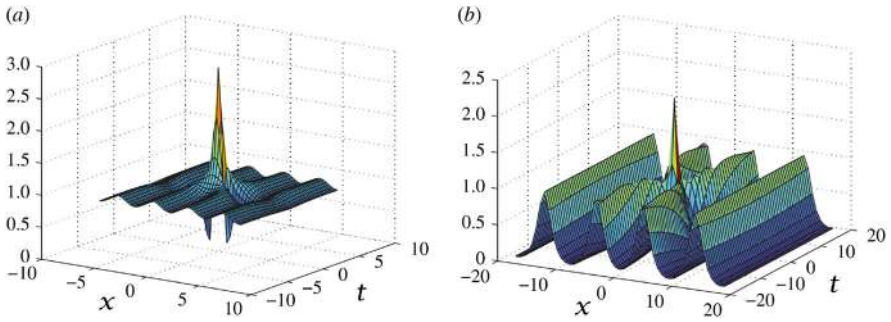

Fig. 5.1 The fundamental rogue wave (5.19) on a dn-periodic background in the NLS equation (5.1) for $k = 0.5$ (**a**) and $k = 0.999$ (**b**). Taken from Chen and Pelinovsky (2018)

and $\mathrm{sn}(x, k)$ is another Jacobian elliptic function (elliptic sine). This solution is nonperiodic in x but approaches a spatially translated dn wave when $x, t \to \pm\infty$. Thus, it is a rogue wave on the dn-periodic background. One can show that the maximum of $|\tilde{u}(x, t)|$ occurs at $(x, t) = (0, 0)$, where $|\tilde{u}(0, 0)| = 2 + \sqrt{1 - k^2}$. As the maximum of $\mathrm{dn}(x; k)$ is one, the magnification factor of the rogue dn-periodic wave is $2+\sqrt{1 - k^2}$. This solution for two values of $k = 0.5$ and 0.999 are displayed in Fig. 5.1.

Using similar techniques, fundamental rogue waves on cn-periodic backgrounds can also be derived, and their expressions are

$$\tilde{u}(x, t) = \left[k\,\mathrm{cn}(x; k) + \frac{\widehat{F}(x, t)}{\widehat{G}(x, t)} \right] e^{\mathrm{i}(2k^2-1)t}, \tag{5.20}$$

where

$$\begin{aligned}
\widehat{F}(x, t) &= k \left(1 - 2\mathrm{iIm}\{\theta(\mathrm{x}, \mathrm{t})\} - |\theta(\mathrm{x}, \mathrm{t})|^2 \right) \\
&\quad \times \left(\mathrm{cn}(x; k)\mathrm{dn}(x; k) + \mathrm{i}\sqrt{1 - k^2}\,\mathrm{sn}(x; k) \right), \\
\widehat{G}(x, t) &= \left(|\theta(x, t)|^2 + 1 \right) \mathrm{dn}(x; k) + 2\mathrm{Re}\{\theta(x, t)\} k\,\mathrm{sn}(x; k)\mathrm{cn}(x; k), \\
\theta(x, t) &= -\left[k^2 \mathrm{cn}(x; k)^2 + \mathrm{i}k\sqrt{1 - k^2} \right] \times \\
&\quad \times \left[2(k + \mathrm{i}\sqrt{1 - k^2}) \int_0^x \frac{k^2 \mathrm{cn}(y; k)^2}{\left(k^2 \mathrm{cn}(y; k)^2 + \mathrm{i}k\sqrt{1 - k^2} \right)^2} dy + 2\mathrm{i}t \right].
\end{aligned}$$

One can show that the maximum of this $|\tilde{u}(x, t)|$ occurs at $(x, t) = (0, 0)$, where $|\tilde{u}(0, 0)| = 2k$. As the maximum of $\mathrm{cn}(x; k)$ is one, the magnification factor of this fundamental rogue cn-periodic wave is 2 uniformly for all $k \in (0, 1)$. This solution for two values of $k = 0.5$ and 0.999 are displayed in Fig. 5.2.

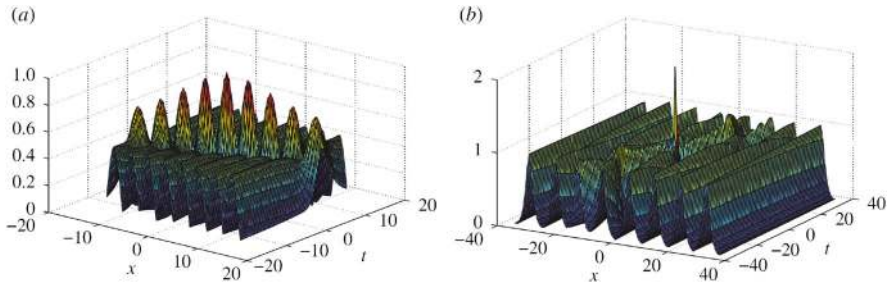

Fig. 5.2 The fundamental rogue wave (5.20) on a cn-periodic background in the NLS equation (5.1) for $k = 0.5$ (**a**) and $k = 0.999$ (**b**). Taken from Chen and Pelinovsky (2018)

Second-order rogue waves on dn- and cn-periodic backgrounds can also be derived by employing twofold Darboux transformation; see Chen and Pelinovsky (2018) for details.

5.1.2 Experimental Observation in Water tanks

Rogue waves that were observed in the water-tank experiments of Sect. 4.2 were all arising from the uniform background (i.e., from waves with constant amplitudes). The above rogue waves arising from nonuniform dn- and cn-backgrounds have been observed in water tanks as well by Xu et al. (2020), and their experiments are described below.

For these experiments, the spatial-evolution form of the NLS equation for water surface elevations was used to make theoretical predictions. This NLS equation is (1.44), i.e.,

$$\mathrm{i}\frac{\partial \tilde{u}}{\partial \tilde{x}} + \frac{1}{2}\frac{\partial^2 \tilde{u}}{\partial \tilde{t}^2} + |\tilde{u}|^2\tilde{u} = 0, \tag{5.21}$$

where

$$\tilde{u} = u/a, \quad \tilde{x} = -k^3a^2x, \quad \tilde{t} = (gk^3a^2/2)^{1/2}\,(t - x/c_g), \tag{5.22}$$

$c_g = \omega/2k$, $\omega = \sqrt{gk}$, and a is a representative wave-amplitude parameter which we will set as the peak amplitude of the background nonuniform wave. The water surface elevation $\zeta(x,t)$ is related to the variable $u(x,t)$ as (1.34) to the second order of wave steepness, i.e.,

$$\zeta(x,t) = \mathrm{Re}\left\{u(x,t)e^{\mathrm{i}(kx-\omega t)} + \frac{1}{2}ku^2(x,t)e^{2\mathrm{i}(kx-\omega t)}\right\}. \tag{5.23}$$

By converting the notations of the NLS equation (5.1) to those in (5.21), we see that Eq. (5.21) admits a nonuniform $\tilde{t}$-periodic background solution

$$\tilde{u}(\tilde{t},\tilde{x}) = \mathrm{dn}(\tilde{t},\alpha)\, e^{\mathrm{i}(1-\alpha^2/2)\tilde{x}}, \tag{5.24}$$

where α is a background parameter, and dn is a Jacobi elliptic function. Note that this background solution's peak amplitude $|\tilde{u}|_{max}$ is unity due to our normalization (5.22). From this nonuniform background, rogue waves can arise. The simplest such rogue wave has been given in Eq. (5.19) of the previous subsection. Converting to the present notations, this rogue wave is

$$\tilde{u}(\tilde{t},\tilde{x}) = \left[\mathrm{dn}(\tilde{t},\alpha) + \frac{F(\tilde{t},\tilde{x})}{G(\tilde{t},\tilde{x})}\right] e^{\mathrm{i}(1-\alpha^2/2)\tilde{x}}, \tag{5.25}$$

where

$$\begin{aligned}
F(\tilde{t},\tilde{x}) &= \left[1 - 2\mathrm{i}\,\mathrm{Im}\{\theta(\tilde{t},\tilde{x})\} - |\theta(\tilde{t},\tilde{x})|^2\right]\left[\mathrm{dn}(\tilde{t},\alpha)^2 + \sqrt{1-\alpha^2}\right], \\
G(\tilde{t},\tilde{x}) &= \left[|\theta(\tilde{t},\tilde{x})|^2 + 1\right]\mathrm{dn}(\tilde{t},\alpha) \\
&\quad + 2\left(1 - \sqrt{1-\alpha^2}\right)\mathrm{Re}\{\theta(\tilde{t},\tilde{x})\}\mathrm{sn}(\tilde{t},\alpha)\mathrm{cn}(\tilde{t},\alpha), \\
\theta(\tilde{t},\tilde{x}) &= -\left[\mathrm{dn}(\tilde{t},\alpha)^2 + \sqrt{1-\alpha^2}\right] \times \\
&\quad \times \left[2(1+\sqrt{1-\alpha^2})\int_0^{\tilde{t}} \frac{\mathrm{dn}(\tau,\alpha)^2}{[\mathrm{dn}(\tau,\alpha)^2 + \sqrt{1-\alpha^2}]^2} d\tau + \mathrm{i}\tilde{x}\right].
\end{aligned}$$

For two parameter choices of $\alpha = 0.3$ and 0.9, this rogue solution is plotted in Fig. 5.3a and b respectively. From this analytical solution as well as the variable scalings (5.22), the physical solution $u(x,t)$ in Eq. (5.21) would be obtained.

The experiments to observe these rogue waves were conducted in a $30 \times 1 \times 1\mathrm{m}^3$ water tank under deep-water conditions (Xu et al. 2020). The initial periodic wave profiles were shaped with a piston wave generator located at one end of the tank. An electric signal drove the piston to directly modulate the surface height in the time domain according to the exact mathematical expression for the surface elevation. A wave-absorbing beach is installed at the opposite end to avoid the influence of reflected waves. Seven wave gauges were then placed at distinct distances from the wave excitation to record the evolution of surface elevation in the longitudinal direction of wave propagation. A key to successful experiments is to accurately generate the surface elevation profile in the boundary condition, as described by the theory. The theoretical surface elevation is calculated from the NLS wave envelope $u(x,t)$ of Eq. (5.21) to the second order in steepness by the formula (5.23).

In the experiments, the carrier amplitude was chosen as $a = 0.01$ m. The carrier frequency was chosen as $\omega = 10.68$ rad/s, which corresponds to a carrier wave

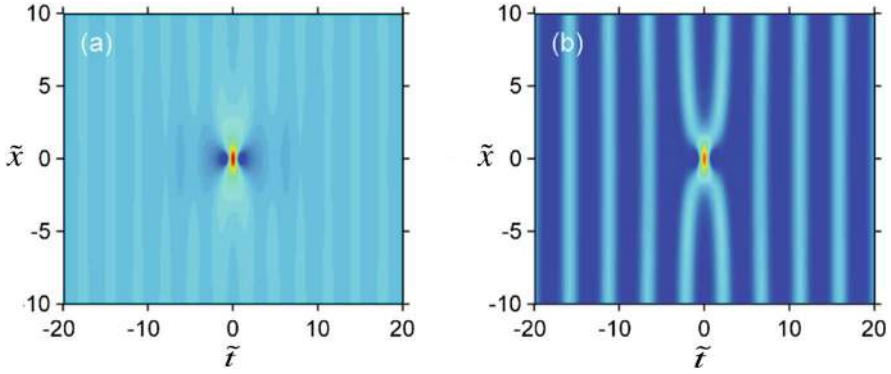

Fig. 5.3 Theoretical space-time dynamics $|\tilde{u}(\tilde{t}, \tilde{x})|$ of the rogue solution (5.25) on a periodic dn background in the NLS equation (5.21). (**a**) $\alpha = 0.3$; (**b**) $\alpha = 0.9$. Taken from Xu et al. (2020)

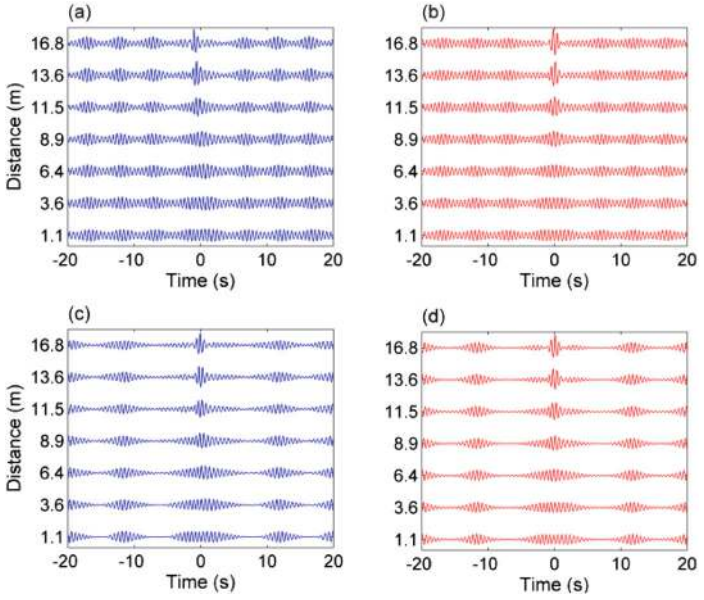

Fig. 5.4 Observation of rogue waves on dn-periodic backgrounds in a water tank. Left panels: evolution of time series of surface elevation measurement with propagation distance. Right panels: corresponding theory. (**a**), (**b**) Rogue dn-periodic wave ($\alpha = 0.8$). (**c**), (**d**) Rogue dn-periodic wave ($\alpha = 0.99$). The time axis of each wave profile is shifted by the amount of x/c_g. Taken from Xu et al. (2020)

number $k = 11.63$/m. The attenuation rate was estimated about 0.25% per meter (in amplitude).

Figure 5.4 shows the results of experiments by shaping an initial localized perturbation centered at $t = 0$ onto the dn-periodic waves for $\tilde{x} = -2.6$. The two cases in panels (a) and (c) report the longitudinal evolution of perturbation for these

periodic waves when $\alpha = 0.8$ and 0.99 until reaching the maximal amplification after 16.8 m. For both cases, theoretical predictions of surface elevations at the same positions are shown in panels (b) and (d) respectively. It can be seen that the measurements agree very well with theory.

Rogue waves arising from cn-periodic backgrounds in the NLS equation (5.21) were also observed by Xu et al. (2020), and details are omitted.

5.1.3 Experimental Observation in Optical Fibers

Rogue waves on dn- and cn-periodic backgrounds of the NLS equation have also been observed in optical fibers by Xu et al. (2020). In this case, the normalized NLS equation is (1.96), i.e.,

$$\mathrm{i}u_\xi + \frac{1}{2}u_{TT} + |u|^2 u = 0, \tag{5.26}$$

where u is the complex envelope of the light's electric field normalized by $P_0^{1/2}$, ξ is the propagation distance z normalized by $(\gamma P_0)^{-1}$, $T \equiv t - \beta_1 z$ is the retarded time normalized by $(|\beta_2|/\gamma P_0)^{1/2}$, P_0 is a characteristic light power, β_1^{-1} is the carrier wave's group velocity, β_2 is the group-velocity-dispersion parameter which is negative in the anomalous-dispersion regime, and γ is the nonlinear coefficient. Rogue waves on dn- and cn-periodic backgrounds of this NLS equation have been presented in an earlier subsection (after change of notations).

The experimental setup by Xu et al. (2020) is given in Fig. 5.5. It is based on the propagation of arbitrarily shaped light waves in optical fibers, and is capable of synthesizing nontrivial exact periodic wave profiles in the temporal domain. The initial state is obtained through the optical pulse shaping with phase and amplitude controls in the spectral domains. This specific processing of a home-made optical frequency comb source (centered at wavenumber $\lambda_p = 1550$ nm) allows generation of exact wave profiles with a specific period fixed by the frequency spacing of the optical comb. Nonlinear propagation is then studied in different lengths of the same standard single-mode fiber SMF-28 (with $\beta_2 = -2.1 \times 10^{-26}\mathrm{s}^2\mathrm{m}^{-1}$ and $\gamma = 0.0012\,\mathrm{W}^{-1}\mathrm{m}^{-1}$ at λ_p) by an appropriate choice of the input average power. The fiber loss is about 5% per kilometer (in power). At fiber output, the power profiles are characterized in both time and frequency domains by means of an ultrafast optical sampling oscilloscope (with subpicosecond resolution) and an optical spectrum analyzer (with 2.5 GHz resolution).

To observe rogue waves on the dn-periodic background, the exact solution (5.19) with $k = 0.7$ was used to shape the input periodic wave with the correct localized perturbation. According to the maximal propagation distance that can be reached, suitable initial conditions (at a normalized ξ value) were chosen to observe the maximum amplification. Specifically, a 13-GHz frequency comb was used to shape the exact solution (5.19) with $\xi = -2.3$ at fiber input. The frequency interval for

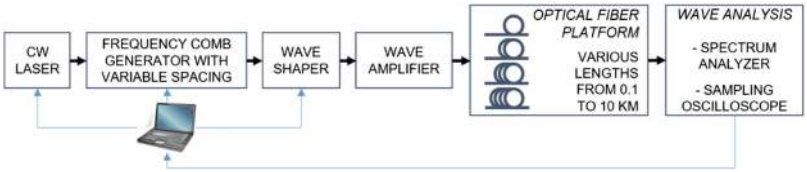

Fig. 5.5 Experimental setup for observation of rogue waves on dn-periodic background in optical fibers. Taken from Xu et al. (2020)

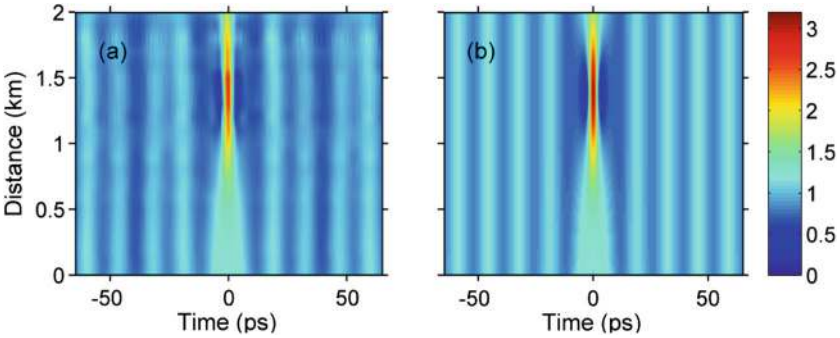

Fig. 5.6 Experimental observation of a rogue wave on a dn-periodic background ($k = 0.7$) in an optical fiber. Plotted are longitudinal evolution of the optical envelope $|u(z,t)|$ obtained from experiment (**a**) and theory (**b**). Taken from Xu et al. (2020)

the dn-periodic wave was 78 GHz. Figure 5.6a presents spatiotemporal evolution measured for the rogue wave on the dn-periodic wave. This figure clearly reveals that the localized perturbation (centered at $t = 0$) grows as predicted by the theory in Fig. 5.6b. After 1.4 km propagation, the optical rogue wave reaches a maximum amplitude nearly 3 $W^{1/2}$, which is close to the theoretical prediction $\sqrt{P_0}(2+\sqrt{1-k^2})$ despite fiber losses (here $P_0 = 1.38$ W). Subsequently, the rogue wave's decay just before 2 km is also seen.

5.2 Robustness of Rogue Waves Under Perturbations

One important question we need to ask is, how robust are rogue waves under perturbations? Since rogue waves can only arise from linearly-unstable backgrounds, the instability of those backgrounds will necessarily affect the evolution of rogue waves and render them unstable. This instability of rogue waves has been further examined by Cuevas-Maraver et al. (2017) from the point of view of spectral stability. However, rogue waves have been observed in experiments of various physical systems as we have shown in Chap. 4. Then, how can we understand the observability of rogue waves given that they are supposed to be unstable?

In this section, we will numerically simulate the evolution of rogue waves under random-noise perturbations in order to determine how robust they are. For brevity, we will only show this for several rogue waves in the NLS equation.

The NLS equation we will numerically simulate is

$$\mathrm{i}u_t + \frac{1}{2}u_{xx} + |u|^2 u = 0. \tag{5.27}$$

The numerical scheme we will use is the pseudo-spectral method, together with the fourth-order Runge-Kutta method to advance in time (Yang 2010). The x-interval is taken as $-50 \le x \le 50$, which is discretized by 1024 grid points. The time-step is taken as $\Delta t = 0.002$, which satisfies the numerical-stability condition.

The first rogue wave we will consider is the Peregrine wave, which is

$$u_p(x,t) = \left(1 - \frac{4(1+2\mathrm{i}t)}{1+4x^2+4t^2}\right) e^{\mathrm{i}t}. \tag{5.28}$$

We will take this Peregrine wave at $t_0 = -3$, and perturb it by random noise. Specifically, the initial condition of our simulation is

$$u(x,t_0) = u_p(x,t_0) + \epsilon\, R(x), \tag{5.29}$$

where $R(x)$ is a random complex function of x with unit peak amplitude, and ϵ is the strength of this random-noise perturbation.

When $\epsilon = 0.015$, i.e., with 1.5% random-noise perturbation, the simulation result for one typical realization of the random-noise function $R(x)$ is displayed in the left column of Fig. 5.7. Panel (a) displays the undisturbed initial Peregrine wave $|u_p(x,t_0)|$ at $t_0 = -3$. Panel (b) displays the disturbed initial Peregrine wave $|u(x,t_0)|$ from Eq. (5.29), which is our initial condition. Notice that this perturbation is clearly visible even though it is only 1.5%. Panel (c) displays the evolution result for this perturbed state. We can see that instability eventually develops on the background, which is not surprising since the uniform background is linearly unstable. However, the instability on the background becomes noticeable only after the Peregrine wave has run its dynamical course and is ready to disappear. For this reason, the Peregrine wave is observable even though it is unstable.

What if the perturbation is stronger? To answer this question, we next choose $\epsilon = 0.05$, i.e., with 5% random-noise perturbation. The simulation result under one typical realization of the random-noise function $R(x)$ is displayed in the right column of Fig. 5.7. It is seen that even though the perturbation is now much stronger, the qualitative feature of the simulation result remains the same. That is, the Peregrine wave still runs its course before the background instability shows up.

Two other rogue waves we will consider are the two second-order rogue waves as shown in Fig. 4.7 of the previous chapter, one being a super rogue wave, and the other being a rogue triplet. For these two rogue waves, we also take them at $t_0 = -3$, and perturb them by random noises similar to Eq. (5.29), with $\epsilon = 0.03$,

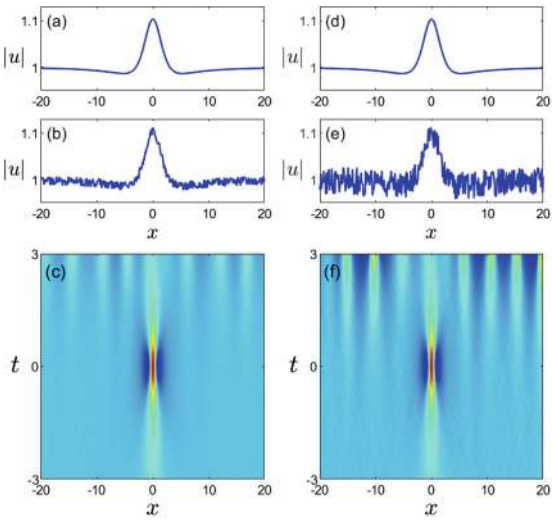

Fig. 5.7 Evolution of the Peregrine wave under perturbations. The perturbation is a random noise imposed on the Peregrine wave at $t = -3$, see Eq. (5.29). Left column: 1.5% perturbation; right column: 5% perturbation. Top row: unperturbed Peregrine waves at $t = -3$; middle row: perturbed Peregrine waves; bottom row: evolutions of perturbed Peregrine waves in the NLS equation

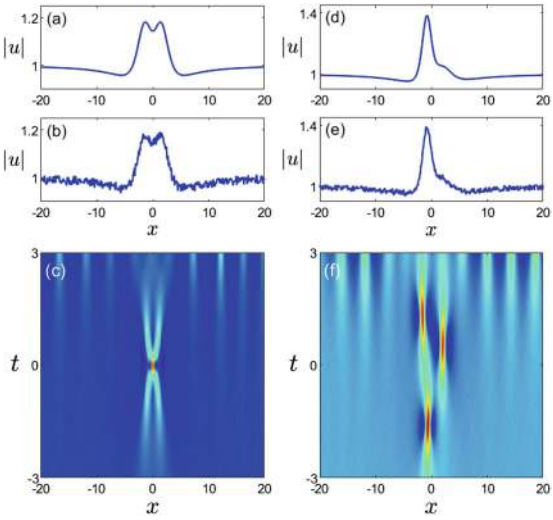

Fig. 5.8 Evolutions of two 2nd-order NLS rogue waves under perturbations. The perturbations are 3% random noises imposed on these rogue waves at $t = -3$. Left column: the super rogue wave case; right column: a rogue triplet case. Top row: unperturbed rogue waves at $t = -3$; middle row: perturbed rogue waves; bottom row: evolutions of perturbed rogue waves in the NLS equation

i.e., with 3% random noise perturbations. Evolution results of these perturbed rogue waves are displayed in the left and right columns of Fig. 5.8, respectively. As can be seen, despite perturbations, these two rogue waves are also able to display their key dynamical features before background instabilities kick in. In physical terms, this means that in the presence of perturbations, rogue waves can still appear and disappear in nature, consistent with experiments of the previous chapter.

It is noted that this type of robustness simulations for rogue waves have been done before in many articles for a wide array of integrable systems, such as the long-wave-short-wave interaction model (Chen et al. 2014a), the coupled Hirota equations (Chan and Chow 2017), generalized derivative NLS equations (Chen et

al. 2019), the NLS equation (Calini et al. 2019), a system of nonconventionally coupled NLS equations (Sun et al. 2021), and others. Our conclusions above are consistent with those earlier articles.

In situations where two spatial dimensions are involved, then the transverse stability of one-dimensional rogue waves with respect to the second spatial dimension is also an issue to consider. For example, in deep water where there are two spatial dimensions on the water surface, the (2+1)-dimensional NLS equation is the appropriate mathematical model. In this case, while rogue waves in the (1+1)-dimensional NLS equation (5.27) also satisfy this (2+1)-dimensional model, whether they are stable or robust against transverse perturbations in this (2+1)-dimensional model remains a question. For the Peregrine wave, its transverse stability in the (2+1)-dimensional NLS equation was investigated by Ablowitz and Cole (2021). It was found that the Peregrine wave suffers transverse instability, and this instability coincides with that of the background plane wave. In optical fibers and narrow water tanks where many of the rogue experiments have been performed, the second spatial dimension either does not exist or can be ignored. In such cases, transverse instability of rogue waves is irrelevant.

5.3 Partial-Rogue Waves in the Sasa-Satsuma Equation

Rogue waves is the focus of this book. These are "waves that come from nowhere and leave without a trace" (Akhmediev et al. 2009b), i.e., they are localized wave excitations that arise from the constant-amplitude background, reach higher amplitude, and then retreat back to the same background, as time progresses.

However, there exists another type of waves that are different from but closely related to rogue waves. These other waves "come from nowhere but leave with a trace". Specifically, these waves also arise from the constant-amplitude background (thus "come from nowhere"), stay localized, and reach higher amplitude. Afterwards, instead of retreating back to the same constant background with no trace, they evolve into localized waves on the constant background that persist at large time, thus leaving a trace. Such peculiar waves were first reported by Ohta and Yang (2013) for the Davey-Stewartson-II equation, where a two-dimensional localized wave arose from the constant background and then split into two localized lumps at large time (see Fig. 4 of that paper). Later, a similar but one-dimensional solution was reported by Zhao et al. (2016b) for the Sasa-Satsuma equation. These peculiar waves resemble rogue waves in the first half of evolution, but contrast them in the second half of evolution. Due to these peculiar behaviors, we call them partial-rogue waves.

Asymptotic prediction of such partial-rogue waves was made by Yang and Yang (2023b) in the Sasa-Satsuma equation. It was shown that among a class of rational solutions in this equation that can be expressed through determinants of Schur polynomials with index jumps of three, partial-rogue waves arise if and only if these rational solutions are of certain orders, where the associated generalized Okamoto

polynomials have real but no purely-imaginary roots, or have purely-imaginary but no real roots (we will call such purely-imaginary roots simply as imaginary roots for brevity in later text). It was further shown that at large negative time, these partial-rogue waves approach the constant-amplitude background, but at large positive time, they split into several fundamental rational solitons, whose numbers are determined by the number of real or imaginary roots in the underlying generalized Okamoto polynomial. We present partial-rogue waves and their asymptotic predictions in the Sasa-Satsuma equation below.

The Sasa-Satsuma equation was proposed as a higher-order nonlinear Schödinger equation for optical pulses that includes some additional physical effects such as third-order dispersion and self-steepening (Kodama and Hasegawa 1987; Sasa and Satsuma 1991). Through a variable transformation, this equation can be written as

$$u_t = u_{xxx} + 6|u|^2 u_x + 3u(|u|^2)_x. \tag{5.30}$$

Sasa and Satsuma (1991) showed that this equation is integrable.

5.3.1 A Class of Rational Solutions

Soliton solutions on the zero background in this equation were derived by Sasa and Satsuma (1991). Later, rational solutions on a nonzero background, including rogue waves, were also derived (Bandelow and Akhmediev 2012; Chen 2013; Zhao et al. 2014, 2016b; Ling 2016; Mu and Qin 2016; Mu et al. 2020; Feng et al. 2022b; Wu et al. 2022). The solutions that are relevant to partial-rogue waves are a certain class of rational solutions, whose τ functions are determinants of Schur polynomials with index jumps of three (which will be called determinants of 3-reduced Schur polynomials). These solutions are different from Sasa-Satsuma rogue waves derived by Feng et al. (2022b) and Wu et al. (2022), which are determinants of 2-reduced Schur polynomials. These determinant solutions of 3-reduced Schur polynomials in the bilinear framework correspond to the solutions with the scattering matrix admitting a triple eigenvalue in the framework of Darboux transformation. Such solutions from Darboux transformation have been studied by Zhao et al. (2016b) and Ling (2016). However, their solutions are not general nor explicit for our purpose. For this reason, we will first present general and explicit expressions for this class of rational solutions through Schur polynomials.

These rational solutions are sitting on a nonzero constant-amplitude background. Through variable scalings, we can normalize the background amplitude to be unity. Then, this background can be written as

$$u_{bg}(x,t) = e^{\mathrm{i}[\alpha(x+6t)-\alpha^3 t]}, \tag{5.31}$$

where α is a wavenumber parameter. When $\alpha = 1/2$, the Sasa-Satsuma equation (5.30) admits general rational solutions whose τ functions are determinants of

3-reduced Schur polynomials, and such solutions are given by the following theorem (Yang and Yang 2023b).

Theorem 5.1 *When $\alpha = 1/2$, the Sasa-Satsuma equation (5.30) admits bounded (N_1, N_2)-th order rational solutions*

$$u_{N_1,N_2}(x,t) = \frac{g_{N_1,N_2}}{f_{N_1,N_2}} e^{\mathrm{i}[\alpha(x+6t)-\alpha^3 t]}, \tag{5.32}$$

where N_1 and N_2 are arbitrary non-negative integers,

$$f_{N_1,N_2} = \sigma_{0,0}, \quad g_{N_1,N_2} = \sigma_{1,0}, \tag{5.33}$$

$$\sigma_{k,l} = \det \begin{pmatrix} \sigma_{k,l}^{[1,1]} & \sigma_{k,l}^{[1,2]} \\ \sigma_{k,l}^{[2,1]} & \sigma_{k,l}^{[2,2]} \end{pmatrix}, \tag{5.34}$$

$$\sigma_{k,l}^{[I,J]} = \left(\phi_{3i-I,\,3j-J}^{(k,l\,I,J)} \right)_{1\le i\le N_I,\,1\le j\le N_J}, \tag{5.35}$$

matrix elements in $\sigma_{k,l}^{[I,J]}$ are defined by

$$\phi_{i,j}^{(k,l,I,J)} = \sum_{\nu=0}^{\min(i,j)} \left(\frac{p_1^2}{4p_0^2} \right)^{\nu} S_{i-\nu}(\mathbf{x}_I^+(k,l) + \nu\mathbf{s})\, S_{j-\nu}(\mathbf{x}_J^-(k,l) + \nu\mathbf{s}), \tag{5.36}$$

vectors $\mathbf{x}_I^{\pm}(k,l) = (x_{1,I}^{\pm}, x_{2,I}^{\pm}, \cdots)$ are given by

$$x_{r,I}^{+}(k,l) = p_r(x+6t) + \beta_r t + k\theta_r + l\theta_r^* + a_{r,I}, \tag{5.37}$$

$$x_{r,J}^{-}(k,l) = p_r(x+6t) + \beta_r t - k\theta_r^* - l\theta_r + a_{r,J}, \tag{5.38}$$

β_r and θ_r are coefficients from expansions

$$p^3(\kappa) = \sum_{r=0}^{\infty} \beta_r \kappa^r, \ \ln\left[\frac{p(\kappa) - \mathrm{i}\alpha}{p_0 - \mathrm{i}\alpha} \right] = \sum_{r=1}^{\infty} \theta_r \kappa^r, \tag{5.39}$$

the function $p(\kappa)$ with expansion $p(\kappa) = \sum_{r=0}^{\infty} p_r \kappa^r$ and real expansion coefficients p_r is defined by the equation

$$Q_1[p(\kappa)] = \frac{Q_1(p_0)}{3} \left[e^{\kappa} + 2e^{-\kappa/2} \cos\left(\frac{\sqrt{3}}{2}\kappa \right) \right], \tag{5.40}$$

with

$$Q_1(p) \equiv \frac{1}{p - \mathrm{i}\alpha} + \frac{1}{p + \mathrm{i}\alpha} + p, \tag{5.41}$$

$p_0 = \pm\sqrt{3}/2$, the real vector $\mathbf{s} = (s_1, s_2, \cdots)$ is defined by the expansion

$$\ln\left[\left(\frac{2p_0}{p_1\kappa}\right)\left(\frac{p(\kappa) - p_0}{p(\kappa) + p_0}\right)\right] = \sum_{r=1}^{\infty} s_r \kappa^r, \tag{5.42}$$

the asterisk '' represents complex conjugation, and*

$$(a_{1,1}, \cdots, a_{3N_1-1,1}),\ (a_{1,2}, \cdots, a_{3N_2-2,2}) \tag{5.43}$$

are free real constants.

The proof of this theorem can be found in Yang and Yang (2023b).

Note 1 When we choose $p_0 = \sqrt{3}/2$, the first few coefficients of p_r, β_r, θ_r, and s_r are

$$p_1 = \frac{12^{1/6}}{2}, \quad p_2 = \frac{12^{-1/6}}{2}, \quad p_3 = \frac{1}{4\sqrt{3}}, \tag{5.44}$$

$$\beta_1 = \frac{9}{8}12^{1/6}, \quad \beta_2 = \frac{9}{8}\cdot\frac{3^{5/6}}{2^{1/3}}, \quad \beta_3 = \frac{19\sqrt{3}}{16}, \tag{5.45}$$

$$\theta_1 = \frac{12^{1/6}}{\sqrt{3} - \mathrm{i}}, \quad \theta_2 = \frac{-\mathrm{i}}{12^{1/6}\left(\sqrt{3} - \mathrm{i}\right)^2}, \quad \theta_3 = 0, \tag{5.46}$$

$$s_1 = 0, \quad s_2 = 0, \quad s_3 = -\frac{1}{40}. \tag{5.47}$$

If we choose $p_0 = -\sqrt{3}/2$, then p_r and β_r would switch sign, θ_r change to θ_r^*, and s_r remain the same.

Note 2 If we choose $p_0 = -\sqrt{3}/2$ and keep all internal parameters $(a_{r,1}, a_{r,2})$ unchanged, then the resulting solution $\tilde{u}(x,t)$ would be related to the solution $u(x,t)$ with $p_0 = \sqrt{3}/2$ as $\tilde{u}(x,t) = u^*(-x,-t)$.

Note 3 Internal parameters $a_{3n,1}$ and $a_{3n,2}$ $(n = 1, 2, \cdots)$ do not affect solutions in Theorem 5.1, for reasons which can be found in Yang and Yang (2021b). Thus, we will set them as zero in later text.

The simplest solution of this class—the fundamental rational soliton, is obtained when we set $N_1 = 0$ and $N_2 = 1$ in Theorem 5.1. In this case, the solution has a single real parameter $a_{1,2}$, which can be normalized to zero through a shift of the x axis. The resulting solution, for both $p_0 = \pm\sqrt{3}/2$, is

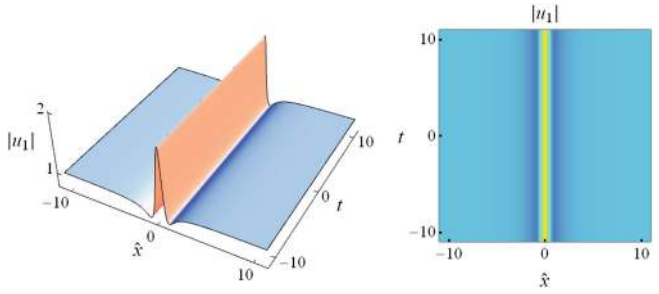

Fig. 5.9 Graph of the fundamental rational soliton (5.48) in the Sasa-Satsuma equation (5.30). Left: 3D plot. Right: density plot. The horizontal axes are $\hat{x} = x + (33/4)t$

$$u_1(x,t) = \hat{u}_1(x,t)e^{\mathrm{i}[\frac{1}{2}(x+6t)-\frac{1}{8}t]}, \tag{5.48}$$

where

$$\hat{u}_1(x,t) = \frac{3\hat{x}^2 + 3\mathrm{i}\hat{x} - 2}{3\hat{x}^2 + 1}, \tag{5.49}$$

and

$$\hat{x} \equiv x + (33/4)t \tag{5.50}$$

is a moving coordinate. The graph of this solution is plotted in Fig. 5.9. This solution is a rational soliton moving on the constant-amplitude background (5.31) with velocity $-33/4$. Its height, i.e., $\max(|u_1|)$, is 2.

5.3.2 *Generalized Okamoto Polynomials*

We will show in later text that rational solutions in Theorem 5.1 contain partial-rogue waves but are not all partial-rogue waves. The question of what solutions in Theorem 5.1 are partial-rogue waves turns out to be closely related to root properties of generalized Okamoto polynomials. So, we will introduce these polynomials and examine their root structures next.

Original Okamoto polynomials arose in Okamoto's study of rational solutions to the Painlevé IV equation (Okamoto 1986). He showed that a class of such rational solutions can be expressed as the logarithmic derivative of certain special polynomials, which are now called Okamoto polynomials. These original polynomials were later generalized, and the generalized Okamoto polynomials provide a more complete set of rational solutions to the Painlevé IV equation. In addition, determinant expressions for the original and generalized Okamoto polynomials

were discovered (Kajiwara and Ohta 1998; Noumi and Yamada 1999; Clarkson 2003, 2006).

Let $p_j(z)$ be Schur polynomials defined by

$$\sum_{j=0}^{\infty} p_j(z)\epsilon^j = \exp\left(z\epsilon + \epsilon^2\right), \tag{5.51}$$

with $p_j(z) \equiv 0$ for $j < 0$. Then, generalized Okamoto polynomials $Q_{N_1,N_2}(z)$, with N_1, N_2 being nonnegative integers, are defined as

$$Q_{N_1,N_2}(z) = \mathrm{Wron}[p_2, p_5, \cdots, p_{3N_1-1}, p_1, p_4, \cdots, p_{3N_2-2}], \tag{5.52}$$

or equivalently,

$$Q_{N_1,N_2}(z) = \begin{vmatrix} p_2 & p_1 & \cdots & p_{3-N_1-N_2} \\ \vdots & \vdots & \vdots & \vdots \\ p_{3N_1-1} & p_{3N_1-2} & \cdots & p_{2N_1-N_2} \\ p_1 & p_0 & \cdots & p_{2-N_1-N_2} \\ \vdots & \vdots & \vdots & \vdots \\ p_{3N_2-2} & p_{3N_2-3} & \cdots & p_{2N_2-N_1-1} \end{vmatrix}, \tag{5.53}$$

since $p'_{j+1}(z) = p_j(z)$ from the definition of $p_j(z)$ in Eq. (5.51), where the prime represents differentiation. The first few $Q_{N_1,N_2}(z)$ polynomials are

$$\begin{aligned} Q_{1,0}(z) &= \frac{1}{2}(z^2+2), \\ Q_{2,0}(z) &= \frac{1}{80}(z^6+10z^4+20z^2+40), \\ Q_{0,1}(z) &= z, \\ Q_{1,1}(z) &= \frac{1}{2}(-z^2+2) \\ Q_{2,1}(z) &= \frac{1}{20}z(z^4-20), \\ Q_{0,2}(z) &= \frac{1}{8}(z^4+4z^2-4), \\ Q_{1,2}(z) &= \frac{1}{8}(-z^4+4z^2+4), \\ Q_{2,2}(z) &= \frac{1}{80}(-z^6+10z^4-20z^2+40). \end{aligned}$$

Note that our definition of generalized Okamoto polynomials is different from that by Clarkson (2003, 2006). Denoting the $Q_{m,n}(z)$ polynomial introduced in Clarkson (2003, 2006) as $Q^{[C]}_{m,n}(z)$, then our polynomial $Q_{N_1,N_2}(z)$ is related to $Q^{[C]}_{m,n}(z)$ as

$$Q_{N_1,N_2}(z) = \begin{cases} \gamma^{(1)}_{N_1,N_2} Q^{[C]}_{N_2-N_1,-N_2}\left(\sqrt{3}\,z/2\right), & N_1 \geq N_2, \\ \gamma^{(2)}_{N_1,N_2} Q^{[C]}_{N_2-N_1,N_1+1}\left(\sqrt{3}\,z/2\right), & N_1 \leq N_2, \end{cases} \tag{5.54}$$

where $\gamma^{(1)}_{N_1,N_2}$ and $\gamma^{(2)}_{N_1,N_2}$ are certain real constants.

Clarkson (2003) observed an interesting symmetry relation between $Q^{[C]}_{n,m}(z)$ and $Q^{[C]}_{m,n}(\mathrm{i}z)$ based on examples. Using that symmetry and the above polynomial connection (5.54), we obtain symmetry relations for our polynomials $Q_{N_1,N_2}(z)$ as

$$Q_{N_1,N_1-N_2}(z) = b_1 e^{-\frac{1}{2}\mathrm{i}\pi d_{N_1,N_2}} Q_{N_1,N_2}(\mathrm{i}z), \quad N_1 \geq N_2, \tag{5.55}$$

$$Q_{N_2-N_1-1,N_2}(z) = b_2 e^{-\frac{1}{2}\mathrm{i}\pi d_{N_1,N_2}} Q_{N_1,N_2}(\mathrm{i}z), \quad N_1 < N_2, \tag{5.56}$$

where

$$d_{N_1,N_2} = N_1^2 + N_2^2 - N_1N_2 + N_1 \tag{5.57}$$

is the degree of the $Q_{N_1,N_2}(z)$ polynomial, $b_1 = \pm 1$ is the sign of the ratio between coefficients of the highest z-power terms in $Q_{N_1,N_2}(z)$ and $Q_{N_1,N_1-N_2}(z)$, while $b_2 = \pm 1$ is the sign of the ratio between coefficients of the highest z-power terms in $Q_{N_1,N_2}(z)$ and $Q_{N_2-N_1-1,N_2}(z)$. In the special case of $N_2 = 0$, the symmetry (5.55) further reduces to

$$Q_{N_1,N_1}(z) = Q_{N_1,0}(\mathrm{i}z). \tag{5.58}$$

Root properties of generalized Okamoto polynomials $Q_{N_1,N_2}(z)$ are important for our partial-rogue wave problem. It is easy to see from Eq. (5.51) that $p_j(-z) = (-1)^j p_j(z)$. Thus, $Q_{N_1,N_2}(-z) = (-1)^\gamma Q_{N_1,N_2}(z)$, where γ is a certain integer. As a result, roots of $Q_{N_1,N_2}(z)$ come in $\pm z$ pairs. In addition, since the polynomial $Q_{N_1,N_2}(z)$ has real coefficients, roots of $Q_{N_1,N_2}(z)$ also come as complex-conjugate pairs.

For our partial-rogue wave problem, it turns out from later text that we need generalized Okamoto polynomials which have either real or imaginary roots, but not both. In addition, zero cannot be a root. Multiplicity of these real or imaginary roots also has important consequences. These root questions of generalized Okamoto polynomials were answered by Roffelsen and Stokes (2024), who obtained the following results.

Theorem 5.2 *Every root of the generalized Okamoto polynomial $Q_{N_1,N_2}(z)$ is simple. In addition, treating zero as both a real root and an imaginary root, then*

the numbers of real and imaginary roots of $Q_{N_1,N_2}(z)$ *are*

$$\rho_{re}(N_1, N_2) = \begin{cases} N_2, & \text{if } N_1 \text{ even and } N_1 \le N_2 - 1, \\ N_1 + 1, & \text{if } N_1 \text{ odd and } N_1 \le N_2 - 1, \\ N_2, & \text{if } N_2 \text{ even and } N_2 \le N_1, \\ N_1 + 1, & \text{if } N_2 \text{ odd and } N_2 \le N_1, \end{cases} \tag{5.59}$$

and

$$\rho_{im}(N_1, N_2) = \begin{cases} N_2 - N_1, & \text{if } N_2 - N_1 \text{ even and } N_1 \le N_2 - 1, \\ N_2, & \text{if } N_2 - N_1 \text{ odd and } N_1 \le N_2 - 1, \\ N_1 - N_2, & \text{if } N_1 - N_2 \text{ even and } N_2 \le N_1, \\ N_1 + 1, & \text{if } N_1 - N_2 \text{ odd and } N_2 \le N_1. \end{cases} \tag{5.60}$$

From this theorem, we can easily see that the only $Q_{N_1,N_2}(z)$ polynomials which have real but no imaginary roots are $Q_{N_1,N_1}(z)$, where the number of real roots is N_1 when N_1 is even and $N_1 + 1$ when N_1 is odd; and the only $Q_{N_1,N_2}(z)$ polynomials which have imaginary but no real roots are $Q_{N_1,0}(z)$, where the number of imaginary roots is N_1 when N_1 is even and $N_1 + 1$ when N_1 is odd.

To verify these results, we plot in Fig. 5.10 roots of $Q_{N_1,N_2}(z)$ in the complex z plane for $0 \le N_1, N_2 \le 3$. We can see from this figure that the $Q_{N_1,0}(z)$ polynomials in the first column have only imaginary roots but no real roots. The $Q_{N_1,N_1}(z)$ polynomials on the diagonal have only real roots but no imaginary roots, which is not surprising given the connection between Q_{N_1,N_1} and $Q_{N_1,0}$ polynomials in Eq. (5.58). For both polynomials, zero is not a root. All other polynomials in Fig. 5.10 have both real and imaginary roots, and are thus not useful for the partial-rogue problem. These root structures in Fig. 5.10 are consistent with Theorem 5.2 and the two symmetries of generalized Okamoto polynomials in Eqs. (5.55)–(5.56).

We have also checked that every root in Fig. 5.10 is simple, consistent with Theorem 5.2.

5.3.3 *Large-Time Predictions of Partial-Rogue Waves*

According to our definition, partial-rogue waves are localized waves that "come from nowhere but leave with a trace". Thus, we impose the following boundary conditions

$$u(x, t) \to e^{\mathrm{i}[\alpha(x+6t)-\alpha^3 t]}, \quad t \to -\infty \text{ or } x \to \pm\infty, \tag{5.61}$$

where $\alpha = 1/2$. In addition, we require $u(x, t)$ not to approach this constant-amplitude background as $t \to +\infty$.

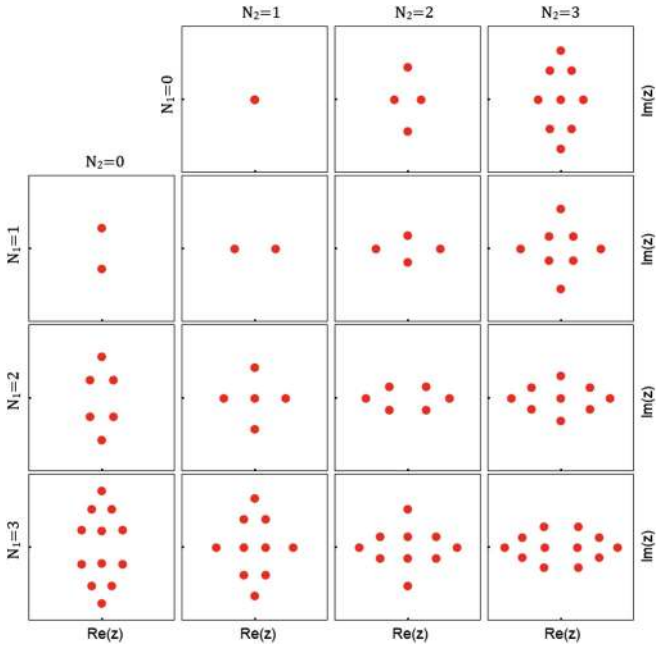

Fig. 5.10 Roots of generalized Okamoto polynomials $Q_{N_1,N_2}(z)$ in the complex z plane for $0 \le N_1, N_2 \le 3$. In all panels, $-5 \le \mathrm{Re}(z), \mathrm{Im}(z) \le 5$

Only a small portion of rational solutions in Theorem 5.1 are partial-rogue waves. This is not surprising, since the fundamental rational soliton in Fig. 5.9 is not a partial-rogue wave already. We will show that a rational solution in Theorem 5.1 is a partial-rogue wave only if the associated generalized Okamoto polynomial has either imaginary or real roots, but not both. This result is summarized in the following two theorems, for imaginary roots and real roots, respectively (Yang and Yang 2023b).

Theorem 5.3 *If the generalized Okamoto polynomial $Q_{N_1,N_2}(z)$ has imaginary but no real roots, then the rational solution $u_{N_1,N_2}(x,t)$ in Theorem 5.1 with $p_0 = -\sqrt{3}/2$ is a partial-rogue wave. In addition, when $t \gg 1$, this solution splits into n fundamental rational solitons $\hat{u}_1(x - x_0^{(k)}, t)\, e^{\mathrm{i}[\frac{1}{2}(x+6t)-\frac{1}{8}t]}$, where n is the number of imaginary roots in $Q_{N_1,N_2}(z)$, and $1 \le k \le n$. The location $x_0^{(k)}$ of the k-th fundamental rational soliton is given by*

$$x_0^{(k)} = -\frac{33}{4}t - \mathrm{i}z_0^{(k)}\frac{3^{3/4}}{2^{1/2}}t^{1/2} + \frac{2}{12^{1/6}}\Delta^{(k)}, \tag{5.62}$$

where $z_0^{(k)}$ is the k-th imaginary root of $Q_{N_1,N_2}(z)$, and $\Delta^{(k)}$ is a $z_0^{(k)}$-dependent $O(1)$ quantity. The error of this fundamental rational soliton approximation is

$O(|t|^{-1/2})$. *Expressed mathematically, if* $t \gg 1$, *and* x *is in an* $O(1)$ *neighborhood of a certain* $x_0^{(k)}$, *i.e.,* $|x - x_0^{(k)}| = O(1)$, *then*

$$u_{N_1,N_2}(x,t) = \hat{u}_1(x - x_0^{(k)}, t)\, e^{\mathrm{i}[\frac{1}{2}(x+6t)-\frac{1}{8}t]} + O(|t|^{-1/2}). \tag{5.63}$$

When $t \to +\infty$ *and* x *is not in an* $O(1)$ *neighborhood of any* $x_0^{(k)}$, *or when* $t \to -\infty$ *for all* x, *the solution approaches the constant-amplitude background (5.31), i.e.,*

$$u_{N_1,N_2}(x,t) \to e^{\mathrm{i}[\frac{1}{2}(x+6t)-\frac{1}{8}t]}. \tag{5.64}$$

Theorem 5.4 *If the generalized Okamoto polynomial* $Q_{N_1,N_2}(z)$ *has real but no imaginary roots, and each real root is nonzero, then the rational solution* $u_{N_1,N_2}(x,t)$ *in Theorem 5.1 with* $p_0 = \sqrt{3}/2$ *is a partial-rogue wave. In addition, when* $t \gg 1$, *this solution splits into* n *fundamental rational solitons* $\hat{u}_1(x - x_0^{(k)}, t)\, e^{\mathrm{i}[\frac{1}{2}(x+6t)-\frac{1}{8}t]}$, *where* n *is the number of real roots in* $Q_{N_1,N_2}(z)$, *and* $1 \le k \le n$. *The location* $x_0^{(k)}$ *of the* k*-th fundamental rational soliton is given by*

$$x_0^{(k)} = -\frac{33}{4}t + z_0^{(k)}\frac{3^{3/4}}{2^{1/2}}t^{1/2} - \frac{2}{12^{1/6}}\Delta^{(k)}, \tag{5.65}$$

where $z_0^{(k)}$ *is the* k*-th real root of* $Q_{N_1,N_2}(z)$, *and* $\Delta^{(k)}$ *is a* $z_0^{(k)}$*-dependent* $O(1)$ *quantity. The error of this fundamental rational soliton approximation is* $O(|t|^{-1/2})$. *Mathematical expressions of these results are the same as in Eqs. (5.63)–(5.64) of Theorem 5.3, except for the different formula (5.65) for the soliton's location* $x_0^{(k)}$.

Proofs of these two theorems can be found in Yang and Yang (2023b).

These two theorems, together with Theorem 5.2 and Fig. 5.10 on root properties of generalized Okamoto polynomials, immediately lead to the following corollary.

Corollary 5.1 *Rational solutions* $u_{N_1,0}(x,t)$ $(N_1 \ge 1)$ *with* $p_0 = -\sqrt{3}/2$, *and* $u_{N_1,N_1}(x,t)$ $(N_1 \ge 1)$ *with* $p_0 = \sqrt{3}/2$, *in the Sasa-Satsuma equation (5.30) are partial-rogue waves. As* $t \to +\infty$, *these solutions split into several fundamental rational solitons, whose number is equal to* N_1 *when* N_1 *is even and* $N_1 + 1$ *when* N_1 *is odd.*

The results in this corollary are not dependent on values of internal parameters $a_{r,1}, a_{r,2}$ $(r = 1, 2, \cdots)$. This is not surprising, since when $|t| \gg 1$, those internal parameters in the solution will play a less significant role.

5.3.4 Numerical Verification of Theoretical Predictions

The simplest partial-rogue wave in the $u_{N_1,0}(x,t)$ family is $u_{1,0}(x,t)$ with $p_0 = -\sqrt{3}/2$. This solution contains two free real parameters $a_{1,1}$ and $a_{2,1}$. Through a shift of the (x,t) axes, we can normalize

$$a_{1,1} = a_{2,1} = 0 \tag{5.66}$$

without loss of generality. In fact, this zero normalization of $a_{1,1}$ and $a_{2,1}$ can be achieved for all partial-rogue waves $u_{N_1,0}(x,t)$ and $u_{N_1,N_1}(x,t)$. Under this parameter normalization, the $u_{1,0}(x,t)$ solution can be written out as

$$u_{1,0}(x,t) = \frac{\sigma_{1,0}(\hat{x},t)}{\sigma_{0,0}(\hat{x},t)} e^{\mathrm{i}[\frac{1}{2}(x+6t)-\frac{1}{8}t]}, \tag{5.67}$$

where

$$\sigma_{0,0}(\hat{x},t) = 4 + 243t^2 + 24\hat{x}^2 - 12\sqrt{3}\hat{x}^3 + 9\hat{x}^4 + 54t\hat{x}\left(2 - \sqrt{3}\hat{x}\right), \tag{5.68}$$

$$\begin{aligned}\sigma_{1,0}(\hat{x},t) = {} & -2 + 6\mathrm{i}\sqrt{3} + 243t^2 - 12\mathrm{i}\hat{x} - \left(3 + 9\mathrm{i}\sqrt{3}\right)\hat{x}^2 + 6\left(3\mathrm{i} - 2\sqrt{3}\right)\hat{x}^3 \\ & + 9\hat{x}^4 - 27t\left[\mathrm{i} + \sqrt{3} + 2\mathrm{i}\left(2\mathrm{i} + \sqrt{3}\right)\hat{x} + 2\sqrt{3}\hat{x}^2\right],\end{aligned} \tag{5.69}$$

and $\hat{x} = x + (33/4)t$. The graph of this solution, in the $(\hat{x},t)$ plane, is plotted in Fig. 5.11a. As one can see, this is indeed a partial-rogue wave. As $t \to +\infty$, it splits into two fundamental rational solitons, consistent with Corollary 5.1.

The next two solutions in the $u_{N_1,0}(x,t)$ family are $u_{2,0}(x,t)$ and $u_{3,0}(x,t)$ with $p_0 = -\sqrt{3}/2$. Under the parameter normalization (5.66), the $u_{2,0}(x,t)$ solution contains additional free real parameters $(a_{4,1}, a_{5,1})$, while the $u_{3,0}(x,t)$ solution contains additional free real parameters $(a_{4,1}, a_{5,1}, a_{7,1}, a_{8,1})$. When we choose

$$a_{4,1} = 2,\ a_{5,1} = -3 \tag{5.70}$$

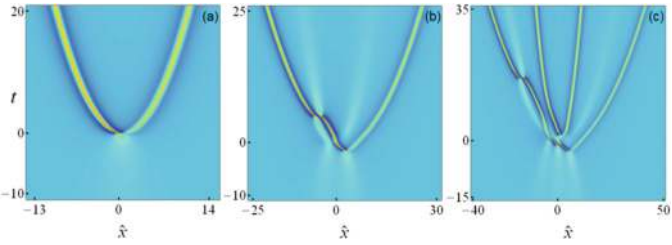

Fig. 5.11 Density plots of partial-rogue waves $|u_{1,0}(x,t)|$ (**a**), $|u_{2,0}(x,t)|$ (**b**), and $|u_{3,0}(x,t)|$ (**c**), with $p_0 = -\sqrt{3}/2$ in the Sasa-Satsuma equation (5.30). Parameter values in (**b**) and (**c**) are given in Eqs. (5.70) and (5.71) respectively. The horizontal axes are $\hat{x} = x + (33/4)t$

in $u_{2,0}(x,t)$ and

$$a_{4,1}=2,\ a_{5,1}=-3,\ a_{7,1}=a_{8,1}=0 \tag{5.71}$$

in $u_{3,0}(x,t)$, the corresponding true solutions are plotted from Theorem 5.1 and displayed in Fig. 5.11b and c respectively. Again, these are indeed partial-rogue waves. When $t\to+\infty$, they split into two and four fundamental rational solitons respectively, consistent with Corollary 5.1 as well.

The reader may notice that individual fundamental solitons at large time in Fig. 5.11 appear to have different heights, while Theorem 5.3 predicts these fundamental solitons should approach the same height. It turns out that this discrepancy is due to the fact that the time shown in Fig. 5.11 is not large enough. We have checked that as time increases further, all these humps indeed approach the same height 2, which is the height of the fundamental rational soliton (5.48).

The simplest partial-rogue wave in the $u_{N_1,N_1}(x,t)$ family is $u_{1,1}(x,t)$ with $p_0=\sqrt{3}/2$. Under parameter normalization (5.66), this $u_{1,1}(x,t)$ solution still contains a free real parameter $a_{1,2}$. However, we have found that this $u_{1,1}(x,t)$ solution can be written as

$$u_{1,1}(x,t)=\frac{\sigma_{1,0}(\tilde{x},\tilde{t})}{\sigma_{0,0}(\tilde{x},\tilde{t})}e^{\mathrm{i}[\frac{1}{2}(x+6t)-\frac{1}{8}t]}, \tag{5.72}$$

where functions $\sigma_{0,0}$ and $\sigma_{1,0}$ are as given in Eqs. (5.68)–(5.69), and

$$\tilde{x}=\hat{x}+\frac{2^{2/3}}{3^{1/6}}a_{1,2},\quad \tilde{t}=t-\frac{2^{5/3}}{3^{13/6}}a_{1,2}+\frac{2^{4/3}}{3^{11/6}}a_{1,2}^2. \tag{5.73}$$

Thus, after a shift of the $(\hat{x},t)$ axes, this $u_{1,1}(x,t)$ solution with free parameter $a_{1,2}$ is equivalent to the $u_{1,0}(x,t)$ solution given in Eqs. (5.67)–(5.69). This $u_{1,1}(x,t)$ solution, in the $(\hat{x},t)$ plane with $a_{1,2}=3$, is plotted in Fig. 5.12a. This is certainly a partial-rogue wave.

The next two solutions in the $u_{N_1,N_1}(x,t)$ family are $u_{2,2}(x,t)$ and $u_{3,3}(x,t)$ with $p_0=\sqrt{3}/2$. Under parameter normalization (5.66), these solutions still contain a number of free real parameters. When we choose

$$a_{4,1}=a_{5,1}=0,\ a_{1,2}=a_{2,2}=a_{4,2}=3 \tag{5.74}$$

in $u_{2,2}(x,t)$ and

$$a_{4,1}=a_{5,1}=a_{7,1}=a_{8,1}=0,\quad a_{1,2}=a_{2,2}=a_{4,2}=a_{5,2}=a_{7,2}=3 \tag{5.75}$$

in $u_{3,3}(x,t)$, the corresponding true solutions are plotted from Theorem 5.1 and displayed in Fig. 5.12b and c respectively. Again, these are indeed partial-rogue waves. When $t\to+\infty$, they split into two and four fundamental rational solitons respectively, consistent with Corollary 5.1.

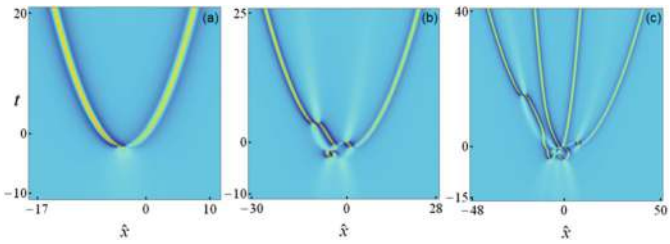

Fig. 5.12 Density plots of partial-rogue waves $|u_{1,1}(x,t)|$ (**a**), $|u_{2,2}(x,t)|$ (**b**), and $|u_{3,3}(x,t)|$ (**c**), with $p_0 = \sqrt{3}/2$ in the Sasa-Satsuma equation (5.30). In (**a**), $a_{1,2} = 3$. Parameter values in (**b**) and (**c**) are given in Eqs. (5.74) and (5.75), respectively. The horizontal axes are $\hat{x} = x + (33/4)t$

5.4 Large-Time Patterns of Higher-Order Lumps in the Kadomtsev-Petviashvili I Equation

In this section, we discuss large-time patterns of higher-order lumps in the Kadomtsev-Petviashvili (KP) I equation. This topic seems quite different from rogue waves. However, we will show that these higher-order lumps exhibit interesting patterns which are also described asymptotically by root structures of certain types of polynomials, analogous to rogue wave patterns. In addition, analytical treatments for lump patterns and rogue patterns have a lot in common.

The KP equation arose in Kadomtsev and Petviashvili's (1970) investigation on the stability of a Korteweg-de Vries soliton with respect to long transverse perturbations. This equation has two types, KP-I and KP-II, and our interest here is KP-I. This KP-I equation is

$$(u_t + 6uu_x + u_{xxx})_x - 3u_{yy} = 0. \tag{5.76}$$

It models two-dimensional evolution of weakly nonlinear shallow water waves under large surface tension (Ablowitz and Segur 1979). It also arises in other branches of physics, such as nonlinear optics (Pelinovsky et al. 1995) and Bose-Einstein condensates (Barashenkov and Makhankov 1988; Tsuchiya et al. 2008).

The KP-I equation (5.76) is solvable by the inverse scattering transform (Novikov et al. 1984; Ablowitz and Clarkson 1991). It admits stable fundamental lump solutions that are bounded rational functions decaying in all spatial directions (Petviashvili 1976; Manakov et al. 1977; Satsuma and Ablowitz 1979). It also admits a broad class of rational solutions that describe the interactions of these lumps. If individual lumps have distinct asymptotic velocities, then they would pass through each other without change in velocities or phases (Manakov et al. 1977; Satsuma and Ablowitz 1979). But if they have the same asymptotic velocities, they would undergo novel anomalous scattering, where the lumps would separate from each other in new spatial directions that are very different from their original incoming directions (Gorshkov et al. 1993; Ablowitz and Villarroel 1997; Ablowitz et al. 2000). In this section, we are concerned with this latter type of solutions, which

we call higher-order lumps. They are also called multi-pole lumps in the literature (Ablowitz and Villarroel 1997; Ablowitz et al. 2000).

5.4.1 Higher-Order Lump Solutions

Analytical expressions of higher-order lumps have been derived by a wide variety of methods before (Pelinovsky and Stepanyants 1993; Gorshkov et al. 1993; Ablowitz and Villarroel 1997; Ablowitz et al. 2000; Dubard et al. 2010; Dubard and Matveev 2013; Clarkson and Dowie 2017). Most of those solutions were special solutions, except for Ablowitz et al. (2000) where general higher-order lump solutions were derived by Darboux transformation. Those general solutions were given through determinants whose matrix elements involve differential operators with respect to the spectral parameter. More explicit expressions of general higher-order lumps were derived by Yang and Yang (2022b) using the bilinear method, and those explicit expressions are given in the following theorem.

Theorem 5.5 *General N-th order lumps of the KP-I equation (5.76) are*

$$u_{\Lambda}(x, y, t) = 2\partial_x^2 \ln \sigma, \tag{5.77}$$

where

$$\sigma(x, y, t) = \det_{1 \le i, j \le N} \left(m_{i,j}\right), \tag{5.78}$$

$$m_{i,j} = \sum_{\nu=0}^{\min(n_i, n_j)} \left(\frac{|p|^2}{(p+p^*)^2}\right)^{\nu} S_{n_i-\nu}\left(\mathbf{x}^+ + \nu \mathbf{s} + \mathbf{a}_i\right) S_{n_j-\nu}\left((\mathbf{x}^+)^* + \nu \mathbf{s}^* + \mathbf{a}_j^*\right), \tag{5.79}$$

N is an arbitrary positive integer, $\Lambda \equiv (n_1, n_2, \cdots n_N)$ is a vector of arbitrary positive integers, p is an arbitrary non-imaginary complex number, the asterisk '$*$' represents complex conjugation, the vector $\mathbf{x}^+ = \left(x_1^+, x_2^+, \cdots\right)$ is defined by

$$x_k^+ = p\frac{1}{k!}x + p^2\frac{2^k}{k!}\mathrm{i}y + p^3\frac{3^k}{k!}(-4)t, \tag{5.80}$$

the vector $\mathbf{s} = (s_1, s_2, \cdots)$ is defined through the expansion

$$\ln\left(\frac{e^{\kappa}-1}{\kappa}\frac{p+p^*}{p\,e^{\kappa}+p^*}\right) = \sum_{j=1}^{\infty} s_j\,\kappa^j, \tag{5.81}$$

vectors $\mathbf{a}_i$ are

$$\mathbf{a}_i = \left(a_{i,1}, a_{i,2}, \cdots, a_{i,n_i}\right), \tag{5.82}$$

and $a_{i,j}$ $(1 \le i \le N, 1 \le j \le n_i)$ *are free complex constants.*

The proof of this theorem can be found in Yang and Yang (2022b).

The fundamental lump can be obtained from Theorem 5.5 by taking $N = 1$ and $n_1 = 1$. Through a shift of the (x, y) axes, we can normalize $a_{1,1} = 0$. In addition, we can take $p = 1$ without loss of generality (Yang and Yang 2022b). In this case, the fundamental lump's expression is

$$u_1(x, y, t) = 2\partial_x^2 \ln\left((x - 12t)^2 + 4y^2 + \frac{1}{4}\right). \tag{5.83}$$

This is a single lump with peak amplitude 16 that is moving at velocity 12.

5.4.2 *Wronskian-Hermite Polynomials and Their Root Structures*

At large time, patterns of higher-order lumps turn out to be closely related to root structures of Yablonskii-Vorob'ev polynomials and Wronskian-Hermite polynomials. Yablonskii-Vorob'ev polynomials and their root structures have been introduced in Sect. 3.1.1. Here, we introduce Wronskian-Hermite polynomials and their root structures.

Let $q_k(z)$ be polynomials defined by

$$\sum_{k=0}^{\infty} q_k(z)\epsilon^k = \exp\left(z\epsilon + \epsilon^2\right). \tag{5.84}$$

These $q_k(z)$ polynomials are related to Hermite polynomials through simple variable scalings. Then, for any positive integer N and index vector $\Lambda = (n_1, n_2, \ldots, n_N)$, where $\{n_i\}$ are positive and distinct integers in ascending order, i.e., $n_1 < n_2 < \cdots < n_N$, the Wronskian-Hermite polynomial $W_\Lambda(z)$ is defined as the Wronskian

$$W_\Lambda(z) = \mathrm{Wron}\left[q_{n_1}(z), q_{n_2}(z), \ldots, q_{n_N}(z)\right], \tag{5.85}$$

or equivalently,

$$W_\Lambda(z) = \begin{vmatrix} q_{n_1}(z) & q_{n_1-1}(z) & \cdots & q_{n_1-N+1}(z) \\ q_{n_2}(z) & q_{n_2-1}(z) & \cdots & q_{n_2-N+1}(z) \\ \vdots & \vdots & \vdots & \vdots \\ q_{n_N}(z) & q_{n_N-1}(z) & \cdots & q_{n_N-N+1}(z) \end{vmatrix}, \tag{5.86}$$

since we can see $q'_{k+1}(z) = q_k(z)$ from the definition (5.84). In the above determinant, $q_k(z) \equiv 0$ when $k < 0$.

Regarding root structures of Wronskian-Hermite polynomials $W_\Lambda(z)$, we have the following facts.

1. The degree of the polynomial $W_\Lambda(z)$ is

$$\rho = \sum_{i=1}^{N} n_i - \frac{N(N-1)}{2}. \tag{5.87}$$

   This fact can be seen from the definition (5.86).
2. The multiplicity of the zero root in $W_\Lambda(z)$ is a triangular number and equal to $d(d+1)/2$, where

$$d = k_{odd} - k_{even}, \tag{5.88}$$

   and k_{odd}, k_{even} are the numbers of odd and even elements in the index vector $(n_1, n_2, \ldots, n_N)$ respectively. This fact was mentioned in Felder et al. (2012) and García-Ferrero and Gómez-Ullate (2015) and proved in Bonneux et al. (2020). If $d(d+1)/2 = 0$, i.e., $d = 0$ or -1, then zero is not a root of $W_\Lambda(z)$.
3. The polynomial $W_\Lambda(z)$ can be factored as $W_\Lambda(z) = z^{d(d+1)/2} f(\zeta)$, where d is given in Eq. (5.88), $\zeta \equiv z^2$, and $f(\zeta)$ is a polynomial of ζ with real coefficients and a nonzero constant term (Bonneux et al. 2020).
4. If z_0 is a root of $W_\Lambda(z)$, so are $-z_0$, z_0^* and $-z_0^*$. This quartet root symmetry can be seen from the above factorization of $W_\Lambda(z)$ and the fact that the coefficients of the polynomial $W_\Lambda(z)$ are real. As a consequence of this quartet symmetry, the root structure of $W_\Lambda(z)$ is non-triangular. This contrasts Yablonskii–Vorob'ev polynomials, which feature triangular root structures.
5. The polynomial $W_\Lambda(z)$ has only zero roots if and only if $(n_1, n_2, \ldots, n_N) = (1, 3, 5, \cdots, 2N-1)$ (Yang and Yang 2022b).

On roots of Wronskian-Hermite polynomials, beside the above facts, it has also been conjectured that all roots of every Wronskian-Hermite polynomial $W_\Lambda(z)$ are simple, except possibly the zero root (Felder et al. 2012). If this conjecture holds, then the number of nonzero roots in $W_\Lambda(z)$ would be

$$N_W = \rho - \frac{d(d+1)}{2}, \tag{5.89}$$

where ρ is the degree of polynomial $W_\Lambda(z)$ given in Eq. (5.87).

To illustrate root structures of Wronskian-Hermite polynomials, we choose two index vectors

$$\Lambda_1 = (2, 3, 4, 5), \quad \Lambda_2 = (3, 4, 5, 7, 9). \tag{5.90}$$

For Λ_1, $d = 2 - 2 = 0$, and thus zero is not a root of $W_{\Lambda_1}(z)$ according to the second fact in the earlier text. For Λ_2, $d = 4 - 1 = 3$, and thus zero is a root of

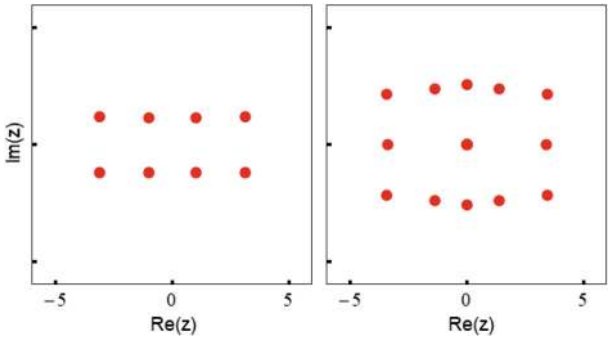

Fig. 5.13 Root structures of Wronskian-Hermite polynomials $W_{\Lambda_1}(z)$ (left) and $W_{\Lambda_2}(z)$ (right) in the complex plane z, where index vectors Λ_1 and Λ_2 are given in Eq. (5.90)

multiplicity six in $W_{\Lambda_2}(z)$. Indeed, the full expressions of these two polynomials are

$$W_{\Lambda_1}(z) = \frac{z^8 - 16z^6 + 120z^4 + 720}{2880},$$
$$W_{\Lambda_2}(z) = -\frac{z^6\left(z^{12} - 12z^{10} + 180z^8 + 672z^6 - 7056z^4 - 181440z^2 - 1270080\right)}{2743372800},$$

where we can clearly see zero is not a root of $W_{\Lambda_1}(z)$ and is a root of multiplicity six in $W_{\Lambda_2}(z)$. Full root structures of these two polynomials are plotted in Fig. 5.13. It is seen that for the first polynomial, its root structure is rectangular (it is not an exact rectangle, but close). For the second polynomial, its root structure is quasi-rectangular with a zero root in the center. All nonzero roots in these two polynomials are simple.

5.4.3 *Large-Time Patterns of Higher-Order Lumps*

Now, we consider patterns of higher-order lumps at large times. In this study, we will set $n_1 < n_2 < \cdots < n_N$ and $p = 1$ without loss of generality (Yang and Yang 2022b). In this case, the constant factor in Eq. (5.79) simplifies to $1/4^{\nu}$.

It turns out that pattern analysis of lumps depends on whether vector elements $a_{i,j}$ of internal parameters $\{\boldsymbol{a}_i\}$ depend on the i index. Here, we only consider the case where $a_{i,j}$ is independent of the i index. In this case, since the length of vector $\boldsymbol{a}_i$ is n_i, and $n_1 < n_2 < \cdots < n_N$, then, each $\boldsymbol{a}_i$ for $i < N$ is just a truncation of the longest vector $\boldsymbol{a}_N$. Since every $\boldsymbol{a}_i$ can be extended to the full $\boldsymbol{a}_N$, and the extended parts are dummy parameters which do not appear in the actual solution formulae, by performing this $\boldsymbol{a}_i$ extension, we can say all $\{\boldsymbol{a}_i\}$ vectors are the same in this case and thus denote $\boldsymbol{a}_i = \boldsymbol{a}$. The first element a_1 of $\boldsymbol{a}$ can be further absorbed into (x, y) through a coordinate shift of

$$x + \Re(a_1) \to x, \quad y + \frac{1}{2}\Im(a_1) \to y, \tag{5.91}$$

where $\Re$ and $\Im$ represent the real and imaginary parts of a complex number. Then, our parameter choices will be

$$\boldsymbol{a}_i = \boldsymbol{a} = (0, a_2, a_3, \cdots). \tag{5.92}$$

Under these parameters, our theorem on patterns of higher-order lumps at large times is stated below (Yang and Yang 2022b).

Theorem 5.6 *For $|t| \gg 1$, the following asymptotics on the higher-order lump solution $u_\Lambda(x, y, t)$ holds.*

1. *If $W_\Lambda(z)$ has nonzero roots that are all simple, then there will be an outer region that is $O\left(|t|^{1/2}\right)$ away from the wave center of $(x, y) = (12t, 0)$, or $\sqrt{(x-12t)^2 + y^2} = O\left(|t|^{1/2}\right)$. In this outer region, the higher-order lump $u_\Lambda(x, y, t)$ asymptotically separates into N_W fundamental lumps $u_1(x - x_0, y - y_0, t)$, where N_W is given in Eq. (5.89), $u_1(x, y, t)$ is given in Eq. (5.83), the lump positions (x_0, y_0) are given by*

$$x_0 = \Re\left(z_0(-12t)^{1/2}\right) - \Re(\Delta), \quad y_0 = \frac{\Im\left(z_0(-12t)^{1/2}\right)}{2} - \frac{\Im(\Delta)}{2}, \tag{5.93}$$

z_0 is each of the N_W nonzero simple roots of $W_\Lambda(z)$, and $\Delta = \Delta(\Lambda, z_0)$ is an $O(1)$ complex constant given by

$$\begin{aligned}\Delta = \frac{1}{W'_\Lambda(z_0)} \Bigg\{ & \lambda \sum_{j=1}^{N} \det_{1\le i\le N} \left(q_{n_i}, \cdots, q_{n_i-(j-2)},\right. \\ & \left. q_{n_i-(j-1)-2}, q_{n_i-j}, \cdots, q_{n_i-(N-1)}\right)_{z=z_0} \\ & + \frac{4}{3} \sum_{j=1}^{N} \det_{1\le i\le N} \left(q_{n_i}, \cdots, q_{n_i-(j-2)}, q_{n_i-(j-1)-3},\right. \\ & \left. q_{n_i-j}, \cdots, q_{n_i-(N-1)}\right)_{z=z_0} \Bigg\}, \end{aligned} \tag{5.94}$$

and

$$\lambda = \begin{cases} \frac{1}{2}\Re(z_0) + \mathrm{i}\Im(z_0), & \text{when } t < 0, \\ \Re(z_0) + \frac{1}{2}\mathrm{i}\Im(z_0), & \text{when } t > 0. \end{cases} \tag{5.95}$$

The absolute error of this fundamental-lump approximation is $O(|t|^{-1/2})$. Expressed mathematically, when (x, y) is in the neighborhood of each of these outer fundamental lumps, i.e., $(x - 12t - x_0)^2 + (y - y_0)^2 = O(1)$ with (x_0, y_0)

given in (5.93), we have the following solution asymptotics

$$u_{\Lambda}(x, y, t) = u_1(x - x_0,\ y - y_0, t) + O\left(|t|^{-1/2}\right), \quad |t| \gg 1. \tag{5.96}$$

2. *If $W_{\Lambda}(z)$ has a zero root, i.e., $d \neq 0$ and $d \neq -1$, where d is as defined in Eq. (5.88), then there will be an inner region that is within $O(|t|^{1/3})$ of the wave center $(x, y) = (12t, 0)$, or $\sqrt{(x-12t)^2 + y^2} \leq O\left(|t|^{1/3}\right)$. In this inner region lies $d(d+1)/2$ fundamental lumps $u_1(x - x_0,\ y - y_0, t)$, where $u_1(x, y, t)$ is given in Eq. (5.83), the lump positions (x_0, y_0) are given by*

$$x_0 = \Re(z_0)\,(12t)^{1/3} - \Re(\hat{\Delta}), \quad y_0 = \frac{\Im(z_0)}{2}(12t)^{1/3} - \frac{1}{2}\Im(\hat{\Delta}), \tag{5.97}$$

z_0 is each of the $d(d+1)/2$ simple roots of the Yablonskii–Vorob'ev polynomial $Q_{\hat{d}}(z)$, with $\hat{d}$ defined as

$$\hat{d} = \begin{cases} d, & \text{when } d \geq 0, \\ |d| - 1, & \text{when } d \leq -1, \end{cases} \tag{5.98}$$

and $\hat{\Delta} = \hat{\Delta}(\Lambda, z_0)$ is an $O(1)$ complex constant whose expression can be found in Yang and Yang (2022b). The absolute error of this fundamental-lump approximation is $O(|t|^{-1/3})$ when $z_0 \neq 0$ and $O(t^{-1})$ when zero is a root of $Q_{\hat{d}}(z)$ and $z_0 = 0$. Expressed mathematically, when (x, y) is in the neighborhood of each of these inner fundamental lumps, i.e., $(x - 12t - x_0)^2 + (y - y_0)^2 = O(1)$, with (x_0, y_0) given in (5.97), we have the following solution asymptotics for $|t| \gg 1$,

$$u_{\Lambda}(x, y, t) = \begin{cases} u_1(x - x_0,\ y - y_0, t) + O\left(|t|^{-1/3}\right), & \text{if } z_0 \neq 0, \\ u_1(x - x_0,\ y - y_0, t) + O\left(t^{-1}\right), & \text{if } z_0 = 0. \end{cases} \tag{5.99}$$

3. *When (x, y) is not in the neighborhood of any of the above fundamental lumps specified by Eqs. (5.93) and (5.97) in the (x, y) plane, including when (x, y) is between the outer and inner regions, $u_{\Lambda}(x, y, t)$ asymptotically approaches zero as $|t| \to \infty$.*

Now, we explain what Theorem 5.6 says regarding solution patterns at large times. The theorem indicates that, the whole wave field is generically split up into two regions featuring different patterns.

1. The outer region is the region that is $O(|t|^{1/2})$ away from the wave center $(x, y) = (12t, 0)$. This region would exist if $W_{\Lambda}(z)$ has nonzero roots, i.e., when $\Lambda \neq (1, 3, 5, \ldots, 2N - 1)$. In this region, there are N_W well-separated fundamental lumps. Relative to the moving frame of x-direction velocity 12, positions (x_0, y_0) of these fundamental lumps, to the leading order of large time, are just a linear transformation of $W_{\Lambda}(z)$'s nonzero-root structure. When t is

large negative, these fundamental-lump positions to the leading order are

$$\begin{pmatrix} x_0^- \\ y_0^- \end{pmatrix} = (12|t|)^{1/2} \begin{pmatrix} 1 & 0 \\ 0 & \frac{1}{2} \end{pmatrix} \begin{pmatrix} \Re(z_0) \\ \Im(z_0) \end{pmatrix}, \tag{5.100}$$

where z_0 is any nonzero root of $W_\Lambda(z)$. However, when t is large positive, these lump positions become

$$\begin{pmatrix} x_0^+ \\ y_0^+ \end{pmatrix} = (12|t|)^{1/2} \begin{pmatrix} 0 & -1 \\ \frac{1}{2} & 0 \end{pmatrix} \begin{pmatrix} \Re(z_0) \\ \Im(z_0) \end{pmatrix}. \tag{5.101}$$

In the former case, the wave pattern formed by these fundamental lumps is simply a stretching of the Wronskian-Hermite nonzero-root structure along both horizontal and vertical directions. But in the latter case, on top of this stretching, the horizontal and vertical directions are also swapped. In both cases, the resulting wave patterns from transformations (5.100)–(5.101) are non-triangular since the root structure of $W_\Lambda(z)$ is non-triangular.

From the above two transformations, we see that fundamental lumps at large negative time $-t$ and large positive time $+t$ in the outer region are related as

$$\begin{pmatrix} x_0^+ \\ y_0^+ \end{pmatrix} = \begin{pmatrix} 0 & -2 \\ \frac{1}{2} & 0 \end{pmatrix} \begin{pmatrix} x_0^- \\ y_0^- \end{pmatrix}. \tag{5.102}$$

Thus, when time goes from large negative to large positive, outer-region lump patterns in the (x, y) plane have swapped horizontal and vertical directions. In addition, stretching of different amounts has also occurred along the two directions. For certain single-line patterns of fundamental lumps, a change from a vertical line to a horizontal line in the (x, y) plane has been graphically reported in Chen et al. (2016) and analytically explained in Chang (2018). Here, we proved this fact for the general case.

In this outer region, fundamental lumps separate from each other in proportion to $|t|^{1/2}$ at large time.

2. The inner region is the region that is within $O(|t|^{1/3})$ of the wave center $(x, y) = (12t, 0)$. This region would exist if $W_\Lambda(z)$ has a zero root, whose multiplicity is necessarily a triangular number of the form $d(d+1)/2$ for an integer d defined in Eq. (5.88) that is not 0 and -1. In this inner region, the solution $u_\Lambda(x, y, t)$ at large time would comprise $d(d+1)/2$ well-separated fundamental lumps. Relative to the moving frame of x-direction velocity 12, positions (x_0, y_0) of these fundamental lumps, to the leading order of large time, are just a linear transformation of $Q_{\hat{d}}(z)$'s root structure, i.e.,

$$\begin{pmatrix} x_0 \\ y_0 \end{pmatrix} = (12t)^{1/3} \begin{pmatrix} 1 & 0 \\ 0 & \frac{1}{2} \end{pmatrix} \begin{pmatrix} \Re(z_0) \\ \Im(z_0) \end{pmatrix}, \tag{5.103}$$

where $\hat{d}$ is defined in Eq. (5.98), and z_0 is each of the $d(d+1)/2$ simple roots of $Q_{\hat{d}}(z)$. The reader is reminded that $\hat{d}(\hat{d}+1)/2 = d(d+1)/2$. Thus, the pattern of these $d(d+1)/2$ fundamental lumps in the inner region at large time is a simple stretching of $Q_{\hat{d}}(z)$'s root structure, which is triangular if $\hat{d} > 1$. In addition, as time evolves from large negative to large positive, these triangular lump patterns would reverse direction along the x-axis. Furthermore, fundamental lumps in this inner region separate from each other in proportion to $|t|^{1/3}$ at large time.

The above results reveal that, the pattern of the solution $u_{\Lambda}(x, y, t)$ at large time generically comprises an outer region featuring the non-triangular shape of the stretched nonzero-root structure of the Wronskian-Hermite polynomial $W_{\Lambda}(z)$, and an inner region featuring the triangular shape of the stretched root structure of the Yablonskii–Vorob'ev polynomial $Q_{\hat{d}}(z)$. As time changes from large negative to large positive, the outer pattern swaps horizontal and vertical directions with certain stretching, while the inner pattern reverses the horizontal direction. These different types of pattern transformations in the outer and inner regions of the same solution are fascinating.

When $\Lambda = (1, 3, 5, \ldots, 2N-1)$, the outer pattern disappears. When $d = 0$ or -1, the inner region disappears. In other situations, both regions would arise.

Ablowitz et al. (2000) reported that at large time, fundamental lumps in the higher-order lump complex separate from each other in proportion to $|t|^q$, where $\frac{1}{3} \le q \le \frac{1}{2}$. Our results indicate that when $\boldsymbol{a}_i = \boldsymbol{a}$, this q value can only be $1/3$ or $1/2$, nothing in between.

5.4.4 Comparison Between True Lump Patterns and Analytical Predictions

Next, we compare our analytical predictions of lump patterns with true solutions. As an example, we choose $N = 5$ and $\Lambda = (3, 4, 5, 7, 9)$. In this case, $d = 3$, and thus zero is a root of multiplicity six in $W_{\Lambda}(z)$, and the inner region is present. Since $\Lambda \neq (1, 3, 5, \ldots, 2N-1)$, the outer region exists as well.

Root structure of the corresponding Wronskian-Hermite polynomial has been displayed in Fig. 5.13 (right panel). It is seen that this $W_{\Lambda}(z)$ admits 12 simple nonzero roots which form a quasi-rectangular shape, plus the zero root of multiplicity six at the center of the quasi-rectangle. Using formula (5.94), we find that for these twelve nonzero roots z_0 of $W_{\Lambda}(z)$ in the right panel of Fig. 5.13, from the left to right,

$$\begin{aligned}\Delta(\Lambda, z_0) \approx\ & -3.9717 \pm 0.4315\mathrm{i}, -3.6158, -2.0475 \pm 1.0544\mathrm{i}, -0.6449, \\ & -0.6449, -2.0475 \pm 1.0544\mathrm{i}, -3.6158, -3.9717 \pm 0.4315\mathrm{i}\end{aligned}$$

when $t > 0$, and

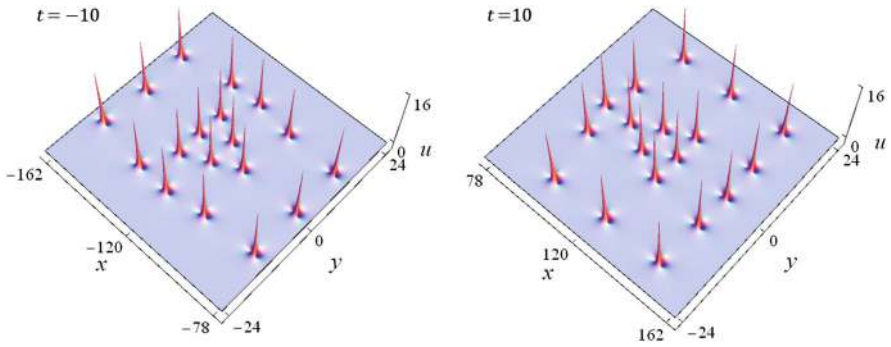

Fig. 5.14 Predicted solutions $u_{\Lambda}(x, y, t)$ with $\Lambda = (3, 4, 5, 7, 9)$ at time values of $t = -10$ (left) and $t = 10$ (right) in the KP-I equation

$$\Delta(\Lambda, z_0) \approx 0.1826 \pm 0.4315\mathrm{i}, -0.6956, -0.1160 \pm 1.0544\mathrm{i}, 1.0043,$$
$$1.0043, -0.1160 \pm 1.0544\mathrm{i}, -0.6956, 0.1826 \pm 0.4315\mathrm{i}$$

when $t < 0$. Since these Δ values are different for different roots, outer lumps would experience different amounts of $O(1)$ position shifts according to formula (5.93).

The zero root of multiplicity six in $W_{\Lambda}(z)$ gives rise to an inner region of six fundamental lumps, whose positions are predicted by the roots of $Q_3(z)$ from Eq. (5.97). Here, we find from $\hat{\Delta}$'s formula in Yang and Yang (2022b) that

$$\hat{\Delta} = 8/7,$$

which is independent of the root z_0 of $Q_3(z)$. Since this $\hat{\Delta}$ value is the same for all six roots of $Q_3(z)$, the six lumps in the inner region would experience the same amount of $O(1)$ position shift from formula (5.97).

Using the nonzero roots of $W_{\Lambda}(z)$ and roots of $Q_3(z)$, together with the above Δ and $\hat{\Delta}$ values, we can predict fundamental-lump locations from formulae (5.93) and (5.97) of Theorem 5.6, for the outer and inner regions, respectively. From that, we can draw the predicted solution in the (x, y) plane at any large time. When $t = \pm 10$, these predicted solutions are plotted in the left and right panels of Fig. 5.14, respectively. The predicted patterns contain twelve fundamental lumps which form a quasi-rectangular pattern in the outer region of the (x, y) plane, plus six fundamental lumps which form a triangle in the inner region. At $t = -10$, the outer lump pattern is roughly a stretching of $W_{\Lambda}(z)$'s nonzero-root structure, while the inner lump pattern is a stretching of $Q_3(z)$'s root structure. At $t = 10$, however, the predicted outer lump pattern has swapped its (x, y) axes from the $t = -10$ state [plus additional (x, y)-direction stretching], while the predicted inner triangular lump pattern has reversed its direction along the x-axis.

To confirm these asymptotic predictions, we plot in Fig. 5.15 the corresponding true solutions $u_{\Lambda}(x, y, t)$ at six time values of $t = -10, -2, -0.2, 0, 2$ and 10.

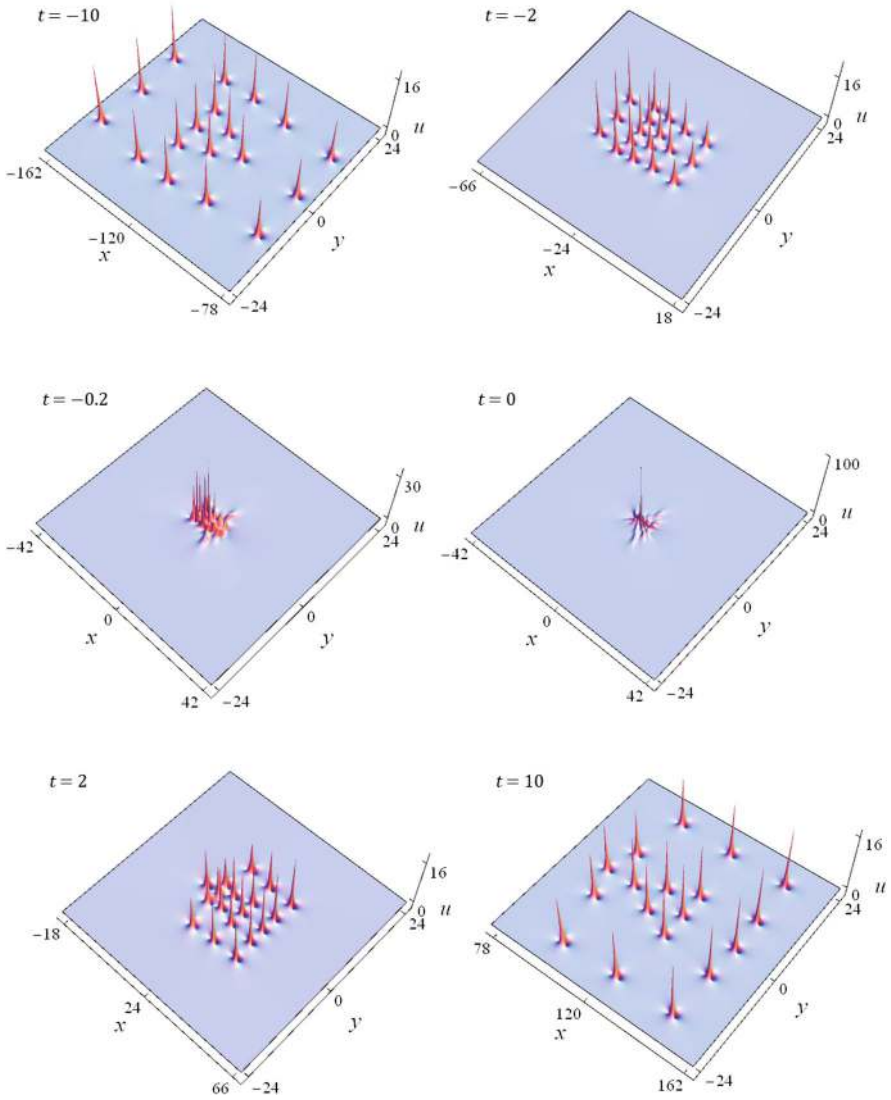

Fig. 5.15 True solutions $u_{\Lambda}(x, y, t)$ with $\Lambda = (3, 4, 5, 7, 9)$ and $\boldsymbol{a} = (0, 0, 0, 0, 0, 0, 0, 0, 0)$, at various times whose values are shown inside the panels

In these true solutions, we have selected all-zero internal parameters of $\boldsymbol{a} = (0, 0, 0, 0, 0, 0, 0, 0, 0)$. It is seen that at large times of $t = \pm 10$, the true solutions closely resemble our predictions in the previous figure. Specifically, the true solutions at these large times also split into outer and inner regions, with outer

patterns quasi-rectangular and inner patterns triangular; and as time changes from $t = -10$ to $t = 10$, the outer pattern swaps its (x, y) orientations, while the inner pattern reverses in x-direction. All these features of the true solution match exactly our predictions in Fig. 5.14.

True solution graphs at intermediate time values in Fig. 5.15 reveal how these striking pattern transformations in outer and inner regions take place. It is seen that all fundamental lumps in the inner and outer regions at large negative time first move toward each other. Then they merge and coalesce at $t \approx 0$. Afterwards, all these fundamental lumps re-emerge and move away from each other, but not returning to their pre-merging state. Instead, the quasi-rectangular outer lumps have swapped their x and y directions, and the triangular inner lumps have reversed the x-direction. These pattern transformations are visually miraculous and mysterious. But due to our Theorem 5.6, they can now be completely understood from a mathematical point of view.

Error decay rates in the outer and inner regions as predicted in Theorem 5.6 have also been numerically verified. See Yang and Yang (2022b) for details.

References

M.J. Ablowitz, P.A. Clarkson, *Solitons, Nonlinear Evolution Equations and Inverse Scattering* (Cambridge University Press, Cambridge, 1991)

M.J. Ablowitz, J.T. Cole, Transverse instability of rogue waves. Phys. Rev. Lett. **127**, 104101 (2021)

M.J. Ablowitz, J.F. Ladik, A nonlinear difference scheme and inverse scattering. Stud. Appl. Math. **55**, 213 (1976)

M.J. Ablowitz, Z.H. Musslimani, Integrable nonlocal nonlinear Schrödinger equation. Phys. Rev. Lett. **110**, 064105 (2013)

M.J. Ablowitz, Z.H. Musslimani, Inverse scattering transform for the integrable nonlocal nonlinear Schrödinger equation. Nonlinearity **29**, 915 (2016)

M.J. Ablowitz, H. Segur, On the evolution of packets of water waves. J. Fluid Mech. **92**, 691 (1979)

M.J. Ablowitz, H. Segur, *Solitons and the Inverse Scattering Transform* (SIAM, Philadelphia, 1981)

M.J. Ablowitz, J. Villarroel, Solutions to the time dependent Schrödinger and the Kadomtsev-Petviashvili equations. Phys. Rev. Lett. **78**, 570 (1997)

M.J. Ablowitz, S. Chakravarty, A.D. Trubatch, J. Villarroel, A novel class of solutions of the non-stationary Schrödinger and the Kadomtsev-Petviashvili I equations. Phys. Lett. A **267**, 132 (2000)

A.B. Aceves, S.Wabnitz, Self-induced transparency solitons in nonlinear refractive periodic media. Phys. Lett. A **141**, 37 (1989)

M. Adler, J. Moser, On a class of polynomials associated with the Korteweg de Vries equation. Commun. Math. Phys. **61**, 1 (1978)

D.S. Agafontsev, V.E. Zakharov, Integrable turbulence generated from modulational instability of cnoidal waves. Nonlinearity **29**, 3551 (2016)

G.P. Agrawal, *Nonlinear Fiber Optics*, 3rd edn. (Academic Press, San Diego, 2001)

N. Akhmediev, V.I. Korneev, Modulation instability and periodic solutions of the nonlinear Schrödinger equation. Theor. Math. Phys. **69**, 1089 (1986)

N. Akhmediev, A. Ankiewicz, J.M. Soto-Crespo, Rogue waves and rational solutions of the nonlinear Schrödinger equation. Phys. Rev. E **80**, 026601 (2009a)

N. Akhmediev, A. Ankiewicz, M. Taki, Waves that appear from nowhere and disappear without a trace. Phys. Lett. A **373**, 675 (2009b)

H. Alfvén, Existence of electromagnetic-hydrodynamic waves. Nature **150**, 405 (1942)

P.A. Altin, G. McDonald, D. Döring, J.E. Debs, T.H. Barter, J.D. Close, N.P. Robins, S.A. Haine, T.M. Hanna, R.P. Anderson, Optically trapped atom interferometry using the clock transition of large ^{87}Rb Bose-Einstein condensates. New J. Phys. **13**, 065020 (2011)

B. Yang, J. Yang, *Rogue Waves in Integrable Systems*,
https://doi.org/10.1007/978-3-031-66793-0

M.H. Anderson, J.R. Ensher, M.R. Matthews, C.E. Wieman, E.A. Cornell, Observation of Bose-Einstein condensation in a dilute atomic vapor. Science **269**, 198 (1995)
A. Ankiewicz, N. Akhmediev, J.M. Soto-Crespo, Discrete rogue waves of the Ablowitz-Ladik and Hirota equations. Phys. Rev. E **82**, 026602 (2010a)
A. Ankiewicz, J.M. Soto-Crespo, N. Akhmediev, Rogue waves and rational solutions of the Hirota equation. Phys. Rev. E **81**, 046602 (2010b)
A. Ankiewicz, D.J. Kedziora, N. Akhmediev, Rogue wave triplets. Phys. Lett. A **375**, 2782 (2011)
H. Aref, Vortices and polynomials. Fluid Dynam. Res. **39**, 5 (2007)
H. Bailung, Y. Nakamura, Observation of modulational instability in a multi-component plasma with negative ions. J. Plasma Phys. **50**, 231 (1993)
H. Bailung, S.K. Sharma, Y. Nakamura, Observation of Peregrine solitons in a multicomponent plasma with negative ions. Phys. Rev. Lett. **107**, 255005 (2011)
B. Bakkali-Hassani, C. Maury, Y.Q. Zou, É. Le Cerf, R. Saint-Jalm, P.C.M. Castilho, S. Nascimbene, J. Dalibard, J. Beugnon, Realization of a Townes soliton in a two-component planar Bose gas. Phys. Rev. Lett. **127**, 023603 (2021)
F. Balogh, M. Bertola, T. Bothner, Hankel determinant approach to generalized Vorob'ev-Yablonski polynomials and their roots. Constr. Approx. **44**, 417 (2016)
U. Bandelow, N. Akhmediev, Sasa-Satsuma equation: Soliton on a background and its limiting cases. Phys. Rev. E **86**, 026606 (2012)
P.P. Banerjee, A. Korpel, Subharmonic generation by resonant three-wave interaction of deep-water capillary waves. Phys. Fluids **25**, 1938 (1982)
I.V. Barashenkov, V.G. Makhankov, Soliton-like bubbles in the system of interacting bosons. Phys. Lett. A **128**, 52 (1988)
F. Baronio, A. Degasperis, M. Conforti, S. Wabnitz, Solutions of the vector nonlinear Schrödinger equations: evidence for deterministic rogue waves. Phys. Rev. Lett. **109**, 044102 (2012)
F. Baronio, M. Conforti, A. Degasperis, S. Lombardo, Rogue waves emerging from the resonant interaction of three waves. Phys. Rev. Lett. **111**, 114101 (2013)
F. Baronio, M. Conforti, A. Degasperis, S. Lombardo, M. Onorato, S. Wabnitz, Vector rogue waves and baseband modulation instability in the defocusing regime. Phys. Rev. Lett. **113**, 034101 (2014)
F. Baronio, B. Frisquet, S. Chen, G. Millot, S. Wabnitz, B. Kibler, Observation of a group of dark rogue waves in a telecommunication optical fiber. Phys. Rev. A **97**, 013852 (2018)
T.B. Benjamin, Instability of periodic wavetrains in nonlinear dispersive systems. Proc. R. Soc. Lond. A **299**, 59 (1967)
T.B. Benjamin, J.E. Feir, The disintegration of wave trains on deep water Part 1. Theory. J. Fluid Mech. **27**, 417 (1967)
D.J. Benney, A general theory for interactions between short and long waves. Stud. Appl. Math. **56**, 81 (1977)
D.J. Benney, A.C. Newell, Nonlinear wave envelopes. J. Math. Phys. **46**, 133 (1967)
D.J. Benney, G.J. Roskes, Wave instabilities. Stud. Appl. Math. **48**, 377 (1969)
M. Bertola, G.A. El, A. Tovbis, Rogue waves in multiphase solutions of the focusing nonlinear Schrödinger equation. Proc. R. Soc. A **472**, 20160340 (2016)
M. Bertola, A. Tovbis, Maximal amplitudes of finite-gap solutions for the focusing nonlinear Schrödinger equation. Commun. Math. Phys. **354**, 525 (2017)
D. Bian, B.L. Guo, L.M. Ling, High-order soliton solution of Landau-Lifshitz equation. Stud. Appl. Math. **134**, 181 (2015)
D. Bilman, P.D. Miller, A robust inverse scattering transform for the focusing nonlinear Schrödinger equation. Commun. Pure Appl. Math. **72**, 1722 (2019)
D. Bilman, L.M. Ling, P.D. Miller, Extreme superposition: Rogue waves of infinite order and the Painlevé-III hierarchy. Duke Math. J. **169**, 671 (2020)
N. Bonneux, C. Dunning, M. Stevens, Coefficients of Wronskian Hermite polynomials. Stud. Appl. Math. **144**, 245 (2020)
J. Boussinesq, Theorie de I'intumescence Liquid, Appleteonde Solitaire au de Translation, se Propageantdansun Canal Rectangulaire. Comptes Rendus **72**, 755 (1871)

J. Boussinesq, Théorie des ondes et des remous qui se propagent le long d'un canal rectangulaire horizontal, en communiquant au liquide contenu dans ce canal des vitesses sensiblement pareilles de la surface au fond. J. Pure Appl. **17**, 55 (1872)
R.W. Boyd, *Nonlinear Optics*, 3rd edn. (Academic Press, San Diego, 2008)
R.J. Buckingham, P.D. Miller, Large-degree asymptotics of rational Painlevé-II functions: noncritical behaviour. Nonlinearity **27**, 2489 (2014)
R.A. Cairns, The role of negative energy waves in some instabilities of parallel flows. J. Fluid Mech. **92**, 1 (1979)
A. Calini, C.M. Schober, Characterizing JONSWAP rogue waves and their statistics via inverse spectral data. Wave Motion **71**, 5 (2017)
A. Calini, C.M. Schober, M. Strawn, Linear instability of the Peregrine breather: numerical and analytical investigations. Appl. Numer. Math. **141**, 36 (2019)
K.M. Case, S.C. Chiu, Three-wave resonant interactions of gravity-capillary waves. Phys. Fluids **20**, 742 (1977)
A. Chabchoub, N. Akhmediev, Observation of rogue wave triplets in water waves. Phys. Lett. A **377**, 2590 (2013)
A. Chabchoub, R. Grimshaw, The hydrodynamic nonlinear Schrödinger equation: space and time. Fluids **1**, 23 (2016)
A. Chabchoub, N. Hoffmann, N. Akhmediev, Rogue wave observation in a water wave tank. Phys. Rev. Lett. **106**, 204502 (2011)
A. Chabchoub, N. Hoffmann, M. Onorato, N. Akhmediev, Super rogue waves: observation of a higher-order breather in water waves. Phys. Rev. X **2**, 011015 (2012a)
A. Chabchoub, N. Hoffmann, M. Onorato, A. Slunyaev, A. Sergeeva, E. Pelinovsky, N. Akhmediev, Observation of a hierarchy of up to fifth-order rogue waves in a water tank. Phys. Rev. E **86**, 056601 (2012b)
H.N. Chan, K.W. Chow, Rogue waves for an alternative system of coupled Hirota equations: structural robustness and modulation instabilities. Stud. Appl. Math. **139**, 78 (2017)
H.N. Chan, K.W. Chow, D.J. Kedziora, R. Grimshaw, E. Ding, Rogue wave modes for a derivative nonlinear Schrödinger model. Phys. Rev. E **89**, 032914 (2014)
J.H. Chang, Asymptotic analysis of multilump solutions of the Kadomtsev-Petviashvili-I equation. Theor. Math. Phys. **195**, 676 (2018)
S. Chen, Twisted rogue-wave pairs in the Sasa-Satsuma equation. Phys. Rev. E **88**, 023202 (2013)
S. Chen, Darboux transformation and dark rogue wave states arising from two-wave resonance interaction. Phys. Lett. A **378**, 1095 (2014)
S. Chen, D. Mihalache, Vector rogue waves in the Manakov system: diversity and compossibility. J. Phys. A **48**, 215202 (2015)
J. Chen, D. Pelinovsky, Rogue periodic waves of the focusing nonlinear Schrödinger equation. Proc. R. Soc. A **474**, 20170814 (2018)
H.H. Chen, Y.C. Lee, C.S. Liu, Integrability of nonlinear Hamiltonian systems by inverse scattering method. Phys. Scr. **20**, 490 (1979)
Z. Chen, M. Segev, T.H. Coskun, D.N. Christodoulides, Y.S. Kivshar, Coupled photorefractive spatial-soliton pairs. J. Opt. Soc. Am. B **14**, 3066 (1997)
S. Chen, P. Grelu, J.M. Soto-Crespo, Dark- and bright-rogue-wave solutions for media with long-wave-short-wave resonance. Phys. Rev. E **89**, 011201 (2014a)
S. Chen, J.M. Soto-Crespo, P. Grelu, Dark three-sister rogue waves in normally dispersive optical fibers with random birefringence. Opt. Express **22**, 27632 (2014b)
S. Chen, J.M. Soto-Crespo, P. Grelu, Watch-hand-like optical rogue waves in three-wave interactions. Optics Express **23**, 349 (2015)
S. Chen, P. Grelu, D. Mihalache, F. Baronio, Families of rational soliton solutions of the Kadomtsev-Petviashvili I equation. Rom. Rep. Phys. **68**, 1407 (2016)
J. Chen, Y. Chen, B.F. Feng, K. Maruno, Y. Ohta, General high-order rogue waves of the (1+1)-dimensional Yajima-Oikawa system. J. Phys. Soc. Jpn. **87**, 094007 (2018a)
J. Chen, B.F. Feng, K. Maruno, Y. Ohta, The derivative Yajima-Oikawa system: bright, dark soliton and breather solutions. Stud. Appl. Math. **141**, 145 (2018b)

S. Chen, Y. Zhou, L. Bu, F. Baronio, J.M. Soto-Crespo, D. Mihalache, Super chirped rogue waves in optical fibers. Opt. Express **27**, 11370 (2019)
J. Chen, B. Yang, B.F. Feng, Rogue waves in the massive Thirring model. Stud. Appl. Math. **151**, 1020 (2023)
K.W. Chow, H.N. Chan, D.J. Kedziora, R. Grimshaw, Rogue wave modes for the long wave short wave resonance model. J. Phys. Soc. Jpn. **82**, 074001 (2013)
A. Chowdhury, J.A. Tataronis, Long wave short wave resonance in nonlinear negative refractive index media. Phys. Rev. Lett. **100**, 153905 (2008)
D.N. Christodoulides, R.I. Joseph, Discrete self-focusing in nonlinear arrays of coupled waveguides. Opt. Lett. **13**, 794 (1988)
D.N. Christodoulides, R.I. Joseph, Slow bragg solitons in nonlinear periodic structures. Phys. Rev. Lett. **62**, 1746 (1989)
P.A. Clarkson, The fourth Painlevé equation and associated special polynomials. J. Math. Phys. **44**, 5350 (2003)
P.A. Clarkson, Special polynomials associated with rational solutions of the defocusing nonlinear Schrödinger equation and the fourth Painlevé equation. Eur. J. Appl. Math. **17**, 293 (2006)
P.A. Clarkson, Vortices and polynomials. Stud. Appl. Math. **123**, 37 (2009)
P.A. Clarkson, C.M. Cosgrove, Painlevé analysis of the nonlinear Schrödinger family of equations. J. Phys. A **20**, 2003 (1987)
P.A. Clarkson, E. Dowie, Rational solutions of the Boussinesq equation and applications to rogue waves. Trans. Math. Appl. **1**, 1 (2017)
P.A. Clarkson, E.L. Mansfield, The second Painlevé equation, its hierarchy and associated special polynomials. Nonlinearity **16**, R1 (2003)
A.D. Craik, *Wave Interactions and Fluid Flows* (Cambridge University Press, Cambridge, 1985)
A.D. Craik, J.A. Adam, Explosive resonant wave interactions in a three-layer fluid flow. J. Fluid Mech. **92**, 15 (1979)
J. Cuevas-Maraver, P.G. Kevrekidis, D.J. Frantzeskakis, N.I. Karachalios, M. Haragus, G. James, Floquet analysis of Kuznetsov-Ma breathers: A path towards spectral stability of rogue waves. Phys. Rev. E **96**, 012202 (2017)
A. Davey, K. Stewartson, On three-dimensional packets of surface waves. Proc. R. Soc. Lond. A. **338**, 101 (1974)
B.C. Davidson, *Methods in Nonlinear Plasma Theory* (Academic Press, New York, 1972)
K.B. Davis, M.O. Mewes, M.R. Andrews, N.J. van Druten, D.S. Durfee, D.M. Kurn, W. Ketterle, Bose-Einstein condensation in a gas of sodium atoms. Phys. Rev. Lett. **75**, 3969 (1995)
A. Degasperis, Darboux polynomial matrices: the classical massive Thirring model as a study case. J. Phys. A **48**, 235204 (2015)
A. Degasperis, S. Lombardo, Rational solitons of wave resonant-interaction models. Phys. Rev. E **88**, 052914 (2013)
A. Degasperis, S. Wabnitz, A.B. Aceves, Bragg grating rogue wave. Phys. Lett. A **379**, 1067 (2015)
V.D. Djordjevic, L.G. Redekopp, On two-dimensional packets of capillary-gravity waves. J. Fluid Mech. **79**, 703 (1977)
P. Dubard, V.B. Matveev, Multi-rogue waves solutions: from the NLS to the KP-I equation. Nonlinearity **26**, R93 (2013)
P. Dubard, P. Gaillard, C. Klein, V.B. Matveev, On multi-rogue wave solutions of the NLS equation and positon solutions of the KdV equation. Eur. Phys. J. Spec. Top. **185**, 247 (2010)
Z. Dutton, C.W. Clark, Effective one-component description of two-component Bose-Einstein condensate dynamics. Phys. Rev. A **71**, 063618 (2005)
K. Dysthe, H.E. Krogstad, P. Müller, Oceanic rogue waves. Annu. Rev. Fluid Mech. **40**, 287 (2008)
B.J. Eggleton, C.M. de Sterke, R.E. Slusher, Bragg solitons in the nonlinear Schrödinger limit: experiment and theory. J. Opt. Soc. Am. B **16**, 587 (1999)
M. Erkintalo, K. Hammani, B. Kibler, C. Finot, N. Akhmediev, J.M. Dudley, G. Genty, Higher-order modulation instability in nonlinear fiber optics. Phys. Rev. Lett. **107**, 253901 (2011)
S.G. Evangelides, L.F. Mollenauer, J.P. Gordon, N.S. Bergano, Polarization multiplexing with solitons. J. Lightwave Technol. **10**, 28 (1992)

G. Felder, A.D. Hemery, A.P. Veselov, Zeros of Wronskians of Hermite polynomials and Young diagrams. Physica D **241**, 2131 (2012)
B.F. Feng, Complex short pulse and coupled complex short pulse equations. Physica D **297**, 62 (2015)
B.F. Feng, K. Maruno, Y. Ohta, Geometric formulation and multi-dark soliton solution to the defocusing complex short pulse equation. Stud. Appl. Math. **138**, 343 (2017)
B.F. Feng, X.D. Luo, M.J. Ablowitz, Z.H. Musslimani, General soliton solution to a nonlocal nonlinear Schrödinger equation with zero and nonzero boundary conditions. Nonlinearity **31**, 5385 (2018)
B.F. Feng, R. Ma, Y. Zhang, General breather and rogue wave solutions to the complex short pulse equation. Physica D **439**, 133360 (2022a)
B.F. Feng, C. Shi, G. Zhang, C. Wu, Higher-order rogue wave solutions of the Sasa-Satsuma equation. J. Phys. A **55**, 235701 (2022b)
P.A. Franken, A.E. Hill, C.W. Peters, G. Weinreich, Generation of optical harmonics. Phys. Rev. Lett. **7**, 118 (1961)
B. Frisquet, B. Kibler, P. Morin, F. Baronio, M. Conforti, G. Millot, S. Wabnitz, Optical dark rogue waves. Sci. Rep. **6**, 20785 (2016)
S. Fukutani, K. Okamoto, H. Umemura, Special polynomials and the Hirota bilinear relations of the second and the fourth Painlevé equations. Nagoya Math. J. **159**, 179 (2000)
M. Funakoshi, M. Oikawa, The resonant interaction between a long internal gravity wave and a surface gravity wave packet. J. Phys. Soc. Jpn. **52**, 1982 (1983)
T.A. Gadzhimuradov, A.M. Agalarov, Towards a gauge-equivalent magnetic structure of the nonlocal nonlinear Schrödinger equation. Phys. Rev. A **93**, 062124 (2016)
M. García-Ferrero, D. Gómez-Ullate, Oscillation theorems for the Wronskian of an arbitrary sequence of eigenfunctions of Schrödinger's equation. Lett. Math. Phys. **105**, 551 (2015)
V.S. Gerdjikov, I. Ivanov, A quadratic pencil of general type and nonlinear evolution equations. II. Hierarchies of Hamiltonian structures. Bulg. J. Phys. **10**, 130 (1983)
V.S. Gerdjikov, A. Saxena, Complete integrability of nonlocal nonlinear Schrödinger equation. J. Math. Phys. **58**, 013502 (2017)
O. Gorbacheva, L. Ostrovsky, Nonlinear vector waves in a mechanical model of a molecular chain. Physica D **8**, 223 (1983)
K.A. Gorshkov, D.E. Pelinovsky, Y.A. Stepanyants, Normal and anomalous scattering, formation and decay of bound states of two-dimensional solitons described by the Kadomtsev-Petviashvili equation. J. Exp. Theor. Phys. **77**, 237 (1993)
R. Grimshaw, The modulation of an internal gravity-wave packet and the resonance with the mean motion. Stud. Appl. Math. **56**, 241 (1977)
E.P. Gross, Structure of a quantized vortex in boson systems. Il Nuovo Cimento **20**, 454 (1961)
B.L. Guo, L.M. Ling, Q.P. Liu, Nonlinear Schrödinger equation: generalized Darboux transformation and rogue wave solutions. Phys. Rev. E **85**, 026607 (2012)
B.L. Guo, L.M. Ling, Q.P. Liu, High-order solutions and generalized Darboux transformations of derivative nonlinear Schrödinger equations. Stud. Appl. Math. **130**, 317 (2013)
L.J. Guo, Y.S. Zhang, S.W. Xu, Z.W. Wu, J.S. He, The higher order rogue wave solutions of the Gerdjikov-Ivanov equation. Phys. Scr. **89**, 035501 (2014)
L. Guo, L.Wang, Y. Cheng, J. He, High-order rogue wave solutions of the classical massive Thirring model equations. Commun. Nonlinear Sci. Numer. Simulat. **52**, 11 (2017)
K. Hammani, B. Kibler, C. Finot, P. Morin, J. Fatome, J.M. Dudley, G. Millot, Peregrine soliton generation and breakup in standard telecommunications fiber. Opt. Lett. **36**, 112 (2011)
A. Hasegawa, Y. Kodama, *Solitons in Fiber Communications* (Clarendon Press, Oxford, 1995)
A. Hasegawa, F. Tappert, Transmission of stationary nonlinear optical pulses in dispersive dielectric fibers. Appl. Phys. Lett. **23**, 142 (1973)
H. Hasimoto, J. Ono, Nonlinear modulation of gravity waves. J. Phys. Soc. Jpn. **33**, 805 (1972)
J.S. He, H.R. Zhang, L.H. Wang, K. Porsezian, A.S. Fokas, Generating mechanism for higher-order rogue waves. Phys. Rev. E **87**, 052914 (2013)

J.S. He, L. Wang, L. Li, K. Porsezian, R. Erdélyi, Few-cycle optical rogue waves: complex modified Korteweg de Vries equation. Phys. Rev. E **89**, 062917 (2014)
A. He, P. Huang, G. Zhang, J. Huang, Revisit of rogue wave solutions in the Yajima-Oikawa system. Nonlinear Dyn. **111**, 9439 (2023)
D.M. Henderson, J.L. Hammack, Experiments on ripple instabilities. Part 1. Resonant triads. J. Fluid Mech. **184**, 15 (1987)
R. Hirota, Exact N-soliton solutions of the wave equation of long waves in shallow-water and in nonlinear lattices. J. Math. Phys. **14**, 810 (1973)
R. Hirota, *The Direct Method in Soliton Theory* (Cambridge University Press, Cambridge, 2004)
M.A. Hoefer, J.J. Chang, C. Hamner, P. Engels, Dark-dark solitons and modulational instability in miscible two-component Bose-Einstein condensates. Phys. Rev. A **84**, 041605(R) (2011)
X. Huang, L.M. Ling, Soliton solutions for the nonlocal nonlinear Schrodinger equation. Eur. Phys. J. Plus **131**, 148 (2016)
E. Infeld, G. Rowlands, *Nonlinear Waves, Solitons and Chaos* (Cambridge University Press, Cambridge, 1990)
M. Jimbo, T. Miwa, Solitons and infinite dimensional Lie algebras. Publ. RIMS, Kyoto Univ. **19**, 943 (1983)
B.B. Kadomtsev, V.I. Petviashvili, On the stability of solitary waves in weakly dispersive media. Sov. Phys. Dokl. **15**, 539 (1970)
K. Kajiwara, Y. Ohta, Determinant structure of the rational solutions for the Painlevé II equation. J. Math. Phys. **37**, 4693 (1996)
K. Kajiwara, Y. Ohta, Determinant structure of the rational solutions for the Painlevé IV equation. J. Phys. A **31**, 2431 (1998)
S. Kakei, N. Sasa, J. Satsuma, Bilinearization of a generalized derivative nonlinear Schrödinger equation. J. Phys. Soc. Jpn. **64**, 1519 (1995)
T. Kakutani, H. Ono, T. Taniuti, C.C. Wei, Reductive perturbation method in nonlinear wave propagation II. Application to hytromagnetic waves in cold plasma. J. Phys. Soc. Jpn. **24**, 1159 (1968)
Y. Kametaka, On poles of the rational solution of the Toda equation of Painlevé-IV type. Proc. Jpn. Acad. A **59**, 453 (1983)
J.U. Kang, G.I. Stegeman, J.S. Aitchison, N. Akhmediev, Observation of Manakov spatial solitons in AlGaAs planar waveguides. Phys. Rev. Lett. **76**, 3699 (1996)
D.J. Kaup, A.C. Newell, An exact solution for a derivative nonlinear Schrödinger equation. J. Math. Phys. **19**, 798 (1978)
D.J. Kaup, A. Reiman, A. Bers, Space-time evolution of nonlinear three-wave interactions. I. Interaction in a homogeneous medium. Rev. Mod. Phys. **51**, 275 (1979)
D.J. Kedziora, A. Ankiewicz, N. Akhmediev, Circular rogue wave clusters. Phys. Rev. E **84**, 056611 (2011)
D.J. Kedziora, A. Ankiewicz, N. Akhmediev, Classifying the hierarchy of nonlinear-Schrödinger-equation rogue-wave solutions. Phys. Rev. E **88**, 013207 (2013)
D.J. Kedziora, A. Ankiewicz, N. Akhmediev, Rogue waves and solitons on a cnoidal background. Eur. Phys. J. Spec. Topics **223**, 43 (2014)
P.G. Kevrekidis, D.J. Frantzeskakis, R. Carretero-Gonzalez, *Emergent Nonlinear Phenomena in Bose-Einstein Condensates: Theory and Experiment* (Springer, Berlin, 2008)
C. Kharif, E. Pelinovsky, A. Slunyaev, *Rogue Waves in the Ocean* (Springer, Berlin, 2009)
B. Kibler, J. Fatome, C. Finot, G. Millot, F. Dias, G. Genty, N. Akhmediev, J.M. Dudley, The Peregrine soliton in nonlinear fibre optics. Nat. Phys. **6**, 790 (2010)
Y.S. Kivshar, Stable vector solitons composed of bright and dark pulses. Opt. Lett. **17**, 1322 (1992)
Y. Kodama, A. Hasegawa, Nonlinear pulse propagation in a monomode dielectric guide. IEEE J. Quantum Electron. **23**, 510 (1987)
V.V. Konotop, J. Yang, D.A. Zezyulin, Nonlinear waves in $\mathcal{PT}$-symmetric systems. Rev. Mod. Phys. **88**, 035002 (2016)
A. Kundu, Landau-Lifshitz and higher-order nonlinear systems gauge generated from nonlinear Schrödinger-type equations. J. Math. Phys. **25**, 3433 (1984)

E.A. Kuznetsov, A.V. Mikhailov, On the completely integrability of the two-dimensional classical Thirring model. Teor. Mat. Fiz. **30**, 193 (1977)
L.M. Ling, The algebraic representation for high order solution of Sasa-Satsuma equation. Discrete Contin. Dyn. Syst. S **9**, 1975 (2016)
L.M. Ling, B.L. Guo, L.C. Zhao, High-order rogue waves in vector nonlinear Schrödinger equations. Phys Rev E, **89**, 041201(R) (2014)
S.V. Manakov, On the theory of two-dimensional stationary self-focusing of electromagnetic waves. Zh. Eksp. Teor. Fiz. **65**, 505 (1973). Sov. Phys. J. Exp. Theor. Phys. **38**, 248 (1974)
S.V. Manakov, V.E. Zakharov, L.A. Bordag, A.R. Its, V.B. Matveev, Two-dimensional solitons of the Kadomtsev-Petviashvili equation and their interaction. Phys. Lett. A **63**, 205 (1977)
V.B. Matveev, M.A. Salle, *Darboux Transformations and Solitons* (Springer-Verlag, Berlin, 1991)
L.F. McGoldrick, Resonant interactions among capillary-gravity waves. J. Fluid Mech. **21**, 305 (1965)
L.F. McGoldrick, An experiment on second order capillary-gravity resonant interactions. J. Fluid Mech. **40**, 251 (1970)
C.R. Menyuk, Nonlinear pulse propagation in birefringent optical fibers. IEEE J. Quantum Electron. **23**, 174 (1987)
A.V. Mikhailov, Integrability of the two-dimensional Thirring model. J. Exp. Theor. Phys. Lett. **23**, 320 (1976)
K. Mio, T. Ogino, K. Minami, S. Takeda, Modified nonlinear Schrödinger equation for Alfvén waves propagating along the magnetic field in cold plasma. J. Phys. Soc. Jpn. **41**, 265 (1976)
J. Moses, B.A. Malomed, F.W. Wise, Self-steepening of ultrashort optical pulses without self-phase-modulation. Phys. Rev. A **76**, 021802(R) (2007)
G. Mu, Z. Qin, Dynamic patterns of high-order rogue waves for Sasa-Satsuma equation. Nonlinear Anal. Real World Appl. **31**, 179 (2016)
G. Mu, Z. Qin, R. Grimshaw, N. Akhmediev, Intricate dynamics of rogue waves governed by the Sasa-Satsuma equation. Physica D **402**, 132252 (2020)
M. Noumi, Y. Yamada, Symmetries in the fourth Painlevé equation and Okamoto polynomials. Nagoya Math. J. **153**, 53 (1999)
S. Novikov, S.V. Manakov, L.P. Pitaevskii, V.E. Zakharov, *Theory of Solitons: The Inverse Scattering Method* (Plenum, New York, 1984)
Y. Ohta, J. Yang, General high-order rogue waves and their dynamics in the nonlinear Schrödinger equation. Proc. R. Soc. A **468**, 1716 (2012a)
Y. Ohta, J. Yang, Rogue waves in the Davey-Stewartson-I equation. Phys. Rev. E **86**, 036604 (2012b)
Y. Ohta, J. Yang, Dynamics of rogue waves in the Davey-Stewartson II equation. J. Phys. A **46**, 105202 (2013)
Y. Ohta, J. Yang, General rogue waves in the focusing and defocusing Ablowitz-Ladik equations. J. Phys. A **47**, 255201 (2014)
Y. Ohta, D. S. Wang, J. Yang, General N-dark-dark solitons in the coupled nonlinear Schrödinger equations. Stud. Appl. Math. **127**, 345 (2011)
K. Okamoto, Studies on the Painlevé equations. III. Second and fourth Painlevé equations, P_{II} and P_{IV}. Math. Ann. **275**, 221 (1986)
D.E. Pelinovsky, Y.A. Stepanyants, New multisoliton solutions of the Kadomtsev-Petviashvili equation. J. Exp. Theor. Phys. Lett. **57**, 24 (1993)
D.E. Pelinovsky, Y.A. Stepanyants, Y.A. Kivshar, Self-focusing of plane dark solitons in nonlinear defocusing media. Phys. Rev. E **51**, 5016 (1995)
D.H. Peregrine, Water waves, nonlinear Schrödinger equations and their solutions. J. Aust. Math. Soc. B **25**, 16 (1983)
V.I. Petviashvili, Equation of an extraordinary soliton. Sov. J. Plasma Phys. **2**, 257 (1976)
O.M. Phillips, Nonlinear dispersive waves. Ann. Rev. Fluid Mech. **6**, 93 (1974)
L.P. Pitaevskii, Vortex lines in an imperfect Bose gas. Sov. Phys. J. Exp. Theor. Phys. **13**, 451 (1961)

J. Rao, Y. Liu, C. Qian, J.S. He, Rogue waves and hybrid solutions of the Boussinesq equation. Z. Naturforsch. A **72**, 307 (2017)
P. Roffelsen, A. Stokes, On real and imaginary roots of generalised Okamoto polynomials (2024). arXiv:2402.15887 [nlin.SI]
A. Romero-Ros, G.C. Katsimiga, S.I. Mistakidis, B. Prinari, G. Biondini, P. Schmelcher, P.G. Kevrekidis, Theoretical and numerical evidence for the potential realization of the Peregrine soliton in repulsive two-component Bose-Einstein condensates. Phys. Rev. A **105**, 053306 (2022)
A. Romero-Ros, G.C. Katsimiga, S.I. Mistakidis, S. Mossman, G. Biondini, P. Schmelcher, P. Engels, P.G. Kevrekidis, Experimental realization of the Peregrine soliton in repulsive two-component Bose-Einstein condensates. Phys. Rev. Lett. **132**, 033402 (2024)
M. Saito, S. Watanabe, H. Tanaca, Modulation instability of ion wave in plasma with negative ion. J. Phys. Soc. Jpn. **53**, 2304 (1984)
P.M. Santini, The periodic Cauchy problem for $\mathcal{PT}$-symmetric NLS, I: the first appearance of rogue waves, regular behavior or blow up at finite times. J. Phys. A **51**, 495207 (2018)
N. Sasa, J. Satsuma, New-type of solutions for a higher-order nonlinear evolution equation. J. Phys. Soc. Jpn. **60**, 409 (1991)
J. Satsuma, M.J. Ablowitz, Two-dimensional lumps in nonlinear dispersive systems. J. Math. Phys. **20**, 1496 (1979)
A.C. Scott, The application of Bäcklund transforms to physical problems, in *Bäcklund Transformations*, ed. by R.M. Miura. Lecture Notes in Mathematics, vol. 515 (Springer-Verlag, Berlin, 1975), pp. 80–105
K. Shimizu, Y.H. Ichikawa, Automodulation of ion oscillation modes in plasma. J. Phys. Soc. Jpn. **33**, 789 (1972)
W.F. Simmons, A variational method for weak resonant wave interactions. Proc. R. Soc. Lond. A **309**, 551 (1969)
S.R. Spangler, J.P. Sheerin, Properties of Alfvén solitons in a finite-Beta plasma. J. Plasma Phys. **27**, 193 (1982)
G.G. Stokes, On the theory of oscillatory waves. Trans. Cambridge Philos. Soc. **8**, 441 (1847)
R. Sugaya, M. Sugawa, H. Nomoto, Experimental observation of explosive instability due to a helical electron beam. Phys. Rev. Lett. **39**, 27 (1977)
W. Sun, L. Liu, P.G. Kevrekidis, Rogue waves of ultra-high peak amplitude: a mechanism for reaching up to a thousand times the background level. Proc. R. Soc. A **477**, 20200842 (2021)
M. Tajiri, T. Arai, Growing-and-decaying mode solution to the Davey-Stewartson equation. Phys. Rev. E **60**, 2297 (1999)
M. Tajiri, Y. Murakami, Rational growing mode: exact solutions to the Boussinesq equation. J. Phys. Soc. Jpn. **60**, 2791 (1991)
W.E. Thirring, A soluble relativistic field theory. Ann. Phys. **3**, 91 (1958)
M. Taneda, Remarks on the Yablonskii-Vorob'ev polynomials. Nagoya Math. J. **159**, 87 (2000)
M. Toda, Studies of a nonlinear lattice. Phys. Rep. **8**, 1 (1975)
S. Tsuchiya, F. Dalfovo, L.P. Pitaevskii, Solitons in two-dimensional Bose-Einstein condensates. Phys. Rev. A **77**, 045601 (2008)
H. Umemura, H. Watanabe, Solutions of the second and fourth Painlevé equations. Nagoya Math. J. **151**, 1 (1998)
F. Ursell, The long-wave paradox in the theory of gravity waves. Proc. Camb. Phil. Soc. **49**, 685 (1953)
A.P. Vorob'ev, On rational solutions of the second Painlevé equation. Differ. Eqn. **1**, 58 (1965)
P.K.A. Wai, C.R. Menyuk, Polarization mode dispersion, decorrelation, and diffusion in optical fibers with randomly varying birefringence. J. Lightwave Technol. **14**, 148 (1996)
D. Wang, D. Zhang, J. Yang, Integrable properties of the general coupled nonlinear Schrödinger equations. J. Math. Phys. **51**, 023510 (2010)
X. Wang, J. Cao, Y. Chen, Higher-order rogue wave solutions of the three-wave resonant interaction equation via the generalized Darboux transformation. Phys. Scr. **90**, 105201 (2015)

L. Wang, C.H. Yang, J. Wang, J.S. He, The height of an nth-order fundamental rogue wave for the nonlinear Schrödinger equation. Phys. Lett. A **381**, 1714 (2017)
X.Y. Wen, Z. Yan, Y. Yang, Dynamics of higher-order rational solitons for the nonlocal nonlinear Schrödinger equation with the self-induced parity-time-symmetric potential. Chaos **26**, 063123 (2016)
G.B. Whitham, Nonlinear dispersion of water waves. J. Fluid Mech. **27**, 399 (1967)
H.G. Winful, G.D. Cooperman, Self-pulsing and chaos in distributed feedback bistable optical devices. Appl. Phys. Lett. **40**, 298 (1982)
O.C. Wright, Effective integration of ultra-elliptic solutions of the focusing nonlinear Schrödinger equation. Physica D **321**, 16 (2016)
C. Wu, G. Zhang, C. Shi, B.F. Feng, General rogue wave solutions to the Sasa-Satsuma equation (2022). arXiv:2206.02210 [nlin.SI]
S.W. Xu, J.S. He, The rogue wave and breather solution of the Gerdjikov-Ivanov equation. J. Math. Phys. **53**, 063507 (2012)
S.W. Xu, J.S. He, L.H. Wang, The Darboux transformation of the derivative nonlinear Schrödinger equation. J. Phys. A **44**, 305203 (2011)
G. Xu, K. Hammani, A. Chabchoub, J.M. Dudley, B. Kibler, C. Finot, Phase evolution of Peregrine-like breathers in optics and hydrodynamics. Phys. Rev. E **99**, 012207 (2019)
G. Xu, A. Chabchoub, D.E. Pelinovsky, B. Kibler, Observation of modulation instability and rogue breathers on stationary periodic waves. Phys. Rev. Res. **2**, 033528 (2020)
A.I. Yablonskii, On rational solutions of the second Painlevé equation. Vesti Akad. Navuk. BSSR Ser. Fiz. Tkh. Nauk. **3**, 30 (1959) (in Russian)
N. Yajima, M. Oikawa, Formation and interaction of sonic-Langmuir solitons: inverse scattering method. Prog. Theor. Phys. **56**, 1719 (1976)
J. Yang, *Nonlinear Waves in Integrable and Nonintegrable Systems* (SIAM, Philadelphia, 2010)
J. Yang, General N-solitons and their dynamics in several nonlocal nonlinear Schrödinger equations. Phys. Lett. A **383**, 328 (2018)
B. Yang, J. Yang, Rogue waves in the nonlocal $\mathcal{PT}$-symmetric nonlinear Schrödinger equation. Lett. Math. Phys. **109**, 945 (2019)
B. Yang, J. Yang, General rogue waves in the Boussinesq equation. J. Phys. Soc. Jpn. **89**, 024003 (2020a)
B. Yang, J. Yang, On general rogue waves in the parity-time-symmetric nonlinear Schrödinger equation. J. Math. Anal. Appl. 124023 (2020b)
B. Yang, J. Yang, Rogue wave patterns in the nonlinear Schrödinger equation. Physica D **419**, 132850 (2021a)
B. Yang, J. Yang, General rogue waves in the three-wave resonant interaction systems. IMA J. Appl. Math. **86**, 378 (2021b)
B. Yang, J. Yang, Universal rogue wave patterns associated with the Yablonskii-Vorob'ev polynomial hierarchy. Physica D **425**, 132958 (2021c)
B. Yang, J. Yang, Rogue waves in (2+1)-dimensional three-wave resonant interactions. Physica D **432**, 133160 (2022a)
B. Yang, J. Yang, Pattern transformation in higher-order lumps of the Kadomtsev-Petviashvili I equation. J. Nonl. Sci. **32**, 52 (2022b)
B. Yang, J. Yang, Overview of the Kadomtsev-Petviashvili-hierarchy reduction method for solitons. Partial Differ. Equ. Appl. Math. **5**, 100346 (2022c)
B. Yang, J. Yang, Rogue wave patterns associated with Okamoto polynomial hierarchies. Stud. Appl. Math. **151**, 60 (2023a)
B. Yang, J. Yang, Partial-rogue waves that come from nowhere but leave with a trace in the Sasa-Satsuma equation. Phys. Lett. A **458**, 128573 (2023b)
B. Yang, J. Yang, Rogue wave patterns associated with Adler-Moser polynomials in the nonlinear Schrödinger equation. Appl. Math. Lett. **148**, 108871 (2024a)
B. Yang, J. Yang, Rogue curves in the Davey-Stewartson I equation (2024b). Chaos **34**, 073148 (2024)

B. Yang, J. Chen, J. Yang, Rogue waves in the generalized derivative nonlinear Schrödinger equations. J. Nonl. Sci. **30**, 3027 (2020)

A. Yariv, *Quantum Electronics*, 2nd edn. (John Wiley & Sons, New York, 1975)

Y.L. Ye, L.L. Bu, C.C. Pan, S.H. Chen, D. Mihalache, F. Baronio, Super rogue wave states in the classical massive Thirring model system. Rom. Rep. Phys. **73**, 117 (2021)

N.J. Zabusky, A synergetic approach to problems of nonlinear dispersive wave propagation and interaction, in *Nonlinear Partial Differential Equations*, ed. by W.F. Ames (Academic Press, New York, 1967), pp. 233–258

V.E. Zakharov, Stability of periodic waves of finite amplitude on the surface of a deep fluid. Zh. Prikl. Mekh. Tekh. Fiz **9**, 86 (1968) (Transl. in J. Appl. Mech. Tech. Phys. 9, 190)

V.E. Zakharov, On stochastization of one-dimensional chains of nonlinear oscillators. Zh. Eksp. Teor. Fiz. **65**, 219 (1973). Sov. Phys. J. Exp. Theor. Phys. **38**, 108 (1974)

V.E. Zakharov, A.B. Shabat, Exact theory of two-dimensional self-focusing and one-dimensional self-modulation of waves in nonlinear media. Zh. E'ksp. Teor. Fiz. **61**, 118 (1971). Sov. Phys. J. Exp. Theor. Phys. **34**, 62 (1972)

Y.S. Zhang, L.J. Guo, A. Chabchoub, J.S. He, Higher-order rogue wave dynamics for a derivative nonlinear Schrödinger equation. Rom. J. Phys. **62**, 102 (2017)

G. Zhang, Z. Yan, X.Y. Wen, Three-wave resonant interactions: Multi-dark-dark-dark solitons, breathers, rogue waves, and their interactions and dynamics. Physica D **366**, 27 (2018)

L.C. Zhao, S.C. Li, L.M. Ling, Rational W-shaped solitons on a continuous-wave background in the Sasa-Satsuma equation. Phys. Rev. E **89**, 023210 (2014)

L.C. Zhao, B.L. Guo, L.M. Ling, High-order rogue wave solutions for the coupled nonlinear Schrödinger equations-II. J. Math. Phys. **57**, 043508 (2016a)

L.C. Zhao, S.C. Li, L.M. Ling, W-shaped solitons generated from a weak modulation in the Sasa-Satsuma equation. Phys. Rev. E **93**, 032215 (2016b)

Zhaqilao, *N*th-order rogue wave solutions of the complex modified Korteweg-de Vries equation. Phys. Scr. **87**, 065401 (2013)

Index

B. Yang, J. Yang, *Rogue Waves in Integrable Systems*,
https://doi.org/10.1007/978-3-031-66793-0